UNIVERSIDAD NACIONAL AUTÓNOMA DE MÉXICO

Maestría y Doctorado en Ciencias Bioquímicas

PROTEÓMICA Y LIPIDÓMICA DE LA MICROALGA OLEAGINOSA
Ettlia oleoabundans

TESIS

QUE PARA OPTAR POR EL GRADO DE:

Doctor en Ciencias

PRESENTA:
M. en C. ADRIANA GARIBAY HERNÁNDEZ

DR. OMAR HOMERO PANTOJA AYALA
Instituto de Biotecnología, Universidad Nacional Autónoma de México

DR. OTTO GEIGER
Centro de Ciencias Genómicas, Universidad Nacional Autónoma de México

DR. RAFAEL VÁZQUEZ DUHALT
Centro de Nanociencias y Nanotecnología, Universidad Nacional Autónoma de México

Ciudad de México. Agosto, 2019

Proteómica y lipidómica de la microalga oleaginosa Ettlia oleoabundans

Proteomics and lipidomics of the oleaginous microalga Ettlia oleoabundans

M. en C. Adriana Garibay Hernández

El presente trabajo se realizó en el Departamento de Biología Molecular de Plantas del Instituto de Biotecnología de la Universidad Nacional Autónoma de México. Para la realización del mismo se contó con financiamiento por parte del Consejo Nacional de Ciencia y Tecnología (CONACyT) y del Programa de Apoyo a los Estudios de Posgrado (PAEP)

Instituto de Biotecnología
UNIVERSIDAD NACIONAL AUTÓNOMA DE MÉXICO

M. EN C. ADRIANA GARIBAY HERNANDEZ

Por medio del presente me permito informar a usted que en la reunión del día 03 de diciembre del 2018 el Subcomité Académico acordó nombrar el siguiente jurado para Examen de Doctorado en Ciencias, con **No.de cuenta 508012855** con la tesis titulada, **"Proteómica y lipidómica de la microalga oleaginosa *Ettlia oleoabundans*"** dirigida por el **Dr. Omar Homero Pantoja**

Presidente	Dra.	Patricia León Mejía
Secretario	Dra.	Marina Gavilanes Ruiz
Vocal	Dra.	Rosa Victoria Pando Robles
Vocal	Dr.	Diego González Halphen
Vocal	Dr.	Christian Sohlenkamp

Sin más por el momento me es grato enviarle un cordial saludo.

A T E N T A M E N T E
"POR MI RAZA HABLARA EL ESPIRITU"
Cuernavaca, Mor. a 03 de diciembre de 2018

Dra. Marcela Ayala Aceves
Coordinadora de Docencia

En un plazo máximo de **tres semanas**, contados a partir del momento en que el sinodal designado oficialmente reciba la tesis, éste deberá dar su voto fundamentado por escrito, el cual será comunicado al comité académico. Si considera que le será imposible cumplir con esta obligación deberá indicarlo al alumno para ser sustituido de inmediato.

AV. UNIVERSIDAD 2001. COL. CHAMILPA
C.P. 62210 CUERNAVACA, MORELOS, MÉXICO
TELS. (5255) 5622 7600 - (777) 329 1600
www.ibt.unam.mx

A mi familia, con amor, por supuesto

“Tal es, para decirlo con la frase de Ortega y Gasset, el ‘tema de nuestro tiempo’: ***la sustancia de nuestros sueños y el sentido de nuestros actos****.*

El hombre moderno tiene la pretensión de pensar despierto. Pero este despierto pensamiento nos ha llevado por los corredores de una sinuosa pesadilla, en donde los espejos de la razón multiplican las cámaras de tortura. Al salir, acaso, descubriremos que habíamos soñado con los ojos abiertos y que los sueños de la razón son atroces. Quizá, entonces, empezaremos a soñar otra vez con los ojos cerrados.”

Octavio Paz, *El laberinto de la soledad*

Agradecimientos / Acknowledgements

Antes que nada, y al final de todo, a mi familia. Gracias mamá y papá por su esfuerzo y dedicación para darme la posibilidad de un futuro mejor. Gracias por su apoyo y amor incondicional, a pesar de que estoy consciente de que la estaban pasando mal. Disculpen el obstinarme en ser como soy, pero nunca duden que en el proceso de perseguir la posibilidad de ser yo misma, intento ser fiel a lo poco que ingratamente les he aprendido: trabajar duro e intentar ser una persona de bien.

Gracias Beto y Miguel, por quererme y estar conmigo. A todos lados siempre los llevo en el corazón. Los quiero mucho hermanitos.

A Benjamín, por apoyarme en gran parte de este largo y complicado proceso. A pesar del tedio, sabes que eres parte de este resultado y te lo agradezco enormemente.

Al Dr. Omar Pantoja. Gracias Boss por recibirme en su laboratorio y por, a pesar de lo inusual de mi situación, haberme apoyado en el desarrollo de este proyecto. Muchas gracias por creer en mí, por su paciencia, y por darme palabras de aliento, en persona o a distancia, especialmente cuando ya no podía seguir adelante. Gracias por transmitirme su pasión y compromiso con la ciencia, por contribuir a la formación del científico que en algún momento quisiera llegar a ser. ¡Muchas gracias por introducirme al mundo de la biología de membranas!

To Dr. Bronwyn Barkla. Thank you for adopting me as a non-official pupil, and for all your support, knowledge and opportunities that you have provided me despite the huge distance between us. I am very thankful for having the opportunity to learn so much from you, as a person and as a woman in science.

Gracias Omar y Bronwyn por siempre estar disponibles, por su tiempo, sus consejos y su ejemplo.

A los miembros de mi Comité Tutoral, Dr. Rafael Vázquez Duhalt y Dr. Otto Geiger. Les agradezco enormemente su comprensión, compromiso, y apoyo a lo largo de las distintas etapas de este proceso. Muchas gracias por su paciencia, accesibilidad, recomendaciones y enseñanzas durante mi formación como doctorante. Gracias por siempre haber tenido las puertas de sus oficinas abiertas para mí y por recibirme en sus laboratorios como uno más de sus estudiantes. Gracias por haberme permitido aprender de ustedes.

A los miembros del jurado. Muchas gracias por su accesibilidad para llevar a cabo la revisión de la tesis, así como por sus comentarios y recomendaciones, los cuales definitivamente han contribuido a la discusión y mejoramiento de la misma.

To Dr. Hans-Peter Mock. I am not able to find the words to express how thankful I am for the opportunity of working at the IPK. Thank you for opening the doors of your group and for providing me the unique possibility to re-start/continue my path in science. Thank you for your patience, for listening to me, especially in the difficult times, for teaching me, and for the great opportunity of learning so much.

To Dr. Michael Schroda. Thank you for contributing to the opportunity to continue my scientific career in Germany. Having met you and every of the discussions we have had, keep me always motivated.

Gracias a cada una de las personas que durante mi estancia en el IBt-UNAM me regalaron parte de su tiempo para acompañarme, apoyarme y/o alentarme durante este periodo. A muchos de ustedes tengo la gran fortuna de tenerlos como amigos y les agradezco enormemente sus palabras, así como el hacer especiales, a veces divertidos y a veces llevaderos, mis días de trabajo.

A miembros (previos y actuales) del Laboratorio del Dr. Omar Pantoja: Delia Narváez, Gustavo Lastiri, Ruth García, Daniel Lagunas, Carolina Yáñez, Paul Rosas y Guadalupe Muñoz.

A miembros del laboratorio vecino: Gustavo Rodríguez, Ramcés García, Mayra López y Héctor Torres.

A miembros (previos y actuales) del Laboratorio de Ingeniería de Vías Metabólicas: Alberto Rodríguez, Andrés Martínez, José de Jesús González, Carmen Espinoza, Cinthia Ávila, Mitsue León, Iván Muñoz, José Utrilla, Estefanía Sierra, Berenice Trujillo, Cessna Moss, Alejandra Aquino, Luis Caspeta, Marco Tulio Fernández, Alejandra Vargas, Luz Ma. Martínez, Delia Caro, Mercedes Enzaldo y Aurelia Ocampo.

A todos los miembros del laboratorio del Dr. Lorenzo Segovia y la Dra. Claudia Martínez, alias “mi laboratorio adoptivo”. La “infiltrada” les agradece su compañía y buenos momentos con mucho cariño. Muchas gracias, Delia Narváez (sí, de nuevo), Omar Tovar, Iris Bravo, Blanca Ramos, Mabel Rodríguez, Fernando García y Rafael López.

A Mario Alberto Caro de la Unidad de Escalamiento y Planta Piloto por su enorme apoyo y cariño.

A la Dra. Carmen Beltrán. Muchas gracias por su amistad y palabras de aliento.

A la Unidad de Docencia del IBt-UNAM por siempre apoyarme en todos mis trámites durante este largo periodo.

Part of this long journey has occurred during my stay at the IPK-Gatersleben. Therefore, I would also like to thank to every person that has supported me in this new adventure in Germany.

To the members of the ABC group: Anna Jozefowicz, Anna-Lena Gippert, Sina Marquardt, Paul Solórzano, Nandhakumar Shanmugaraj, Elena Brückner, Annegret Wolf and Petra Linow. Thank you for being so nice colleagues, for contributing to such a friendly and collaborative working atmosphere, and for making so enjoyable my work in the group.

Thanks to Ricardo Giehl, Yudelsy Tandrón, Jonathan Brassac and Anna Jozefowicz for believing in me, for your patience, for staying in the difficult times, and for being my adoptive family in Gatersleben. ¡Muchas gracias amigos!

Contents

Resumen

Ettlia oleoabundans (sinónimo taxonómico de *Neochloris oleoabundans*) es una microalga verde oleaginosa cuyo genoma no ha sido secuenciado. A pesar del renovado interés en el uso de sus lípidos para la generación de productos de valor agregado, el conocimiento de su fisiología y bioquímica es aún limitado, particularmente cuando crece bajo deficiencia de nitrógeno (N), condición caracterizada por inducir la acumulación de lípidos. Con el propósito de comprender los mecanismos relacionados con la síntesis y acumulación de lípidos en *E. oleoabundans*, superando las limitaciones inherentes al estudio de organismos no modelo, en el presente trabajo se realizó un análisis cuantitativo utilizando tecnologías ómicas, complementado con un enfoque multidisciplinario. El estudio se centró en el análisis de los lípidos y proteínas de membrana con el objetivo de determinar los mecanismos a través de los cuales las membranas biológicas contribuyen a la respuesta inducida por deficiencia de N.

Los resultados de este trabajo sustentan la reasignación taxonómica de *E. oleoabundans* de la clase *Chlorophyceae*, en la cual originalmente se encontraba clasificada, a la clase *Trebouxiophyceae*, impactando directamente la interpretación de los procesos fisiológicos que ocurren en la microalga. La curación manual del proteoma de membrana, generado mediante un enfoque basado en RNA-Seq, posibilitó proveer una descripción detallada de los procesos biológicos que acontecen en las membranas de *E. oleoabundans* crecida bajo deficiencia de N, con un enfoque en el metabolismo lipídico. Esto permitió la identificación de proteínas consideradas exclusivas de organismos fotosintéticos superiores (PSBS y MPH1: Photosynthetic II Subunit S y Maintenance of Photosystem II under High Light1), así como de la nueva proteína RP2-CLC (Retinitis Pigmentosa Type 2-Clathrin Light Chain), cuya arquitectura no ha sido descrita. Asimismo, se demostró la existencia del lípido de betaína, diacilgliceril-*N,N,N*-trimetilhomoserina en *E. oleoabundans*, además de su capacidad de sintetizar fosfatidilcolina mediante la *N*-metilación de fosfatidiletanolamina dependiente de *S*-adenosil-L-metionina (SAM).

Fundamentándose en los resultados de este trabajo, se propone un modelo tentativo para los complejos procesos biológicos que acontecen en *E. oleoabundans* ante condiciones de deficiencia de N. Se postula que la acumulación de lípidos es acompañada por cinco eventos mayoritarios, los cuales no necesariamente ocurren de modo secuencial: (1) adaptación de la actividad fotosintética y reajuste de la disponibilidad de ATP/NADPH para reducir el daño foto-oxidativo; (2) producción de especies reactivas de oxígeno en el

cloroplasto y remodelación de sus membranas, procesos que a su vez podrían inducir un mecanismo de autofagia; (3) regulación del metabolismo lipídico a nivel del metabolismo de ácidos grasos (biosíntesis *de novo* y catabolismo); (4) remodelación de los lípidos extra-cloroplásticos, acompañada por una mayor *N*-metilación de glicerolípidos dependiente de SAM; y, (5) coordinación inter-organelar de la respuesta a deficiencia de N mediada por el estado redox de la célula.

El estudio presentado en este documento provee nuevos hallazgos referentes a la fisiología de *E. oleoabundans*, así como un panorama integral de los complejos procesos celulares que acontecen en las membranas de la microalga en respuesta a la deficiencia de N, acompañados por la consecuente acumulación de lípidos.

Abstract

Ettlia oleoabundans (taxonomic synonym of *Neochloris oleoabundans*) is a non-sequenced oleaginous green microalga. Despite the interest in the use of this organism to produce value-added compounds from its acyl-lipids, a basic understanding of its physiology and biochemistry is lacking, especially under nitrogen (N) deprivation conditions known to trigger lipid accumulation. To overcome the limitations inherent to non-model organisms and understand the mechanisms underlying changes in the lipid metabolism and storage of *E. oleoabundans*, a quantitative omics-based study, complemented with multidisciplinary approaches, was performed. A special focus on lipid and protein membrane constituents was conducted to understand how these are involved in the functions of biological membranes to cope with N deprivation.

The present work provides compelling evidence supporting the taxonomical reclassification of *E. oleoabundans* within the *Trebouxiophyceae* class of green microalgae, rather than in the *Chlorophyceae* class, therefore influencing the interpretation of its physiology. Using an RNA-Seq-based proteomics approach, the manual annotation of the membrane protein components enabled an accurate description of the cellular processes occurring on the membranes of this microalga upon N deprivation, with special focus on lipid metabolism. The detailed analysis of both protein and membrane components proved essential to uncover novel aspects of its physiology. These included the identification of membrane proteins considered exclusive to higher photosynthetic organisms (Photosynthetic II Subunit S and Maintenance of Photosystem II under High Light1) and the novel protein Retinitis Pigmentosa Type 2-Clathrin Light Chain. The existence of the betaine lipid diacylglyceryl-*N,N,N*-trimethylhomoserine and the capability of *E. oleoabundans* to synthesize phosphatidylcholine via the *S*-adenosyl-L-methionine (SAM)-dependent *N*-methylation of phosphatidylethanolamine were also discovered.

A working model is postulated based on the results from this study. A complex response, summarized in five major events not necessarily occurring in sequence, is proposed to accompany lipid accumulation in N-deprived *E. oleoabundans*: (1) fine-tuning of photosynthesis and adjustment of ATP/NADPH ratios to reduce photo-oxidative damage; (2) active production of reactive oxygen species in the plastid, accompanied by chloroplast membrane remodeling, and likely triggering an autophagic flux; (3) regulation of lipid metabolism at the acyl-lipid level (*de novo* FA biosynthesis and catabolism); (4) remodeling of extra-chloroplastic lipids, supported by the induction of SAM-dependent glycerolipid *N*-

methylation; and (5) inter-organellar redox-mediated coordination of the cellular response to N stress.

This study uncovers novel physiological features of *E. oleoabundans* and provides new insights into the complex cellular basis of N stress response and lipid metabolism in this non-model oleaginous microalga.

1. Introduction

Microalgae represent an exceptionally diverse but highly specialized group of microorganisms adapted to various ecological habitats (Hu et al., 2008). In recent years, oleaginous microalgae (lipid contents higher than 20% w/w of their dry weight) have attracted renewed interest owing to the potential of using their acyl-lipids as energy-rich feedstocks for the sustainable production of biofuels and countless value added compounds (nutraceuticals, lubricants, plastics, paints, natural insecticides, cosmetics, etc.) (Hu et al., 2008; Liu and Benning, 2013; Horn and Benning, 2016).

Ettlia oleoabundans is a non-sequenced oleaginous green microalga, that despite its potential biotechnological application, a basic understanding of its physiology and biochemistry is lacking, especially under nitrogen (N) deprivation conditions known to trigger lipid accumulation (Tornabene et al., 1983; Li et al., 2008; Pruvost et al., 2009; Breuer et al., 2012; Garibay-Hernández et al., 2013). To understand the mechanisms underlying changes in lipid metabolism in response to N depletion, comparative mass-spectrometry (MS)-based shotgun proteomics and lipidomics analyses were performed, together with microscopy and lipid kinetic labeling experiments, as well as classic biochemical approaches.

1.1. *Ettlia oleoabundans*

Ettlia oleoabundans (taxonomic synonym of *Neochloris oleoabundans*) is a unicellular edaphic green microalga isolated from the top of sand dunes in Saudi Arabia that belongs to the *Chlorophyta* phylum and is placed within the *Chlorophyceae* class (Chantanachat and Bold, 1962; Deason et al., 1991). It was initially classified within the genus *Neochloris* (Starr, 1955), from which this and other species showing uninucleate vegetative cells were reclassified into the genus *Ettlia* (Komárek, 1989; Deason et al., 1991). The classification of coccoid green algae, such as *E. oleoabundans*, is described as a “taxonomic nightmare”, because the ultrastructural features in which it has largely relied have not resolved their polyphyleticism, resulting in cases of either cryptic diversity or similarity. Therefore, a taxonomic revision of the species within the *Ettlia* genus is still pendant (Pegg et al., 2015).

The knowledge of the *E. oleoabundans* cell architecture is minimal, being limited to the characters defining the *Ettlia* genus that are based on its type species *E. carotinosa*: spherical/subspherical uninucleate vegetative cells showing a parietal chloroplast that comprises at least one pyrenoid; and thin-walled zoospores, with clockwise orientation of

the flagellar apparatus (Deason et al., 1991). It remains to be determined if all of these features are present in *E. oleoabundans*, because its ultrastructure was not studied when moved into the *Ettlia* genus and current information is limited to its coccoid (unicellular, non-motile) phase. Nonetheless, being a photosynthetic eukaryote derived from a single primary endosymbiotic event, *E. oleoabundans* cells are expected to have the following intracellular components: double membrane-bound chloroplast, nucleus, mitochondria, microbodies (peroxisomes), vacuole, endoplasmic reticulum, Golgi apparatus and cytoplasmic vesicles (Lewis and McCourt, 2004; Harris, 2009). Based on the diagnostic features for both, the *Neochloris* and *Ettlia* genera (Deason et al., 1991), *E. oleoabundans* is expected to present a pyrenoid, which is a plastidic microcompartment easily visible by light microscopy, whose known function is to enhance the photosynthetic CO_2 fixation by the ribulose-1,5-biphosphate carboxylase/oxygenase (Zhan et al., 2018). All embryophytes (except for hornworts) lack pyrenoids, whereas their presence/absence in algae is phylogenetically meaningful (Lewis and McCourt, 2004). Besides the energy-producing organelles, the characterization of intracellular compartments such as vacuoles and peroxisomes has received little attention in microalgae. In the last six years only few reports, together with this work, are providing the first insights into *E. oleoabundans* cell architecture (Baldisserotto et al., 2012; Giovanardi, 2013; Sabia et al., 2015; Rashidi and Trindale, 2018).

Due to its high lipid content (up to 56% w/w of its dry weight), *E. oleoabundans* is classified as an oleaginous microalga (Gouveia et al., 2009). It is a highly versatile organism as it can grow in freshwater, wastewater (Levine et al., 2011; Wang and Lan, 2011; Yang et al., 2011), and in culture media with salt concentrations up to sea water levels (Arredondo-Vega et al., 1995; Baldisserotto et al., 2012; Popovich et al., 2012). Moreover, it is able to grow under phototrophic, mixotrophic (Giovanardi et al., 2013; Baldisserotto et al., 2016) and heterotrophic (Wu et al., 2011; Morales-Sánchez et al., 2013) conditions. Owing to its high lipid content and growth versatility, *E. oleoabundans* is an organism of biotechnological interest.

Many microalgae alter their lipid biosynthetic pathways towards the formation and accumulation of neutral lipids under stress conditions imposed by chemical or physical environmental stimuli, either acting individually or in combination. Amongst these, N limitation has proved to be the most critical condition triggering lipid storage in numerous microalgae of different taxa (Hu et al., 2008). In line with this, a large extent of microalgal research has not focused on understanding N assimilation mechanisms, but on using this stress to alter lipid metabolism. Most research in *E. oleoabundans* has thus centered on

improving its lipid yield and productivity under N deficiency conditions through different culture strategies (Tornabene et al., 1983; Li et al., 2008; Pruvost et al., 2009; Breuer et al., 2012; Garibay-Hernández et al., 2013), and evaluating how other environmental factors (*e.g.* light intensity, pH, temperature, salinity, oxygen and CO_2 supply) additionally control lipid production (Gouveia et al., 2009; Wang and Lan, 2011; Yang et al., 2011; Popovich et al., 2012; Santos et al., 2012; Sousa et al., 2012). A decreased cell proliferation, accompanied by an increased biomass on a per cell basis owing to the accumulation of storage compounds, mainly triacylglycerols (TAG) but also starch, has proved to be a hallmark of N-deprived *E. oleoabundans* (Breuer et al., 2012; Rismani-Yazdi et al., 2012; Garibay-Hernández et al., 2013). Another characteristic feature of *E. oleoabundans* upon N stress is an increased saturation of its fatty acid (FA) profile due to the higher content of 18:0 (number of carbon atoms:number of double bonds in the FA), but mainly 18:1, together with decreased levels of 18:2 and 18:3 FA (Levine et al., 2011; Breuer et al., 2012; Rismani-Yazdi et al., 2012; Garibay-Hernández et al., 2013).

Despite the existing research on improving neutral lipid yield in *E. oleoabundans*, its membrane lipid composition and its lipid metabolism, remain understudied. Prior to this project, the glycerolipid composition of this microalga was qualitatively assessed in a single study according to which *E. oleoabundans* comprises steryl-esters, mono-, di- and triacylglycerides within its neutral lipids, as well as the polar glycerolipids: monogalactosyldiacylglycerol (MGDG), digalactosyldiacylglycerol (DGDG), phosphatidylcholine (PC), phosphatidylethanolamine (PE), phosphatidylserine (PS), phosphatidylinositol (PI), phosphatidylglycerol (PG) and cardiolipin (CL) (Tornabene et al., 1983). Only recently, together with the work described hereby, insights into the biology and biochemistry behind N deficiency and lipid accumulation are being provided (Rismani-Yazdi et al., 2012; Benvenuti et al., 2015; Baldisserotto et al., 2016; Matich et al., 2016, 2018; Goh et al., 2017; Sturme et al., 2018), emphasizing the lack of knowledge of the physiology from *E. oleoabundans*.

1.2. General aspects of microalgal lipid metabolism

In contrast with other eukaryotes such as animals, yeast and land plants, lipid metabolism and neutral lipid accumulation in algae have remained largely unexplored. The state-of-the-art knowledge of microalgal lipid metabolism at the beginning of this work is summarized by Hu et al., 2008. Due to the limited evidence at that moment, the basic pathways of lipid

metabolism in algae were considered analogous to those in higher plants. Along the last ten years, this status has been updated by the wealth of data provided through omics approaches, showing that many aspects of lipid metabolism in microalgae deviate from plants (Merchant et al., 2012; Liu and Benning, 2013; Zienkiewicz et al., 2016; Li-Beisson et al., 2019). Most knowledge on algal lipid metabolism though, is still based on non-experimentally verified genome predictions and orthologous relationships to enzymes of known function in other eukaryotes, mainly in the model plant *Arabidopsis thaliana*, and to a lesser extent, it is supported by direct studies in algal systems (Stern, 2009; Khozin-Goldberg and Cohen, 2011; Merchant et al., 2012; Liu and Benning, 2013; Zienkiewicz et al., 2016; Li-Beisson et al., 2019).

The main differences between the lipid metabolism of land plants and microalgae are summarized in Table 1.1. Firstly, striking differences in their glycerolipid composition do exist, as contrary to land plants, betaine lipids (non-phosphorous zwitterionic ether-linked glycerolipids) are frequently present in microalgae species, several of which either lack or contain few PC (Riekhof et al., 2005; Guschina and Harwood, 2006; Liu and Benning, 2013), a membrane bilayer-forming molecule central to lipid metabolism in plants, where it is the most abundant extraplastic glycerolipid (Bates et al., 2007; Bates, 2016; Nakamura, 2017). Land plants and microalgae also differ in their FA composition, being the latter able to synthesize several species of very long chain polyunsaturated FA (VLCPUFA) in high amounts (*e.g.* eicosapentaenoic, docosahexaenoic and arachidonic acids) (Harwood and Guschina, 2009; Nakamura and Li-Beisson, 2016).

Second, the genetic complexity underlying lipid metabolism is often higher in land plants when compared to microalgae (Hu et al., 2008; Merchant et al., 2012). However, exceptions do exist, as homology-based analyses have shown that some lipid metabolism proteins (*e.g.* the acyl-coenzyme A:diacylglycerol acyltransferase, DGAT) are encoded by more gene copies in microalgae than in land plants (Liu and Benning, 2013). Third, lipid accumulation in microalgae takes place in single photosynthetically active cells, whereas in plants it generally occurs in specialized tissues that are often not photosynthetically active (*e.g.* seeds, fruits, pollen grains). Finally, lipid accumulation in microalgae is triggered by environmental stressors, while in specialized tissues/organs of land plants it is usually subjected to developmental control (Liu and Benning, 2013; Zienkiewicz et al., 2016).

Table 1.1. Major aspects differing between the lipid metabolism of microalgae and land plants.

Aspect	Land plants	Microalgae
Lipid composition	*PC is the most abundant extraplastic lipid, central to lipid metabolism. VLCPUFA are not produced in significant amounts.*	*Betaine lipids are present in species with low amounts or lacking PC. Algae can produce large quantities of VLCPUFA.*
Genetic complexity	*Multiple genes encoding proteins with redundant activities.*	*Smaller number of gene homologs predicted for a specific function.*
TAG synthesis location	*Occurs in specialized individual tissues/organs.*	*Occurs, from CO_2 fixation to TAG synthesis, in a single cell.*
TAG accumulation	*Subjected to developmental control in specialized tissues/organs.*	*Triggered by environmental stressors.*

Chlamydomonas reinhardtii is a green microalga belonging to the *Chlorophyceae* class, which currently provides the best model for microalgal lipid research (Merchant et al., 2012; Liu and Benning, 2013). Compared with other microalgae, the physiology of *C. reinhardtii* has been thoroughly studied, it accounts with a fully sequenced and annotated genome, as well as with a molecular toolkit enabling its study through genetic approaches (Stern, 2009; Merchant et al., 2012; Liu and Benning, 2013; Li-Beisson et al., 2015; Crozet et al., 2018). The lipid composition of *C. reinhardtii* has been fully characterized and its physiology upon N deprivation has been studied using multiple approaches (Giroud et al., 1988; Miller et al., 2010; Boyle et al., 2012; Longworth et al., 2012; Msanne et al., 2012; Schmollinger et al., 2014; Li-Beisson et al., 2015).

Although differences exist between *C. reinhardtii* and land plants, their major pathways for acyl-lipid metabolism are predicted to be conserved, and can be dissected intro three simplified phases indicated in Fig. 1.1 (Stern, 2009; Li-Beisson et al., 2015; Nakamura, 2017; Li-Beisson et al., 2019). The first phase is *de novo* FA biosynthesis that is presumed to occur exclusively in the chloroplast. Its first committing step consists on the irreversible ATP-dependent carboxylation of acetyl-CoA, the direct carbon precursor for acyl-lipid biosynthesis, catalyzed by a multi-subunit bacterial-type acetyl-CoA carboxylase (ACCase) comprised by four different polypeptides: biotin carboxylase, biotin carboxyl carrier protein, α- and β-carboxyltransferase. A new ACCase subunit, termed BADC (biotin attachment domain-containing), was recently identified in land plants and in a limited subset of green algae. This protein acts as an ACCase negative regulator (Salie et al., 2016; Li-Beisson et al., 2019). Further carbon-chain elongation steps to produce 16- and 18-carbon FA are performed by the multipartite fatty acid synthase (FAS), which involves four different

enzymes: ketoacyl-acyl carrier protein (ACP) synthase, ketoacyl-ACP reductase, hydroxyacyl-ACP dehydrase and enoyl-ACP reductase.

The second phase consists on the first steps of the Kennedy pathway. These steps take place either, in the chloroplast or endoplasmic reticulum (ER) membranes, where acyltransferases sequentially attach ACP- or CoA-activated FA, respectively, into G3P to produce LPA and then, PA. The dephosphorylation of PA generates DAG, which is the penultimate intermediate of the Kennedy pathway. In the third phase, DAG is used either in its free form or as activated cytidine diphosphate (CDP-DAG) for the synthesis of glycerolipids. In this third phase, regarding neutral glycerolipids, TAG formation resembles that on yeast and land plants, as homologs for two enzymes directly-involved in its synthesis from free DAG, the DGAT and the phospholipid:DAG acyltransferase (PDAT), have been identified in *C. reinhardtii* (Boyle et al., 2012; Li-Beisson et al., 2015; Zienkiewicz et al., 2016). However, if TAG assembly in microalgae takes place in the ER and/or chloroplast membranes is still under debate (Wang et al., 2009; Fan et al., 2011; Davidi et al., 2015; Zienkiewicz et al., 2016; Moriyama et al., 2018).

In land plants, the assembly of the complex polar glycerolipids occurs by attaching different polar headgroups to the DAG backbone; PI, PG and CL are synthesized from CDP-DAG, whereas free DAG is the precursor of PC, PE, PS, SQDG, MGDG and DGDG (Nakamura, 2017). The major pathways for these membrane glycerolipids are apparently conserved between *C. reinhardtii* and land plants (Li-Beisson et al., 2015; 2019). Owing to the absence of PS and PC in *C. reinhardtii* (Li-Beisson et al., 2015; Sato et al., 2016), the biosynthesis of these glycerolipids in microalgae remains understudied, despite PC being central to acyl-lipid metabolism in land plants (Bates et al., 2007; Bates, 2016), and crucial for formation, growth, and stability of the lipid droplets where TAG are accumulated (Penno et al., 2013; Goold et al., 2015).

As mentioned above, microalgae species either lacking or containing few PC often contain betaine lipids as major membrane constituents, where they are believed to replace PC as an alternative zwitterionic lipid (Guschina and Harwood, 2006; Liu and Benning, 2013; Li-Beisson et al., 2019). Among these, DGTS is the most common in nature and frequently present in green algae species (Cañavate et al., 2017; Li-Beisson et al., 2019). In *C. reinhardtii*, it is a significant extraplastidic membrane component, where its synthesis from DAG by the bifunctional protein, betaine lipid synthase (BTA1), has been characterized (Riekhof et al., 2005). Contrary to *C. reinhardtii*, PC and PS, but not betaine lipids, have been detected in *E. oleoabundans* (Tornabene et al., 1983; Matich et al., 2016, 2018; Goh

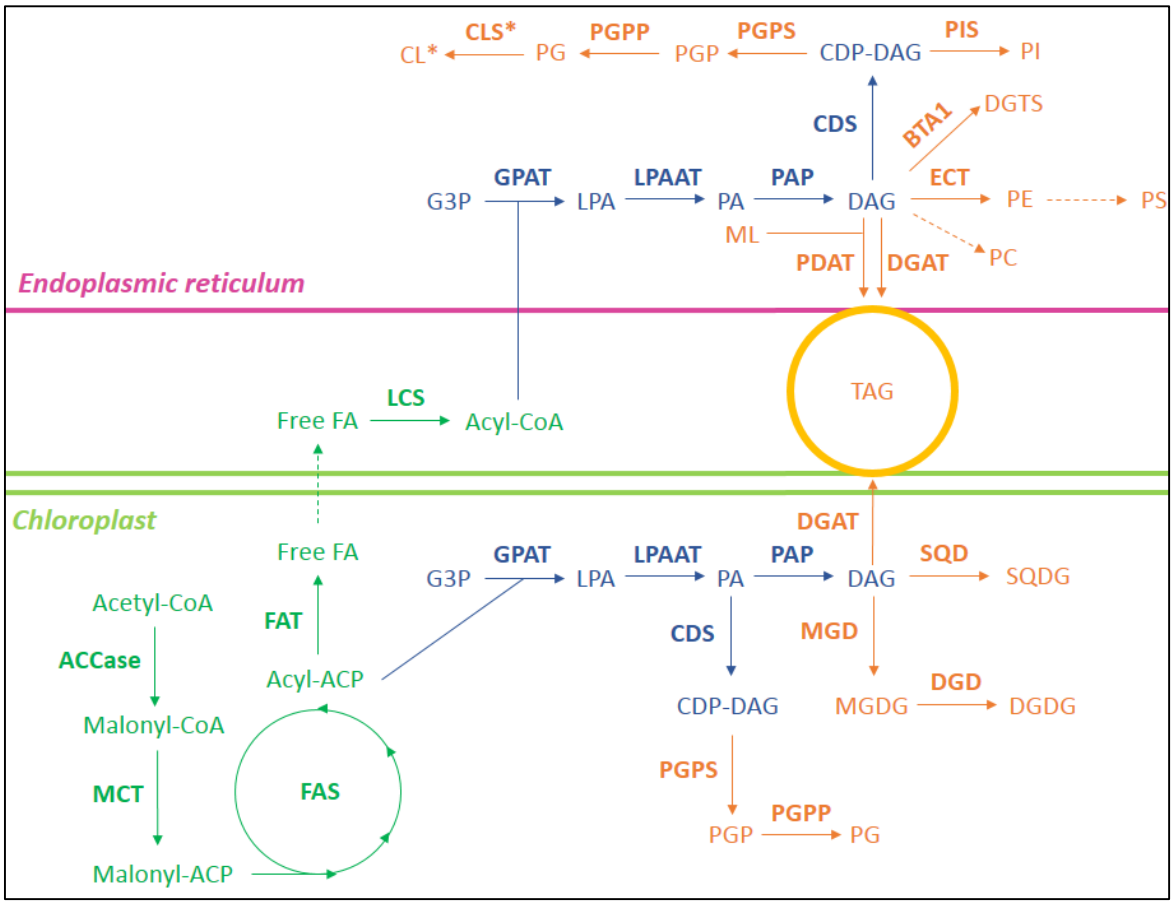

Fig. 1.1. Acyl-lipid metabolism in green microalgae. It is conceptually divided into three phases: (1) *de novo* FA synthesis (green); (2) formation of free or cytidine diphosphate (CDP)-activated DAG (blue); (3) assembly of neutral and polar glycerolipids (orange). Scheme based on Li-Beisson et al., 2019. Compound abbreviations: CL, DGDG, FA, MGDG, PC, PE, PG, PI, PS, TAG, are described in the text; CoA, coenzyme A; DAG, diacylglycerol; DGTS, diacylglyceryl-*N,N,N*-trimethylhomoserine; G3P, glycerol-3-phosphate; LPA, lysophosphatidic acid; PA, phosphatidic acid; PGP, PG-phosphate; ML, membrane glycerolipid (several glycerolipids can be acyl donors according to *in vitro* assays); SQDG, sulfoquinovosyldiacylglycerol. Enzyme abbreviations (bold letters): ACCase, ACP, BTA1, DGAT, FAS, PDAT, are given in the text; CDS, CDP-DAG synthase; CLS, CL synthase (*cardiolipin synthesis occurs in the mitochondria); DGD, DGDG synthase; ECT, CDP-ethanolamine:DAG ethanolamine phosphotransferase; FAT, acyl-ACP thioesterase; GPAT, G3P acyltransferase; LCS, long-chain acyl-CoA synthetase; LPAAT, LPA acyltransferase; MCT, malonyl-CoA:ACP malonyltransferase; MGD, MGDG synthase; PAP, PA phosphatase; PGPP, PGP phosphatase; PGPS, PGP synthase; PIS, PI synthase; SQD, SQDG synthase.

et al., 2017). Even though *C. reinhardtii* has enabled addressing relevant mechanistic questions in microalgae lipid biology, it is not an oleaginous microalga. This, together with its unusual membrane lipid composition, and the differences identified in the lipid metabolism of distinct species of oleaginous microalgae (Liu and Benning, 2013; Li-Beisson et al., 2019), underscore the need to perform microalgae strain-specific studies in order to understand the diversity and commonalities behind the biological processes supporting lipid accumulation.

1.3. Omics approaches: a tool to understand microalgae physiology

At the beginning of this project, only the outcomes from the 18-year (1978-1996) research funded by the US Department of Energy's Aquatic Species Program (ASP) provided the most comprehensive effort for algal strain isolation, characterization, genetic engineering and further process development for their biotechnological application. The ASP studies on microalgal physiology and biochemistry, centered on the ability to induce lipid accumulation upon nutrient stress, uncovering the need to understand the mechanisms underlying lipid storage to develop highly productive strains (Sheehan et al., 1998; Hu et al., 2008). Although lipid biosynthesis pathways were known to exist in *C. reinhardtii* as described above, even for this model microalga no concerted efforts to characterize its response under nutrient stress were available. Only in the last ten years, rapidly developing post-genomics, systems biology approaches such as transcriptomics, proteomics and metabolomics have been performed, becoming essential for understanding the physiology of microalgae (Jinkerson et al., 2011; Ndimba et al., 2013).

The first studies on the mechanisms underlying lipid accumulation consisted on a comparative transcriptomic analysis of the premier microalgal model *C. reinhardtii*, using N deprivation to induce high TAG levels (Miller et al., 2010). As shown by N limitation studies in this microalga (González-Ballester et al., 2004; Stern, 2009), many genes involved in N import and assimilation were induced following N deprivation, including nitrate transporters and reductases, as well as transport systems for ammonia and organic N sources; though, genes from biosynthetic pathways utilizing the assimilated N remained relatively unaffected. This transcriptional analysis provided the basis for what is currently accepted as a "typical" N limitation response in green microalgae: up-regulation of genes associated to N import, N assimilation and lipid metabolism, alongside with the down-regulation of those involved in protein biosynthesis and photosynthesis. These results have been supported and enriched by studies performed during the past ten years using multiple omics approaches (Schmollinger et al., 2014; Valledor et al., 2014; López García de Lomana et al., 2015; Gargouri et al., 2015; Yang et al., 2015; Juergens et al., 2016; Légeret et al., 2016), in which the current knowledge on microalgal lipid metabolism is mostly based (Li-Beisson et al., 2015; 2019). Nonetheless, it must be kept in mind that species-specific studies are necessary as *C. reinhardtii* is not an archetype of green oleaginous microalgae.

Preliminary insights into *E. oleoabundans* physiology upon lipid accumulation conditions started to be provided alongside with the very beginning of the work described hereby. An initial transcriptomic approach proved that it shows a "typical" N deprivation

response (Rismani-Yazdi et al., 2012): enrichment of transcripts involved in N transport and assimilation, lipid biosynthesis/metabolism and NADPH regeneration, together with a reduction of those related to photosynthesis, carbon fixation, protein machinery and cell growth. This study established the foundations for the *in silico* analysis of *E. oleoabundans* lipid metabolism. During the last four years additional lipidomics and transcriptomic studies have emerged (Matich et al., 2016, 2018; Goh et al., 2017; de Jaeger et al., 2018; Sturme et al., 2018), in two of which different environmental conditions known to trigger lipid accumulation (N deprivation and osmotic stress) were exploited to identify core features of TAG production. Altogether, the outcomes from these studies are not always consistent, but already suggest that lipid accumulation might be supported by an increased availability of direct carbon precursors (acetyl-CoA) and reducing equivalents partitioned towards an increased acyl-lipid biosynthesis, which is accompanied by transcriptional changes in lipid catabolism genes. Nonetheless, these investigations have neither provided novel insights into *E. oleoabundans* physiology, nor identified features distinguishing oleaginous from non-oleaginous microalgae. The complementary omics-based approaches employed in the present work are therefore necessary to understand the processes behind lipid metabolism and accumulation in *E. oleoabundans*.

Most of the proteomic studies performed on non-model microalgae are limited to the analysis of total protein extracts, and therefore the most abundant soluble proteins will be over-represented. These approaches overlook the role played by microalgal membrane proteins, which have remained understudied despite the fact that the majority of lipid metabolism proteins have been proposed to be membrane-associated (Natter et al., 2005; Joyard et al., 2010; Wang and Benning, 2012), and that N starvation is known to exert ultrastructural changes in microalgal cells (Moellering and Benning, 2010), including membrane lipid remodeling, turnover and degradation (Li et al., 2012; Yoon et al., 2012; Li et al., 2014a). Accordingly, in the present work, the membrane protein components, together with its lipid constituents are investigated to understand how these compounds shape the function of biological membranes and contribute to the response of *E. oleoabundans* upon N starvation, as well as to the sustained accumulation of lipids triggered by this stress condition.

2. Hypothesis

The membrane components of the oleaginous microalga *E. oleoabundans* play critical roles in the response to nitrogen deprivation, supporting the accumulation of lipids, which is an intrinsic feature of nitrogen-starved *E. oleoabundans*.

3. Objectives

3.1. Main objective

Identify the biological processes taking place in *E. oleoabundans* membranes and provide insights on how its components are involved in the response to nitrogen (N) deprivation and support lipid accumulation by using a multidisciplinary approach.

3.1. Specific objectives

- Develop and implement methods for: 1) reproducible cultivation of *E. oleoabundans* under control (N sufficiency) and stress (N deprivation) conditions, and 2) isolation of microsomal membranes for further analysis.
- Study of the ultrastructural changes induced upon N deprivation and lipid droplet formation dynamics by transmission electron and confocal fluorescence microscopy of *E. oleoabundans*.
- Quantitative profiling of *E. oleoabundans* glycerolipids and membrane proteins under N sufficiency and N deprivation conditions.
- Identification of the biological processes occurring in the membranes of N-deprived cells using an RNA-Seq-based proteomics approach for protein identification.
- Compartmentalization analysis of biological processes of interest through microsome fractionation, followed by protein profiling of individual membrane fractions.
- Short-term kinetic analysis of lipid dynamics through radioactive labeling.
- Data integration for the identification of membrane-localized cellular processes responsive to N stress, contributing to cope with this condition and supporting the sustained accumulation of lipids in *E. oleaobundans*.

4. Membrane proteomic insights into the physiology and taxonomy of an oleaginous green microalga

This chapter is published as:

Adriana Garibay-Hernández, Bronwyn J. Barkla, Rosario Vera-Estrella, Alfredo Martinez and Omar Pantoja (2017) Membrane proteomic insights into the physiology and taxonomy of an oleaginous microalga. Plant Physiology **173**: 390-416

Abstract

Ettlia oleoabundans is a non-sequenced oleaginous green microalga. Despite the significant biotechnological interest in producing value-added compounds from the acyl-lipids of this microalga, a basic understanding of the physiology and biochemistry of oleaginous microalgae is lacking, especially under nitrogen deprivation conditions known to trigger lipid accumulation. Using an RNA-Seq-based proteomics approach together with manual annotation, we are able to provide the first membrane proteome of an oleaginous microalga. This approach allowed the identification of novel proteins in *E. oleoabundans*, including two photoprotection-related proteins, Photosystem II Subunit S and Maintenance of Photosystem II under High Light1, which were considered exclusive to higher photosynthetic organisms, as well as Retinitis Pigmentosa Type 2-Clathrin Light Chain, a membrane protein with a novel domain architecture. Free flow zonal electrophoresis of microalgal membranes coupled to LC-MS/MS proved to be a useful technique for determining the intracellular location of proteins of interest. Carbon flow compartmentalization in *E. oleoabundans* was modeled using this information. Molecular phylogenetic analysis of protein markers and 18S (r)DNA, support the reclassification of *E. oleoabundans* within *Trebouxiophycean* microalgae, rather than with the *Chlorophyceae* class in which it is currently classified, indicating it may not be closely related to the model green alga *Chlamydomonas reinhardtii*. A detailed survey of biological processes taking place in the membranes of nitrogen-deprived *E. oleoabundans,* including lipid metabolism, provides insights into the basic biology of this non-model organism.

4.1. Introduction

Ettlia oleoabundans (taxonomic synonym of *Neochloris oleoabundans*) is a unicellular edaphic green microalga that belongs to the *Chlorophyta* phylum and is currently placed within the *Chlorophyceae* class (Chantanachat and Bold, 1962; Deason et al., 1991). It is a non-sequenced microalga classified as oleaginous due to its high lipid content (up to 56% w/w of its dry weight) (Gouveia et al., 2009). Several abiotic stress conditions such as high temperature (Yang et al., 2013), high salinity (Arredondo-Vega et al., 1995) and nitrogen (N) deficiency (Tornabene et al., 1983; Li et al., 2008; Pruvost et al., 2009; Garibay-Hernández et al., 2013) trigger neutral lipid accumulation in this microalga. *E. oleoabundans* is a highly versatile organism as it can grow in freshwater, wastewater (Levine et al., 2011; Wang and Lan, 2011; Yang et al., 2011; Olguín et al., 2015), and in culture media with salt concentrations up to sea water levels (Arredondo-Vega et al., 1995; Baldisserotto et al., 2012; Popovich et al., 2012). Moreover, it is able to grow under phototrophic, mixotrophic (Giovanardi et al., 2013; Baldisserotto et al., 2016) and heterotrophic (Wu et al., 2011; Morales-Sánchez et al., 2013) conditions. Owing to its high lipid content and growth versatility, *E. oleoabundans* is an organism of biotechnological interest. However, a basic understanding of its physiology is currently lacking, as most reports have focused on improving the lipid yield and productivity of *E. oleoabundans* under N deficiency conditions through different culture strategies, and evaluating how other environmental factors additionally control lipid production. At present, only few reports have assessed the biology and biochemistry behind N deficiency and lipid accumulation in *E. oleoabundans* (Rismani-Yazdi et al., 2012; Benvenuti et al., 2015; Baldisserotto et al., 2016; Matich et al., 2016).

Rapidly developing post-genomics, systems biology approaches such as transcriptomics, proteomics and metabolomics, have become essential for understanding the physiology of different organisms, including microalgae (Jinkerson et al., 2011; Ndimba et al., 2013). Algal proteomics has been primarily performed with the model green alga *Chlamydomonas reinhardtii* for the analysis of subcellular compartments (Schmidt et al., 2006; Atteia et al., 2009; Terashima et al., 2010) and characterization of the proteome under stress conditions (Chen et al., 2010; Baba et al., 2011; Castruita et al., 2011; Mühlhaus et al., 2011), including N starvation (Schmollinger et al., 2014; Valledor et al., 2014; Wase et al., 2014). Although *C. reinhardtii* currently provides the best model for microalgal lipid research (Liu and Benning, 2013), it is not an oleaginous species and may not represent the physiology of other species of biotechnological interest, as microalgae comprise an extremely diverse group of photosynthetic microorganisms (Hu et al., 2008). In recent years,

a limited number of proteomics studies have been performed on non-model oleaginous strains such as *Chlorella protothecoides* (Gao et al., 2014)*, Chlorella sorokiniana* (Ma et al., 2013)*, Chlorella vulgaris* (Guarnieri et al., 2011; Guarnieri et al., 2013)*, Isochrysis galbana* (Song et al., 2013), and *Nannochloropsis oceanica* (Dong et al., 2013). However, proteomic analysis of non-model microalgae is still challenging as the lack of a sequenced genome in most of them compromises the quality and quantity of the generated data (Ndimba et al., 2013; Wang et al., 2014).

Most of the proteomic studies performed on non-model microalgae are limited to the analysis of total protein extracts, and therefore the most abundant soluble proteins will be over-represented. These approaches overlook the role played by microalgal membrane proteins, which have remained understudied despite the fact that the majority of lipid metabolism proteins have been proposed to be membrane-associated (Natter et al., 2005; Joyard et al., 2010; Wang and Benning, 2012), and that N starvation is known to exert ultrastructural changes in microalgal cells (Moellering and Benning, 2010), including membrane lipid remodeling, turnover and degradation (Li et al., 2012; Yoon et al., 2012; Li et al., 2014a).

In this study, microsomal membranes from *E. oleoabundans* cells submitted to N deprivation were analyzed via an RNA-Seq-based proteomics approach (Wang et al., 2014), using the *E. oleoabundans* transcriptome generated by Rismani-Yazdi and collaborators (Rismani-Yazdi et al., 2012). To overcome the typical limitations of membrane proteomics due to the heterogeneous, hydrophobic and low abundance nature of membrane proteins (Tan et al., 2008), a gel-free shotgun proteomics strategy was employed. In parallel, free-flow zonal electrophoresis (FFZE), a liquid-based matrix-free separation technology (Barkla et al., 2007; Wildgruber et al., 2014), was coupled to shotgun proteomics and uniquely employed to assess the intracellular location of novel identified proteins, as well as to provide a detailed survey of biological processes related to energy and carbon flux in N-deprived *E. oleoabundans*, giving insights into the basic biology of this organism. Molecular phylogenetic analysis of proteins identified in this work and of 18S (r)DNA, raised concerns regarding the taxonomic status of *E. oleoabundans*, as they support a close alliance between *E. oleoabundans* and species of the *Trebouxiophyceae* class, which is contrary to its current classification.

4.2. Results and discussion

4.2.1. *Ettlia oleoabundans* membrane proteome

To study the membrane proteome of the non-sequenced oleaginous microalga, *E. oleoabundans*, microsomes from 4-d N-deprived cultures, were isolated and subsequently analyzed using gel-free liquid chromatography tandem-mass spectrometry (LC-MS/MS).

As a first approach, product ion data was searched against the *Viridiplantae* protein database (TaxID 33090, unknown version, 677107 entries) using the Mascot search program (Matrix Science, London, UK). A total of 45 proteins (1,057 spectra) were identified with two or more unique peptides, from which only 30 were detected in at least two of four biological replicates. The small number of identified proteins can be attributed to the typical limitations of studying membrane proteins (Tan et al., 2008), but mostly to the lack of sequence data for non-sequenced organisms (Ndimba et al., 2013; Wang et al., 2014), such as *E. oleoabundans*. To overcome these limitations, an RNA-Seq-based proteomics strategy was established, using as a guide the *E. oleoabundans de novo* sequenced transcriptome (Rismani-Yazdi et al., 2012). The *E. oleoabundans* transcriptome comprises 56,550 non-redundant transcripts and was obtained from cells cultured under both, N replete and deprived conditions (Rismani-Yazdi et al., 2012). In order to generate an *E. oleoabundans* protein database, an *in silico* six-frame translation of the transcriptome was performed, yielding 54,652 non-redundant putative protein sequences. The *E. oleoabundans* protein database (unknown version, 53,921 entries) was merged with the *Viridiplantae* database and subsequently used for peptide and protein identification. Using this approach, 551 proteins (18,902 spectra) were identified, from which only 404 complied with the stringency described above. This was a 13.5-fold increase in identifications over using only the *Viridiplantae* database. This result shows that use of the *E. oleoabundans* translated transcriptome significantly improved protein identification and highlights the advantages of integrating *de novo* transcriptomic and proteomic analyses to study non-model microalgae (Guarnieri et al., 2011).

In order to describe the composition of the *E. oleoabundans* membrane proteome, the sequences from the 404 identified proteins were analyzed with transmembrane helices (HMMTOP v.2.0, TMHMM v.2.0) and beta-barrel membrane protein (MCMBB, TMBETADISC-RBF) prediction programs (Krogh et al., 2001; Tusnády and Simon, 2001; Bagos et al., 2004; Ou et al., 2008). Proteins predicted to possess a transmembrane region

by any of the four prediction programs were considered as integral membrane proteins. This analysis demonstrated that 57% of the *E. oleoabundans* membrane proteome is comprised by integral membrane proteins; the remaining 43% can be classified as peripheral membrane proteins which do not transverse the membrane, but may be associated with the membrane surface to varying extents (Tan et al., 2008).

4.2.2. Functional annotation of *E. oleoabundans* membrane proteome

To address the biological significance of the identified membrane proteins, we initially performed a functional annotation based on sequence similarity using the Blast2GO suite (Götz et al., 2008). From the total of 404 proteins, 391 returned a significant Blastp match (E-value cut-off ≤ 0.001) against the NCBI non-redundant protein sequences database. The majority of the proteins (92%) had best-hit homologs in species from the *Trebouxiophycean* class, whereas only 3% possessed best-hit homologs with members of the *Chlorophycean* class (Fig. S4.1). This result resembles those obtained from the analysis of the *E. oleoabundans* transcriptome (Rismani-Yazdi et al., 2012), suggesting a closer proximity of *E. oleoabundans* to the *Trebouxiophycean Chlorella* species.

Although automatic annotations have been shown to be more reliable than generally believed (Škunca et al., 2012), and there is a demonstrated good performance of Blast2GO (Götz et al., 2008), functional miss-annotation in computational analysis remains a significant concern (Schnoes et al., 2009). To improve protein annotation, each of the 404 identified proteins were manually curated as described in Materials and Methods.

Following manual curation, the cellular location of 85% of the identified proteins was predicted (Fig. S4.2A). The majority of the membrane proteins (41%) were located to the chloroplast, not surprising as this organelle occupies most of the microalga's cell volume (Giovanardi et al., 2013). Despite this, most of the cellular compartments were represented in the membrane proteome, including the lipid droplets (LDs), which are structures induced by N deprivation (Davis et al., 2012; Popovich et al., 2012; Giovanardi et al., 2013). Cytoplasmic proteins comprised only 9% of the membrane proteome (Fig. S4.2A). The majority of identified proteins (82%) were categorized into known biological processes (Fig. S4.2B), which were grouped into three broad categories: protein and N metabolism (28%), energy production and homeostasis (23%), and carbon metabolism (15%). All the identified proteins are described in Tables S1-S15 and classified according to the biological process to which they are related. The corresponding protein homologs in the model organisms

Chlamydomonas reinhardtii and *Arabidopsis thaliana* are also indicated, as well as the predictions and the experimental evidence for the cellular location of these proteins.

4.2.3. Novel occurrence of the photosynthesis-related proteins, PSBS and MPH1, in green microalgae

Photosystem II subunit S or 22 kDa protein (PSBS) and Maintenance of Photosystem II under High Light 1 (MPH1) are proteins related to well characterized photoprotective responses that have been considered exclusive to higher photosynthetic organisms.

In this work, the *E. oleoabundans* PSBS protein (*Eo*PSBS, m.395061, Table S4.1) was identified in all four biological replicates with up to seven unique peptides, and a maximum coverage of 29% of the predicted protein sequence. *Eo*PSBS is comprised by 252 amino acids with an estimated molecular weight (MW) of 28 kDa considering the predicted chloroplast transit peptide (CTP) (Fig. 4.1A), and of 25 kDa following transit peptide cleavage. Similar to *A. thaliana* PSBS (*At*PSBS), *Eo*PSBS comprises a chlorophyll a/b binding protein domain (Fig. 4.1A), four membrane-spanning alpha-helixes (Kyte-Doolittle, Fig. 4.1B; HMMTOP v2.0, Fig. 4.1A and S4.3A), and a predicted N-terminal CTP (28 aa, PredAlgo, Fig. 4.1A and S4.3A). The two symmetrically arranged lumen-exposed glutamate residues that are necessary for the PSBS pH-sensing mechanism and thus, its function in land plants (Glu-122 and Glu-226, in *At*PSBS) (Li et al., 2002; Li et al., 2004), are both conserved in *Eo*PSBS (Glu-120 and Glu-224, Fig. 4.1A and S4.3A). *Eo*PSBS homologs from higher plants and green algae species were retrieved from the UniProtKB database (Fig. 4.1C and S4.3A), although PSBS transcripts (Miller et al., 2010; Gerotto and Morosinotto, 2013), but not the corresponding protein (Bonente et al., 2008), have been identified in green microalgae until very recently when PSBS was detected in *C. reinhardtii* upon high light acclimation (Correa-Galvis et al., 2016; Tibiletti et al., 2016). *Eo*PSBS shares 75% identity with the predicted protein from *Chlorella variabilis* (class *Trebouxiophyceae*), and 46% with the corresponding proteins from *Chlorophycean* species; in contrast, only 30% identity is shared with PSBS from land plants (Fig. S4.3B). Phylogenetic analysis showed that PSBS is conserved along the green lineage (*Viridiplantae*), however PSBS from green algae and land plants clustered into two distinct clades (Fig. 4.1C). This result suggests that PSBS was present in the common ancestor of extant green algae and land plants but that it evolved separately in these two phylogenetic groups, as it has been suggested in previous

evolutionary analysis of genomic and transcriptomic PSBS sequences (Koziol et al., 2007; Bonente et al., 2008; Gerotto and Morosinotto, 2013).

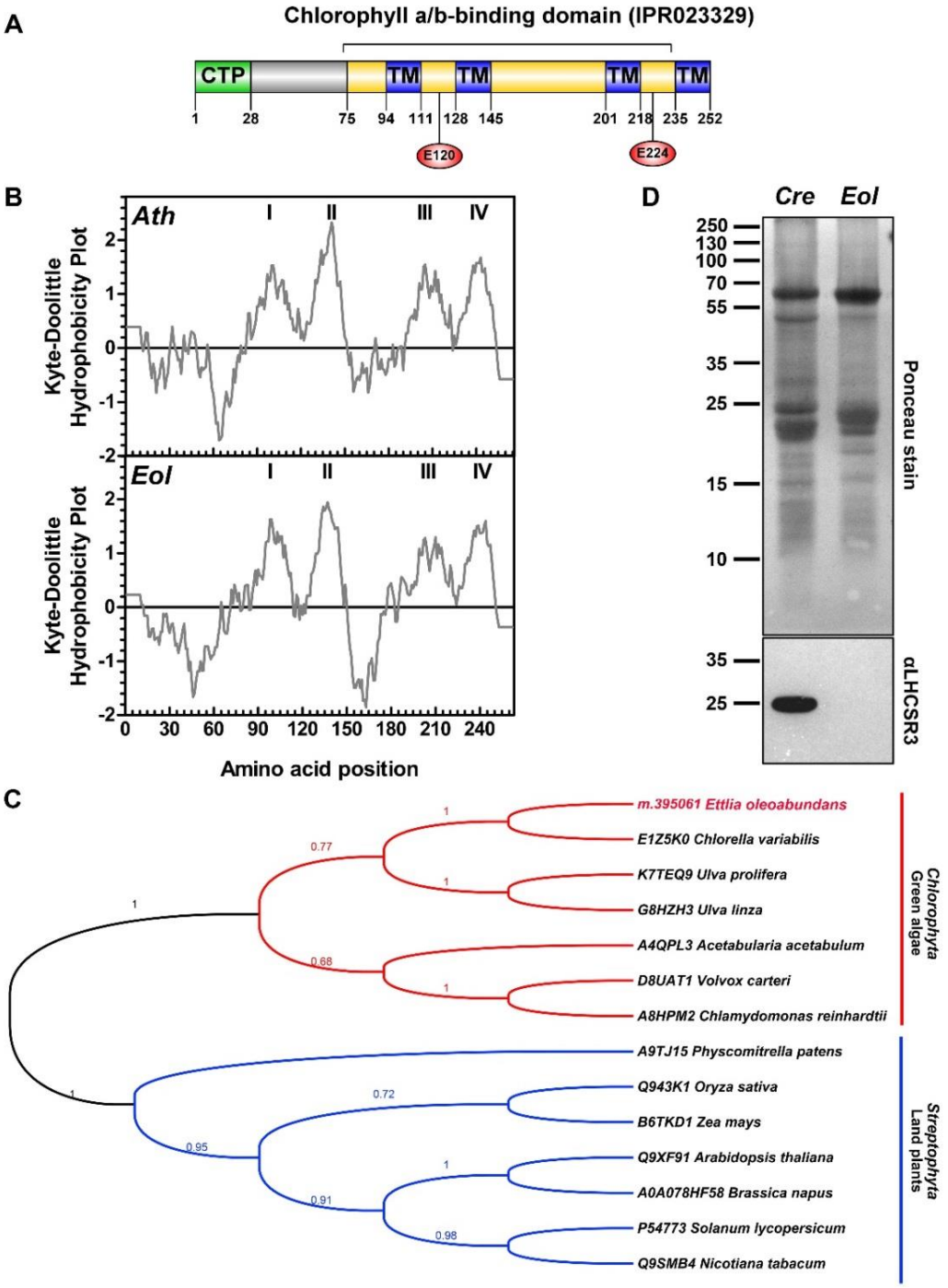

Figure 4.1. Analysis of qE effector proteins (PSBS and LHCSR) in N-depleted *E. oleoabundans*. (A) Protein architecture of *Eo*PSBS. The identified protein domain signatures (InterPro; yellow), the predicted chloroplast transit peptide (PredAlgo; CTP, green) and transmembrane domains (HMMTOP v2.0; TM, blue) are indicated. The conserved residues involved in the PSBS pH-sensing mechanism are shown (red circles). (B) Hydrophobicity comparison of PSBS from *E. oleoabundans* (*Eol*) and *A. thaliana* (*Ath*). Probable TM domains (values > 0) are shown in the Kyte-Doolittle hydrophobicity plots (window size: 19). (C) Phylogenetic analysis of PSBS homologs. Aligned sequences (Fig. S4.3) were submitted for maximum likelihood (ML) analysis. The topology of the ML tree with the highest log likelihood (-3122.6386) is shown. Bootstrap (MLb) values are shown next to the branches. UniProtKB accession numbers for PSBS homologs are provided. (D) Immunological detection of LHCSR in microsomes from *Eol* and *Cre* (*C. reinhardtii*). SDS-PAGE 12.5% (w/v) acrylamide gel, loaded with 20 µg protein per lane.

Vascular plants rely on PSBS for the pH-regulated activation of the energy-dependent feedback de-excitation component (qE) of non-photochemical quenching (NPQ) for photoprotection (Li et al., 2000; Niyogi and Truong, 2013). In contrast, eukaryotic algae, except for red algae, cryptophytes (Dittami et al., 2010) and peridinin-containing dinoflagellates (Boldt et al., 2012), commonly depend on LHC-like protein Stress Related (LHCSR, LI818 or LHCSX) for qE induction (Peers et al., 2009; Bailleul et al., 2010). Despite pH regulation of qE being restricted to LHCSR in *C. reinhardtii*, recent evidence has shown that its full NPQ capacity is also dependent on PSBS, whose substoichiometric accumulation is a prerequisite for further activation of the LHCSR-dependent qE mechanism (Correa-Galvis et al., 2016). These two mechanisms apparently overlapped at some point during evolution as both proteins, LHCSR and PSBS, have also been identified in organisms that represent transitional states between green algae and vascular plants, where, contrary to what has been found in *C. reinhardtii*, these proteins function independently and additively in qE regulation (Alboresi et al., 2010; Gerotto et al., 2012; Mou et al., 2013; Zhang et al., 2013a). In view of this, we searched for the presence of LHCSR in *E. oleoabundans* to determine if both qE effector proteins were present. An LHCSR homolog was not identified by searching the transcriptome (Rismani-Yazdi et al., 2012) and the corresponding *in-silico* translated proteome of *E. oleoabundans*. Absence of LHCSR was further confirmed by western blot analysis of microsomes from N-deprived *E. oleoabundans* (Fig. 4.1D). The absence of an LHCSR homolog in *E. oleoabundans* questions the conservation of qE mechanisms within green microalgae.

MPH1 is a proline-rich intrinsic thylakoid protein that participates in protection and stabilization of photosystem II (PSII) against photooxidative damage in *A. thaliana* under high-light stress (Liu and Last, 2015a; Liu and Last, 2015b). Identification of an MPH1 homolog in the membranes of N-deprived *E. oleoabundans* (*Eo*MPH1, m.337748, Table S4.1) was also unexpected since MPH1 has been reported as a protein specific to land plants (Liu and Last, 2015a; Liu and Last, 2015b). In this study, *Eo*MPH1 was identified in three out of four biological replicates, with up to three unique peptides, and a maximum coverage of 19% of the predicted protein sequence. *Eo*MPH1 is comprised of 164 amino acids with an estimated MW of 16.2 kDa considering the CTP (Fig. 4.2A), and of 13.6 kDa following its cleavage. It shares 15 to 20% sequence identity with MPH1 sequences from higher plants (Fig. S4.4B), including structural features predicted for *At*MPH1 (Liu and Last, 2015b): a single transmembrane domain (Kyte-Doolittle, Fig. 4.2B; TMHMM v2.0, Fig. 4.2A and S4.4A), an N-terminal CTP (25 aa, PredAlgo, Fig. 4.2A and S4.4A), and a high-proline

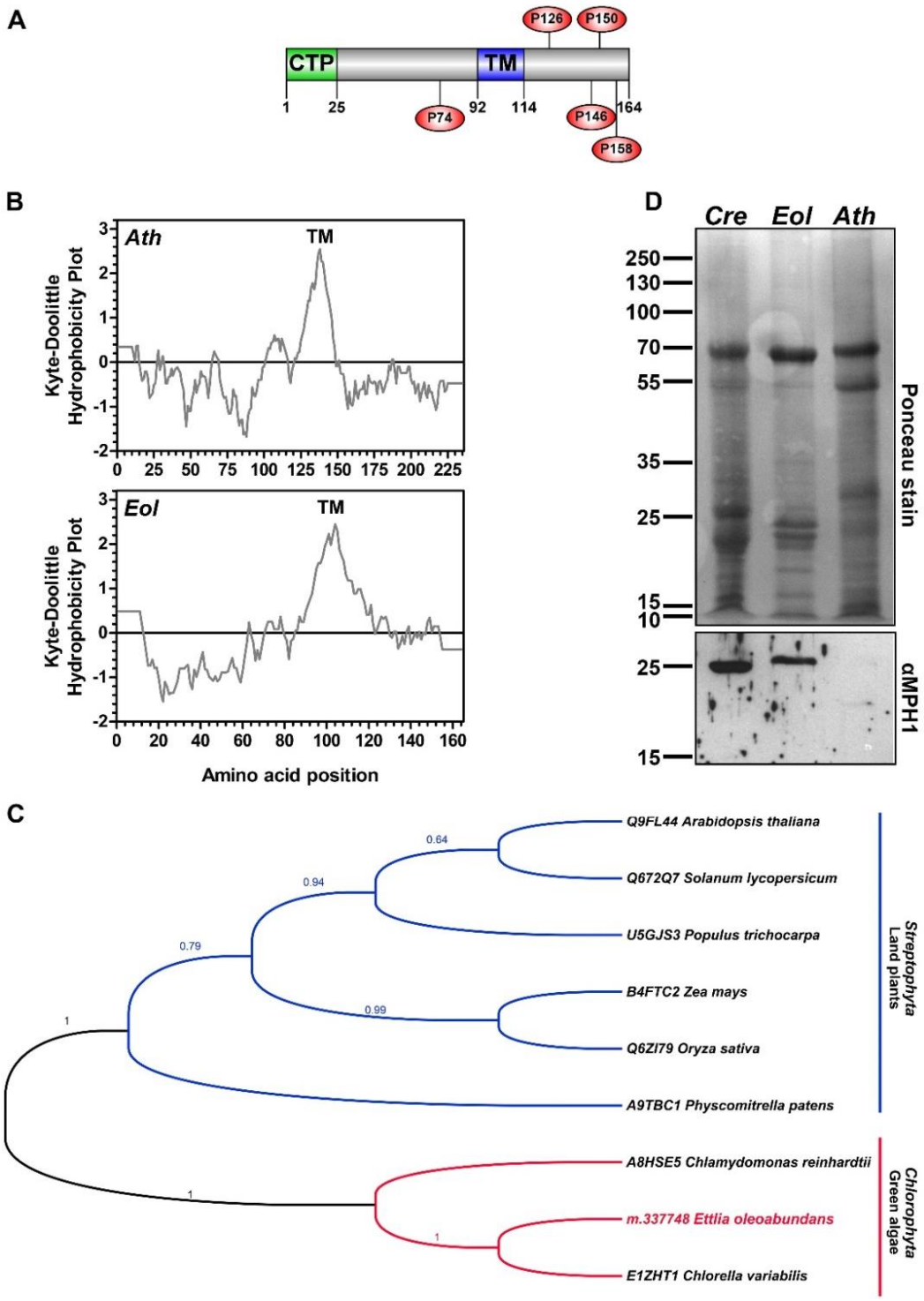

Figure 4.2. MPH1 sequence analysis and identification in green microalgae membranes. (A) Protein architecture of *Eo*MPH1. The predicted CTP (PredAlgo; green) and TM domain (TMHMM v2.0; blue) are indicated. Conserved proline residues are shown (red circles). (B) Hydrophobicity comparison of MPH1 from *E. oleoabundans* (*Eol*) and *A. thaliana* (*Ath*). Probable TM domains (values > 1.6) are shown in the Kyte-Doolittle hydrophobicity plots (window size: 19). (C) Phylogenetic analysis of MPH1 homologs. Aligned sequences (Fig. S4.4) were submitted for ML analysis. The topology of the ML tree with the highest log likelihood (-2177.6951) is shown. MLb values are shown next to the branches. UniProtKB accession numbers for MPH1 homologs are provided. (D) Immunological detection of MPH1 in microsomes from *Ath* (positive control; red box), *Eol* and *Cre* (*C. reinhardtii*). SDS-PAGE 12.5% (w/v) acrylamide gel, 20 µg protein per lane.

content (6% of the protein), from which some interspersed proline residues are conserved (Fig. 4.2A and S4.4A). Based on the presence of MPH1 in *E. oleoabundans*, we searched for unreported homologs from other green microalgae species. Results identified predicted sequences from *C. variabilis* (class *Trebouxiophyceae*) and *C. reinhardtii* (class *Chlorophyceae*), which shared 68% and 28% identity, respectively, with *Eo*MPH1 (Fig. S4.4). Phylogenetic analysis showed that MPH1 sequences from green algae and land plants clustered into two distinct clades (Fig. 4.2C). To confirm the presence of MPH1 in membranes of green microalgae, microsomes from *E. oleoabundans* and *C. reinhardtii* were probed using a polyclonal antibody raised against *At*MPH1 (Liu and Last, 2015b). A single band of approximately 25 kDa was identified on the blot in both cases (Fig. 4.2D). Considering that both homologs have a predicted MW close to 13 kDa, this result suggests that microalgal MPH1 may form dimers. Contrary to this finding, a single band corresponding to the *At*MPH1 predicted MW (20 kDa) was identified (Fig. 4.2D) in *A. thaliana* membranes, whose low intensity may be attributed to its low abundance.

4.2.4. RP2-CLC, a novel domain architecture protein identified in *E. oleoabundans* membranes

The proteomic analysis of *E. oleoabundans* membranes resulted in the detection of several unknown proteins. Among them, we identified protein m.397619 (Table S4.9), which presents a domain architecture that has not been described previously. This protein comprises 368 amino acids, contains an N-terminal region corresponding to the Retinitis Pigmentosa type 2 (RP2) protein family, and a C-terminus that comprises a clathrin light chain (CLC) domain (Fig. 4.3A). Accordingly, we named this protein *Eo*RP2-CLC. A survey of proteins with this architecture in the UniProtKB database showed that they are limited to certain unicellular eukaryotes, such as green microalgae from both *Trebouxiophyceae* and *Chlorophyceae* classes, several ciliated protozoa, and mould species from the *Oomycetes* class, but are not present in higher eukaryotes.

*Eo*RP2-CLC is a Tubulin Binding Cofactor C (TBCC) domain-containing protein, as it comprises a predicted TBCC-like domain within the N-terminal RP2 region (Fig. 4.3A). Three protein families with TBCC domains (Fig. 4.3B) have been described (Stephan et al., 2007).The first (Clade 1/TBCC) is the canonical TBCC, which is essential for *de novo* native α/β-tubulin heterodimer formation by stimulating GTP hydrolysis in β-tubulin (Lundin et al., 2010); this clade comprises proteins from a diverse range of eukaryotes. The second (Clade

2/RP2) contains homologs of human RP2, which are apparently restricted to eukaryotes capable of forming cilium/flagellum (Stephan et al., 2007). The third (Clade 3/TBCCd1) comprises non-canonical TBCC domain-containing proteins, which lack a conserved catalytic arginine responsible for GTPase-activating protein (GAP) activity (Bartolini et al., 2002). However, an arginine residue located close to the arginine finger position in TBCC and RP2-like proteins (Fig. S4.5) has been suggested to suffice for GAP activity in TBCCd1 proteins (Feldman and Marshall, 2009). *E. oleoabundans* has predicted protein homologs for each clade (Fig. 4.3B), however, only *Eo*RP2-CLC was identified in the membrane proteome. *Eo*RP2-CLC, together with the protein homolog from *C. variabilis* (UniProtKB: E1ZN89), which is characterized by autosporic reproduction (Huss et al., 1999), clustered within the RP2 clade (Fig. 4.3B). Thus, the RP2 clade may not be restricted to cilium/flagellum-forming eukaryotes as previously proposed (Stephan et al., 2007). Sequence analysis showed that only the TBCC domains from *E. oleoabundans* and *C. variabilis* RP2 sequences do not present the conserved catalytic arginine, but instead showed a homologous substitution with a lysine residue (Fig. 4.3A and S4.5), which may suffice for GAP activity.

Presence of RP2-CLC proteins in the microsomes from both *E. oleoabundans* and *C. reinhardtii* were confirmed using a polyclonal antibody raised against *Homo sapiens* RP2 (*Hs*RP2) (Fig. 4.3C). A single protein band with a MW slightly higher than that predicted for *Eo*RP2-CLC (39 kDa) was identified in *E. oleoabundans*. In *C. reinhardtii*, two protein bands around the MW predicted for *Cr*RP2-CLC (Cre06.g293250.t1.1, 58 kDa) were detected, where one of these bands may correspond to a post-translationally modified *Cr*RP2-CLC, similar to *Hs*RP2 that is known to be subjected to dual N-terminal acylation (Chapple et al., 2000).

RP2-CLC proteins have a domain architecture that differs from currently characterized RP2 proteins and are present in both, flagellated and non-flagellated microalgae (Fig. 4.3B), suggesting they may be involved in other non-cilia/flagella-specific functions. Contrary to microalgae of the *Chlorophyceae* class, no obvious homologs to currently known CLC proteins were identified in either the *E. oleoabundans in-silico* translated protein database, or in the predicted proteins for *C. variabilis* (pico-PLAZA; Vandepoele et al., 2013). CLC has also been shown to be absent in other unicellular eukaryotes such as *Cyanidioschyzon merolae* (Misumi et al., 2005), *Entamoeba histolytica,* and *Giardia lamblia* (Manna et al., 2015), however, this might be due to the high divergence of CLC sequences among eukaryotes (Wang et al., 2003). The existence of *No*RP2-CLC as the only candidate for a

CLC-harboring protein in *E. oleoabundans*, together with current evidence that supports a role of *Hs*RP2 in post-Golgi trafficking (Evans et al., 2010), suggests that *Eo*RP2-CLC may play a role in formation/trafficking of clathrin-coated vesicles in *E. oleoabundans* cells.

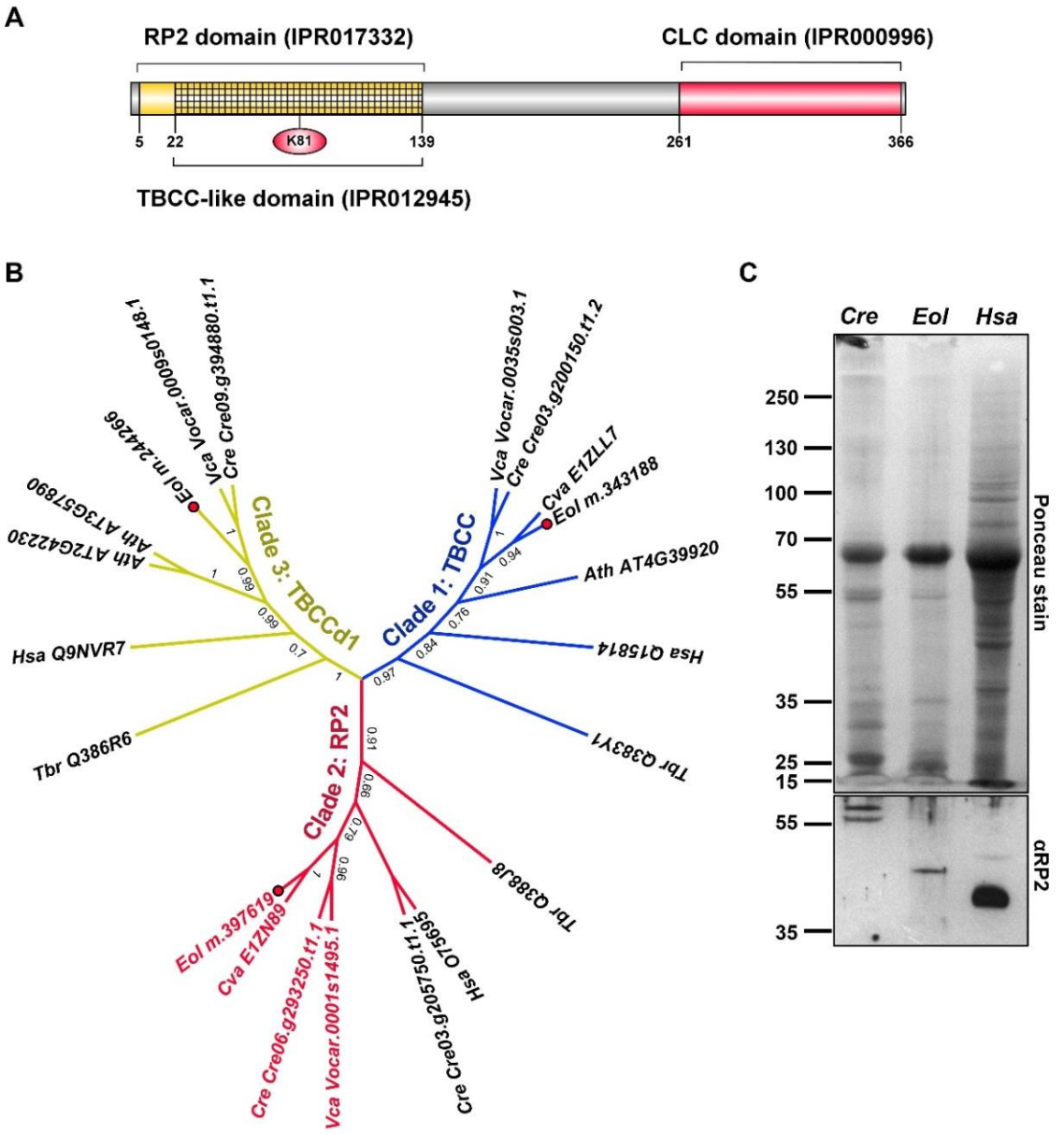

Figure 4.3. *Eo*RP2-CLC, a membrane TBCC-domain containing protein with a novel domain architecture. (A) Protein architecture of *Eo*RP2-CLC. The identified InterPro signatures and the lysine residue (red circle) that may correspond to a homologous substitution of the key arginine residue for GAP activity are indicated. (B) ML analysis of TBCC-domain containing proteins. Clade 1/TBCC (blue), clade 2/RP2 (red), clade 3/TBCCd1 (yellow). RP2-CLC domain architecture proteins are highlighted in red text. Amino acid sequences were aligned with webPRANK. The topology of the ML tree with the highest log likelihood (-8226.6668) is shown. MLb values are shown next to the branches. Accession numbers are provided: UniProtKB (*Hsa, Tbr, Cva*), Phytozome v10 (*Cre, Vca*), TAIR (*Ath*). *Ath A. thaliana, Cre C. reinhardtii, Cva C. variabilis, Hsa H. sapiens, Eol E. oleoabundans* (red dots)*, Tbr Trypanosoma brucei, Vca Volvox carteri.* (C) Immunological detection of RP2-like proteins in microsomes from *Cre* and *Eol.* SDS-PAGE 10% (w/v) acrylamide gel, 20 µg protein per lane. Total protein extracts (10 µl) from human (*Hsa*) C2BBe1 cells (clone of Caco-2) were analyzed as a positive control, where the 40 kDa RP2 human protein was identified.

4.2.5. Determining the subcellular location of novel proteins via FFZE membrane fractionation coupled to MS-based analysis

To assess the subcellular location of the novel microalgal proteins identified in this work, we employed a membrane fractionation approach. In this study, we avoided traditional fractionation techniques by using free-flow zonal electrophoresis (FFZE), a liquid-based high resolution membrane separation technique based on surface charge that has been proved useful for subcellular proteome sample preparation (Barkla et al., 2007; Wildgruber et al., 2014; de Michele et al., 2016).

E. oleoabundans microsomes from N-deprived cultures were separated into 96 individual FFZE fractions (Fig. 4.4A) and each fraction was subjected to either, direct chlorophyll measurements (Fig. 4.4B), or western blot analysis against protein markers for both, the chloroplast and the plasma membrane (Fig. 4.4C). Chloroplast membranes were detected in fractions 51 to 58, while more positively charged fractions (56 to 67) comprised the plasma membrane (Fig. 4.4C). Individual FFZE fractions, from 45 to 67, were then subjected to shotgun proteomics analysis to gain a more comprehensive overview of the protein profile of each of these fractions. A spectral counting-based quantitative approach, expressed in terms of the Normalized Spectral Abundance Factor (NSAF; Zhang et al., 2010), was used to determine the distribution of protein markers specific for different subcellular compartments among the analyzed FFZE fractions (Fig. 4.4D). Similarly to the protein blot analysis, the MS-based analysis confirmed the presence of two different membrane populations, but showed that the chloroplast fractions were also enriched in mitochondrial membranes (fractions 45 to 58) whereas the plasma membrane fractions co-migrated with vacuolar membranes (fractions 56 to 67) (Fig. 4.4D).

The MS-based analysis of the FFZE fractions was further employed to assess the subcellular location of *Eo*PSBS and *Eo*MPH1. Peptides for these proteins were detected and their distribution profiles within the FFZE fractions were mapped with those from known marker proteins. These two photosynthesis-related proteins presented similar distributions to that shown by the chloroplast-enriched membrane fractions (Fig. 4.4E). These results, together with the evidence that both proteins possess a predicted N-terminal CTP (Fig. 4.1A and 4.2A), confirmed that *Eo*PSBS and *Eo*MPH1 are chloroplastic membrane proteins, as has been demonstrated for their land plant homologs (Li et al., 2000; Ferro et al., 2010; Liu and Last, 2015b). Similar analysis for the distribution of *Eo*RP2-CLC among the FFZE fractions, showed that this protein was more abundant in the plasma membrane-enriched

fractions (Fig. 4.4E), an observation that agrees with the RP2 plasma membrane localization in vertebrates (Chapple et al., 2002; Grayson et al., 2002).

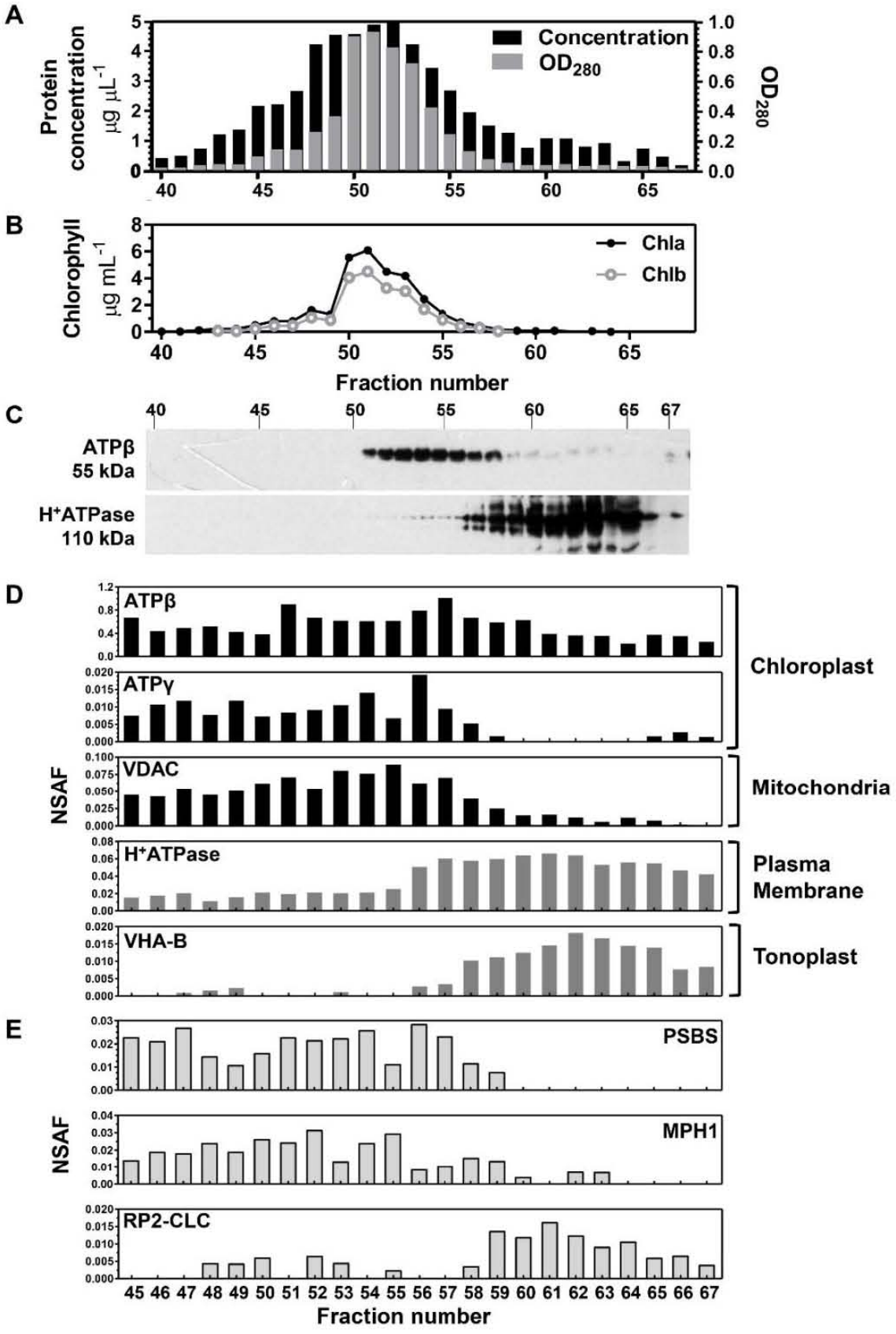

Figure 4.4. Subcellular location of novel proteins from *E. oleoabundans* via FFZE fractionation coupled to MS-based analysis. Microsomal membranes from N-deficient cultures were separated by FFZE. (A) Protein profile of FFZE fractions. (B) Chlorophyll a and b concentrations in FFZE fractions. (C) Immunological detection in the respective fractions of ATPβ (chloroplast marker) and H^+-ATPase (plasma membrane marker). SDS-PAGE 10% (w/v) acrylamide gel, 15 µg protein per lane. The approximate MWs of the detected proteins are shown. (D) Graphical representation of the normalized spectral count (NSAF values) of protein markers specific for subcellular compartments among the FFZE fractions. Individual FFZE fractions were analyzed by LC-MS/MS. The identification numbers for the surveyed protein markers are: gi|416678 (ATPβ); m.392881 (ATPγ); m.378383 (VDAC); m.363780 (H^+-ATPase); m.395664 (VHA-B). (E) Graphical representation of the NSAF values of PSBS, MPH1, and RP2-CLC among the FFZE fractions.

4.2.6. Molecular phylogenetic analysis of identified proteins places *E. oleoabundans* within *Trebouxiophycean* algae

E. oleoabundans is a coccoid green microalga with a complex taxonomic history. It was initially classified within the *Neochloris* genus (*Sphaeropleales*), but later reclassified into the *Ettlia* genus (*Chlamydomonadales*) which comprised uninucleate cells with thin-walled zoospores (Deason et al., 1991; Guiry and Guiry, 1996). Despite that most researchers commonly refer to this microalga as *Neochloris oleoabundans*, it is currently classified as *Ettlia oleoabundans*, which is placed within the *Chlorophyceae* class according to the classification of the *Ettlia* genus type species, *Ettlia carotinosa* (Guiry and Guiry, 1996; Pegg et al., 2015).

The results from this work raised concerns regarding the taxonomic status of *E. oleoabundans*. Most of the identified proteins (>90%) had best-hit homologs in species from the *Trebouxiophycean* class (Fig. S4.1) and phylogenetic analysis of identified proteins, including PSBS (Fig. 4.1C), MPH1 (Fig. 4.2C), TBCC, RP2-CLC (Fig. 4.3B), and enolase (Fig. S4.7), showed a closer relationship between *E. oleoabundans* and *C. variabilis* (*Trebouxiophyceae*), rather than with *Chlorophycean* species. Moreover, evidence for zoospore formation in several *Ettlia* species is lacking (Yoo et al., 2013), including *E. oleoabundans* for which only autosporic reproduction has been observed, similar to *Chlorella* species of the *Trebouxiophycean* class (Huss et al., 1999).

To assess the taxonomy of *E. oleoabundans*, a molecular phylogenetic analysis based on a multi-gene approach was performed. This has proved to increase the power of discrimination and robustness of the phylogenetic analysis compared to single-gene analysis (Moreira et al., 2000; Gontcharov et al., 2002; Tippery et al., 2012). Six proteins proposed as microalgal phylogenetic markers (Moreira et al., 2000; Tippery et al., 2012; Wei et al., 2013) were chosen, two per genome (Table S4.16): nuclear-encoded, actin and elongation factor 1-alpha (EF-1α); plastid-encoded, photosystem II D1 (PSBA) and

RuBisCO large chain (RBCL); mitochondria-encoded, cytochrome oxidase subunits 1 (COX1) and 2 (COX2). Amino acid sequences representative for the three green microalgae classes, *Chlorophyceae*, *Trebouxiophyceae* and *Prasinophyceae* (outgroup), were retrieved, aligned and concatenated. Phylogenetic analysis of concatenated markers placed *E. oleoabundans* as a close relative of the *Chlorella* species within the *Trebouxiophyceae* class (Fig. 4.5A), a relationship that was strongly supported by the bootstrap value from the maximum likelihood analysis (MLb=0.79). The relationship of *E. oleoabundans* with *Trebouxiophycean* algae, rather than with the *Chlorophycean* class is reinforced by the analysis of *E. oleoabundans* COX2 (*Eo*COX2, m.110997, Table S4.2). *E. oleoabundans* contains an orthodox intact mitochondria-encoded COX2, identified in this study by a single polypeptide, which lacks a predicted N-terminal mitochondrial targeting sequence (PredAlgo). This protein showed around 80% identity to orthodox COX2 homologs from members of the *Trebouxiophycean* class (Fig. S4.6B). Phylogenetic analysis confirmed the close relationship of *Eo*COX2 with orthodox COX2 from *Chlorella* species, rather than with homologs from *Chlorophycean* algae, which clustered into a different clade (Fig. S4.6A). *Eo*COX2 clearly differs from its homologs in *Chlorophycean* algae, characterized by exhibiting an atypical COX2 heterodimer as a consequence of a lineage-specific fragmentation and nuclear relocation of the mitochondrial *COX2* gene (Pérez-Martinez et al., 2001; Rodríguez-Salinas et al., 2012).

Due to the reduced availability of completely sequenced microalgal genomes, the multi-gene approach was performed with a reduced taxon sampling. To improve the accuracy of the analysis, we performed an 18S (r)DNA phylogenetic analysis with increased taxon sampling, which included three independent 18S partial sequences for *E. oleoabundans*, one of them obtained in this work (Fig. 4.5B, Table S4.17). Two major taxa within the *Chlorophyceae* class, where species of the *Neochloris* and *Ettlia* genus are currently classified (*Sphaeropleales* and *Chlamydomonadales*), were highly represented. Taxon sampling was also increased for the diverse *Trebouxiophycean* class. The 18S phylogeny confirmed the extremely close relationship between *E. oleoabundans* and *Trebouxiophyceaen* microalgae, as all three 18S *E. oleoabundans* sequences clustered together within this class, particularly in the well-defined *Chlorellales* lineage supported by a robust bootstrapping score (MLb=0.76, Fig. 4.5B). Other *Ettlia* species considered in this analysis were still placed in several groups within the *Chlorophycean* class, supporting previous concerns regarding the classification of the species from this genus (Pegg et al., 2015).

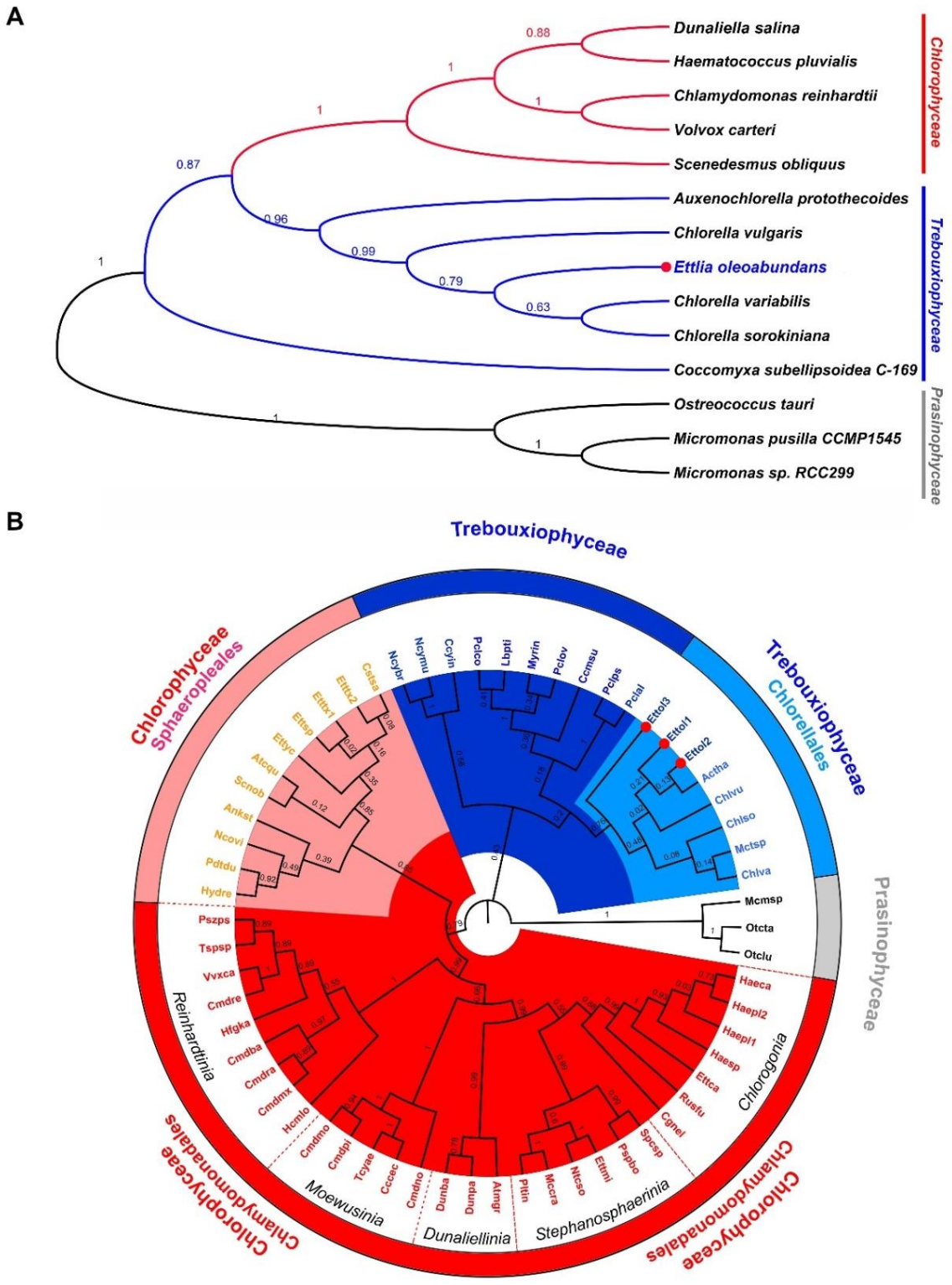

Figure 4.5. Molecular phylogenetic analysis of *E. oleoabundans*. (A) ML analysis of concatenated nuclear- (EF-1α, actin), plastid- (PSBA, RBCL), and mitochondria-encoded (COX1, COX2) amino acid sequences (Table S16). The topology of the ML tree with the highest log likelihood (-20458.0427) is shown. (B) ML analysis of 18S (r)DNA nucleotide sequences (Table S4.17); Ettol2 corresponds to the sequence obtained in this work. The topology of the ML tree with the highest log likelihood (-12721.9945) is shown. MLb values are shown next to the branches. *E. oleoabundans* sequences are highlighted (red dots). Green microalgae classes are denoted as follows: *Chlorophyceae* (red), *Trebouxiophyceae* (blue), *Prasinophyceae* (gray; outgroup). Major taxa represented within these classes are denoted in (B).

Altogether, our results provide compelling evidence for reclassifying *E. oleoabundans* into the *Trebouxiophycean* class, close to the *Chlorellales* lineage, and indicate that it is not closely related to *Chlorophycean* microalgae.

4.2.7. Lipid metabolism represented in the *E. oleoabundans* membrane proteome

E. oleoabundans has shown potential for biotechnological applications, as its lipid acyl-chains are considered an energy-rich feedstock for the production of biofuels and value-added compounds (Hu et al., 2008; Liu and Benning, 2012; Garibay-Hernández et al., 2013). Analysis of the *E. oleoabundans* membrane proteome under lipid accumulation conditions (N deprivation) presents an opportunity to study proteins related to lipid metabolism, since many of them are membrane-associated (Natter et al., 2005; Joyard et al., 2009; Wang and Benning, 2012). Table 4.1 lists the proteins involved in acetyl-CoA synthesis and lipid metabolism identified in this study.

Acetyl-CoA synthesis

The direct carbon precursor for *de novo* fatty acid synthesis in photosynthetic organisms is plastidic acetyl-CoA, which is directly synthesized by the activity of the chloroplastic pyruvate dehydrogenase (PDH) complex, via the oxidative decarboxylation of glycolysis-derived pyruvate (Shtaida et al., 2015). We identified the four subunits of the chloroplastic PDH complex in the membranes of N-deprived *E. oleoabundans* (E1α, E1β, E2, and E3; Table 4.1, Fig. 4.6). Cytoplasmic production of acetyl-CoA was also represented by the identification of the ATP-citrate synthase alpha and beta subunits (Table 4.1, Fig. 4.6), whose cytoplasmic location has been demonstrated in *A. thaliana* (Fatland et al., 2002). The ATP-citrate synthase has been proposed as a key enzyme for lipid accumulation in mammals, oleaginous yeast, fungi (Courchesne et al., 2009), and *C. reinhardtii* (Wase et al., 2014).

Lipid metabolism

The membrane proteome of *E. oleoabundans* was comprised of 3.5% of proteins related to lipid metabolism (Table 4.1). A similar amount of lipid metabolism-related proteins (Table 4.1, proteins highlighted with an asterisk) were additionally identified in only one replicate of the total microsomal samples and/or through MS analysis of the FFZE fractions where

sample complexity was reduced. This demonstrates that the low abundance of lipid biosynthetic proteins hindered their identification in *E. oleoabundans* membranes.

Among the proteins identified in *E. oleoabundans* membranes, the committed step for fatty acid biosynthesis catalyzed by the heteromeric acetyl-CoA carboxylase (ACC) (Stern, 2009) was represented. Two ACC chloroplast-targeted components, alpha-carboxyl transferase and biotin carboxylase (Table 4.1), were identified in total microsomal samples, whereas the chloroplast-encoded beta-carboxyl transferase subunit (Table 4.1) was exclusively detected through MS analysis of the FFZE fractions. The fourth ACC component, biotin carboxyl carrier protein, was not detected, probably due to its low abundance and low MW (26 kDa) predicted from its transcript (Rismani-Yazdi et al., 2012). Incomplete detection of the ACC constituents is more frequent than expected, as only a few subunits have been identified in several proteomics studies performed in *A. thaliana* (Ferro et al., 2003; Froehlich et al., 2003; Kleffmann et al., 2004; Peltier et al., 2006) and *C. reinhardtii* (Bienvenut et al., 2011; Schmollinger et al., 2014). The chloroplastic fatty acid synthesis was also represented in this work by the identification of the 3-hydroxyacyl-ACP dehydratase and the enoyl-ACP reductase (Table 4.1), which are components of the multipartite (type II) fatty acid synthase complex (Li-Beisson et al., 2015). In agreement with the existence of very long chain fatty acids (acyl-chain length beyond 18C) in N-deprived *E. oleoabundans* (Tornabene et al., 1983; Garibay-Hernández et al., 2013; Matich et al., 2016), we identified a homolog of the beta-ketoacyl-CoA reductase (Table 4.1), a component of the endoplasmic reticulum-bound multienzymatic fatty acid elongase complex (Haslam and Kunst, 2013). Three long chain acyl-CoA synthetase isoforms (Table 4.1), required for the activation of free fatty acids to acyl-CoA thioesters (Li-Beisson et al., 2015), were also identified.

Glycerolipid metabolism was represented in *E. oleoabundans* microsomes by the glycerol-3-phosphate acyltransferase (GPAT) and the 1-acyl-sn-glycerol-3-phosphate acyltransferase (Table 4.1), which catalyze the first two reactions common to glycerolipid synthesis leading to phosphatidic acid formation (Li-Beisson et al., 2015). The GPAT identified in this work is a homolog of a *C. reinhardtii* LD-associated protein (Nguyen et al., 2011), but also of plant GPAT9 proteins (Shockey et al., 2016) and thus, may be involved in *E. oleoabundans* triacylglycerol biosynthesis as has been demonstrated for its homologs in *Parietochloris incisa* (*Trebouxiophyceae*) and *A. thaliana* (Iskandarov et al., 2016; Shockey et al., 2016; Singer et al., 2016).

Table 4.1. Acetyl-CoA and lipid metabolism proteins identified in membranes of N-depleted *E. oleoabundans*. Acetyl-CoA and lipid metabolism proteins identified with at least two unique peptides in two or more biological replicates of total microsomal membrane samples are described. Very low abundant proteins that were exclusively identified in one biological replicate and/or in FFZE membrane fractions are highlighted with an asterisk. The calculated MWs are shown, together with the corresponding protein homologs in the model organisms *C. reinhardtii* (Cr) and *A. thaliana* (At), and their corresponding % identity values (%ID). Common abbreviations (Abbr.) of the identified proteins are provided. Subcellular localizations were predicted (Pr) using PredAlgo. Curated cell locations (Cu) were established according to the protein homologs. References are provided for protein homologs whose cell location has been experimentally demonstrated (NA, Not Available). [a] Experimental evidence of subcellular location is available; [b] Experimental evidence of subcellular location is not available; [c] Protein identified in only one biological replicate of total microsomal samples; [d] Protein exclusively identified in FFZE membrane fractions; [e] Protein identified in one biological replicate of total microsomal samples and in FFZE membrane fractions. C, Chloroplast; Cy, Cytoplasm; FAE, Fatty Acid Elongase complex; FAS, Fatty Acid Synthase complex; LD, Lipid Droplet; M, Mitochondria; O, Other; PM, Plasma Membrane; PX, Peroxisome; SP, Signal Peptide.

Protein ID	Curated description	Abbr.	MW kDa	E.C. number	Best Cr homolog		Best At homolog		Subcellular localization		
					JGI v5.5 ID	%ID	TAIR10 ID	%ID	Pr	Cu	Reference
Acetyl-CoA synthesis											
m.73526	Pyruvate dehydrogenase E1 component subunit alpha, chloroplastic*[d]	PDH E1α	47	1.2.4.1.	Cre02.g099850.t1.1	75	AT1G01090	70	**C**	**C[a]**	Terashima et al., 2010
m.371437	Pyruvate dehydrogenase E1 component subunit beta, chloroplastic	PDH E1β	41	1.2.4.1.	Cre03.g194200.t1.2	86	AT1G30120	69	**C**	**C[a]**	Terashima et al., 2010
m.130266	Pyruvate dehydrogenase E2 component, chloroplastic	PDH E2	50	2.3.1.12	Cre03.g158900.t1.2	74	AT3G25860	54	**C**	**C[a]**	Terashima et al., 2010
m.324850	Pyruvate dehydrogenase E3 component, chloroplastic	PDH E3	63	1.8.1.4.	Cre01.g016514.t1.1	72	AT3G16950	60	**C**	**C[a]**	Terashima et al., 2010
m.396299	ATP-citrate synthase alpha chain protein*[e]	ACLA	47	2.3.3.8.	Cre05.g241850.t1.2	62	AT1G10670	65	**SP**	**Cy[a]**	Fatland et al., 2002
m.391431	ATP-citrate synthase beta chain protein	ACLB	76	2.3.3.8.	Cre02.g088600.t1.2	77	AT5G49460	75	**O**	**Cy[a]**	Fatland et al., 2002
Lipid Metabolism											
Acyl-lipid biosynthesis											
m.212887	Acetyl-CoA carboxylase carboxyl transferase subunit alpha, chloroplastic	ACC α-CT	60	6.4.1.2.	Cre12.g519100.t1.2	73	AT2G38040	54	**C**	**C[a]**	Terashima et al., 2010
gi|3023244	Acetyl-CoA carboxylase carboxyl transferase subunit beta, chloroplastic*[d]	ACC β-CT	47	6.4.1.2.	Cre12.g484000.t1.1	75	ATCG00500	61	**O**	**C[a]**	Terashima et al., 2010
m.390372	Biotin carboxylase, chloroplastic	ACC BCR	61	6.3.4.14 6.4.1.2.	Cre08.g359350.t1.2	80	AT5G35360	74	**C**	**C[a]**	Terashima et al., 2010

Protein ID	Curated description	Abbr.	MW kDa	E.C. number	Best Cr homolog		Best At homolog		Subcellular localization		
					JGI v5.5 ID	%ID	TAIR10 ID	%ID	Pr	Cu	Reference
m.332618	3-Hydroxyacyl-[acyl-carrier-protein] dehydratase, chloroplastic*[d]	FAS HAD	25	4.2.1.59.	Cre03.g208050.t1.2	70	AT5G10160	54	**M**	**C[a]**	Terashima et al., 2010
m.179214	Enoyl-[acyl-carrier-protein] reductase [NADH], chloroplastic*[e]	FAS ENR	39	1.3.1.9.	Cre06.g294950.t1.1	82	AT2G05990	76	**C**	**C[a]**	Terashima et al., 2010
m.84123	Beta-ketoacyl-CoA reductase*[e]	FAE KCR	39	1.1.1.330.	Cre09.g392430.t1.1	32	AT1G67730	43	**SP**	**E[a]**	Beaudoin et al., 2009
m.368848	Long chain acyl-CoA synthetase_A	LCS	71	6.2.1.3	Cre13.g566650.t2.1	58	AT4G23850	48	**O**	**LD[a]**	Moellering and Benning, 2010
m.224985	Long chain acyl-CoA synthetase_B	LCS	76	6.2.1.3	Cre13.g566650.t2.1	47	AT4G11030	43	**SP**	**LD[a]**	Moellering and Benning, 2010
m.371326	Long chain acyl-CoA synthetase_C	LCS	67	6.2.1.3	Cre12.g507400.t1.2	63	AT5G27600	53	**M**	**M[b]**	NA
Isoprenoid biosynthesis via the mevalonate pathway											
m.149328	Acetyl-CoA acetyltransferase*[d]	ACAT	51	2.3.1.9.	Cre02.g146050.t1.2	64	AT5G47720	59	**M**	**Cy[a]**	Carrie et al., 2007
Glycerolipid biosynthesis											
m.241864	Glycerol-3-phosphate acyltransferase*[c]	GPAT	54	2.3.1.15.	Cre06.g273250.t1.2	55	AT5G60620	60	**O**	**E[a], LD[a]**	Gidda et al., 2009; Nguyen et al., 2011
m.357823	1-Acyl-sn-glycerol-3-phosphate acyltransferase, chloroplastic*[d]	LPAAT	37	2.3.1.51.	Cre09.g398289.t1.1	63	AT4G30580	56	**C**	**C[a], LD[a]**	Ferro et al., 2010; Nguyen et al., 2011
m.250190	Acyltransferase family protein*[e]		54	NA	NA	NA	NA	NA	**C**	**U**	NA
Lipid signaling											
m.34057	Phosphatidylinositol 4-kinase alpha*[d]	PI4Kα	213	2.7.1.67.	Cre05.g245550.t1.1	45	AT1G49340	39	**O**	**PM[a], LD[a]**	Nguyen et al., 2011; Zhang et al., 2011
m.226782	Sac1p-like phosphoinositide phosphatase*[d]	SAC1	69	3.1.1.-	Cre09.g388750.t1.2	43	AT3G51460	39	**O**	**E[a], LD[a]**	Despres et al., 2003; Nguyen et al., 2011
Lipid Droplet structural proteins											
m.413736	Major lipid droplet protein	MLDP	28	NA	Cre12.g491550.t1.2	24	NA	NA	**O**	**LD[a]**	Davidi et al., 2012
m.392627	Probable plastid-lipid associated protein_A, chloroplastic	PLAP	59	NA	Cre07.g325736.t1.1	42	AT5G19940	32	**M**	**C[a]**	Terashima et al., 2010
m.50827	Probable plastid-lipid associated protein_B, chloroplastic	PLAP	42	NA	Cre03.g189300.t1.1	44	AT4G04020	48	**M**	**C[a]**	Ferro et al., 2010

Protein ID	Curated description	Abbr.	MW kDa	E.C. number	Best Cr homolog		Best At homolog		Subcellular localization		
					JGI v5.5 ID	%ID	TAIR10 ID	%ID	Pr	Cu	Reference
m.244306	Probable plastid-lipid associated protein_C, chloroplastic	PLAP	23	NA	Cre03.g188650.t1.2	62	AT3G26070	58	**C**	**C**[a]	Terashima et al., 2010
gi|132270	Rubber elongation factor protein*[d]	REF	15	NA	NA	NA	AT3G05500	48	**O**	**LD**[a]	Horn et al., 2013
Lipid trafficking											
m.216464	Membrane-associated 30 kDa protein, chloroplastic	VIPP1	33	NA	Cre13.g583550.t1.2	54	AT1G65260	54	**C**	**C**[a]	Nordhues et al., 2012
m.362261	Protein Trigalactosyldiacylglycerol 2, chloroplastic	TGD2	44	NA	Cre16.g694400.t1.2	57	AT3G20320	40	**O**	**C**[a]	Terashima et al., 2010
m.116135	Phospholipid-transporting ATPase*[d]	ALA	159	3.6.3.1.	Cre16.g656500.t1.1	32	AT1G59820	33	**O**	**E**[a], **PM**[a]	Poulsen et al., 2008; Mitra et al., 2009
m.417181	ABC transporter G family member_A	ABCG	70	3.6.3.-	Cre07.g313250.t1.2	57	AT3G55100	31	**O**	**PM**[b]	NA
m.306564	ABC transporter G family member_C	ABCG	69	3.6.3.-	Cre07.g313250.t1.2	55	AT3G55100	29	**O**	**PM**[b]	NA
m.117336	Chloroplast J-like domain-containing protein	CJD1	30	NA	Cre03.g171100.t1.1	34	AT1G08640	26	**C**	**C**[a]	Ajjawi et al., 2011
Lipases and fatty acid β-oxidation											
m.419400	Putative triacylglycerol lipase*[d]	TGL	47	3.1.1.3.	Cre07.g348550.t1.1	42	AT5G67050	37.3	**SP**	**Cy**[b]	NA
m.225854	Acyl-CoA oxidase_A, peroxisomal*[d]	ACX	75	1.3.3.6.	Cre05.g232002.t1.1	66	AT5G65110	57.9	**O**	**PX**[a]	Stabenau et al., 1984
m.366023	Acyl-CoA oxidase_B, peroxisomal*[c]	ACX	74	1.3.3.6.	Cre11.g467350.t1.2	62	AT1G06290	36	**O**	**PX**[a]	Stabenau et al., 1984
m.420224	Fatty acid beta-oxidation multifunctional protein, peroxisomal*[e]	MFP	77	4.2.1.17. 1.1.1.35.	Cre16.g695050.t1.2	66	AT3G06860	55	**SP**	**PX**[a]	Stabenau et al., 1984
m.356362	2,4-dienoyl-CoA reductase, peroxisomal*[e]	RED	35	1.3.1.4.	Cre17.g731850.t1.2	64	AT3G12800	53	**SP**	**PX**[a]	Reumann et al., 2007

Regarding the metabolism of membrane lipids, two phosphoinositide (PI: phosphorylated derivatives of phosphatidylinositol) signaling proteins were identified in *E. oleoabundans* membranes: phosphatidylinositol 4-kinase alpha and Sac1p-like phosphoinositide phosphatase (Table 4.1). These proteins are likely to be involved in the ultrastructural changes required for LD formation in N-deprived *E. oleoabundans* (Giovanardi et al., 2013). Evidence shows that phosphatidylinositol levels are responsive to N depletion in *E. oleoabundans* (Matich et al., 2016) and changes in PI dynamics have been observed in other microalgae species under environmental stress (Einspahr et al., 1988; Heilmann et al., 2001). Moreover, homologs of both PI signaling proteins have been identified in *C. reinhardtii* LDs (Moellering and Benning, 2010; Nguyen et al., 2011) and a link between PI signaling and LD homeostasis has been demonstrated in yeast (Ren et al., 2014).

In accordance with LD formation in N-deprived *E. oleoabundans* (Popovich et al., 2012; Giovanardi et al., 2013), homologs for LD structural proteins were detected in this work (Table 4.1), including members of the probable Plastid-Lipid Associated Protein family (PLAP; Singh and McNellis, 2011), a rubber elongation factor protein (Horn et al., 2013; Berthelot et al., 2014), and a putative Major Lipid Droplet Protein (MLDP) that shares around 25% identity with current characterized MLDPs from *Haematococcus pluvialis* (Peled et al., 2011)*, C. reinhardtii* (Moellering and Benning, 2010), and *Dunaliella* species (Davidi et al., 2012).

We also identified proteins involved in lipid trafficking (Table 4.1) including the membrane-associated 30 kDa Vesicle Inducing Protein in Plastids (VIPP1), the trigalactosyldiacylglycerol chloroplastic protein (TG2), and an aminophoshopholipid-transporting ATPase (ALA). VIPP1 has been suggested to play a role in thylakoid membrane formation via membrane vesicles (Nordhues et al., 2012), whereas TG2 is a homolog of the substrate binding component of a prokaryotic-type ABC transporter located in the chloroplast envelope that is proposed to participate in chloroplast import of lipids derived from the endoplasmic reticulum (Awai et al., 2006; Li et al., 2016a). ALAs are P4-ATPases implicated in the translocation of specific phospholipids within the two leaflets of biological membranes, a process proposed to generate the local curvature that precedes vesicle budding (Poulsen et al., 2008; Zhou and Graham, 2009). Two homologs of half-sized ABCG transporters were also identified (Table 4.1), which may be involved in lipid trafficking in *E. oleoabundans*, as ABCG transporters have been related to the transport of lipophilic molecules in other organisms (Verrier et al., 2008; Li et al., 2016a).

Our results suggest that lipid degradation is still active in N-deprived *E. oleoabundans* despite the massive oil accumulation triggered by this stress condition (Tornabene et al., 1983; Li et al., 2008; Pruvost et al., 2009; Garibay-Hernández et al., 2013). We identified a putative triacylglycerol lipase probably involved in the release of fatty acids from neutral glycerolipids, as well as homologs of both, core and auxiliary plant peroxisomal proteins that participate in the beta-oxidation reactions for degradation of saturated and unsaturated fatty acids (Table 4.1). In *E. oleoabundans*, beta-oxidation probably takes place in unspecialized peroxisomes (microbodies) lacking the glycolate metabolic enzymes, similar to what has been proposed for *Eremosphaera* (Stabenau et al., 1984) and *Dunaliella* (Stabenau et al., 1993) green microalgae species. The identification of lipid catabolism-related proteins in N-deprived *E. oleoabundans* supports the idea that fatty acid turnover is constitutive and that a continuous balance between oil synthesis and degradation exists even under N stress (Li-Beisson et al., 2015).

The coverage of the lipid metabolic pathways in this work was still limited although additional lipid metabolism-related proteins were identified in the FFZE fractions and/or in only a single total microsomal sample. Incomplete detection of the entire lipid metabolism machinery may be attributed to their low abundance or lack of similarity with current annotated sequences, which prevents their positive identification, but may also reflect their complete absence in the analyzed samples. Our results suggest that the amount of membrane associated lipid metabolism proteins may be lower than has been proposed (Natter et al., 2005; Joyard et al., 2010; Wang and Benning, 2012), as many have been identified to a major extent in total soluble protein extracts from other microalgae (Guarnieri et al., 2011; Gao et al., 2014).

4.2.8. Carbon metabolism proteins in *.E. oleoabundans* membranes

Additional biological processes were covered almost to their entirety in the *E. oleoabundans* membrane proteome, including central carbon metabolism and electron transport. A comprehensive description is provided in this study to better understand the major metabolic constraints of carbon partitioning in this microalga. Other biological processes typically related to N deprivation, including N acquisition, protein turnover, and oxidative stress responses, were also represented in *E. oleoabundans* membrane proteome, as well as processes related to pigment metabolism, transcription regulation, and signaling, which are all described in the Supplementary Information.

Carbon metabolism was represented in the membranes of N-depleted *E. oleoabundans* by 13% of the total proteome (Fig. S4.2, Table S4.4). Not all carbon metabolism-related proteins were identified in the analysis of total microsomal samples; however, the remainder were identified through MS analysis of the FFZE fractions due to the decrease in sample complexity by fractionation (Fig. 4.6, Table S4.4, proteins highlighted with an asterisk).

Inorganic carbon acquisition and assimilation

The CO_2 concentrating mechanism appears to be active in N-limited *E. oleoabundans* (Fig. 4.6, orange; Table S4.4), as we identified proteins involved in active inorganic carbon uptake (High Light Activated 3 [HLA3]), as well as in its interconversion (CO_2/HCO_3^-), recapture, and concentration within the cell (α-type carbonic anhydrases, Limiting CO_2-Inducible B [LCIB]-like proteins). Key regulators of the Calvin cycle (CP12, RuBisCO activase) and almost half (5/11) of its chloroplastic enzymes were identified (Table S4.4), including phosphoglycerate kinase (PGK), glyceraldehyde-3-phosphate dehydrogenase (GPDH), and aldolase, enzymes that are shared with the chloroplast glycolytic pathway (Fig. 4.6, green). Photorespiration and one carbon metabolism proteins were also present in membranes of N-deprived *E. oleoabundans* (Table S4.4).

Biosynthesis of photosynthetic carbon precursors via a compartmentalized glycolytic pathway

The complete glycolytic pathway, with the exception of glucose-6-phosphate isomerase, were identified in this work (Fig. 4.6, green and blue; Table S4.4), demonstrating this pathway is active in N-deprived *E. oleoabundans*. This suggests that glycolysis may be the major contributor for pyruvate production, which is presumed to be the primary carbon source for fatty acid biosynthesis (Chapman et al., 2013; Shtaida et al., 2015).

Identification of most of the glycolytic proteins in *E. oleoabundans* membranes is not as surprising as it may first appear. Membrane association of some or all of the glycolytic pathway components and their sequestration within different organelles are the most usual forms of glycolytic compartmentalization for regulating central carbon metabolism (Ginger et al., 2010; Johnson and Alric, 2013). Several modes of glycolytic compartmentalization

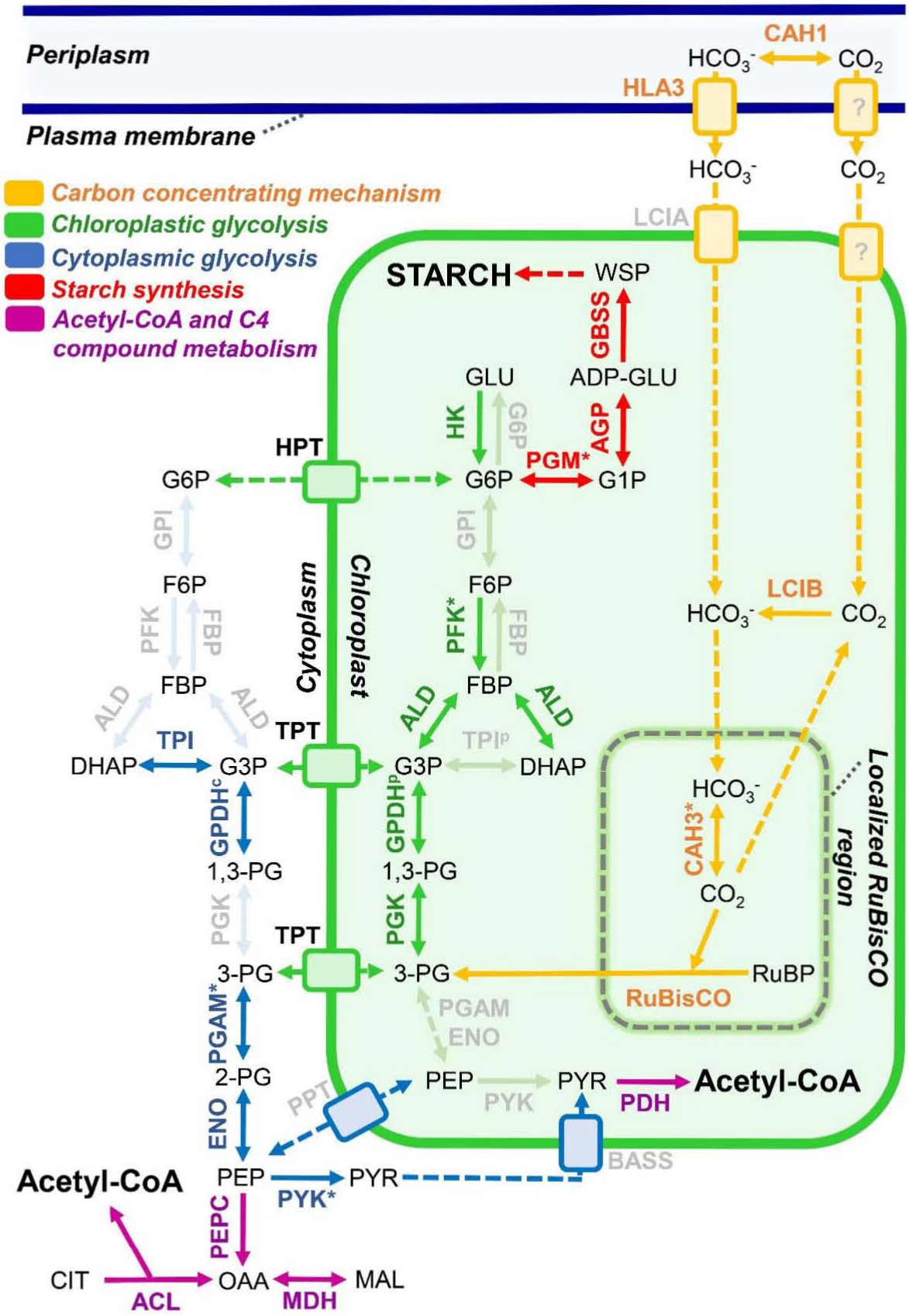

Figure 4.6. Carbon metabolism in N-deficient *E. oleoabundans*. Graphical representation of the carbon metabolism proteins identified by LC-MS/MS in the membrane proteome of *E. oleoabundans.* All proteins were identified in FFZE fractions except HK, which was exclusively identified in total microsome samples. Very low abundant proteins that were exclusively identified in FFZE fractions and not in total microsomes are highlighted with an asterisk (*). Not identified proteins are shown in a clear gray color.

Subcellular locations were predicted using PredAlgo together with experimental evidence available for the corresponding homologs. Identified proteins are described in Table S4.4.

Protein abbreviations: ACL, ATP-citrate synthase; AGP, G1P adenylyltransferase; ALD, aldolase; BASS, sodium/pyruvate cotransporter; CAH1, carbonic anhydrase, periplasmic; CAH3, carbonic anhydrase, chloroplastic; ENO, enolase; FBP, fructose-1,6-biphosphatase; G6P, glucose-6-phosphatase; GBSS, granule-bound starch synthase; GPDH^{c}, G3P dehydrogenase, cytosolic; GPDH^{p}, G3P dehydrogenase A, chloroplastic; GPI, glucose-6-phosphate isomerase; HLA3, probable inorganic carbon transporter HLA3; HK, hexokinase; HPT, UhpC-type hexose phosphate translocator; LCIA, putative inorganic carbon transporter LCIA; LCIB, LCIB family protein; MDH, malate dehydrogenase, cytoplasmic; PDH, pyruvate dehydrogenase; PEPC, PEP carboxylase; PFK, phosphofructokinase; PGAM, phosphoglycerate mutase; PGK, phosphoglycerate kinase; PGM, phosphoglucomutase; PPT, phosphoenolpyruvate/phosphate translocator; PYK, pyruvate kinase; TPI, triosephosphate isomerase; TPT, triose phosphate/phosphate translocator; RuBisCO, RuBP carboxylase. **Compound abbreviations:** 1,3-PG, 1,3-biphosphoglycerate; 2-PG, 2-phosphoglycerate; 3-PG, 3-phosphoglycerate; ADP-GLU, adenosine diphosphate glucose; CIT, citrate; DHAP, dihydroxyacetone phosphate; FBP, fructose-1,6-biphosphate; F6P, fructose-6-phosphate; G3P, glyceraldehyde-3-phosphate; GLU, glucose; G1P, glucose-1-phosphate; G6P, glucose-6-phosphate; MAL, malate; OAA, oxaloacetate; PEP, phosphoenolpyruvate; PYR, pyruvate; RuBP, ribulose-1,5-biphosphate; WSP, water soluble polysaccharide.

have emerged in microalgae (Ginger et al., 2010; Smith et al., 2012), where a comprehensive view only exists for *C. reinhardtii* (Klein, 1986; Johnson and Alric, 2013), and some diatoms (Smith et al., 2012). To assess carbon flow compartmentalization in *E. oleoabundans*, we manually curated the subcellular location of glycolytic proteins (Fig. 4.6, Table S4.4). Accordingly, the enzymes from the upper part of glycolysis (from hexokinase to PGK; Fig. 4.6, green) are apparently targeted to the chloroplast, and those from the lower part (from phosphoglycerate mutase to pyruvate kinase; Fig. 4.6, blue) may be associated to the cytoplasmic face of membranes due to the lack of a predicted target peptide.

In order to confirm the compartmentalization of the glycolytic pathway, we analyzed the distribution of the glycolytic enzymes in the FFZE fractions using an MS-based approach (Fig. 4.7). Enzymes from the lower part of glycolysis separated similar to the fractions enriched in tonoplast and plasma membrane (fractions 56 to 67), indicating their possible association to the cytoplasmic side of these membranes. In contrast, chloroplastic GPDH and PGK, two enzymes of the upper part of glycolysis, were highly abundant in fractions 56 to 59, which were also enriched with the protein marker of the outer chloroplast envelope (TOC75), and to a lesser extent, with markers of the thylakoid (ATP synthase subunit γ) and inner chloroplast membranes (TIC110) (Fig. 4.7). This suggests that chloroplastic GPDH and PGK may be associated to the chloroplast envelope, as demonstrated for their counterparts in *A. thaliana* (Ferro et al., 2010). The two other enzymes from the upper part of glycolysis, phosphofructokinase and aldolase, showed a distribution profile similar to that from the tonoplast and plasma membrane, but were still detected in envelope-enriched fractions (Fig. 4.7). Thus, we suggest they may be targeted to both, chloroplast and

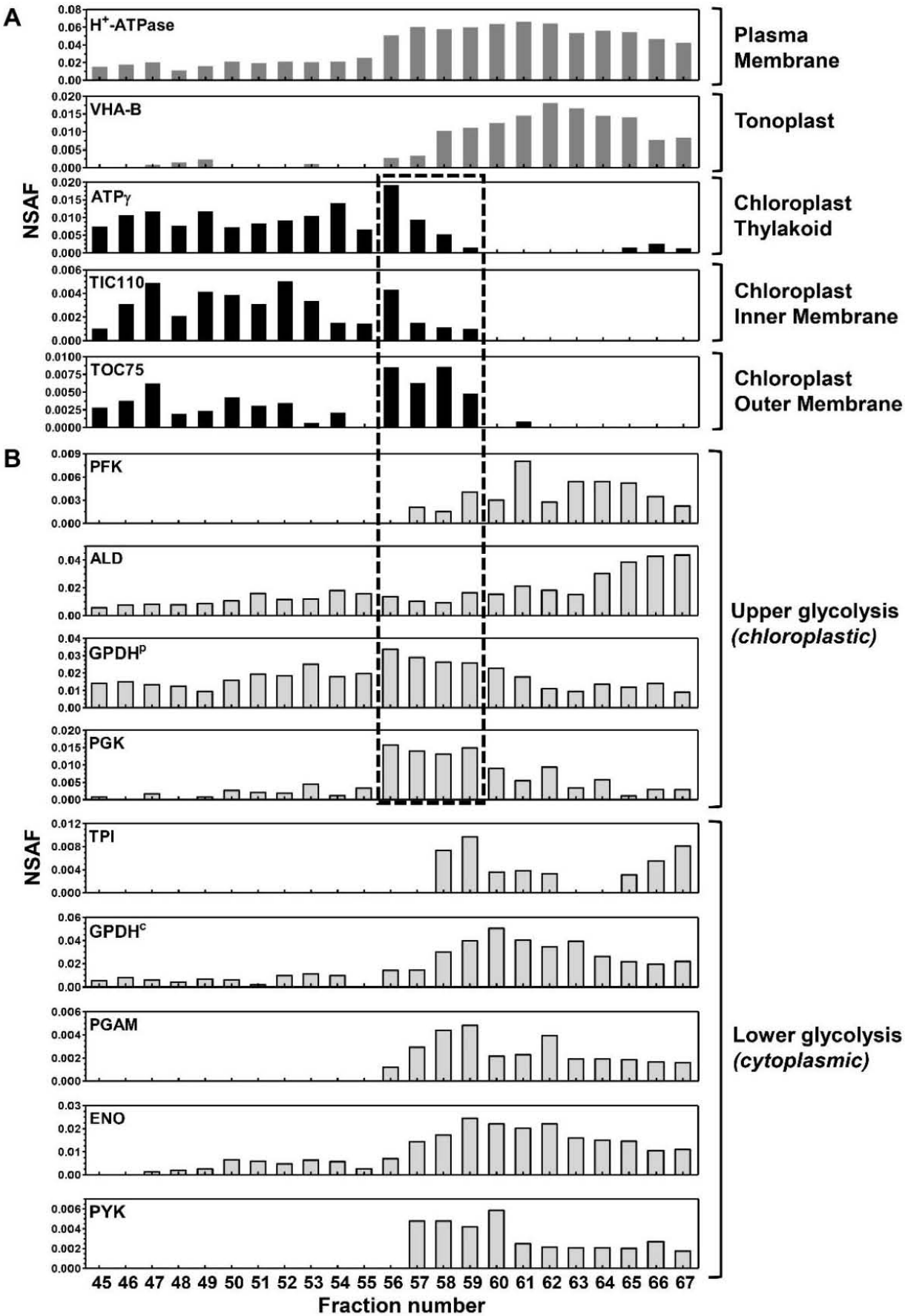

Figure 4.7. FFZE profiles of glycolytic enzymes suggest their targeting to multiple cellular locations. Individual FFZE fractions were analyzed by LC-MS/MS and surveyed for proteins of interest. (A) Graphical representation of NSAF values of protein markers specific for subcellular compartments among the FFZE fractions. The surveyed compartment markers are: m.363780 (H^+-ATPase); m.392881

(ATPγ); m.227792 (TIC110); m.134654 (TOC75). (B) Graphical representation of NSAF values of glycolytic enzymes among the FFZE fractions. According to their predicted cellular location, proteins are grouped into upper and lower glycolytic pathway enzymes. These proteins are described in Table S4.4. FFZE fractions enriched with the outer chloroplast membrane are enclosed in the box (fractions 56 to 59).

cytoplasmic locations, similar to their *C. reinhardtii* homologs (Klein, 1986; Johnson and Alric, 2013). Additional targeting of glycolytic proteins to other cell locations such as the tonoplast is possible, as demonstrated for enolase and aldolase in the salt-tolerant plant *Mesembryanthemum crystallinum*, where they are targeted to the tonoplast to perform moonlighting functions (Barkla et al., 2009).

Glycolysis compartmentalization in *E. oleoabundans* is reinforced by the identification of triose-phosphate and hexose-phosphate translocators that may communicate the two parts of glycolysis across the chloroplast envelope (Fig. 4.6, Table S4.4). Phosphoenolpyruvate and pyruvate transporters were not identified in this work, however, homologs of a phosphonelolpyruvate/phosphate translocator and a sodium/pyruvate cotransporter (PPT, BASS [Bile Acid:Na^+ Symporter]; Fig. 4.6) have been shown to be transcribed in N-deprived *E. oleoabundans* (Rismani-Yazdi et al., 2012). Altogether, our results support the compartmentalization of the glycolytic proteins in *E. oleoabundans*, however, additional experiments for determining their specific localization and dynamics are necessary.

Among the identified glycolytic proteins, it is worth highlighting enolase (*Eo*ENO; Table S4.4, Fig. S4.7), whose presence in *E. oleoabundans* membranes was confirmed by western blot (Fig. S4.7D). Sequence analysis of *Eo*ENO and its homologs, revealed that enolases from *Trebouxiophycean* and *Chlorophycean* microalgae present an additional N-terminal region (InterPro: IPR003117) that corresponds to the RIIa domain (Canaves and Taylor, 2002) (Fig. S4.7A and S4.7B). Phylogenetic analysis confirmed that RIIa-containing enolases are exclusive to *Trebouxiophycean* and *Chlorophycean* species, clustering separately from enolases of land plants and *Prasinophyceaen* microalgae (Fig. S4.7C). The RIIa domain mediates homodimerization of the regulatory subunit of cAMP-dependent protein kinases (PKA) and high affinity binding to AKAP (A-kinase anchoring protein) scaffold proteins, required for the integration of signaling pathways and for the subcellular compartmentalization of its components (Newlon et al., 2001). This suggests that in green microalgae the RIIa domain may be involved in enolase dimerization and/or anchoring to AKAPs for intracellular targeting and regulatory purposes, similar to the non-PKA RIIa-containing Radial Spoke Protein 11 (RSP11; Yang et al., 2006).

Starch synthesis

Starch synthesis was represented in the *E. oleoabundans* membrane proteome by glucose-1-phosphate adenylyltransferase, one of the major rate controlling enzymes, and by other key enzymes involved in green algal starch metabolism including the plastidial phosphoglucomutase and the granule-bound starch synthase (Fig. 4.6, red; Table S4.4). This suggests that starch synthesis is still active in this microalga after prolonged N stress, which agrees with the increase in both lipid and starch content that has been previously reported for N-deprived *E. oleoabundans* (Rismani-Yazdi et al., 2012; Garibay-Hernández et al., 2013).

4.2.9. Photosynthetic and mitochondrial electron transport in *E. oleoabundans*

Analysis of the *E. oleoabundans* membrane proteome allowed us to provide a survey of the components of the photosynthetic and respiratory electron transport chains (Fig. 4.8, Tables S1-S3), essential for supplying energy to the processes taking place during N deprivation.

The mitochondrial respiratory chain

Each of the five complexes of the mitochondrial respiratory chain were represented in the *E. oleoabundans* membrane proteome (Fig. 4.8, Table S4.2). However, comparison of the identified subunits to the oxidative phosphorylation proteome in *C. reinhardtii* (Stern, 2009), shows that important differences do exist. Contrary to *Chlorophycean* microalgae, *E. oleoabundans* has an orthodox intact mitochondria-encoded COX2 (Fig. S4.6) and a classical mitochondrial ATP synthase (Complex V). The latter is supported by identification of subunit *d* (Table S4.2), which is known to be absent from the non-canonical mitochondrial ATP synthases of the *Chlorophycean* lineage (Vázquez-Acevedo et al., 2006; Vázquez-Acevedo et al., 2016). In addition, sequence analysis of the identified mitochondrial ATPase constituents (*α, β, γ, δ, d*; Fig. 4.8, Table S4.2) suggests they are encoded by both, nuclear and mitochondrial genomes, contrary to the *Chlorophycean* lineage where all ATPase subunits are nuclear-encoded (Vázquez-Acevedo et al., 2006; Vázquez-Acevedo et al., 2016).

Photosynthesis and photoprotective mechanisms

All the photosynthetic complexes, PSI-LHCI, cytochrome *b6f*, PSII-LHCII, and ATP synthase, were represented in membranes of N-deprived *E. oleoabundans* (Fig. 4.8, Table S4.1). At least 45% of the protein subunits comprising each of the complexes were identified, including several low molecular mass PSII proteins (PSBE, PSBH, PSBR, PSB27, PSB29, PSB32, PSB33; Table S4.1), which have proven difficult to detect owing to their low abundance, small size, and hydrophobicity (Shi and Schröder, 2004; Shi et al., 2012). Compared to glycolysis and lipid metabolism-related proteins, whose low abundance hindered their detection in *E. oleoabundans* membranes, the identification of low molecular mass PSII proteins in this work can be attributed to the high proportion of chloroplast-localized proteins that comprised the *E. oleoabundans* membrane proteome (41%; Fig. S4.2A). The identified photosynthesis-related proteins are homologs of the corresponding proteins in the model green alga *C. reinhardtii* (Stern, 2009; Minagawa and Tokutsu, 2015), suggesting that, contrary to what is observed for the mitochondrial respiratory chain, the composition of the core photosynthetic complexes is highly conserved among green algae.

In agreement with the diminished integrity of the photosynthetic apparatus that has been reported for N-deprived *E. oleoabundans* (Benvenuti et al., 2015), proteins directly involved in synthesis and turnover of the D1 subunit (FTSH ATP-dependent zinc metalloproteases, Low PSII Accumulation 1, atypical short-chain dehydrogenase HCF244), as well as in PSI (YCF4) and PSII assembly, stability, and/or repair (peptidyl- prolyl cis-trans isomerase CYP38, M-Enriched Thylakoid 1, MPH1, rubredoxin), were identified in this work (Table S4.1). Additional photoprotective responses appeared to be active in N-deprived *E. oleoabundans*, as we were able to identify key molecular effectors of the short-term components of NPQ (Table S4.1): energy-dependent feedback de-excitation quenching (qE: calcium sensing receptor CAS, PSBS), zeaxanthin-dependent quenching (qZ: violaxanthin de-epoxidase), and state-transition-dependent quenching (qT: serine/threonine protein kinase STT7) (Erickson et al., 2015; Minagawa and Tokutsu, 2015). Key components of the two proposed cyclic electron flow pathways (Iwai et al., 2010; Johnson and Alric, 2013), the NADPH dehydrogenase (NDH-2), and the ferredoxin (ferredoxin-NADP reductase, PGR5-

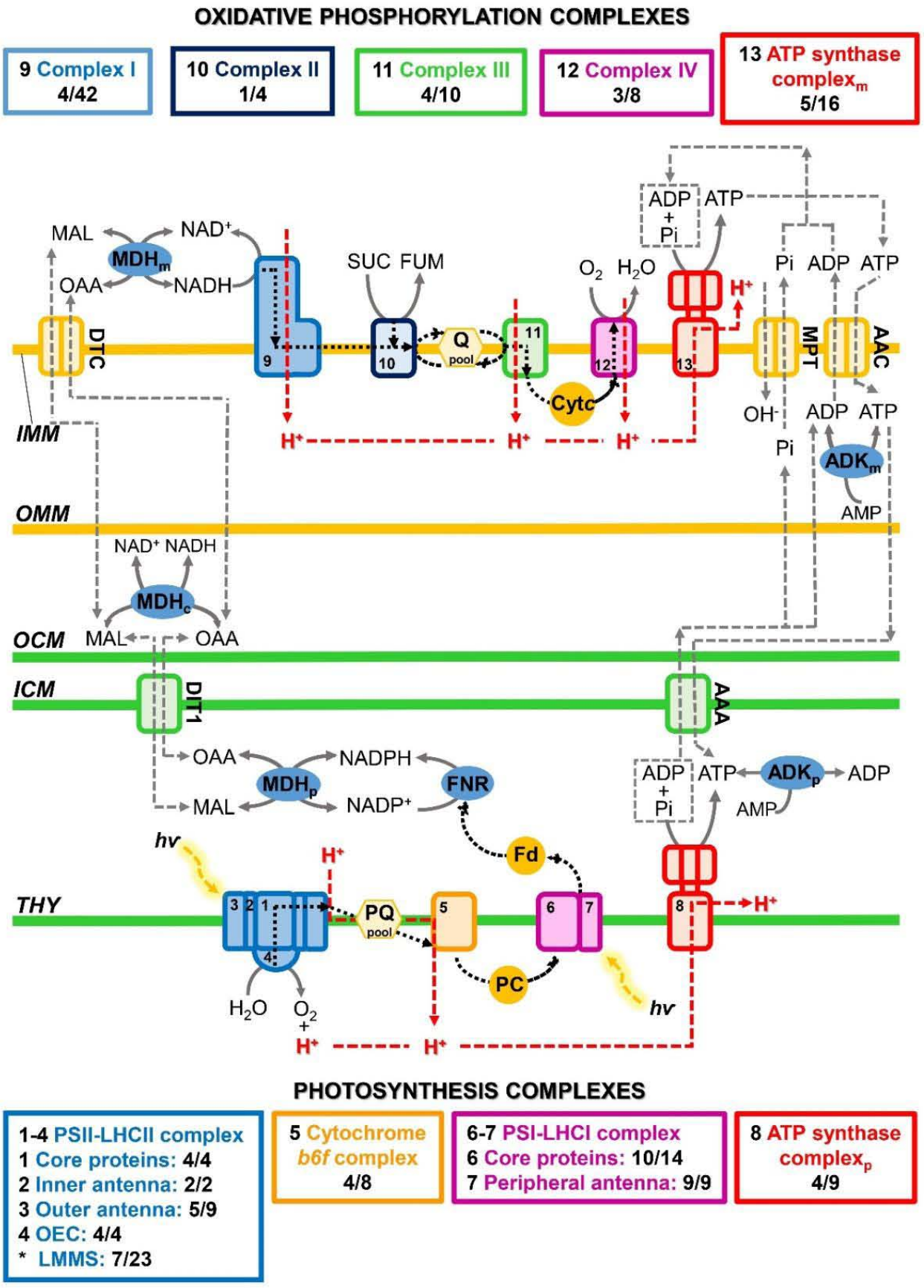

Figure 4.8. Photosynthesis and oxidative phosphorylation in the membrane proteome of N-deficient *E. oleoabundans*. Graphical representation of the proteins identified by LC-MS/MS in the membrane proteome of *E. oleoabundans* involved in energy conversion and homeostasis. Identified proteins are described in Table S4.1 (Photosynthesis), S4.2 (Oxidative phosphorylation) and S4.3 (Energy and reducing power homeostasis). The number of proteins detected in *E. oleoabundans* from each of the

complexes of the chloroplastic and mitochondrial electron transfer chains, are shown in colored boxes and compared to the number of proteins identified in the complexes of the model alga *C. reinhardtii*. In Complex IV, *Cr*COX2 is considered as a non-split subunit. In the *E. oleoabundans* ATP synthase mitochondrial complex, the N- and C- terminal peptides of subunit d are considered as a unique non-split protein. Black dashed lines indicate electron transfer; red dashed lines indicate proton translocation.

c, cytoplasmic; m, mitochondrial; p, chloroplastic; *, proteins associated to any part of the PSII-LHCII supercomplex; AAA, ADP/ATP carrier protein, chloroplastic; AAC, ADP/ATP carrier protein, mitochondrial; ADK, adenylate kinase; Cyt*c*, cytochrome c; DIT1, dicarboxylate transporter 1, chloroplastic; DTC, mitochondrial dicarboxylate/tricarboxylate carrier; Fd, ferredoxin; FNR, ferredoxin-NADP reductase; FUM, fumarate; ICM, inner chloroplast membrane; IMM, inner mitochondrial membrane; LHCI, light harvesting complex of PSI; LHCII, light harvesting complex of PSII; LMMS, low molecular mass subunits; MAL, malate; MDH, malate dehydrogenase; MPT, mitochondrial phosphate carrier protein; OAA, oxaloacetate; OCM, outer chloroplast membrane; OEC, oxygen evolving complex; OMM, outer mitochondrial membrane; PC, plastocyanin; PQ, plastoquinone; PSI, photosystem I; PSII, photosystem II; Q, ubiquinone; SUC, succinate; THY, thylakoid membrane.

like protein 1) dependent pathways, were also identified (Table S4.1 and Table S4.3). This supports that alternative electron pathways may be active in N-deprived *E. oleoabundans* for photoprotection and for satisfying the varying demand for ATP/NADPH under abiotic stress conditions.

Additional mechanisms known to modulate the redox potential and ATP concentration in different cellular compartments, particularly under fluctuating environmental conditions (Cardol et al., 2003; Johnson and Alric, 2013; Erickson et al., 2015), were represented in N-deprived *E. oleoabundans*. We were able to identify the main effectors of the malate shunt (malate dehydrogenase isoforms, dicarboxylate transporter, mitochondrial dicarboxylate/tricarboxylate carrier) and proteins necessary for regulating ATP concentrations within the chloroplast and the mitochondria (adenylate kinase isoforms, mitochondrial and chloroplastic ADP/ATP carrier proteins, mitochondrial phosphate carrier protein) (Fig. 4.8, Table S4.3).

4.3. Conclusion

The results from this work provide a detailed survey of the membrane proteome of an oleaginous microalga. Combining gel-free shotgun proteomics together with searching against an organism-specific RNA-Seq-based protein database, considerably improved protein identification. This approach overcame both, the typical limitations of studying membrane proteins, and the difficulty of working with non-sequenced organisms for which the quality and quantity of the data available in reference databases is neither complete nor specific. Although manual annotation may be a time-consuming strategy, we demonstrated

its usefulness for analyzing non-sequenced organisms, as it significantly improved the number of identified proteins, as well as the accuracy and reliability of their annotations.

This approach allowed the novel identification in *E. oleoabundans* of the photosynthesis-related proteins, MPH1 and PSBS, both thought to be exclusive to higher photosynthetic organisms. These findings suggest that photoprotective mechanisms, including NPQ, are active after prolonged N deprivation, and indicate that in *E. oleoabundans* these mechanisms are more closely related to higher photosynthetic organisms than previously proposed. The identification of PSBS and the presumed absence of an LHCSR homolog in *E. oleoabundans* is contrary to what has been observed in *C. reinhardtii*. In *C. reinhardtii*, a light-inducible PSBS was recently identified and was demonstrated to be essential for activation of an LHCSR-dependent qE mechanism to which most of the microalgal NPQ capability has been attributed (Peers et al., 2009; Niyogi and Truong, 2013; Correa-Galvis et al., 2016; Tibiletti et al., 2016). This result questions the conservation of qE mechanisms within green microalgae, where the specific role played by PSBS in *E. oleoabundans* NPQ must be determined. In addition to the photosynthesis-related proteins, we also detected RP2-CLC, a novel domain architecture protein that is likely involved in intracellular trafficking of clathrin-coated vesicles in lower eukaryotes, a process that apparently has its own peculiarities in these understudied organisms. Using FFZE fractionation of membranes, we confirmed the chloroplastic location of PSBS and MPH1, together with the enrichment of RP2-CLC in the plasma membrane. Using this strategy also contributed to the identification of very low abundant proteins related to *E. oleoabundans* lipid metabolism, allowing us to identify a detailed list of proteins involved in the major steps of acyl-lipid metabolism, lipid trafficking, lipid signaling, and LD formation in *E. oleoabundans*. An MS-based analysis of FFZE fractions additionally supported the compartmentalization of glycolytic proteins in *E. oleoabundans*, which is an important constraint that appears to govern central carbon metabolism and partitioning.

Finally, through molecular phylogenetic approaches, we provide compelling evidence for the phylogenetic grouping of this microalga with the *Chlorellales* lineage of the *Trebouxiophycean* class of green microalgae, rather than with the *Chlorophycean* class in which it is currently classified. Our results provide an important platform for studying *E. oleoabundans* and underscore the importance of studying non-model organisms, as the analysis of specific features in *E. oleoabundans* demonstrates that its biology differs from that of non-oleoaginous model organisms.

4.4. Materials and methods

4.4.1. Microalgae strains and culture conditions

Ettlia oleoabundans UTEX 1185 was grown under phototrophic conditions in 2.8 L Fernbach glass flasks with a working volume of 40%, using modified Bold's Basal Media (mBBM) (Garibay-Hernández et al., 2013). Axenic cultures with an initial cell density of 1-2 x 10^6 cells mL^{-1} were maintained for 7 d at 25±0.5°C, under continuous orbital agitation (300 rpm), and white fluorescent light illumination (100 µE m^{-2} s^{-1}). To induce N deprivation, 7-d cultures were individually centrifuged for 10 min (10,000 *g*, 4°C), washed once with 200 mL of N-free mBBM, resuspended in 1.12 L of N-free mBBM, and transferred into Fernbach flasks. Axenic N-deprived cultures with an initial cell density of 10-15 x 10^6 cells mL^{-1} were maintained during 4 d under the aforementioned conditions.

Chlamydomonas reinhardtii wall-less strain *cw15 mt+* was grown under mixotrophic conditions in 0.5 L Erlenmeyer glass flasks with a 40% working volume, using Tris-acetate-phosphate medium (Harris, 2009). Axenic cultures with an initial cell density of 1-2 x 10^6 cells mL^{-1} were maintained for 4 d at 24±2°C, under white fluorescent light illumination (50-100 µE m^{-2} s^{-1}, 16:8 light-dark cycles), and continuous orbital agitation (80 rpm).

Cell density was determined by direct microscopic cell count using a Neubauer chamber. Cultures were tested for the absence of bacteria in glucose-free Luria broth agar (1.5% w/v) medium plates (Bertani, 1951), incubated at 37°C for at least 24 h.

4.4.2. Microsomal membrane isolation

All the operations in this protocol were performed at 4°C. N-deprived *E. oleoabundans* cultures (1.12 L) or *C. reinhardtii* cultures (0.4 L) were used for microsome isolation. Cultures were centrifuged for 10 min (10,000 *g*, 4°C), washed once with 0.1 M HEPES-KOH pH 7.5 (50/500 mL of centrifuged culture), and resuspended in 2.5 mL of homogenization medium (400 mM mannitol, 10% w/v glycerol, 5% w/v PVP-10, 0.5% w/v BSA, 1 mM PMSF, 30 mM Tris, 2 mM DTT, 5 mM EGTA, 5 mM $MgSO_4$, 0.5 mM BHT, 0.25 mM dibucaine, 1 mM benzamidine, 26 mM K^+-metabisulfite; adjusted to pH 8.0 with NaOH). Cells were homogenized by passing the cell suspension five times through a French press (Thermo Spectronic, Model FA-078) at 20 kpsi, using a mini pressure cell. Microsomal membranes were isolated as described in Barkla et al. (1995). Briefly, the homogenate was centrifuged

for 20 min (10,000 *g*, 4°C) and the pellet was discarded. To concentrate the microsomes, the supernatant was centrifuged (80,000 g_{rmin}, 50 min, 4°C; Beckman 45 Ti rotor, L8-M ultra-centrifuge). The microsomal pellet was resuspended in suspension medium (400 mM mannitol, 10% w/v glycerol, 6 mM Tris/MES pH 8.0, 2 mM DTT) using a 10 mL glass teflon homogenizer. Samples were frozen in liquid N_2 for storage at -80°C. Microsomes from *Arabidopsis thaliana* were isolated as described in Barkla et al. (2007).

4.4.3. FFZE

Microsomal membranes from N-deprived *E. oleoabundans* were fractionated by FFZE using the BD FFE system (BD proteomics) as described in Barkla et al. (2007). Briefly, prior to fractionation, the microsomal sample was diluted 2:1 (v/v) in separation medium (10 mM triethanol amine [TEA], 10 mM acetic acid, 2 mM KCl, 250 mM sucrose) and centrifuged for 20 min (14,000*g*, 4°C). The sample was supplemented with Mg-ATP (3 mM final concentration) to enhance membrane separation during FFZE (Barkla et al., 2007). The sample was injected continuously via a peristaltic pump at 1.2 mL h^{-1} using the anodic sample inlet. Media inlets 2 to 6 and counter flow inlets C1, C2, and C3, contained separation medium, whereas inlets 1 and 7 comprised stabilization medium (40 mM TEA, 40 mM acetic acid, 8 mM KCl, 180 mM sucrose). The cathodic and anionic circuit electrolyte solutions consisted of 100 mM TEA, 100 mM acetic acid, and 20 mM KCl adjusted to pH 7.4 (NaOH); 0.4% formaldehyde was added to the anodic solution to prevent loss of chloride by anodic oxidation.

FFZE was performed in horizontal mode at 5°C, 750 V (150 mA), with media and counter flow rates of 250 mL h^{-1}. Following separation in the chamber, membrane fractions were collected continually in 96-deep well microtiter plates (4 mL per well). Fractions from sequential plates corresponding to the same well were pooled; 1.2 mL aliquots were collected per pooled fraction, frozen in liquid N_2, and stored at -80°C for LC-MS/MS analysis. The remaining volume of each collected fraction was ultra-centrifuged (100,000 *g,* 50 min, 4°C; Beckman 55.2 Ti rotor, L8-M ultra-centrifuge) for membrane concentration. Membrane pellets corresponding to each fraction were resuspended in 25-200 µL of suspension buffer (250 mM mannitol, 10% w/v glycerol, 10 mM Tris/MES pH 8.0, 2 mM DTT) and frozen in liquid N_2 for storage at -80°C. FFZE separation was monitored by collecting microtiter plates (250 µL per well) at several time points and measuring protein (OD_{280}) using a microplate scanning spectrophotometer (Power $Wave_X$; Bio-Tek Instruments).

4.4.4. Protein and chlorophyll concentration measurements

Protein in microsomal and concentrated FFZE fractions was measured by a modification of the Bradford method (Bradford, 1976). Membrane protein was partially solubilized with 0.5% v/v Triton X-100 for 5 min, prior to dilution and addition of the dye reagent concentrate; final Triton X-100 concentration in the assay was 0.05%. BSA was used as the protein standard.

Chlorophyll in FFZE fractions, prior to concentration, was measured according to the method of Arnon (1949), with some modifications, using a microplate scanning spectrophotometer (Power Wave$_X$; Bio-Tek Instruments). Absorbance was directly measured at 645 and 663 nm, and calculations were made according to the following equations.

$$\text{Chl}a\ (\mu g\ mL^{-1}) = 12.7A_{663} - 2.69A_{645}$$

$$\text{Chl}b\ (\mu g\ mL^{-1}) = 22.9A_{645} - 4.68A_{663}$$

4.4.5. SDS-PAGE, staining, and immunoblotting

For protein precipitation, total microsome samples and concentrated FFZE fractions were diluted 50-fold in 1:1 v/v ethanol:acetone and incubated overnight at -20°C according to Parry et al. (1989). Samples were then centrifuged for 20 min (14,000 *g*, 4°C). Pellets were air dried, resuspended in Laemmli buffer (Laemlli, 1970), and heated (60°C, 2 min) before loading (15 to 20 µg protein per lane) onto 10 to12.5% (w/v) linear acrylamide gels as indicated. After electrophoresis, SDS-PAGE separated proteins were either fixed and stained with Coomassie R250, or electrophoretically transferred onto nitrocellulose membranes (ECL, GE Lifesciences) for immunoblot analysis as described by Vera-Estrella et al. (2004). Digital images were captured using the Gel Doc XR+ System (Bio-Rad). Primary antibodies, either commercially available or custom made, and dilutions employed in this study were as follows: *A. thaliana* anti-MPH1 (1/200) (Liu and Last, 2015b); *C. reinhardtii* anti-LHCSR3 (1/1000) (Agrisera, AS14 2766); *Homo sapiens* anti-enolase (1/1000) (Santa Cruz Biotechnology, sc-7455); *H. sapiens* anti-RP2 (1/3000) (Chapple et al., 2000); *Spinacia oleracea* anti-AtpB (1/10,000) (McCormac and Barkan, 1999); global anti-H^+ATPase (1/1000) (Agrisera, AS07 260).

4.4.6. Shotgun proteomics analysis

For sample preparation prior to proteomic analysis, total microsome samples (100 µg per replicate; four independent biological replicates) and FFZE fractions (1.2 mL per fraction; 23 individual FFZE fractions) were suspended in TE buffer (10 mM Tris/HCl pH 7.6, 1 mM EDTA pH 8.0, 0.3% sodium deoxycholate), precipitated with 72% trichloroacetic acid (9% final TCA concentration; 4°C, 1 h) and, after recovering the precipitated protein, submitted to an additional precipitation step with 90% acetone (-30°C, overnight). The preparation (solubilization, reduction, alkylation, and trypsin digestion) of the vacuum-dried protein extracts and their further manipulation (re-solubilization and desalting) prior to LC-MS/MS analysis, were performed as described in detail by Barkla et al. (2012).

LC-MS/MS analysis was performed at the proteomics discovery platform of the Institut de Recherches Cliniques de Montréal using the LC-MS/MS equipment described in detail by Barkla et al. (2012). Chromatography buffers were 0.2% formic acid (FA) (buffer A) and 100% acetonitrile/0.2% FA (buffer B). Peptide samples were loaded on-column (600 nL min^{-1}) and eluted (250 nL min^{-1}) with a two slope gradient: buffer B first increased from 2 to 40% (85 min), and then from 40 to 80% (15 min). LC-MS/MS data acquisition was accomplished using an eleven scan event cycle, comprised of a full MS scan for scan event 1 acquired in the Orbitrap. Mass resolution for MS was set to 60,000 (at *m/z* 400) and used to trigger the ten additional MS/MS events acquired in parallel in the linear ion trap for the top ten most intense ions. Mass over charge ratio range was from 360 to 1700 for MS scanning with a target value of 1,000,000 charges, and from ~1/3 of parent *m/z* ratio to 2,000 for MS/MS scanning with a target value of 10,000 charges. Data-dependent scan events used a maximum ion fill time of 100 ms and one microscan. Target ions already selected for MS/MS were dynamically excluded for 31 s after two counts. Nanospray and S-lens voltages were set to 1.3–1.8 kV and 50 V, respectively. Capillary temperature was set to 250°C. MS/MS conditions were: normalized collision energy, 35 V; activation Q, 0.25; activation time, 10 ms.

An *E. oleoabundans* protein database was generated at the Unidad Universitaria de Apoyo Bioinformático-UNAM (Cuernavaca, Mexico), through *in silico* six-frame translation of the *E. oleoabundans* non-redundant transcriptome database (56,550 transcripts) (Rismani-Yazdi et al., 2012). TransDecoder (Haas et al., 2013) was used to identify the candidate protein-coding regions based on nucleotide composition and open reading frame length. For database search, peak list files were generated with Proteome Discoverer (version 1.4) using the following parameters: minimum mass, 500 Da; maximum mass, 6000

Da; no grouping of MS/MS spectra; precursor charge, auto; minimum number of fragment ions, 5. All MS/MS spectra were analyzed with Mascot 2.3 (Matrix Science, London, UK) against the *Viridiplantae* (TaxID 33090, unknown version, 677107 entries) and/or the *E. oleoabundans* (unknown version, 53921 entries) protein databases assuming trypsin digestion. The mass tolerances for precursor and fragment ions were set to 10 ppm and 0.6 Da, respectively. Cysteine carbamidomethylation was specified as a fixed modification, and methionine oxidation as a variable modification.

Scaffold (Scaffold 4.3.4, Proteome Software Inc., Portland, OR, USA) was used to validate MS/MS based peptide and protein identifications. Scaffold parameters were set to a minimum of two peptides per protein, with minimum probabilities of 99% at the protein level (Protein Prophet algorithm, Nesvizhskii et al., 2003) and 95% at the corresponding peptide level (Scaffold Local FDR algorithm). Proteins containing similar peptides that could not be differentiated based on MS/MS analysis alone were grouped to satisfy the principles of parsimony.

4.4.7. Protein functional annotation

Proteins were annotated if they complied with the above mentioned Scaffold parameters and if they were identified with two or more unique peptides in at least two of four biological replicates unless otherwise stated. Automatic annotation based on sequence similarity was initially performed using the Blast2GO suite (version 2.8; April 2014) with the default parameters (Götz et al., 2008). To improve protein annotation, each of the identified proteins were individually curated during the period comprised within May 2014 and May 2015. Manual curation was initially based on the results provided by the Blast2GO analysis and additionally supported by the following resources: experimental evidence available in the literature for protein homologs; detailed sequence analysis in the PredAlgo subcellular localization prediction tool (Tardif et al., 2012) and in multiple databases including, ARAMEMNON v.8.0 (Schwacke et al., 2003), InterPro (Mitchell et al., 2015), Phytozome v.10.2 (Goodstein et al., 2012), SUBA3 (Tanz et al., 2013), TCDB (Saier et al., 2014), UniProtKB (SwissProt and TrEMBL entries) (The UniProt Consortium, 2014), as well as ARALIP (Li-Beisson et al., 2010), AT_CHLORO (Ferro et al., 2010), MEROPS v.9.9 (Rawlings et al., 2014) and PlnTFDB (Pérez-Rodríguez et al., 2010), depending on the requirements. Functional assignments were additionally verified using the IntEnz (Fleischmann et al., 2004) and QuickGO (Binns et al., 2008) databases. A protein sequence

from *E. oleoabundans* was manually annotated as a specific protein, only if it contained the domains required for the function that was being assigned or at least the signatures necessary for being allocated to a specific protein family, otherwise, proteins were annotated as unknown even if they were electronically inferred as a known protein.

4.4.8. Genomic DNA extraction and 18S (r)DNA sequencing

Genomic DNA was extracted from 25 mL of N-sufficient *E. oleoabundans* cultures as follows. Cells were pelleted by centrifugation (10,000 *g*, 10 min, room temperature [RT]), frozen in liquid N_2, and ground with mortar and pestle. Ground cells were suspended in TE buffer to an initial working volume of 600 µL to which 180 µL of lysozyme (50 mg mL^{-1}) were added, and incubated for 30 min at RT. Then, 120 µL of 10% SDS and 3 µL of proteinase K (20 mg mL^{-1}) were added to the sample and incubated for 1 h at 37°C with agitation. After this, 100 µL of 5 M NaCl and 80 µL of CTAB/NaCl (10%/0.7 M) were added to the sample, which was mixed and incubated for a further 10 min at 65°C with agitation. DNA was extracted with one volume (1V) CH_3Cl:isoamyl alcohol (24:1 v/v). The upper phase was recovered by centrifugation (14,000 *g*, 5 min, RT) and combined with 1V of phenol:CH_3Cl:isoamyl alcohol (25:24:1 v/v/v). For DNA precipitation, the upper phase was recovered by centrifugation, combined with 0.6V of isopropanol, and incubated for 15 min at -30°C. The precipitate was collected by centrifugation (14,000 *g*, 10 min, 4°C), washed with 1 mL cold 75% ethanol, dried, and resuspended in 50 µL TE. Then, genomic DNA was treated with 3 µL of RNAse A (20 mg mL^{-1}; 30 min, 37°C, agitation), taken to a final volume of 300 µL by adding water, and re-extracted with 1V of phenol:CH_3Cl:isoamyl alcohol (25:24:1 v/v/v). The upper phase was recovered by centrifugation and DNA was precipitated with 0.1V of 7.5 M ammonium acetate plus 2.5V of absolute ethanol (15 min, -30°C). The precipitate was collected, washed, dried, and dissolved as aforementioned. Genomic DNA quality was assessed by agarose gel electrophoresis, and by A_{260}/A_{280} and A_{260}/A_{230} ratios (NanoDrop spectrophotometer).

The *E. oleoabundans* 18S rRNA gene was amplified by PCR (35 cycles; Long PCR enzyme mix, ThermoFisher Scientific) using genomic DNA as a template and the oligonucleotide primers (5'-ACCTGGTTGATCCTGCCAG-3', 5'-TGATCCTTCYGCAGGTTCAC-3') according to Moon-van der Staay et al. (2001). A PCR product of approximately 2.5 kbp was amplified and purified from an agarose gel using the High pure PCR product purification kit (Roche Diagnostics), whose quality was verified as

aforementioned. A partial 18S (r)DNA sequence was obtained by sequencing (3730, Perkin-Elmer/Applied Biosystems) and deposited in the NCBI GenBank database under the accession number KX350066.

4.4.9. Molecular phylogenetic analysis

To perform a molecular phylogenetic analysis using a multi-gene approach, two nuclear (actin, EF-1α), two chloroplastic (PSBA, RBCL), and two mitochondria-encoded (COX1, COX2) protein markers were selected. The amino acid sequences retrieved for the analysis are described in Table S4.16. Each set of proteins was individually aligned using Clustal Omega (Sievers et al., 2011). The resulting alignments were manually inspected using MEGA7 (Kumar et al., 2016), where all positions with less than 70% site coverage were removed. The verified alignments per each of the six proteins were concatenated using CLC Genomics Workbench 9.0 (QIAGEN Bioinformatics). The evolutionary analysis was conducted in MEGA7 using the Maximum Likelihood (ML) method based on the JTT matrix-based model (Jones et al., 1992). The initial tree was made automatically using the default method (NJ/BioNJ). The nodal support was estimated by bootstrap values (Felsenstein, 1985) based on 1000 replications. Additional phylogenetic analysis of proteins identified in this work were conducted in MEGA7 as described above, where all positions with less than 70% site coverage were eliminated.

Phylogenetic analysis of 18S (r)DNA data was performed with an increased taxon sampling, mostly based on Pegg et al. (2015), that comprised 62 different 18S (r)DNA nucleotide sequences (complete and partial) retrieved from the NCBI nucleotide database (Table S4.17). Sequences were aligned using Clustal Omega. The evolutionary analysis was conducted in MEGA7 using the ML method based on the Tamura-Nei model (Tamura and Nei, 1993), where all positions with less than 70% site coverage were eliminated. The initial tree construction and the estimation of the nodal support were performed as above mentioned.

4.4.10. Accession numbers

Sequence data from this article can be found in the GenBank / EMBL data libraries under accession number KX350066 [18S ribosomal RNA gene, partial sequence]. The *E. oleoabundans* protein database and the mass spectrometry proteomics data have been

deposited to the ProteomeXchange Consortium (http://www.proteomexchange.org) via the MassiVE (Mass Spectrometry Interactive Virtual Environment) partner repository (http://massive.ucsd.edu) with the dataset MassiVE identifier MSV000079977. Additional protein and peptide information from LC-MS/MS analysis of FFZE membrane fractions is provided in Table S4.18.

4.5. Acknowledgements

Authors thank Dr. Denis Faubert and Marguerite Boulos at Institut de Recherches Cliniques de Montréal-Proteomics Discovery Platform for LC-MS/MS analysis. We also thank Dr. Jordan Peccia (Yale University, USA) and Dr. Berat Z. Haznedaroglu (Boğaziçi University, TR) for providing the *E. oleoabundans* transcriptome. Dr. Alejandro Sanchez-Flores and Karel Estrada at Unidad Universitaria de Apoyo Bioinformático-UNAM (Universidad Nacional Autónoma de México) are also acknowledged for generating the *E. oleoabundans* protein database. The gifts of the *C. reinhardtii* strain from Dr. Diego Gonzalez-Halphen (UNAM), the C2BBe1 cells from Dr. Carlos F. Arias (UNAM), the anti-MPH1 antibody from Dr. Robert L. Last (Michigan State University, USA), the anti-RP2 antibody from Dr. Michael Cheetham (University College London, UK), and the anti-AtpB antibody from Dr. Patricia Leon (UNAM), are acknowledged. We also thank Luz María Martínez, Mario A. Caro Bermúdez, Mercedes Enzaldo Cruz, and Ma. Guadalupe Muñoz García for technical assistance. Support in phylogenetic analysis from Gustavo Rodriguez-Alonso is acknowledged.

4.6. Supplemental data

Supplemental material is provided in Appendix A.

5. SAM-dependent glycerolipid *N*-methylation and membrane remodeling in an oleaginous microalga upon nitrogen deprivation

Adriana Garibay-Hernández, Bronwyn J. Barkla, Rosario Vera-Estrella, Diana Ximena Sahonero-Canavesi, Otto Geiger and Omar Pantoja

Abstract

Microalgae comprise an exceptionally diverse group of organisms, whose ecological success relies on their ability to cope with different stressors. Amongst these, nitrogen (N) deprivation has been of utmost importance as it triggers neutral lipid accumulation in some species, turning these organisms into subjects of biotechnological interest. *Ettlia oleoabundans* is a non-sequenced oleaginous green microalga from which we have provided a detailed survey of the biological processes taking place in its membranes during N deprivation. To get a comprehensive view of the cellular processes underlying lipid accumulation, a multidisciplinary approach was performed by combining confocal fluorescence and transmission electron microscopy, mass spectrometry-based profiling of lipid and membrane protein components, short-term lipid kinetic labeling, and classical biochemical strategies.

N-starved cells showed an increased cell size and alterations in cell ultrastructure, accompanied by the formation of lipid droplets. Induction of lipid metabolism at the acyl-lipid level may enable the sustained accumulation of lipids. An extensive remodeling of lipid and protein membrane components supported the morphological changes observed upon N deprivation. These changes may be accompanied by a chloroplast stress response and likely trigger an autophagic process. This study revealed the synthesis of phosphatidylcholine via phosphatidylethanolamine *N*-methylation, and the existence of the betaine lipid diacylglyceryl-*N,N,N*-trimethylhomoserine (DGTS) in *E. oleoabundans*. We suggest that glycerolipid *S*-adenosyl-L-methionine (SAM)-dependent *N*-methylation is favored during N deprivation, probably to regulate the intracellular SAM/SAH ratio (SAH: *S*-adenosyl-L-homocysteine) and cope with oxidative stress.

5.1. Introduction

Microalgae represent an exceptionally diverse but highly specialized group of microorganisms adapted to various ecological habitats, whose ecological success relies on their remarkable ability to cope with different stressors. Nutrient deprivation, especially nitrogen (N) starvation, has been thoroughly studied as it triggers the accumulation of lipids in different microalgae strains, turning these into feedstocks of interest to produce value-added compounds (Hu et al., 2008).

The edaphic green microalga *Etttlia oleoabundans* (class *Trebouxiophyceae*) has gained special attention, owing to its high lipid content (up to 56% [w/w] of its dry weight) (Gouveia et al., 2009), metabolic flexibility (Garibay-Hernández et al., 2013; Morales-Sánchez et al., 2013; Ferroni et al., 2018), and capability to thrive either in freshwater, wastewater (Levine et al., 2011; Wang and Lan, 2011; Yang et al., 2011) or sea water (Arredondo-Vega et al., 1995; Baldisserotto et al., 2012; Popovich et al., 2012). Most research though, has focused on improving its lipid yield (Tornabene et al., 1983; Li et al., 2008; Pruvost et al., 2009; Breuer et al., 2012; Garibay-Hernández et al., 2013) rather than on understanding its response to nutrient stress.

Only recently, insights into the biology and biochemistry behind N deprivation and lipid accumulation in *E. oleoabundans* are being provided (Rismani-Yazdi et al., 2012; Benvenuti et al., 2015; Baldisserotto et al., 2016; Matich et al., 2016, 2018; Garibay-Hernández et al., 2017; Goh et al., 2017; Sturme et al., 2018). Current knowledge on this microalga supports that chloroplast lipids are responsive to N starvation, and triacylglycerol (TAG) biosynthesis is induced at the transcriptional level during N stress. These observations though, have not uncovered features distinguishing oleaginous from non-oleaginous microalgae, nor provided a specific understanding of *E. oleoabundans* physiology.

Most of the knowledge on algal lipid metabolism still relies on genome predictions and orthologous relationships to enzymes of known function in other eukaryotes, mainly in the model plant *Arabidopsis thaliana* and the green microalga *Chlamydomonas reinhardtii* (Stern, 2009; Khozin-Goldberg and Cohen, 2011; Merchant et al., 2012; Liu and Benning, 2013; Zienkiewicz et al., 2016; Li-Beisson et al., 2019). Although this approach has proved useful, it has its limitations. Firstly, the lipid metabolism in microalgae cannot be directly compared to that in land plants, as it takes place in single photosynthetically active cells where the bulk of TAG synthesis is induced upon abiotic stressors, whereas in land plants neutral lipid accumulation is mostly limited to specialized tissues and subjected to developmental control (Liu and Benning, 2013; Zienkiewicz et al., 2016). Second, lipid

composition within microalgae is tremendously diverse (Hu et al., 2008; Harwood and Guschina, 2009). When compared to *C. reinhardtii* (class *Chlorophyceae*), *E. oleoabundans* belongs to a different taxonomical group, and differences in key components of photoprotection and oxidative phosphorylation processes have already been identified (Garibay-Hernández et al., 2017). Moreover, contrary to *C. reinhardtii* (Li-Beisson et al., 2015), phosphatidylcholine (PC) and phosphatidylserine (PS) are both present in *E. oleoabundans* (Tornabene et al., 1983; Matich et al., 2016). Despite PC being central to acyl-lipid metabolism in land plants (Bates et al., 2007; Bates, 2016), and crucial for formation, growth and stability of the lipid droplets (LD) where TAG are accumulated (Penno et al., 2013; Goold et al., 2015), the metabolic pathways and the role played by this N-containing phospholipid in microalgae has not been studied.

Here, to investigate the cellular processes behind *E. oleoabundans* response to N deprivation, we use a multidisciplinary approach that combines confocal fluorescence microscopy (CFM), transmission electron microscopy (TEM), MS-based protein and lipid profiling, kinetic radioactive labeling and classical biochemical approaches. A special focus was made on how lipid and membrane protein components are involved in the function of biological membranes and contribute to the cellular response in N starvation. This work uncovers the capability of *E. oleoabundans* to synthesize PC via the *N*-methylation of phosphatidylethanolamine (PE), and the existence of the betaine lipid diacylglyceryl-*N,N,N*-trimethylhomoserine (DGTS). Our results suggest a role for *S*-adenosyl-L-methionine (SAM)-dependent glycerolipid methylation on the N stress response. Our results provide a more comprehensive and integrated view of the cellular processes resulting in a sustained accumulation of neutral lipids enabling *E. oleoabundans* to cope with N stress.

5.2. Results

5.2.1. Morphological features behind lipid accumulation in nitrogen-deprived cells

Phototrophic batch *E. oleoabundans* cultures under N sufficiency and N deprivation conditions were firstly characterized through a kinetic analysis. This analysis confirmed the typical behavior of phototrophic N-depleted *E. oleoabundans* cultures (Li et al., 2008; Pruvost et al., 2009; Rismani-Yazdi et al., 2012; Garibay-Hernández et al., 2013). N deprivation resulted in lower chlorophyll levels and a decrease in cell proliferation (Fig. S5.1). Despite a lowered cell division, N deprivation promoted higher biomass content on a per cell basis (Fig. S5.1). Higher cell mass under N-deprived conditions has been attributed to the accumulation of storage compounds, mainly TAG, but also starch (Pruvost et al.,

2009; Breuer et al., 2012; Rismani-Yazdi et al., 2012; Garibay-Hernández et al., 2013; Klok et al., 2013). Differences in cell growth kinetic parameters between both tested conditions were statistically significant after four days (4 d) (Fig. 5.1A). This time point was therefore selected for further analysis.

To understand the cell biology behind the effects of N deprivation on *E. oleoabundans*, the morphology of 4-d N-sufficient and N-deprived cells was analyzed by TEM. As shown in Fig. 5.1B, N deprivation induced ultrastructural changes, with the most obvious differences observed in cell size and chloroplast morphology. The N-deprived cells showed an increased size; their chloroplasts were enlarged and amorphic, with a less defined pyrenoid, and showed starch grains distributed within disorganized thylakoid membranes. Despite these changes, merged thylakoid membrane tubules traversing the pyrenoid were still clearly identified in N-deprived microalgae (Fig. 5.1B, magnification views). These pyrenoid tubules physically bridge the sites of light-dependent photosynthesis (thylakoids) and light-independent carbon fixation (pyrenoid), being therefore proposed as conduits of ATP and carbon molecules (Engel et al., 2015). Preservation of these structures during N deprivation highlights their importance for maintaining photosynthetic carbon fixation under stress conditions, enabling this microalga to reach biomass concentrations comparable to those attained under N sufficiency, but with a lower number of cells Fig. S5.1). Most N-depleted cells displayed electron-lucent cytosolic structures (Fig. 5.1B) attributed to LD, which were occasionally detected in N-sufficient cells.

To investigate LD formation, a comparative time-course analysis between N-sufficient and N-depleted conditions was performed by CFM (Fig. S5.2). Owing to its specific interaction with hydrophobic molecules (Greenspan et al., 1985), Nile Red (NR) was used as a LD probe, as it has proved reliable for visualization and quantification of intracellular neutral lipid content in microalgae (Yan et al., 2013), including *E. oleoabundans* (Gouveia et al., 2009; da Silva et al., 2009). Microalgae cells were monitored through chlorophyll autofluorescence, as chloroplasts comprise most of the cells' volume (Fig. 5.1B). This analysis demonstrated that LD formation in *E. oleoabundans* cells is independent of the N availability condition (Fig. 5.1C). However, N depletion induced faster LD formation, since LD appeared in most cells within the first hour of N deprivation (Fig. 5.1C), whereas LD were occasionally detected after 3 h in N-sufficient conditions (Fig. S5.2). Quantitative image analysis confirmed an increased size of N-deprived cells, which was already suggested by both kinetic and TEM analysis (Fig. 5.1A,B). Increased cell size (Fig. 5.1A) was consistent with the higher lipid content under N deprivation, which compared to N sufficiency, triggered

a sustained accumulation of lipids on a per cell basis, even 4 d after the onset of the stress (Fig. 5.1C,D). A sustained increase in the number of LD per cell was quantified, as well as an increase in LD size after 4 d of N deprivation (Fig. 5.1D). These results indicated that both the number of LD, as well as their size, contribute to the higher amounts of lipids observed in N-deprived cells (Fig. 5.1D).

A detailed analysis of LD size showed that LD populations were highly varied, independent of N availability (Fig. S5.2 and S5.3). LD radiuses (r) ranged from 0.1 to 1.2 μm. Based on the frequency distributions of LD populations, three classes were defined: small ($r<0.2$ μm), medium ($0.2\leq r\leq 0.6$ μm), and large ($r>0.6$ μm), with the majority of the LD (at least 75%) falling within the medium range, probably corresponding to a population of growing LD in the cells (Fig. S5.3). Small LD might correspond to new droplets, likely formed as precursors of LD of greater dimensions, whereas large LD might result from a continued increase of *in situ* neutral lipid synthesis and/or fusion of droplets of smaller sizes, as supported by TEM images (Fig. 5.1B). After 4 d of N deprivation, approximately 10% of the LD population was comprised by large LD, which contributed to statistically higher median LD size values when compared to N-sufficient cells at this time point (Fig. 5.1D). However, around 10% of the LD population was also comprised by small-sized LD (Fig. 5.1D). This result suggests that the lipid content attained under N deprivation is not only a consequence of larger LD, but also supported by the sustained generation of small-sized LD.

The properties of *E. oleoabundans* membranes were analyzed to get insights into the morphological changes exerted by N deprivation. For this purpose, the separation profile of microsomes from N-sufficient cells was evaluated using Free Flow Zonal Electrophoresis (FFZE), a liquid-based high-resolution membrane separation technique based on surface charge (Wildgruber et al., 2014; Barkla, 2007). Individual FFZE fractions were subjected to protein and chlorophyll measurements, or western blot analysis against protein markers for different cell compartments. The FFZE profile of membranes from N-sufficient cultures was compared to that already reported for N-deprived *E. oleoabundans* (Garibay-Hernández et al., 2017). In comparison to N-sufficient cells, membrane fractions from N-depleted cells showed a markedly shifted electrophoretic mobility and a more distinct separation of subcellular compartments (Fig. S5.4). These results suggested that N depletion induces biochemical changes in *E. oleoabundans* membranes, which significantly alter their net surface charge. Therefore, subsequent analyses focused on studying changes in membrane components.

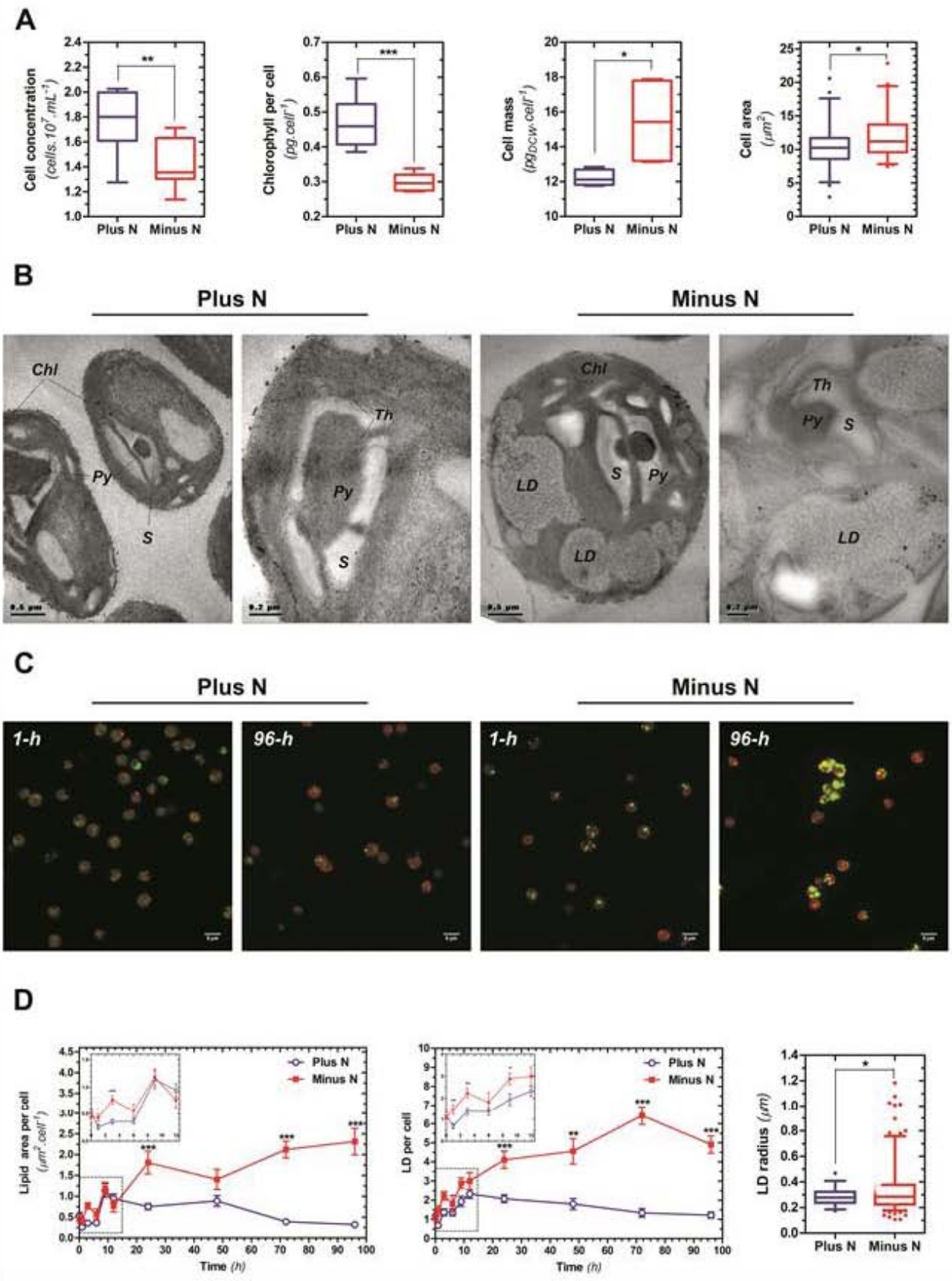

Figure 5.1. Cell growth and morphological characterization of N-deprived *E. oleoabundans*. Data correspond to cells after 4 d under N deprivation (minus N) or N sufficiency (plus N). (A) Cell growth parameters. Cell size is represented as cell area (quantified by CFM image analysis; n = 46 plus N, 41 minus N). (B) Cell ultrastructure analyzed by TEM (Chl, chloroplast; LD, lipid droplet; Py, pyrenoid; S, starch granules). (C) LD visualization by CFM. Representative z-stack merged images correspond to one- and 96-h-treated cells. Green: neutral lipids (NR, λ Exc/Em 488/520 nm); red: chloroplasts (chlorophyll, λ

Exc/Em 635/668 nm). (D) Quantitative time-course CFM image analysis of LD dynamics (0 to 96 h). Data are mean ± standard error of the mean (SEM) of n = 25-90 cells. For LD size distribution: n = 61, plus N; 201, minus N). Statistical analyses were performed through unpaired two-tailed Student's *t*-tests. Statistically significant changes are indicated with asterisks: *p*-value < 0.05, *; < 0.01, **; < 0.001, ***. In box plots, boxes indicate the lower, median and upper quartiles, whiskers extend from the 5th to the 95th percentiles, and data points out of this range are indicated (circles).

5.2.2. Characterization of *E. oleoabundans* glycerolipidome

The unique functions and properties of biological membranes are shaped by the tight regulation of their lipid and protein components, yet most research has focused largely on the latter. To address the effect of N availability on *E. oleoabundans* membrane lipid composition, total lipid extracts from N-sufficient and N-deprived conditions were analyzed by two-dimensional thin layer chromatography (2D-TLC), which resolves the major polar lipid classes. Polar lipids were characterized based on their specific staining for functional groups (Fig. S5.5). Lipid identification was supported by evaluation of lipid spot migration in two previously characterized 2D-TLC systems (Benning et al., 1995; Vences-Guzmán et al., 2008) (Fig. S5.5), and by earlier knowledge of *E. oleoabundans* polar lipid composition (Tornabene et al., 1983). In this analysis, the four canonical photosynthetic glycerolipids were identified, monogalactosyldiacylglycerol (MGDG), digalactosyldiacylglycerol (DGDG), sulfoquinovosyldiacylglycerol (SQDG), and phosphatidilglycerol (PG), together with three phospholipids (PC, PE, PS) known to be predominant in extraplastidic membranes (Nakamura and Li-Beisson, 2016). An additional polar lipid (U, Fig. 5.2A) co-migrating with DGDG and positive for Dragendorff staining, as well as two lipid spots positive to α-naftol (UG, Fig. 5.2A) were detected, which may correspond to not fully identified lipids earlier reported for *E. oleoabundans* (Tornabene et al., 1983), either containing unidentified amino compounds or sugar (D-glucose, heptose, or unknown sugar compounds) moieties, respectively. Comparison by 2D-TLC of equal lipid extract amounts from N-sufficient and N-deprived cells, highlighted changes in the abundance of membrane polar lipids, particularly in PG and MGDG (Fig. 5.2A). Using a one-dimensional (1D)-TLC system to resolve neutral lipids (Fan et al., 2011), a higher TAG content was observed under N deprivation (Fig. 5.2B).

Total lipid extracts from N-sufficient and N-deprived *E. oleoabundans* cells were further analyzed through a targeted lipidomics approach using direct-infusion electrospray ionization triple quadrupole tandem MS (ESI-TQ-MS/MS). Results from the MS-based analysis confirmed the presence of the glycerolipids identified by 2D-TLC (DGDG, MGDG, SQDG, PG, PC, PE, PS), as well as the presence of phosphatidylinositol (PI), phosphatidic

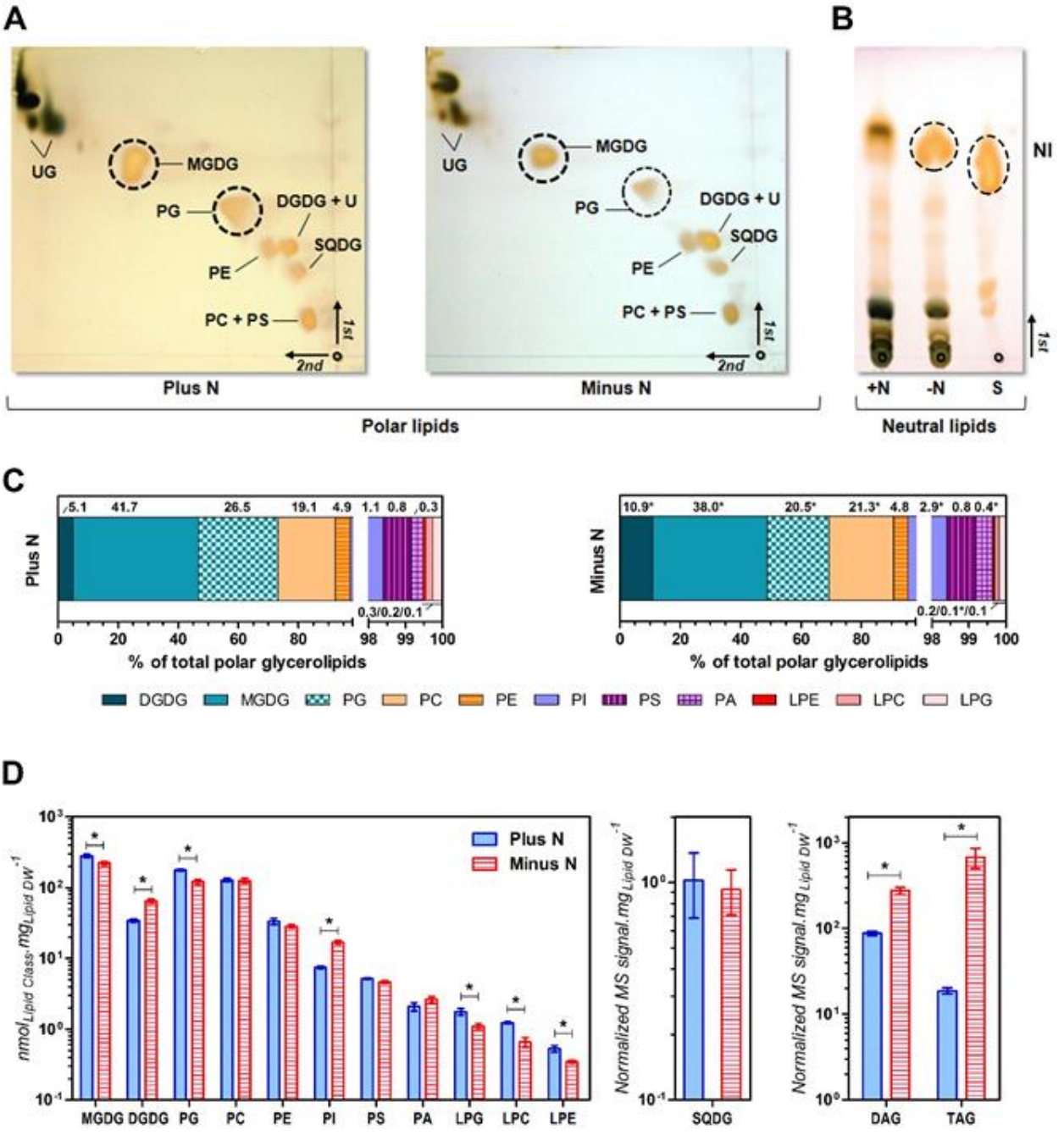

Figure 5.2. Lipid composition of *E. oleoabundans* under N sufficiency and N deprivation conditions. (A, B) TLC of total lipid extracts from N-sufficient (plus N) and N-deprived (minus N) microalgae. Developed TLC plates exposed to iodine vapor for lipid visualization are shown. (A) 2D-TLC of polar lipids based on Vences-Guzmán et al. (2008) Lipids were assigned as described in Fig. S5.5. U, unknown lipid; UG, unknown glycolipid. (B) 1D-TLC of neutral lipids based on Fan et al. (2011). Cooking vegetable oil (S) was used as reference for neutral lipids (Nl). (C) Amount of each polar glycerolipid class relative to the total polar glycerolipids. The corresponding percentage values are indicated. (D) Amount of each glycerolipid class relative to the total weight of analyzed lipids (lipid DW). Data in (C) and (D) were quantified by ESI-TQ-MS/MS and are mean ± SEM of five biological replicates. Statistical analyses was performed by unpaired two-tailed Student's *t*-test. Statistically significant changes (*p*-value < 0.05) are indicated (asterisks).

acid (PA), and the monoacyl glycerolipid classes (lysoglycerolipids) lysoPE (LPE), lysoPC (LPC), and lysoPG (LPG) (Fig. 5.2C). The neutral lipids, diacylglycerol (DAG) and TAG, were also analyzed using this approach. It was not possible to determine the specific contribution of every glycerolipid class to the total amount of measured glycerolipids, as the response factors for some classes (SQDG, DAG, TAG) could not be calculated due to the variability within the molar responses of the molecular species comprising them. We could describe the specific contributions among polar glycerolipids, with the exception of SQDG (Fig. 5.2C). Independent of N availability, photosynthetic glycerolipids comprised around 70% of the total polar membrane lipids, among which MGDG was the most abundant (Fig. 5.2C). This is not surprising as the chloroplast occupies most of the microalga's cell volume (Fig. 5.1B,C). Accordingly, PG, the only chloroplast-synthesized phospholipid proved indispensable for photosynthetic function (Nakamura, 2017), together with PC, were the most abundant phospholipid classes (Fig. 5.2C). Lower fractions were comprised by PE (~5%) and PI (~1-3%), followed by PS, PA and the lysoglycerolipid classes, each of which comprised less than 1% of the total polar glycerolipids (Fig. 5.2C).

The chemical diversity of glycerolipids is not only shaped by the different polar headgroups, but also by the combination of the acyl groups attached to the glycerol backbone (Nakamura, 2017). A total of 283 polar glycerolipid molecular species (referred as total number of carbons:total number of unsaturations of all the acyl chains) were identified in this work (Table S5.1). Contrary to polar lipids, neutral glycerolipid molecular species were repetitively analyzed through multiple neutral loss scans per every acyl group they contained; for example, a 52:3 TAG molecule comprising 16:0/18:2/18:1 would be detected in three different scans for 16:0, 18:2 and 18:1. While this impedes determining the specific number of neutral glycerolipid molecular species, we can confirm that at least 100 (22 DAG and 78 TAG species) were identified in this study (Table S5.1).

Independent of N availability, 34- and 36-acyl-carbon-containing species (34-C and 36-C) comprised the majority of every polar glycerolipid class (from 67 to up to 95%), where 34-C lipid species were generally the most abundant, except for PC, which was mainly composed by 36-C lipid molecules (Fig. 5.3A). A high proportion of the two anionic chloroplast glycerolipids, SQDG and PG (approximately 30 and 10%, respectively), were comprised by 32-C lipids, mainly by the saturated molecular species (32:0), being more abundant than 36-C lipids which were barely detected in PG (<0.5%; Fig. 5.3A). The neutral glycerolipid DAG was also largely comprised by 32-C molecular species (from 7.6 to up to 21%), which

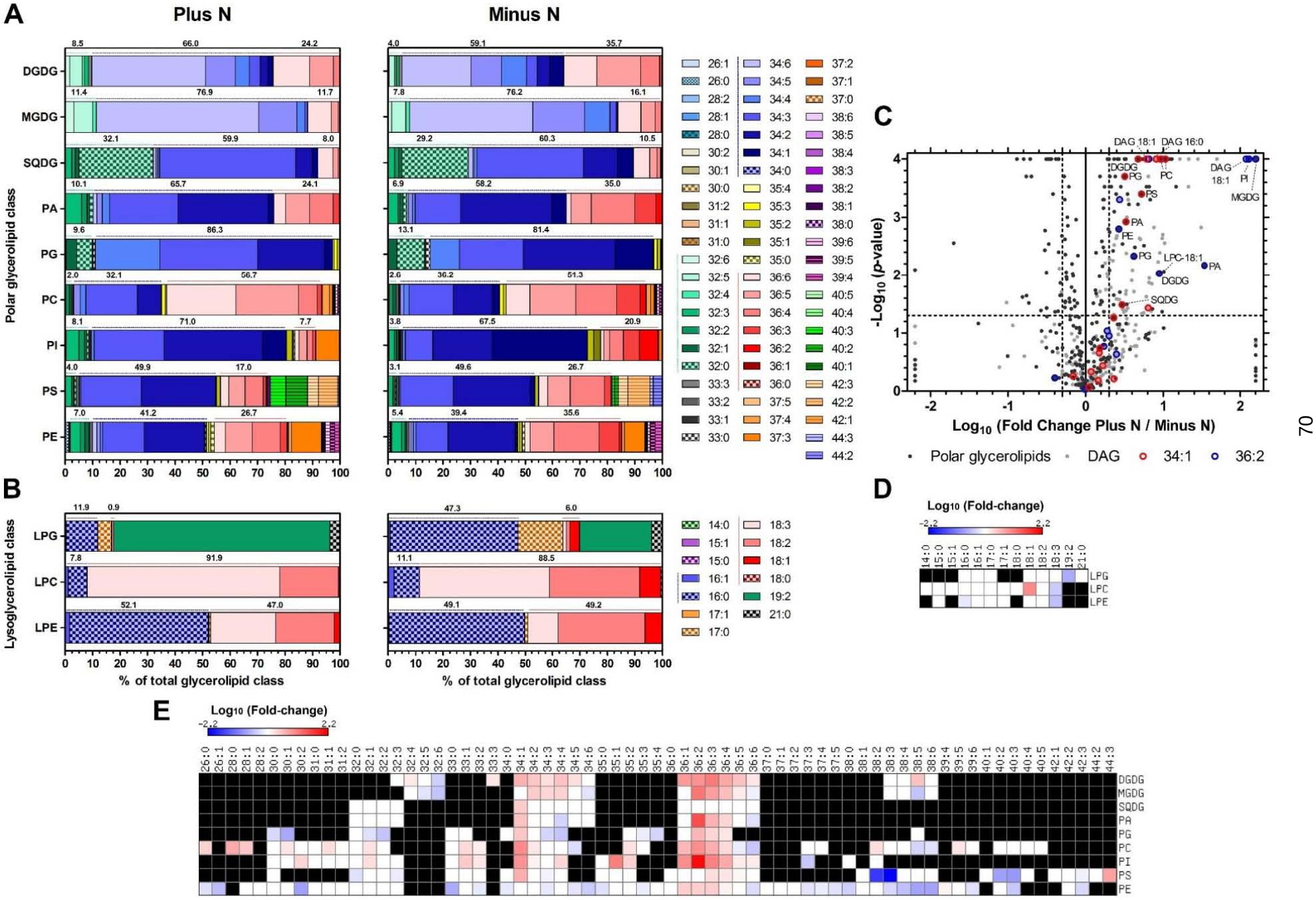
A
Plus N
Minus N
Polar glycerolipid class
DGDG
MGDG
SQDG
PA
PG
PC
PI
PS
PE
% of total glycerolipid class
B
Lysoglycerolipid class
LPG
LPC
LPE
% of total glycerolipid class
C
DAG 18:1
DAG 16:0
DGDG
PG
PC
PS
PA
PE
LPC-18:1
SQDG
DAG 18:1
PI
MGDG
-Log10 (p-value)
Log10 (Fold Change Plus N / Minus N)
Polar glycerolipids
DAG
34:1
36:2
D
Log10 (Fold-change)
E
Log10 (Fold-change)

Figure 5.3. N deprivation-induced changes in polar membrane glycerolipids. (A, B) Bar plots representing the relative abundance of each lipid molecular species comprised within a polar glycerolipid class under N sufficiency (plus N) and N deprivation (minus N) (*e.g.*, MGDG 34:6 comprised 59.2% and 45.1% of the total measured MGDG pool under plus and minus N, respectively). Molecular species within a glycerolipid class are ordered, from left to right, according to increasing total acyl-carbon values; within a total acyl-carbon group, species are shown from higher to lower unsaturation values (left to right). Completely saturated species are represented by squared patterns. Lipid species with total acyl-carbon values higher than 38 are indicated with horizontal-lined patterns. The proportions comprised by 32, 34, and 36 acyl-carbon-containing molecular species within a glycerolipid class (A), or by 16- and 18-C FA-containing species in a lysoglycerolipid group (B), are indicated with lines next to their corresponding percentage values (*e.g.* MGDG 34-C species comprised 66% and 59.1% of the total measured MGDG pool under plus and minus N conditions, respectively). (C) Volcano plot of polar glycerolipid and DAG molecular species with FC and Student's *t*-test *p*-value thresholds of two and 0.05, respectively (dashed lines); both FC and *p*-values are log10-transformed. (D, E) Heat maps showing N deprivation-induced changes relative to N sufficiency, in polar glycerolipid (E) and lysoglycerolipid (D) molecular species. Colors represent log10 values of statistically significant (*p*-value < 0.05) FC. Non-statistically-significant changes are indicated with log10 values of zero (white). Not-detected molecular lipid species are black-colored. Molecular glycerolipid species are denoted as total acyl chain-carbons:total double bonds. Values are mean of five biological replicates.

together with the 34-C (>39%) and 36-C (>17%) lipid species, comprised 96% of the total DAG signal under both N availability conditions (Fig. 5.4A). Molecular species containing less than 32 acyl-carbons were identified in DAG and all phospholipid species, except PA (Fig. 5.3 and 5.4). Moreover, only DAG and N-containing phospholipids (PC, PE and PS) included molecular species with more than 38 acyl-carbons, all of which were unsaturated (Fig. 5.3 and 5.4). This result agrees with findings in plant cells, where very long chain FA (>18-C) are primarily found in PC, PE, and especially highly enriched in PS (Murata et al., 1984; Vincent et al., 2001). In this work, 20:1-containing TAG species were also identified (Fig. 5.4B). Although the specific FA composition of every glycerolipid molecular species could not be determined through our lipidomics approach, its prediction is still possible when the overall FA profile is available. Analysis of the lysoglycerolipid composition (Fig. 5.3B) and the FA revealed by the neutral loss scans of DAG and TAG molecules (Fig. 5.4B), together with previous reports for *E. oleoabundans* (Tornabene et al., 1983; Gouveia et al., 2009; Breuer et al., 2012; Popovich et al., 2012; Garibay-Hernández et al., 2013; Matich et al., 2016; Sturme et al., 2018), support complex total FA profiles with a chain-length ranging from 6- to 24-C, comprised mainly (>94%) by acyl chains of 16- and 18-C. Accordingly, at least 80% of the neutral glycerolipid signal corresponded to 16- and 18-C-containing molecular species (Fig. 5.4B).

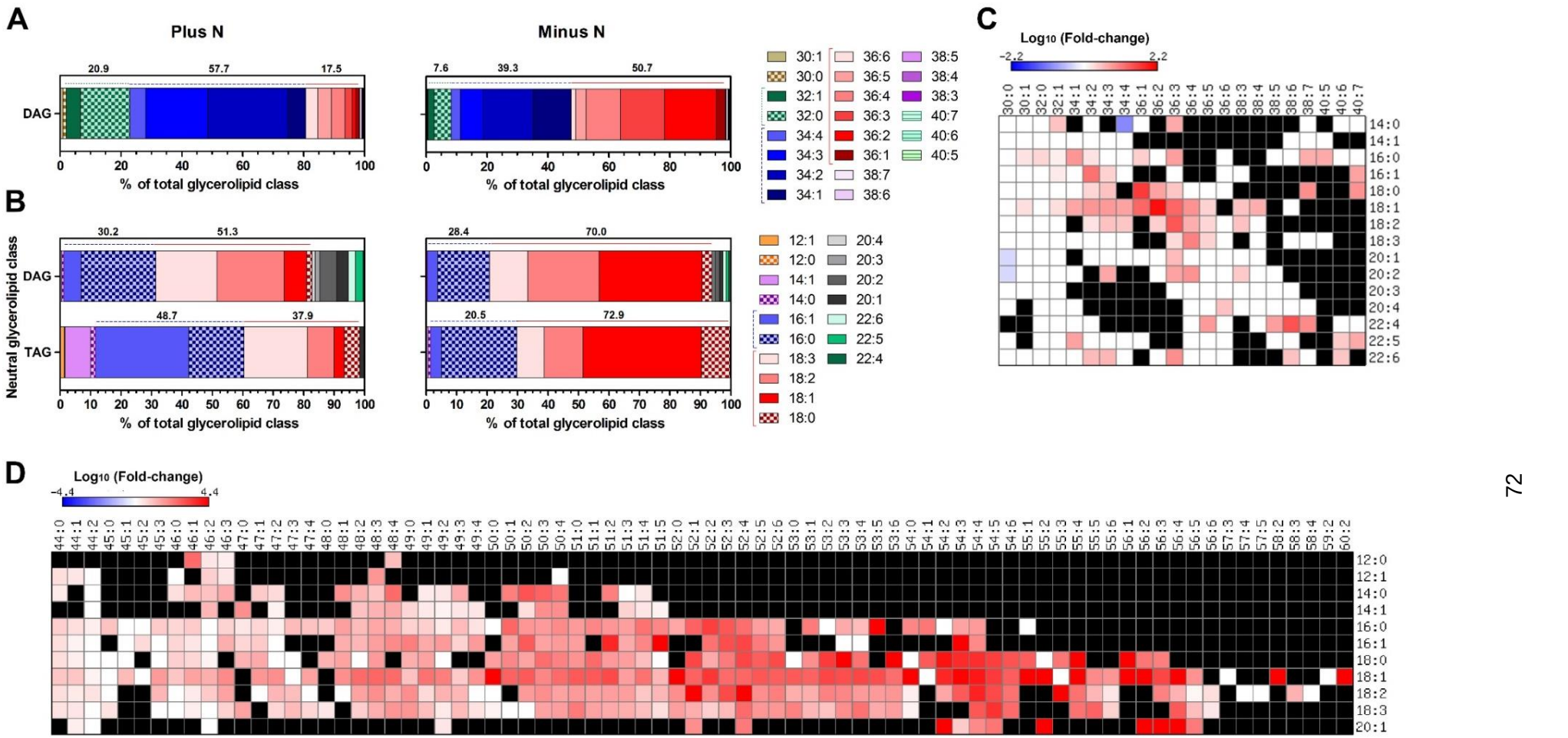

Figure 5.4. N deprivation-induced changes in neutral glycerolipids. (A) Bar plots representing the relative proportion of the total DAG signal comprised by the identified DAG molecular species. Bar plots are as described in Fig. 5.3. (B) Bar plots representing the proportion comprised by molecular species containing a specific FA, relative to the total signal of the corresponding neutral glycerolipid class (DAG or TAG) (*e.g.* 18:3-containing TAG comprised 20.8% and 8.94% of the total measured TAG under plus and minus N conditions, respectively). The proportions comprised by 16- and 18-C FA-containing neutral glycerolipid species are indicated with lines next to their corresponding percentage values (*e.g.* 16-C-containing TAG comprised 48.7% and 20.5% of the total measured TAG under plus and minus N conditions, respectively). (C, D) Heat maps showing changes in DAG (C), and TAG (D) molecular species**.** Neutral glycerolipid species were identified by the neutral loss of one FA group (rows) and the mass of the intact neutral lipid molecule from which this fatty acid was released (columns; total acyl chain carbons:total double bonds). The coloring of heat maps is as described in Fig. 5.3. Values are mean of five biological replicates.

5.2.3. Quantitative analysis of *E. oleoabundans* glycerolipidome supports induction of membrane lipid remodeling and neutral lipid accumulation during nitrogen deprivation

Nitrogen deprivation in *E. oleoabundans* resulted in changes in its glycerolipid composition. All major polar glycerolipid classes (DGDG, MGDG, PG, PC) and some low abundant phospholipid classes (PA, PI, and LPG) were responsive when analyzed relative to the total amount of polar glycerolipids (Fig. 5.2B). The decrease in MGDG and PG confirmed the changes from 2D-TLC analysis (Fig. 5.2A). Data were also analyzed relative to the total weight of extracted lipids (Lipid DW; Fig. 5.2D) to provide a different perspective and enable the comparison of SQDG, DAG and TAG contents between N-sufficient and N-deprived conditions. In contrast to the other chloroplast glycerolipids (DGDG, increased 1.9-fold; MGDG and PG, decreased 0.8- and 0.7-fold, respectively), the total amount of SQDG did not change (Fig. 5.2D). A three- and 36-fold increase in the total MS signal from DAG and TAG, respectively (Fig. 5.2D), confirms neutral lipid accumulation in N-deprived *E. oleoabundans*, in agreement with our results using 1D-TLC (Fig. 5.2B) and microscopy (Fig. 5.1). The changes in the contributions of DGDG, MGDG, PG, LPG and PI to the total lipid content of N-deprived microalgae remained significant (Fig. 5.2D). Moreover, the contribution of not only LPG, but all of the lysophospholipid classes were decreased (Fig. 5.2D). When expressed on a per lipid weight basis, the amounts of PC and PA were not changed after N deprivation (Fig. 5.2D), suggesting that their proportion within polar lipids was increased (Fig. 5.2C), in order to maintain their overall contribution to the total lipid content, which would be otherwise decreased due to the accumulation of neutral lipids.

A total of 131 polar glycerolipid molecular species were statistically changed under N deprivation, 51 of which showed at least a two-fold increase, whereas 32 were decreased more than two-fold (Fig. 5.3C-E). All of the responsive neutral glycerolipid species were increased after N stress, with the exception of three DAG species (Fig. 5.4C,D).The N deprivation-responsive species were distributed among all the glycerolipid classes, indicating that while the overall amount of a specific class did not change under this condition, the molecular species which comprise it are still responsive. Nitrogen deprivation induced an overall increase of 34- and 36-C DAG (Fig. 5.4C) and polar glycerolipid molecules (Fig. 5.3C,E). The most increased were the 36:2 species (Fig. 5.3C), showing more than a 100-fold change (FC) in DAG, PI, and even in MGDG, whose overall amount was reduced in N stress (Fig. 5.2). Moreover, 36:2, 36:3, and 36:4 species were increased among DAG and all polar glycerolipids, except for SQDG, where only 34:1 was altered (Fig.

5.3E and 5.4C). Together with 36:2, 34:1 were amongst the most responsive species, having increased at least three-fold in DAG and all polar glycerolipids, excluding PE and MGDG (Fig. 5.3C,E and 5.4C). Further analysis showed that N stress-responsive 34:1 and 36:2 DAG mainly corresponded to 16:0 and 18:1-containing species (Fig. 5.3C and 5.4C), being therefore comprised by 16:0/18:1 and 18:1/18:1, respectively. In addition, 18:1-LPC augmented ten-fold despite that the remaining lysoglycerolipid species were either decreased or unchanged (Fig. 5.3C,D). All of the acyl-containing TAG groups were increased under N deprivation, where the proportion comprised by the 16:0- and 18:1-containing species within the total TAG (1.4- and 11.5-fold, respectively) was enriched (Fig. 5.4B,D). Altogether, our data show that N deprivation triggers an increase of 16:0, but mainly 18:1 FA, in all the glycerolipid classes. As these two FA are the main products of *de novo* FA biosynthesis in the plastid (Koo et al., 2004; Li-Beisson et al., 2015), these results suggested this pathway was induced in N-deprived cells.

Analysis of the decreased lipid molecules shows that despite not displaying the highest FC values, polyunsaturated 34-C species were those that contributed the most to the overall reduction of both MGDG and PG (Fig. 5.3A,E). Surprisingly, 56% of the decreased molecular species corresponded to N-containing phospholipids (PE, PS, PC; Fig. 5.3E), despite their overall amounts did not change under N deprivation (Fig. 5.2). Most of the decreased N-containing phospholipids were PE species, however, four of the five species that decreased the most corresponded to PS (38:2, 38:3, 40:2, 40:3) (Fig. 5.3C,E). The acyl chain length of PS has been correlated with both plant lifespan (Li et al., 2014b), and to membrane nanodomain formation through either lateral or across the bilayer lipid-lipid interactions (Harayama and Riezman, 2018). Whether the changes observed in N-deprived *E. oleoabundans* are related to these processes remains to be addressed. As most lipid research has focused on studying lipids based on their head group chemistry, a better understanding of the influence of the glycerolipid acyl chain length and its degree of unsaturation is necessary.

5.2.4. Short-term lipid dynamics reveal a link between PE and PC during nitrogen deprivation

To understand the dynamics of acyl-lipid metabolism, kinetic labeling experiments were performed using [^{14}C]acetate, which was rapidly incorporated into the lipid fraction (Fig. S5.6A), enabling to label the acyl chains with minimal incorporation into head groups (Bates

et al., 2007). In both N sufficiency and N deprivation conditions, label concentrations in the media were reduced to at least 40 and 80%, eight and 48 h after the onset of the labeling, respectively (Fig. S5.6A). Kinetic labeling experiments at the glycerol backbone level were not possible as [^{14}C]glycerol was barely incorporated (Fig. S5.6A-B).

Polar lipid labeling kinetics over a 48 h period showed that from 27 to up to 47% of the [^{14}C]acetate was exclusively incorporated into glycolipid species (Fig. 5.5A; spots 1, 3, 5; Fig. S5.6B). Amongst these, the highest label amounts (N sufficiency: 47%; N deprivation: 36%) were comprised by MGDG (Fig. 5.5A), the most abundant glycolipid in *E. oleoabundans* (Fig. 5.2C-D). In contrast to glycolipids, higher proportions of [^{14}C]acetate were incorporated into phospholipids under both, N sufficiency (48-60%) and N deprivation (61-67%) conditions. Comparison between N sufficiency and N deprivation conditions showed that the former supported higher proportions of [^{14}C]acetate-labeled glycolipids, whereas higher amounts of phospholipids were labeled under N deprivation. Differences between the labeling kinetics of both conditions were not observed for glycolipids, but only for phospholipids (Fig. 5.5A). chloroplast for further extra-plastidic glycerolipid assembly (Wang et al., 2017).

PG was the major [^{14}C]acetate-labeled glycerolipid under N sufficiency with over 28% of the label incorporated at all time points, increasing to maximum values of 47% (Fig. 5.5A). Rapid [^{14}C]acetate labeling of PG implies the incorporation of early *de novo*-synthesized FA into this glycerolipid. This suggests a role of PG in acyl editing of *E. oleoabundans* plastid lipids: similar to land plants, nascent acyl groups may be cycled through PG contributing to their export from the Compared to N sufficiency, PG labeling was decreased under N deprivation, comprising from 21 to 29% of the [^{14}C]acetate during the assay (Fig. 5.5A). Thus, nascent FA-cycling through PG may not be a major process in N-deprived *E. oleoabundans*.

Despite the MS data evidence that the endogenous levels of N-containing phospholipids did not change after 4 d (Fig. 5.2), differences in their labeling kinetics and higher [^{14}C]acetate-labeling of these phospholipids under N deprivation were observed when compared to N sufficiency (Fig. 5.5A). PE was immediately labeled in N-sufficient conditions, reaching 25% at 15 min and exponentially decreasing to about 3%, 4 h after the onset of the assay; whereas PC was gradually labeled from 6%, increasing to 13% after 48 h. In contrast, N deprivation induced higher labeling of both PE and PC, from 31% steadily falling to 19%, and from 9% increasing to 18%, respectively (Fig. 5.5A). Greater

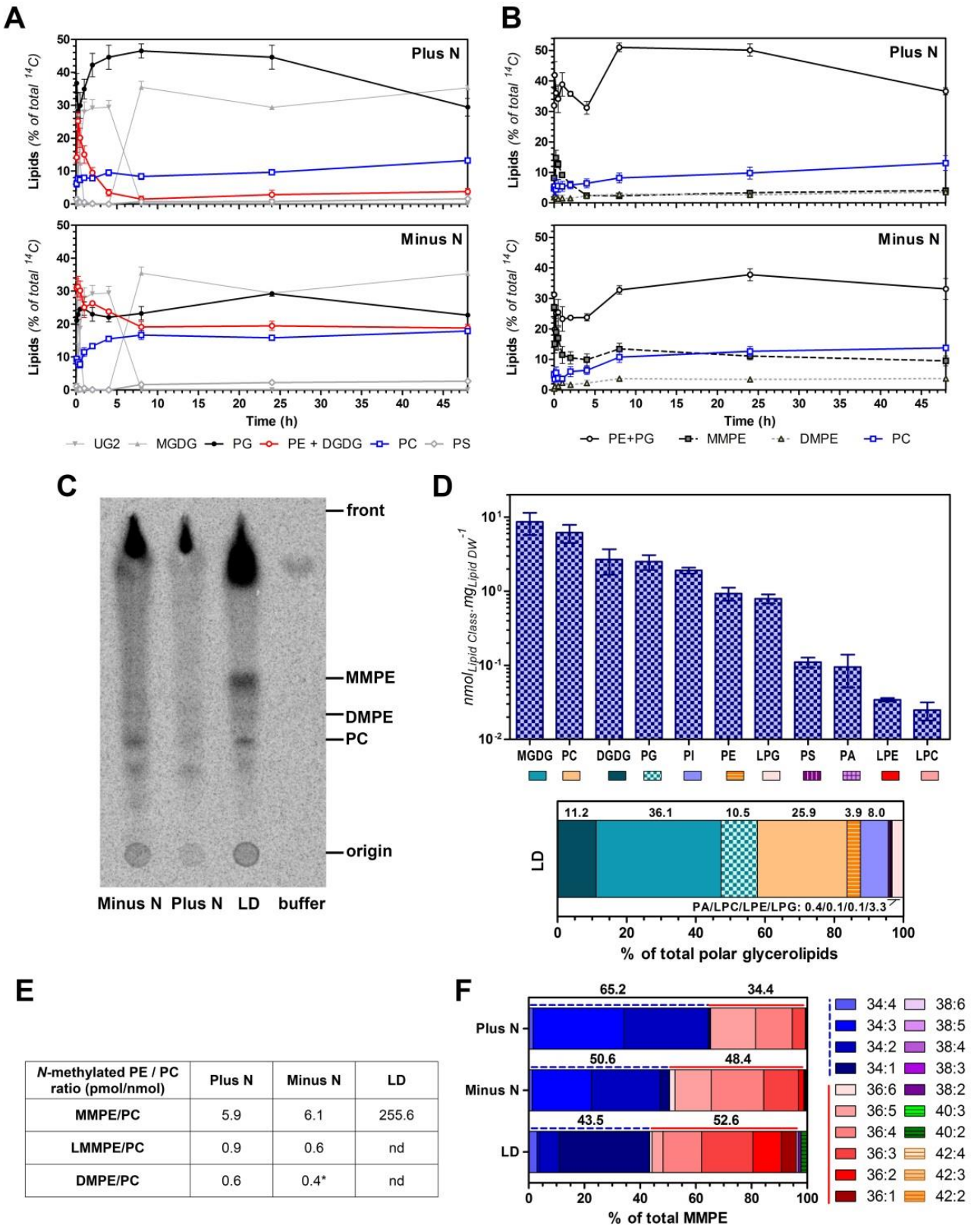

N-methylated PE / PC ratio (pmol/nmol)	Plus N	Minus N	LD
MMPE/PC	5.9	6.1	255.6
LMMPE/PC	0.9	0.6	nd
DMPE/PC	0.6	0.4*	nd

Figure 5.5. *E. oleoabundans* synthesizes PC via SAM-dependent PE methylation. (A, B) Kinetics of [^{14}C]acetate glycerolipid labeling under N sufficiency (plus N) and N deprivation (minus N). [^{14}C]acetate-labeled lipids were separated using two different 1D-TLC systems to analyze: (A) major polar glycerolipids; (B) *N*-methylated PE derivatives. The percentages of glycerolipid species per total [^{14}C]acetate-labeled lipids from each time point are shown. Data are mean of three biological replicates. (C) Lipid *N*-methyltransferase assay performed with LD, and microsomes from plus N and minus N conditions, using *S*-adenosyl-L-[methyl-^{14}C]methionine. The relative mobilities of PE, MMPE, DMPE and PC are indicated. (D) Polar glycerolipid composition (ESI-TQ-MS/MS) of LD from cells under minus N after 4 d. The amounts of glycerolipid classes are expressed relative to the total weight of analyzed lipids (nmol $mg_{LipidDW}^{-1}$), and as

percentages of the total amount of polar glycerolipids in the LD. SQDG was also detected (0.17 normalized MS signal $mg_{LipidDW}^{-1}$). Data are mean of five biological replicates. (E) Quantitative targeted ESI-TQ-MS/MS analysis of PE *N*-methylated derivatives in LD and total cell lipid extracts. Statistically significant changes (unpaired two-tailed Student's *t*-test; *p*-value < 0.05) between plus N and minus N are indicated (asterisks); nd: below detection limit. (F) Bar plots representing the relative abundance of the lipid molecular species comprising MMPE in the LD and total cell lipid extracts. Bar plots are as described in Fig. 5.3. Data in (E) and (F) are mean of five biological replicates, except for LD (pool from five LD preparations). Error bars represent SEM.

PS labeling (1.7-fold) was also supported under N deprivation (Fig. 5.5A). Although changes in PE kinetics could also be influenced by DGDG, owing to their co-migration in the TLC system (Fig. S5.6B), the reciprocal behavior between PE and PC labeling kinetics under N deprivation, suggests a precursor-product relationship between them.

5.2.5. *E. oleoabundans* synthesizes *N*-methylated glycerolipids: PC via SAM-dependent PE methylation and the betaine lipid DGTS

Despite being one of the most common phospholipids in eukaryotes, PC biosynthesis in algae remains unclear. Existence of the PE *N*-methylation pathway in *E. oleoabundans* to synthesize PC could explain the [^{14}C]acetate-labeling dynamics observed between PE and PC during N deprivation (Fig. 5.5A).

In eukaryotes, successive PE methylation is catalyzed by either PE and/or phospholipid *N*-methyltransferases (PEMT and/or PLMT), both of which are integral membrane enzymes using SAM as a methyl donor (Hirashima et al., 2018). Microsomes from N-sufficient and N-deprived *E. oleoabundans*, as well as LD isolated from the latter, were tested for lipid *N*-methyltransferase activity in the presence of endogenous PE and *S*-adenosyl-L-[*methyl-^{14}C*]methionine based on de Rudder et al. (1997). Lipid separation by 1D-TLC showed [^{14}C]-methylated lipid products with relative mobilities corresponding to all three successive *N*-methylated derivatives of PE: phosphatidylmonomethylethanolamine (MMPE), phosphatidyldimethylethanolamine (DMPE) and PC (Fig. 5.5C). The evidence from this *in vitro* enzymatic assay indicates that PC synthesis can occur in *E. oleoabundans* membranes and LD via the PE methylation pathway. Additional incorporation of the radioactive label into unknown lipid species migrating close to the solvent front was observed in this assay (Fig. 5.5C), similar to de Rudder et al. (1997).

The *in vivo* formation of the PE methylation pathway intermediates was analyzed by 1D-TLC separation of [^{14}C]acetate-labeled lipids. Lipid spots with relative mobilities corresponding to MMPE and DMPE were detected in total lipid extracts from N-sufficient

and N-deprived cells (Fig. S5.6C). Using a 1D-TLC system for methylated lipids, [^{14}C]acetate-labeling kinetics over a 48 h period showed that higher proportions of [^{14}C]acetate (from 12 to up to 23% of the radioactive label) were incorporated into the PE methylated intermediates, particularly into MMPE, during N deprivation (Fig. 5.5B). The *in vivo* incorporation of methyl groups into PE could not be further investigated as *E. oleoabundans* did not assimilate L-[*methyl*-^{14}C]methionine after incubation for 48 h (data not shown). Using targeted ESI-TQ-MS/MS, the existence of PE *N*-methylated derivatives in total lipid extracts from 4-d N-sufficient and N-deprived cultures was confirmed (Fig. 5.5E,F). The MMPE and DMPE positive ion species were identified by the neutral loss of 155.02 and 169.02 Da, corresponding to their characteristic head group fragments (monomethylphosphoethanolamine and dimethylphosphoethanolamine, respectively). This approach also confirmed the presence of MMPE in LD, where the MMPE to PC ratio was 42 times higher to that observed in total lipid extracts of N-deprived cells (Fig. 5.5E,F). Further analysis of the LD polar lipid composition showed that compared to total lipid extracts (19-21%, Fig. 5.2C), the proportion of PC is higher within the polar glycerolipids of the LD (26%, Fig. 5.5D). These results suggest an enriched PE *N*-methylation activity in the LD of N-deprived *E. oleoabundans*, probably to maintain the high levels of PC in these discrete organelles.

Amino acid sequence-based search for lipid *N*-methyltransferases in the *in silico* translated *E. oleoabundans* protein database (Garibay-Hernández et al., 2017) showed that this microalga possesses a homolog for PLMT (*Eo*PLMT; m.314600), but not for PEMT, which is consistent with recent homology searches in other green microalgae (Hirashima et al., 2018). The predicted *Eo*PLMT is 181 amino acids in size and shares at least 23% of sequence identity with homologs (Fig. S5.7), from algae to humans, which have been proven to have phospholipid *N*-methyltransferase activity (Kodaki and Yamashita, 1987; Shield et al., 2003; Keogh et al., 2009; Hirashima et al., 2018). *Eo*PLMT is predicted to be an integral membrane protein and its sequence alignment shows it has the two conserved residues (Fig. S5.7A) necessary for SAM binding in the human homolog (Shield et al., 2003). Surprisingly, another homolog for a lipid *N*-methyltransferase, the betaine lipid synthase BTA1 (*Eo*BTA1; m.387277), was also identified in the *E. oleoabundans* proteome database. This protein is required for the synthesis of the betaine lipid diacylglyceryl-*N,N,N*-trimethylhomoserine (DGTS) in *C. reinhardtii* (Riekhof et al., 2005). The putative *Eo*BTA1 (Fig. 5.6A) has 744 amino acids, shares 61% identity with *Cr*BTA1 and contains the two

amino acids critical for SAM binding and DGTS synthesis in *C. reinhardtii* (Riekhof et al., 2005).

The identification of a predicted BTA1 homolog in *E. oleoabundans* was completely unexpected as the corresponding lipid product (DGTS) has never been reported for this microalga (Tornabene et al., 1983; Matich et al., 2016, 2018; Goh et al., 2017). In this work, we identified DGTS by accurate quadrupole time-of-flight (QTOF)-MS-based detection of its characteristic positive fragment ions in total lipid extracts from N-sufficient and N-deprived cells (Fig. 5.6B-D): $[C_{10}H_{22}O_5N]^+$ at *m/z* 236.1492, corresponding to the DGTS backbone after the removal of both FA; and $[C_7H_{14}O_2N]^+$ at *m/z* 144.1019, corresponding to the polar headgroup (Li et al., 2017). Contrary to PE *N*-methylation intermediates, DGTS was not detected in LD as the corresponding signal was in the noise range. Direct infusion MS/MS precursor ion scan of all parents of *m/z* 236.1 showed DGTS is comprised by unsaturated 34- and 36-C lipid species (Fig. 5.6F), likely constituted by 16/18 and 18/18 FA, respectively, as indicated by the fragmentation patterns of the most abundant precursor ions (data not shown). Comparison of the DGTS signal relative to PC in total cell lipid extracts from N-sufficient and N-deprived conditions, suggested higher abundance of DGTS during N deprivation (Fig. 5.6E). This, together with the higher proportion of [^{14}C]acetate-labeled MMPE during N stress (Fig. 5.5B), and the enriched PE *N*-methylation activity in LD (Fig. 5.5C,E), suggested that N deprivation induces SAM-dependent lipid *N*-methylation in *E. oleoabundans*.

5.2.6. Identification of nitrogen depletion-responsive proteins in *E. oleoabundans* membranes

To get insights into the membrane-associated mechanisms underlying *E. oleoabundans* response to N stress, including regulation of lipid metabolism, microsomes from cells under N deprivation and N sufficiency conditions were analyzed using a quantitative label-free MS shotgun proteomics approach. In total, 619 proteins (37,210 spectra) were identified with not less than two unique peptides in at least one of the eight analyzed samples, by applying protein and peptide score-thresholds of 99 and 95 percent, respectively.

Label-free quantitative methods rely on different metrics from MS data to estimate protein abundances. The precursor intensity (PI)-based methods rely on the integrated peptide ion intensities from the precursor ion spectra (MS1). The spectral counting (SpC)

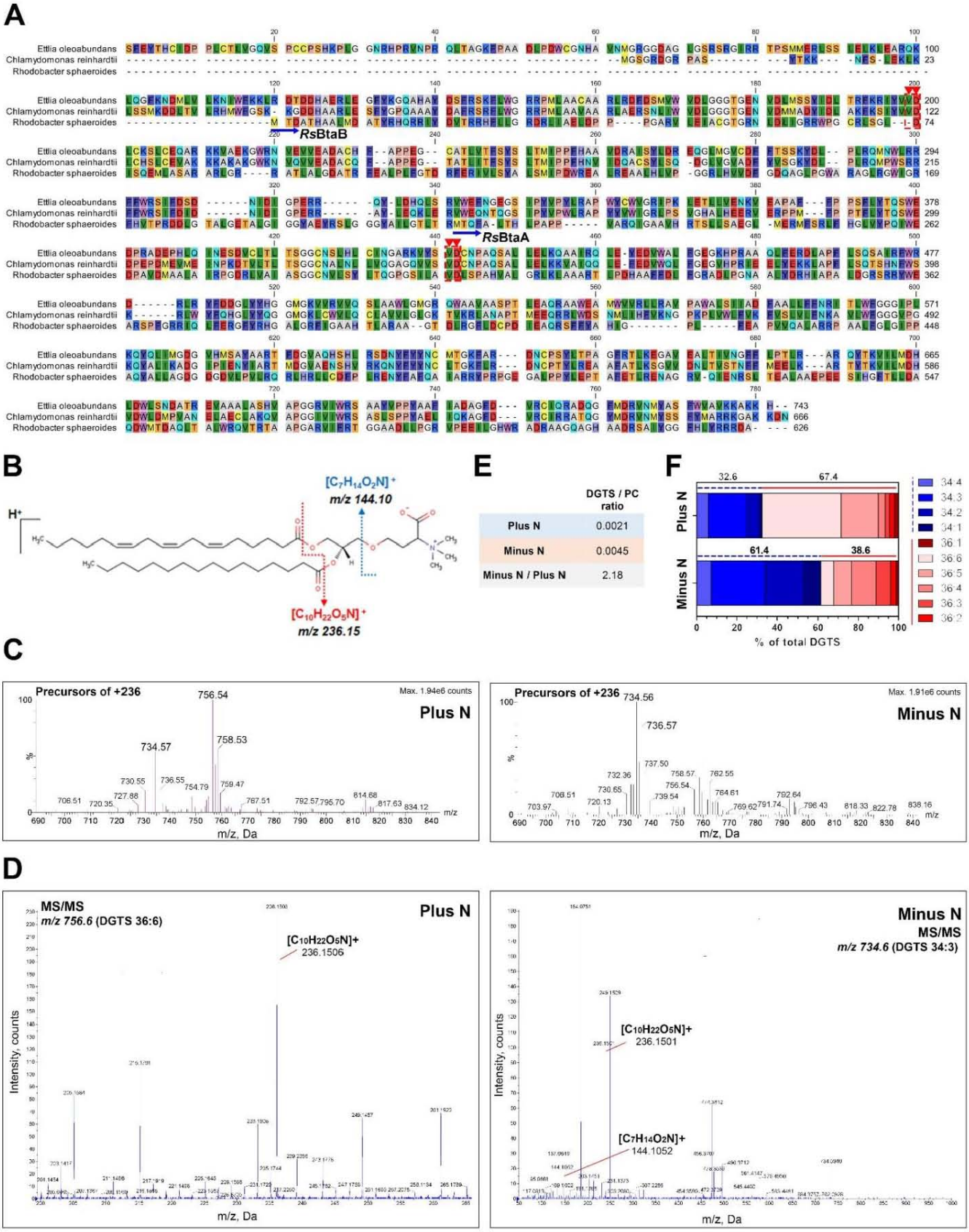

Figure 5.6. Identification of DGTS in *E. oleoabundans*. (A) Sequence alignment of *Eo*BTA1 (m.387277) and its counterparts in *C. renhardtii* (*Cr*BTA1: Q6DN05) and *R. sphaeroides* (*Rs*BtaA: Q93TQ1; *Rs*BtaB: Q6DN05; Uniprot accession numbers are provided). The conserved residues for SAM binding are highlighted (red arrows). Full-length amino acid sequences were aligned with Clustal Omega. The sequences *Rs*BtaA and *Rs*BtaB were treated as a single entity; the starting methionine of each is indicated (blue arrows). Amino acids are colored according to the RasMol color scheme. (B) MS fragmentation pattern of DGTS in positive ionization mode. (C) ESI-TQ-MS/MS precursor ion scan of *m/z* 236 in total lipid extracts from N-

sufficient (plus N) and N-deprived (minus N) conditions. (D) High resolution ESI-QTOF-MS/MS spectra of most abundant DGTS precursor ions identified in plus N and minus N (*m/z* 756.6 and *m/z* 734.6, respectively). Characteristic DGTS fragments from (A) are indicated (error < 10 ppm). (E) Abundance of DGTS in total lipid extracts. DGTS amounts are expressed as normalized MS signal per pmol of PC. DGTS was below the detection limit in LD. (F) Bar plots representing the relative abundance of the lipid molecular species comprising DGTS in total lipid extracts. Bar plots are as described in Fig. 5.3.

methods are based on the number of MS/MS spectra identified for all the peptides assigned to a protein; SpC methods have diversified to take into account the spectra shared among proteins, the observable tryptic peptides, or the length of a protein (WSpC, weighted SpC; emPAI, exponentially modified protein abundance index; and NSAF, normalized spectral abundance factor, respectively). Additional label-free approaches, such as total ion count (TIC), have combined the features of PI and SpC-based methods by measuring the intensity of fragment MS/MS ions (Neilson et al., 2011; Ahrné et al., 2013). In this study, relative protein quantification was performed using WSpC, emPAI, NSAF, Top3 PI, and Top3 TIC (Top3: sum of the three highest intensity values), as previous studies have proved that combining label-free approaches increases the power for detecting protein changes in shotgun experiments (Old et al., 2005; Freund and Prenni, 2013; Bubis et al., 2017). After applying the stringency parameters described in Materials and Methods, a total of 157 proteins were responsive in at least one of the five label-free approaches; of these, 34 proteins denoted as ‘core proteins’ were significant according to all five methods (Fig. 5.7A).

To explore the quantitative data from all five label-free approaches used in this work and their relationship with both N availability conditions, a multivariate principal component analysis (PCA) was performed. The PCA shows (Fig. 5.7B,C) that most of data variance (83%) is explained by the first principal component (PC1), along which samples are clearly distinguished based on the label-free quantification method; whereas the second uncorrelated principal component (PC2) accounts for 5% of the variance, enabling further differentiation between N-depleted and N-sufficient samples. Once the main source of data variation from PC1 was dismissed, samples could be discriminated according to their treatment along PC2, which together with PC3, explain 54% of the remaining variation. (Fig. 5.7C, inset). When the specific weight with which every protein contributes to the first two principal components is visualized in the loadings plot, proteins extend along PC2 based on their changes under N deprivation (Fig. 5.7D). The increased core proteins (red) are distributed in the upper half of the plot, while the decreased ones (blue) are spread in the lower half. When analyzed individually, all of the five methods could discriminate between N-depleted and N-sufficient samples (Fig. S5.9A). The combination of label-free quantitative

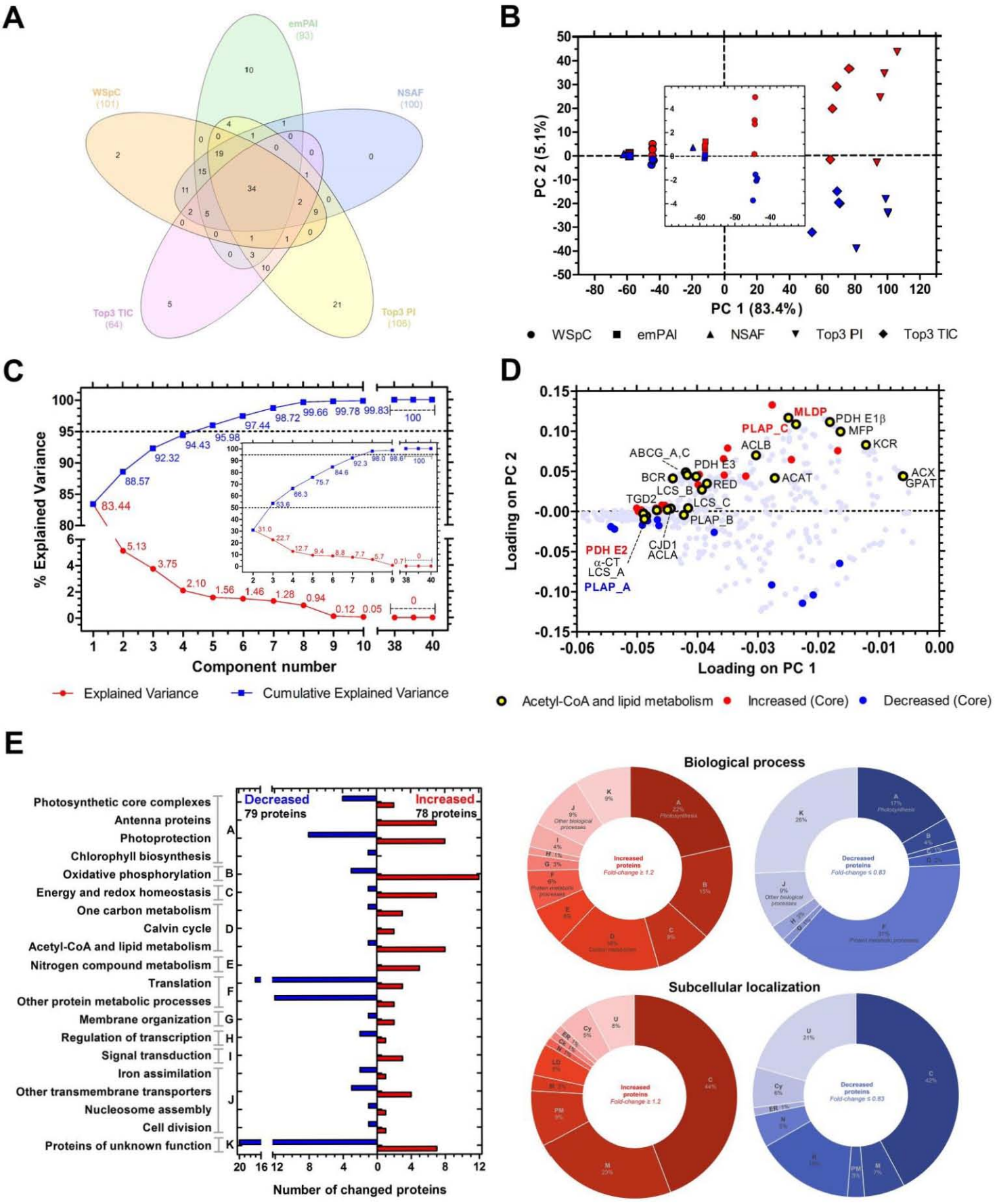

Figure 5.7. Label-free quantitative shotgun proteomics of *E. oleoabundans* membranes. (A) N deprivation-responsive proteins according to different label-free quantification approaches: WSpC, emPAI, NSAF, Top3 TIC, and Top3 PI. The central intersect of the Venn diagram defines

the responsive proteins common to all methods (core proteins). (B) PCA scores plot of the membrane proteome analyzed through five label-free approaches. The points represent each of the biological replicates (red, minus N; blue, plus N) quantified by a specific label-free method. The X and Y coordinates represent PC1 and PC2, respectively. The region corresponding to the spectral counting-based label-free methods is magnified in the inset. (C) PCA scree plot representing the proportion of variance explained by each principal component (red) and the corresponding cumulative variance values (blue). The contribution of each principal component to the total dataset variance, once the percentage from PC1 has been removed, is indicated in the graph inset. Dashed lines indicate 95% of total variance explained (50% in the graph inset). (D) PCA loadings plot. Each point represents one of the 619 identified proteins. The core proteins are highlighted (red, increased; blue, decreased).

Identified acetyl-CoA and lipid metabolism proteins are indicated (yellow) together with their abbreviations; among these proteins, the labels of those comprised within the core proteins are highlighted (red, increased; blue, decreased). α-CT, Acetyl-CoA carboxylase carboxyl transferase subunit α, chloroplastic (m.212887); ACAT, Acetyl-CoA acetyltransferase (m.149328); ACLA, ATP-citrate synthase α-chain protein (m.396299); ACX, Acyl-CoA oxidase B, peroxisomal (m.366023); BCR, Biotin carboxylase, chloroplastic (m.390372); CJD1, Chloroplast J-like domain-containing protein (m.117336); GPAT, Glycerol-3-phosphate acyltransferase (m.241864); KCR, β-Ketoacyl-CoA reductase (m.84123); PLAP_B, Probable plastid-lipid associated protein B, chloroplastic (m.50827); RED, 2,4-Dienoyl-CoA reductase, peroxisomal (m.356362); TGD2, Protein trigalactosyldiacylglycerol 2, chloroplastic (m.362261); the remaining abbreviations are depicted in Table 5.1. (E) Biological process and subcellular localization of responsive proteins. The bar graph shows the biological process distribution of responsive proteins. The circular graphs show the distributions of the responsive proteins relative to the total of increased (red) or decreased (blue) proteins, respectively. Biological process labels: bar graph; subcellular localization labels: C, chloroplast; Ck, cytoskeleton; Cy, cytoplasm; ER, endoplasmic reticulum; LD, lipid droplet; M, mitochondria; N, nucleus; PM, plasma membrane; R, cytosolic ribosome; U, unknown. Each protein is represented by a single biological process and cell compartment term.

approaches proved advantageous, as compared to the amount of N-responsive proteins exclusively identified by all five methods (34 core proteins), this strategy increased the number of detected proteins that were significantly responsive to N stress (157 proteins).

To address the biological significance of the proteomic changes observed after N-deprivation, the 157 responsive proteins (79 increased, 78 decreased) were annotated based on Garibay-Hernández et al. (2017), and manually curated to include recent updates (Table S5.2). Most responsive membrane proteins were categorized into known biological processes, and cellular location was predicted for the majority (Table S5.2); however, 17% of them remained as proteins of unknown function. Results supported the remodeling of membrane functions after N deprivation (Fig. 5.2E). Compared to N sufficiency, the fraction of proteins involved in N assimilation, bioenergetic processes, and carbon metabolism, particularly lipid metabolism, was increased under N deprivation, whereas the proportion of those related to protein metabolic processes, mainly cytoplasmic translation, was decreased.

The relative amount of proteins located to LD, as well as in energy-converting organelles, mainly the mitochondria, was expanded after N depletion, while the fraction of cytosolic ribosomal proteins was markedly diminished. The strong contribution of lipid metabolism-related proteins to the changes observed in the membrane proteome is

supported by PCA, as in the loadings plots most of these proteins were distributed in the upper part of PC2, corresponding to the distribution of N-deprived samples in the scores plots (Fig. 5.7B,D and S5.9). This indicates that the higher abundance of lipid metabolism proteins is a distinctive feature of N-deprived microalgae, in agreement with their oleaginous phenotype (Fig. 5.1). Most of these proteins were statistically increased under N stress, four of which were common to all label free quantitative methods (Fig. S5.8).

Transcriptomic data corresponding to each of the identified responsive proteins was retrieved from Rismani-Yazdi et al. (2012) (Table S5.2). Only half of the retrieved transcripts were found to be statistically changed under N deprivation (Benjamini and Hochberg adusted *p*-value: *q*-value ≤ 0.05), among which 41 out of 78 showed a coordinated response with their respective proteins, indicating that abundance of these proteins may be controlled at the transcriptional level. In contrast, the remaining 37 transcripts displayed a correlation pattern opposite to the protein response (contra-regulated) (Fig. S5.10). Previous studies have found that transcript levels commonly explain less than half of protein changes, suggesting that, for discordant transcript-protein pairs, protein abundance may be regulated at post-transcriptional and/or post-translational levels (Castruita et al., 2011; Dyhrman et al., 2012; Haider and Pal, 2013; Schmollinger et al., 2014; Wang et al., 2014; Fan et al., 2017). Low transcript-protein correlation can also be attributed to differences between the transcript and protein half-lives, technical limitations on detection of low-abundance transcripts/proteins, and variations between the experimental conditions under which omics data were gathered (Dyhrman et al., 2012; Haider and Pal, 2013).

5.3. Discussion

5.3.1. Nitrogen-sparing, photoprotection and energy balance mechanisms are induced in nitrogen-deprived *E. oleoabundans*

The quantitative membrane proteomics analysis uncovered the occurrence of the main hallmark processes of N deprivation, including those involved in increased N uptake (Table S5.2). Ammonium (AMT1) and nitrate (NRT2) high affinity transporters were unique to N-depleted cells. Although *E. oleoabundans* has not been reported to uptake organic N sources except for urea (Li et al., 2008), an intermediate-affinity choline transporter-like protein (CTL) was exclusively detected under N deprivation. CTLs are required for

phospholipid biosynthesis in animals (Michel et al., 2006), however, their role in photosynthetic organisms is yet unclear (Dettmer et al., 2014). Induction of intracellular ammonia assimilation via the glutamine synthetase-glutamate synthase (GS-GOGAT) and urea cycles was also suggested by the increased abundance of GS and the carbamoyl phosphate synthetase (CARB), respectively. A reduced chloroplastic and cytosolic protein synthesis capacity in N deprivation was suggested by the decreased abundance of large ribosomal subunit components, translation initiation and elongation factors, as well as several proteins with targeting functions (Table S5.2).

In agreement with the lower chlorophyll content of N-deprived cells (Fig. 5.1A), the abundance of the protochlorophyllide reductase (POR) enzyme, which catalyzes light-dependent chlorophyll biosynthesis, was decreased (Stern, 2009). Diminished photosynthetic efficiency of this microalga under N deprivation (Klok et al., 2013; Benvenuti et al., 2015), is also consistent with changes observed in photosynthesis-related proteins (Fig. 5.7E and Table S5.2). In line with the photosystem II (PSII) susceptibility to oxidative damage under stress (Benvenuti et al., 2015; Erickson et al., 2015), Thylakoid Formation 1 (THF1/PSB29) and a chloroplast rubredoxin, necessary for PSII turnover (Bečková et al., 2017) and its assembly/stability (Calderon et al., 2013), respectively, were increased under N deprivation. Two chloroplastic voltage-dependent chloride channels (VCCN), which in *A. thaliana* have been shown to play an important role in rapidly adjusting electron transport and activating photoprotective mechanisms, also increased in abundance after N starvation (Herdean et al., 2016).

Despite activation of photoprotective mechanisms, photosystem I (PSI) photodamage under N deprivation was indicated by changes to its functional reaction center stoichiometry with decreases in proteins mediating PSI electron transfer (PSI reaction center subunits II [PSAB], IV [PSAE], N [PSAN]; Haldrup et al., 1999; Stern, 2009). Synthesis of chloroplastic ATP is likewise affected as the abundance of the catalytic β subunit from the chloroplast ATP synthase was lowered. Our data suggest that *E. oleoabundans* copes with the energy imbalance caused by N shortage and ameliorates photodamage through alternative electron transport pathways. Induction of both NADPH dehydrogenase- and ferredoxin-dependent cyclic electron flow pathways was indicated by the increased abundance of several of their protein components (Table S5.2). An increased abundance of core constituents of mitochondrial complexes, including catalytic components of cytochrome bc_1, cytochrome *c* oxidase, and ATP synthase (Fig. 5.7E and Table S5.2), suggested a bioenergetic preference for respiration in N-starved cells. Amongst 15 oxidative

phosphorylation-related proteins responsive to N deprivation, only three accessory proteins from the NADH:ubiquinone oxidoreductase and cytochrome *c* oxidase complexes were decreased (Table S5.2). Under N starvation, a higher oxidative phosphorylation may provide an additional ATP source to maintain carbon fixation, as proteins necessary for ATP exchange between the mitochondria and the chloroplast (mitochondrial and chloroplastic ADP/ATP carriers, and a mitochondrial phosphate carrier) were increased. An augmented respiratory metabolism may represent an economical use of N, especially when degradative processes generate substrates for respiration (Schmollinger et al., 2014).

5.3.2. Nitrogen deprivation alters chloroplast morphology and triggers a chloroplast stress response

Our results indicate that *E. oleoabundans* N starvation is characterized by an increased cell size and profound alterations in its cellular ultrastructure, mainly in the chloroplast (Fig. 5.1B), accompanied by changes in its membrane properties (Fig. S5.4). As both, the plastid photosynthetic activity and membrane architecture are highly dependent on its lipid composition (Nakamura and Li-Beisson, 2016), particularly on the specific contribution of DGDG (Holzl et al., 2009; Demé et al., 2014), the morphological alterations in N-deprived cells are partially explained by the major changes in its chloroplast glycerolipids. Despite the decrease in PG (0.7-fold), N deprivation induced a lower ratio of hexagonal (MGDG) to bilayer (DGDG, PG, SQDG)-forming chloroplast lipids, owing to the changes in both major galactolipids, MGDG and DGDG (0.8 and 1.9-fold, respectively; Fig. 5.2D). This resulted in a lower MGDG/DGDG ratio that may prevent formation of non-bilayer phases and bilayer rupture (Demé et al., 2014), likely stabilizing chloroplast membranes during N starvation. Chloroplast membrane remodeling and lowered MGDG/DGDG ratios may help to cope with abiotic stressors, as recently confirmed in *C. reinhardtii* (Du et al., 2018).

The strong decrease in abundance of the ATP-independent metalloprotease EGY1 (Ethyl-dependent Gravitropism-deficient and Yellow-green1) and the membrane-remodeling GTPase FZL (FuZzy onions-Like) in N-deprived cells (Table S5.2), may also contribute to their altered chloroplast ultrastructure. These membrane components have proved essential for correct chloroplast morphology (Chen et al., 2005; Gao et al., 2006), and mutations in these proteins trigger early senescence responses in *A. thaliana* (Landoni et al., 2013; Chen et al., 2016; Tremblay et al., 2016). Moreover, FZL and the Hypersensitive Induced Reaction (HIR) protein, which contrary to FZL, was increased under N stress (Table S5.2), have been

proposed as negative (Landoni et al., 2013; Tremblay et al., 2016) and positive (Ishikawa et al., 2015) regulators, respectively, of cell death through the reactive oxygen species (ROS) and salicylic acid-mediated hypersensitive response (HR) pathway. The loss of chloroplast integrity in *A. thaliana*'s FZL mutants has been linked to the activation of HR cell death through chloroplast-generated ROS (Landoni et al., 2013). Therefore, the altered chloroplast ultrastructure in N-starved cells could be accompanied by a chloroplast stress response, which is supported by the higher abundance of the chloroplast proteins 2-cys peroxiredoxin and glutaredoxin (Table S5.2), which are central to the main plastidic ROS detoxification/signaling systems (Foyer and Noctor, 2011; Vaseghi et al., 2018). Induction of a chloroplast stress response is also suggested by the increased levels of THF1 (Huang et al., 2013b; Zhan et al., 2016; Bečková et al., 2017) and the Vesicle-Inducing Protein in Plastids1 (VIPP1) (Kroll et al., 2001; Nordhues et al., 2012; Zhang et al., 2016; Gutu et al., 2018; Theis and Schroda, 2019) (Table S5.2), which play a crucial role in the biogenesis and repair of thylakoid membrane complexes, and in the coping with chloroplast membrane stress.

In addition to chloroplast membrane stress, autophagy-related markers were responsive to N deprivation. The ribosomal protein RPL37, whose degradation is a landmark of autophagic flux activation in *C. reinhardtii* (Couso et al., 2018), was decreased in N-starved cells (Table S5.2). Compared to N-sufficient cells where FZL was detected, its absence from the membranes of N-deprived microalgae (Table S5.2), agrees with the activation of autophagy in *A. thaliana*'s FZL mutants, besides its known effect on altered chloroplast morphology and cell death (Tremblay et al., 2016). These results, together with the transcriptional upregulation of AuTophaGy-related (ATG) components of the ubiquitin-like conjugation machinery (ATG3, ATG4, ATG5, ATG7, ATG8, ATG12) previously reported for *E. oleoabundans* upon N starvation (Rismani-Yazdi et al., 2012), suggest the activation of an autophagic response in N-depleted cells.

Altogether, we propose that the chloroplast morphological changes occurring in N-deprived *E. oleoabundans* may be accompanied by a chloroplast oxidative response and trigger an autophagic process, as recently described for *C. reinhardtii* (Heredia-Martinez et al., 2018). An increased autophagic flux may allow recycling of unneeded or damaged material to maintain cell survival upon N stress, and may be necessary for TAG synthesis and LD formation, as shown for *C. reinhardtii* under nutrient deprivation (Couso et al., 2018).

5.3.3. Carbon metabolism proteins responsive to nitrogen deprivation support an increased photosynthetic carbon flux towards acyl-lipid metabolism

The high representation of carbon metabolism within the N depletion-responsive proteins (10%; Fig. 5.7E), suggests changes in carbon partitioning, which are likely coupled to modifications in N metabolism. Growth kinetics showed that total carbon fixation was the same in N-sufficient and N-deprived cultures (both reached the same biomass concentration after 4 d: 0.22 g/L), whereas carbon fixation on a per cell basis was increased during N stress, as higher cell mass values were attained (Fig. S5.1) despite the profound alterations in chloroplast morphology and function. A higher carbon fixation per cell may be supported by the ultrastructural preservation of pyrenoid tubules in N-deprived cells (Fig. 5.1B), the increased abundance of the plasma membrane inorganic carbon transporter HLA3 (High Light Activated3), as well as two chloroplastic Calvin cycle enzymes, transketolase and phosphoglycerate kinase (Table S5.2). The abundance of the thylakoid carbonic anhydrase CAH3 was decreased in membranes of N-deprived cells (Table S5.2). This may be attributed to a relocation of CAH3 to the pyrenoid for improving carbon fixation (Blanco-Rivero et al., 2012; Mitchell et al., 2014), rather than to its lowered abundance during N starvation, as its attachment to the thylakoid membranes to increase PSII activity (Benlloch et al., 2015) may be unnecessary owing to the affected PSII efficiency of N-deprived cells (Benvenuti et al., 2015). Altogether, an increased photosynthetic fixation of CO_2 may be a strategy to ameliorate chloroplast ROS production in N-deprived microalgae, as proved for *C. reinhardtii* (Du et al., 2018).

Our quantitative proteomics analysis suggested that N-deprived cells divert the increased photosynthetic carbon flux towards acetyl-CoA synthesis, the direct precursor of FA biosynthesis, supporting the idea that TAG accumulation capacity of green oleaginous microalgae strongly depends on enhanced production of acetyl-CoA (Avidan et al., 2015; Avidan and Pick, 2015). An increased synthesis of both, plastidic and cytoplasmic acetyl-CoA, is indicated by our data. A higher abundance in N-deprived cells of three out of the four subunits (E1β, E2, E3; Table 5.1) that compose the chloroplastic pyruvate dehydrogenase complex (PDH) supported an enhanced synthesis of plastidic acetyl-CoA, whereas the increase of the ATP-citrate synthase β-subunit (ACLB; Table 5.1) suggested that cytoplasmic acetyl-CoA production is also enhanced.

Long-chain acyl-CoA synthetases (LCS) activate free FA to acyl-CoA thioesters for their utilization in most lipid metabolic pathways, including FA elongation and desaturation, glycerolipid biosynthesis, and β-oxidation (Shockey et al., 2002). The three LCS isoforms

identified in *E. oleoabundans* membranes (Garibay-Hernández et al., 2017) were increased under N stress (Table 5.1). Two of them (LCS_A, LCS_B), are close homologs of *C. reinhardtii* LCS2 (*Cr*LCS2) which was detected in LD (Moellering and Benning, 2010; Nguyen et al., 2011) and has been shown to be involved in channeling *de novo* synthesized acyl groups into TAG (Li et al., 2016b). Together with the overall increase of 16:0 and 18:1 FA-containing glycerolipid classes during N starvation (Fig. 5.3 and 5.4), this result underscores the enhanced activation of newly synthesized FA in the chloroplast, as a key control point to drive FA export and incorporation into TAG (Li et al., 2016a,b). LCS_C, the third increased LCS, is a homolog of *C. reinhardtii* ACS2 and is closely related to *A. thaliana* LCS6 and LCS7, all of which have been associated to β-oxidation of FA, probably derived from TAG (Fulda et al., 2002; Shockey et al., 2002; Jia et al., 2016). This indicates that FA degradation is still active in N-deprived cells and is supported by detection of the FA β-oxidation multifunctional protein (MFP) exclusively in N-starved cells (Table 5.1). A continuous balance between oil synthesis and degradation during N stress is thus suggested.

In line with the increased LCS-mediated FA activation, known to be the driving force for FA membrane transport (Li et al., 2016a), two half-sized ATP-Binding Cassette transporters of subfamily G (ABCG), also named White-Brown Complex (WBC) homologues (Verrier et al., 2008), were increased at least 5-fold during N stress (Table 5.1). These proteins are likely candidates for transporting lipophilic molecules across the membranes in *E. oleoabundans*, as plant WBC homologues are involved in translocation of cuticular wax and suberin monomers, as well as sporopollenin and other lipidic monomers during pollen development (Verrier et al., 2008; Do et al., 2017).

A homolog of the green alga lineage-specific Major Lipid Droplet Protein (MLDP), whose abundance positively correlates with TAG accumulation during abiotic stress (Peled et al., 2011; Davidi et al., 2012; Tsai et al., 2015; Javee et al., 2016; Siegler et al., 2017), was detected solely in membranes from N-deprived cells (Table 5.1). The identification of MLDP in *E. oleoabundans* microsomes indicates that it is not specific to LD, but that it resides in other cell membranes as well, probably in ER-LD connection subdomains, as previously proposed (Huang et al., 2013a; Tsai et al., 2015; Siegler et al., 2017). MLDP has proved to play a structural role in LD size, and a functional role in *C. reinhardtii* by recruiting proteins to the LD surface, including lipid metabolism-related proteins such as *Cr*LCS2 (Tsai et al., 2015; Siegler et al., 2017). Two probable Plastid Lipid-Associated Proteins (PLAP)

Table 5.1. Acetyl-CoA and lipid metabolism proteins responsive to N deprivation in *E. oleoabundans* membranes. The protein FC (N deprivation, -N, relative to N sufficiency, +N) is shown for each label-free quantification method, together with the corresponding *p*-values. Data represent four biological replicates per tested condition; the number of biological replicates in which proteins were identified by at least two unique peptides (UP) is indicated. The label-free methods where proteins were significantly changed (*p*-value ≤ 0.05) are highlighted in gray. The average of statistically significant FC are given; for proteins exclusively detected under -N, FC are reported as infinity (INF). The corresponding transcripts and their regulation under -N are indicated according to Rismani-Yazdi et al. (2010). Statistically significant (*q*-value < 0.05) transcript Log_2 FC are highlighted (gray cells). Common abbreviations (Abbr.) are shown, together with the calculated protein molecular masses (MM, in kDa). Curated cell localizations are provided (Garibay-Hernández et al., 2017). [a] Experimental evidence of subcellular localization is available for protein homologs; [b] Experimental evidence of subcellular localization is not available. C, chloroplast; Cy, cytoplasm; LD, lipid droplet; M, mitochondria; O, other; PX, peroxisome; SP, signal peptide; U, unknown.

Protein Identifier	Curated Description	Abbr.	MM	Curated Cell Location	Replicates ≥ 2 UP –N / +N	Protein Abundance FC –N / +N (*p*-value)						Transcript regulation	
						Average	WSpC	emPAI	NSAF	Top3 PI	Top3 TIC	ID	Log_2 FC -N / +N (*q*-value)
Acetyl-CoA biosynthesis													
m.371437	Pyruvate dehydrogenase E1 component subunit β, chloroplastic	PDH E1β	41	C[a]	3 / 0	INF	INF (0.028)	INF (0.037)	INF (0.028)	INF (0.08)	INF (0.12)	Locus_1487_Transcript_1/1_Confidence_1.000_Length_1601_k23	1.25 (0.00000)
m.130266	Pyruvate dehydrogenase E2 component, chloroplastic	PDH E2	50	C[a]	4 / 4	1.78	1.7 (0.02)	2.3 (0.0051)	1.8 (0.017)	1.5 (0.04)	1.6 (0.037)	Locus_5688_Transcript_3/3_Confidence_0.800_Length_2288_k23	0.93 (0.00055)
m.324850	Pyruvate dehydrogenase E3 component, chloroplastic	PDH E3	63	C[a]	4 / 2	3.35	3.1 (0.044)	3.2 (0.025)	3.1 (0.037)	4.0 (0.033)	2.8 (0.082)	Locus_8019_Transcript_4/4_Confidence_0.625_Length_2140_k33	1.12 (0.00002)
m.391431	ATP-citrate synthase β-chain protein	ACLB	76	Cy[a]	2 / 0	7.40	4.8 (0.06)	7.4 (0.038)	4.9 (0.06)	54.0 (0.2)	31.0 (0.22)	Locus_3990_Transcript_4/5_Confidence_0.667_Length_4120_k23	-0.54 (0.14221)
Acyl-lipid biosynthesis													
m.368848	Long-chain acyl-CoA synthetase A	LCS	71	LD[a]	4 / 4	1.70	1.3 (0.074)	1.7 (0.032)	1.4 (0.08)	1.4 (0.32)	1.3 (0.41)	Locus_1272_Transcript_3/3_Confidence_0.714_Length_2813_k23	0.51 (0.24833)
m.224985	Long chain acyl-CoA synthetase B	LCS	76	LD[a]	4 / 1	7.03	4.5 (0.035)	4.7 (0.059)	4.6 (0.038)	9.4 (0.07)	12.0 (0.0096)	Locus_1196_Transcript_14/19_Confidence_0.304_Length_3552_k33	-0.81 (0.00727)

Protein Identifier	Curated Description	Abbr.	MM	Curated Cell Location	Replicates ≥ 2 UP –N / +N	Protein Abundance FC –N / +N (*p*-value)						Transcript regulation	
						Average	WSpC	emPAI	NSAF	Top3 PI	Top3 TIC	ID	Log_2 FC -N / +N (*q*-value)
m.371326	Long chain acyl-CoA synthetase C	LCS	67	M[b]	2 / 0	3.00	1.8 (0.08)	1.9 (0.12)	1.8 (0.085)	3.3 (0.061)	3.0 (0.01)	Locus_1473_Transcript_2/3_Confidence_0.667_Length_2217_k23	-0.86 (0.00673)
LD structural proteins													
m.413736	Major lipid droplet protein	MLDP	34	LD[a]	4 / 0	INF	INF (0.0002)	INF (0.00029)	INF (0.00024)	INF (0.026)	INF (0.0055)	Locus_72_Transcript_2/2_Confidence_1.000_Length_1313_k23	0.49 (0.28114)
m.392627	Probable plastid-lipid associated protein A, chloroplastic	PLAP	59	C[a]	4 / 4	0.62	0.6 (0.0016)	0.6 (0.0025)	0.6 (0.002)	0.6 (0.028)	0.7 (0.028)	Locus_4259_Transcript_1/6_Confidence_0.706_Length_3966_k23	0.10 (0.86550)
m.244306	Probable plastid-lipid associated protein_C, chloroplastic	PLAP	23	C[a]	4 / 0	INF	INF (0.0006)	INF (0.002)	INF (0.0011)	INF (0.0012)	INF (0.021)	Locus_2168_Transcript_4/6_Confidence_0.722_Length_2327_k33	0.81 (0.00347)
Lipid trafficking													
m.417181	ABC transporter G family member A	ABCG	70	U	4 / 1	6.23	5.4 (0.0013)	7.8 (0.03)	5.5 (0.0016)	12 (0.053)	6.1 (0.09)	Locus_1110_Transcript_3/3_Confidence_0.333_Length_2710_k23	1.41 (0.00041)
m.306564	ABC transporter G family member C	ABCG	69	U	2 / 1	5.30	2.0 (0.2)	3.7 (0.049)	2.1 (0.19)	8.2 (0.018)	4 (0.0038)	Locus_6123_Transcript_1/2_Confidence_1.000_Length_3300_k33	0.86 (0.00079)
Fatty acid β-oxidation													
m.420224	Fatty acid β-oxidation multifunctional protein, peroxisomal	MFP	77	PX[a]	1 / 0	INF	INF (0.039)	INF (0.039)	INF (0.042)	INF (0.14)	INF (0.16)	Locus_3608_Transcript_1/1_Confidence_1.000_Length_2333_k23	-0.03 (0.96850)

were also responsive to N-deprivation (Table 5.1). PLAP are considered as the major structural proteins specific to plastoglobules, which are not LD, but small lipophilic particles attached to thylakoid membranes (Lohscheider and Río Bártulos, 2016; Moriyama et al., 2018). Whether changes in PLAP abundance are related to lipid accumulation in N-deprived *E. oleoabundans* remains to be studied.

Altogether, the changes in acetyl-CoA and lipid metabolism-related proteins (Table 5.1) indicate that lipid accumulation in N-deprived *E. oleoabundans* is supported by induction of lipid metabolism at the acyl-lipid level (i.e. increased acyl-CoA feeding into FA biosynthesis and their enhanced ATP-dependent activation) and modulation of LD dynamics/structure through LD-specific proteins.

5.3.4. SAM-dependent glycerolipid *N*-methylation may contribute to LD formation and to oxidative stress protection during nitrogen deprivation

The results from this work demonstrate that *E. oleoabundans* can synthesize PC via the SAM-dependent *N*-methylation of PE, potentially through the activity of a putative PLMT homolog. *In vitro* enzymatic assays, identification of the pathway intermediates in lipid extracts, and sequence homology-based analysis (Fig. 5 and S5.7), support this conclusion. The novel existence in *E. oleoabundans* of the ether-linked *N*-methylated glycerolipid, DGTS, was also demonstrated.

Our results resemble recent findings in species from the *Chlamydomonas* genus (class *Chlorophyceae*), where all three PE methylations are catalyzed by a single PLMT (Hirashima et al., 2018). However, besides chloroplast galactolipids, PC is the dominant polar glycerolipid in *E. oleoabundans* (Fig. 5.2), whereas PC is either missing or a minor component in *Chlamydomonas* species, where DGTS has been detected as the main non-chloroplastic polar lipid (Harwood et al., 2009; Sakurai et al., 2014). It has been suggested that being a non-phosphorous zwitterionic glycerolipid, DGTS could replace PC either in microalgae containing no or very low levels of PC (Riekhof et al., 2005; Sakurai et al., 2014), or under low phosphorous availability as a strategy to cope with phospholipid degradation (Benning et al., 2015, Zavaleta-Pastor et al., 2010; Shemi et al., 2016; Cañavate et al., 2017). In *E. oleoabundans*, it is not likely that DGTS replaces PC or other N-containing phospholipids, as their total amounts were not decreased under N deprivation, and contrary to PC, DGTS was not detected in the LD. Despite these differences, conservation of the PE methylation pathway across algae lineages, supports the hypothesis for a vertical

inheritance of the PC biosynthetic mechanisms in *Viridiplantae,* followed by the diversification of their substrate preferences during evolution (Hirashima et al., 2018). The existence of additional PC biosynthetic pathways in *E. oleoabundans* remains to be studied.

Despite the lack of a comprehensive understanding of the biological functions of betaine lipids, our results suggesting an increase in PE *N*-methylation and its LD enrichment in N-deprived *E. oleoabundans* (Fig. 5.5), together with the relative increase in DGTS abundance (Fig. 5.7E), indicate that glycerolipid SAM-dependent *N*-methylation may play an important role during N stress. This is supported by the increased abundance in N-deprived cells of the *S*-adenosyl-L-homocysteine (SAH) hydrolase (SAH1; 11-fold) and a glutaredoxin homolog (6-fold) (Table S5.2), where the latter is a disulfide oxidoreductase that uses glutathione as an electron donor. In non-photosynthetic eukaryotes, beyond its function for PC biosynthesis, PE methylation has proved to be the major SAM-consuming reaction and thus, a major producer of SAH, a product and inhibitor of SAM-dependent methyltransferases (Malanovic et al., 2008; Vance, 2014; Ye et al., 2017). A higher SAH turnover into critical sulfur-containing metabolites (i.e. cystathionine, cysteine, glutathione) by inducing SAH1 has been shown to accompany increased PE methylation to alleviate the inhibition of methyltransferases, and to protect cells against oxidative stress by shunting methionine and SAM into the synthesis of the antioxidant glutathione (Ye et al., 2017). Based on this evidence and our results, we propose that glycerolipid SAM-dependent *N*-methylation is increased in *E. oleoabundans* to regulate the intracellular SAM/SAH ratio and to cope with the oxidative stress to which N-deprived cells are subjected. Moreover, an increased SAH1 may be involved in the regulation of TAG homeostasis in N-starved microalgae, as demonstrated in non-photosynthetic eukaryotes (Malanovic et al., 2008; Vance, 2014; Visram et al., 2018) and suggested by the identification of a SAH1 homolog in *C. reinhardtii* LD (Moellering and Benning, 2010). Being PC the most abundant phospholipid in *E. oleoabundans* LD (Fig. 5D), the PE *N*-methyltransferase activity detected in the LD may support PC biosynthesis and contribute to the formation and stabilization of these organelles, as demonstrated in adipocytes (Hörl et al., 2011).

5.3.5. Nitrogen deprivation induces changes in membrane-associated regulatory proteins

Several proteins involved in regulatory functions were responsive to N deprivation. The abundance of an ErbB-3 Binding Protein1 (EBP1) homolog was decreased (Table S5.2),

which may be related to the reduced cell proliferation of N-deprived cells (Fig. 5.1A and S5.1), as EBP1 is a conserved dose-dependent regulator of cell growth that stimulates cell division in land plants (Horváth et al., 2006; Wang et al., 2016). The exclusive identification of a DUF155 domain-containing protein (m.391974, Table S5.2) in N-deprived samples may indicate that there is an impaired cell cycle progression contributing to a lower cell division during N deprivation. The DUF155 domain-containing proteins, like Retarded Root Growth in *A. thaliana,* have been proposed as basic components of the cell division machinery (Zhou et al., 2011a), whose homologs in *Saccharomyces cerevisiae* (RMD1, RMD8) are essential for sporulation (Enyenihi and Saunders, 2003).

A calcium-dependent protein kinase (CDPK) and a phosphopeptide-binding 14-3-3 protein were increased in N-deprived cells (Table S5.2), as was reported for N-deprived *C. reinhardtii* (Motiwalla et al., 2014; Valledor et al., 2014; Wase et al., 2014). Both signal transduction proteins are involved in diverse biological processes in land plants, including regulation of carbon and N metabolism through a complex relationship between 14-3-3 proteins, CDPK, and CDPK clients (Swatek et al., 2014). Furthermore, 14-3-3 proteins have been shown to increase plant oil biosynthesis through interaction with the AP2/EREB family transcription factor WRInkled1 (WRI1) (Ma et al., 2016). Considering that AP2/EREB family members are responsive to N stress in several microalgae including *E. oleoabundans* (Rismani-Yazdi et al., 2012), and their transcriptional regulation correlates with that of lipid synthesis-related genes in *C. reinhardtii* (Gargouri et al., 2015) and *Nannochloropsis* spp. (Hu et al., 2014), it is likely that 14-3-3 proteins may also regulate oil biosynthesis in N-deprived microalgae.

Two transcription regulators (TR), a GCN5-related *N*-acetyltransferase (GNAT) and the stress-responsive High Light Activated8 (HLA8) nuclease, were increased and decreased, respectively, upon N stress. Analysis of their homologs in the *C. reinhardtii* transcriptional regulatory network (Chlamy Network Portal; López García de Lomana et al., 2015), shows that their expression under N stress concurs with the protein changes observed in this work. Both TR homologs belong to co-regulated transcriptional modules comprising N assimilation and lipid metabolism genes (Gargouri et al., 2015; López García de Lomana et al., 2015): the *Cr*GNAT homolog is co-regulated with AMT1, CARB and a diacylglycerol acyltransferase, whereas *Cr*HLA8 is co-expressed with NAD-dependent glycerol-3-phosphate dehydrogenase, β-ketoacyl synthase, and 1-acyl-glycerol-3-phosphate acyltransferase genes. It is possible that these membrane-associated TR will

orchestrate the transcriptional response of *E. oleoabundans* to N deprivation in order to control the phenotypic transition into lipid accumulation.

This work unveils the high complexity of the N stress response, comprising diverse biological processes: from ultrastructural changes to membrane remodeling, signaling, redox homeostasis and metabolic regulation. Therefore, not only the neutral lipids accumulated in the LD but multiple membrane components at specific subcellular locations, play key roles in the integration and tight coordination of this cellular response. The novel findings on the metabolism of *N*-containing glycerolipids in the green microalga *E. oleoabundans*, pinpoint that lipid metabolism does not only result into changes in the membrane composition during N deprivation, but that it may contribute to the integration of the stress response by modulating the SAM/SAH turnover, likely impacting the redox status of the cell.

5.4. Materials and methods

5.4.1. Microalgae strains, culture conditions and cell growth analysis

Ettlia oleoabundans (taxonomic synonym of *Neochloris oleoabundans*) UTEX 1185 was grown under phototrophic conditions in 2.8-L Fernbach glass flasks with a working volume of 40%, using modified Bold's Basal Media (mBBM) (Garibay-Hernández et al., 2013). Axenic cultures with an initial cell concentration of 1-2 x 10^6 cells mL^{-1} were maintained for 7 d at 25±0.5°C, under continuous orbital agitation (300 rpm), and white fluorescent light illumination (100 µE m^{-2} s^{-1}). To evaluate N sufficiency or N deprivation conditions, 7-d cultures were individually centrifuged (10 min, 10,000 *g*, 4°C), washed once with 200 mL of N-free mBBM, and resuspended in 1.12 L of either standard (2.94 mM $NaNO_3$) or N-free mBBM. The resuspended cells were transferred into Fernbach flasks with an initial cell concentration of 10-15 x 10^6 cells mL^{-1} and maintained over 4 d under the aforementioned conditions.

Microalgal growth was analyzed in terms of dry weight, chlorophyll and cell concentrations, as described in Garibay-Hernández et al. (2013). Briefly, cell concentration was determined by direct microscopic cell count using a Neubauer chamber. Dry weight (biomass) concentration was measured gravimetrically by filtering 10 mL of microalgal culture through previously tared nylon filters (47 mm diameter; 0.45 µm pore size), which

were then dried at 80°C for 48 h, cooled in a desiccator and weighted. Chlorophyll concentration in microalgal cultures was determined spectrophotometrically according to Pruvost et al. (2009). Culture samples (1.5 mL) were centrifuged (13,000 rpm, 5 min) and the cell pellet was extracted with methanol (1.5 mL) for 30 min in the dark at 45°C. The extracts were centrifuged and the absorbance values ($A_{Wavelength}$) of the supernatant were collected at 652, 665 and 750 nm. Chlorophyll concentration was calculated based on the equations: Chlorophyll *a* (μg mL^{-1}) = 16.5169 A_{665} - 8.0962 A_{652} - A_{750}; Chlorophyll *b* (μg mL^{-1}) = 27.4405 A_{652} – 12.1688 A_{665} - A_{750}; Total chlorophyll (μg mL^{-1}) = chlorophyll *a* + chlorophyll *b*. Biomass (cell mass) and chlorophyll content on a per cell basis were calculated dividing these values by the corresponding cell concentration.

Cultures were tested for the absence of bacteria in glucose-free Luria broth agar (1.5% w/v) medium plates (Bertani, 1951), incubated at 37°C for at least 24 h.

5.4.2. Microsomal membranes and LD isolation

Microsomal membrane isolation from *E. oleoabundans* cultures (1.12 L) under N sufficiency and N deprivation conditions was performed as described by Garibay-Hernández et al. (2017).

LD were isolated from N-deprived cultures by sucrose gradient flotation. All steps were performed at 4°C. Cells were harvested by centrifugation (10,000 *g*, 10 min) and resuspended in 2.5 mL of lysis medium (20 mM tricine, 300 mM sucrose pH 7.8, 1 mM phenylmethylsulfonyl fluoride, 2 mM dithiothreitol). Cells were ruptured by passing the cell suspension five times through a French press (Thermo Spectronic; model FA-078) at 20 k.p.s.i. using a mini pressure cell. The cell homogenate was brought to a final volume of 20 mL with lysis medium and centrifuged (10,000 *g*, 20 min); the pellet was discarded. In a new tube, the sucrose gradient was prepared: the supernatant (20 mL) was overlaid with 5 mL of buffer 2 (20 mM tricine, 150 mM sucrose pH 7.8, 2 mM dithiothreitol), followed by 5 mL of flotation buffer (20 mM HEPES, 100 mM KCl, 2 mM $MgCl_2$, 2 mM dithiothreitol). The sucrose gradient was centrifuged at 100,000 *g* for 1 h (Beckman SW40 Ti swinging-bucket rotor, L8-M ultracentrifuge). LD floating in the upper gradient were carefully collected with a syringe, transferred into a 1.5-mL Eppendorf tube and centrifuged (14,000 rpm, 10 min). The floating LD were concentrated by carefully removing the underlying liquid with a syringe. To wash the LD suspension, it was diluted with flotation buffer to a final volume of 500 μL and centrifuged (14,000 rpm, 10 min); the underlying liquid was removed. The LD suspension

was washed a second time, but after removal of the underlying liquid, it was resuspended with resuspension buffer (400 mM mannitol, 10% [w/v] glycerol, 6 mM Tris-MES pH 8.0, 2 mM dithiothreitol) to a final volume of 50-250 µL. Samples were frozen in liquid N_2 for storage at -80°C. Chlorophyll contamination of the LD isolated by this method was assessed by comparing their absorption spectra at 430 and 675 nm to that shown by total microsomal membranes from N-sufficient conditions.

5.4.3. FFZE

Microsomal membranes from N-sufficient and N-deprived conditions were fractionated by FFZE as described by Garibay-Hernández et al. (2017), where the methods for monitoring FFZE separation via spectrophotometry and immunoblotting techniques are also described.

5.4.4. Protein concentration measurements

Protein in microsomal and FFZE fractions, as well as in isolated LD, was measured by a modification of the Bradford method (Bradford, 1976) as described in Garibay-Hernández et al., (2017).

5.4.5. TEM

Microalgae cells (50 mL) were harvested and fixed (4% paraformaldehyde and 2.5% glutaraldehyde in 0.16 M cacodylate buffer pH 7.4) for 12 h at 4°C. Cells were centrifuged (3500 rpm, 5 min) and washed with cacodylate buffer at 4°C. Cells were post-fixed with 1% OsO_4 in the dark (1 h, 4°C), and washed twice with cacodylate buffer at 4°C. Samples were dehydrated with increasing concentrations of ethanol (10 min in each concentration: 30%, 50%, 70%, 80%, 96% and 100% -twice-), infiltrated with increasing concentrations of EPON resin, and polymerized at 60°C for 24-48 h in BEEM capsules. Ultrathin sections (60 nm) were generated by using a Leica Ultracut R microtome, post-stained with 2% uranyl acetate and lead citrate 0.3%, and examined using a Carl Zeiss Libra 120 PLUS TEM, operating at 80 kV. Images were recorded on a Gatan CCD camera.

5.4.6. Analysis of LD formation by CFM

Aliquots (12 mL) from N-sufficient and N-deprived cultures were taken at different time points: 0, 1, 3, 6, 9, 12, 24, 48, 72 and 96 h. Cells were harvested (13,000 rpm, 10 min, room temperature –RT-) and resuspended in 3.6 mL of phosphate-buffered saline (PBS, in g L^{-1}: NaCl, 80; KCl, 2; Na_2HPO_4, 14.4; KH_2PO_4, 2.4; pH 7.4). Cells were chemically fixed by adding 0.4 mL of formaldehyde 10% (v/v) and incubated for 15 min at RT. Cells were washed three times (each with 4 mL PBS), resuspended (1.2 mL PBS) and stored in the dark at 4°C prior to staining.

For CFM, fixed cells (250 µL) were stained with 7.5 µL of Nile Red (NR; 5 mM stock in acetone), followed by incubation in the dark (10 min, 37°C). Cells were washed once and resuspended (250 µL PBS). Stained cells (50 µL) were mixed 1:1 (v/v) with 1% (w/v) low-temperature melting point agarose kept at 40°C, applied to the microscope slide and overlaid with a cover slide. Images were acquired with an Olympus FV1000 inverted multiphoton confocal microscope (Upright BX61WI) equipped with a 60X oil immersion objective (UPLSAPO 60X S NA 1.30) using a digital zoom value of three. For neutral lipid-specific detection of NR fluorescence and chlorophyll autofluorescence, the excitation/emission wavelengths were 488/520 and 635/668 nm, respectively. As controls, CFM images from non-stained-fixed cells were acquired at every time point.

The CFM images were processed and analyzed using ImageJ software (Abràmoff et al., 2004). For apparent LD area quantitation, 32-bit maximum projection Z-stacks from the NR acquisition channel were analyzed using the Lipid Droplet Counter plugin. The processing parameters were defined based on the fluorescence of non-stained controls: bandpass: maximal and minimal feature size, 50 and 1, respectively; watershed: x, y and z radius of one, invert option; segment analyzer: area, maximum and connect thresholds, 0.05, 0.3 and 0.9, respectively. The output of every analysis was manually inspected and non-LD areas were removed. LD radiuses were calculated assuming that LD are round.

Microalgal cells were detected in the CFM images based on chlorophyll autofluorescence. Composite images (18-bit), generated by merging the maximum projection Z-stacks from the NR and chlorophyll channels, were used to quantitate the number of LD per cell. The coordinates from every measured LD using the Lipid Droplet Counter were retrieved and transferred into the corresponding composite image and the LD per cell were manually quantified. Cell size (area) was measured by processing these composite images using the ROI (Region Of Interest) manager tool. The cells (ROI) were

defined by transforming the composite into binary images using the Huang threshold (Huang and Wang, 1995).

5.4.7. Lipid extraction

Lipids were extracted from either cells or LD, isolated from N-deprived or N-sufficient cultures. For total cell lipid extraction, cells were harvested (10,000 *g*, 10 min, 4°C) and resuspended in 7 mL of isopropanol with 0.01% (w/v) BHT (butyl hydroxytoluene). For the isolated LD, 1.5 mL of isopropanol with 0.01% (w/v) BHT were added. The resuspended samples were then incubated at 75°C for 15 min to inactivate phospholipases. Afterwards, all steps were performed at 4°C. Each sample was thoroughly homogenized using a glass Teflon homogenizer and transferred into a Teflon tube. The homogenizer was rinsed with one volume (V) of chloroform and one V of methanol; these volumes were pooled with the isopropanol homogenate and combined with 0.8 V of water. The single phase was then combined with one V of chloroform and one V of water, agitated and centrifuged (10,000 *g*, 3 min) to separate the two phases. The lower organic phase was recovered in a new Teflon tube. The remaining aqueous phase was re-extracted two more times, each with one V of chloroform. The lower phase from all extractions were pooled. The lipids comprised in the organic phase were concentrated by vacuum-drying at 40°C and transferred into pre-weighed 2-mL screw-capped glass vials, where they were dried under N_2 flux. The amount of extracted lipids was determined gravimetrically. For storage, lipids were resuspended in chloroform and kept at -80°C.

5.4.8. TLC-based characterization of total lipid composition

Total cell lipid extracts were analyzed on high-performance TLC aluminum sheets (silica gel 60; Merck). Neutral lipids were separated by 1D-TLC using hexane:diethyl ether:acetic acid (70:30:1, by volume) as a mobile phase (Fan et al., 2011). Polar lipids were separated by 2D-TLC using two different solvent systems (Fig. S5.5). In the first system (Benning et al., 1995), silica plates were impregnated with 0.25 M $(NH_4)_2SO_4$ and activated at 120°C (30 min) prior to lipid separation; 1D, chloroform:methanol:water (70:30:5, by volume); 2D, chloroform:acetone:methanol:acetic acid:water (50:20:10:10:5, by volume). In the second system (Vences-Guzmán et al., 2008), lipids were separated on untreated silica plates: 1D, chloroform:methanol:water (70:30:5, by volume); 2D, chloroform:methanol:acetic acid

(65:25:10, by volume). Total lipid extracts from N-deprived and N-sufficient cells were loaded on an equal dry weight basis and visualized by reversible stain with iodine vapor, and by spraying with 50% (v/v) sulfuric acid followed by heating at 120°C. Polar lipids were characterized by staining with diagnostic spray reagents specific for quaternary ammonium groups (Dragendorff's reagent), free amino groups (0.1% w/v ninhydrin in acetone), and sugar residues (2.4% w/v α-naphtol in 10% v/v sulfuric acid, 80% v/v ethanol); when using the latter two reagents, spraying was followed by heating at 120°C.

5.4.9. Profiling of glycerolipid molecular species by ESI-TQ-MS/MS

Polar and neutral glycerolipids were analyzed by ESI-TQ-MS/MS at the Kansas Lipidomics Research Center (KLRC). Dried lipid extracts were dissolved in chloroform and aliquots of 10-20 µL were used for analysis. For polar glycerolipids, precise amounts of phospholipid and galactolipid internal standards obtained and quantified as described by Welti et al. (2002), were added according to Xiao et al. (2010). For DAG and TAG, the internal standards DAG 15:0 (4.64 nmol per sample) and TAG 17:1 (3.1 nmol per sample) were added. The sample and internal standard mixtures were combined with solvents, such that the ratio of chloroform:methanol:300 mM ammonium acetate in water was 300:665:35 (by volume). The final volume was 1.2 mL for most analyses, except for DAG (1.4 mL).

For all the glycerolipids described in this work, except for DGTS, lipid extracts were introduced by continuous infusion into the ESI source of the TQ-MS (API4000/4000QTRAP, Applied Biosystems, or Waters Xevo TQS), by using an autosampler fitted with the required injection loop for the acquisition time and presented to the ESI needle at 30 µL min^{-1}.

The molecular species from the polar glycerolipids PE, PC, LysoPC, PI, PS, PA, PG, LysoPG, MGDG, and DGDG were analyzed according to Xiao et al. (2010). LysoPE, MMPE, LysoMMPE, and DMPE were analyzed as indicated by Bibis et al. (2014). SQDG was measured with the scan described by Welti et al. (2003). The molecular species of these lipids were defined by the presence of a head group detected by sequential precursor and neutral loss scans as follows: PE and LysoPE, $[M+H]^+$, neutral loss of 141.0 (NL141.0); MMPE and LysoMMPE, $[M+H]^+$, NL155.02; DMPE, $[M+H]^+$, NL169.02; PC and lysoPC, $[M+H]^+$, precursors of *m/z* 184.1; PI, $[M+NH_4]^+$, NL277.0; PS, $[M+H]^+$, NL185.0; PA, $[M+NH_4]^+$, NL115.0; PG, $[M+NH_4]^+$, NL189.0; LysoPG, $[M-H]^-$, precursors of *m/z* 152.9; MGDG, $[M+NH_4]^+$, NL179.1; DGDG, $[M+NH_4]^+$, NL341.1; and SQDG, $[M-H]^-$, precursors of *m/z* 225.0. In these analyses, individual FA species were not determined; instead, polar

lipids were identified at the level of class, total number of acyl carbons, and total number of acyl-double bonds. All analyzed polar lipids were quantified in molar amounts by comparison with two polar lipid standards of the same class, except for SQDG, MMPE, LysoMMPE, and DMPE, which were quantified in comparison to internal standards of other classes (LPG 18:0 for SQDG, and PE 24:0 for the others) and are expressed in terms of normalized MS signal, where a signal of one is the same signal as one nmol of standard.

Neutral glycerolipids (DAG and TAG) were detected as $[M+NH_4]^+$ ions by a series of NL scans as described by Li et al. (2014b). The scans targeted losses of FA as neutral ammoniated fragments: NL217.2 (12:0); NL215.2 (12:1); NL245.2 (14:0); NL243.2 (14:1); NL259.2 (15:0, for DAG internal standard); NL273.3 (16:0); NL271.3 (16:1); NL285.3 (17:1, for TAG internal standard); NL301.3 (18:0); NL299.3 (18:1); NL297.3 (18:2); NL295.3 (18:3); NL327.3 (20:1); NL325.3 (20:2); NL323.3 (20:3); NL321.3 (20:4); NL349.3 (22:4); NL347.3 (22:5); and NL345.3 (22:6). The DAG and TAG molecular species were identified by the mass of one FA group and the mass of the intact molecule (i.e. total acyl carbons:total acyl-double bonds), which means that most of neutral glycerolipid species were repetitively analyzed, as they were scanned per each of the FA they contained. In neutral lipids, MS responses vary depending on chain length and double bond number. Here, response corrections were not determined or applied to the neutral glycerolipid data, which were expressed in terms of normalized MS signal, in comparison to the indicated internal standard.

The molecular species of the betaine lipid DGTS were profiled using a Xevo TQ-S MS (Waters Corporation) equipped with an ESI source operating in direct-infusion mode. Samples were prepared with internal standard mixtures for polar glycerolipids and combined with solvents as described above. Samples were injected into a 300-µl PEEK sample loop with a 2777 autosampler (Waters Corporation). The injection volume was set at 400 µl. The sample in the loop was infused to the MS with an Acquity pump (Waters Corporation). Data for DGTS (precursor of *m/z* 236.0; collision energy 30) and PC (precursor of *m/z* 184.1; collision energy 28) were acquired to express DGTS abundance in terms of PC. The settings of the Xevo TQ-S MS were: capillary voltage, ±2.8 kV; source offset voltage, ±30.0 V; cone voltage, ±40.0 V; source temperature, 150°C; desolvation temperature, 250°C; cone gas flow, 150 L h^{-1}; desolvation gas flow, 650 L h^{-1}; collision gas flow, 0.14 mL min^{-1}; nebulizer gas pressure, 7 bar; low mass 1 and 2 resolution, 2.5; high mass 1 and 2 resolution, 14.5; ion energy 1 and 2, 1.0.

For data processing, the background of each spectrum was subtracted, the data were smoothed, peak areas integrated, and data exported as peak lists. The LipidomeDB Data Calculation Environment (Zhou et al., 2011b) was used to locate target compound peak data, deconvolute isotopes, and quantify lipids in each class in comparison with internal standards. Correction for chemical and/or instrumental noise was performed as described by Xiao et al. (2010). The data were corrected for the fraction of the sample analyzed and when required, normalized to the sample dry weight. Statistical analyses were performed through unpaired two-tailed Student's *t*-test.

5.4.10. Quadrupole Time-Of-Flight (QTOF) MS for identification of DGTS

The identification of DGTS was performed at the KLRC. Dried lipid extracts were dissolved in chloroform and 20 µl aliquots of the pooled samples were combined with solvents such that the ratio of chloroform:methanol:300 mM ammonium acetate in water was 300:665:35 (by volume). Spectra were acquired on a QStar Elite hybrid QTOF-MS (Sciex/Applied Biosystems). Samples were introduced by continuous infusion into the ESI source at a rate of 30 µl min^{-1} using an integrated Harvard syringe pump. The MS/MS product ion scans were carried out with individual fragmentation of $[M+H]^+$ ions from intact DGTS species that were detected in the TQ-MS precursor scans. The QTOF-MS/MS settings were: ion spray voltage: 5.0 kV; source temperature: 150°C; curtain gas: 25 (arbitrary units); ion source gases: 20 and 30 (arbitrary units); declustering potential: 80 V; declustering potential 2: 15 V; focusing potential: 300 V; collision gas (N_2): 3 (arbitrary units); collision energy: 50 V. Data were collected over the range of *m/z* 50 to 1000, resulting in 300-600 cumulative scans during acquisition for 5-10 min. Data were collected and smoothed using the Analyst QS 2.0 software. Resultant positive ion fragments were identified and formulas determined. Accurate masses of the product ions were determined to ten thousandths of a mass unit.

5.4.11. *In vivo* lipid labeling with [^{14}C]acetate

Microalgal cultures were prepared from 100-mL pre-cultures with a final cell density of 3 x 10^7 cells/mL, grown for 4 d in mBBM (40% working volume), under the phototrophic conditions described in 5.4.1. Cells were harvested (10,000 *g*, 10 min, 4°C), washed with 25 mL of N-free mBBM, and resuspended to a final concentration of 3 x 10^7 cells mL^{-1} in mBBM or N-free mBBM, for N-sufficient or N-deprived conditions, respectively. Two-mL cultures

were labeled with 2 µCi [1-^{14}C]acetate (1 µCi mL^{-1}; 55 mCi mmol^{-1}) and incubated for 48 h. During this period, 200 µL aliquots were taken at different time points (0, 5, 15, 30 min, 1, 2, 4, 8, 24 and 48 h). Cells were harvested (14,000 *g*, 10 min, RT) and resuspended in 100 µL of water for further lipid extraction. Aliquots (5 µL) from the supernatant were collected for radioactivity incorporation measurements.

Lipids were extracted according to Bligh and Dyer (1959). Briefly, 375 µL of methanol:chloroform (2:1, by volume) were added to the water-resuspended cells and mixed. The supernatant was recovered by centrifugation (14,000 *g*, 5 min, RT) and combined with water (125 µL) and chloroform (125 µL). After mixing, the lower organic phase was recovered by centrifugation (14,000 *g*, 5 min, RT) and dried. Dried lipids were resuspended in 20 µL of methanol:chloroform (1:1, by volume) and stored at -20°C for further analysis.

Radioactive label incorporation was determined by quantification in both the supernatant (5 µL) and extracted lipids (5 µL) through liquid scintillation counting (Beckman Coulter LS 65000 Liquid Scintillation Counter). Lipid extracts (5 µL) were analyzed by 1D-TLC on high-performance TLC aluminum sheets (silica gel 60; Merck) using chloroform:methanol:acetic acid (130:50:20, by volume) as a mobile phase (Sahonero-Canavesi et al., 2015). For the analysis of PE methylated derivatives, *n*-propyl alcohol:propionic acid:chloroform:water (75:50:50:25, by volume) was employed as the mobile phase (de Rudder et al., 1997). Radioactive-labeled lipids were visualized using a Phosphor-Imager (Storm 820; Molecular Dynamics) and quantified with the software ImageQuant TL (Amersham Biosciences). In addition to [1-^{14}C]acetate, labeling experiments were performed with [U-^{14}C]glycerol (0.5 µCi mL^{-1}; 143 mCi mmol^{-1}) and L-[*methyl*-^{14}C]methionine (1 µCi mL^{-1}; 55 mCi mmol^{-1}), however only negligible incorporation of these substrates was observed.

5.4.12. Phospholipid methyltransferase activity

To measure the phospholipid methyltransferase activity, endogenous PE was isolated via preparative TLC. Microalgal cells were grown in 100 mL of mBBM for 5 d under the phototrophic conditions described in 5.4.1. After harvesting (10,000 *g*, 10 min, 4°C), total lipids were extracted as described by Bligh and Dyer (1959). Concentrated lipid extracts were separated by 1D-TLC on high-performance TLC aluminum sheets (silica gel 60; Merck) using chloroform:methanol:acetic acid (130:50:20, by volume) as a mobile phase

(Sahonero-Canavesi et al., 2015). Iodine-stained material, positive to ninhydrin staining and with a relative mobility corresponding to PE, was scraped from the TLC plate and the lipids were extracted according to Bligh and Dyer (1959). To reduce the presence of non-PE lipids, the PE-enriched lipid extract was separated a second time using the same 1D-TLC system, and the material corresponding to PE was isolated as described above. The purified PE was dried with N_2 flux and quantified gravimetrically. PE was resuspended in chloroform:methanol 1:1 (by volume) to a concentration of 10 µg μL^{-1}.

Microsomes from N-sufficient and N-deprived *E. oleoabundans*, as well as LD isolated from the latter, were tested for phospholipid *N*-methyltransferase activity in the presence of endogenous PE and *S*-adenosyl-L-[*methyl-^{14}C*]methionine based on de Rudder et al. (1997). The reaction mixture contained 100 µg of endogenous PE, 12 nCi of *S*-adenosyl-L-[*methyl-^{14}C*]methionine (58 nCi $nmol^{-1}$), 0.2% (v/v) Triton X-100 (final concentration) and 90 µg of protein (either from microsomes or LD) in 100 mM Tris-HCl (pH 8.0), in a total volume of 180 µL. The mixtures were incubated for 4 h in a 28°C water bath, and the reactions were stopped by addition of 750 µL ice-cold chloroform:methanol 2:1 (by volume). Lipids were extracted as described by Bligh and Dyer (1959). Dried lipids were resuspended in 20 µL of methanol:chloroform (1:1, by volume) and stored at -20°C for further analysis. The 1D-TLC separation for analysis of PE methylated derivatives and the visualization of radioactive-labeled lipids was performed as described in the previous section.

5.4.13. Quantitative label-free shotgun proteomics

Total microsomes (100 µg protein per sample) from four independent biological replicates of 4-d cultures under N deprivation and N sufficiency conditions were analyzed using liquid chromatography (LC)-MS/MS using an Easy-nanoLC II system (Proxeon Biosystems) coupled to a linear trap quadrupole orbitrap Velos hybrid MS (ThermoFisher Scientific). Sample preparation and LC-MS/MS analyses were performed at the proteomics discovery platform of the Institut de Recherches Cliniques de Montréal as previously described (Garibay-Hernández et al., 2017).

The generation of peak list files and product ion search against the Viridiplantae protein database (TaxID 33090, unknown version; 677,107 entries) merged with the *E. oleoabundans* protein database (unknown version; 53,921 entries) were performed as described by Garibay-Hernández et al. (2017). Validation of MS/MS-based peptide and

protein identifications was carried out with Scaffold 4.3.4 (Proteome Software) according to Garibay-Hernández et al. (2017).

Scaffold 4.3.4 (Proteome Software) was employed for label-free relative quantitation using five methods: WSpC, emPAI, NSAF, Top3 PI, and Top3 TIC. Data were normalized at the sample level, which means that the sum of the selected quantitative value for all the proteins within each sample was adjusted to a common value. The significance of relative quantification by each method was evaluated through Student's *t*-tests with a *p*-value threshold ≤ 0.05. All statistically significant FC (ratio of N–deprived relative to N-sufficient conditions) were either ≥ 1.2 or ≤ 0.83; hence, these were established as FC thresholds (Fig. S5.8). Only statistical-significant proteins detected by at least two unique peptides in not less than three out of four biological replicates from either N-depleted or N-sufficient conditions were considered as responsive.

The ClustVis web tool (Metsalu and Vilo, 2015) was used for multivariate PCA. The quantitative data from each of the five label-free approaches was analyzed by PCA using individual data matrices of 619 x 8 (619 proteins with their corresponding quantitative values in every biological replicate, four per tested condition). To explore the quantitative data from all five label-free approaches together and their relationship with both N availability conditions, a single data matrix of 610 x 40 (AllData) was also analyzed by PCA. For multivariate analysis, quantitative data were pretreated as follows: WSpC, glog-transformed/non-scaled; emPAI, non-transformed/variance-scaled; NSAF, non-transformed/Pareto-scaled; Top3 PI, glog-transformed/non-scaled; Top3 TIC, glog-transformed/non-scaled; AllData, glog-transformed/non-scaled. When required, generalized log (glog) data transformation was done before analysis in ClustVis; $glog = \log[(x + \sqrt{(x\text{^}2 + 1)})/2]$ (where *x* is protein quantitative value). Singular Value Decomposition (SVD) with imputation was used to calculate principal components.

5.4.14. Protein functional annotation

Annotations for proteins responsive to N deprivation were retrieved from Garibay-Hernández et al. (2017) and manually curated to include recent updates. A detailed description of these proteins according to their biological process is provided in Table S5.2, where data corresponding to their transcriptional regulation according to Rismani-Yazdi et al. (2012) is also indicated.

5.5. Acknowledgements

MS-based lipid analyses were performed at the KLRC, where instrument acquisition and method development was supported by NSF grants MCB 0455318 and 0920663 and DBI 0521587, and NSF EPSCoR grant EPS-0236913 with matching support from the State of Kansas through Kansas Technology Enterprise Corporation and Kansas State University. The KLRC is also supported by K-INBRE (NIH Grant P20 RR16475 from the INBRE program of the National Center for Research Resources). The protein LC-MS/MS analysis was carried out at the Institut de Recherches Cliniques de Montréal-Proteomics Discovery Platform with the support of Dr. Denis Faubert and Marguerite Boulos. We thank Dr. Guadalupe Trinidad Zavala for her support with TEM at the Universidad Nacional Autónoma de México (UNAM); Dr. Arturo Pimentel for his support on image analysis and, together with Andrés Saralegui, for their support with CFM at the National Laboratory of Advanced Microscopy-UNAM. M. Guadalupe Muñoz García is also acknowledged for technical assistance. Special thanks to Dr. Ruth Welti (KRLC) for stimulating discussions regarding the lipidomic analysis of microalgae.

5.6. Supplemental data

Supplemental material is provided in Appendix B.

6. General discussion

During the last ten years, interest in the use of microalgae to produce value-added compounds from their acyl-lipids has triggered intensive research on algal lipid metabolism, focusing on the identification of factors involved in TAG metabolism, on the subcellular organization of lipid pathways, and on the interactions between organelles. Most of this research has been performed in a few model algal species, mostly the green microalga *Chlamydomonas reinhardtii*, but also in the marine diatom *Phaeodactylum tricornutum* and species of the brown algae-related genus *Nannochloropsis* (Li-Beisson et al., 2019). After an overall survey of the data provided by omics approaches in recent years, it is still assumed that lipid metabolism pathways identified in higher plants are followed in eukaryotic algae. It should be noted though, that just for few putative lipid metabolism homologues, their enzymatic activity, regulatory mechanisms, or their subcellular localization, have been experimentally verified (Li-Beisson et al., 2019). Moreover, the significant advances in microalgal lipid research are not always relevant to all microalgae species, given their polyphyletic origin that is manifested in their diverse and complex lipid biochemistry (Guschina and Harwood, 2006; Li-Beisson et al., 2019).

Part of this knowledge gap requires to be addressed by species-specific approaches, highlighting the relevance of the study described herein. The present work provides compelling evidence, which supports the taxonomical reclassification of *Ettlia oleoabundans* within the *Chlorellales* lineage of the Trebouxiophyceae class of green microalgae, rather than in the Chlorophyceae class, where it was previously classified (Garibay-Hernández et al., 2017). This finding will influence the identification of gene homologs, data curation and the interpretation of the physiology of this microalga, since it belongs to a different taxonomical class than that of the model *C. reinhardtii* (class Chlorophyceae).

The present study has enabled a detailed description of the cellular processes occurring on the membranes of *E. oleoabundans* under N deprivation (Garibay-Hernández et al., 2017). These include photosynthesis, oxidative phosphorylation, and carbon metabolism, with a particular focus on inorganic carbon acquisition and assimilation, glycolysis, starch synthesis and acyl-lipid metabolism. Using a subcellular approach, the compartmentalization of the carbon metabolism was addressed, together with the subcellular location of particular proteins of interest. Future analysis of the individual membrane fractions isolated in this work by targeting proteins involved in specific processes (*e.g.* lipid metabolism), will undoubtedly give further insights into their compartmentalization

within specific membrane domains and/or organelles, and their interactions with other cellular processes. The focus employed in this work enabled the identification of N deprivation response components common to eukaryotic phototrophs and revealed novel aspects of the physiology of this microalga. These include the identification of membrane proteins previously considered exclusive to higher photosynthetic organisms, proteins displaying a novel architecture, and new roles played by N-containing glycerolipids in the N stress response.

Based on results obtained from this study and current literature, a tentative working model is postulated. Five events are proposed, not necessarily occurring in sequence, which lead or support lipid accumulation in N-deprived *E. oleoabundans* (**Figure 6.1**): (1) fine-tuning of photosynthesis and adjustment of ATP/NADPH ratios; (2) chloroplast membrane remodeling, plastid reactive oxygen species (ROS) production and induction of autophagy; (3) regulation of lipid metabolism at the acyl-lipid level (*de novo* FA biosynthesis and catabolism); (4) remodeling of extrachloroplastic lipids supported by the induction of *S*-adenosyl-L-methionine (SAM)-dependent glycerolipid *N*-methylation; and (5) interorganellar redox-mediated coordination of the cellular response to N stress. The evidence supporting these events is provided below.

(1) Fine-tuning of photosynthetic electron transport and CO_2 fixation in response to N deprivation

To withstand the sudden removal of N, *E. oleoabundans* must adjust its photosynthetic machinery to alleviate the detrimental effects of excess light (Erickson et al., 2015). The changes observed in photosynthesis-related proteins (**Chapter 5**) support the activation of early photoprotective mechanisms involved in energy thermal dissipation (non-photochemical quenching: NPQ) and alternative electron transport, as well as in the activation of mechanisms to cope with ROS, repair of the reaction centers, and regulation of their stoichiometry. The adjustment of the photosynthetic electron transport chain results in the re-equilibration of the NADPH/ATP ratio, which must be tightly coordinated to downstream metabolic reactions of CO_2 assimilation (Erickson et al., 2015). In N-deprived microalgae, it has often been thought that diversion of the carbon supply towards storage compounds (starch, but mainly TAG) acts as an electron sink to accommodate an over-reduced chloroplast (Hu et al., 2008; Li-Beisson et al., 2019). During N depletion under phototrophic conditions, *E. oleoabundans* showed higher carbon fixation on a per cell basis

together with an increased lipid content (**Chapter 5**). This result agrees with a recent study in *C. reinhardtii* that underscores the need to expand the prevalent “electron sink” hypothesis: an increased photosynthetic carbon fixation, rather than only the diversion of the carbon flux towards storage compounds, prevents the oxidative damage of the chloroplast by using the reducing equivalents and ATP provided by the photosynthetic electron transport chain (Du et al., 2018).

In this context, a question remains open. How can N-deprived microalgae cells show an increase in CO_2 fixation despite having a reduced photosynthetic efficiency? The activation of photoprotection strategies that initially lower the light-harvesting capacity of photosystem II (PSII), is considered to reduce an organism’s overall photosynthetic efficiency (Erickson *et al.*, 2015; Tian et al., 2019), defined as the fraction of light energy fixed as chemical energy (Wijffels, 2008). In line with this, lower efficiencies in light utilization (*i.e.* decreased PSII maximum quantum yields) are characteristic of N-deprived microalgae, including *E. oleoabundans* (Benvenuti et al., 2015). Despite showing an altered chloroplast ultrastructure, the preservation of the pyrenoid tubules (**Chapter 5**) shows the relevance of maintaining the photosynthetic carbon and ATP supply in N-deprived cells, which eventually results on the accumulation of storage compounds. A detailed analysis of the mechanisms fine-tuning the photochemical reactions upon N deprivation might provide the first molecular insights into the link between photosynthetic efficiency and lipid accumulation.

Performing a comprehensive study on the unequal distribution of PSBS (PSII Subunit S) and LHCSR (Light Harvesting Complex-like protein Stress Related) within microalgae species already provides an exciting starting point. The PSBS and LHCSR proteins trigger the pH-regulated activation of NPQ (the first, mainly in vascular plants, the latter, mostly in lower eukaryotic photrotrophs), but through different molecular mechanisms (Niyogi and Truong, 2013). Recent studies show that the PSBS protein is present in *C. reinhardtii* but only transiently and in very low abundance (Correa-Galvis et al., 2016; Tibiletti et al., 2016), and that NPQ activation relies on the LHCSR proteins (Tian et al., 2019). In contrast, the results from this work question the conservation of NPQ mechanisms in microalgae, as PSBS was abundant in *E. oleoabundans* membranes, whereas neither the protein product nor the transcript of a LHCSR homolog were detected (**Chapter 4**). The identification of these mechanistic differences underlying the fine-tuning of photosynthesis between microalgae species will help in understanding the molecular basis behind their contrasting photosynthetic activities and hence, lipid productivities, that have been observed during N starvation (Benvenuti et al., 2015).

(2) N deprivation induces chloroplast membrane remodeling and may trigger ROS-mediated autophagy

To withstand N deprivation, not only the photosynthetic electron flow and CO_2 fixation are adjusted in *E. oleoabundans* cells, but their chloroplast membranes are remodeled as well. As described in **Chapter 5**, membrane remodeling is indicated by the ultrastructural alterations observed through transmission electron microscopy, by the differences in electrophoretic mobility of the chloroplast membranes, and by the changes in their protein and lipid components. Upon N stress, changes in the major galactolipids were reflected in lower MGDG/DGDG ratios, thought to stabilize chloroplast membranes by preventing the formation of non-bilayer phases and bilayer rupture (Demé et al., 2014). This agrees with recent results in *C. reinhardtii* where MGDG turnover by the specific lipase PGD1 (Plastid Galactoglycerolipid Degradation1) adjusts the thylakoid membrane composition, protecting the chloroplast against oxidative stress upon N deprivation (Du et al., 2018). Whether lower MGDG levels in N-starved *E. oleoabundans* are due to a decreased MGDG synthesis, as recently suggested by downregulation of the MGDG synthase in this microalga (Sturme et al., 2018), and/or due to a higher MGDG turnover, remains to be determined.

The lower abundance of the sole chloroplast-synthesized phospholipid, PG (**Chapter 5**), may also influence chloroplast ultrastructure and function under N stress, as it has proven indispensable for photosynthetic function (Nakamura and Li-Beisson, 2015). Short-term labeling dynamics additionally suggest a role for PG in editing/cycling nascent FA, probably through a mechanism similar to that lead by PLP1 (Plastid Lipase1) in *A. thaliana*'s developing embryos (Wang et al., 2017).

Despite showing different glycerolipid specificities, *At*PLIP1 shares a close similarity to *Cr*PGD1 (31% identity; Clustal Omega). Thus, it is not surprising that the same three candidate sequences (m.370664, m.241306, m.370683) are retrieved from the *E. oleoabundans in silico* protein database (**Chapter 4**), when using either *At*PLIP1 or *Cr*PGD1 as bait. The three retrieved putative proteins have predicted N-terminal chloroplast transit peptides (22 amino acids; PredAlgo), comprise the conserved catalytic triad Ser-Asp-His typical for α/β-hydrolases (IPR029058; InterPro), and all of them share 43% sequence identity with *Cr*PGD1, and 33% with *At*PLIP1. Their protein products however, were not detected in *E. oleoabundans* membranes and, contrary to *Cr*PGD1 (Du et al., 2018), their corresponding transcripts are downregulated more than two-fold during N deprivation according to Rismani-Yazdi et al., 2012. A detailed analysis of the biochemical activity and physiological function of these candidate plastidic lipases in *E. oleoabundans* will

undoubtedly provide molecular insights into chloroplast membrane remodeling and its relevance during abiotic stress.

As discussed in **Chapter 5**, although photoprotective strategies are triggered upon N deprivation, an increase in chloroplastic ROS production may not be completely avoided, as suggested by the higher abundance of plastid proteins involved in ROS scavenging and signaling, and proteins thought to cope with chloroplast membrane stress. Within these, a glutaredoxin and a 2-cys peroxiredoxin proteins were increased, which are central to the two main chloroplastic ROS detoxification/signaling systems, the ascorbate/glutathione (Meyer et al., 2007; Foyer and Noctor, 2011) and the 2-cys peroxiredoxin/thioredoxin system (Vaseghi et al., 2018), respectively. Considering recent evidence in *C. reinhardtii* (Du et al., 2018; Heredia-Martínez et al., 2018), the outcomes from this work (**Chapter 5**) suggest a link between chloroplast membrane remodeling, plastid ROS production, and induction of an autophagic process. In addition to the glycerolipid turnover discussed above, this link is supported by changes in chloroplastic proteins that have been related to ROS-mediated cell death induction in land plants, and the identification of *bona fide* autophagy markers in N-deprived *E. oleoabundans*. These markers include the decrease in the ribosomal protein RPL37, which is specifically degraded via autophagy in N-deprived *C. reinhardtii* cells (Couso et al., 2018), and the transcriptional upregulation of AuTophaGy-related (ATG) components of the ubiquitin-like conjugation machinery (Rismani-Yazdi et al., 2012). Moreover, a study already indicates that autophagy might be required for the deposition of lipid droplets (LD) in N-starved *C. reinhardtii* (Couso et al., 2018).

Autophagy is a major catabolic process that allows eukaryotic cells to recycle unneeded or damaged material to maintain cellular homeostasis. This intracellular highly dynamic process is visualized as a sequence of membrane-dependent events, characterized by the formation of double-membrane vesicles called autophagosomes, which engulf and deliver the cargo to an endolytic compartment (Bozkhov, 2018; Couso et al., 2018). The plant-specific mechanisms and functions involved in autophagy are hotly debated, and fundamental questions remain to be addressed: for example, the conservation of autophagy mechanisms in phototrophs when compared to yeast and animals; the extent to which autophagy is critical in cell resource management and the balance between cell survival and death; the direct participation of autophagy in the turnover of lipid stores; and the crosstalk between autophagy and photosynthesis (Bozkhov, 2018). Dissection of the link within chloroplast membranes, ROS and autophagy, indicated by studies in N-deprived microalgae, including this work, give exciting insights into the current challenges in the field

of autophagy in eukaryotic phototrophs. The N deprivation-responsive chloroplast membrane-remodeling GTPase, FZL (FuZzy onions-Like), which was shown to be involved in chloroplast morphology and cell death in *A. thaliana* (Tremblay et al., 2016), is a good candidate for studying this process. Recent characterization of the FZL homolog in *C. reinhardtii* highlighted the relevance of this dynamin-related-protein for microalgal chloroplast morphology (Findinier et al., 2019).

(3) Induction of lipid metabolism at the acyl-lipid level

Upon N deprivation, coupling higher photosynthetic CO_2 fixation to downstream metabolic reactions, results in the accumulation of storage compounds in *E. oleoabundans*. This work shows that these compounds primarily take the form of neutral glycerolipids (DAG, TAG), but also there is some accumulation of starch (**Chapter 5**). The quantitative analysis of the starch and lipid metabolism proteins identified in *E. oleoabundans* membranes (**Chapter 4**), showed that the former were not responsive, whereas the latter were increased during N deprivation (**Chapter 5**). This supports the preferential accumulation of lipids in N-deprived *E. oleoabundans*, with starch serving as a transient reserve compound (Breuer et al., 2012; Garibay-Hernández et al., 2013; Sturme et al., 2018). The increased transcription of the sucrose non-fermenting-related kinase 1 (SnRK1) homolog in this N-deprived microalga (Rismani-Yazdi et al., 2012; Sturme et al., 2018), suggests it may play a key role in the regulation of carbon partitioning. The SnRK1 kinase is an evolutionarily conserved key regulator of cellular metabolism during starvation, stress and growth-promoting conditions, whose role as a master regulator of energy signaling in land plants is well-known (Nukarinen et al, 2016; Wurzinger et al., 2018), but whose function in microalgae remains to be characterized (Colina et al., 2019). Accordingly, the mechanisms controlling the carbon allocation ratios between carbohydrate and lipid reserves in microalgae, which are species-dependent (*e.g.* starch is the predominant storage compound in *C. reinhardtii*, whereas lipids are in *E. oleoabundans*), are not fully understood. It has been proposed that stressed microalgae synthesize TAG whenever the carbon supply outstrips the starch synthesis capacity, where the size of the starch pool would then define lipid accumulation. Current evidence though, indicates that this interplay is beyond the mere competition for carbon allocation, likely also relying on complex interactions with the changing levels of ATP and reducing equivalents (Li-Beisson et al., 2019). Thus, once again, understanding the diversity of photosynthesis fine-tuning mechanisms within microalgae species may provide the key to understand their contrasting carbon allocation preferences.

Altogether, this work shows that upon N deprivation, lipid metabolism is induced at the acyl-lipid level via enhanced production of chloroplastic acetyl-CoA, followed by a higher ATP-dependent activation of *de novo* synthesized FA by long chain acyl-CoA synthetases. An increase in lipid transport and an active FA catabolism upon N deprivation are also indicated. As discussed in **Chapter 5**, these results are partially supported by the transcriptomic analysis of N-deprived *E. oleoabundans* performed by Rismani-Yazdi et al., 2012, whose main findings are consistent with a recent time-series transcriptomic analysis (Sturme et al., 2018). Increased synthesis of acetyl-CoA and activation of FA are also supported by transcriptional data. However, the abundance of proteins directly involved in *de novo* FA and glycerolipid synthesis (*e.g.* acetyl-CoA carboxylase subunits, FA synthetase complex components, glycerol acyltransferases) remained unchanged in *E. oleoabundans* membranes, though they have shown to be transcriptionally upregulated. Contrary to the transcriptional downregulation of FA catabolism indicated by Rismani-Yazdi et al., 2012, the membrane proteomics data suggest an active β-oxidation pathway.

Compared to the current literature, these results pinpoint two processes whose roles in microalgae lipid metabolism have remained overlooked: (1) the influence of an increased FA synthesis and activation as a driving force for their membrane export and interorganellar traffic; and, (2) the effect of an active FA β-oxidation on lipid accumulation in N-deprived microalgae. In line with this, recent evidence demonstrated the existence of a peroxisomal pathway for FA degradation in *C. reinhardtii* (Kong et al., 2017), which proved necessary for coping with N deprivation (Kong et al., 2018).

This work also indicates that the modulation of LD dynamics, probably by structural proteins such as the green alga lineage-specific Major Lipid Droplet Protein (MLDP), and the metabolism of the polar lipids comprising the LD monolayer, are relevant for lipid accumulation. In recent years, research on the composition, formation and function of microalgal LD, with special focus on MLDP, has been performed (Goold et al., 2015). Nevertheless, the dynamics and functions of these organelles, as well as the specific role played by MLDP, are not clear yet. In *E. oleoabundans*, the first insights into these discrete organelles are provided by this work, and thus, further research is needed.

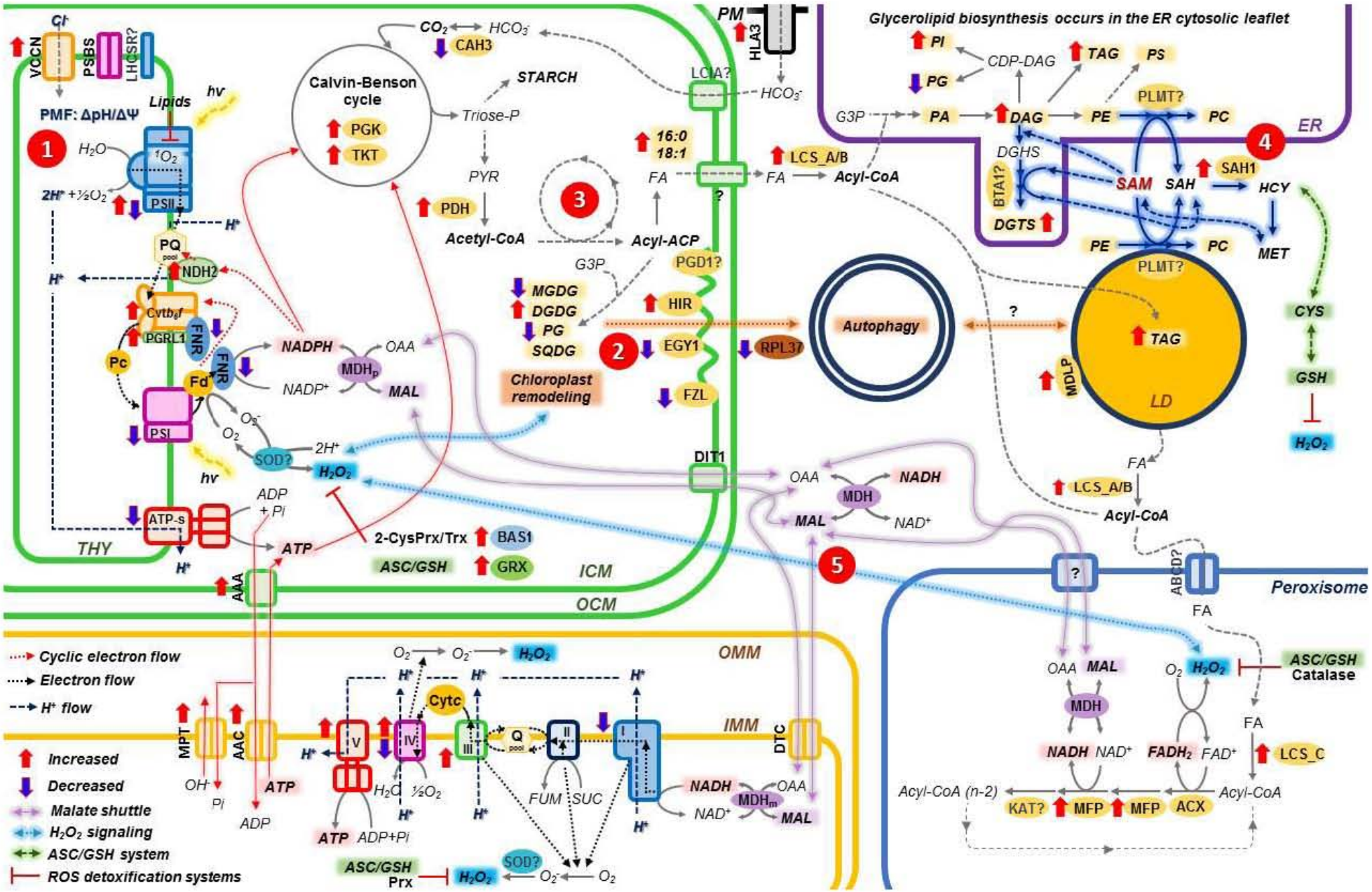
Glycerolipid biosynthesis occurs in the ER cytosolic leaflet
Calvin-Benson cycle
PMF: ΔpH/ΔΨ
Lipids
STARCH
Triose-P
PYR
Acetyl-CoA
Acyl-ACP
Acyl-CoA
CDP-DAG
PA
DAG
PE
PC
PS
PI
PG
TAG
PLMT?
SAM
SAH
SAH1
HCY
MET
CYS
GSH
DGHS
BTA1?
DGTS
ER
LD
MDLP
Autophagy
Chloroplast remodeling
MGDG
DGDG
PG
SQDG
HIR
EGY1
FZL
RPL37
PGD1?
NADPH
NADP+
OAA
MAL
MDH
NADH
Peroxisome
ABCD?
LCS_A/B
LCS_C
ACX
MFP
KAT?
FADH2
FAD+
Acyl-CoA (n-2)
ASC/GSH
Catalase
2-CysPrx/Trx
BAS1
GRX
SOD?
DIT1
HLA3
LCIA?
CAH3
PGK
TKT
PDH
NDH2
PQ
Cytb6f
PGRL1
FNR
Fd
PSI
PSII
Pc
VCCN
PSBS
LHCSR?
ATP-s
THY
ICM
OCM
OMM
IMM
MPT
AAC
DTC
Cytc
Q pool
FUM
SUC
Prx
Cyclic electron flow
Electron flow
H+ flow
Increased
Decreased
Malate shuttle
H2O2 signaling
ASC/GSH system
ROS detoxification systems

Figure 6.1. Tentative model of events related to lipid accumulation occurring in N-deprived *E. oleoabundans*. A complex response accompanies lipid accumulation in N-deprived *E.oleoabundans*. Five different major events are proposed to occur (not necessarily occurring in sequence). **(1)** After N starvation, fine-tuning of photosynthesis occurs to reduce photooxidative damage. **(2)** Plastid ROS-scavenging/signaling systems are active and accompanied by changes in the chloroplast membrane composition. These may trigger an autophagic flux. **(3)** Increased CO_2 fixation results in higher production of acetyl-CoA channeled towards *de novo* synthesis of FA. Lipid metabolism is regulated at the acyl-lipid level (biosynthesis and catabolism) and by LD dynamics. **(4)** Changes in membrane glycerolipids are accompanied by an increased SAM-dependent glycerolipid *N*-methylation, resulting in a higher SAM turnover. **(5)** A redox-based interorganellar communication might coordinate the response to N deprivation.

The glycerolipids and the proteins identified in this work, which are relevant for the model, are indicated. Question marks pinpoint proteins that were not identified, but whose corresponding transcripts are present in the microalga with exception of ABCD, KAT, LCIA, LHCSR, SOD. The quantified changes in membrane components (membrane proteins, lipids) are indicated with arrows. Compound (italics) abbreviations: ASC, ascorbate; CDP, cytidine diphosphate; CYS, cysteine; DAG, diacylglycerol; DGDG, digalactosyldiacylglycerol; DGHS, diacylglycerolhomoserine; DGTS, diacylglyceryl-N,N,N-trimethylhomoserine; FA, fatty acid; FUM, fumarate; G3P, glycerol-3-P; GSH, glutathione; HCY, homocysteine; MAL, malate; MET, methionine; MGDG, monogalactosyldiacylglycerol; OAA, oxalacetate; P, phosphate; PA, phosphatidic acid; PC, phosphatidylcholine; PE, phosphatidylethanolamine; PG, phosphatidylglycerol; PI, phosphatidylinositol; PS, phosphatidylserine; PQ, plastoquinone; PYR, pyruvate; Q, ubiquinone; TAG, triacylglycerol; SAH, S-adenosyl-L-homocysteine; SAM, S-adenosyl-L-methionine; SQDG, sulfoquinovosyldiacylglycerol; SUC, succinate. Protein abbreviations: 2-Cys-Prx, 2-cys peroxiredoxin; I-V, oxidative phosphorylation complexes; AAA, ADP/ATP carrier protein, chloroplastic; AAC, ADP/ATP carrier protein, mitochondrial; ABCD, ABC transporter D family member; ACP, acyl carrier protein; ACX, acyl-CoA oxidase; ATP-s, ATP synthase complex; BAS1, 2-Cys-Prx BAS1; BTA1, betaine lipid synthase; CAH3, carbonic anhydrase; Cyt b6f, cytochrome b6f complex; Cyt c, cytochrome c; DIT1, dicarboxylate transporter 1; DTC, mitochondrial dicarboxylate/tricarboxylate transporter; EGY1, probable zinc metalloprotease EGY1; Fd, ferredoxin; FNR, Fd-NADP reductase; GRX, glutaredoxin; HIR, hypersensitive-induced response protein; HLA3, probable inorganic carbon transporter HLA3; LCIA, putative inorganic carbon transporter LCIA; KAT. ketoacyl-CoA thiolase; MDH, malate dehydrogenase (p, chloroplastic; m, mitochondrial); MFP, FA β-oxidation multifunctional protein; LCS, long-chain acyl-CoA synthetase; MPT, mitochondrial phosphate carrier protein; NDH2, type-II NAD(P)H dehydrogenase; Pc, plastocyanin; PDH, pyruvate dehydrogenase; PGRL1, PGR5-like protein; PGK, phosphoglycerate kinase; PLMT, phospholipid N-methyltransferase; RPL37, 60S ribosomal protein L37; SOD, superoxide dismutase; TKT, transketolase; Trx, thioredoxin; VCCN, voltage dependent chloride channel; LHCSR, FZL, MLDP, PGD1, PSBS, are described in the text. ER, endoplasmic reticulum; ICM, inner chloroplast membrane; IMM, inner mitochondrial membrane; OCM, outer chloroplast membrane; OMM, outer chloroplast membrane; PM, plasma membrane; PMF, proton motif force; THY, thylakoid membrane

(4) Remodeling of extrachloroplastic glycerolipids accompanied by induction of SAM-dependent glycerolipid *N*-methylation

Upon N deprivation, *E. oleoabundans* lipid metabolism is not only induced at the acyl-lipid level but is accompanied by changes in the glycerolipid composition. The detailed glycerolipid characterization performed in this work using both, thin layer chromatography- and mass spectrometry (**Chapter 5**), provides direct confirmation of results and compensates for the limitations between these techniques (Degraeve-Guibault et al., 2017; Jouhet et al., 2017).

The glycerolipid analysis showed remodeling of chloroplastic glycerolipids and alterations of glycerolipids present in other organellar membranes. Changes in the membrane glycerolipids of N-deprived *E. oleoabundans* have been described in recent MS-

based studies (Matich et al., 2016, 2018; Goh et al., 2017). Nevertheless, important classes were not considered in these analyses (*e.g.* PS, PI, PA, DGDG), preventing a comprehensive understanding of their role in this microalga. The changes in membrane glycerolipids upon N deprivation may be related to multiple cellular processes, likely including autophagy: a process known to require membrane dynamics and remodeling events, where the identities and functions of the involved lipid species remains scarce (Enrique Gomez, et al., 2017).

Considering that the lack of nutrients such as phosphorous, triggers the replacement of phospholipids for non-phosphorous-containing glycerolipids (Zavaleta-Pastor et al., 2010; Mühlroth et al., 2017), it is surprising that neither the biosynthetic pathways, nor the dynamics and cellular functions of N-containing glycerolipids (*i.e.* PC, PE, PS) have been assessed in microalgae, particularly under N deprivation conditions. It is even more striking that these glycerolipids have remained overlooked despite being widely distributed (Li-Beisson et al., 2019) and playing key roles in membrane structure and function (Nakamura, 2017). This work provides novel insights into the metabolism and dynamics of N-containing glycerolipids in *E. oleoabundans* and green microalgae as well. First, N deprivation triggers changes in the short-term dynamics, but not in in the overall amounts of N-containing glycerolipids (particularly PC and PE), which suggests that maintaining their abundance may be critical for cell function. Second, *E. oleoabundans* is able to synthesize PC via the sequential SAM-dependent *N*-methylation of PE. This is relevant because PC biosynthesis in microalgae remained unknown until very recently, when insights for *Chlamydomonas* species containing minimal amounts of PC were provided by Hirashima et al. (2018). However, these may not be representative of species such as *E. oleoabundans*, where PC is the major extrachloroplastic glycerolipid. Third, PE *N*-methylation activity is located not only to the microsomes but also to the LD, whose major polar glycerolipid is PC. This suggests a key role of the PC biosynthetic pathway in LD formation and hence, in neutral lipid accumulation. Fourth, in addition to the PE-derivatives, *E. oleobundans* contains the *N*-methylated betaine lipid DGTS, which was not previously identified in this microalga (Tornabene et al., 1983; Matich et al., 2016, 2018; Goh et al., 2017). Fifth, N deprivation induces SAM-dependent glycerolipid *N*-methylation, likely increasing the turnover of its reaction product (SAH: *S*-adenosyl-L-homocysteine) to alleviate the inhibition of methyltransferases and to maintain the synthesis of the membrane structural lipid PC, as well as higher DGTS levels.

As discussed in **Chapter 5**, induction of SAM-dependent glycerolipid *N*-methylation might play a role beyond glycerolipid metabolism, underscoring the relevance of membrane lipids as integration hubs for cellular processes. Based on evidence in non-photosynthetic eukaryotes, the results from this work suggest that an increased SAM-dependent glycerolipid *N*-methylation may be a major consumer of SAM, not only facilitating its turnover into SAH, but also into sulfur-containing metabolites, including glutathione, thus enabling the microalga to cope with oxidative stress. Whether this lipid metabolic pathway is linked to histone methylation and gene expression reprogramming as shown in *Saccharomyces cerevisiae* (Ye et al., 2017), remains to be investigated. This hypothesis already provides a stimulating starting point to assess the mechanisms underlying the link between membrane lipid metabolism and the cellular response to N deprivation in microalgae.

(5) Redox signaling-mediated integration of the cellular response to N deprivation

The light-capturing and biosynthetic reactions from the chloroplast, including the formation of energy-rich compounds such as starch and FA, must be tightly coordinated with those occurring in other cell compartments to ensure cell growth and survival. The events described above for N-deprived *E. oleoabundans* point towards ROS and/or reducing equivalents, which define the cell's redox potential, as central players for orchestrating the stress response through interorganellar communication. This agrees with reports for several green microalgae that showed a link between the accumulation of lipids upon N deprivation and an oxidative stress response (Zhang et al., 2013b; Yilancioglu et al., 2014; Du et al., 2018; Heredia-Martínez et al., 2018).

The membrane proteome data obtained from N-deprived *E. oleoabundans* provide evidence for cooperation between the chloroplast and the mitochondria through alternative electron transport pathways and trafficking of ATP/ADP and reducing equivalents (malate shunt) across subcellular membranes to adjust the redox potential. This agrees with current knowledge from green algae where the export of excess reducing equivalents to the mitochondria has proved to balance the chloroplast redox poise (Dang et al., 2014). The results from this work also suggest plastidic ROS-based signaling during N starvation. How the chloroplastic ROS are involved in the interplay with the mitochondria remains to be determined. Current evidence points towards 3'-phosphoadenosine 5'-phosphate (PAP) as an evolutionarily-conserved candidate mediator of ROS-dependent chloroplast-mitochondria crosstalk and retrograde signaling (Waszczak et al., 2018). In land

phototrophs, the accumulation of PAP in the chloroplast acts a retrograde signal that relays information of the plastid redox state to the nucleus (Estavillo et al., 2011; Chan et al., 2016; Zhao et al., 2019). Hence, the dual-targeting to the chloroplast and the mitochondria of proteins involved in PAP turnover and organellar import (Estavillo et al., 2011; Ashykhmina et al., 2019), as well as their conserved sequence similarity from chlorophytes to streptophytes (Zhao et al., 2019), support this hypothesis.

Peroxisomes are also involved in energetic metabolism. Despite their characteristic oxidation reactions leading to H_2O_2 production, the role of peroxisome-derived H_2O_2 in ROS signaling and the communication with other energy-producing organelles is poorly understood. Only recent evidence in *C. reinhardtii* supports a redox-based communication between peroxisomes and chloroplasts, where the peroxisomal malate dehydrogenase transmits its redox state to the chloroplast by means of the malate shuttle and H_2O_2-based signaling: upon N starvation, the sustained H_2O_2 and higher malate levels generated through an active peroxisomal FA β-oxidation, proved necessary to regulate chloroplast metabolism, downregulate photosynthesis and attenuate oxidative stress, thus enabling cell survival (Kong et al., 2018). A similar regulation of chloroplast performance through peroxisomal malate/H_2O_2-based signaling may occur in N-deprived *E. oleoabundans*, as evidence points to an active FA β-oxidation and malate shunt in this work.

The role of the glutathione poise and thus, that of the SAM-dependent glycerolipid *N*-methylation, in the interorganellar coordination of the response to N deprivation remains to be determined. It is worth mentioning that additional mechanisms to redox-based signaling, such as those mediated by the membrane-associated regulatory proteins changed upon N stress (**Chapter 5**), may enable the identification of key hubs integrating signals from distinct pathways and/or cell compartments to orchestrate the corresponding responses leading to lipid accumulation.

7. Conclusion

Insights into the high complexity of the cellular responses to N deprivation in *E. oleoabundans* are provided by this work through the integration of multiple approaches and technologies. These results underscore that not only the lipids accumulated in LD, but multiple molecular components at specific subcellular locations, are involved at different levels in the response to N deprivation. A working model is provided which sheds light into the major cellular processes leading to this coordinated stress response, where specific areas are postulated for further study. A detailed analysis of proposed molecular components will undoubtedly enable a better understanding of the underlying mechanisms, will provide insight into the coupling of different cell compartments to cope with abiotic stress, and will help identify the key elements behind the contrasting performances observed within microalgae species. The results from this study will be complemented by those from an ongoing project focused on the characterization of *E. oleoabundans* LD.

Finally, the extendibility of these outcomes to other photosynthetic organisms will provide a better understanding into either the conservation and/or diversification of the stress responses along the evolution of phototrophs and within their different ecological contexts.

This work unveils exciting questions to be addressed, some of which are indicated below.

- Is the novel protein RP2-CLC (Retinitis Pigmentosa Type 2-Clathrin Light Chain) involved in the intracellular trafficking mediated by clathrin-coated vesicles in lower eukaryotes?
- Within green microalgae, how are the photosynthesis fine-tuning mechanisms influenced by the differential distribution of the NPQ molecular effectors PSBS and LHCSR?
- How is the microalgal FZL homolog involved in the changes triggered by N deprivation on chloroplast morphology and autophagy?
- What is the contribution of the lipase homologs *Cr*PGD1 and *At*PLIP1 to membrane remodeling and abiotic stress tolerance in *E. oleoabundans*?
- Which are the specific roles played by the responsive LCS proteins in *E. oleoabundans* acyl-lipid biosynthesis, transport and degradation?
- Can PC be synthesized by alternative metabolic pathways? How are these regulated upon stress?

- What is the role of DGTS in *E. oleoabundans*?
- Which specific organelles directly contribute to LD formation and by which mechanisms?
- Which are the compartment-specific ROS and reducing equivalent dynamics triggered by N deprivation? How would these contribute to interorganellar communication?

References

Abràmoff MD, Magalhães PJ, Ram SJ (2004) Image processing with ImageJ. Biophotonics Int **11**: 36–42

Ahrné E, Molzahn L, Glatter T, Schmidt A (2013) Critical assessment of proteome-wide label-free absolute abundance estimation strategies. Proteomics **13**: 2567–2578

Ajjawi I, Coku A, Froehlich JE, Yang Y, Osteryoung KW, Benning C, Last RL (2011) A J-like protein influences fatty acid composition of chloroplast lipids in Arabidopsis. PLoS One **6**: e25368

Aker J, Hesselink R, Engel R, Karlova R, Borst JW, Visser AJ, de Vries SC (2007) In vivo hexamerization and characterization of the Arabidopsis AAA ATPase CDC48A complex using Förster resonance energy transfer-fluorescence lifetime imaging microscopy and fluorescence correlation spectroscopy. Plant Physiol **145**: 339–350

Alboresi A, Gerotto C, Giacometti GM, Bassi R, Morosinotto T (2010) *Physcomitrella patens* mutants affected on heat dissipation clarify the evolution of photoprotection mechanisms upon land colonization. Proc Natl Acad Sci U S A **107**: 11128–11133

Almeida CM, Pereira C, da Costa DS, Pereira S, Pissarra J, Simoes I, Faro C (2012) Chlapsin, a chloroplastidial aspartic proteinase from the green algae *Chlamydomonas reinhardtii.* Planta **236**: 283–296

Arnon DI (1949) Copper enzymes in isolated chloroplasts. Polyphenoloxidase in *Beta vulgaris*. Plant Physiol **24**: 1–15

Arredondo-Vega BO, Band CJ, Vazquez-Duhalt R (1995) Biochemical composition of *Neochloris oleoabundans* adapted to marine medium. Cytobios **83**: 201–205

Ashykhmina N, Lorenz M, Frerigmann H, Koprivova A, Hofsetz E, Stührwohldt N, Flügge U-I, Haferkamp I, Kopriva S, Gigolashvili T (2019) PAPST2 plays critical roles in removing the stress signaling molecule 3'-phosphoadenosine 5'-phosphate from the cytosol and its subsequent degradation in plastids and mitochondria. Plant Cell **31**: 231–249

Atteia A, Adrait A, Brugière S, Tardif M, van Lis R, Deusch O, Dagan T, Kuhn L, Gontero B, Martin W, et al (2009) A proteomic survey of *Chlamydomonas reinhardtii* mitochondria sheds new light on the metabolic plasticity of the organelle and on the nature of the α-proteobacterial mitochondrial ancestor. Mol Biol Evol **26**: 1533–1548

Avci U, Petzold HE, Ismail IO, Beers EP, Haigler CH (2008) Cysteine proteases XCP1 and XCP2 aid micro-autolysis within the intact central vacuole during xylogenesis in Arabidopsis roots. Plant J **56**: 303–315

Avidan O, Brandis A, Rogachev I, Pick U (2015) Enhanced acetyl-CoA production is associated with increased triglyceride accumulation in the green alga *Chlorella desiccata*. J Exp Bot **66**: 3725–3735

Avidan O, Pick U (2015) Acetyl-CoA synthetase is activated as part of the PDH-bypass in the oleaginous green alga *Chlorella desiccata*. J Exp Bot **66**: 7287–7298

Awai K, Xu C, Tamot B, Benning C (2006) A phosphatidic acid-binding protein of the chloroplast inner envelope membrane involved in lipid trafficking. Proc Natl Acad Sci U S A **103**: 10817–10822

Baba M, Suzuki I, Shiraiwa Y (2011) Proteomic analysis of high-CO_2-inducible extracellular proteins in the unicellular green alga, *Chlamydomonas reinhardtii*. Plant Cell Physiol **52**: 1302–1314

Bagos PG, Liakopoulos TD, Hamodrakas SJ (2004) Finding beta-barrel outer membrane proteins with a Markov chain model. WSEAS Trans Biol Biomed **2**: 186–189

Bailleul B, Rogato A lessandra, de Martino A, Coesel S, Cardol P, Bowler C, Falciatore A, Finazzi G (2010) An atypical member of the light harvesting complex stress related protein family modulates diatom responses to light. Proc Natl Acad Sci U S A **107**: 18214–18219

Baldisserotto C, Ferroni L, Giovanardi M, Boccaletti L, Pantaleoni L, Pancaldi S (2012) Salinity promotes growth of freshwater *Neochloris oleoabundans* UTEX 1185 (Sphaeropleales, Chlorophyta): Morphophysiological aspects. Phycologia **51**: 700–710

Baldisserotto C, Popovich C, Giovanardi M, Sabia A, Ferroni L, Constenla D, Leonardi P, Pancaldi S (2016) Photosynthetic aspects and lipid profiles in the mixotrophic alga *Neochloris oleoabundans* as useful parameters for biodiesel production. Algal Res **16**: 255–265

Barkla BJ, Vera-Estrella R, Hernández-Coronado M, Pantoja O (2009) Quantitative proteomics of the tonoplast reveals a role for glycolytic enzymes in salt tolerance. Plant Cell **21**: 4044–4058

Barkla BJ, Vera-Estrella R, Pantoja O (2007) Enhanced separation of membranes during free flow zonal electrophoresis in plants. Anal Chem **79**: 5181–5187

Barkla BJ, Vera-Estrella R, Pantoja O (2012) Protein profiling of epidermal bladder cells from the halophyte *Mesembryanthemum crystallinum*. Proteomics **12**: 2862–5

Barkla BJ, Zingarelli L, Blumwald E, Smith JAC (1995) Tonoplast Na+/H+ antiport activity and its energization by the vacuolar H+-ATPase in the halophytic plant *Mesembryanthemum crystallinum*. Plant Physiol **109**: 549–556

Barneche F, Steinmetz F, Echeverría M (2000) Fibrillarin genes encode both a conserved nucleolar protein and a novel small nucleolar RNA involved in ribosomal RNA methylation in *Arabidopsis thaliana*. J Biol Chem **275**: 27212–27220

Bartolini F, Bhamidipati A, Thomas S, Schwahn U, Lewis SA, Cowan NJ (2002) Functional overlap between Retinitis Pigmentosa 2 protein and the Tubulin-specific Chaperone Cofactor C. J Biol Chem **277**: 14629–14634

Bates PD (2016) Understanding the control of acyl flux through the lipid metabolic network of plant oil biosynthesis. Biochim Biophys Acta - Mol Cell Biol Lipids **1861**: 1214–1225

Bates PD, Ohlrogge JB, Pollard M (2007) Incorporation of newly synthesized fatty acids into cytosolic glycerolipids in pea leaves occurs via acyl editing. J Biol Chem **282**: 31206–31216

Batoko H, Zheng H-Q, Hawes C, Moore I (2000) A Rab1 GTPase is required for transport between the endoplasmic reticulum and Golgi apparatus and for normal Golgi movement in plants. Plant Cell **12**: 2201–2218

Bauer M, Dietrich C, Nowak K, Sierralta WD, Papenbrock J (2004) Intracellular localization of Arabidopsis sulfurtransferases. Plant Physiol **135**: 916–926

Beaudoin F, Wu X, Li F, Haslam RP, Markham JE, Zheng H, Napier JA, Kunst L (2009) Functional characterization of the Arabidopsis beta-ketoacyl-coenzyme A reductase candidates of the fatty acid elongase. Plant Physiol **150**: 1174–1191

Bečková M, Yu J, Krynická V, Kozlo A, Shao S, Koník P, Komenda J, Murray JW, Nixon PJ (2017) Structure of Psb29/Thf1 and its association with the FtsH protease complex involved in photosystem II repair in cyanobacteria. Philos Trans R Soc B Biol Sci **372**: 20160394

Benlloch R, Shevela D, Hainzl T, Grundström C, Shutova T, Messinger J, Samuelsson G, Sauer-Eriksson AE (2015) Crystal structure and functional characterization of photosystem II-associated carbonic anhydrase CAH3 in *Chlamydomonas reinhardtii*. Plant Physiol **167**: 950–962

Benning C, Huang Z-H, Gage DA (1995) Accumulation of a novel glycolipid and betaine lipid in cells of *Rhodobacter sphaeroides* grown under phosphate limitation. Arch Biochem Biophys **317**: 103–111

Benvenuti G, Bosma R, Cuaresma M, Janssen M, Barbosa MJ, Wijffels RH (2015) Selecting microalgae with high lipid productivity and photosynthetic activity under nitrogen starvation. J Appl Phycol **27**: 1425–1431

Bertani G (1951) Studies on lysogenesis. I. The mode of phage liberation by lysogenic *Escherichia coli*. J Bacteriol **62**: 293–300

Berthelot K, Lecomte S, Estevez Y, Peruch F (2014) *Hevea brasiliensis* REF (Hev b 1) and SRPP (Hev b 3): an overview on rubber particle proteins. Biochimie **106**: 1–9

Bhuiyan NH, Friso G, Poliakov A, Ponnala L, van Wijk KJ (2015) MET1 is a thylakoid-associated TPR protein involved in photosystem II supercomplex formation and repair in Arabidopsis. Plant Cell **27**: 262–285

Bibis SS, Dahlstrom K, Zhu T, Zufferey R (2014) Characterization of Leishmania major phosphatidylethanolamine methyltransferases LmjPEM1 and LmjPEM2 and their inhibition by choline analogs. Mol Biochem Parasitol **196**: 90–99

Bienvenut W V, Espagne C, Martinez A, Majeran W, Valot B, Zivy M, Vallon O, Adam Z, Meinnel T, Giglione C (2011) Dynamics of post-translational modifications and protein stability in the stroma of *Chlamydomonas reinhardtii* chloroplasts. Proteomics **11**: 1734–1750

Binns D, Dimmer E, Huntley R, Barrell D, O'Donovan C, Apweiler R (2008) QuickGO: A web-based tool for gene ontology searching. Bioinformatics **25**: 3045–3046

Blanco-Rivero A, Shutova T, Román MJ, Villarejo A, Martinez F (2012) Phosphorylation controls the localization and activation of the lumenal carbonic anhydrase in *Chlamydomonas reinhardtii*. PLoS One **7**: e49063

Bligh EG, Dyer WJ (1959) A rapid method of total lipid extraction. Can J Biochem Physiol **37**: 911–917

Boldt L, Yellowlees D, Leggat W (2012) Hyperdiversity of genes encoding integral light-harvesting proteins in the dinoflagellate *Symbiodinium* sp. PLoS One **7**: e47456

Bonente G, Passarini F, Cazzaniga S, Mancone C, Buia MC, Tripodi M, Bassi R, Caffarri S (2008) The occurrence of the psbs gene product in *Chlamydomonas reinhardtii* and in other photosynthetic organisms and its correlation with energy quenching. Photochem Photobiol **84**: 1359–1370

Borkhsenious ON, Mason CB, Moroney J V (1998) The intracellular localization of ribulose-1,5-bisphosphate carboxylase/oxygenase in *Chlamydomonas reinhardtii*. Plant Physiol **116**: 1585–1591

Bouvier F, Linka N, Isner J-C, Mutterer J, Weber APM, Camara B (2006) Arabidopsis SAMT1 defines a plastid transporter regulating plastid biogenesis and plant development. Plant Cell **18**: 3088–105

Boyle NR, Page MD, Liu B, Blaby IK, Casero D, Kropat J, Cokus S, Hong-Hermesdorf A, Shaw J, Karpowicz SJ, et al (2012) Three acyltransferases and a nitrogen responsive regulator are implicated in nitrogen starvation-induced triacylglycerol accumulation in Chlamydomonas. J Biol Chem **287**: 15811–15825

Bozhkov PV (2018) Plant autophagy: Mechanisms and functions. J Exp Bot **69**: 1281-1285

Bradford MM (1976) A rapid and sensitive method for the quantitation of microgram quantities of protein utilizing the principle of protein-dye binding. Anal Biochem **72**: 248–254

Breuer G, Lamers PP, Martens DE, Draaisma RB, Wijffels RH (2012) The impact of nitrogen starvation on the dynamics of triacylglycerol accumulation in nine microalgae strains. Biores Technol **124**: 217–226

Brugière S, Kowalski S, Ferro M, Seigneurin-Berny D, Miras S, Salvi D, Ravanel S, D'Hérin P, Garin J, Bourguignon J, et al (2004) The hydrophobic proteome of mitochondrial membranes from Arabidopsis cell suspensions. Phytochemistry **65**: 1693–1707

Bubis JA, Levitsky LI, Ivanov M V., Tarasova IA, Gorshkov M V. (2017) Comparative evaluation of label-free quantification methods for shotgun proteomics. Rapid Commun Mass Spectrom **31**: 606–612

Busch A, Rimbauld B, Naumann B, Rensch S, Hippler M (2008) Ferritin is required for rapid remodeling of the photosynthetic apparatus and minimizes photo-oxidative stress in response to iron availability in *Chlamydomonas reinhardtii*. Plant J **55**: 201–211

Calderon RH, García-Cerdán JG, Malnoë A, Cook R, Russell JJ, Gaw C, Dent RM, De Vitry C, Niyogi KK (2013) A conserved rubredoxin is necessary for photosystem II accumulation in diverse oxygenic photoautotrophs. J Biol Chem **288**: 26688–26696

Cañavate JP, Armada I, Hachero-Cruzado I (2017) Interspecific variability in phosphorus-induced lipid remodelling among marine eukaryotic phytoplankton. New Phytol **213**: 700–713

Canaves JM, Taylor SS (2002) Classification and phylogenetic analysis of the cAMP-dependent protein kinase regulatory subunit family. J Mol Evol **54**: 17–29

Cardol P, Gloire G, Havaux M, Remacle C, Matagne R, Franck F (2003) Photosynthesis and state transitions in mitochondrial mutants of *Chlamydomonas reinhardtii* affected in respiration. Plant Physiol **133**: 2010–2020

Carrie C, Murcha MW, Millar HA, Smith SM, Whelan J (2007) Nine 3-ketoacyl-CoA thiolases (KATs) and acetoacetyl-CoA thiolases (ACATs) encoded by five genes in *Arabidopsis thaliana* are targeted either to peroxisomes or cytosol but not to mitochondria. Plant Mol Biol **63**: 97–108

Carroll AJ, Heazlewood JL, Ito J, Millar AH (2008) Analysis of the Arabidopsis cytosolic ribosome proteome provides detailed insights into its components and their post-translational modification. Mol Cell Proteomics **7**: 347–369

Carter C, Pan S, Zouhar J, Avila EL, Girke T, Raikhel N V (2004) The vegetative vacuole proteome of *Arabidopsis thaliana* reveals predicted and unexpected proteins. Plant Cell **16**: 3285–3303

Castruita M, Casero D, Karpowicz SJ, Kropat J, Vieler A, Hsieh SI, Yan W, Cokus S, Loo JA, Benning C, et al (2011) Systems biology approach in Chlamydomonas reveals connections between copper nutrition and multiple metabolic steps. Plant Cell **23**: 1273–1292

Chan KX, Mabbitt PD, Phua SY, Mueller JW, Nisar N, Gigolashvili T, Stroeher E, Grassl J, Arlt W, Estavillo G, Jackson CJ, Pogson BJ (2016) Sensing and signaling of oxidative stress in chloroplasts by inactivation of the SAL1 phosphoadenosine phosphatase. Proc Natl Acad Sci U S A **113**: E4567-76

Chantanachat S, Bold HC (1962) Phycological studies II. Some algae from arid soils. Univ Texas Publ **6218**: 1–74

Chapman KD, Dyer JM, Mullen RT (2013) Commentary: Why don't plant leaves get fat? Plant Sci **207**: 128–134

Chapple JP, Hardcastle AJ, Grayson C, Spackman LA, Willison KR, Cheetham ME (2000) Mutations in the N-terminus of the X-linked retinitis pigmentosa protein RP2 interfere with the normal targeting of the protein to the plasma membrane. Hum Mol Genet **9**: 1919–1926

Chapple JP, Hardcastle AJ, Grayson C, Willison KR, Cheetham ME (2002) Delineation of the plasma membrane targeting domain of the X-linked retinitis pigmentosa protein RP2. Integr Ophtalmol Vis Sci **43**: 2015–2020

Chen C, Wang J, Zhao X (2016) Leaf senescence induced by EGY1 defection was partially restored by glucose in *Arabidopsis thaliana*. Bot Stud **57**: 5

Chen G, Bi YR, Li N (2005) EGY1 encodes a membrane-associated and ATP-independent metalloprotease that is required for chloroplast development. Plant J **41**: 364–375

Chen M, Zhao L, Sun Y-L, Cui S-X, Zhang L-F, Yang B, Wang J, Kuang T-Y, Huang F (2010) Proteomic analysis of hydrogen photoproduction in sulfur-deprived Chlamydomonas cells. J Proteome Res **9**: 3854–3866

Coleman JR, Grossman AR (1984) Biosynthesis of carbonic anhydrase in *Chlamydomonas reinhardtii* during adaptation to low CO_2. Proc Natl Acad Sci U S A **81**: 6049–6053

Colina F, Amaral J, Carbó M, Pinto G, Soares A, Cañal MJ, Valledor L (2019) Genome-wide identification and characterization of CKIN/SnRK gene in *Chlamydomonas reinhardtii*. Sci Rep **9**: 350

Conner M, Krell T, Lindsay JG (1996) Identification and purification of a distinct dihydrolipoamide dehydrogenase from pea chloroplasts. Planta **200**: 195–202

Correa-Galvis V, Redekop P, Guan K, Griess A, Truong TB, Wakao S, Niyogi KK, Jahns P (2016) Photosystem II subunit PsbS is involved in the induction of LHCSR protein-dependent energy dissipation in *Chlamydomonas reinhardtii*. J Biol Chem **291**: 17478–17487

Courchesne NMD, Parisien A, Wang B, Lan CQ (2009) Enhancement of lipid production using biochemical, genetic and transcription factor engineering approaches. J Biotechnol **141**: 31–41

Couso I, Pérez-Pérez ME, Martínez-Force E, Kim H-S, He Y, Umen JG, Crespo JL (2018) Autophagic flux is required for the synthesis of triacylglycerols and ribosomal protein turnover in Chlamydomonas. J Exp Bot **69**: 1355–1367

Crozet P, Navarro FJ, Willmund F, Mehrshahi P, Bakowski K, Lauersen KJ, Pérez-Pérez M-E, Auroy P, Gorchs Rovira A, Sauret-Gueto S, et al (2018) Birth of a photosynthetic chassis: A MoClo toolkit enabling synthetic biology in the microalga *Chlamydomonas reinhardtii*. ACS Synth Biol **7**: 2074–2086

da Silva TL, Reis A, Medeiros R, Oliveira AC, Gouveia L (2009) Oil production towards biofuel from autotrophic microalgae semicontinuous cultivations monitorized by flow cytometry. Appl Biochem Biotechnol **159**: 568–578

Dammann C, Ichida A, Hong B, Romanowsky SM, Hrabak EM, Harmon AC, Pickard BG, Harper JF (2003) Subcellular targeting of nine calcium-dependent protein kinase isoforms from Arabidopsis. Plant Physiol **132**: 1840–1848

Dang K-V, Plet J, Tolleter D, Jokel M, Cuiné S, Carrier P, Auroy P, Richaud P, Johnson X, Alric J, Allahverdiyeva Y, Peltier G (2014) Combined increases in mitochondrial cooperation and oxygen photoreduction compensate for deficiency in cyclic electron flow in *Chlamydomonas reinhardtii*. Plant Cell 26: 3036-3050

Davidi L, Katz A, Pick U (2012) Characterization of major lipid droplet proteins from Dunaliella. Planta **236**: 19–33

Davidi L, Levin Y, Ben-Dor S, Pick U (2015) Proteome analysis of cytoplasmatic and plastidic β-carotene lipid droplets in *Dunaliella bardawil*. Plant Physiol **167**: 60–79

Davis RW, Volponi J V, Jones HDT, Carvalho BJ, Wu H, Singh S (2012) Multiplex fluorometric assessment of nutrient limitation as a strategy for enhanced lipid enrichment and harvesting of *Neochloris oleoabundans*. Biotechnol Bioeng **109**: 2503–2512

de Jaeger L, Carreres BM, Springer J, Schaap PJ, Eggink G, Martins Dos Santos VAP, Wijffels RH, Martens DE (2018) *Neochloris oleoabundans* is worth its salt: Transcriptomic analysis under salt and nitrogen stress. PLoS One **13**: e0194834

de Michele R, McFarlane HE, Parsons HT, Meents MJ, Lao J, González Fernández-Niño SM, Petzold CJ, Frommer WB, Samuels AL, Heazlewood JL (2016) Free-flow electrophoresis of plasma membrane vesicles enriched by two-phase partitioning enhances the quality of the proteome from Arabidopsis seedlings. J Proteome Res **15**: 900–913

de Rudder KE, Thomas-Oates JE, Geiger O (1997) Rhizobium meliloti mutants deficient in phospholipid N-methyltransferase still contain phosphatidylcholine. J Bacteriol **179**: 6921–6928

Deason T., Silva PC, Watanabe S, Floyd GL (1991) Taxonomic status of the species of the green algal genus Neochloris. Plant Syst Evol **177**: 213–219

Degraeve-Guilbault C, Bréhélin C, Haslam R, Sayanova O, Marie-Luce G, Jouhet J, Corellou F (2017) Glycerolipid characterization and nutrient deprivation-associated changes in the green picoalga *Ostreococcus tauri*. Plant Physiol **173**: 2060-2080

Demé B, Cataye C, Block MA, Maréchal E, Jouhet J (2014) Contribution of galactoglycerolipids to the 3-dimensional architecture of thylakoids. FASEB J **28**: 3373–3383

Depège N, Bellafiore S, Rochaix J-D (2003) Role of chloroplast protein kinase Stt7 in LHCII phosphorylation and state transition in Chlamydomonas. Science **299**: 1572–1575

Despres B, Bouissonnié F, Wu H-J, Gomord V, Guilleminot J, Grellet F, Berger F, Delseny M, Devic M (2003) Three SAC1-like genes show overlapping patterns of expression in Arabidopsis but are remarkably silent during embryo development. Plant J **34**: 293–306

Dettmer J, Ursache R, Campilho A, Miyashima S, Belevich I, O'Regan S, Mullendore DL, Yadav SR, Lanz C, Beverina L, et al (2014) CHOLINE TRANSPORTER-LIKE1 is required for sieve plate development to mediate long-distance cell-to-cell communication. Nat Commun **5**: 4276

Dewez D, Park S, García-Cerdán JG, Lindberg P, Melis A (2009) Mechanism of REP27 protein action in the D1 protein turnover and photosystem II repair from photodamage. Plant Physiol **151**: 88–99

Dittami SM, Michel G, Collén J, Boyen C, Tonon T (2010) Chlorophyll-binding proteins revisited - a multigenic family of light-harvesting and stress proteins from a brown algal perspective. BMC Evol Biol **10**: 365

Do THT, Martinoia E, Lee Y (2017) Functions of ABC transporters in plant growth and development. Curr Opin Plant Biol **41**: 32–38

Dong H-P, Williams E, Wang D, Xie Z-X, Hsia R, Jenck A, Halden R, Li J, Chen F, Place AR (2013) Responses of *Nannochloropsis oceanica* IMET1 to long-term nitrogen starvation and recovery. Plant Physiol **162**: 1110–26

Du Z-Y, Lucker BF, Zienkiewicz K, Miller TE, Zienkiewicz A, Sears BB, Kramer DM, Benning C (2018) Galactoglycerolipid lipase PGD1 is involved in thylakoid membrane remodeling in response to adverse environmental conditions in Chlamydomonas. Plant Cell **30**: 447–465

Duchêne A-M, Giritch A, Hoffmann B, Cognat V, Lancelin D, Peeters NM, Zaepfel M, Maréchal-Drouard L, Small ID (2005) Dual targeting is the rule for organellar aminoacyl-tRNA synthetases in *Arabidopsis thaliana*. Proc Natl Acad Sci U S A **102**: 16484–16489

Dunkley TPJ, Hester S, Shadforth IP, Runions J, Weimar T, Hanton SL, Griffin JL, Bessant C, Brandizzi F, Hawes C, et al (2006) Mapping the Arabidopsis organelle proteome. Proc Natl Acad Sci U S A **103**: 6518–6523

Dyhrman ST, Jenkins BD, Rynearson TA, Saito MA, Mercier ML, Alexander H, Whitney LP, Drzewianowski A, Bulygin V V., Bertrand EM, et al (2012) The transcriptome and proteome of the diatom *Thalassiosira pseudonana* reveal a diverse phosphorus stress response. PLoS One **7**: e33768

Dymek EE, Goduti D, Kramer T, Smith EF (2006) A kinesin-like calmodulin-binding protein in Chlamydomonas: Evidence for a role in cell division and flagellar functions. J Cell Sci **119**: 3107–3116

Einspahr KJ, Peeler TC, Thompson GA (1988) Rapid changes in polyphosphoinositide metabolism associated with the response of *Dunaliella salina* to hypoosmotic shock. J Biol Chem **263**: 5775–5779

Engel BD, Schaffer M, Cuellar LK, Villa E, Plitzko JM, Baumeister W (2015) Native architecture of the Chlamydomonas chloroplast revealed by in situ cryo-electron tomography. Elife **2015**: 1–29

Enrique Gomez R, Joubès J, Valentin N, Batoko H, Satiat-Jeunemaître B, Bernard A (2017) Lipids in membrane dynamics during autophagy in plants. J Exp Bot **69**: 1287-1299

Enyenihi AH, Saunders WS (2003) Large-scale functional genomic analysis of sporulation and meiosis in *Saccharomyces cerevisiae*. Genetics **163**: 47–54

Erickson E, Wakao S, Niyogi KK (2015) Light stress and photoprotection in *Chlamydomonas reinhardtii*. Plant J **82**: 449–465

Estavillo GM, Crisp PA, Pornsiriwong W, Wirtz M, Collinge D, Carrie C, Giraud E, Whelan J, David P, Javot H, Brearley C, Hell R, Marin E, Pogson BJ (2011) Evidence for a SAL1-PAP chloroplast retrograde pathway that functions in drought and high light signaling in Arabidopsis. Plant Cell **23**: 3992-4012

Evans RJ, Schwarz N, Nagel-Wolfrum K, Wolfrum U, Hardcastle AJ, Cheetham ME (2010) The retinitis pigmentosa protein RP2 links pericentriolar vesicle transport between the Golgi and the primary cilium. Hum Mol Genet **19**: 1358–1367

Facchinelli F, Colleoni C, Ball SG, Weber AP (2013) Chlamydia, cyanobiont, or host: Who was on top in the ménage à trois? Trends Plant Sci **18**: 673–679

Fan J, Andre C, Xu C (2011) A chloroplast pathway for the de novo biosynthesis of triacylglycerol in *Chlamydomonas reinhardtii*. FEBS Lett **585**: 1985–1991

Fan M, Sun X, Xu N, Liao Z, Li Y, Wang J, Fan Y, Cui D, Li P, Miao Z (2017) Integration of deep transcriptome and proteome analyses of salicylic acid regulation high temperature stress in *Ulva prolifera*. Sci Rep **7**: 11052

Fatland BL, Ke J, Anderson MD, Mentzen WI, Cui LW, Allred CC, Johnston JL, Nikolau BJ, Wurtele ES (2002) Molecular characterization of a heteromeric ATP-citrate lyase that generates cytosolic acetyl-coenzyme A in Arabidopsis. Plant Cell **130**: 740–756

Feldman JL, Marshall WF (2009) ASQ2 encodes a TBCC-like protein required for mother-daughter centriole linkage and mitotic spindle orientation. Curr Biol **19**: 1238–1243

Felsenstein J (1985) Confidence limits on phylogenies: An approach using the bootstrap. Evolution **39**: 783–791

Ferro M, Brugière S, Salvi D, Seigneurin-Berny D, Court M, Moyet L, Ramus C, Miras S, Mellal M, Le Gall S, et al (2010) AT_CHLORO, a comprehensive chloroplast proteome database with subplastidial localization and curated information on envelope proteins. Mol Cell Proteomics **9**: 1063–1084

Ferro M, Salvi D, Brugière S, Miras S, Kowalski S, Louwagie M, Garin J, Joyard J, Rolland N (2003) Proteomics of the chloroplast envelope membranes from *Arabidopsis thaliana*. Mol Cell Proteomics **2**: 325–345

Ferroni L, Giovanardi M, Poggioli M, Baldisserotto C, Pancaldi S (2018) Enhanced photosynthetic linear electron flow in mixotrophic green microalga *Ettlia oleoabundans* UTEX 1185. Plant Physiol Biochem **130**: 215–223

Findinier J, Delevoye C, Cohen MM (2019) The dynamin-like protein Fzl promotes thylakoid fusion and resistance to light stress in *Chlamydomonas reinhardtii*. PLoS Genet **15**: e1008047

Fisher M, Gokhman I, Pick U, Zamir A (1997) A structurally novel transferrin-like protein accumulates in the plasma membrane of the unicellular green alga *Dunaliella salina* grown in high salinities. J Biol Chem **272**: 1565–1570

Fleischmann A, Darsow M, Degtyarenko K, Fleischmann W, Boyce S, Axelsen KB, Bairoch A, Schomburg D, Tipton KF, Apweiler R (2004) IntEnz, the integrated relational enzyme database. Nucleic Acids Res **32**: D434–D437

Foyer CH, Noctor G (2011) Ascorbate and glutathione: the heart of the redox hub. Plant Physiol **155**: 2-18

Freund DM, Prenni JE (2013) Improved detection of quantitative differences using a combination of spectral counting and MS/MS total ion current. J Proteome Res **12**: 1996–2004

Froehlich JE, Wilkerson CG, Ray WK, McAndrew RS, Osteryoung KW, Gage DA, Phinney BS (2003) Proteomic study of the *Arabidopsis thaliana* chloroplastic envelope membrane utilizing alternatives to traditional two dimensional electrophoresis. J Proteome Res **2**: 413–425

Fujimoto M, Arimura S-I, Ueda T, Takanashi H, Hayashi Y, Nakano A, Tsutsumi N (2010) Arabidopsis dynamin-related proteins DRP2B and DRP1A participate together in clathrin-coated vesicle formation during endocytosis. Proc Natl Acad Sci U S A **107**: 6094–6099

Fulda M, Shockey J, Werber M, Wolter FP, Heinz E (2002) Two long-chain acyl-CoA synthetases from *Arabidopsis thaliana* involved in peroxisomal fatty acid β-oxidation. Plant J **32**: 93–103

Gao C, Wang Y, Shen Y, Yan D, He X, Dai J, Wu Q (2014) Oil accumulation mechanisms of the oleaginous microalga *Chlorella protothecoides* revealed through its genome, transcriptomes, and proteomes. BMC Genomics **15**: 582

Gao H, Sage TL, Osteryoung KW (2006) FZL, an FZO-like protein in plants, is a determinant of thylakoid and chloroplast morphology. Proc Natl Acad Sci U S A **103**: 6759–6764

Gao H, Wang Y, Fei X, Wright DA, Spalding MH (2015) Expression activation and functional analysis of HLA3, a putative inorganic carbon transporter in *Chlamydomonas reinhardtii*. Plant J **82**: 1–11

Gargouri M, Park J-J, Holguin FO, Kim M-J, Wang H, Deshpande RR, Shachar-Hill Y, Hicks LM, Gang DR (2015) Identification of regulatory network hubs that control lipid metabolism in *Chlamydomonas reinhardtii*. J Exp Bot **66**: 4551–4566

Garibay-Hernández A, Barkla BJ, Vera-Estrella R, Martinez A, Pantoja O (2017) Membrane proteomic insights into the physiology and taxonomy of an oleaginous green microalga. Plant Physiol **173**: 390–416

Garibay-Hernández A, Vazquez-Duhalt R, Serrano-Carreón L, Martinez A (2013) Nitrogen limitation in *Neochloris oleoabundans*: A reassessment of its effect on cell growth and biochemical composition. Appl Biochem Biotechnol **171**: 1775–91

Gerotto C, Alboresi A, Giacometti GM, Bassi R, Morosinotto T (2012) Coexistence of plant and algal energy dissipation mechanisms in the moss *Physcomitrella patens*. New Phytol **196**: 763–773

Gerotto C, Morosinotto T (2013) Evolution of photoprotection mechanisms upon land colonization: Evidence of PSBS-dependent NPQ in late Streptophyte algae. Physiol Plant **149**: 583–598

Gidda SK, Shockey JM, Rothstein SJ, Dyer JM, Mullen RT (2009) *Arabidopsis thaliana* GPAT8 and GPAT9 are localized to the ER and possess distinct ER retrieval signals: Functional divergence of the dilysine ER retrieval motif in plant cells. Plant Physiol Biochem **47**: 867–879

Ginger ML, McFadden GI, Michels PAM (2010) Rewiring and regulation of cross-compartmentalized metabolism in protists. Phil Trans R Soc B **365**: 831–845

Giovanardi M, Ferroni L, Baldisserotto C, Tedeschi P, Maietti A, Pantaleoni L, Pancaldi S (2013) Morphophysiological analyses of *Neochloris oleoabundans* (Chlorophyta) grown mixotrophically in a carbon-rich waste product. Protoplasma **250**: 161–74

Giroud C, Gerber A, Eichenberger W (1988) Lipids of *Chlamydomonas reinhardtii*. Analysis of molecular species and intracellular site(s) of biosynthesis. Plant Cell Physiol **29**: 587–595

Goh FQY, Jeyakani J, Cazenave-Gassiot A, Tipthara P, Yeo Z, Wenk M, Clarke ND (2017) Core features of triacylglyceride production in *Ettlia oleoabundans* revealed by lipidomic and gene expression profiling under distinct induction conditions. Algal Res **26**: 453–462

Gontcharov AA, Marin B, Melkonian M (2002) Are combined analyses better than single gene phylogenies? A case study using SSU rDNA and rbcL sequence comparisons in the Zygnematophyceae (Streptophyta). Mol Biol Evol **21**: 612–624

González-Ballester D, Camargo A, Fernández E (2004) Ammonium transporter genes in Chlamydomonas: The nitrate-specific regulatory gene Nit2 is involved in Amt1;1 expression. Plant Mol Biol **56**: 863-878

Goodstein DM, Shu S, Howson R, Neupane R, Hayes RD, Fazo J, Mitros T, Dirks W, Hellsten U, Putnam N, et al (2012) Phytozome: A comparative platform for green plant genomics. Nucleic Acids Res **40**: 1178–1186

Goold H, Beisson F, Peltier G, Li-Beisson Y (2015) Microalgal lipid droplets: Composition, diversity, biogenesis and functions. Plant Cell Rep **34**: 545–555

Götz S, García-Gómez JM, Terol J, Williams TD, Nagaraj SH, Nueda MJ, Robles M, Talón M, Dopazo J, Conesa A (2008) High-throughput functional annotation and data mining with the Blast2GO suite. Nucleic Acids Res **36**: 3420–3435

Gouveia L, Marques AE, da Silva TL, Reis A (2009) *Neochloris oleabundans* UTEX #1185: A suitable renewable lipid source for biofuel production. J Ind Microbiol Biotechnol **36**: 821–826

Grayson C, Bartolini F, Chapple JP, Willison KR, Bhamidipati A, Lewis SA, Luthert PJ, Hardcastle AJ, Cowan NJ, Cheetham ME (2002) Localization in the human retina of the X-linked retinitis pigmentosa protein RP2, its homologue cofactor C and the RP2 interacting protein Arl3. Hum Mol Genet **11**: 3065–3074

Greenspan P, Mayer EP, Fowler SD (1985) Nile red: a selective fluorescent stain for intracellular lipid droplets. J Cell Biol **100**: 965 LP-973

Grossman A, Takahashi H (2001) Macronutrient utilization by photosynthetic eukaryotes and the fabric of interactions. Annu Rev Plant Physiol Plant Mol Biol **52**: 163–210

Guarnieri MT, Nag A, Smolinski SL, Darzins A, Seibert M, Pienkos PT (2011) Examination of triacylglycerol biosynthetic pathways via de novo transcriptomic and proteomic analyses in an unsequenced microalga. PLoS One **6**: e25851

Guarnieri MT, Nag A, Yang S, Pienkos PT (2013) Proteomic analysis of *Chlorella vulgaris*: Potential targets for enhanced lipid accumulation. J Proteomics **93**: 245–253

Guiry MD, Guiry GM (1996) AlgaeBase. World-wide electronic publication. Natl. Univ. Ireland, Galway, http://www.algaebase.org

Guschina IA, Harwood JL (2006) Lipids and lipid metabolism in eukaryotic algae. Prog Lip Res **45**: 160-186

Gutu A, Chang F, O'Shea EK (2018) Dynamical localization of a thylakoid membrane binding protein is required for acquisition of photosynthetic competency. Mol Microbiol **108**: 16–31

Haas BJ, Papanicolaou A, Yassour M, Grabherr M, Blood PD, Bowden J, Couger MB, Eccles D, Li B, Lieber M, et al (2013) *De novo* transcript sequence reconstruction from RNA-Seq: Reference generation and analysis with Trinity. Nat Protoc **8**: 1494–1512

Haider S, Pal R (2013) Integrated analysis of transcriptomic and proteomic data. Curr Genomics **14**: 91–110

Haldrup A, Naver H, Scheller HV (1999) The interaction between plastocyanin and photosystem I is inefficient in transgenic Arabidopsis plants lacking the PSI-N subunit of photosystem I. Plant J **17**: 689–698

Harayama T, Riezman H (2018) Understanding the diversity of membrane lipid composition. Nat Rev Mol Cell Biol **19**: 281–296

Harris EH (2009) The Chlamydomonas sourcebook: Introduction to Chlamydomonas and its laboratory use, 2nd ed. Elsevier Academic Press, Canada

Harwood JL, Guschina IA (2009) The versatility of algae and their lipid metabolism. Biochimie **91**: 679–684

Haslam TM, Kunst L (2013) Extending the story of very-long-chain fatty acid elongation. Plant Sci **210**: 93–107

Heazlewood JL, Tonti-Filippini JS, Gout AM, Day DA, Whelan J, Millar AH (2004) Experimental analysis of the Arabidopsis mitochondrial proteome highlights signaling and regulatory components, provides assessment of targeting prediction programs, and indicates plant-specific mitochondrial proteins. Plant Cell **16**: 241–56

Heilmann I, Perera IY, Gross W, Boss WF (2001) Plasma membrane phosphatidylinositol 4,5-bisphosphate levels decrease with time in culture. Plant Physiol **126**: 1507–1518

Herdean A, Teardo E, Nilsson AK, Pfeil BE, Johansson ON, Ünnep R, Nagy G, Zsiros O, Dana S, Solymosi K, et al (2016) A voltage-dependent chloride channel fine-tunes photosynthesis in plants. Nat Commun **7**: 11654

Heredia-Martínez LG, Andrés-Garrido A, Martínez-Force E, Pérez-Pérez ME, Crespo JL (2018) Chloroplast damage induced by the inhibition of fatty acid synthesis triggers autophagy in Chlamydomonas. Plant Physiol **178**: 1112-1129

Hirashima T, Toyoshima M, Moriyama T, Sato N (2018) Evolution of the phosphatidylcholine biosynthesis pathways in green algae: Combinatorial diversity of methyltransferases. J Mol Evol **86**: 68–76

Hölzl G, Witt S, Gaude N, Melzer M, Schottler MA, Dormann P (2009) The role of diglycosyl lipids in photosynthesis and membrane lipid homeostasis in Arabidopsis. Plant Physiol **150**: 1147–1159

Hörl G, Wagner A, Cole LK, Malli R, Reicher H, Kotzbeck P, Köfeler H, Höfler G, Frank S, Bogner-Strauss JG, et al (2011) Sequential synthesis and methylation of phosphatidylethanolamine promote lipid droplet biosynthesis and stability in tissue culture and in vivo. J Biol Chem **286**: 17338–17350

Hörmann F, Küchler M, Sveshnikov D, Oppermann U, Li Y, Soll J (2004) Tic32, an essential component in chloroplast biogenesis. J Biol Chem **279**: 34756–34762

Horn PJ, Benning C (2016) The plant lipidome in human and environmental health. Science **353**: 1228-32

Horn PJ, James CN, Gidda SK, Kilaru A, Dyer JM, Mullen RT, Ohlrogge JB, Chapman KD (2013) Identification of a new class of lipid droplet-associated proteins in plants. Plant Physiol **162**: 1926–1936

Horváth BM, Magyar Z, Zhang Y, Hamburger AW, Bakó L, Visser RGF, Bachem CWB, Bögre L (2006) EBP1 regulates organ size through cell growth and proliferation in plants. EMBO J **25**: 4909–4920

Hu J, Wang D, Li J, Jing G, Ning K, Xu J (2014) Genome-wide identification of transcription factors and transcription-factor binding sites in oleaginous microalgae Nannochloropsis. Sci Rep **4**: 5454

Hu Q, Sommerfeld M, Jarvis E, Ghirardi M, Posewitz M, Seibert M, Darzins A (2008) Microalgal triacylglycerols as feedstocks for biofuel production: Perspectives and advances. Plant J **54**: 621–639

Huang K, Kunkel T, Beck CF (2004) Localization of the blue-light receptor phototropin to the flagella of the green alga *Chlamydomonas reinhardtii*. Mol Biol Cell **15**: 3605–3614

Huang N-L, Huang M-D, Chen T-LL, Huang AHC (2013a) Oleosin of subcellular lipid droplets evolved in green algae. Plant Physiol **161**: 1862–1874

Huang W, Chen Q, Zhu Y, Hu F, Zhang L, Ma Z, He Z, Huang J (2013b) Arabidopsis Thylakoid Formation 1 is a critical regulator for dynamics of PSII-LHCII complexes in leaf senescence and excess light. Mol Plant **6**: 1673–1691

Huss VAR, Frank C, Hartmann EC, Hirmer M, Kloboucek A, Seidel BM, Wenzeler P, Kessler E (1999) Biochemical taxonomy and molecular phylogeny of the genus Chlorella sensu lato (Chlorophyta). J Phycol **35**: 587–598

Iliev D, Voytsekh O, Schmidt E-M, Fiedler M, Nykytenko A, Mittag M (2006) A heteromeric RNA-binding protein is involved in maintaining acrophase and period of the circadian clock. Plant Physiol **142**: 797–806

Im C-S, Eberhard S, Huang K, Beck CF, Grossman AR (2006) Phototropin involvement in the expression of genes encoding chlorophyll and carotenoid biosynthesis enzymes and LHC apoproteins in *Chlamydomonas reinhardtii*. Plant J **48**: 1–16

Ishikawa T, Aki T, Yanagisawa S, Uchimiya H, Kawai-Yamada M (2015) Overexpression of BAX INHIBITOR-1 links plasma membrane microdomain proteins to stress. Plant Physiol **169**: 1333–1343

Iskandarov U, Sitnik S, Shtaida N, Didi-Cohen S, Leu S, Khozin-Goldberg I, Cohen Z, Boussiba S (2016) Cloning and characterization of a GPAT-like gene from the microalga *Lobosphaera incisa* (Trebouxiophyceae): Overexpression in *Chlamydomonas reinhardtii* enhances TAG production. J Appl Phycol **28**: 907–919

Ito J, Batth TS, Petzold CJ, Redding-Johanson AM, Mukhopadhyay A, Verboom R, Meyer EH, Millar AH, Heazlewood JL (2011) Analysis of the Arabidopsis cytosolic proteome highlights subcellular partitioning of central plant metabolism. J Proteome Res **10**: 1571–1582

Iwai M, Takizawa K, Tokutsu R, Okamuro A, Takahashi Y, Minagawa J (2010) Isolation of the elusive supercomplex that drives cyclic electron flow in photosynthesis. Nature **464**: 1210–1213

Javee A, Sulochana SB, Pallissery SJ, Arumugam M (2016) Major Lipid Body Protein: A conserved structural component of lipid body accumulated during abiotic stress in *S. quadricauda* CASA-CC202. Front Energy Res **4**: 37

Jia B, Song Y, Wu M, Lin B, Xiao K, Hu Z, Huang Y (2016) Characterization of long-chain acyl-CoA synthetases which stimulate secretion of fatty acids in green algae *Chlamydomonas reinhardtii*. Biotechnol Biofuels **9**: 184

Jinkerson RE, Subramanian V, Posewitz MC (2011) Improving biofuel production in phototrophic microorganisms with systems biology. Biofuels **2**: 125–144

Johnson X, Alric J (2013) Central carbon metabolism and electron transport in *Chlamydomonas reinhardtii*: Metabolic constraints for carbon partitioning between oil and starch. Eukaryot Cell **12**: 776–793

Jones DT, Taylor WR, Thornton JM (1992) The rapid generation of mutation data matrices from protein sequences. Comput Appl Biosci **8**: 275–282

Jouhet J, Lupette J, Clerc O, Magneschi L, Bedhomme M, Collin S, Roy S, Maréchal E, Rébeillé F (2017) LC-MS/MS versus TLC plus GC methods: consistency of glycerolipid and fatty acid profiles in microalgae and higher plant cells and effect of a nitrogen starvation. PloS One **12**: e0182423

Joyard J, Ferro M, Masselon C, Seigneurin-Berny D, Salvi D, Garin J, Rolland N (2010) Chloroplast proteomics highlights the subcellular compartmentation of lipid metabolism. Prog Lipid Res **49**: 128–158

Juergens MT, Disbrow B, Shachar-Hill Y (2016) The relationship of triacylglycerol and starch accumulation to carbon and energy flows during nutrient deprivation in *Chlamydomonas reinhardtii*. Plant Physiol **171**: 2445-2457

Karlsson J, Clarke AK, Chen Z-Y, Hugghins SY, Park Y-I, Husic HD, Moroney J V, Samuelsson G (1998) A novel alpha-type carbonic anhydrase associated with the thylakoid membrane in *Chlamydomonas reinhardtii* is required for growth at ambient CO_2. EMBO J **17**: 1208–1216

Kato-Minoura T, Hirono M, Kamiya R (1997) Chlamydomonas inner-arm dynein mutant, ida5, has a mutation in an actin-encoding gene. J Cell Biol **137**: 649–656

Keller LC, Romijn EP, Zamora I, Yates III JR, Marshall WF (2005) Proteomic analysis of isolated Chlamydomonas centrioles reveals orthologs of ciliary-disease genes. Curr Biol **15**: 1090–1098

Keogh MR, Courtney PD, Kinney AJ, Dewey RE (2009) Functional characterization of phospholipid *N*-methyltransferases from Arabidopsis and soybean. J Biol Chem **284**: 15439–15447

Khozin-Goldberg I, Cohen Z (2011) Unraveling algal lipid metabolism: Recent advances in gene identification. Biochimie **93**: 91–100

Kianianmomeni A, Hallmann A (2014) Algal photoreceptors: *in vivo* functions and potential applications. Planta **239**: 1–26

Kiba T, Feria-Bourrellier A-B, Lafouge F, Lezhneva L, Boutet-Mercey S, Orsel M, Bréhaut V, Miller A, Daniel-Vedele F, Sakakibara H, et al (2012) The Arabidopsis nitrate transporter NRT2.4 plays a double role in roots and shoots of nitrogen-starved plants. Plant Cell **24**: 245–58

Kleffmann T, Russenberger D, von Zychlinski A, Christopher W, Gruissem W, Baginsky S (2004) The *Arabidopsis thaliana* chloroplast proteome reveals pathway abundance and novel protein functions. Curr Biol **14**: 354–362

Klein U (1986) Compartmentation of glycolysis and of the oxidative pentose-phosphate pathway in *Chlamydomonas reinhardii*. Planta **167**: 81–86

Klok AJ, Martens DE, Wijffels RH, Lamers PP (2013) Simultaneous growth and neutral lipid accumulation in microalgae. Bioresour Technol **134**: 233–243

Kodaki T, Yamashita S (1987) Yeast phosphatidylethanolamine methylation pathway. Cloning and characterization of two distinct methyltransferase genes. J Biol Chem **262**: 15428–15435

Kojima S, Bohner A, Gassert B, Yuan L, von Wirén N (2007) AtDUR3 represents the major transporter for high-affinity urea transport across the plasma membrane of nitrogen-deficient Arabidopsis roots. Plant J **52**: 30–40

Komárek J (1989) Polynuclearity of vegetative cells in coccal green algae from the family Neochloridaceae. Arch Protistenk **137**: 255-273

Kong F, Liang Y, Légeret B, Beyly-Adriano A, Blangy S, Haslam RP, Napier JA, Beisson F, Peltier G, Li-Beisson Y (2017) Chlamydomonas carries out fatty acid β-oxidation in ancestral peroxisomes using a bona fide acyl-CoA oxidase. Plant J **90**: 358-371

Kong F, Burlacot A, Liang Y, Légeret B, Alseekh S, Brotman Y, Fernie AR, Krieger-Liszkay A, Beisson F, Peltier G, Li-Beisson Y (2018) Interorganelle communication: Peroxisomal MALATE DEHYDROGENASE2 connects lipid catabolism to photosynthesis through redox coupling in Chlamydomonas. Plant Cell **3**0: 1824-1847

Koo AJK, Ohlrogge JB, Pollard M (2004) On the export of fatty acids from the chloroplast. J Biol Chem **279**: 16101–16110

Koziol AG, Borza T, Ishida K-I, Keeling P, Lee RW, Durnford DG (2007) Tracing the evolution of the light-harvesting antennae in chlorophyll a/b-containing organisms. Plant Physiol **143**: 1802–1816

Krahmer N, Guo Y, Wilfling F, Hilger M, Lingrell S, Heger K, Newman HW, Schmidt-Supprian M, Vance DE, Mann M, et al (2011) Phosphatidylcholine synthesis for lipid droplet expansion is mediated by localized activation of CTP:phosphocholine cytidylyltransferase. Cell Metab **14**: 504–515

Krogh A, Larsson B, von Heijne G, Sonnhammer ELL (2001) Predicting transmembrane protein topology with a hidden Markov model: Application to complete genomes. J Mol Biol **305**: 567–580

Kroll D, Meierhoff K, Bechtold N, Kinoshita M, Westphal S, Vothknecht UC, Soll J, Westhoff P (2001) VIPP1, a nuclear gene of *Arabidopsis thaliana* essential for thylakoid membrane formation. Proc Natl Acad Sci U S A **98**: 4238–4242

Kumar S, Stecher G, Tamura K (2016) MEGA7: Molecular evolutionary genetics analysis version 7.0 for bigger datasets. Mol Biol Evol **33**: 1870–1874

Laemlli UK (1970) Cleavage of structural proteins during the assembly of the head of bacteriophage T4. Nature **227**: 680–685

Landoni M, De Francesco A, Bellatti S, Delledonne M, Ferrarini A, Venturini L, Pilu R, Bononi M, Tonelli C (2013) A mutation in the FZL gene of Arabidopsis causing alteration in chloroplast morphology results in a lesion mimic phenotype. J Exp Bot **64**: 4313–4328

Lange PR, Geserick C, Tischendorf G, Zrenner R (2008) Functions of chloroplastic adenylate kinases in Arabidopsis. Plant Physiol **146**: 492–504

Légeret B, Schulz-Raffelt M, Nguyen HM, Auroy P, Beisson F, Peltier G, Blanc G, Li-Beisson Y (2016) Lipidomic and transcriptomic analyses of *Chlamydomonas reinhardtii* under heat stress unveil a direct route for the conversion of membrane lipids into storage lipids. Plant Cell Environ **39**: 834-847

Lermontova I, Schubert V, Börnke F, Macas J, Schubert I (2007) Arabidopsis CBF5 interacts with the H/ACA snoRNP assembly factor NAF1. Plant Mol Biol **65**: 615–626

Levine RB, Costanza-Robinson MS, Spatafora GA (2011) *Neochloris oleoabundans* grown on anaerobically digested dairy manure for concomitant nutrient removal and biodiesel feedstock production. Biomass Bioenerg **35**: 40–49

Levitan A, Trebitsh T, Kiss V, Pereg Y, Dangoor I, Danon A (2005) Dual targeting of the protein disulfide isomerase RB60 to the chloroplast and the endoplasmic reticulum. Proc Natl Acad Sci U S A **102**: 6225–30

Lewis LA, McCourt RM (2004) Green algae and the origin of land plants. Am J Bot **91**: 1535-1556

Li J, Han D, Wang D, Ning K, Jia J, Wei L, Jing X, Huang S, Chen J, Li Y, et al (2014a) Choreography of transcriptomes and lipidomes of Nannochloropsis reveals the mechanisms of oil synthesis in microalgae. Plant Cell **26**: 1645–1665

Li N, Xu C, Li-Beisson Y, Philippar K (2016a) Fatty acid and lipid transport in plant cells. Trends Plant Sci **21**: 145–158

Li X, Moellering ER, Liu B, Johnny C, Fedewa M, Sears BB, Kuo M-H, Benning C (2012) A galactoglycerolipid lipase is required for triacylglycerol accumulation and survival following nitrogen deprivation in *Chlamydomonas reinhardtii*. Plant Cell **24**: 4670–86

Li X, Zhang R, Patena W, Gang SS, Blum SR, Ivanova N, Yue R, Robertson JM, Lefebvre PA, Fitz-Gibbon ST, et al (2016b) An indexed, mapped mutant library enables reverse genetics studies of biological processes in *Chlamydomonas reinhardtii*. Plant Cell **28**: 367–387

Li X-P, Björkman O, Shih C, Grossman AR, Rosenquist M, Jansson S, Niyogi KK (2000) A pigment-binding protein essential for regulation of photosynthetic light harvesting. Nature **403**: 391–395

Li X-P, Gilmore AM, Caffarri S, Bassi R, Golan T, Kramer D, Niyogi KK (2004) Regulation of photosynthetic light harvesting involves intrathylakoid lumen pH sensing by the PsbS protein. J Biol Chem **279**: 22866–22874

Li X-P, Phippard A, Pasari J, Niyogi KK (2002) Structure-function analysis of photosystem II subunit S (PsbS) *in vivo*. Funct Plant Biol **29**: 1131–1139

Li Y, Horsman M, Wang B, Wu N, Lan CQ (2008) Effects of nitrogen sources on cell growth and lipid accumulation of green alga *Neochloris oleoabundans*. Appl Microbiol Biotechnol **81**: 629–636

Li Y, Lou Y, Mu T, Xu J, Zhou C, Yan X (2017) Simultaneous structural identification of diacylglyceryl-N-trimethylhomoserine (DGTS) and diacylglycerylhydroxymethyl-N,N,N-trimethyl-β-alanine (DGTA) in microalgae using dual Li+/H+adduct ion mode by ultra-performance liquid chromatography/quadrupole time-of-flight mass spectrometry. Rapid Commun Mass Spectrom **31**: 457–468

Li Y, Zheng G, Jia Y, Yu X, Zhang X, Yu B, Wang D, Zheng Y, Tian X, Li W (2014b) Acyl chain length of phosophatidylserine is correlated with plant lifespan. PLoS One **9**: e103227

Li-Beisson Y, Beisson F, Riekhof W (2015) Metabolism of acyl-lipids in *Chlamydomonas reinhardtii*. Plant J **82**: 504–522

Li-Beisson Y, Shorrosh B, Beisson F, Andersson MX, Arondel V, Bates PD, Baud S, Bird D, Debono A, Durrett TP, et al (2010) Acyl-Lipid Metabolism. Arab. B. American Society of Plant Biologists, Rockville, MD, p e0133

Li-Beisson Y, Thelen JJ, Fedosejevs E, Harwood JL (2019) The lipid biochemistry of eukaryotic algae. Prog Lip Res **74**: 31-68

Link S, Engelmann K, Meierhoff K, Westhoff P (2012) The atypical short-chain dehydrogenases HCF173 and HCF244 are jointly involved in translational initiation of the psbA mRNA of Arabidopsis. Plant Physiol **160**: 2202–2218

Liu B, Benning C (2013) Lipid metabolism in microalgae distinguishes itself. Curr Opin Biotechnol **24**: 300–9

Liu J, Last RL (2015a) MPH1 is a thylakoid membrane protein involved in protecting photosystem II from photodamage in land plants. Plant Signal Behav **10**: e1076602

Liu J, Last RL (2015b) A land plant-specific thylakoid membrane protein contributes to photosystem II maintenance in *Arabidopsis thaliana*. Plant J **82**: 731–743

Lohscheider JN, Río Bártulos C (2016) Plastoglobules in algae: A comprehensive comparative study of the presence of major structural and functional components in complex plastids. Mar Genomics **28**: 127–136

Longworth J, Noirel J, Pandhal J, Wright PC, Vaidyanathan S (2012) HILIC- and SCX-based quantitative proteomics of *Chlamydomonas reinhardtii* during nitrogen starvation induced lipid and carbohydrate accumulation. J Proteome Res **11**: 5959–5971

López García de Lomana A, Schäuble S, Valenzuela J, Imam S, Carter W, Bilgin DD, Yohn CB, Turkarslan S, Reiss DJ, Orellana M V., et al (2015) Transcriptional program for nitrogen starvation-induced lipid accumulation in *Chlamydomonas reinhardtii*. Biotechnol Biofuels **8**: 207

Lorković ZJ, Hilscher J, Barta A (2004) Use of fluorescent protein tags to study nuclear organization of the spliceosomal machinery in transiently transformed living plant cells. Mol Biol Cell **15**: 3233–3243

Luciński R, Jackowski G (2013) AtFtsH heterocomplex-mediated degradation of apoproteins of the major light harvesting complex of photosystem II (LHCII) in response to stresses. J Plant Physiol **170**: 1082–1089

Lundin VF, Leroux MR, Stirling PC (2010) Quality control of cytoskeletal proteins and human disease. Trends Biochem Sci **35**: 288–297

Ma Q, Wang J, Lu S, Lv Y, Yuan Y (2013) Quantitative proteomic profiling reveals photosynthesis responsible for inoculum size dependent variation in *Chlorella sorokiniana*. Biotechnol Bioeng **110**: 773–784

Ma W, Kong Q, Mantyla JJ, Yang Y, Ohlrogge JB, Benning C (2016) 14-3-3 protein mediates plant seed oil biosynthesis through interaction with AtWRI1. Plant J **88**: 228–235

Malanovic N, Streith I, Wolinski H, Rechberger G, Kohlwein SD, Tehlivets O (2008) *S*-adenosyl-L-homocysteine hydrolase, key enzyme of methylation metabolism, regulates phosphatidylcholine synthesis and triacylglycerol homeostasis in yeast: Implications for homocysteine as a risk factor of atherosclerosis. J Biol Chem **283**: 23989–23999

Manna PT, Gadelha C, Puttick AE, Field MC (2015) ENTH and ANTH domain proteins participate in AP2-independent clathrin-mediated endocytosis. J Cell Sci **128**: 2130–2142

Marmagne A, Ferro M, Meinnel T, Bruley C, Kuhn L, Garin J, Barbier-Brygoo H, Ephritikhine G (2007) A high content in lipid-modified peripheral proteins and integral receptor kinases features in the Arabidopsis plasma membrane proteome. Mol Cell Proteomics **6**: 1980–1996

Matich EK, Butryn DM, Ghafari M, del Solar V, Camgoz E, Pfeifer BA, Aga DS, Haznedaroglu BZ, Atilla-Gokcumen GE (2016) Mass spectrometry-based metabolomics of value-added biochemicals from *Ettlia oleoabundans*. Algal Res **19**: 146–154

Matich EK, Ghafari M, Camgoz E, Caliskan E, Pfeifer BA, Haznedaroglu BZ, Atilla-Gokcumen GE (2018) Time-series lipidomic analysis of the oleaginous green microalga species *Ettlia oleoabundans* under nutrient stress. Biotechnol Biofuels **11**: 29

McCormac DJ, Barkan A (1999) A nuclear gene in maize required for the translation of the chloroplast atpB/E mRNA. Plant Cell **11**: 1709–16

McKay RML, Gibbs SP, Vaughn KC (1991) Rubisco activase is present in the pyrenoid of green algae. Protoplasma **162**: 38–45

Merchant SS, Kropat J, Liu B, Shaw J, Warakanont J (2012) TAG, you're it! Chlamydomonas as a reference organism for understanding algal triacylglycerol accumulation. Curr Opin Biotechnol

Metsalu T, Vilo J (2015) ClustVis: A web tool for visualizing clustering of multivariate data using Principal Component Analysis and heatmap. Nucleic Acids Res **43**: W566–W570

Meyer AJ, Brach T, Marty L, Kreye S, Rouhier N, Jacquot J-P, Hell R (2007) Redox-sensitive GFP in *Arabidopsis thaliana* is a quantitative biosensor for the redox potential of the cellular glutathione redox buffer. Plant J **52**: 973-986

Michel V, Yuan Z, Ramsubir S, Bakovic M (2006) Choline transport for phospholipid synthesis. Exp Biol Med **231**: 490–504

Millar AH, Sweetlove LJ, Giegé P, Leaver CJ (2001) Analysis of the Arabidopsis mitochondrial proteome. Plant Physiol **127**: 1711–1727

Miller R, Wu G, Deshpande RR, Vieler A, Gärtner K, Li X, Moellering ER, Zäuner S, Cornish AJ, Liu B, et al (2010) Changes in transcript abundance in *Chlamydomonas reinhardtii* following nitrogen deprivation predict diversion of metabolism. Plant Physiol **154**: 1737–1752

Minagawa J, Tokutsu R (2015) Dynamic regulation of photosynthesis in *Chlamydomonas reinhardtii*. Plant J **82**: 413–28

Misumi O, Matsuzaki M, Nozaki H, Miyagishima S, Mori T, Nishida K, Yagisawa F, Yoshida Y, Kuroiwa H, Kuroiwa T (2005) *Cyanidioschyzon merolae* genome. A tool for facilitating comparable studies on organelle biogenesis in photosynthetic eukaryotes. Plant Physiol **137**: 567–585

Mitchell A, Chang H-Y, Daugherty L, Fraser M, Hunter S, Lopez R, McAnulla C, McMenamin C, Nuka G, Pesseat S, et al (2015) The InterPro protein families database: The classification resource after 15 years. Nucleic Acids Res **43**: D213–D221

Mitchell MC, Meyer MT, Griffiths H (2014) Dynamics of carbon-concentrating mechanism induction and protein relocalization during the dark-to-light transition in synchronized *Chlamydomonas reinhardtii*. Plant Physiol **166**: 1073–1082

Mitra SK, Walters BT, Clouse SD, Goshe MB (2009) An efficient organic solvent based extraction method for the proteomic analysis of Arabidopsis plasma membranes. J Proteome Res **8**: 2752–2767

Moellering ER, Benning C (2010) RNA interference silencing of a major lipid droplet protein affects lipid droplet size in *Chlamydomonas reinhardtii*. Eukaryot Cell **9**: 97–106

Monneuse J-M, Sugano M, Becue T, Santoni V, Hem S, Rossignol M (2011) Towards the profiling of the *Arabidopsis thaliana* plasma membrane transportome by targeted proteomics. Proteomics **11**: 1789–1797

Moon-van der Staay SY, de Wachter R, Vaulot D (2001) Oceanic 18S rDNA sequences from picoplankton reveal unsuspected eukaryotic diversity. Nature **409**: 607–610

Morales-Sánchez D, Tinoco-Valencia R, Kyndt J, Martinez A (2013) Heterotrophic growth of *Neochloris oleoabundans* using glucose as a carbon source. Biotechnol Biofuels **6**: 100

Moreira D, Le Guyader H, Philippe H (2000) The origin of red algae and the evolution of chloroplasts. Nature **405**: 69–72

Moriyama T, Toyoshima M, Saito M, Wada H, Sato N (2018) Revisiting the algal "Chloroplast Lipid Droplet": The absence of an entity that is unlikely to exist. Plant Physiol **176**: 1519–1530

Motiwalla MJ, Sequeira MP, D'Souza JS (2014) Two calcium-dependent protein kinases from *Chlamydomonas reinhardtii* are transcriptionally regulated by nutrient starvation. Plant Signal Behav **9**: e27969

Mou S, Zhang X, Dong M, Fan X, Xu J, Cao S, Xu D, Wang W, Ye N (2013) Photoprotection in the green tidal alga *Ulva prolifera*: Role of LHCSR and PsbS proteins in response to high light stress. Plant Biol **15**: 1033–9

Msanne J, Xu D, Konda AR, Casas-Mollano JA, Awada T, Cahoon EB, Cerutti H (2012) Metabolic and gene expression changes triggered by nitrogen deprivation in the photoautotrophically grown microalgae *Chlamydomonas reinhardtii* and *Coccomyxa* sp. C-169. Phytochemistry **75**: 50–59

Mueller SJ, Lang D, Hoernstein SNW, Lang EGE, Schuessele C, Schmidt A, Fluck M, Leisibach D, Niegl C, Zimmer AD, et al (2014) Quantitative analysis of the mitochondrial and plastid proteomes of the moss *Physcomitrella patens* reveals protein macrocompartmentation and microcompartmentation. Plant Physiol **164**: 2081–2095

Mühlhaus T, Weiss J, Hemme D, Sommer F, Schroda M (2011) Quantitative shotgun proteomics using a uniform ^{15}N-labeled standard to monitor proteome dynamics in time course experiments reveals new insights into the heat stress response of *Chlamydomonas reinhardtii*. Mol Cell Proteomics **10**: M110.004739, 1–27

Mühlroth A, Winge P, El Assimi A, Jouhet J, Maréchal E, Hohmann-Marriott MF, Vadstein O, Bones AM (2017) Mechanisms of phosphorus acquisition and lipid class remodeling under P limitation in a marine microalga. Plant Physiol **175**: 1543-1559

Murata N, Sato N, Takahashi N (1984) Very-long-chain saturated fatty acids in phosphatidylserine from higher plant tissues. Biochim Biophys Acta **795**: 147–150

Nakamura Y (2017) Plant phospholipid diversity: Emerging functions in metabolism and protein–lipid interactions. Trends Plant Sci **22**: 1027–1040

Nakamura Y, Li-Beisson Y (2016) Lipids in plant and algae development, 1st ed. Springer International Publishing, Switzerland

Natter K, Leitner P, Faschinger A, Wolinski H, McCraith S, Fields S, Kohlwein SD (2005) The spatial organization of lipid synthesis in the yeast *Saccharomyces cerevisiae* derived from large scale green fluorescent protein tagging and high resolution microscopy. Mol Cell Proteomics **4**: 662–672

Ndimba BK, Ndimba RJ, Johnson TS, Waditee-Sirisattha R, Baba M, Sirisattha S, Shiraiwa Y, Agrawal GK, Rakwal R (2013) Biofuels as a sustainable energy source: An update of the applications of proteomics in bioenergy crops and algae. J Proteomics **93**: 234–244

Neilson KA, Ali NA, Muralidharan S, Mirzaei M, Mariani M, Assadourian G, Lee A, van Sluyter SC, Haynes PA (2011) Less label, more free: approaches in label-free quantitative mass spectrometry. Proteomics **11**: 535–553

Nesvizhskii AI, Keller A, Kolker E, Aebersold R (2003) A statistical model for identifying proteins by tandem mass spectrometry. Anal Chem **75**: 4646–4658

Newlon MG, Roy M, Morikis D, Carr DW, Westphal R, Scott JD, Jennings PA (2001) A novel mechanism of PKA anchoring revealed by solution structures of anchoring complexes. EMBO J **20**: 1651–1662

Nguyen HM, Baudet M, Cuiné S, Adriano J-M, Barthe D, Billon E, Bruley C, Beisson F, Peltier G, Ferro M, et al (2011) Proteomic profiling of oil bodies isolated from the unicellular green microalga *Chlamydomonas reinhardtii*: With focus on proteins involved in lipid metabolism. Proteomics **11**: 4266–4273

Nielsen E, Cheung AY, Ueda T (2008) The regulatory RAB and ARF GTPases for vesicular trafficking. Plant Physiol **147**: 1516–1526

Nikolovski N, Rubtsov D, Segura MP, Miles GP, Stevens TJ, Dunkley TPJ, Munro S, Lilley KS, Dupree P (2012) Putative glycosyltransferases and other plant Golgi apparatus proteins are revealed by LOPIT proteomics. Plant Physiol **160**: 1037–1051

Niyogi KK, Truong TB (2013) Evolution of flexible non-photochemical quenching mechanisms that regulate light harvesting in oxygenic photosynthesis. Curr Opin Plant Biol **16**: 307–314

Nogaj LA, Srivastava A, van Lis R, Beale SI (2005) Cellular levels of glutamyl-tRNA reductase and glutamate-1-semialdehyde aminotransferase do not control chlorophyll synthesis in *Chlamydomonas reinhardtii*. Plant Physiol **139**: 389–396

Nordhues A, Schöttler MA, Unger A-K, Geimer S, Schönfelder S, Schmollinger S, Rütgers M, Finazzi G, Soppa B, Sommer F, et al (2012) Evidence for a role of VIPP1 in the structural organization of the photosynthetic apparatus in Chlamydomonas. Plant Cell **24**: 637–59

Nühse TS, Stensballe A, Jensen ON, Peck SC (2004) Phosphoproteomics of the Arabidopsis plasma membrane and a new phosphorylation site database. Plant Cell **16**: 2394–405

Nukarinen E, Nägele T, Pedrotti L, Wurzinger B, Mair A, Landgraf R, Börnke F, Hanson J, Teige M, Baena-Gonzalez E, Dröge-Laser W, Weckwerth W (2016) Quantitative phosphoproteomics reveals a role of the AMPK plant ortholog SnRK1 as a metabolic master regulator under energy deprivation. Sci Rep **6**: 31697

Old WM, Meyer-Arendt K, Aveline-Wolf L, Pierce KG, Mendoza A, Sevinsky JR, Resing KA, Ahn NG (2005) Comparison of label-free methods for quantifying human proteins by shotgun proteomics. Mol Cell Proteomics **4**: 1487–1502

Olguín EJ, Castillo OS, Mendoza A, Tapia K, González-Portela RE, Hernández-Landa VJ (2015) Dual purpose system that treats anaerobic effluents from pig waste and produce *Neochloris oleoabundans* as lipid rich biomass. N Biotechnol **32**: 387–395

Ou Y-Y, Gromiha MM, Chen S-A, Suwa M (2008) TMBETADISC-RBF: Discrimination of beta-barrel membrane proteins using RBF networks and PSSM profiles. Comput Biol Chem **32**: 227–231

Ozawa S, Nield J, Terao A, Stauber EJ, Hippler M, Koike H, Rochaix J-D, Takahashi Y (2009) Biochemical and structural studies of the large Ycf4-photosystem I assembly complex of the green alga *Chlamydomonas reinhardtii*. Plant Cell **21**: 2424–2442

Palmieri L, Arrigoni R, Blanco E, Carrari F, Zanor MI, Studart-Guimaraes C, Fernie AR, Palmieri F (2006) Molecular identification of an Arabidopsis *S*-adenosylmethionine transporter. Analysis of organ distribution, bacterial expression, reconstitution into liposomes, and functional characterization. Plant Physiol **142**: 855–65

Parry R V, Turner JC, Rea PA (1989) High purity preparations of higher plant vacuolar H^+-ATPase reveal additional subunits. Revised subunit composition. J Biol Chem **264**: 20025–32

Parsons HT, Christiansen K, Knierim B, Carroll A, Ito J, Batth TS, Smith-Moritz AM, Morrison S, McInerney P, Hadi MZ, et al (2012) Isolation and proteomic characterization of the Arabidopsis Golgi defines functional and novel components involved in plant cell wall biosynthesis. Plant Physiol **159**: 12–26

Peers G, Truong TB, Ostendorf E, Busch A, Elrad D, Grossman AR, Hippler M, Niyogi KK (2009) An ancient light-harvesting protein is critical for the regulation of algal photosynthesis. Nature **462**: 518–521

Pegg C, Wolf M, Alanagreh L, Portman R, Buchheim MA (2015) Morphological diversity masks phylogenetic similarity of Ettlia and Haematococcus (Chlorophyceae). Phycologia **54**: 385–397

Peled E, Leu S, Zarka A, Weiss M, Pick U, Khozin-Goldberg I, Boussiba S (2011) Isolation of a novel oil globule protein from the green alga *Haematococcus pluvialis* (Chlorophyceae). Lipids **46**: 851–861

Peltier J-B, Cai Y, Sun Q, Zabrouskov V, Giacomelli L, Rudella A, Ytterberg AJ, Rutschow H, van Wijk KJ (2006) The oligomeric stromal proteome of *Arabidopsis thaliana* chloroplasts. Mol Cell Proteomics **5**: 114–133

Penno A, Hackenbroich G, Thiele C (2013) Phospholipids and lipid droplets. Biochim Biophys Acta - Mol Cell Biol Lipids **1831**: 589–594

Pérez-Martinez X, Antaramian A, Vázquez-Acevedo M, Funes S, Tolkunova E, D'Alayer J, Claros MG, Davidson E, King MP, González-Halphen D (2001) Subunit II of cytochrome c oxidase in Chlamydomonad algae is a heterodimer encoded by two independent nuclear genes. J Biol Chem **276**: 11302–11309

Pérez-Rodríguez P, Riaño-Pachón DM, Corrêa LGG, Rensing SA, Kersten B, Mueller-Roeber B (2010) PlnTFDB: Updated content and new features of the plant transcription factor database. Nucleic Acids Res **38**: D822–827

Peters K, Belt K, Braun H-P (2013) 3D Gel Map of Arabidopsis Complex I. Front Plant Sci **4**: 153

Petroutsos D, Busch A, Janssen I, Trompelt K, Bergner SV, Weinl S, Holtkamp M, Karst U, Kudla J, Hippler M (2011) The chloroplast calcium sensor CAS is required for photoacclimation in *Chlamydomonas reinhardtii*. Plant Cell **23**: 2950–2963

Pohlmeyer K, Soll J, Grimm R, Hill K, Wagner R (1998) A high-conductance solute channel in the chloroplastic outer envelope from pea. Plant Cell **10**: 1207–1216

Popovich CA, Damiani C, Constenla D, Martínez AM, Freije H, Giovanardi M, Pancaldi S, Leonardi PI (2012) *Neochloris oleoabundans* grown in enriched natural seawater for biodiesel feedstock: Evaluation of its growth and biochemical composition. Bioresour Technol **114**: 287–293

Poulsen LR, López-Marqués RL, McDowell SC, Okkeri J, Licht D, Schulz A, Pomorski T, Harper JF, Palmgren MG (2008) The Arabidopsis P4-ATPase ALA3 localizes to the Golgi and requires a beta-subunit to function in lipid translocation and secretory vesicle formation. Plant Cell **20**: 658–676

Pruvost J, Van Vooren G, Cogne G, Legrand J (2009) Investigation of biomass and lipids production with *Neochloris oleoabundans* in photobioreactor. Bioresour Technol **100**: 5988–5995

Qi Y, Tsuda K, Nguyen L V, Wang X, Lin J, Murphy AS, Glazebrook J, Thordal-Christensen H, Katagiri F (2011) Physical association of Arabidopsis hypersensitive induced reaction proteins (HIRs) with the immune receptor RPS2. J Biol Chem **286**: 31297–31307

Rashidi B, Trindade LM (2018) Detailed biochemical and morphologic characteristics of the green microalga *Neochloris oleoabundans* cell wall. Algal Res **35**: 152-159

Rawlings ND, Waller M, Barrett AJ, Bateman A (2014) MEROPS: The database of proteolytic enzymes, their substrates and inhibitors. Nucleic Acids Res **42**: D503–509

Ren J, Lin CP-C, Pathak MC, Temple BRS, Nile AH, Mousley CJ, Duncan MC, Eckert DM, Leiker TJ, Ivanova PT, et al (2014) A phosphatidylinositol transfer protein integrates phosphoinositide signaling with lipid droplet metabolism to regulate a developmental program of nutrient stress–induced membrane biogenesis. Mol Biol Cell **25**: 712–727

Reumann S, Quan S, Aung K, Yang P, Manandhar-Shrestha K, Holbrook D, Linka N, Switzenberg R, Wilkerson CG, Weber APM, et al (2009) In-depth proteome analysis of Arabidopsis leaf peroxisomes combined with in vivo subcellular targeting verification indicates novel metabolic and regulatory functions of peroxisomes. Plant Physiol **150**: 125–143

Riekhof WR, Sears BB, Benning C (2005) Annotation of genes involved in glycerolipid biosynthesis in *Chlamydomonas reinhardtii*: Discovery of the betaine lipid synthase BTA1Cr. Eukaryot Cell **4**: 242–252

Rismani-Yazdi H, Haznedaroglu BZ, Hsin C, Peccia J (2012) Transcriptomic analysis of the oleaginous microalga *Neochloris oleoabundans* reveals metabolic insights into triacylglyceride accumulation. Biotechnol Biofuels **5**: 74

Rodrigues RB, Sabat G, Minkoff BB, Burch HL, Nguyen TT, Sussman MR (2014) Expression of a translationally fused TAP-tagged plasma membrane proton pump in *Arabidopsis thaliana*. Biochemistry **53**: 566–578

Rodríguez-Salinas E, Riveros-Rosas H, Li Z, Fuciková K, Brand JJ, Lewis LA, González-Halphen D (2012) Lineage-specific fragmentation and nuclear relocation of the mitochondrial cox2 gene in chlorophycean green algae (Chlorophyta). Mol Phylogenet Evol **64**: 166–176

Sabia A, Baldisserotto C, Biondi S, Marchesini R, Tedeschi P, Maietti A, Giovanardi M, Ferroni L, Pancaldi S (2015) Re-cultivation of *Neochloris oleoabundans* in exhausted autotrophic and mixotrophic media: the potential role of polyamines and free fatty acids. Appl Microbiol Biotechnol **99**: 10597-10609

Sahonero-Canavesi DX, Sohlenkamp C, Sandoval-Calderón M, Lamsa A, Pogliano K, López-Lara IM, Geiger O (2015) Fatty acid-releasing activities in *Sinorhizobium meliloti* include unusual diacylglycerol lipase. Environ Microbiol **17**: 3391–3406

Saier MH, Reddy VS, Tamang DG, Västermark Å (2014) The transporter classification database. Nucleic Acids Res **42**: D251–258

Salie MJ, Zhang N, Lancikova V, Xu D, Thelen JJ (2016) A family of negative regulators targets the committed step of de novo fatty acid biosynthesis. Plant Cell **28**: 2312-2325

Sakurai K, Mori N, Sato N (2014) Detection and characterization of phosphatidylcholine in various strains of the genus Chlamydomonas (Volvocales, Chlorophyceae). J Plant Res **127**: 641–650

Santos AM, Janssen M, Lamers PP, Evers W a C, Wijffels RH (2012) Growth of oil accumulating microalga *Neochloris oleoabundans* under alkaline-saline conditions. Bioresour Technol **104**: 593–599

Sato N, Mori N, Hirashima T, Moriyama T (2016) Diverse pathways of phosphatidylcholine biosynthesis in algae as estimated by labeling studies and genomic sequence analysis. Plant J **87**: 281–292

Schmidt M, Gessner G, Luff M, Heiland I, Wagner V, Kaminski M, Geimer S, Eitzinger N, Reissenweber T, Voytsekh O, et al (2006) Proteomic analysis of the eyespot of *Chlamydomonas reinhardtii* provides novel insights into its components and tactic movements. Plant Cell **18**: 1908–1930

Schmollinger S, Mühlhaus T, Boyle NR, Blaby IK, Casero D, Mettler T, Moseley JL, Kropat J, Sommer F, Strenkert D, et al (2014) Nitrogen-sparing mechanisms in Chlamydomonas affect the transcriptome, the proteome, and photosynthetic metabolism. Plant Cell **26**: 1410–1435

Schnoes AM, Brown SD, Dodevski I, Babbitt PC (2009) Annotation error in public databases: Misannotation of molecular function in enzyme superfamilies. PLoS Comput Biol **5**: e1000605

Schottkowski M, Peters M, Zhan Y, Rifai O, Zhang Y, Zerges W (2012) Biogenic membranes of the chloroplast in *Chlamydomonas reinhardtii*. Proc Natl Acad Sci U S A **109**: 19286–19291

Schwacke R, Schneider A, van der Graaff E, Fischer K, Catoni E, Desimone M, Frommer WB, Flügge U-I, Kunze R (2003) ARAMEMNON, a novel database for Arabidopsis integral membrane proteins. Plant Physiol **131**: 16–26

Seitz SB, Weisheit W, Mittag M (2010) Multiple roles and interaction factors of an E-box element in *Chlamydomonas reinhardtii*. Plant Physiol **152**: 2243–2257

Sheehan J, Dunahay T, Benemann J, Roessler PG (1998) A look back at the US Department of Energy's Aquatic Species Program - Biodiesel from algae, close out report TP-580-24190. Golden, CO: National Renewable Laboratory.

Shemi A, Schatz D, Fredricks HF, Van Mooy BAS, Porat Z, Vardi A (2016) Phosphorus starvation induces membrane remodeling and recycling in *Emiliania huxleyi*. New Phytol **211**: 886–898

Shi L-X, Hall M, Funk C, Schröder WP (2012) Photosystem II, a growing complex: Updates on newly discovered components and low molecular mass proteins. Biochim Biophys Acta **1817**: 13–25

Shi L-X, Schröder WP (2004) The low molecular mass subunits of the photosynthetic supracomplex, photosystem II. Biochim Biophys Acta **1608**: 75–96

Shields DJ, Altarejos JY, Wang X, Agellon LB, Vance DE (2003) Molecular dissection of the *S*-adenosylmethionine-binding site of phosphatidylethanolamine *N*-methyltransferase. J Biol Chem **278**: 35826–35836

Shockey J, Regmi A, Cotton K, Adhikari N, Browse J, Bates PD (2016) Identification of Arabidopsis GPAT9 (At5g60620) as an essential gene involved in triacylglycerol biosynthesis. Plant Physiol **170**: 163–179

Shockey JM, Fulda MS, Browse JA (2002) Arabidopsis contains nine long-chain acyl-coenzyme A synthetase genes that participate in fatty acid and glycerolipid metabolism. Plant Physiol **129**: 1710–1722

Shtaida N, Khozin-Goldberg I, Boussiba S (2015) The role of pyruvate hub enzymes in supplying carbon precursors for fatty acid synthesis in photosynthetic microalgae. Photosynth Res **125**: 407–422

Siegler H, Valerius O, Ischebeck T, Popko J, Tourasse NJ, Vallon O, Khozin-Goldberg I, Braus GH, Feussner I (2017) Analysis of the lipid body proteome of the oleaginous alga *Lobosphaera incisa*. BMC Plant Biol **17**: 98

Sievers F, Wilm A, Dineen D, Gibson TJ, Karplus K, Li W, Lopez R, McWilliam H, Remmert M, Söding J, et al (2011) Fast, scalable generation of high-quality protein multiple sequence alignments using Clustal Omega. Mol Syst Biol **7**: 539

Singer SD, Chen G, Mietkiewska E, Tomasi P, Jayawardhane K, Dyer JM, Weselake RJ (2016) Arabidopsis GPAT9 contributes to synthesis of intracellular glycerolipids but not surface lipids. J Exp Bot **67**: 4627–4638

Singh DK, McNellis TW (2011) Fibrillin protein function: The tip of the iceberg? Trends Plant Sci **16**: 432–441

Škunca N, Altenhoff A, Dessimoz C (2012) Quality of computationally inferred gene ontology annotations. PLoS Comput Biol **8**: e1002533

Smith SR, Abbriano RM, Hildebrand M (2012) Comparative analysis of diatom genomes reveals substantial differences in the organization of carbon partitioning pathways. Algal Res **1**: 2–16

Song P, Li L, Liu J (2013) Proteomic analysis in nitrogen-deprived Isochrysis galbana during lipid accumulation. PLoS One **8**: e82188

Sousa C, de Winter L, Janssen M, Vermuë MH, Wijffels RH (2012) Growth of the microalgae *Neochloris oleoabundans* at high partial oxygen pressures and sub-saturating light intensity. Bioresour Technol **104**: 565–570

Sparkes I, Tolley N, Aller I, Svozil J, Osterrieder A, Botchway S, Mueller C, Frigerio L, Hawes C (2010) Five Arabidopsis reticulon isoforms share endoplasmic reticulum location, topology, and membrane-shaping properties. Plant Cell **22**: 1333–43

Stabenau H, Winkler U, Säftel W (1984) Enzymes of beta-oxidation in different types of algal microbodies. Plant Physiol **75**: 531–533

Stabenau H, Winkler U, Säftel W (1993) Localization of glycolate dehydrogenase in two species of Dunaliella. Planta **191**: 362–364

Starr RC (1955) A comparative study of *Chlorococcum meneghini* and other spherical, zoospore-producing genera of the Chlorococcales. Indiana Univ Publ Sci Ser No. **20**: 1-11

Stauber EJ, Fink A, Markert C, Kruse O, Johanningmeier U, Hippler M (2003) Proteomics of *Chlamydomonas reinhardtii* light-harvesting proteins. Eukaryot Cell **2**: 978–994

Stephan A, Vaughan S, Shaw MK, Gull K, McKean PG (2007) An essential quality control mechanism at the eukaryotic basal body prior to intraflagellar transport. Traffic **8**: 1323–1330

Stern D (2009) The Chlamydomonas sourcebook: Organellar and metabolic processes, 2nd ed. Elsevier Academic Press, Canada

Sturme MHJ, Gong Y, Heinrich JM, Klok AJ, Eggink G, Wang D, Xu J, Wijffels RH (2018) Transcriptome analysis reveals the genetic foundation for the dynamics of starch and lipid production in *Ettlia oleoabundans*. Algal Res **33**: 142-155

Swatek KN, Wilson RS, Ahsan N, Tritz RL, Thelen JJ (2014) Multisite phosphorylation of 14-3-3 proteins by calcium-dependent protein kinases. Biochem J **459**: 15–25

Tamura K, Nei M (1993) Estimation of the number of nucleotide substitutions in the control region of mitochondrial DNA in humans and chimpanzees. Mol Biol Evol **10**: 512–526

Tan S, Tan HT, Chung MCM (2008) Membrane proteins and membrane proteomics. Proteomics **8**: 3924–3932

Tanz SK, Castleden I, Hooper CM, Vacher M, Small I, Millar H a. (2013) SUBA3: A database for integrating experimentation and prediction to define the subcellular location of proteins in Arabidopsis. Nucleic Acids Res **41**: 1185–1191

Tardif M, Atteia A, Specht M, Cogne G, Rolland N, Brugière S, Hippler M, Ferro M, Bruley C, Peltier G, et al (2012) PredAlgo: A new subcellular localization prediction tool dedicated to green algae. Mol Biol Evol **29**: 3625–3639

Terashima M, Specht M, Naumann B, Hippler M (2010) Characterizing the anaerobic response of *Chlamydomonas reinhardtii* by quantitative proteomics. Mol Cell Proteomics **9**: 1514–1532

The UniProt Consortium (2014) UniProt: a hub for protein information. Nucleic Acids Res **43**: D204–212

Theis J, Schroda M (2019) VIPP2 interacts with HSP22E/F at chloroplast membrane and modulates retrograde signal for HSP22E/F gene expression in *Chlamydomonas reinhardtii*. Plant Cell Environ. Submitted:

Tian L, Nawrocki WJ, Liu X, Polukhina I, van Stokkum IHM, Croce R (2019) pH dependence, kinetics and light-harvesting regulation of nonphotochemical quenching in Chlamydomonas. Proc Natl Acad Sci U S A **116**: 8320-8325

Tibiletti T, Auroy P, Peltier G, Caffarri S (2016) *Chlamydomonas reinhardtii* PsbS protein is functional and accumulates rapidly and transiently under high light. Plant Physiol **171**: 2717–2730

Tippery NP, Fuciková K, Lewis PO, Lewis LA (2012) Probing the monophyly of the Sphaeropleales (Chlorophyceae) using data from five genes. J Phycol **48**: 1482–1493

Tornabene TG, Holzer G, Lien S, Burris N (1983) Lipid composition of the nitrogen starved green alga *Neochloris oleoabundans*. Enzym Microb Technol **5**: 435–440

Tremblay A, Seabolt S, Zeng H, Zhang C, Böckler S, Tate DN, Duong VT, Yao N, Lu H (2016) A role of the FUZZY ONIONS LIKE gene in regulating cell death and defense in Arabidopsis. Sci Rep **6**: 37797

Tsai C-H, Zienkiewicz K, Amstutz CL, Brink BG, Warakanont J, Roston R, Benning C (2015) Dynamics of protein and polar lipid recruitment during lipid droplet assembly in *Chlamydomonas reinhardtii*. Plant J **83**: 650–660

Tusnády GE, Simon I (2001) The HMMTOP transmembrane topology prediction server. Bioinformatics **17**: 849–850

Urreta I, Ikaran Z, Janices I, Ibañez E, Castro-Puyana M, Castañón S, Suárez-Alvarez S (2014) Revalorization of *Neochloris oleoabundans* biomass as source of biodiesel by concurrent production of lipids and carotenoids. Algal Res **5**: 16–22

Valledor L, Furuhashi T, Recuenco-Muñoz L, Wienkoop S, Weckwerth W (2014) System-level network analysis of nitrogen starvation and recovery in *Chlamydomonas reinhardtii* reveals potential new targets for increased lipid accumulation. Biotechnol Biofuels **7**: 171

van Lis R, Atteia A, Nogaj LA, Beale SI (2005) Subcellular localization and light-regulated expression of protoporphyrinogen IX oxidase and ferrochelatase in *Chlamydomonas reinhardtii*. Plant Physiol **139**: 1946–1958

Vance DE (2014) Phospholipid methylation in mammals: From biochemistry to physiological function. Biochim Biophys Acta - Biomembr **1838**: 1477–1487

Vandepoele K, Van Bel M, Richard G, Van Landeghem S, Verhelst B, Moreau H, Van de Peer Y, Grimsley N, Piganeau G (2013) pico-PLAZA, a genome database of microbial photosynthetic eukaryotes. Environ Microbiol **15**: 2147–2153

Vaseghi M-J, Chibani K, Telman W, Liebthal MF, Gerken M, Schnitzer H, Mueller SM, Dietz K-J (2018) The chloroplast 2-cysteine peroxiredoxin functions as thioredoxin oxidase in redox regulation of chloroplast metabolism. eLife **7**: e38194

Vázquez-Acevedo M, Cardol P, Cano-Estrada A, Lapaille M, Remacle C, González-Halphen D (2006) The mitochondrial ATP synthase of chlorophycean algae contains eight subunits of unknown origin involved in the formation of an atypical stator-stalk and in the dimerization of the complex. J Bioenerg Biomembr **38**: 271–282

Vázquez-Acevedo M, Vega-deLuna F, Sánchez-Vásquez L, Colina-Tenorio L, Remacle C, Cardol P, Miranda-Astudillo H, González-Halphen D (2016) Dissecting the peripheral stalk of the mitochondrial ATP synthase of chlorophycean algae. Biochim Biophys Acta - Bioenerg **1857**: 1183–1190

Vences-Guzmán MA, Geiger O, Sohlenkamp C (2008) *Sinorhizobium meliloti* mutants deficient in phosphatidylserine decarboxylase accumulate phosphatidylserine and are strongly affected during symbiosis with Alfalfa. J Bacteriol **190**: 6846–6856

Vera-Estrella R, Barkla BJ, Bohnert HJ, Pantoja O (2004) Novel regulation of aquaporins during osmotic stress. Plant Physiol **135**: 2318–2329

Verrier PJ, Bird D, Burla B, Dassa E, Forestier C, Geisler M, Klein M, Kolukisaoglu Ü, Lee Y, Martinoia E, et al (2008) Plant ABC proteins - A unified nomenclature and updated inventory. Trends Plant Sci **13**: 151–159

Vincent P, Maneta-Peyret L, Cassagne C, Moreau P (2001) Phosphatidylserine delivery to endoplasmic reticulum-derived vesicles of plant cells depends on two biosynthetic pathways. FEBS Lett **498**: 32–36

Visram M, Radulovic M, Steiner S, Malanovic N, Eichmann TO, Wolinski H, Rechberger GN, Tehlivets O (2018) Homocysteine regulates fatty acid and lipid metabolism in yeast. J Biol Chem **293**: 5544–5555

Voigt J, Liebich I, Kiess M, Frank R (2001) Subcellular distribution of 14-3-3 proteins in the unicellular green alga *Chlamydomonas reinhardtii*. Eur J Biochem **268**: 6449–6457

Wang B, Lan CQ (2011) Biomass production and nitrogen and phosphorus removal by the green alga *Neochloris oleoabundans* in simulated wastewater and secondary municipal wastewater effluent. Biores Technol **102**: 5639–5644

Wang J, Virta VC, Riddelle-Spencer K, O'Halloran TJ (2003) Compromise of clathrin function and membrane association by clathrin light chain deletion. Traffic **4**: 891–901

Wang K, Froehlich JE, Zienkiewicz A, Hersh HL, Benning C (2017) A Plastid Phosphatidylglycerol Lipase contributes to the export of acyl groups from plastids for seed oil biosynthesis. Plant Cell **29**: 1678 LP-1696

Wang T, Sui Z, Liu X, Li Y, Li H, Xing J, Song F, Zhang Y, Sun Q, Ni Z (2016) Ectopic expression of a maize hybrid up-regulated gene, ErbB-3 binding Protein 1 (ZmEBP1), increases organ size by promoting cell proliferation in Arabidopsis. Plant Sci **243**: 23–34

Wang X, Liu Q, Zhang B (2014) Leveraging the complementary nature of RNA-Seq and shotgun proteomics data. Proteomics **14**: 2676–2687

Wang Z, Benning C (2012) Chloroplast lipid synthesis and lipid trafficking through ER-plastid membrane contact sites. Biochem Soc Trans **40**: 457–463

Wang ZT, Ullrich N, Joo S, Waffenschmidt S, Goodenough U (2009) Algal lipid bodies: stress induction, purification, and biochemical characterization in wild-type and starch-less *Chlamydomonas reinhardtii*. Eukaryot Cell **8**: 1856–1868

Wase N, Black PN, Stanley BA, DiRusso CC (2014) Integrated quantitative analysis of nitrogen stress response in *Chlamydomonas reinhardtii* using metabolite and protein profiling. J Proteome Res **13**: 1373–1396

Waszczak C, Carmody M, Kangasjärvi J (2018) Reactive oxygen species in plant signaling. Annu Rev Plant Biol **69**: 209-236

Waterborg JH, Robertson AJ, Tatar DL, Borza CM, Davie JR (1995) Histones of *Chlamydomonas reinhardtii*. Synthesis, acetylation, and methylation. Plant Physiol **109**: 393–407

Wei L, Xin Y, Wang D, Jing X, Zhou Q, Su X, Jia J, Ning K, Chen F, Hu Q, et al (2013) Nannochloropsis plastid and mitochondrial phylogenomes reveal organelle diversification mechanism and intragenus phylotyping strategy in microalgae. BMC Genomics **14**: 534

Welti R, Li W, Li M, Sang Y, Biesiada H, Zhou HE, Rajashekar CB, Williams TD, Wang X (2002) Profiling membrane lipids in plant stress responses: Role of phospholipase Dα in freezing-induced lipid changes in Arabidopsis. J Biol Chem **277**: 31994–32002

Welti R, Wang X, Williams TD (2003) Electrospray ionization tandem mass spectrometry scan modes for plant chloroplast lipids. Anal Biochem **314**: 149–152

Wetzel CM, Harmacek LD, Yuan LH, Wopereis JLM, Chubb R, Turini P (2009) Loss of chloroplast protease SPPA function alters high light acclimation processes in *Arabidopsis thaliana* L. (Heynh.). J Exp Bot **60**: 1715–1727

Wijffels RH (2008) Potential of sponges and microalgae for marine biotechnology. Trends Biotechnol **26**: 26-31

Wildgruber R, Weber G, Wise P, Grimm D, Bauer J (2014) Free-flow electrophoresis in proteome sample preparation. Proteomics **14**: 629–636

Willmund F, Dorn K V, Schulz-Raffelt M, Schroda M (2008) The chloroplast DnaJ homolog CDJ1 of *Chlamydomonas reinhardtii* is part of a multichaperone complex containing HSP70B, CGE1, and HSP90C. Plant Physiol **148**: 2070–82

Wu N, Li Y, Lan CQ (2011) Production and rheological studies of microalgal extracellular biopolymer from lactose using the green alga *Neochloris oleoabundans*. J Polym Env **19**: 935–942

Wurzinger B, Nukarinen E, Nägele T, Weckwerth W, Teige M (2018) The SnRK1 kinase as a central mediator of energy signaling between different organelles. Plant Physiol **176:** 1085-1094

Xiao S, Gao W, Chen Q-F, Chan S-W, Zheng S-X, Ma J, Wang M, Welti R, Chye M-L (2010) Overexpression of Arabidopsis Acyl-CoA Binding Protein ACBP3 promotes starvation-induced and age-dependent leaf senescence. Plant Cell **22**: 1463–1482

Xue H, Tokutsu R, Bergner SV, Scholz M, Minagawa J, Hippler M (2015) PHOTOSYSTEM II SUBUNIT R is required for efficient binding of LIGHT-HARVESTING COMPLEX STRESS-RELATED PROTEIN3 to photosystem II-light-harvesting supercomplexes in *Chlamydomonas reinhardtii*. Plant Physiol **167**: 1566–78

Yamaguchi K, Beligni MV, Prieto S, Haynes PA, McDonald WH, Yates III JR, Mayfield SP (2003) Proteomic characterization of the *Chlamydomonas reinhardtii* chloroplast ribosome: Identification of proteins unique to the 70 S ribosome. J Biol Chem **278**: 33774–33785

Yamano T, Tsujikawa T, Hatano K, Ozawa S, Takahashi Y, Fukuzawa H (2010) Light and low-CO_2-dependent LCIB-LCIC complex localization in the chloroplast supports the carbon-concentrating mechanism in *Chlamydomonas reinhardtii*. Plant Cell Physiol **51**: 1453–1468

Yan C, Fan J, Xu C (2013) Chapter 5 - Analysis of oil droplets in microalgae. *In* H Yang, PBT-M in CB Li, eds, Lipid Droplets. Academic Press, pp 71–82

Yang D, Song D, Kind T, Ma Y, Hoefkens J, Fiehn O (2015) Lipidomic analysis of *Chlamydomonas reinhardtii* under nitrogen and sulfur deprivation. PLoS One **10**: e0137948

Yang P, Diener DR, Yang C, Kohno T, Pazour GJ, Dienes JM, Agrin NS, King SM, Sale WS, Kamiya R, et al (2006) Radial spoke proteins of Chlamydomonas flagella. J Cell Sci **119**: 1165–1174

Yang Y, Mininberg B, Tarbet A, Weathers P (2013) At high temperature lipid production in *Ettlia oleoabundans* occurs before nitrate depletion. Appl Microbiol Biotechnol **97**: 2263–2273

Yang Y, Xu J, Vail D, Weathers P (2011) *Ettlia oleoabundans* growth and oil production on agricultural anaerobic waste effluents. Bioresour Technol **102**: 5076–5082

Ye C, Sutter BM, Wang Y, Kuang Z, Tu BP (2017) A metabolic function for phospholipid and histone methylation. Mol Cell **66**: 180–193

Yilancioglu K, Cokol M, Pastirmaci I, Erman B, Cetiner S (2014) Oxidative stress is a mediator for increased lipid accumulation in a newly isolated *Dunaliella salina* strain. PLoS One **9**: e91957

Yohn CB, Cohen A, Danon A, Mayfield SP (1998) A poly(A) binding protein functions in the chloroplast as a message-specific translation factor. Proc Natl Acad Sci U S A **95**: 2238–43

Yoo C, Choi G-G, Kim S-C, Oh H-M (2013) *Ettlia* sp. YC001 showing high growth rate and lipid content under high CO_2. Bioresour Technol **127**: 482–488

Yoon K, Han D, Li Y, Sommerfeld M, Hu Q (2012) Phospholipid:diacylglycerol acyltransferase is a multifunctional enzyme involved in membrane lipid turnover and degradation while synthesizing triacylglycerol in the unicellular green microalga *Chlamydomonas reinhardtii*. Plant Cell **24**: 3708–3724

Yoshida K, Ohnishi M, Fukao Y, Okazaki Y, Fujiwara M, Song C, Nakanishi Y, Saito K, Shimmen T, Suzaki T, et al (2013) Studies on vacuolar membrane microdomains isolated from Arabidopsis suspension-cultured cells: Local distribution of vacuolar membrane proteins. Plant Cell Physiol **54**: 1571–1584

Zavaleta-Pastor M, Sohlenkamp C, Gao J-L, Guan Z, Zaheer R, Finan TM, Raetz CRH, Lopez-Lara IM, Geiger O (2010) *Sinorhizobium meliloti* phospholipase C required for lipid remodeling during phosphorus limitation. Proc Natl Acad Sci **107**: 302–307

Zhan J, Zhu X, Zhou W, Chen H, He C, Wang Q (2016) Thf1 interacts with PS I and stabilizes the PS I complex in *Synechococcus* sp. PCC7942. Mol Microbiol **102**: 738–751

Zhan Y, Marchand CH, Maes A, Mauries A, Sun Y, Dhaliwal JS, Uniacke J, Arragain S, Jiang H, Gold ND, Martin VJJ, Lemaire SD, Zerges W (2018) Pyrenoid functions revealed by proteomics in *Chlamydomonas reinhardtii*. PLoS One **13**: e0185039

Zhang L, Kondo H, Kamikubo H, Kataoka M, Sakamoto W (2016) VIPP1 has a disordered C-terminal tail necessary for protecting photosynthetic membranes against stress. Plant Physiol **171**: 1983–95

Zhang X, Ye N, Mou S, Xu D, Fan X (2013a) Occurrence of the PsbS and LhcSR products in the green alga *Ulva linza* and their correlation with excitation pressure. Plant Physiol Biochem **70**: 336–341

Zhang Y, Wen Z, Washburn MP, Florens L (2010) Refinements to label free proteome quantitation: How to deal with peptides shared by multiple proteins. Anal Chem **82**: 2272–2281

Zhang Y-M, Chen H, He C-L, Wang Q (2013b) Nitrogen starvation induced oxidative stress in an oil-producing green alga *Chlorella sorokiniana* C3. PLoS One **8**: e69225

Zhang ZJ, Peck SC (2011) Simplified enrichment of plasma membrane proteins for proteomic analyses in *Arabidopsis thaliana*. Proteomics **11**: 1780–1788

Zhao C, Wang Y, Chan KX, Marchant DB, Franks PJ, Randall D, Tee EE, Chen G, Ramesh S, Phua SY, et al. (2019) Evolution of chloroplast retrograde signaling facilitates green plant adaptation to land. Proc Natl Acad Sci U S A **116**: 5015–5020

Zhou X, Graham TR (2009) Reconstitution of phospholipid translocase activity with purified Drs2p, a type-IV P-type ATPase from budding yeast. Proc Natl Acad Sci **106**: 16586–16591

Zhou X, Li Q, Chen X, Liu J, Zhang Q, Liu Y, Liu K, Xu J (2011a) The Arabidopsis RETARDED ROOT GROWTH gene encodes a mitochondria-localized protein that is required for cell division in the root meristem. Plant Physiol **157**: 1793–804

Zhou Z, Marepally S, Nune D, Pallakollu P, Ragan G, Roth MR, Wang L, Lushington G, Visvanathan M, Welti R (2011b) LipidomeDB data calculation environment: online processing of direct-infusion mass spectral data for lipid profiles. Lipids **46**: 879–884

Zienkiewicz K, Du Z-Y, Ma W, Vollheyde K, Benning C (2016) Stress-induced neutral lipid biosynthesis in microalgae — Molecular, cellular and physiological insights. Biochim Biophys Acta - Mol Cell Biol Lipids **1861**: 1269–1281

Zybailov B, Rutschow H, Friso G, Rudella A, Emanuelsson O, Sun Q, van Wijk KJ (2008) Sorting signals, N-terminal modifications and abundance of the chloroplast proteome. PLoS One **3**: e1994

APPENDIX A

Supplemental material from Chapter 4

A.1. Supplemental information. Additional biological processes represented in the *Ettlia oleoabundans* membrane proteome.

Several biological processes associated to *E. oleoabundans* membranes corresponded to typical responses of microalgae to N-deficient conditions. Accordingly, transporters for the uptake of both, typical and alternative N sources such as nitrate, ammonia, urea, and choline, were identified together with enzymes involved in ammonia assimilation, such as glutamine synthetase and carbamoyl-phosphate synthetase (Table S4.6). Protein turnover was also represented by proteolysis-related proteins, including membrane-bound chloroplast proteases involved in photoprotection (Table S4.1), such as FTSH ATP-dependent zinc metalloproteases and the SPPA serine protease (Stern, 2009; Wetzel et al., 2009; Luciński and Jackowski, 2013), as well as aspartic and cysteine proteinases, and specific inhibitors of both, cysteine and serine proteases (Table S4.8). In addition, we were able to identify several members of the major chaperone families (Hsp70, Hsp60, Hsp100/Clp, sHsp), which appeared to be targeted to different cell locations (chloroplast, mitochondria, endoplasmic reticulum [ER]), together with other proteins with chaperone functions, including the peptidyl-prolyl cis-trans isomerase, protein disulfide isomerase, and calnexin/calreticulin (Table S4.8). Identification of these proteins supports the existence of protein quality control and degradation mechanisms in different cell compartments of N-deprived *E. oleoabundans*. The functioning of the protein machinery did not seem to be compromised under N deprivation, as it was represented in *E. oleoabundans* membranes by both, cytosolic (53 out of 80 proteins) and chloroplastic (6 out of 51 proteins) ribosomal proteins, translation initiation and elongation factors, translational regulators, an alanine-tRNA ligase, and members of the ER and chloroplast translocons (Table S4.7 and S4.8). Protection against oxidative stress, to which N-deprived microalgae are submitted as a consequence of macronutrient limitation (Grossman and Takahashi, 2001; Schmollinger et al., 2014), was represented by proteins involved in removal of reactive oxygen species and redox signaling responses (Table S4.13), including an m-type thioredoxin, a glutaredoxin, and peroxidases, such as a thioredoxin-dependent 2-cys peroxidase, a cytochrome c peroxidase, and a probable L-ascorbate peroxidase.

A decrease in the chlorophyll content of N-deprived *E. oleoabundans* has been documented previously (Pruvost et al., 2009; Rismani-Yazdi et al., 2012). Despite the chlorosis phenotype, the chlorophyll biosynthesis pathway was well represented in the microsomes of N-deficient *E. oleabundans* (Table S4.5) by proteins common to the biosynthesis of all tetrapyrroles as well as some specific to chlorophyll biosynthesis. Moreover, Ferrochelatase, which is a protein exclusive to heme biosynthesis (Stern, 2009), was also identified; this finding is consistent with maintenance of the respiratory and photosynthetic electron transport in N-deficient cells. This conclusion is supported by the fact that photosynthesis and mitochondrial respiration were some of the most well-covered biological processes in this work. Carotenoid biosynthesis was also represented in this study (Table S4.5) despite the decrease that has been observed in the total carotenoid content of *E. oleoabundans* cultures under nitrate deficiency (Urreta et al., 2014).

The identification of proteins related to calcium and light-mediated signal transduction mechanisms (Table S4.11), suggests that they are active in *E. oleoabundans* under N stress. The detection of a 14-3-3 protein, together with several calcium-binding proteins, agrees with previous results in N-deficient *Chlamydomonas reinhardtii*, where these type of signaling proteins are present in high abundance (Motiwalla et al., 2014; Valledor et al., 2014; Wase et al., 2014). Additionally, two photoreceptors were identified in N-starved *E. oleoabundans*: a phototropin and an opsin-like protein. Phototrophin has been associated with a variety of blue-light-regulated physiological processes, including the expression of genes encoding chlorophyll-binding proteins as well as chlorophyll and carotenoid biosynthesis enzymes (Im et al., 2006). The identified opsin-like protein in *E. oleoabundans* is a homolog of the animal-type rhodopsins chlamyopsin-2 (COP2) and volvoxopsin-1 from *C. reinhardtii* and *Volvox carteri*, respectively. The function of these proteins has been related to photosynthesis (Kianianmomeni and Hallmann, 2014), as COP2 has been proposed to regulate the biogenesis of the photosystem I complex in response to varying light conditions (Ozawa et al., 2009).

Transcription regulation in N-deprived *E. oleoabundans* may be also active, as indicated by the identification of proteins related to transcriptional control, together with other RNA-processing and binding proteins (Table S4.10). These proteins include a transcription factor of the CSD (Cold Shock Domain) family, a transcriptional regulator of the GNAT (GCN5-related *N*-acetyltransferase) family, and a homolog of the HLA8 (High Light Activated 8) protein from *C. reinhardtii*, which has been proposed to perform as a transcriptional co-regulator via an E-box regulatory element (Seitz et al., 2010). Members of both, the CSD

and GNAT families, have been identified as regulatory hubs that control lipid accumulation during N deprivation in *C. reinhardtii* (Gargouri et al., 2015). Accordingly, their *E. oleoabundans* homologs may also be relevant for the microalga's oleaginous phenotype.

A.2. Supplemental figures

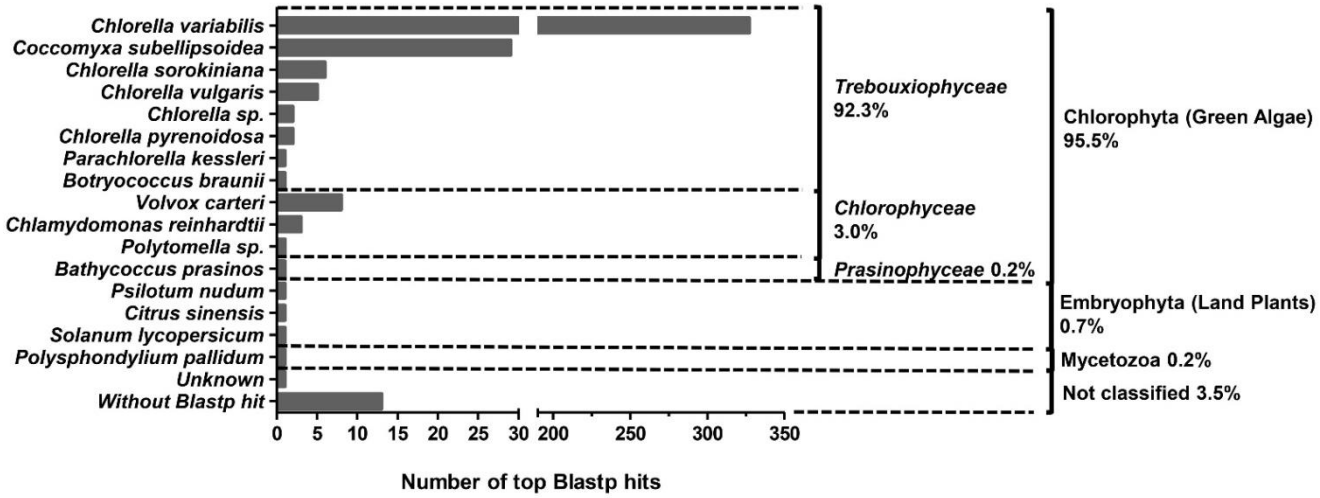

Figure S4.1. Blastp best hits for *E. oleoabundans* membrane proteins Top-hit species distribution of the Blastp analysis of the membrane proteome of N-deficient *E. oleoabundans*. The number of top-hits per specie is shown. For taxonomic groups of interest, the amount of top-hits is represented as a percentage with respect to the total of identified proteins (404).

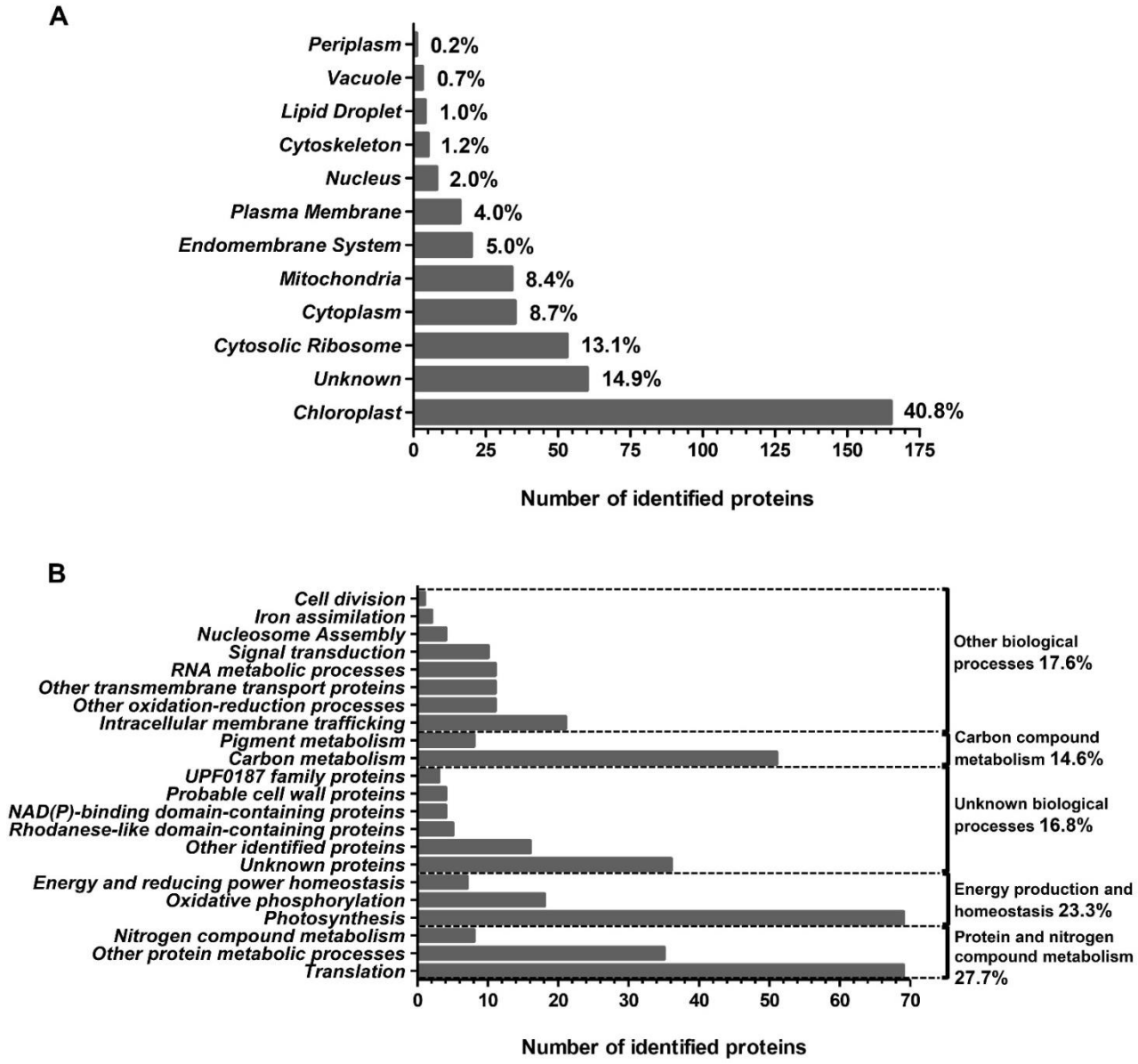

Figure S4.2. Cellular component (A) and biological process (B) distributions of identified proteins. Assignments were initially performed using the Blast2GO and QuickGO tools for Gene Ontology searching and then manually curated as described in the Methods section. Each protein is represented only once by either a cell compartment and a biological process term, according to the principal cell location in which the protein performs its main biological process. Well-known cytosolic proteins and those targeted to several cellular locations, including chloroplast-mitochondria dual-targeted proteins, were classified as cytoplasmic. The number of proteins represented in each term is indicated, as well as their percentage compared to the total of identified proteins (404).

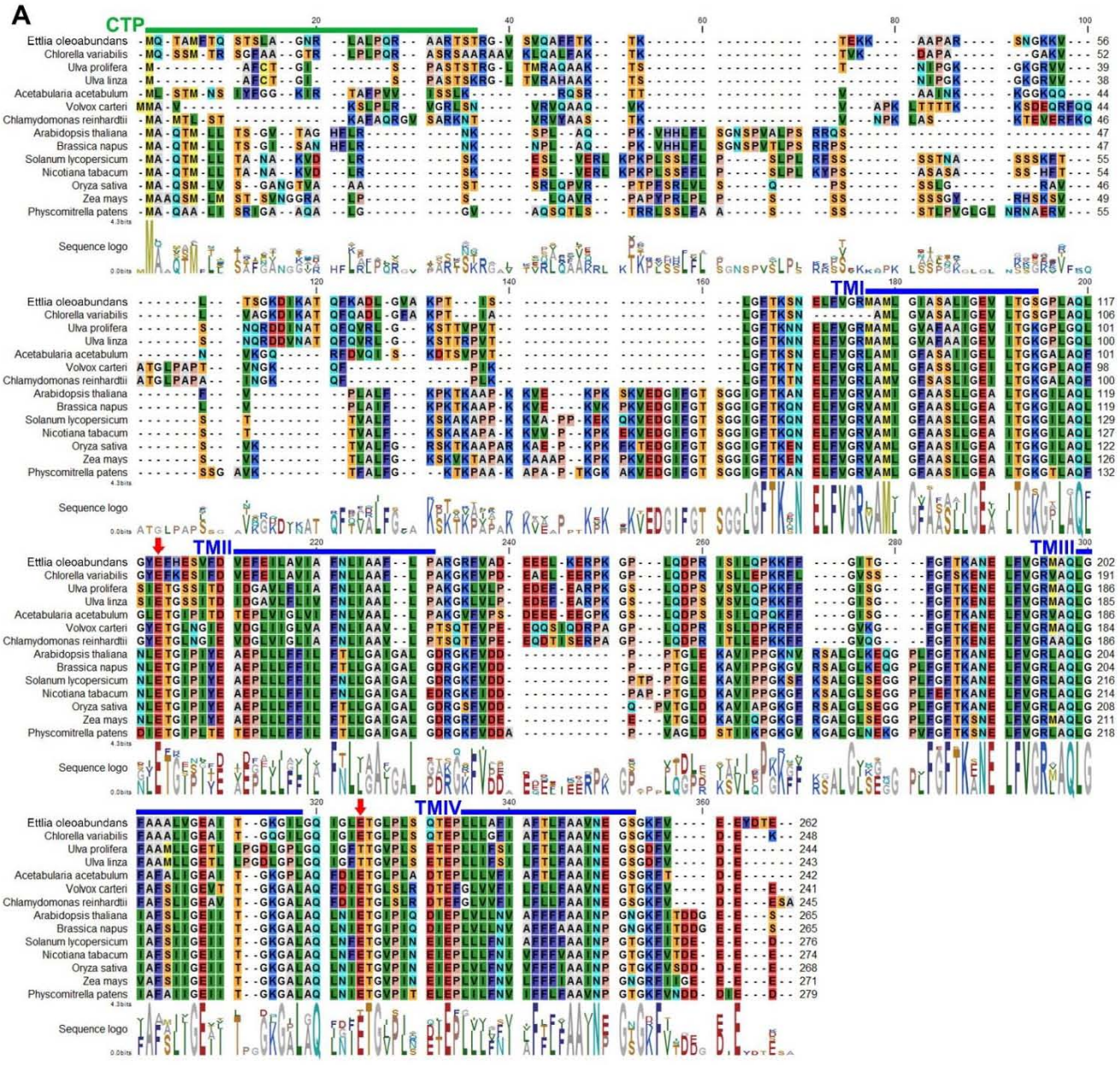

B

		1	2	3	4	5	6	7	8	9	10	11	12	13	14
m.395061 Ettlia oleoabundans	1		74.90	55.06	53.93	52.45	46.59	46.10	30.53	30.22	32.40	31.88	31.21	31.75	31.78
E1Z5K0 Chlorella variabilis	2	197		52.47	51.33	50.96	45.45	43.68	29.62	29.30	29.02	28.48	29.32	28.62	30.28
K7TEQ9 Ulva prolifera	3	147	138		97.13	51.75	42.91	42.18	27.65	27.01	31.51	30.97	33.22	33.11	30.23
G8HZH3 Ulva linza	4	144	135	237		51.36	42.54	41.82	27.97	27.33	31.83	31.29	32.57	32.79	29.90
A4QPL3 Acetabularia acetabulum	5	139	133	133	132		49.81	50.75	34.65	34.65	35.64	34.11	35.81	34.69	34.65
D8UAT1 Volvox carteri	6	130	125	115	114	131		77.51	29.97	29.65	30.60	30.06	30.97	30.77	31.55
A8HPM2 Chlamydomonas reinhardtii	7	130	121	116	115	135	193		30.91	30.60	30.31	30.41	30.77	29.84	30.31
Q9XF91 Arabidopsis thaliana	8	98	93	86	87	105	95	98		95.09	73.59	70.92	69.86	66.55	59.52
A0A078HF58 Brassica napus	9	97	92	84	85	105	94	97	252		73.24	71.28	69.15	66.20	58.84
P54773 Solanum lycopersicum	10	104	92	98	99	108	97	97	209	208		91.30	72.18	71.93	62.33
Q9SMB4 Nicotiana tabacum	11	102	90	96	97	103	95	97	200	201	252		73.05	69.72	60.82
Q943K1 Oryza sativa	12	98	90	101	99	106	96	96	197	195	205	206		80.00	66.67
B6TKD1 Zea mays	13	100	89	101	100	102	96	94	191	190	205	198	220		63.99
A9TJ15 Physcomitrella patens	14	102	96	94	93	105	100	97	175	173	182	177	190	183	

Figure S4.3. Sequence analysis of *Eo*PSBS. (A) Sequence alignment of *Eo*PSBS and its homologs. Full-length amino acid sequences were aligned with webPRANK. Amino acids are colored according to the RasMol color scheme. The predicted CTP (PredAlgo, green line), TM domains (HMMTOP v2.0, blue lines), and conserved residues for PSBS pH-sensing (red arrows) are indicated. The UniProtKB accession numbers are provided in (B). (B) Pairwise comparison among PSBS proteins listed in (A) shows the percentage identity (upper right values) and number of identical residues (bottom left values).

A

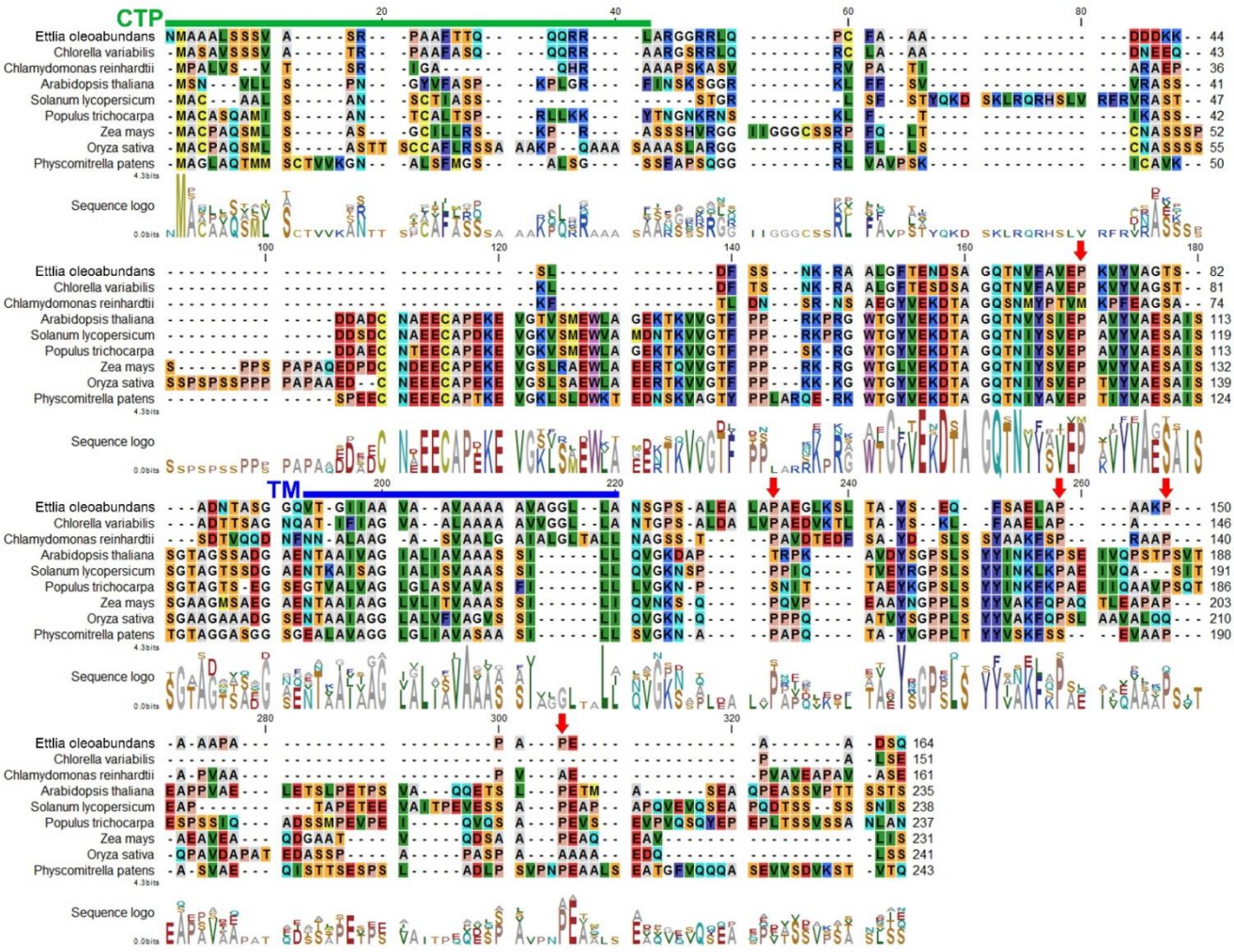

B

		1	2	3	4	5	6	7	8	9
m.337748 Ettlia oleoabundans	1		67.68	28.00	16.42	17.25	17.12	21.03	19.08	17.90
E1ZHT1 Chlorella variabilis	2	111		31.03	19.17	18.50	18.36	18.33	18.39	18.75
A8HSE5 Chlamydomonas reinhardtii	3	49	54		17.84	18.75	19.29	19.84	17.18	21.74
Q672Q7 Solanum lycopersicum	4	45	51	48		58.62	53.41	41.94	38.83	36.69
Q9FL44 Arabidopsis thaliana	5	44	47	48	153		56.56	45.17	42.44	38.22
U5GJS3 Populus trichocarpa	6	44	47	49	141	138		44.40	41.70	40.39
B4FTC2 Zea mays	7	53	46	50	117	117	115		61.75	37.17
Q6ZI79 Oryza sativa	8	50	48	45	113	115	113	155		36.30
A9TBC1 Physcomitrella patens	9	46	48	55	102	99	103	100	102	

Figure S4.4. Sequence analysis of *Eo*MPH1. (A) Sequence alignment of *Eo*MPH1 and its homologs. Full-length amino acid sequences were aligned with webPRANK. Amino acids are colored according to the RasMol color scheme. The predicted CTP (PredAlgo, green line), TM domain (HMMTOP v2.0, blue line), and conserved proline residues (red arrows) are indicated. The UniProtKB accession numbers are provided in (B). (B) Pairwise comparison among MPH1 homologs listed in (A) shows the percentage identity (upper right values) and number of identical residues (bottom left values).

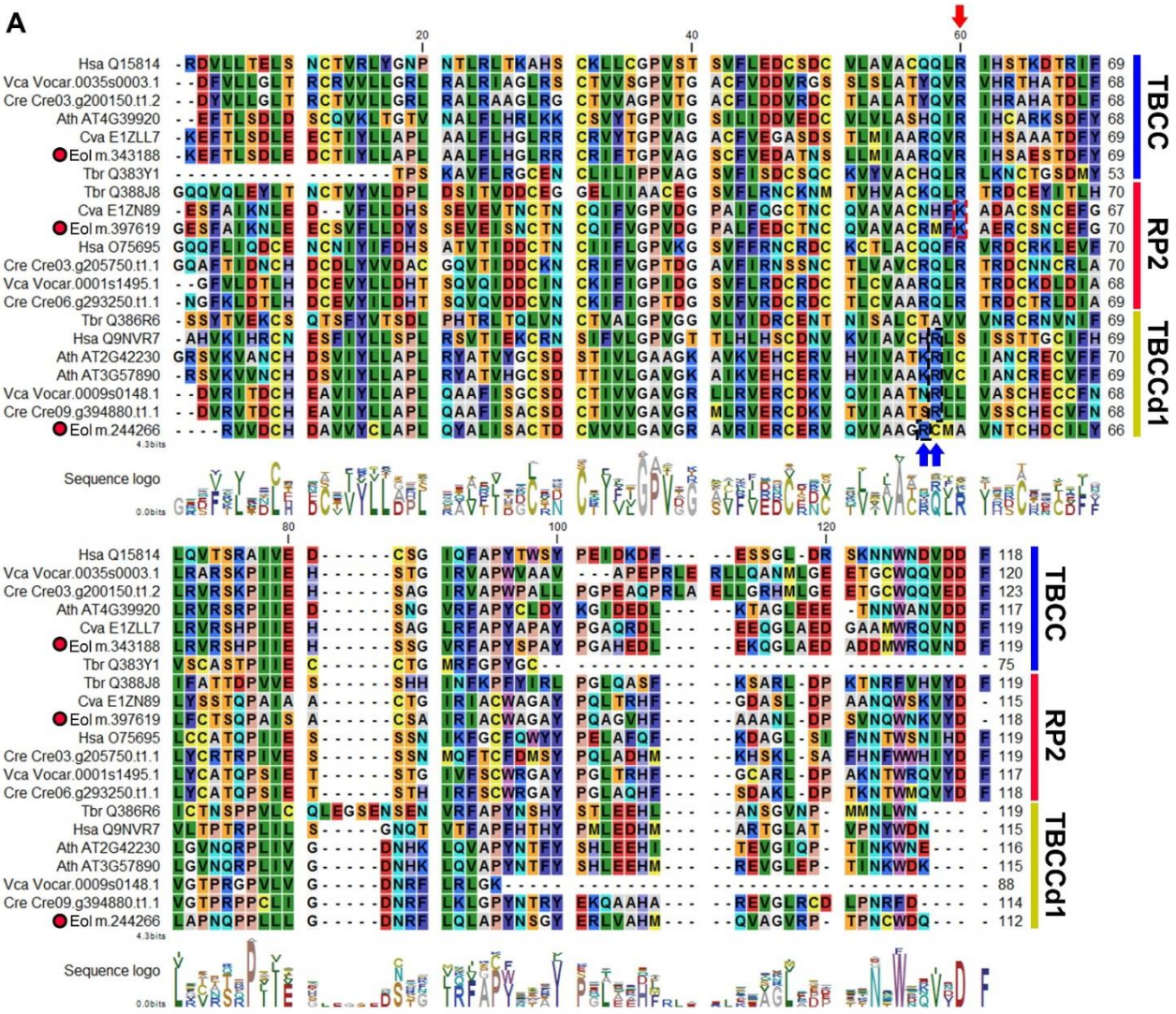

Figure S4.5. Sequence analysis of TBCC domain-containing proteins. (A) Sequence alignment of TBCC-like domains (IPR012945) from proteins present in the TBCC domain-containing protein families: TBCC, RP2, and TBCCd1. Amino acid sequences were aligned with Clustal Omega. Amino acids are colored according to the RasMol color scheme. The conserved arginine residue in TBCC and RP2 classes is highlighted (red arrow). Lysine residues in *Cva* and *Eol* RP2-CLC sequences, probably corresponding to a homologous substitution of the key arginine residue, are highlighted (red dashed square). Arginine residues that may fulfill the same purpose in TBCCd1 proteins are highlighted (black dashed squares, blue arrows). Accession numbers are provided: UniprotKB (*Hsa, Tbr, Cva*), Phytozome v10 (*Cre, Vca*), TAIR (*Ath*). *Hsa Homo sapiens, Vca Volvox carteri, Cre Chlamydomonas reinhardtii, Ath Arabidopsis thaliana, Cva Chlorella variabilis, Eol Ettlia oleoabundans* (red dots), *Tbr Trypanosoma brucei.* (B) Predicted amino acid sequences for *Eol* TBCC and TBCCd1 family proteins. These proteins were not identified in the membranes of N-deprived *Eol*.

A

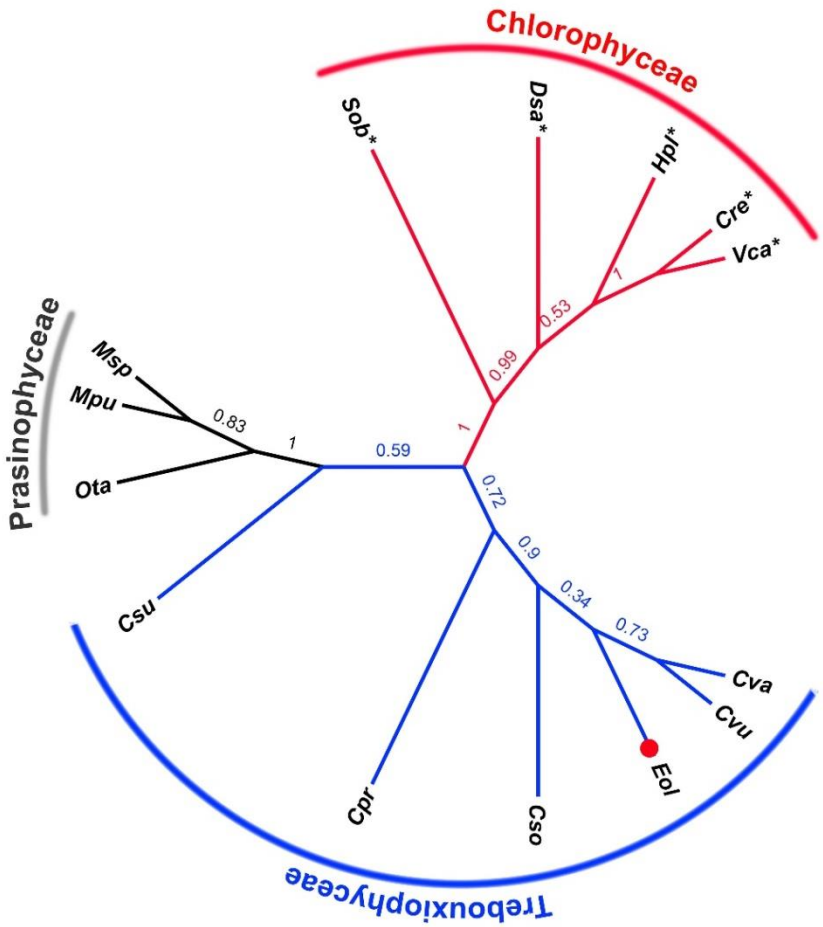

B

	1	2	3	4	5	6	7	8	9	10	11	12	13	14
Ettlia oleoabundans (Eol) 1		83.33	77.13	76.74	72.09	65.50	61.87	55.73	56.00	49.14	46.55	46.12	47.41	41.34
Chlorella vulgaris (Cvu) 2	185		77.91	79.07	71.32	68.60	62.65	58.02	57.82	52.16	48.71	50.43	51.29	44.09
Chlorella sorokiniana (Cso) 3	199	201		94.96	86.43	79.07	74.03	66.67	68.73	49.03	47.88	47.49	47.88	49.81
Chlorella variabilis (Cva) 4	198	204	245		84.50	79.84	73.26	65.93	67.27	50.58	47.49	48.26	47.88	49.42
Chlorella protothecoides (Cpr) 5	186	184	223	218		78.29	72.48	64.44	68.36	49.81	47.49	47.10	47.49	49.42
Coccomyxa subellipsoidea C-169 (Csu) 6	169	177	204	206	202		71.32	66.67	67.27	47.49	45.17	46.72	46.33	50.97
Ostreococcus tauri (Ota) 7	159	161	191	189	187	184		73.33	74.18	47.29	45.35	45.35	44.19	46.51
Micromonas pusilla CCMP1545 (Mpu) 8	146	152	180	178	174	180	198		77.45	47.53	44.11	46.01	45.25	44.98
Micromonas sp. RCC299 (Msp) 9	154	159	189	185	188	185	204	213		44.93	41.67	42.39	42.39	42.03
Dunaliella salina (Dsa*) 10	114	121	127	131	129	123	122	125	124		85.71	82.49	82.03	54.58
Haematococcus pluvialis (Hpl*) 11	108	113	124	123	123	117	117	116	115	186		83.87	83.87	56.57
Chlamydomonas reinhartdtii (Cre*) 12	107	117	123	125	122	121	117	121	117	179	182		93.55	51.79
Volvox carteri (Vca*) 13	110	119	124	124	123	120	114	119	117	178	182	203		52.59
Scenedesmus obliquus (Sob*) 14	105	112	129	128	128	132	120	121	116	137	142	130	132	

Figure S4.6. Sequence analysis of *Eo*COX2. (A) ML analysis of *Eo*COX2 (*Eol*; red dot) and its homologs within green microalgae classes (Table S4.16): *Chlorophyceae* (red), *Trebouxiophyceae* (blue), *Prasinophyceae* (gray). *Chlorophycean* sequences corresponding to the COX2A and COX2B subunits were manually concatenated into a unique bi-domain sequence by removing N- and C-terminal extensions according to Rodríguez-Salinas et al., 2012. The concatenated COX2 sequences from *Chlorophycean* microalgae (highlighted with an asterisk) were aligned with intact orthodox COX2 amino acid sequences using Clustal Omega. The topology of the ML tree with the highest log likelihood (-2555.6238) is shown. MLb values are shown next to the branches. (B) Pairwise comparison among COX2 protein homologs shows the percentage identity (upper right values) and number of identical residues (bottom left values).

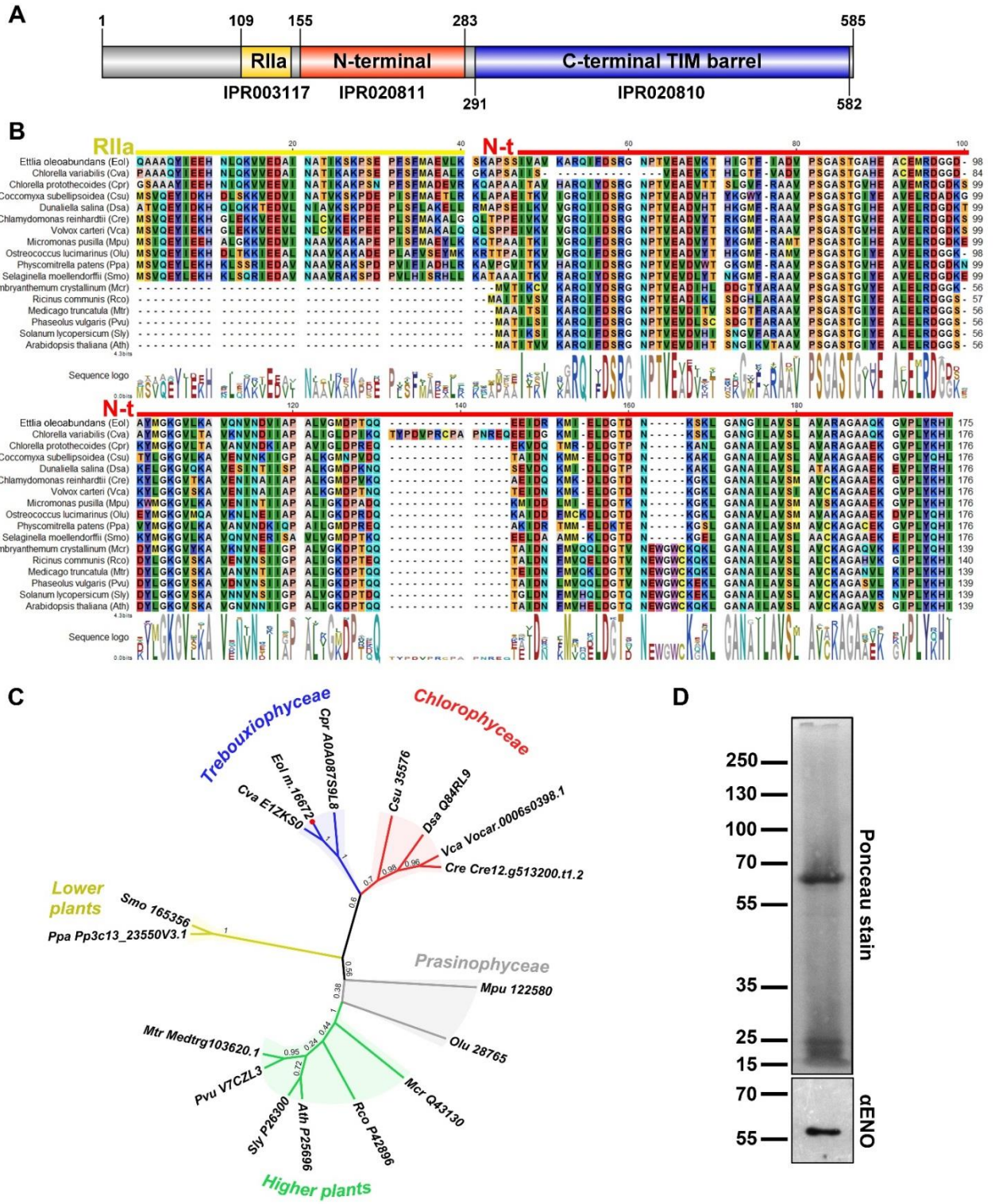

Figure S4.7. Analysis of *Eo*ENO and its homologs in the green lineage. (A) Protein architecture of *Eo*ENO. The identified protein domain signatures (InterPro) are indicated. (B) Sequence alignment of *Eo*ENO and its homologs. Full-length amino acid sequences were aligned with Clustal Omega. Amino acids are colored according to the RasMol color scheme. The alignment region comprising the RIIa (yellow) and N-terminal (red) domains from *Eo*ENO is shown. Accession numbers are provided in (C). (C) ML analysis of ENO homologs. The topology of the ML tree with the highest log likelihood (-6030.8107) is shown. MLb values are shown next to the branches. Accession numbers are provided: UniProtKB (*Cva, Cpr, Dsa, Pvu, Rco, Mcr, Sly, Ath*), Phytozome v10 (*Csu, Cre, Vca, Mpu, Olu, Ppa, Smo, Mtr*). (D) Immunological detection of ENO in *Eol* microsomes. SDS-PAGE 10% (w/v) acrylamide gel, 20 µg protein per lane.

A.3. Supplemental tables

Supplemental Tables S4.1-S4.15. Biological processes represented in membranes of N-deprived *E. oleoabundans*.

The supplementary tables describe the proteins identified in the membrane proteome of N-deficient *E. oleoabundans*, classified according to the biological process to which they are related. The proteins with at least two unique peptides in two or more biological replicates were identified and manually annotated. The calculated molecular weights (MW) of the identified protein sequences are shown, together with their homologs in the model organisms *Chlamydomonas reinhardtii* (*Cr*) and *Arabidopsis thaliana* (*At*) and their corresponding % identity values (%ID). Subcellular localizations were predicted using PredAlgo. Curated cellular locations were established according to the reported location of protein homologs in other species. References are provided for those protein homologs whose cell location has been experimentally demonstrated. Proteins well-known for being cytosolic or targeted to several membrane locations inside the cell, including those dual-targeted to the chloroplast and mitochondria, were considered as cytoplasmic.

[a] Experimental evidence of subcellular location is available; [b] Experimental evidence of subcellular location is not available; [c] UniProtKB accession number. **Abbreviations:** C, Chloroplast; Ck, Cytoskeleton; Cy, Cytoplasm; E, Endomembrane System; LD, Lipid Droplet; M, Mitochondria; N, Nucleus; NA, Not Available; O, Other; P, Periplasm; PM, Plasma Membrane; R, Cytosolic Ribosome; SP, Signal Peptide; U, Unknown; V, Vacuole.

Table S4.1. Photosynthesis.

Protein ID	Curated description	MW (kDa)	E.C. number	Best Cr homolog		Best At homolog		Subcellular localization		
				JGI v5.5 ID	% ID	TAIR10 ID	% ID	Predicted	Curated	Reference
PSI-LHCI supercomplex: PSI core proteins										
m.253814	Photosystem I P700 chlorophyll a apoprotein A1 (PSAA)	83	1.97.1.12.	P12154[c]	93	ATCG00350	86	**O**	**C[a]**	Ferro et al., 2010
m.253815	Photosystem I P700 chlorophyll a apoprotein A2 (PSAB)	82	1.97.1.12.	P09144[c]	90	ATCG00340	85	**O**	**C[a]**	Ferro et al., 2010
gi|21542193	Photosystem I iron-sulfur center (PSAC)	9	1.97.1.12.	Q00914[c]	89	ATCG01060	94	**O**	**C[a]**	Ferro et al., 2010
m.420934	Photosystem I reaction center subunit II (PSAD)	22	NA	Cre05.g238332.t1.1	82	AT1G03130	76	**C**	**C[a]**	Terashima et al., 2010
m.396598	Photosystem I reaction center subunit IV (PSAE)	14	NA	Cre10.g420350.t1.2	77	AT2G20260	70	**C**	**C[a]**	Terashima et al., 2010
m.357923	Photosystem I reaction center subunit III (PSAF)	25	NA	Cre09.g412100.t1.2	71	AT1G31330	55	**C**	**C[a]**	Terashima et al., 2010
m.420947	Photosystem I reaction center subunit V (PSAG)	14	NA	Cre12.g560950.t1.2	48	AT1G55670	53	**C**	**C[a]**	Terashima et al., 2010
m.421406	Photosystem I reaction center subunit VI (PSAH)	16	NA	Cre07.g330250.t1.2	55	AT1G52230	43	**C**	**C[a]**	Terashima et al., 2010
m.372652	Photosystem I reaction center subunit XI (PSAL)	20	NA	Cre12.g486300.t1.2	77	AT4G12800	60	**C**	**C[a]**	Ferro et al., 2010
m.375289	Photosystem I reaction center subunit N (PSAN)	18	NA	Cre02.g082500.t1.1	62	AT5G64040	51	**C**	**C[a]**	Ferro et al., 2010
PSI-LHCI supercomplex: LHCI peripheral antenna										
m.367956	LHCI type I chlorophyll a/b-binding protein LHCA1	23	NA	Cre06.g283050.t1.2	68	AT3G54890	52	**O**	**C[a]**	Stauber et al., 2003
m.419572	LHCI chlorophyll a/b-binding protein LHCA2	26	NA	Cre12.g508750.t1.2	67	AT3G54890	45	**C**	**C[a]**	Stauber et al., 2003
m.416990	LHCI type III chlorophyll a/b-binding protein LHCA3	32	NA	Cre11.g467573.t1.1	57	AT1G61520	64	**C**	**C[a]**	Stauber et al., 2003
m.414848	LHCI chlorophyll a/b-binding protein LHCA4	24	NA	Cre10.g452050.t1.2	48	AT3G47470	45	**O**	**C[a]**	Stauber et al., 2003
m.365254	LHCI chlorophyll a/b-binding protein LHCA5	30	NA	Cre10.g425900.t1.2	70	AT3G47470	49	**C**	**C[a]**	Stauber et al., 2003

m.353942	LHCI chlorophyll a/b-binding protein LHCA6	29	NA	Cre06.g278213.t1.1	69	AT3G47470	49	**C**	**C[a]**	Stauber et al., 2003
m.382652	LHCI chlorophyll a/b-binding protein LHCA7	29	NA	Cre16.g687900.t1.2	48	AT1G45474	45	**C**	**C[a]**	Stauber et al., 2003
m.368979	LHCI chlorophyll a/b-binding protein LHCA8	27	NA	Cre06.g272650.t1.2	56	AT1G45474	44	**C**	**C[a]**	Stauber et al., 2003
m.415631	LHCI chlorophyll a/b-binding protein LHCA9	25	NA	Cre07.g344950.t1.2	67	AT3G47470	40	**C**	**C[a]**	Stauber et al., 2003
PSI-LHCI supercomplex: assembly/disassembly factors										
gi|3025040	Photosystem I assembly protein YCF4	21	NA	O20030[c]	55	ATCG00520	48	**O**	**C[a]**	Ferro et al., 2010
PSII-LHCII supercomplex: PSII core proteins										
m.166963	Photosystem II D1 protein (PSBA)	39	1.10.3.9.	P07753[c]	94	ATCG00020	95	**O**	**C[a]**	Ferro et al., 2010
m.174678	Photosystem II CP47 reaction center protein (PSBB)	56	NA	P37255[c]	86	ATCG00680	82	**O**	**C[a]**	Ferro et al., 2010
m.386649	Photosystem II CP43 reaction center protein (PSBC)	52	NA	P10898[c]	90	ATCG00280	87	**O**	**C[a]**	Ferro et al., 2010
m.386650	Photosystem II D2 protein (PSBD)	39	1.10.3.9.	P06007[c]	94	ATCG00270	93	**O**	**C[a]**	Ferro et al., 2010
PSII-LHCII supercomplex: LHCII inner monomeric antenna										
m.281149	Chlorophyll a/b-binding protein CP26 (LHCB5)	31	NA	Cre16.g673650.t1.1	77	AT4G10340	54	**C**	**C[a]**	Terashima et al., 2010
m.354498	Chlorophyll a/b-binding protein CP29 (LHCB4)	32	NA	Cre17.g720250.t1.2	66	AT5G01530	59	**O**	**C[a]**	Terashima et al., 2010
PSII-LHCII supercomplex: LHCII outer trimeric antenna										
m.416614	Major LHCII type I chlorophyll a/b-binding protein_A	26	NA	Cre06.g283950.t1.2	72	AT2G34430	67	**C**	**C[a]**	Stauber et al., 2003
m.421136	Major LHCII type I chlorophyll a/b-binding protein_B	18	NA	Cre06.g283950.t1.2	83	AT2G05070	75	**O**	**C[a]**	Stauber et al., 2003
m.419129	Major LHCII type I chlorophyll a/b-binding protein_C	26	NA	Cre04.g232104.t1.1	73	AT2G05070	66	**C**	**C[a]**	Stauber et al., 2003
m.418152	Major LHCII type III chlorophyll a/b-binding protein_A	29	NA	Cre12.g548400.t1.2	74	AT2G05100	71	**C**	**C[a]**	Stauber et al., 2003
m.418258	Major LHCII type III chlorophyll a/b-binding protein_B	24	NA	Cre12.g548400.t1.2	74	AT2G05100	69	**O**	**C[a]**	Stauber et al., 2003
PSII-LHCII supercomplex: extrinsic oxygen evolving complex										

m.353310	Oxygen-evolving enhancer protein 1 (PSBO)	31	NA	Cre09.g396213.t1.1	78	AT5G66570	64	**C**	**C[a]**	Bienvenut et al., 2011
m.362592	Oxygen-evolving enhancer protein 2 (PSBP)	27	NA	Cre12.g550850.t1.2	65	AT1G06680	54	**C**	**C[a]**	Bienvenut et al., 2011
m.4569	Oxygen-evolving enhancer protein 3, N-terminal peptide (PSBQ)	13	NA	Cre08.g372450.t1.2	57	NA	NA	**C**	**C[a]**	Bienvenut et al., 2011
m.267881	Oxygen evolving enhancer protein 3, C-terminal peptide (PSBQ)	9	NA	Cre08.g372450.t1.2	65	NA	NA	**O**	**C[a]**	Bienvenut et al., 2011
m.373915	Photosystem II 10 kDa polypeptide (PSBR)[d]	15	NA	Cre06.g261000.t1.2	67	AT1G79040	49	**C**	**C[a]**	Xue et al., 2015
PSII-LHCII supercomplex: low molecular mass subunits										
m.342757	Cytochrome b559 subunit alpha (PSBE)	9	NA	P48268[c]	90	ATCG00580	81	**O**	**C[a]**	Ferro et al., 2010
m.178475	Photosystem II reaction center protein H (PSBH)	9	NA	P22666[c]	71	ATCG00710	79	**O**	**C[a]**	Ferro et al., 2010
m.207905	Photosystem II 11 kDa protein (PSB27)	21	NA	Cre05.g243800.t1.2	53	AT1G03600	45	**C**	**C[a]**	Terashima et al., 2010
m.202007	Protein THYLAKOID FORMATION1 (PSB29)	31	NA	Cre13.g562850.t1.2	52	AT2G20890	44	**C**	**C[a]**	Terashima et al., 2010
m.245409	Thylakoid lumenal 18.3 kDa protein (PSB32)	28	3.1.3.2.	Cre03.g182150.t1.2	53	AT1G54780	43	**C**	**C[a]**	Terashima et al., 2010
m.307142	Photosystem II protein 33 (PSB33)	35	NA	Cre09.g411200.t1.2	73	AT1G71500	50	**C**	**C[a]**	Terashima et al., 2010
PSII-LHCII supercomplex: other biogenesis/repair factors										
m.383182	ATP-dependent zinc metalloprotease FTSH type A_A	76	3.4.24.-	Cre12.g485800.t1.2	84	AT1G50250	79	**C**	**C[a]**	Terashima et al., 2010
gi|412990905	ATP-dependent zinc metalloprotease FTSH type A_B	76	3.4.24.-	Cre12.g485800.t1.2	79	AT1G50250	73	**C**	**C[a]**	Terashima et al., 2010
m.369183	ATP-dependent zinc metalloprotease FTSH type B	74	3.4.24.-	Cre17.g720050.t1.2	78	AT2G30950	79	**C**	**C[a]**	Terashima et al., 2010
m.163337	Atypical short-chain dehydrogenase HCF244	50	NA	Cre02.g142146.t1.1	73	AT4G35250	66	**C**	**C[a]**	Link et al., 2012
m.326095	Peptidyl-prolyl cis-trans isomerase CYP38	56	5.2.1.8.	Cre03.g189800.t1.2	61	AT3G01480	53	**C**	**C[a]**	Bienvenut et al., 2011
m.357603	Photosystem II stability/assembly factor HCF136	43	NA	Cre06.g273700.t1.2	68	AT5G23120	59	**C**	**C[a]**	Bienvenut et al., 2011
m.337748	Probable MPH1 protein	16	NA	A8HSE5[c]	28	AT5G07020	37	**C**	**C[a]**	This work
m.316237	Protein LOW PSII ACCUMULATION 1 (LPA1)	49	NA	Cre10.g430150.t1.2	48	AT1G02910	32	**M**	**C[a]**	Dewez et al., 2009

m.170274	PsbP-like protein 1 (PPL1)	27	NA	Cre12.g509050.t1.1	60	AT3G55330	55	**C**	**C[a]**	Ferro et al., 2010
m.376520	Protein M-ENRICHED THYLAKOID 1 (MET1)	39	NA	Cre01.g031100.t1.2	63	AT1G55480	39	**M**	**C[a]**	Bhuiyan et al., 2015
m.157685	Rubredoxin	22	NA	Cre07.g315150.t1.2	63	AT1G54500	57	**C**	**C[a]**	Terashima et al., 2010
Cytochrome *b6f* complex										
m.189757	Apocytochrome f (PETA)	39	NA	P23577[c]	74	ATCG00540	72	**O**	**C[a]**	Ferro et al., 2010
m.186165	Cytochrome b6 (PETB)	24	NA	Q00471[c]	95	ATCG00720	90	**O**	**C[a]**	Ferro et al., 2010
m.312733	Cytochrome b6-f complex iron-sulfur subunit (PETC)	22	1.10.9.1.	Cre11.g467689.t1.1	73	AT4G03280	69	**C**	**C[a]**	Iwai et al., 2010
m.186166	Cytochrome b6-f complex subunit 4 (PETD)	16	NA	P23230[c]	90	ATCG00730	86	**O**	**C[a]**	Ferro et al., 2010
ATP synthase complex, chloroplastic										
gi|3023328	ATP synthase subunit alpha (ATPA)	55	3.6.3.14.	Cre02.g116750.t1.1	62	ATCG00120	79	**O**	**C[a]**	Ferro et al., 2010
gi|416678	ATP synthase subunit beta (ATPB)	52	3.6.3.14.	Cre17.g698000.t1.2	69	ATCG00480	87	**O**	**C[a]**	Ferro et al., 2010
m.392881	ATP synthase subunit gamma (ATPC)	39	NA	Cre06.g259900.t1.2	71	AT4G04640	66	**C**	**C[a]**	Terashima et al., 2010
m.419593	ATP synthase subunit delta (ATPD)	26	NA	Cre11.g467569.t1.1	64	AT4G09650	45	**C**	**C[a]**	Terashima et al., 2010
Non-photochemical quenching and cyclic electron flow										
m.26479	Calcium sensing receptor (CAS)	47	NA	Cre12.g497300.t2.1	44	AT5G23060	29	**M**	**C[a]**	Petroutsos et al., 2011
m.115949	Ferredoxin-NADP reductase (FNR)	39	1.18.1.2.	Cre11.g476750.t1.2	80	AT4G05390	62	**C**	**C[a]**	Iwai et al., 2010
m.263364	Peroxisomal membrane 22 kDa (Mpv17/PMP22) family protein	23	NA	Cre16.g683750.t1.2	51	AT2G42770	41	**C**	**C[a]**	Terashima et al., 2010
m.264998	PGR5-like protein (PGRL1)	33	NA	Cre07.g340200.t1.1	41	AT4G11960	38	**C**	**C[a]**	Iwai et al., 2010
m.395061	Photosystem II 22 kDa protein (PSBS)	28	NA	Cre01.g016750.t1.2	60	AT1G44575	47	**C**	**C[a]**	This work
m.117393	Serine protease SPPA	80	3.4.21.-	Cre10.g444550.t1.2	56	AT1G73990	50	**SP**	**C[a]**	Terashima et al., 2010
m.304492	Serine/threonine-protein kinase STT7	66	2.7.11.1.	Cre02.g120250.t2.1	50	AT1G68830	47	**C**	**C[a]**	Depège et al., 2003

m.405041	Violaxanthin de-epoxidase (VDE)	50	1.10.99.3.	Cre09.g388060.t1.1	23	AT1G08550	53	**C**	**C[a]**	Ferro et al., 2010

[d] This protein is also considered a PSII low molecular mass subunit.

Table S4.2. Oxidative phosphorylation.

Protein ID	Curated description	MW (kDa)	E.C. number	Best Cr homolog		Best At homolog		Subcellular localization		
				JGI v5.5 ID	% ID	TAIR10 ID	% ID	Predicted	Curated	Reference
Complex I, NADH:ubiquinone oxidoreductase										
m.419475	NADH dehydrogenase [ubiquinone] flavoprotein 1	53	1.6.5.3. 1.6.99.3.	Cre10.g422600.t1.1	90	AT5G08530	81	**M**	**M[a]**	Atteia et al., 2009
m.418591	NADH dehydrogenase [ubiquinone] flavoprotein 2	32	1.6.5.3. 1.6.99.3.	Cre10.g450400.t1.2	68	AT4G02580	57	**M**	**M[a]**	Atteia et al., 2009
m.222860	NADH dehydrogenase [ubiquinone] iron-sulfur protein 1	79	1.6.5.3. 1.6.99.3.	Cre12.g535950.t1.2	67	AT5G37510	57	**M**	**M[a]**	Atteia et al., 2009
m.391195	NADH dehydrogenase [ubiquinone] 1 alpha subcomplex subunit 5	19	NA	Cre13.g568800.t1.2	36	AT5G52840	39	**M**	**M[a]**	Peters et al., 2013
Complex II, succinate:ubiquinone oxidoreductase										
m.206297	Succinate dehydrogenase [ubiquinone] flavoprotein subunit (SDH1)	69	1.3.5.1.	Cre14.g619133.t1.1	81	AT5G66760	78	**C**	**M[a]**	Atteia et al., 2009
Complex III, ubiquinol:cytochrome *c* oxidoreductase										
m.384751	Mitochondrial-processing peptidase subunit alpha (MPPA)	55	3.4.24.64.	Cre17.g722800.t1.2	45	AT3G16480	51	**M**	**M[a]**	Brugière et al., 2004
m.415214	Mitochondrial-processing peptidase subunit beta (QCR1)	54	3.4.24.64.	Cre12.g523850.t1.2	63	AT3G02090	64	**M**	**M[a]**	Atteia et al., 2009
m.365842	Cytochrome b-c1 complex subunit 4 (CYC1)	33	NA	Cre15.g638500.t1.2	65	AT5G40810	79	**M**	**M[a]**	Atteia et al., 2009
m.421237	Cytochrome b-c1 complex subunit Rieske (RIP1)	27	1.10.2.2.	Cre01.g051900.t1.2	62	AT5G13440	72	**M**	**M[a]**	Atteia et al., 2009
Complex IV, cytochrome *c* oxidase										
m.110997	Cytochrome c oxidase subunit 2 (COX2)	23	1.9.3.1.	Cre01.g049500.t1.2	66	ATMG00160	72	**SP**	**M[a]**	Heazlewood et al., 2004
m.363418	Cytochrome c oxidase subunit 5B (COX5B)	19	NA	Cre13.g567600.t1.2	38	AT1G80230	33	**M**	**M[a]**	Atteia et al., 2009
m.356410	Cytochrome c oxidase subunit 6B (COX6B)	16	NA	Cre06.g304350.t1.2	44	AT4G28060	51	**M**	**M[a]**	Atteia et al., 2009
Complex V: ATP synthase										

m.347310	ATP synthase subunit alpha (ATPα)	55	NA	Cre02.g116750.t1.1	72	ATMG01190	73	**O**	**M[a]**	Millar et al., 2001
m.366102	ATP synthase subunit beta (ATPβ)	52	3.6.3.14.	Cre17.g698000.t1.2	85	AT5G08680	81	**O**	**M[a]**	Atteia et al., 2009
m.415370	ATP synthase subunit gamma (ATPγ)	37	NA	Cre15.g635850.t2.1	58	AT2G33040	52	**M**	**M[a]**	Brugière et al., 2004
m.381548	ATP synthase subunit delta' (ATPδ)	22	NA	Cre11.g467707.t1.1	40	AT5G47030	46	**M**	**M[a]**	Brugière et al., 2004
m.161014	ATP synthase subunit d, N-terminal peptide (ATP*d*)	12	NA	Cre02.g107050.t1.1	28	AT3G52300	32	**M**	**M[a]**	Brugière et al., 2004
m.364530	ATP synthase subunit d, C-terminal peptide (ATP*d*)	9	NA	NA	NA	AT3G52300	30	**M**	**M[a]**	Brugière et al., 2004

Table S4.3. Energy and reducing power homeostasis.

Protein ID	Curated description	MW (kDa)	E.C. number	Best Cr homolog		Best At homolog		Subcellular localization		
				JGI v5.5 ID	% ID	TAIR10 ID	% ID	Predicted	Curated	Reference
Energy homeostasis										
m.331511	Adenylate kinase_A, mitochondrial (ADK_m)	28	2.7.4.3.	Cre12.g557600.t1.1	75	AT5G63400	67	**O**	**M[a]**	Atteia et al., 2009
m.419048	Adenylate kinase_B, chloroplastic (ADK_p)	32	2.7.4.3.	Cre12.g494850.t1.2	69	AT5G47840	53	**SP**	**C[a]**	Lange et al., 2008
m.414529	ADP/ATP carrier protein, chloroplastic (AAA)	64	NA	Cre08.g358526.t1.1	73	AT1G80300	71	**C**	**C[a]**	Terashima et al., 2010
m.418026	ADP/ATP carrier protein, mitochondrial (AAC)	37	NA	Cre09.g386650.t1.2	50	AT5G13490	49	**M**	**M[a]**	Brugière et al., 2004
m.358988	Mitochondrial phosphate carrier protein (MPT)	40	NA	Cre03.g172300.t1.2	75	AT5G14040	69	**M**	**M[a]**	Atteia et al., 2009
Reducing power homeostasis										
m.419931	Malate dehydrogenase [NADP], chloroplastic (MDH_p)	48	1.1.1.82.	Cre09.g410700.t1.2	73	AT5G58330	67	**C**	**C[a]**	Bienvenut et al., 2011
m.417023	Malate dehydrogenase, cytoplasmic (MDH_c)	38	1.1.1.37.	Cre02.g145800.t1.2	72	AT1G04410	79	**C**	**Cy[b]**	NA
m.417165	Malate dehydrogenase, mitochondrial (MDH_m)	37	1.1.1.37.	Cre12.g483950.t1.2	78	AT1G53240	72	**M**	**M[a]**	Atteia et al., 2009
m.381983	Dicarboxylate transporter 1, chloroplastic (DIT1)	57	NA	Cre17.g713350.t1.2	74	AT5G12860	64	**C**	**C[a]**	Ferro et al., 2010
m.373251	Mitochondrial dicarboxylate/tricarboxylate carrier (DTC)	32	NA	Cre16.g672650.t1.2	66	AT5G19760	62	**O**	**M[a]**	Atteia et al., 2009
m.377074	NAD(P) transhydrogenase	113	1.6.1.2.	Cre01.g054500.t1.2	68	NA	NA	**C**	**Cy[a]**	Tardif et al., 2012
m.403196	Type-II NAD(P)H dehydrogenase (NDH-2)	67	1.6.5.-	Cre05.g232200.t1.2	63	AT2G29990	34	**C**	**C[a]**	Terashima et al., 2010

Table S4.4. Carbon metabolism. Carbon metabolism proteins with at least two unique peptides in two or more biological replicates are described. Proteins m.310144 and m.352308, which were identified with two unique peptides in only one biological replicate, are also described together with proteins that were not identified in the total microsome samples, but in the FFZE membrane fractions, which are highlighted with an asterisk.

Protein ID	Curated description	MW (kDa)	E.C. number	Best Cr homolog		Best At homolog		Subcellular localization		
				JGI v5.5 ID	% ID	TAIR10 ID	% ID	Predicted	Curated	Reference
Carbon Concentrating Mechanism										
m.370606	Putative inorganic carbon transporter HLA3	149	3.6.3.-	Cre02.g097800.t1.1	51	AT2G34660	30	**O**	**PM**[a]	Gao et al., 2015
m.361344	LCIB family protein_A	55	NA	Cre06.g307500.t1.1	48	NA	NA	**C**	**C**[a]	Yamano et al., 2010
m.421782	LCIB family protein_B	49	NA	Cre06.g307500.t1.1	48	NA	NA	**O**	**C**[a]	Yamano et al., 2010
m.421082	Alpha carbonic anhydrase, periplasmic (CAH1)	39	4.2.1.1.	Cre04.g223100.t1.2	33	AT1G08080	28	**SP**	**P**[a]	Coleman and Grossman, 1984
m.310144	Alpha carbonic anhydrase, chloroplastic***** (CAH3)	39	4.2.1.1.	Cre09.g415700.t1.2	49	AT1G08080	29	**C**	**C**[a]	Karlsson et al., 1998
m.417201	Peptidyl-prolyl cis-trans isomerase CYP1	22	5.2.1.8.	Cre01.g002300.t1.2	81	AT4G34870	75	**O**	**Cy**[a]	Ito et al., 2011
Photosynthetic Carbon Fixation										
m.415694	Ribulose biphosphate carboxylase small chain (RuBisCO)	14	4.1.1.39.	Cre02.g120100.t1.2	66	AT5G38430	47	**SP**	**C**[a]	Borkhsenious et al., 1998
m.384585	Ribulose biphosphate carboxylase large chain (RuBisCO)	53	4.1.1.39.	P00877[c]	94	ATCG00490	89	**O**	**C**[a]	Borkhsenious et al., 1998
m.304273	Ribulose biphosphate carboxylase/oxygenase activase	48	3.6.1.3.	Cre04.g229300.t1.1	84	AT2G39730	73	**C**	**C**[a]	McKay et al., 1991
m.372822	Transketolase	80	2.2.1.1.	Cre02.g080200.t1.2	67	AT3G60750	64	**C**	**C**[a]	Terashima et al., 2010
m.361538	Calvin cycle protein CP12	14	NA	Cre08.g380250.t1.2	47	AT3G62410	54	**C**	**C**[a]	Ferro et al., 2010
Photorespiration										
m.86428	Glycolate dehydrogenase, mitochondrial	120	1.1.99.14.	Cre06.g288700.t1.2	73	AT5G06580	24	**M**	**M**[a]	Atteia et al., 2009
m.276420	Aminomethyltransferase, mitochondrial	45	2.1.2.10.	Cre03.g193750.t1.1	73	AT1G11860	68	**M**	**M**[a]	Atteia et al., 2009

m.380870	Dihydrolipoyl dehydrogenase, mitochondrial	34	1.8.1.4.	Cre18.g749847.t1.1	71	AT1G48030	64	**O**	**M**[a]	Conner et al., 1996
m.352886	Serine hydroxymethyltransferase, mitochondrial	57	2.1.2.1.	Cre16.g664550.t1.2	82	AT4G37930	76	**M**	**M**[a]	Atteia et al., 2009
Glycolysis										
m.352308	Hexokinase[f] (HK)	49	2.7.1.1.	Cre02.g117500.t1.2	39	AT4G29130	39	**O**	**C**[a]	Terashima et al., 2010
m.366318	ATP-dependent 6-phosphofructokinase, chloroplastic* (PFK)	59	2.7.1.11.	Cre06.g262900.t1.2	66	AT2G22480	48	**C**	**C**[a]	Terashima et al., 2010
m.418145	Fructose-bisphosphate aldolase, chloroplastic[d] (ALD)	43	4.1.2.13.	Cre05.g234550.t1.2	77	AT2G01140	74	**C**	**C**[a]	Terashima et al., 2010
m.293516	Triosephosphate isomerase, cytosolic (TPI)	27	5.3.1.1.	Cre01.g029300.t1.2	55	AT3G55440	71	**O**	**Cy**[a]	Ito et al., 2011
m.383891	Glyceraldehyde-3-phosphate dehydrogenase A, chloroplastic[d] ($GPDH_p$)	43	1.2.1.13.	Cre01.g010900.t1.2	85	AT1G42970	71	**C**	**C**[a]	Bienvenut et al., 2011
m.419980	Glyceraldehyde-3-phosphate dehydrogenase, cytosolic ($GPDH_c$)	31	1.2.1.12.	Cre12.g485150.t1.2	72	AT1G16300	72	**O**	**Cy**[b]	NA
m.382809	Phosphoglycerate kinase, chloroplastic[d] (PGK)	50	2.7.2.3.	Cre11.g467770.t1.1	76	AT3G12780	74	**C**	**C**[a]	Bienvenut et al., 2011
m.227839	2,3-bisphosphoglycerate-independent phosphoglycerate mutase* (PGAM)	62	5.4.2.12.	Cre06.g272050.t1.2	72	AT1G09780	60	**O**	**Cy**[a]	Ito et al., 2011
m.16672	Enolase (ENO)	63	4.2.1.11.	Cre12.g513200.t1.2	70	AT2G36530	69	**M**[e]	**Cy**[b]	NA
m.43324	Pyruvate kinase* (PYK)	57	2.7.1.40.	Cre12.g533550.t1.1	75	AT5G08570	70	**O**	**Cy**[a]	Ito et al., 2011
C4 compound metabolism										
m.419931	Malate dehydrogenase [NADP], chloroplastic (MDH_p)	48	1.1.1.82.	Cre09.g410700.t1.2	73	AT5G58330	67	**C**	**C**[a]	Terashima et al., 2010
m.417023	Malate dehydrogenase, cytoplasmic (MDH_c)	38	1.1.1.37.	Cre02.g145800.t1.2	72	AT1G04410	79	**C**	**Cy**[b]	NA
m.417165	Malate dehydrogenase, mitochondrial (MDH_m)	37	1.1.1.37.	Cre12.g483950.t1.2	78	AT1G53240	72	**M**	**M**[a]	Atteia et al., 2009
Starch synthesis										
m.199949	Phosphoglucomutase, chloroplastic* (PGM)	67	5.4.2.2.	Cre06.g278210.t1.1	71	AT5G51820	66	**C**	**C**[a]	Ferro et al., 2010

m.395051	Glucose-1-phosphate adenylyltransferase large subunit, chloroplastic (AGP)	58	2.7.7.27.	Cre13.g567950.t1.2	63	AT5G19220	61	**SP**	**C**[a]	Ferro et al., 2010
m.406951	Granule-bound starch synthase, chloroplastic (GBSS)	65	2.4.1.21.	Cre17.g721500.t1.2	61	AT1G32900	56	**C**	**C**[a]	Terashima et al., 2010
m.89293	Starch-binding domain-containing protein	108	NA	Cre03.g158050.t1.1	47	AT5G01260	44	**M**	**Cy**[b]	NA
One Carbon Metabolism										
m.357300	Adenosylhomocysteinase	54	3.3.1.1.	Cre03.g204250.t1.2	86	AT4G13940	82	**C**	**Cy**[a]	Ito et al., 2011
m.182504	S-adenosylmethionine carrier	42	NA	Cre06.g286250.t1.2	69	AT4G39460	58	**O**	**Cy**[a]	Bouvier et al., 2006; Palmieri et al., 2006
Other metabolite shuttles										
m.373251	Mitochondrial dicarboxylate/tricarboxylate carrier (DTC)	32	NA	Cre16.g672650.t1.2	66	AT5G19760	62	**O**	**M**[a]	Atteia et al., 2009
m.381983	Dicarboxylate transporter 1, chloroplastic (DIT1)	57	NA	Cre17.g713350.t1.2	74	AT5G12860	64	**C**	**C**[a]	Ferro et al., 2010
m.26688	Triose phosphate/phosphate translocator TPT, chloroplastic	42	NA	Cre01.g045550.t1.2	64	AT5G46110	48	**C**	**C**[a]	Ferro et al., 2010
m.29156	UhpC-type hexose phosphate translocator (HPT)	62	NA	Cre16.g688850.t1.1	68	AT4G25220	31	**C**	**C**[a]	Facchinelli et al., 2013

[d] Proteins that also play a role in the Photosynthetic Carbon Fixation.

[e] A mitochondrial transit peptide of 129 amino acids is predicted. Owing to its unfeasibility, this protein is considered without a target peptide in the article discussion.

[f] HK was classified as plastidic because its homologs in *Cr* and *At* have been located in this organelle, even though they also lack a chloroplast transit peptide.

Table S4.5. Pigment metabolism.

Protein ID	Curated description	MW (kDa)	E.C. number	Best Cr homolog		Best At homolog		Subcellular localization		
				JGI v5.5 ID	% ID	TAIR10 ID	% ID	Predicted	Curated	Reference
Chlorophyll metabolism										
m.122796	Glutamate-1-semialdehyde 2,1-aminomutase	52	5.4.3.8.	Cre03.g158000.t1.2	84	AT3G48730	73	**O**	**C[a]**	Nogaj et al., 2005
m.383293	Protoporphyrinogen oxidase	60	1.3.3.4.	Cre09.g396300.t1.2	64	AT4G01690	59	**C**	**C[a]**	van Lis et al., 2005
m.372707	Magnesium protoporphyrin IX methyltransferase	37	2.1.1.11.	Cre12.g498550.t1.1	71	AT4G25080	58	**C**	**C[a]**	Terashima et al., 2010
m.19173	Protochlorophyllide reductase	43	1.3.1.33.	Cre01.g015350.t1.1	73	AT1G03630	71	**C**	**C[a]**	Terashima et al., 2010
m.300057	Geranylgeranyl diphosphate reductase	56	1.3.1.83.	Cre01.g050950.t1.2	83	AT1G74470	71	**C**	**C[a]**	Terashima et al., 2010
m.350458	Light-harvesting-like protein 3	28	NA	Cre03.g199535.t1.1	67	AT4G17600	58	**C**	**C[a]**	Terashima et al., 2010
m.281766	Ferrochelatase	62	4.99.1.1.	Cre07.g339750.t2.1	71	AT2G30390	66	**O**	**C[a]**	van Lis et al., 2005
Carotenoid metabolism										
m.155110	15-cis-phytoene desaturase	62	1.3.5.5.	Cre12.g509650.t1.2	75	AT4G14210	73	**C**	**C[a]**	Terashima et al., 2010
m.405041	Violaxanthin de-epoxidase	50	1.10.99.3.	Cre09.g388060.t1.1	23	AT1G08550	53	**C**	**C[a]**	Ferro et al., 2010

Table S4.6. Nitrogen compound metabolism.

Protein ID	Curated description	MW (kDa)	E.C. number	Best Cr homolog		Best At homolog		Subcellular localization		
				JGI v5.5 ID	% ID	TAIR10 ID	% ID	Predicted	Curated	Reference
Nitrogen assimilation										
m.413648	High affinity nitrate transporter 2	56	NA	Cre09.g410800.t1.2	47	AT5G60770	49	**O**	**PM**[a]	Kiba et al., 2012
m.415635	Glutamine synthetase, cytosolic	41	6.3.1.2.	Cre02.g113200.t1.1	78	AT5G37600	62	**O**	**Cy**[b]	NA
m.360553	Ammonium transporter 1_A	55	NA	Cre03.g159254.t1.2	47	AT3G24300	45	**SP**	**PM**[a]	Monneuse et al., 2011
m.415049	Ammonium transporter 1_B	57	NA	Cre03.g159254.t1.2	38	AT1G64780	42	**O**	**PM**[a]	Monneuse et al., 2011
m.414437	Urea-proton symporter DUR3	78	NA	Cre08.g360200.t1.2	56	AT5G45380	56	**O**	**PM**[a]	Kojima et al., 2007
m.363330	Choline transporter-like protein	58	NA	Cre09.g390467.t1.1	34	AT4G38640	30	**SP**	**PM**[b]	NA
m.223431	Glutamine synthetase, chloroplastic	42	6.3.1.2.	Cre12.g530600.t1.1	75	AT5G35630	54	**C**	**C**[a]	Ferro et al., 2010
Amino acid metabolism										
m.367066	Carbamoyl-phosphate synthase large chain, chloroplastic	132	6.3.5.5.	Cre08.g358580.t1.1	74	AT1G29900	68	**M**	**C**[a]	Bienvenut et al., 2011

Table S4.7. Translation.

Protein ID	Curated description	MW (kDa)	E.C. number	Best Cr homolog		Best At homolog		Subcellular localization		
				JGI v5.5 ID	% ID	TAIR10 ID	% ID	Predicted	Curated	Reference
Chloroplast ribosome, small subunit										
m.309702	30S ribosomal protein S2, N-terminal peptide	16	NA	O47027[c]	41	ATCG00160	45	**O**	**C[a]**	Ferro et al., 2010
m.346015	30S ribosomal protein S2, C-terminal peptide	14	NA	O47027[c]	22	ATCG00160	46	**O**	**C[a]**	Ferro et al., 2010
Chloroplast ribosome, large subunit										
m.68137	50S ribosomal protein L1	35	NA	Cre02.g088900.t1.2	70	AT3G63490	56	**M**	**C[a]**	Yamaguchi et al., 2003
m.331401	50S ribosomal protein L15	24	NA	Cre14.g612450.t1.2	63	AT3G25920	62	**C**	**C[a]**	Yamaguchi et al., 2003
m.192359	50S ribosomal protein L19	16	NA	Cre17.g734450.t1.2	48	AT4G11630	44	**O**	**C[a]**	Yamaguchi et al., 2003
m.408152	50S ribosomal protein L18	19	NA	Cre01.g052100.t1.2	51	AT1G48350	57	**C**	**C[a]**	Yamaguchi et al., 2003
m.203971	50S ribosomal protein L24	20	NA	Cre16.g652550.t1.2	51	AT5G54600	48	**M**	**C[a]**	Yamaguchi et al., 2003
Regulation of chloroplastic translation										
m.405364	Chloroplast elongation factor Ts pro-protein	88	NA	Cre12.g519180.t2.1	61	AT4G29060	59	**C**	**C[a]**	Terashima et al., 2010
m.192357	Elongation factor Tu	42	3.6.5.3.	Cre06.g259150.t1.2	63	AT4G20360	79	**SP**	**C[a]**	Ferro et al., 2010
m.354187	Polyadenylate-binding protein RB47	68	NA	Cre01.g039300.t1.2	69	AT1G49760	62	**O**	**C[a]**	Yohn et al., 1998
Cytosolic ribosome, small subunit										
m.417486	40S ribosomal protein SA	33	NA	Cre10.g432800.t1.2	75	AT1G72370	70	**O**	**R[a]**	Carroll et al., 2008
m.357271	40S ribosomal protein S2	31	NA	Cre01.g039250.t2.1	87	AT3G57490	78	**O**	**R[a]**	Carroll et al., 2008
m.419945	40S ribosomal protein S3	26	NA	Cre02.g102250.t1.2	87	AT2G31610	85	**O**	**R[a]**	Carroll et al., 2008
m.354269	40S ribosomal protein S3a	33	NA	Cre13.g568650.t1.2	82	AT4G34670	74	**O**	**R[a]**	Carroll et al., 2008

m.366080	40S ribosomal protein S4	29	NA	Cre06.g308250.t1.2	78	AT5G58420	69	**O**	**R[a]**	Carroll et al., 2008
m.413725	40S ribosomal protein S5	24	NA	Cre06.g290950.t1.2	86	AT2G37270	82	**M**	**R[a]**	Carroll et al., 2008
m.419710	40S ribosomal protein S6	29	NA	Cre09.g400650.t1.2	79	AT4G31700	73	**O**	**R[a]**	Carroll et al., 2008
m.415493	40S ribosomal protein S7	24	NA	Cre12.g498900.t1.2	74	AT1G48830	67	**C**	**R[a]**	Carroll et al., 2008
m.414798	40S ribosomal protein S8	25	NA	Cre06.g272800.t1.2	72	AT5G59240	73	**M**	**R[a]**	Carroll et al., 2008
m.357965	40S ribosomal protein S9	46	NA	Cre08.g359750.t2.1	86	AT5G15200	77	**SP**	**R[a]**	Carroll et al., 2008
m.415245	40S ribosomal protein S13	19	NA	Cre07.g331900.t1.2	76	AT3G60770	83	**C**	**R[a]**	Carroll et al., 2008
m.419471	40S ribosomal protein S14	18	NA	Cre11.g480150.t1.2	83	AT3G52580	83	**C**	**R[a]**	Carroll et al., 2008
m.415647	40S ribosomal protein S16	16	NA	Cre13.g573351.t1.2	77	AT3G04230	74	**O**	**R[a]**	Carroll et al., 2008
m.416831	40S ribosomal protein S17	16	NA	Cre12.g498250.t1.2	82	AT5G04800	78	**O**	**R[a]**	Carroll et al., 2008
m.414774	40S ribosomal protein S18	18	NA	Cre06.g272950.t1.1	84	AT4G09800	81	**O**	**R[a]**	Carroll et al., 2008
m.415376	40S ribosomal protein S19	19	NA	Cre02.g106600.t1.2	59	AT5G15520	55	**O**	**R[a]**	Carroll et al., 2008
m.414266	40S ribosomal protein S23	15	NA	Cre12.g504200.t1.2	94	AT5G02960	89	**O**	**R[a]**	Carroll et al., 2008
m.367740	40S ribosomal protein S26	10	NA	Cre16.g682300.t1.2	76	AT2G40590	66	**O**	**R[a]**	Carroll et al., 2008
Cytosolic ribosome, large subunit										
m.416054	60S acidic ribosomal protein P0	33	NA	Cre12.g520500.t1.1	62	AT3G09200	63	**C**	**R[a]**	Carroll et al., 2008
m.384792	60S acidic ribosomal protein P2	10	NA	Cre02.g143050.t1.2	67	AT2G27710	53	**O**	**R[a]**	Carroll et al., 2008
m.416977	60S ribosomal protein L3	43	NA	Cre10.g417700.t1.2	81	AT1G61580	70	**O**	**R[a]**	Carroll et al., 2008
m.415487	60S ribosomal protein L4	43	NA	Cre09.g397697.t1.1	70	AT3G09630	63	**O**	**R[a]**	Carroll et al., 2008
m.416634	60S ribosomal protein L5	34	NA	Cre14.g621450.t1.2	68	AT5G39740	63	**O**	**R[a]**	Carroll et al., 2008
m.417233	60S Ribosomal protein L6	27	NA	Cre01.g011000.t1.2	67	AT1G74050	57	**C**	**R[a]**	Carroll et al., 2008
m.358078	60S Ribosomal protein L7	27	NA	Cre12.g537800.t1.2	74	AT2G44120	69	**O**	**R[a]**	Carroll et al., 2008

m.354526	60S ribosomal protein L7a	27	NA	Cre12.g529651.t1.1	80	AT3G62870	68	**O**	**R[a]**	Carroll et al., 2008
m.420513	60S ribosomal protein L8	29	NA	Cre12.g535851.t1.1	83	AT2G18020	78	**C**	**R[a]**	Carroll et al., 2008
m.415229	60S ribosomal protein L9	23	NA	Cre12.g494050.t1.2	77	AT4G10450	62	**C**	**R[a]**	Carroll et al., 2008
m.383519	60S ribosomal protein L10	26	NA	Cre09.g388200.t1.1	76	AT1G26910	78	**O**	**R[a]**	Carroll et al., 2008
m.413488	60S ribosomal protein L11	21	NA	Cre01.g027000.t1.2	77	AT2G42740	79	**O**	**R[a]**	Carroll et al., 2008
m.373292	60S ribosomal protein L12	20	NA	Cre12.g528750.t1.2	73	AT3G53430	79	**C**	**R[a]**	Carroll et al., 2008
m.415074	60S ribosomal protein L13	24	NA	Cre14.g630100.t1.2	57	AT3G49010	61	**O**	**R[a]**	Carroll et al., 2008
m.418267	60S ribosomal protein L13a	23	NA	Cre12.g532550.t1.1	78	AT3G24830	72	**O**	**R[a]**	Carroll et al., 2008
m.414263	60S ribosomal protein L14	16	NA	Cre17.g701200.t1.2	65	AT4G27090	50	**C**	**R[a]**	Carroll et al., 2008
m.360129	60S ribosomal protein L15	25	NA	Cre02.g091100.t1.2	83	AT4G17390	78	**O**	**R[a]**	Carroll et al., 2008
m.418209	60S ribosomal protein L17	21	NA	Cre13.g568900.t1.2	67	AT1G67430	68	**C**	**R[a]**	Carroll et al., 2008
m.415657	60S ribosomal protein L18	21	NA	Cre12.g512600.t1.2	82	AT5G27850	75	**O**	**R[a]**	Carroll et al., 2008
m.357220	60S ribosomal protein L18a	8	NA	Cre01.g047750.t1.2	67	AT1G29965	61	**O**	**R[a]**	Carroll et al., 2008
m.415461	60S ribosomal protein L19	18	NA	Cre02.g075700.t1.2	83	AT3G16780	81	**C**	**R[a]**	Carroll et al., 2008
m.418238	60S ribosomal protein L21	16	NA	Cre06.g278135.t1.1	73	AT1G09690	65	**O**	**R[a]**	Carroll et al., 2008
m.413470	60S ribosomal protein L22	13	NA	Cre07.g357850.t1.2	85	AT3G05560	76	**O**	**R[a]**	Carroll et al., 2008
m.418624	60S ribosomal protein L23	14	NA	Cre04.g211800.t1.2	86	AT3G04400	77	**O**	**R[a]**	Carroll et al., 2008
m.414858	60S ribosomal protein L23a	10	NA	Cre06.g282500.t1.2	80	AT2G39460	82	**O**	**R[a]**	Carroll et al., 2008
m.414201	60S ribosomal protein L26	17	NA	Cre01.g040000.t1.2	73	AT5G67510	72	**C**	**R[a]**	Carroll et al., 2008
m.355110	60S ribosomal protein L27	17	NA	Cre17.g701650.t1.2	77	AT4G15000	66	**C**	**R[a]**	Carroll et al., 2008
m.414616	60S ribosomal protein L27a	18	NA	Cre02.g115200.t1.2	80	AT1G70600	72	**C**	**R[a]**	Carroll et al., 2008
m.415310	60S ribosomal protein L28	13	NA	Cre11.g467578.t1.1	50	AT2G19730	48	**O**	**R[a]**	Carroll et al., 2008

m.353856	60S ribosomal protein L30	7	NA	Cre10.g420750.t1.2	85	AT1G77940	72	**O**	**R[a]**	Carroll et al., 2008
m.417942	60S ribosomal protein L32	14	NA	Cre06.g289550.t1.2	76	AT4G18100	76	**O**	**R[a]**	Carroll et al., 2008
m.416985	60S ribosomal protein L34	13	NA	Cre16.g661050.t1.2	62	AT1G69620	62	**O**	**R[a]**	Carroll et al., 2008
m.415255	60S ribosomal protein L35	14	NA	Cre14.g617900.t1.2	60	AT5G02610	69	**O**	**R[a]**	Carroll et al., 2008
m.417525	60S ribosomal protein L36	12	NA	Cre12.g484050.t1.2	72	AT3G53740	65	**C**	**R[a]**	Carroll et al., 2008
m.416193	60S ribosomal protein L37	10	NA	Cre10.g430400.t1.2	67	AT3G16080	77	**C**	**R[a]**	Carroll et al., 2008
Regulation of cytosolic translation										
m.379239	Circadian RNA-binding protein CHLAMY 1 subunit C1	53	NA	Cre06.g250800.t2.1	50	AT1G33680	36	**O**	**Cy[a]**	Iliev et al., 2006
m.240501	eIF5-mimic protein	54	NA	Cre06.g298350.t1.2	50	AT1G65220	41	**O**	**Cy[b]**	NA
m.414715	Elongation factor 1-alpha	51	3.6.5.3.	Cre06.g263450.t1.2	88	AT1G07930	41	**O**	**Cy[b]**	NA
m.415822	Elongation factor 2	93	3.6.5.3.	Cre12.g516200.t1.2	80	AT1G56070	78	**O**	**Cy[a]**	Ito et al., 2011
m.360936	Eukaryotic initiation factor 4a	49	3.6.4.13.	Cre06.g298650.t1.2	85	AT3G13920	86	**C**	**Cy[a]**	Ito et al., 2011
tRNA synthesis										
m.228428	Alanine--tRNA ligase	108	6.1.1.7.	Cre02.g143200.t1.1	66	AT1G50200	57	**C**	**Cy[a]**	Duchêne et al., 2005

Table S4.8. Other protein metabolic processes.

Protein ID	Curated description	MW (kDa)	E.C. number	Best Cr homolog		Best At homolog		Subcellular localization		
				JGI v5.5 ID	% ID	TAIR10 ID	% ID	Predicted	Curated	Reference
Protein targeting										
m.415162	Nascent polypeptide-associated complex subunit alpha-like protein	15	NA	Cre15.g635600.t1.2	84	AT5G13850	82	**O**	**Cy**[a]	Ito et al., 2011
Endoplasmic Reticulum protein translocation										
m.388079	Protein transport protein Sec61 subunit alpha	54	NA	Cre03.g171350.t1.2	68	AT1G78720	64	**SP**	**E**[a]	Nikolovski et al., 2012
m.258682	Translocon-associated protein subunit beta	26	NA	Cre05.g244950.t1.2	32	AT5G14030	32	**SP**	**E**[a]	Nikolovski et al., 2012
Chloroplast protein translocation										
m.414971	Short chain dehydrogenase TIC 32	41	1.1.1.-	Cre12.g556750.t1.1	46	AT4G11410	38	**O**	**C**[a]	Hörmann et al., 2004
m.181462	Protein TIC 62	61	1.-	Cre06.g269050.t1.2	61	AT3G18890	57	**C**	**C**[a]	Ferro et al., 2010
m.227792	Protein TIC 110	119	NA	Cre10.g452450.t1.2	42	AT1G06950	37	**C**	**C**[a]	Schottkowski et al., 2012
m.153068	Translocase of chloroplast 34	51	3.6.5.-	Cre06.g252200.t1.2	37	AT5G05000	39	**O**	**C**[a]	Terashima et al., 2010
m.134654	Protein TOC 75	87	NA	Cre03.g175200.t1.2	33	AT3G46740	44	**C**	**C**[a]	Schottkowski et al., 2012
m.141978	Translocase of chloroplast 159	106	3.6.5.-	Cre17.g707500.t1.2	26	AT5G20300	29	**O**	**C**[a]	Ferro et al., 2010
Protein modification process										
m.262465	Prolyl 4-hydroxylase	47	1.14.11.2.	Cre10.g443050.t1.2	33	AT5G66060	30	**O**	**E**[a]	Nikolovski et al., 2012
m.408523	Ubiquitin	10	NA	Cre01.g007051.t1.2	93	AT3G52590	99	**O**	**Cy**[b]	NA
Protein folding										
m.293021	ATP-dependent Clp protease ATP-binding subunit clpA-like, chloroplastic	100	NA	Cre10.g465550.t1.1	45	AT5G50920	83	**C**	**C**[a]	Ferro et al., 2010
m.372714	Calnexin homolog	66	NA	Cre07.g357900.t1.2	49	AT5G07340	60	**O**	**E**[a]	Dunkley et al., 2006

m.415324	Chaperone protein DnaJ, chloroplastic	37	NA	Cre12.g507650.t1.2	62	AT2G22360	57	**O**	**C[a]**	Willmund et al., 2008
m.257035	Chaperonin 60 subunit beta, chloroplastic	64	3.6.4.9.	Cre07.g339150.t1.1	76	AT1G55490	72	**C**	**C[a]**	Bienvenut et al., 2011
m.394018	Chaperonin CPN60, mitochondrial	61	3.6.4.9.	Cre06.g309100.t1.2	79	AT3G23990	73	**C**	**M[a]**	Atteia et al., 2009
m.251107	Heat shock 70 kDa protein, chloroplastic	74	3.6.4.10.	Cre06.g250100.t1.2	85	AT4G24280	77	**C**	**C[a]**	Bienvenut et al., 2011
m.351998	Heat shock-related 70 kDa protein_A	49	NA	Cre08.g372100.t1.2	81	AT3G12580	81	**SP**	**U**	NA
m.372648	Heat shock-related 70 kDa protein_B	22	NA	Cre08.g372100.t1.2	82	AT5G02500	83	**O**	**U**	NA
m.357691	Luminal-binding protein	73	3.6.4.10.	Cre02.g080700.t1.2	85	AT5G42020	81	**SP**	**E[a]**	Dunkley et al., 2006
m.72221	Peptidyl-prolyl cis-trans isomerase, chloroplastic	52	5.2.1.8.	Cre06.g303300.t1.2	45	AT3G15520	38	**O**	**C[a]**	Terashima et al., 2010
m.418074	Protein disulfide isomerase	56	5.3.4.1.	Cre02.g088200.t1.2	50	AT5G60640	42	**SP**	**E[a]**	Levitan et al., 2005
m.259240	Small heat shock protein	31	NA	Cre07.g318800.t1.2	38	AT1G07400	42	**M**	**Cy[b]**	NA
Protein degradation										
m.375664	Cell division control protein 48 homolog	88	3.6.1.3.	Cre06.g269950.t1.2	88	AT3G09840	88	**O**	**Cy[a]**	Aker et al., 2007
m.383400	Chlapsin	47	3.4.23.-	Cre04.g226850.t1.2	58	AT1G62290	58	**SP**	**C[a]**	Almeida et al., 2012
m.420384	Cysteine proteinase	45	3.4.22.-	Cre05.g247851.t1.1	52	AT4G35350	51	**SP**	**Cy[a]**	Avci et al., 2008
m.386349	Cysteine proteinase inhibitor	12	NA	Cre16.g685725.t2.1	41	AT5G12140	38	**SP**	**Cy[a]**	Ito et al., 2011
m.288191	Probable carboxypeptidase PM20D1	61	3.4.17.-	Cre12.g508500.t1.2	41	AT1G44820	40	**SP**	**U**	NA
m.362717	Serine protease inhibitor Kazal-type	30	NA	Cre07.g329500.t1.2	37	NA	NA	**SP**	**U**	NA
m.422036	Trypsin-like serine endopeptidase	46	3.4.21.-	Cre01.g045601.t1.2	33	NA	NA	**SP**	**U**	NA
Protein interaction										
m.421481	Calcium/calmodulin dependent protein kinase II association domain-containing protein_A	30	NA	Cre16.g661750.t1.2	48	NA	NA	**C**	**U**	NA

m.372212	Calcium/calmodulin dependent protein kinase II association domain-containing protein_D	17	NA	Cre16.g661750.t1.2	50	NA	NA	**O**	**U**	NA
m.159885	Leucine-rich repeat, ribonuclease inhibitor subfamily protein	55	NA	Cre06.g302700.t1.1	50	AT1G10510	46	**M**	**C**[a]	Ferro et al., 2010
m.49320	Sterile alpha motif domain-containing protein	53	NA	Cre10.g419950.t1.1	28	NA	NA	**O**	**U**	NA
m.400735	Tetratricopeptide repeat-containing protein	21	NA	Cre10.g439350.t1.2	38	AT1G55480	41	**C**	**C**[b]	NA

Table S4.9. Intracellular membrane trafficking.

Protein ID	Curated description	MW (kDa)	E.C. number	Best Cr homolog		Best At homolog		Subcellular localization		
				JGI v5.5 ID	% ID	TAIR10 ID	% ID	Predicted	Curated	Reference
m.353642	Actin	42	NA	Cre13.g603700.t1.2	90	AT2G37620	89	**O**	**Ck[a]**	Kato-Minoura et al., 1997
m.352925	ADP-ribosylation factor	21	3.6.5.2.	Cre12.g486250.t1.2	92	AT1G10630	94	**O**	**E[a]**	Parsons et al., 2012
m.363118	AP-1 complex subunit beta	76	NA	Cre11.g478156.t2.1	71	AT4G23460	74	**O**	**E[b]**	NA
m.391009	Clathrin heavy chain	189	NA	Cre02.g101400.t1.2	69	AT3G08530	64	**O**	**E[a]**	Parsons et al., 2012
m.449	Coatomer subunit alpha	138	NA	Cre13.g565850.t1.1	79	AT1G62020	63	**O**	**E[b]**	NA
m.364595	Coatomer subunit beta	113	NA	Cre04.g217921.t1.1	65	AT4G31490	59	**O**	**E[b]**	NA
m.128169	Coatomer subunit gamma	100	NA	Cre06.g310750.t1.2	68	AT4G34450	62	**O**	**E[b]**	NA
m.214297	Dynamin-related protein	81	NA	Cre02.g079550.t1.2	33	AT1G10290	27	**O**	**U**	NA
m.381765	Dynamin-related protein 1 subfamily member	69	3.6.5.5.	Cre05.g245950.t1.1	51	AT3G60190	46	**O**	**E[a]**	Fujimoto et al., 2010
m.377780	Kinesin-like calmodulin-binding protein, C-terminal peptide	69	3.6.4.5.	Cre06.g278125.t1.1	64	AT5G65930	54	**O**	**Ck[a]**	Dymek et al., 2006
m.419992	Kinesin-like calmodulin-binding protein, N-terminal peptide	66	NA	Cre06.g278125.t1.1	66	AT5G65930	53	**O**	**Ck[a]**	Dymek et al., 2006
m.62529	Putative clathrin assembly protein	74	NA	Cre09.g393136.t1.1	41	AT5G57200	41	**O**	**E[b]**	NA
m.362053	RAB1/RABD/YPT1-related small GTPase	23	3.6.5.2.	Cre12.g560150.t1.2	85	AT1G02130	77	**O**	**E[a]**	Batoko et al., 2000
m.418226	RAB11/RABA/YPT31/32-related small GTPase	24	3.6.5.2.	Cre03.g189250.t1.2	93	AT1G07410	76	**O**	**E[a]**	Nielsen et al., 2008
m.361245	Reticulon-like protein	24	NA	Cre06.g308950.t1.2	33	AT4G11220	30	**O**	**E[a]**	Sparkes et al., 2010
m.397619	RP2-Clathrin light chain family protein (RP2-CLC)	39	NA	Cre06.g293250.t1.1	41	AT4G39920	29	**O**	**PM[a]**	This work
m.221766	Transmembrane 9 superfamily member	80	NA	Cre12.g494350.t1.2	52	AT5G35160	50	**SP**	**E[a]**	Parsons et al., 2012
m.366113	Tubulin alpha chain	50	3.6.5.6.	Cre03.g190950.t1.2	97	AT1G04820	96	**O**	**Ck[a]**	Keller et al., 2005

m.381961	Tubulin beta chain	54	3.6.5.6.	Cre12.g542250.t1.1	93	AT5G62700	90	**O**	**Ck[a]**	Keller et al., 2005
m.314807	Vacuolar protein sorting-associated protein 32 (VPS32)	36	NA	Cre06.g282200.t1.2	48	AT2G19830	51	**SP**	**E[a]**	Yoshida et al., 2013
m.272697	Vesicle-associated protein	27	NA	Cre03.g196900.t1.2	36	AT2G45140	52	**O**	**E[a]**	Dunkley et al., 2006

Table S4.10. RNA metabolic processes.

Protein ID	Curated description	MW (kDa)	E.C. number	Best Cr homolog		Best At homolog		Subcellular localization		
				JGI v5.5 ID	% ID	TAIR10 ID	% ID	Predicted	Curated	Reference
Regulation of transcription										
m.350552	Cold shock protein (CSD)	18	NA	Cre06.g268600.t1.2	78	AT4G36020	58	**O**	**U**	NA
m.323842	GCN5-related N-acetyltransferase (GNAT)	23	2.3.1.-	Cre11.g467526.t1.1	42	NA	NA	**C**	**C**[b]	NA
m.339185	HLA8-like nuclease	21	NA	Cre01.g048150.t1.2	44	AT2G40410	33	**O**	**N**[a]	Seitz et al., 2010
RNA processing										
m.363682	DEAD-box ATP-dependent RNA helicase	68	3.6.4.13.	Cre10.g427700.t1.2	71	AT2G42520	66	**O**	**Cy**[b]	NA
m.24677	H/ACA ribonucleoprotein complex subunit 4	50	5.4.99.-	Cre03.g172950.t1.2	79	AT3G57150	73	**O**	**N**[a]	Lermontova et al., 2007
m.235791	rRNA 2'-O-methyltransferase fibrillarin	33	2.1.1.-	Cre02.g077300.t1.2	87	AT4G25630	81	**O**	**N**[a]	Barneche et al., 2000
m.378433	Serine/arginine-rich splicing factor RSZ	28	NA	Cre17.g712000.t1.1	51	AT2G24590	52	**O**	**N**[a]	Lorkovic et al., 2004
RNA binding										
m.396016	Glycine-rich RNA-binding protein	30	NA	Cre17.g729150.t1.2	48	AT3G26420	46	**O**	**U**	NA
m.222753	KH domain-contaning protein	39	NA	Cre06.g250800.t2.1	27	AT5G04430	22	**C**	**Cy**[b]	NA
m.129410	RNA-binding protein_A	49	NA	Cre03.g169150.t2.1	40	AT4G00830	36	**C**	**Cy**[a]	Ito et al., 2011
m.97418	RNA-binding protein_B	59	NA	Cre16.g656250.t1.1	40	AT2G21660	47	**O**	**U**	NA

Table S4.11. Signal transduction.

Protein ID	Curated description	MW (kDa)	E.C. number	Best Cr homolog		Best At homolog		Subcellular localization		
				JGI v5.5 ID	% ID	TAIR10 ID	% ID	Predicted	Curated	Reference
Cellular response to light										
m.32101	Opsin-like protein	27	NA	Cre01.g002500.t1.2	26	NA	NA	**M**	**U**	NA
m.385313	Phototropin	88	2.7.11.1.	Cre03.g199000.t1.2	64	AT5G58140	44	**O**	**PM**[a]	Huang et al., 2004
Calcium-mediated signaling										
m.26479	Calcium sensing receptor, chloroplastic (CAS)	47	NA	Cre12.g497300.t2.1	44	AT5G23060	29	**M**	**C**[a]	Petroutsos et al., 2011
m.420836	Calcium-dependent protein kinase	60	2.7.11.1.	Cre07.g328900.t1.2	52	AT5G12180	57	**C**	**Cy**[a]	Dammann et al., 2003
m.419212	Calmodulin	21	NA	Cre03.g178150.t1.1	85	AT3G43810	86	**O**	**Cy**[b]	NA
m.291084	EF-hand calcium-binding domain-containing protein_A	39	NA	Cre01.g016300.t1.1	38	NA	NA	**C**	**C**[b]	NA
m.137276	EF-hand calcium-binding domain-containing protein_B	19	NA	Cre02.g108900.t1.2	36	AT1G64850	26	**O**	**U**	NA
Other signaling proteins										
m.413740	14-3-3 protein	29	NA	Cre12.g559250.t1.2	92	AT3G02520	80	**O**	**Cy**[a]	Voigt et al., 2001
m.369331	Guanine nucleotide-binding protein subunit beta-like protein	36	NA	Cre06.g278222.t1.1	83	AT1G48630	68	**O**	**Cy**[a]	Ito et al., 2011
m.245760	Probable protein phosphatase 2C	32	3.1.3.16.	Cre08.g365632.t1.1	61	AT1G43900	35	**O**	**Cy**[b]	NA

Table S4.12. Other transmembrane transport proteins.

Protein ID	Curated description	MW (kDa)	E.C. number	Best Cr homolog		Best At homolog		Subcellular localization		
				JGI v5.5 ID	% ID	TAIR10 ID	% ID	Predicted	Curated	Reference
m.357380	ABC transporter B family member	81	3.6.3.-	Cre17.g725200.t1.2	59	AT1G02530	36	**M**	**PM**[a]	Mitra et al., 2009
m.377402	ABC transporter G family member_B	175	3.6.3.-	Cre16.g655450.t1.1	40	AT1G59870	51	**O**	**PM**[a]	Mitra et al., 2009
m.421753	Outer envelope pore protein 24_A, chloroplastic	29	NA	NA	NA	AT1G45170	19	**SP**	**C**[a]	Pohlmeyer et al., 1998
m.341627	Outer envelope pore protein 24_B, chloroplastic	24	NA	NA	NA	NA	NA	**O**	**C**[a]	Pohlmeyer et al., 1998
m.138922	Probable metabolite transport protein, chloroplastic	30	NA	Cre13.g569250.t1.2	48	AT1G44920	38	**M**	**C**[a]	Ferro et al., 2010
m.352416	Proton-efflux P-type ATPase, plasma membrane-type_A	112	3.6.3.6.	Cre03.g165050.t1.2	63	AT2G18960	41	**O**	**PM**[a]	Rodrigues et al., 2014
m.363780	Proton-efflux P-type ATPase, plasma membrane-type_B	113	3.6.3.6.	Cre10.g459200.t1.2	61	AT3G42640	42	**O**	**PM**[a]	Nühse et al., 2004
m.350079	Pyrophosphate-energized vacuolar membrane proton pump	70	3.6.1.1.	Cre09.g394436.t1.1	78	AT1G15690	73	**O**	**V**[a]	Carter et al., 2004
m.378383	Voltage-dependent anion-selective channel protein	30	NA	Cre05.g241950.t1.2	43	AT5G57490	28	**O**	**M**[a]	Atteia et al., 2009
m.395664	V-type proton ATPase subunit B	55	NA	Cre02.g076350.t1.2	85	AT1G20260	84	**O**	**V**[a]	Carter et al., 2004
m.399358	V-type proton ATPase subunit G	12	NA	Cre11.g468550.t1.2	54	AT4G23710	49	**M**	**V**[a]	Carter et al., 2004

Table S4.13. Other oxidation-reduction processes.

Protein ID	Curated description	MW (kDa)	E.C. number	Best Cr homolog		Best At homolog		Subcellular localization		
				JGI v5.5 ID	% ID	TAIR10 ID	% ID	Predicted	Curated	Reference
Regulation of redox homeostasis										
m.370006	2-cys peroxiredoxin BAS1, chloroplastic	27	1.11.1.15.	Cre06.g257601.t1.2	76	AT5G06290	69	**C**	**C[a]**	Bienvenut et al., 2011
m.418092	Cytochrome c peroxidase, mitochondrial	41	1.11.1.5.	Cre09.g401886.t1.1	70	AT1G07890	48	**M**	**M[a]**	Atteia et al., 2009
m.267965	Glutaredoxin	62	NA	Cre06.g278183.t1.1	47	AT4G08550	35	**C**	**Cy[b]**	NA
m.209382	Probable L-ascorbate peroxidase, chloroplastic	38	1.11.1.11.	Cre05.g233900.t1.2	45	AT4G09010	36	**C**	**C[a]**	Ferro et al., 2010
m.376641	Thioredoxin M-type, chloroplastic	20	NA	Cre01.g052250.t1.2	42	AT3G15360	59	**C**	**C[a]**	Ferro et al., 2010
Other oxidation-reduction proteins										
m.419409	Amine oxidase	43	1.-	Cre13.g587500.t2.1	60	AT4G14210	23	**O**	**C[a]**	Terashima et al., 2010
m.283677	FAD-dependent monooxygenase	58	1.14.13.-	Cre12.g493700.t1.2	29	AT5G67030	29	**O**	**U**	NA
m.339313	Ferredoxin reductase-type FAD-binding and oxidoreductase FAD/NAD(P)-binding domain-containing protein	35	1.-	Cre01.g000350.t1.1	50	AT1G15140	45	**C**	**C[a]**	Terashima et al., 2010
m.419428	Glyoxal/galactose oxidase	48	1.1.3.-	Cre06.g278252.t1.1	25	AT3G57620	30	**O**	**U**	NA
m.261559	Probable Flavodoxin-like quinone reductase	26	1.6.5.2.	Cre10.g456100.t1.2	67	AT5G54500	62	**M**	**PM[a]**	Marmagne et al., 2007
m.414660	Zinc-type alcohol dehydrogenase family protein	37	NA	Cre06.g297400.t1.1	45	AT4G13010	37	**O**	**U**	NA

Table S4.14. Other biological processes.

Protein ID	Curated description	MW (kDa)	E.C. number	Best Cr homolog		Best At homolog		Subcellular localization		
				JGI v5.5 ID	% ID	TAIR10 ID	% ID	Predicted	Curated	Reference
Cell division										
m.391974	Protein RETARDED ROOT GROWTH, mitochondrial	45	NA	Cre09.g394917.t1.1	49	AT1G69380	23	**C**	**M**[a]	Zhou et al., 2011a
Iron assimilation										
m.413714	Ferritin, chloroplastic	31	1.16.3.1.	Cre09.g387800.t1.2	54	AT3G11050	49	**M**	**C**[a]	Busch et al., 2008
m.360182	Transferrin	121	NA	NA	NA	NA	NA	**SP**	**PM**[a]	Fisher et al., 1997
Nucleosome assembly										
m.338764	Histone H2A	14	NA	Cre06.g264950.t1.2	89	AT1G51060	89	**C**	**N**[a]	Waterborg et al., 1995
m.105761	Histone H2B_A	15	NA	Cre06.g271376.t1.1	84	AT3G46030	82	**O**	**N**[a]	Waterborg et al., 1995
m.415729	Histone H2B_B	15	NA	Cre13.g570050.t1.2	87	AT3G45980	87	**C**	**N**[a]	Waterborg et al., 1995
m.166547	Histone H4	14	NA	Cre06.g266600.t1.2	93	AT1G07660	95	**O**	**N**[a]	Waterborg et al., 1995

Table S4.15. Proteins of unknown function.

Protein ID	Curated description	MW (kDa)	E.C. number	Best Cr homolog		Best At homolog		Subcellular localization		
				JGI v5.5 ID	% ID	TAIR10 ID	% ID	Predicted	Curated	Reference
NAD(P)-binding domain-containing proteins										
m.314583	Galactose-binding domain-like, CIA-30 and Rossmann-fold NAD(P)-binding domain-containing protein_A	76	NA	Cre06.g274650.t1.1	53	AT4G18810	33	**C**	**C[a]**	Terashima et al., 2010
m.216711	Galactose-binding domain-like, CIA-30 and Rossmann-fold NAD(P)-binding domain-containing protein_B	67	NA	Cre05.g244800.t1.2	54	AT4G18810	48	**M**	**C[a]**	Ferro et al., 2010
m.13924	NAD(P)-binding Rossmann-fold superfamily protein_B	54	NA	Cre02.g081250.t1.2	30	AT3G18890	25	**C**	**C[a]**	Terashima et al., 2010
m.66681	NAD(P)-binding Rossmann-fold superfamily protein_C	36	NA	Cre06.g279850.t1.2	61	AT2G37660	50	**C**	**C[a]**	Terashima et al., 2010
Probable cell wall proteins										
m.372532	FAS1 domain-containing protein	28	NA	Cre12.g492650.t1.2	35	NA	NA	**O**	**U**	NA
m.94582	Proline-rich extensin signature-containing protein_A	50	NA	NA	NA	AT5G09520	44	**C**	**U**	NA
m.270148	Proline-rich extensin signature-containing protein_B	60	NA	NA	NA	NA	NA	**O**	**U**	NA
m.313614	Proline-rich extensin signature-containing protein_C	38	NA	NA	NA	NA	NA	**SP**	**U**	NA
Rhodanese-like domain-containing proteins										
m.269266	Rhodanese-like domain-containing protein_A	29	NA	Cre13.g602650.t1.2	57	AT4G24750	42	**C**	**C[a]**	Zybailov et al., 2008
m.58086	Rhodanese-like domain containing protein_B	69	NA	Cre05.g247450.t1.2	38	AT3G59780	34	**C**	**C[a]**	Terashima et al., 2010
m.384354	Rhodanese-like domain-containing protein_C	43	NA	Cre09.g401293.t1.1	28	AT3G59780	29	**M**	**C[a]**	Zybailov et al., 2008
m.381311	Rhodanese-like domain-containing protein_D	26	NA	Cre02.g111450.t1.2	43	AT4G27700	31	**C**	**C[a]**	Terashima et al., 2010

m.154074	Rhodanese-like domain-containing protein_E	26	NA	Cre16.g650050.t1.2	42	AT4G27700	38	**C**	**C**[a]	Bauer et al., 2004
UPF0187 family proteins										
m.373663	UPF0187 protein_A, chloroplastic	51	NA	Cre11.g474700.t1.1	43	AT3G61320	32	**M**	**C**[b]	NA
m.388425	UPF0187 protein_B, chloroplastic	50	NA	Cre11.g474700.t1.1	45	AT3G61320	33	**C**	**C**[b]	NA
m.406263	UPF0187 protein_C, chloroplastic	51	NA	Cre11.g474700.t1.1	44	AT2G45870	39	**C**	**C**[b]	NA
Other identified proteins										
m.388849	CreA family protein	28	NA	Cre08.g361850.t1.2	57	NA	NA	**O**	**U**	NA
m.313032	DUF1499 family protein	24	NA	Cre11.g468750.t1.2	61	AT3G60810	48	**C**	**C**[a]	Terashima et al., 2010
m.243853	DUF1517 family protein	47	NA	Cre01.g004450.t1.2	43	AT1G54520	44	**C**	**C**[a]	Ferro et al., 2010
m.230740	DUF1995 domain-containing protein	42	NA	Cre03.g184550.t1.2	24	AT5G35170	47	**O**	**U**	NA
m.413885	Hypersensitive-induced response protein	32	NA	Cre16.g690879.t1.1	58	AT5G62740	55	**O**	**PM**[a]	Qi et al., 2011
m.286009	MORN repeat-containing protein	48	NA	Cre06.g300550.t1.2	46	AT2G35170	45	**O**	**U**	NA
m.326572	Oxidoreductase HTATIP2-like protein	25	NA	Cre16.g672050.t2.1	52	NA	NA	**O**	**M**[a]	Mueller et al., 2014
m.412470	PBP domain-containing protein	45	NA	Cre01.g044300.t1.2	24	NA	NA	**SP**	**U**	NA
m.184707	Pollen allergen Poa pIX/Phl pVI family protein	19	NA	NA	NA	NA	NA	**C**	**U**	NA
m.163579	Probable thylakoid lumenal 16.5 kDa protein, chloroplastic	22	NA	Cre06.g256250.t1.2	48	AT4G02530	31	**C**	**C**[a]	Terashima et al., 2010
m.197305	Pyrophosphate-energized vacuolar membrane proton pump family protein	12	NA	Cre09.g394436.t1.1	55	AT1G15690	40	**SP**	**U**	NA
m.197391	RETICULATA-RELATED family protein, chloroplastic	37	NA	Cre16.g678000.t1.2	57	AT3G08640	52	**C**	**C**[a]	Terashima et al., 2010
m.363941	SOUL heme-binding protein	26	NA	Cre06.g299700.t1.2	48	AT1G17100	33	**SP**	**Cy**[b]	NA
m.393062	START-like domain-containing protein	17	NA	Cre11.g467760.t1.1	41	NA	NA	**O**	**U**	NA
m.178172	Streptococcal non-M secreted SibA family protein	27	NA	NA	NA	NA	NA	**C**	**U**	NA
m.303864	Transmembrane protein 194	49	NA	Cre03.g183800.t1.1	29	NA	NA	**SP**	**U**	NA

Unknown proteins										
m.376839	Unknown protein_A	42	NA	NA	NA	NA	NA	**O**	**U**	NA
m.132404	Unknown protein_AA	66	NA	NA	NA	NA	NA	**M**	**U**	NA
m.412999	Unknown protein_AB	21	NA	NA	NA	NA	NA	**C**	**U**	NA
m.394013	Unknown protein_AC	26	NA	NA	NA	NA	NA	**C**	**U**	NA
m.205316	Unknown protein_AD	8	NA	NA	NA	NA	NA	**SP**	**U**	NA
m.420337	Unknown protein_AE	9	NA	Cre07.g349200.t1.2	38	NA	NA	**O**	**U**	NA
m.383934	Unknown protein_AF	11	NA	NA	NA	NA	NA	**C**	**U**	NA
m.260912	Unknown protein_AG	19	NA	Cre02.g081050.t1.2	36	AT1G65900	38	**O**	**U**	NA
m.352389	Unknown protein_AH	17	NA	Cre05.g233050.t1.2	52	NA	NA	**O**	**U**	NA
m.175026	Unknown protein_AI	31	NA	Cre09.g402950.t1.1	45	AT5G08540	32	**O**	**C**[a]	Ferro et al., 2010
m.248508	Unknown protein_AJ	47	NA	NA	NA	NA	NA	**C**	**U**	NA
m.364059	Unknown protein_AK	30	NA	NA	NA	NA	NA	**O**	**U**	NA
m.418699	Unknown protein_AL	8	NA	NA	NA	NA	NA	**O**	**U**	NA
m.398482	Unknown protein_AM	18	NA	NA	NA	NA	NA	**C**	**U**	NA
m.247758	Unknown protein_AN	34	NA	NA	NA	NA	NA	**SP**	**U**	NA
m.37572	Unknown protein_AO	24	NA	Cre12.g498950.t1.2	40	NA	NA	**O**	**LD**[a]	Moellering and Benning, 2010
m.202466	Unknown protein_AP	25	NA	NA	NA	NA	NA	**O**	**U**	NA
m.261163	Unknown protein_B	39	NA	Cre03.g164000.t1.2	32	NA	NA	**C**	**C**[a]	Terashima et al., 2010
m.146237	Unknown protein_C	43	NA	NA	NA	NA	NA	**C**	**U**	NA
m.317171	Unknown protein_D	31	NA	Cre01.g002750.t2.1	38	NA	NA	**M**	**M**[b]	NA
m.417976	Unknown protein_E	26	NA	NA	NA	AT2G21870	24	**M**	**U**	NA
m.389943	Unknown protein_F	29	NA	NA	NA	NA	NA	**C**	**U**	NA
m.406589	Unknown protein_G	27	NA	Cre06.g279500.t1.1	34	AT5G06130	32	**C**	**C**[b]	NA
m.239299	Unknown protein_J	19	NA	NA	NA	NA	NA	**C**	**U**	NA

m.111503	Unknown protein_M	15	NA	NA	NA	NA	NA	**C**	**U**	NA
m.152339	Unknown protein_O	22	NA	NA	NA	NA	NA	**SP**	**U**	NA
m.169592	Unknown protein_P	16	NA	NA	NA	NA	NA	**C**	**U**	NA
m.413882	Unknown protein_Q	17	NA	Cre07.g349200.t1.2	29	NA	NA	**O**	**U**	NA
m.390039	Unknown protein_R	17	NA	Cre12.g555150.t1.2	22	AT3G18410	47	**M**	**U**	NA
m.403010	Unknown protein_S	40	NA	NA	NA	NA	NA	**SP**	**U**	NA
m.119057	Unknown protein_T	23	NA	NA	NA	NA	NA	**C**	**U**	NA
m.397130	Unknown protein_U	47	NA	NA	NA	NA	NA	**O**	**U**	NA
m.402505	Unknown protein_V	27	NA	NA	NA	NA	NA	**SP**	**U**	NA
m.260921	Unknown protein_W	40	NA	Cre02.g081050.t1.2	36	AT1G65900	31	**SP**	**U**	NA
m.405932	Unknown protein_X	14	NA	Cre06.g278195.t1.1	62	AT1G42960	49	**C**	**C**[a]	Terashima et al., 2010
m.354567	Unknown protein_Z	10	NA	Cre07.g349200.t1.2	40	NA	NA	**O**	**U**	NA

Table S4.16. Molecular phylogenetic analysis based on a multi-gene approach. List of taxa considered for the molecular phylogenetic analysis using concatenated mitochondria- (COX1, COX2), chloroplast- (PSBA, RBCL), and nuclear-encoded (EF-1α, actin) protein sequences UniProtKB accession numbers are provided unless otherwise stated.

Microalga species	COX1	COX2	PSBA	RBCL	EF-1α	Actin
Chlamydomonas reinhardtii [b]	P08681	Cre03.g154350.t1.2[d] Cre01.g049500.t1.2[d]	P07753	P00877	A8HX38	P53498
Chlorella protothecoides	A0A0A6ZEF7	A0A0A6ZEH4	A0A023HHM2	A8TKS7	A0A087SK74	A0A087SSM0
Chlorella sorokiniana	A0A076EAS5	A0A076E9B2	W8SIR2	W8SUA8	GAPD01004391.1[e]	Q8H0E6
Chlorella variabilis	A0A097P5Y8	A0A097P5Y2	F2YGK0	A9ZM80	E1ZBK2	E1ZLQ3
Chlorella vulgaris	P92619	Q6RFG7	P56318	P12466	JK816135.1[e]	Q8H0E5
Coccomyxa subellipsoidea	F1DPN3	F1DPL6	E9NPR9	E9NPX3	I0Z5I8	I0YI95
Dunaliella salina [b]	A0A0C5BWI3	Dusal.0134s00004.1[d] Dusal.0209s00005.1[d]	D0FY08	D0FXZ7	Dusal.0162s00022.1 [d]	Dusal.0175s00014.1 [d]
Ettlia oleoabundans [a]	m.342666[f]	m.110997	m.166963	m.384585	m.414715	m.353642
Haematococcus pluvialis [b]	SRR1040551[c] (read 6774)	DV203769.1[e] DV203283.1[e]	A0A0S2IDG6	A0A0S2IDA4	SRR1040551[c] (read 7797)	SRR1040551[c] (read 13003)
Micromonas pusilla CCMP1545	C1KR95	C1KRA4	C1KRD0	C1MSG5	C1MZI5	C1MYV3
Micromonas sp. CC299	C1KRF3	C1KRF7	C1KR28	C1KR38	C1E8S6	C1E7K7
Ostreococcus tauri	Q0P3F1	Q0P3F9	Q0P3J1	Q0P3J3	A0A096P7Q8	A0A096P7W5

Scenedesmus obliquus [b]	Q9MD20	Q9MD14, H9A5E9	Q1KVU8	Q1KVV0	C0LL60	E3SC86
Volvox carteri [b]	B3GTB1	Vocar.0019s0127.1[d] Vocar.0001s0585.1 [d]	D0VMW3	B8R182	D8THW4	P20904

[a] Sequences are identified with the Protein IDs with which they can be surveyed in Tables S4.1-S4.15.

[b] COX2 from *Chlorophycean* algae that are known to be coded by two different genes. Before performing the alignment of the COX2 dataset, *Chlorophycean* COX2A and COX2B subunits were manually concatenated into one sequence. For this purpose, N-terminal and C-terminal extensions of both, COX2A and COX2B, were removed according to Rodríguez-Salinas et al. (2012).

[c] Reads (cDNA) derived from an RNA-Seq project available at NCBI as a Sequence Read Project (SRA). BioProject: PRJNA22929; SRA: SRP033355; Experiment: SRX384371; Run: SRR1040551. Sequences can be accessed using the read number. Amino acid sequences were obtained by six-frame translation.

[d] Sequences retrieved from the Phytozome database v.10.3.

[e] GenBank accession numbers for cDNA sequences derived from transcriptomic data. Amino acid sequences were obtained by six-frame translation.

[e] *E. oleoabundans* COX1 was not detected in the membrane proteome. However, the translated sequence from the corresponding transcript was used for this analysis.

>m.342666|EoCOX1

MLTRWLYSTNHKDIGTLYLIFAAFSGVLGTAFSALIRLELAQPGNQILGGNHQLYNVIITAHAFLMVFYLVMPALMGGFGNWFLPILIGAPDM
AFPRLNNISFWLLPPSLLLLLSSALVEVGAGTGWTVYPPLSGIASHSGGSVDLAIFSLHLAGASSIMGAINFITTVFNMRAPGMSMHRLPLFV
WSVLITAFLLILALPVLAGGITMLLTDRNFNTTFFDPAGGGDPILYQHLFWFFGHPEVYILILPAFGIVSHVISTFSKKPIFGYLGMVYAMCSIGI
LGFIVWAHHMYTVGLDIDTRAYFTAATMIIAVPTGIKIFSWIATMWGGSLEFRTPMLFAVGFLFLFTVGGLTGVVLANSGLDIAFHDTYYVVG
HFHYVLSMGAVFGMFAGFYYWIGKISGVQYPETLGQIHFWMTFLGVNITFFPMHFLGLAGMPRRIPDYADAYAGWNAIASYGSYLSVLAAL
FFFYVVYKTLTSDETCPRNPWETTPGVSPTLEWMCTSPPSFHTYSEIPAIRTSRKQD*

Table S4.17. 18S (r)DNA molecular phylogenetic analysis. List of taxa for phylogenetic analysis of 18S (r)DNA nucleotide sequences, including the corresponding abbreviations employed for Figure 4.5B. GenBank accession numbers are provided. The partial 18S sequence obtained in this study is highlighted with bold letters. NA, Not Available.

Abbreviation	*Microalga species*	Strain	Accession number
Actha	*Actinastrum hantzschii*	CCAP 200/3	FM205884.1
Ankst	*Ankistrodesmus stipitatus*	SAG 202-5	X56100.1
Atcqu	*Asterarcys quadricellulare*	KNUA020	JQ043183.1
Atmgr	*Asteromonas gracilis*	CCMP 813	DQ009744.1
Cccec	*Chlorococcum echinozygotum*	UTEX 118	U57698.1
Ccmsu	*Coccomyxa subellipsoidea*	SAG 216-13	KF673374.1
Ccyin	*Coenocystis inconstans*	NA	AB017435.1
Cgnel	*Chlorogonium elongatum*	UTEX 11	U70589.1
Chlso	*Chlorella sorokiniana*	SAG 211-31	KF673387.1
Chlva	*Chlorella variabilis*	SAG 211-6	FM205849.1
Chlvu	*Chlorella vulgaris*	CCAP 211/81	FM205854.1
Cmdba	*Chlamydomonas baca*	SAG 24.87	U70781.1
Cmdmo	*Chlamydomonas moewusii*	SAG 11-11	U70786.1
Cmdmx	*Chlamydomonas mexicana*	SAG 11-60a	AF395434.1
Cmdno	*Chlamydomonas noctigama*	SAG 33.72	AJ781311.1
Cmdpi	*Chlamydomonas pitschmannii*	SAG 14.73	U70789.1
Cmdra	*Chlamydomonas rapa*	SAG 48.72	U70790.1
Cmdre	*Chlamydomonas reinhardtii*	CC-1952	AY665727.1
Cstsa	*Coelastrella saipanensis*	NA	AB055800.1
Dunba	*Dunaliella bardawil*	DB1	AF150905.1
Dunpa	*Dunaliella parva*	SAG 19-1	DQ009763.1
Ettca	*Ettlia carotinosa*	SAG 213-4	GU292342.1
Ettmi	*Ettlia minuta*	NA	M62996.1
Ettol1	*Ettlia oleoabundans*	UTEX 1185	KM068042.1
Ettol2	***Ettlia oleoabundans***	**UTEX 1185**	**KX350066.1**
Ettol3	*Ettlia oleoabundans*	UTEX 1185	JX978410.1
Ettsp	*Ettlia sp.*	SP	KF746927.1

Etttx1	*Ettlia texensis*	SAG 79.80	GU292343.1
Etttx2	*Ettlia texensis*	A2	HG328356.1
Ettyc	*Ettlia sp.*	YC001	JQ684664.1
Haeca	*Haematococcus capensis*	KMMCC 1353	JQ315535.1
Haepl1	*Haematococcus pluvialis*	SAG 34-1b	AF159369.1
Haepl2	*Haematococcus pluvialis*	NIES-144	AB360747.1
Haesp	*Haematococcus sp.*	KORDI03	FJ877140.1
Hcmlo	*Heterochlamydomonas lobata*	UTEX 728	AF367858.1
Hfgka	*Hemiflagellochloris kazakhstanica*	NA	AB244244.1
Hydre	*Hydrodictyon reticulatum*	SAG 236-1b	AY780660.1
Lbpti	*Lobosphaera tirolensis*	ASIB S234	AB006051.1
Mccra	*Macrochloris radiosa*	UTEX 1964	KC196723.1
Mcmsp	*Micromonas sp.*	RCC299	HM191693.1
Mctsp	*Micractinium sp.*	Ehime	JX889639.1
Myrin	*Myrmecia incise*	SAG 2007	AY762602.1
Ncovi	*Neochloris vigenis*	NA	M74496.1
Ncybr	*Neocystis brevis*	CCALA 393	JQ920362.1
Ncymu	*Neocystis mucosa*	SAG 40.88	JQ920367.1
Ntcso	*Nautococcus solutus*	SAG 76.80	AB360749.1
Otclu	*Ostreococcus lucimarinus*	RCC798	KT860898.1
Otcta	*Ostreococcus tauri*	NA	AY329635.1
Pclal	*Parietochloris alveolaris*	UTEX 836	EU878373.1
Pclco	*Parietochloris cohaerens*	UTEX 1707	EU878372.1
Pclov	*Parietochloris ovoidea*	ACKU 177-03	EU878374.1
Pclps	*Parietochloris pseudoalveolaris*	NA	M63002.1
Pdtdu	*Pediastrum duplex*	UTEX 1364	AY779859.1
Pltin	*Pleurastrum insigne*	SAG 30.93	Z28972.1
Pspbo	*Protosiphon botryoides*	UTEX 99	U41177.1
Pszps	*Paulschulzia pseudovolvox*	UTEX 167	AF408246.1
Rusfu	*Rusalka fusiformis*	NIES-123	AB360750.1
Scnob	*Scenedesmus obliquus*	SAG 276-3a	X56103.1
Spcsp	*Spongiochloris spongiosa*	UTEX 1	U63107.1

Tcyae	*Tetracystis aeria*	UTEX 1453	U41175.1
Tspsp	*Tetraspora sp.*	NA	U83121.1
Vvxca	*Volvox carteri*	UTEX 1885	X53904.1

Table S4.18. Proteins surveyed in FFZE membrane fractions via LC-MS/MS analysis.

Protein ID / Curated description	No. FFZE fractions (protein)[a]	Best %Protein ID probability[b]	Max. %Sequence coverage[b]	Max. UP/FFZE fraction[b]	Total UP[c]	UP sequence	Best %Peptide ID probability[b]	No. FFZE fractions (peptide)[d]	Max. SpC/FFZE fraction[e]
Subcellular compartment protein markers									
gi|416678 ATP synthase subunit beta *Thylakoid membrane marker* (Table S4.1)	**23**	**100**	**35.3**	**9**	**13**	**K.AHGGVSVFGGVGER.T**	**99.7**	**3**	**1**
						R.AVAMSATDGLMR.G	99.7	14	2
						K.DGSITSIQAVYVPADDLTDPAPATTFAHLDATTVLSR.N	99.7	5	2
						R.FVQAGSEVSALLGR.M	99.7	19	2
						K.GIYPAVDPLDSTSTMLQPWIVGDQHYQCAQNVK.Q	99.7	1	1
						R.MPSAVGYQPTLATEMGGLQER.I	99.7	11	3
						K.NEAGQEISVTCEVQQLLGDHCVR.A	99.7	7	2
						K.QDVLLFIDNIFR.F	99.7	8	2
						R.SAPAFVDLDTK.L	99.7	8	2
						K.TVLIMELINNIAK.A	99.7	23	6
						K.VALVYGQMNEPPGAR.M	99.7	10	2
						K.VVDLLAPYR.R	99.7	8	2
						R.YKELQDIIAILGLDELSEEDR.L	99.7	1	1
m.392881 ATP synthase subunit gamma *Thylakoid membrane marker* (Table S4.1)	**18**	**100**	**37.8**	**7**	**10**	**R.AQDAVVNGRPFAENLVK.V**	**99.7**	**1**	**1**
						K.EAQAIADDIFADFVSQEVDKVELIYTK.F	99.7	5	4
						R.EGQLVVEAEQVR.T	99.7	12	2
						K.FVSLISSSPVIQTLLPLTPSGEVCDINGNCVDAAEDEVFK.L	99.7	1	1
						K.ITTELTEIVAGAASV.-	99.7	7	2
						R.LRVEDVDSPLVAQRPVK.S	99.7	5	2
						R.MNAMNNASDNAAELKR.S	99.7	17	3
						K.SVALVVVTGDR.G	99.7	7	2
						K.VLYGVNQR.L	99	1	2
						R.YAELTGMGIAVR.L	99.7	6	2
m.378383 Voltage-dependent anion-selective channel protein *Mitochondria membrane marker* (Table S4.12)	**22**	**100**	**67.5**	**16**	**18**	**K.DDKLDMALK.G**	**99.7**	**7**	**2**
						R.DLNVGTTTFATGLSK.Q	99.7	17	2
						K.ELAPGLTVGVMGTVPDPDSGK.L	99.7	13	3
						R.FGFGYDLK.-	99	7	2
						K.GAYAADKYNVVATLAQSGK.L	99.7	19	4
						R.LAVSGQFSALDLNKPPR.F	99.7	21	7
						K.LDNAGIVSVLYEQELKPR.N	99.7	13	5
						K.LKLDNAGIVSVLYEQELKPR.N	99.7	21	4
						K.LSIDYTHAHANIK.S	99.7	4	1

						K.LSVAAAYK.E	99	14	2
						K.NTATALLAHK.V	99.7	12	4
						K.QLEGGALTK.L	99.7	7	2
						K.SVVSLTAAPK.V	99.7	16	2
						K.TADGVEFTVNAVGK.D	99.7	5	2
						K.TADGVEFTVNAVGKDDK.L	96.1	1	2
						K.VAFDTTIGAEVTR.D	99.7	15	4
						K.VDVAATTGFEGVTMGGEASYDTSK.S	99.7	16	6
						K.YNVVATLAQSGK.L	99.7	10	2
m.363780 Proton-efflux P-type ATPase, plasma membrane type_B *Plasma membrane marker* (Table S4.12)	**23**	**100**	**48.2**	**42**	**52**	**R.AAALLGSANQEANLQK.V**	**99.7**	**22**	**3**
						K.ADVGVAVAGATDAAR.G	99.7	15	2
						R.AEIEADCTAK.I	99.7	20	4
						K.AKGDGSADPPEGAR.W	99.7	8	8
						K.ALRDGQVQTIDASELVPGDIVIIR.L	99.7	11	3
						K.ALTSALAPK.A	99.7	20	2
						R.CHEMGISVK.M	99.7	8	2
						R.DAVHPCQFCTLSSGGDHPFWSNK.E	99.7	20	6
						K.DGETTVGVTGEEEK.E	99.7	6	2
						K.DGETTVGVTGEEEKEVDFK.E	99.7	16	2
						R.DGQVQTIDASELVPGDIVIIR.L	99.7	23	7
						R.DNATGEIER.V	99.7	13	3
						R.DSLWGESGTYTMAK.F	99.7	15	4
						K.EIGEQEALTILK.A	99.7	22	2
						K.FSGDVAFAGSTIK.Q	99.7	23	4
						K.FVPFNPTDK.Y	98.7	2	1
						K.FVPFNPTDKYTIAFVR.D	99.7	15	6
						R.GAADIVLTAPGLSAIVTAIIGAR.K	99.7	1	1
						K.GAPQVVVR.N	99	22	2
						K.GDGSADPPEGAR.W	99.6	1	1
						R.GEQMGAAANIGINK.M	99.7	14	3
						K.GLTSDEVAK.R	99.7	8	2
						K.GLTSDEVAKR.L	99.2	1	1
						R.HCVVYATGMQTFFGR.A	99.7	16	4
						K.HMVGMTGDGVNDAPALKK.A	99.7	3	3
						K.ILAEEGASGKPEDETPLQCDQAALTGESLPVK.K	99.7	23	4
						K.ILAEEGASGKPEDETPLQCDQAALTGESLPVKK.F	99.7	18	6
						K.KADVGVAVAGATDAAR.G	99.7	22	4
						K.KFSGDVAFAGSTIK.Q	99.7	3	2
						K.KGLTSDEVAK.R	99.7	21	4

						R.KHMVGMTGDGVNDAPALK.K	99.7	20	4
						R.LEQYGYNK.L	99	15	2
						R.LEQYGYNKLPEESR.N	99.7	1	1
						R.LGDIVPADIK.I	99.7	23	2
						K.LTVDHVNCYPLTGHSIEEVLK.Y	99.7	13	4
						K.MITGDQLLIGK.E	99.7	23	3
						K.MITGDQLLIGKETAK.Q	98.9	1	1
						R.MSAVEEMAGMDILCSDK.T	99.7	1	1
						R.MSAVEEMAGMDILCSDKTGTLTLNK.L	99.7	2	2
						R.MVPNAAMLQR.A	99.7	15	5
						R.NSYNRAEIEADCTAK.I	99.7	4	2
						K.QGFGLVEGHASVEDLVVEADGFAEVFPEHK.F	99.7	13	2
						R.QGQTWTSSTPACTIYPEEIEDCSITALQQCIAEQR.Y	99.5	2	2
						K.QLGMGTNMFTTETLLK.A	99.7	22	6
						K.RLEQYGYNK.L	99.7	19	4
						R.SGGMFSNIFR.T	99.7	22	6
						K.TGTLTLNK.L	99	16	2
						R.TRGEQMGAAANIGINK.M	99.7	21	6
						R.VSHGGYQSGGVPGVGGR.M	99.7	19	5
						R.WEMVGLVPLFDPPR.H	99.7	15	7
						R.WEMVGLVPLFDPPRHDTK.E	99.7	3	2
						K.YGAMSANIVTEEPIDMVLHESYPNR.D	99.7	12	8
m.395664 **V-type proton ATPase subunit B** ***Tonoplast marker*** **(Table S4.12)**	**16**	**100**	**28.9**	**9**	**9**	**R.AVVQVFEGTSGIDNR.S**	**99.7**	**13**	**2**
						R.FVNQGLYDNR.S	99.7	13	2
						R.GDHSEVSNQLYANYAIGK.D	99.7	6	2
						K.HGNEDGESEPFAIVFAAMGVNMETAHFFK.Q	99.7	2	1
						K.IPLFSAAGLPHNDIAAQICR.Q	99.7	6	2
						R.STTLEFTGEVLR.T	99.7	10	2
						R.TVGGVAGPLVAVNTVK.K	99.7	10	2
						R.TVLFLNLANDPTIER.I	99.7	9	2
						K.YAEIVNLR.L	99	4	2
m.227792 **Protein TIC 110** ***Inner chloroplast membrane marker*** **(Table S4.8)**	**15**	**100**	**9.2**	**8**	**15**	**K.AEVLGDLVDR.V**	**99.7**	**1**	**1**
						R.AGGESVGESGGGVMK.S	99.7	8	2
						K.ASLGLTDVDAAPAHIEVGR.R	99.7	7	2
						K.DAVNNALAAGIDGFGFEDR.R	97.6	1	1
						K.EAGVDVASVLGEDAR.Q	99.7	1	1
						K.EATEAAEAEIK.E	96.3	1	1
						R.GGQLQADKEFLVGLK.S	99.3	2	1
						K.LIYVSNLVFGDR.Q	99.7	2	2

						R.LTDGTGDFSSER.M	99.7	3	2
						K.LTEEDDASLR.E	99.7	6	2
						R.MLQQLPSELGIDADKAAK.T	96.2	1	1
						K.TLLGLGNR.E	99	4	2
						R.TTLVQAISFLR.Q	99.7	15	2
						R.VFGLTDAQVYVAK.R	99.7	3	2
						K.YGASLATTNPDELK.A	99.7	4	2
m.134654 Protein TOC75 *Outer chloroplast membrane marker* (Table S4.8)	**15**	**100**	**15.6**	**8**	**13**	**R.DTTYLVNGAQVGAR.D**	**99.7**	**1**	**1**
						K.GSSYGMGILFGAIR.A	99.7	3	2
						K.IGNTIGDLPAYDAFLLGGPFSVR.G	99.7	6	2
						K.ISVVHVDEEGNPSK.A	99.4	5	2
						K.NFLAPSDDLSFR.V	98.4	2	1
						R.NLFGNAASIAASINTK.N	99.7	4	3
						R.NSSGTLALVAQEITTR.D	99.7	3	2
						K.TLQNVFALDLFDNVQILPR.Q	99.6	1	1
						R.TTPFGQYLADGPPTALSDK.G	99.7	1	1
						K.VGITEQYSR.N	99.7	13	2
						R.VLSAQGALTR.D	99.7	10	2
						R.VPVLGQQLYAFAEYGSDLGSSAEVR.G	99.7	4	2
						R.YVEAAAELR.V	99.7	3	2
Novel identified proteins									
m.395061 Photosystem II 22 kDa protein (PSBS) (Table S4.1)	**15**	**100**	**25.6**	**6**	**6**	**K.ADLGVAKPTISLGFTK.S**	**99.7**	**12**	**3**
						K.ANELFVGR.M	99	11	2
						K.FFGITGFGFTK.A	99.7	11	2
						R.FVADEEELKERPK.G	97.9	2	1
						K.KFFGITGFGFTK.A	99.7	3	2
						R.MAQLGFAAALVGEAITGK.G	99.7	14	4
m.337748 Probable MPH1 protein (Table S4.1)	**18**	**100**	**18.9**	**3**	**3**	**R.AALGFTENDSAGQTNVFAVEPK.V**	**99.7**	**18**	**8**
						K.SLDFSSNK.R	99	6	2
						K.SLDFSSNKR.A	99.7	11	2
m.397619 RP2-Clathrin light chain family protein (RP2-CLC) (Table S4.9)	**16**	**100**	**20.9**	**5**	**7**	**K.APGSINGESFAIK.N**	**99.7**	**2**	**2**
						R.EASESKGNGELGPSGTTEPER.I	99.7	9	2
						K.GNGELGPSGTTEPER.I	99.7	9	2
						R.IACWAGAYPQAGVHFAAANLDPSVNQWNK.V	99.7	8	3
						R.IISMIDFNLARPNGSDLSR.F	99.7	2	2
						K.QALQAAAAK.Y	98.9	2	1
						K.YLEQFYER.R	99	16	2

Carbon metabolism proteins									
m.310144 Alpha carbonic anhydrase CAH3 (Table S4.4)	**14**	**100**	**17.2**	**3**	**3**	**R.KPGVNARPPQPLVDR.S**	**99.2**	**8**	**3**
						R.NTGHGTMQVNIPEGIEYELGPGGQR.H	99.7	13	4
						R.SAPTSPGAESQLQRPINLQTLLPK.V	99.7	3	2
m.199949 Phospho-glucomutase, chloroplastic (Table S4.4)	**7**	**100**	**4**	**2**	**2**	**K.FNYSSGEPAPEK.I**	**99.7**	**2**	**1**
						R.YDYEGVESEAANK.M	99.7	6	2
m.366318 ATP-dependent 6-phosphofructokinase, chloroplastic (Table S4.4)	**11**	**100**	**5.5**	**2**	**2**	**K.GTDASGNPILQDIGVFLR.D**	**99.7**	**9**	**3**
						K.NATIQLPDFALR.A	99.7	8	2
m.418145 Fructose-bisphosphate aldolase, chloroplastic (Table S4.4)	**23**	**100**	**47.4**	**12**	**14**	**R.ALQNTVLK.T**	**99**	**13**	**2**
						K.ANSDAQLGKYDSAGESAEAAK.G	99.7	4	4
						R.DCAYGLAR.Y	98.6	5	2
						K.GILAMDESNATCGK.R	99.7	5	4
						K.GLHPLANSNGESWCSGLDGLAQR.C	99.7	8	2
						R.LESIGLENTVENR.Q	99.7	16	2
						K.RLESIGLENTVENR.Q	99.7	22	4
						R.SVVSIPAGPSTIAVR.D	99.7	19	2
						R.TLEVAEMTWAETFK.Y	99.7	4	2
						K.TWKGEEANVQAAQDALLK.R	99.7	1	2
						R.YAAIAQNAGLVPIVEPEILLDGDHDINR.T	99.7	17	8
						K.YDSAGESAEAAK.G	99.7	9	2
						K.YLADNNVLFEGILLKPSMVTPGAEHSK.K	99.7	16	8
						K.YLADNNVLFEGILLKPSMVTPGAEHSKK.A	99.7	6	3
m.383891 Glyceraldehyde-3-phosphate dehydrogenase A, chloroplastic (Table S4.4)	**23**	**100**	**35**	**11**	**16**	**R.AAALNIVPTTTGAAK.A**	**99.7**	**13**	**2**
						R.ANSNLEVVAVNDSGGVK.Q	99.7	22	2
						K.AVALVLPK.L	99	11	3
						K.GILGVSDEPLVSCDYR.M	99.7	20	2
						K.GSGIPTYVVGVNEGDYK.H	99.7	19	2
						K.GTMTTTHSYTGDQR.L	99.7	4	1
						K.HSDAIISNASCTTNCLAPFVK.V	97.6	1	1
						R.MTDVSSTIDAALTMVMGDDMVK.V	99.7	2	2
						K.TFAEEVNEAFR.E	99.7	22	2
						K.VLITAPAK.G	99	6	2
						R.VPTPTVSVVDLVVQVEK.K	99.7	4	2

						R.VPTPTVSVVDLVVQVEKK.T	99.7	4	2
						K.VVAWYDNEWGYSQR.V	99.7	4	2
						R.VVDLAEVTATK.W	99.7	9	2
						R.VVDLAEVTATKWE.-	99.7	10	2
						K.YDSTMGTFNADVK.I	99.7	14	2
m.382809 Phosphoglycerate kinase, chloroplastic (Table S4.4)	**21**	**100**	**22.1**	**8**	**12**	**K.ADDCIGDAVTEK.L**	**99.7**	**3**	**2**
						R.ADLNVPLDGDLNITDDTR.I	99.7	1	1
						K.FLSPSVAGFLLQK.E	99.7	9	2
						K.GVEFVLPTDVIVADK.F	99.7	10	2
						K.IGVIESLLEK.C	99.7	16	2
						K.IILGGGMIFTFYK.A	99.7	3	2
						K.LAAPADLYVNDAFGTAHR.A	99.7	4	2
						R.LSELLGMAVEK.A	99.7	1	2
						R.LSELLGMAVEKADDCIGDAVTEK.L	99.7	1	2
						K.MSNGSVLLLENVR.F	99.7	1	1
						K.VLLTSHLGRPK.K	95.4	1	1
						K.VLPGVAALNEADVK.V	99.7	9	2
m.293516 Triosephosphate isomerase, cytosolic (Table S4.4)	**8**	**100**	**17.9**	**2**	**3**	**K.IVIAYEPVWAIGTGK.V**	**99.7**	**5**	**2**
						K.NCGDLAGCPDIDGFLVGGASLKPEFVDIIK.S	99.7	2	2
						K.WLADNVSAEVAAATR.I	99.7	2	3
m.419980 Glyceraldehyde-3-phosphate dehydrogenase, cytosolic (Table S4.4)	**22**	**100**	**49.5**	**10**	**11**	**K.AGIQLSDTFVK.L**	**99.7**	**20**	**4**
						K.EGLMTTVHATTATQK.T	99.7	13	4
						R.FKGEVSHTADSLVVNGK.A	99.7	10	2
						R.GAAQNIIPSSTGAAK.A	99.7	20	2
						K.GVMGFTDEDVVSADFIGDKR.S	99.6	7	2
						K.KVIISAPSK.D	99.7	11	2
						K.MNPEEIPWGEVGADFVCESTGVFTEVGK.A	99.7	1	1
						K.TMDVVSNASCTTNCLAPLAK.V	99.7	6	4
						R.VPTLDVSVVDLTVNLNKPAK.Y	99.7	2	2
						K.VVDDSFGIK.E	99.7	19	2
						K.YADIMSALK.A	99.7	6	3
m.227839 2,3-bisphospho-glycerate-independent phospho-glycerate mutase (Table S4.4)	**12**	**100**	**8.1**	**3**	**4**	**R.FIVTSDHGNADDMAQR.N**	**97.7**	**1**	**1**
						K.FVEELEALLK.E	99.7	4	2
						K.IPKPQGPLLVCVLDGFGENK.I	99.7	11	2
						R.TFVCSETQK.F	99.6	1	1

m.16672 Enolase (Table S4.4)	**21**	**100**	**30.3**	**11**	**12**	**K.APSSIVAVK.A**	**99.6**	**1**	**1**
						K.AVQNVNDVIAPALVGMDPTQQEEIDRK.M	99.7	12	4
						K.GLAQIVGDDLLCTNPTR.V	99.7	11	4
						R.GNPTVEAEVK.T	99.7	5	2
						R.HIADLAGNTK.V	99.7	20	2
						K.IAMDCAASEFYGEDGKYDLAFK.S	99.7	4	2
						R.IEEELGEDAVYAGDNYR.H	99.7	15	2
						R.SGETEDSFIADLAVGLCTGQIK.T	99.7	1	2
						K.SKAPSSIVAVK.A	99.7	4	2
						K.SKPSEPFSFMAEVLK.S	99.7	8	4
						K.VNQIGSLTESIQAVK.M	99.7	16	4
						K.VVEDAINATIK.S	99.7	15	2
m.43324 Pyruvate kinase (Table S4.4)	**11**	**100**	**9.5**	**3**	**4**	**R.ASDSDTTDEILQAALEHAK.D**	**99.7**	**10**	**2**
						R.FNFSHGSHEYHQETLNNLR.A	99.7	3	1
						R.GLVPILAEGSAR.A	99.7	4	2
						R.KGSDLDTIR.Q	99.7	1	2
Acetyl-CoA synthesis proteins									
m.73526 Pyruvate dehydrogenase E1 component subunit aTable 4.1lpha, chloroplastic (Table 4.1)	**7**	**100**	**32.3**	**8**	**9**	**R.ATAPSSLGDNEPWIYK.K**	**99.7**	**7**	**2**
						R.EVAMEAVER.A	99.7	6	2
						R.FRGHSLADPDELR.R	99.7	6	2
						K.GFGIGPDGR.Y	99.7	5	2
						K.MFGFVHLYSGQEAVSTGVIK.A	99.7	6	4
						R.RGEGPTLIEAETYR.F	99.7	7	3
						K.VKEEVDDAVEFAENSPKPDMSQLLENVFADPK.G	99.7	7	3
						K.YMVANGLATESDVQAIEAK.V	99.7	1	1
						R.YRYEQPGFTAGTAEVS.-	99.7	7	2
m.396299 ATP-citrate synthase alpha chain protein (Table 4.1)	**22**	**100**	**12.5**	**4**		**K.KWGDVEFPLPFGR.T**	**99.7**	**1**	**1**
						R.LAGLQLPIAVAQVK.E	99.7	7	2
						R.LAPLLSTLPLELR.G	99.7	20	3
						K.LGYAEAQQFIEAR.M	99.7	8	2
						R.SVSIPTGAEPTSDR.L	99.7	10	2
						R.TLLDAATAHADGR.G	99.6	4	1
						K.VVDMDGTVGR.I	99.7	4	2
Lipid metabolism proteins									
gi|3023244 Acetyl-CoA carboxylase carboxyl transferase subunit beta, chloroplastic (Table 4.1)	**11**	**100**	**5.1**	**2**	**2**	**K.QALSETLTLYK.E**	**99.7**	**11**	**2**
						M.SILSWIENQR.K	99.7	3	2

m.332618 3-hydroxyacyl-ACP dehydratase, chloroplastic (Table 4.1)	**4**	**100**	**24.5**	**4**	**5**	**K.AAEVEAAASGIETK.G** K.ALKDIEEIMTILPHR.Y K.DAAQQNNFFFGGVDNCR.W K.LVSMNEQFFTGHFPQR.A R.YPFLLVDR.V	**99.7** 99.7 99.7 99.7 99	**1** 3 3 1 2	**1** 2 2 1 1
m.179214 Enoyl-ACP reductase [NADH], chloroplastic (Table 4.1)	**4**	**100**	**7.6**	**2**	**3**	**K.AFIAGVADDQGFGWAIAK.C** R.VIPGYGGGMSSAK.A R.YSYENAPVKK.E	**99.7** 98.1 99.7	**1** 1 4	**1** 1 2
m.84123 Beta-ketoacyl-CoA reductase (Table 4.1)	**9**	**100**	**16.8**	**4**	**5**	**K.AFVDTFSR.S** K.EAEAAAAAGGAEEVPPPSETKR.E R.ETSFTPYWFHGIQEAFVTSAPVWLINR.Q R.LDAPTPETWAAAAVR.Q R.QVMSIHQGLR.S	**99** 99.7 99.4 99.7 95.9	**6** 1 2 6 1	**3** 2 2 2 1
m.149328 Acetyl-CoA acetyltransferase (Table 4.1)	**3**	**100**	**8.9**	**2**	**2**	**K.SHLDHARPAQQQEQQQEQR.Q** R.TPLGSFQGGLSHLSATELGAAAIR.A	**96.6** 99.7	**1** 3	**1** 2
m.357823 1-Acyl-sn-glycerol-3-phosphate acyltransferase, chloroplastic (Table 4.1)	**4**	**100**	**15.3**	**3**	**3**	**K.AKVPVVPITLIGTGDLMPNTQEYLLFPGK.V** K.TSNFLIPIIGWSMFLTGHVMINR.L K.VPVVPITLIGTGDLMPNTQEYLLFPGK.V	**99.7** 99.6 99.7	**3** 1 4	**2** 1 3
m.250190 Acyltransferase family protein (Table 4.1)	**4**	**100**	**10**	**2**	**3**	**R.AAGYLPLNDPLTR.G** R.IKPAGTYVASR.V R.LVMTEGVDDEGKPLDTPPQPAGSAALPALALLGITLAR.A	**95.5** 99.2 99.7	**1** 1 4	**1** 2 3
m.34057 Phosphatidyl-inositol 4-kinase alpha (Table 4.1)	**11**	**100**	**5.2**	**5**	**8**	**R.AAASLEAVLPLALFLSK.S** R.ALVALLGSEAAALASK.A R.DVLQALFEAAHQEESEGPDGAAHQR.L R.LLAFLLHELPALQYK.R R.LVVLDAGEAAVQNIPEAAPLLATPAAAK.A R.MLALAGGDEDLAHLVVPLLR.D R.QALLVMLLSAEVER.L R.SHADLTTTFVPLTASALERPESVPTLGR.M	**99.7** 99.7 99.7 97.5 99.7 99.7 99.7 99.7	**9** 2 1 1 2 4 1 1	**2** 2 1 1 1 2 2 1

m.226782 Sac1p-like phosphoinositide phosphatase (Table 4.1)	**23**	**100**	**17.9**	**8**	**12**	**R.DNAGTVAEQHGVFR.T**	**99.7**	**6**	**2**
						R.GSIPLLWSQTPCLK.Y	99.7	3	2
						K.GYSDVFGVLGLAR.L	99.7	12	2
						R.LEAGPALVVVTAVEEAAR.L	99.7	21	12
						K.LSAAYAEAAAGLGASGAGGSTDGTSHAGNTVSFR.L	99.7	2	1
						R.LSVLWGAISNDIHR.F	99.7	10	2
						R.NQTVFESHAR.S	98.2	1	1
						R.SLAQGYQEVVAINLANQTGR.E	99.7	1	1
						R.TNVVQGMLGR.R	96.9	1	1
						R.VAATEVLADTR.N	99.7	20	2
						K.VDKGYSDVFGVLGLAR.L	99.7	7	2
						R.YYLNNFEDGSKQDAIDLVTGAYVVAPGKPAPFHPR.G	99.7	2	1
gi|132270 Rubber elongation factor protein (Table 4.1)	**10**	**100**	**31.9**	**4**	**4**	**K.DASIQVVSAIR.A**	**99.7**	**10**	**2**
						K.DKSGPLQPGVDIIEGPVK.N	99.7	2	2
						K.FVDSTVVASVTIIDR.S	99.7	2	2
						K.SGPLQPGVDIIEGPVK.N	95.4	2	1
m.116135 Phospholipid-transporting ATPase (Table 4.1)	**12**	**100**	**3.8**	**3**	**3**	**K.LKDTAAAAADELLETYLR.R**	**99.7**	**12**	**2**
						K.LQEGVPAAIQTLLDANIR.V	99.7	4	2
						R.NSNLNEDLGKIEYIFSDK.T	99.7	7	2
m.419400 Putative triacylglycerol lipase (Table 4.1)	**6**	**100**	**10.1**	**3**	**3**	**K.DVIPIIPQDSK.N**	**99.7**	**6**	**2**
						R.LLCSAAKPGLYDPPACCMYR.M	99.7	1	2
						K.MGATGTSLVYVPK.I	99.7	2	2
m.225854 Acyl-CoA oxidase_A, peroxisomal (Table 4.1)	**2**	**100**	**7.2**	**3**	**3**	**R.ECCGGHGYAAVNR.L**	**99.7**	**2**	**2**
						R.GVAVPLVDAFAIPDHILR.A	99.6	2	2
						R.TKDEVLVADVHSLSAGLK.A	99.7	1	1
m.420224 Fatty acid beta-oxidation multifunctional protein, peroxisomal (Table 4.1)	**8**	**100**	**17.3**	**7**	**8**	**R.AALELGLVDAVVPPEQLLQAAK.R**	**99.7**	**1**	**2**
						R.ASPDPDLVPLVQQSR.K	99.7	1	1
						R.HLLHPLLCLDAIQYGIEHGGR.A	99.7	1	1
						R.ILGAHFFSPAHVMPLLEIVR.T	99.7	3	1
						R.IQSNLTSR.V	94.7	1	1
						K.MSDQDIAEFIFFPVVNEGSR.V	99.7	4	2
						R.TDKLEALGEALAILQFAR.A	99.7	8	2
						R.VCTPGTSFGLPELQLGIIPGFGGTQR.L	96.6	1	1

m.356362 2,4-dienoyl-CoA reductase, peroxisomal (Table 4.1)	**17**	**100**	**9.2**	**2**	**4**	**R.AVGLAGAGSSSGSGSTPR.S**	**99.7**	**1**	**2**
						K.LAPGSDGAAAVQK.L	99.7	17	2
						R.SLGLEWGHYGIR.T	99.7	2	2
						R.TAGVAPGPIEGTAGMTK.L	97.9	1	1

[a] Number of FFZE fractions, from a total of 23, where the corresponding protein was identified.

[b] Best/maximum value attained within the FFZE membrane fractions where the protein was identified.

[c] Maximum number of exclusive unique peptides (UP) with which the protein was identified in an individual FFZE fraction.

[d] Total number of UPs with which the protein was identified considering all the 23 analyzed FFZE fractions.

[e] Sequence of the UPs with which the protein was detected via LC-MS/MS within all the analyzed FFZE fractions. The amino acid residues appearing before and after the periods correspond to the residues proceeding and following the peptide in the protein sequence.

[f] Best % identification probability value with which the specific UP was identified within the FFZE fractions.

[g] Number of FFZE fractions in which the UP was identified.

[f] Maximum number of spectra with which the corresponding peptide was detected in an individual FFZE fraction.

APPENDIX B.

Supplemental material from Chapter 5

B.1. Supplemental figures

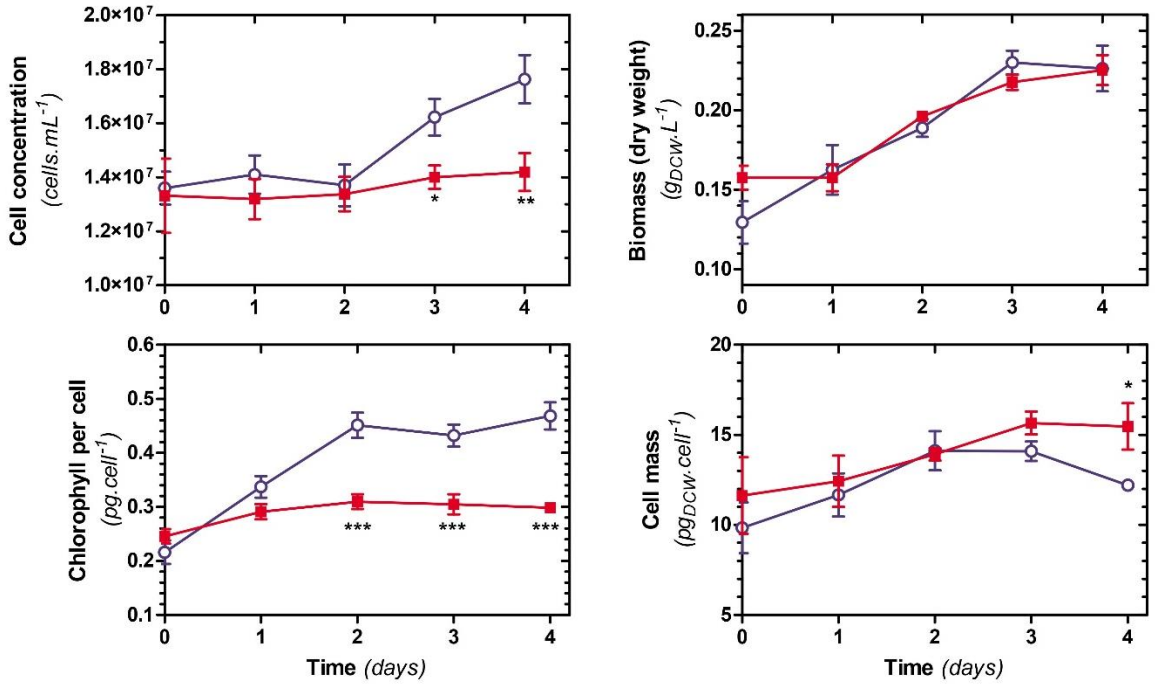

Figure S5.1. Kinetic growth of N-deprived and N-sufficient *E. oleoabundans*. Microalgal growth under N-deprivation (red squares) or N-sufficiency (blue circles) during 4 d. Data are mean ± SEM of at least four biological replicates per tested condition. Statistical analyses were performed per each time point through unpaired two-tailed Student's *t*-tests. Statistically significant changes are indicated with asterisks: *p*-value < 0.05, *; < 0.01, **; < 0.001, ***.

Plus N
Minus N
Plus N
Minus N
0-h
1-h
3-h
6-h
9-h
0-h
1-h
3-h
6-h
9-h
12-h
24-h
48-h
72-h
96-h
12-h
24-h
48-h
72-h
96-h

B-2

Figure S5.2. LD formation time-course analysis. Representative z-stack-merged CFM images for those acquired in each analyzed time point (0 to 96-h) under N sufficiency (plus N) and N deprivation (minus N). Green: neutral lipids (NR, λ Exc/Em 488/520 nm); red: chloroplasts (chlorophyll, λ Exc/Em 635/668 nm). Scale = 5 µm.

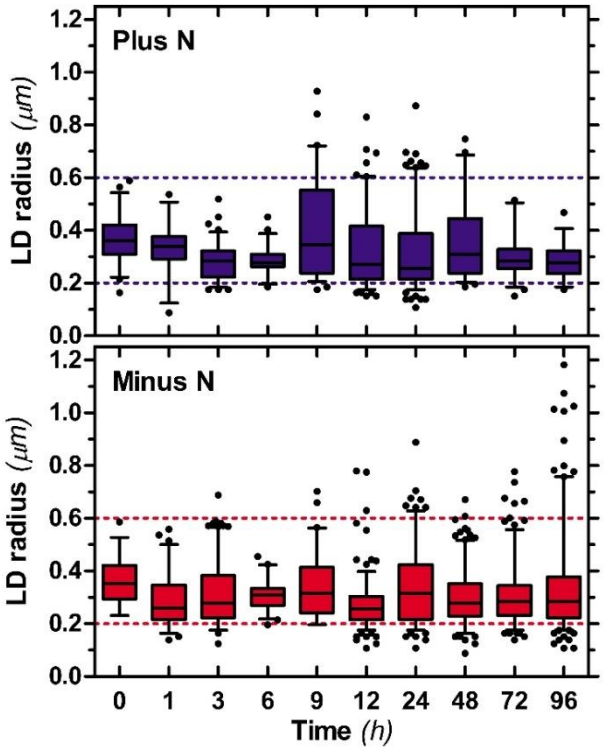

Figure S5.3. LD size distribution. LD size (radius) was quantified through CFM image analysis. From 0 to 96-h, n = 48, 51, 85, 75, 62, 121, 187, 54, 59, 61, and n = 30, 70, 167, 47, 72, 198, 156, 214, 193, 201, for N-sufficient (plus N) and N-deprived (minus N) conditions, respectively. Box plots are as described in Fig. 5.1. Dashed lines indicate the three categories in which LD were classified: small, r<0.2 µm; medium, 0.2≤r≤0.6 µm; and, large, r>0.6 µm.

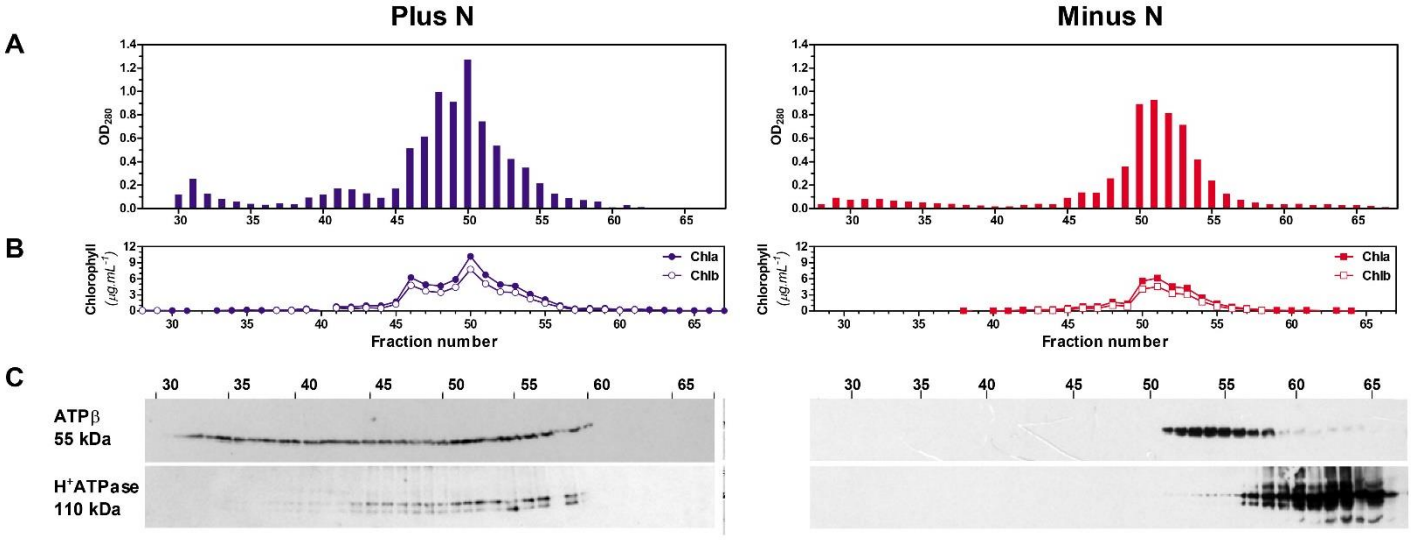

Figure S5.4. Electrophoretic membrane properties analyzed via FFZE. Microsomal membranes from 4-d N-sufficient (plus N) and N-deprived (minus N) cultures were separated by FFZE. (A) Protein profiles of FFZE fractions. OD_{280}, optical density at 280 nm. (B) Chlorophyll *a* and *b* concentrations in FFZE fractions. (C) Immunological detection in the respective fractions of ATPβ (chloroplast marker) and H^+ATPase (plasma membrane marker). Ten percent (w/v) SDS-PAGE acrylamide gels loaded with 15 µg of protein per lane. Figure modified from Garibay-Hernández et al., 2017.

A

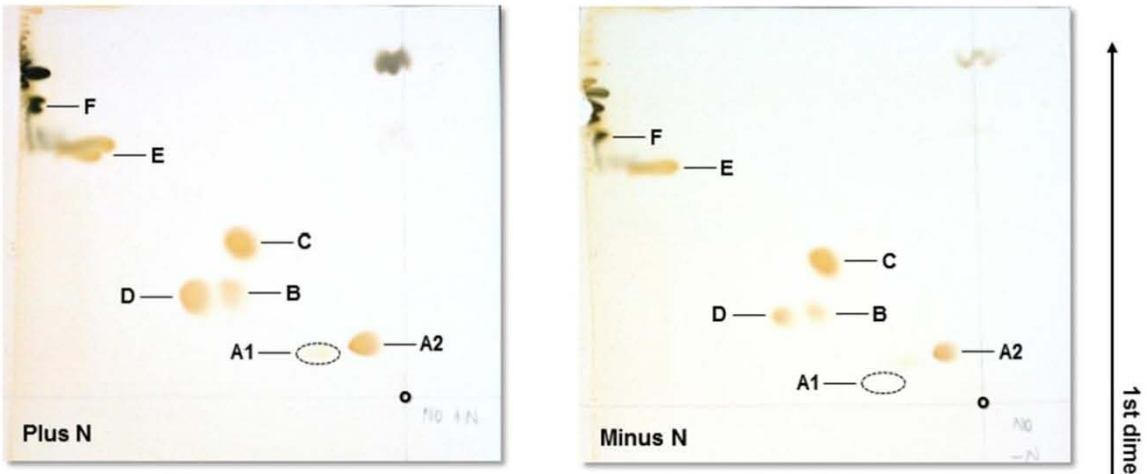

B

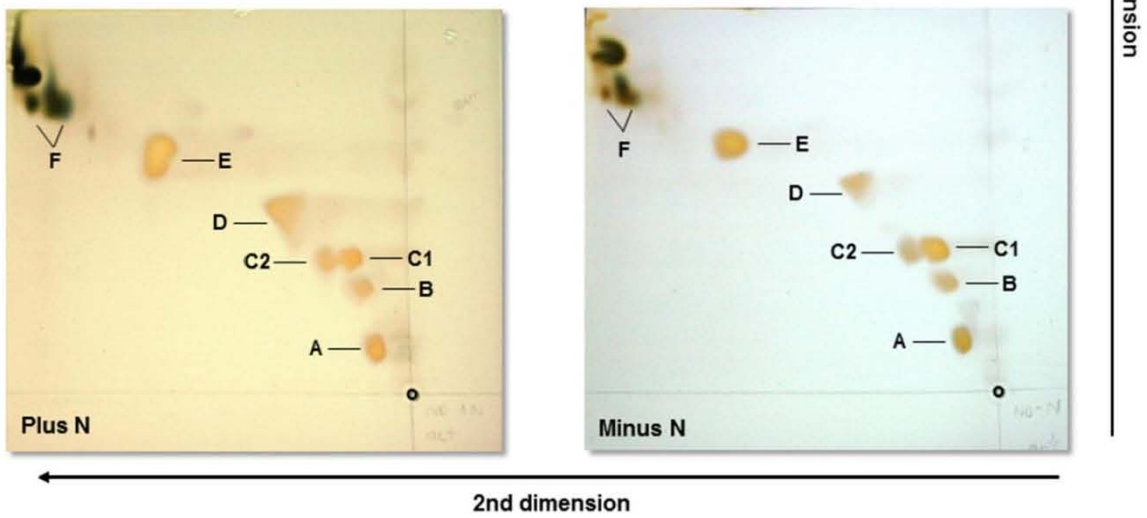

C

Label	Lipid	Ninhydrin	Dragendorff	α-naftol	References
A	PS + PC	+	+	-	Benning et al., 1995
A1	PS	+	-	-	Vences-Guzmán et al., 2008
A2	PC	-	+	-	Vences-Guzmán et al., 2008
B	SQDG	-	-	+	Benning et al., 1995; Vences-Guzmán et al., 2008
C	PE + DGDG + U	+	+	+	NA
C1	DGDG + U	-	+	+	Benning et al., 1995
C2	PE	+	-	-	Benning et al., 1995; Vences-Guzmán et al., 2008
D	PG	-	-	-	Vences-Guzmán et al., 2008
E	MGDG	-	-	+	Benning et al., 1995
F	UG	-	-	+	NA

Figure S5.5. 2D-TLC separation of polar lipids. (A) 2D-TLC based on Vences-Guzmán et al., 2008. (B) 2D-TLC based on Benning et al., 1995. (C) Lipid spot identification based on specific staining of lipids for functional groups and relative lipid mobilities reported on reference TLC systems. NA, not available; U, unknown lipid; UG, unknown glycolipid.

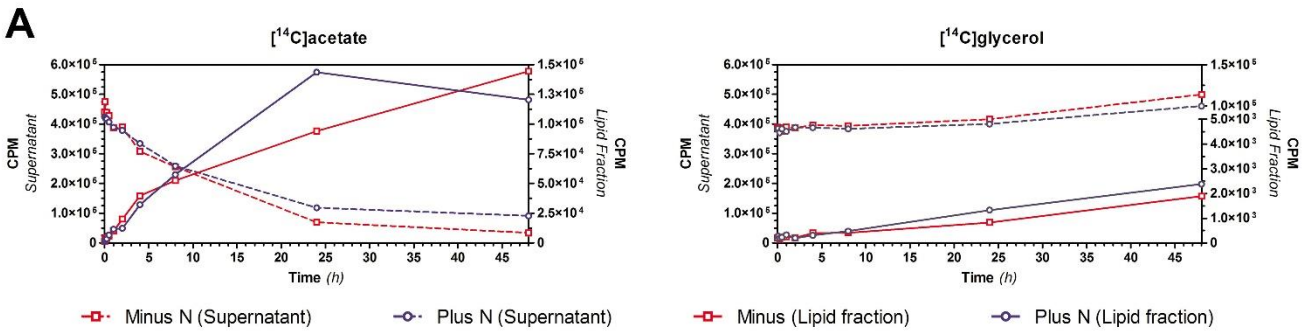

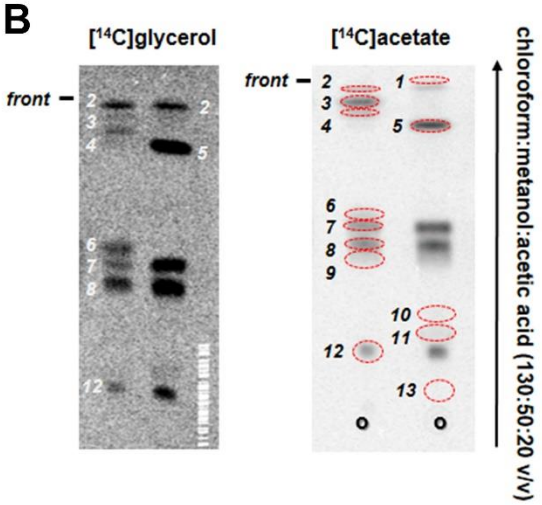

Label	Lipid	Ninhydrin	α-naftol	References
1	UG	-	+	2D-TLC (Suppl Fig. 8)
2	Unknown	-	-	NA
3	UG	-	+	2D-TLC (Suppl Fig. 8)
4	Unknown	-	-	NA
5	MGDG	-	+	2D-TLC (Suppl Fig. 8)
6	Unknown	-	-	NA
7	PG	-	-	Sahonero-Canavesi et al., 2015; 2D-TLC (Suppl Fig. 8)
8	PE + DGDG	+	+	Sahonero-Canavesi et al., 2015; 2D-TLC (Suppl Fig. 8)
9	MMPE	-	-	Sahonero-Canavesi et al., 2015
10	Unknown	-	-	NA
11	PS	+	-	2D-TLC (Suppl Fig. 8)
12	PC	-	-	Sahonero-Canavesi et al., 2015; 2D-TLC (Suppl Fig. 8)
13	Unknown	-	-	NA

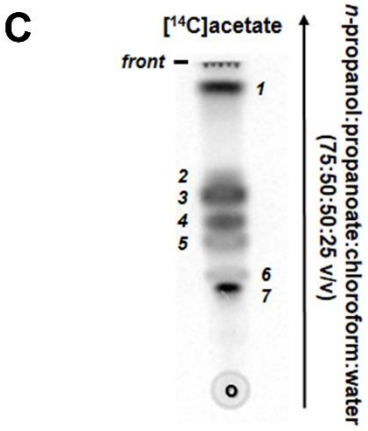

Label	Lipid	Ninhydrin	α-naftol	Standard	References
1	Unknown	-	-	NA	NA
2	PG	-	-	NA	de Rudder et al., 1999
3	PE	+	-	+	de Rudder et al., 1999
4	MMPE	-	-	+	de Rudder et al., 1999
5	DMPE	-	-	+	de Rudder et al., 1999
6	PS?	+	-	NA	NA
7	PC	-	-	+	de Rudder et al., 1999

Figure S5.6. Radioactive labeling of *E. oleoabundans* lipids. (A) Time course incorporation of label from [^{14}C]acetate and [^{14}C]glycerol into the lipid fraction under N sufficiency (plus N) and N deprivation (minus N). The amount of incorporated radioactivity (CPM, counts per minute) is expressed in terms of its decrease in the culture supernatant and its increase in the lipid fraction. (B, C) 1D-TLC separation of either [^{14}C]acetate- or [^{14}C]glycerol-labelled total lipid extracts. Lipid spot identification was based on specific staining of lipids for functional groups and relative lipid mobilities, either reported on reference TLC systems, and/or confirmed with commercial standards when available. NA, not available; UG, unknown glycolipid. (B) 1D-TLC separation at two different time points of major polar lipids based on Sahonero-Canavesi et al. (2015). This dimension corresponds to the 2D of the TLC system described in Fig. S5.5A. (C) 1D-TLC separation of PE *N*-methylated derivatives based on de Rudder et al. (1997).

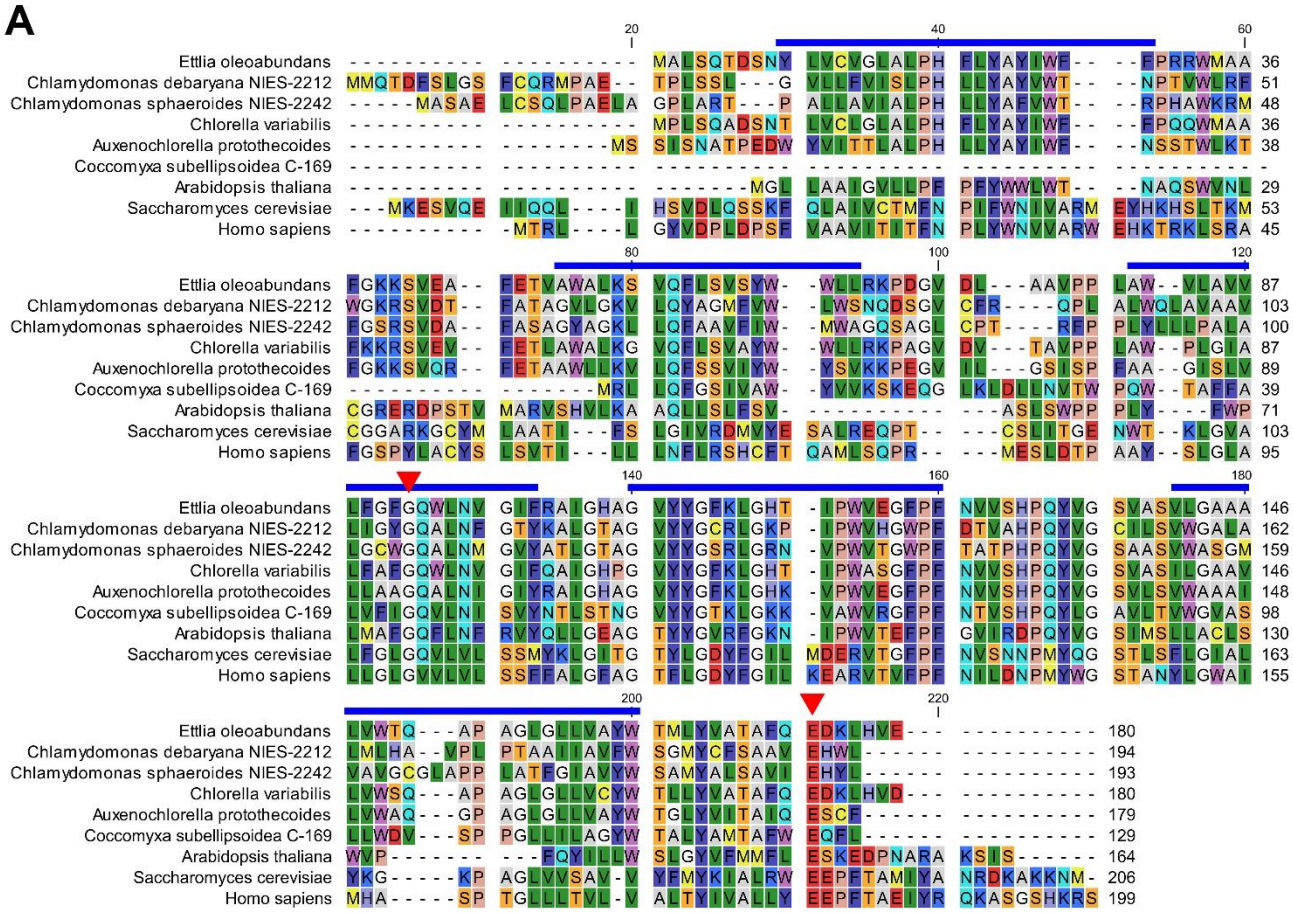

B

	1	2	3	4	5	6	7	8	9
Ettlia oleoabundans	1		34.16	32.34	83.33	61.54	28.96	27.23	18.52	22.49
Chlamydomonas debaryana NIES-2212	2	69		47.98	31.19	34.83	22.73	23.58	15.49	13.66
Chlamydomonas sphaeroides NIES-2242	3	65	95		30.85	33.84	23.86	24.17	16.81	16.89
Chlorella variabilis	4	150	63	62		56.04	28.42	27.23	17.13	20.57
Auxenochlorella protothecoides	5	112	70	67	102		32.42	24.87	16.59	18.57
Coccomyxa subellipsoidea C-169	6	53	45	47	52	59		17.84	15.35	15.38
Arabidopsis thaliana	7	52	50	51	52	48	33		18.10	17.24
Saccharomyces cerevisiae	8	40	35	38	37	36	33	38		40.10
Homo sapiens	9	47	31	38	43	39	32	35	83	

Figure S5.7. *E. oleoabundans* phospholipid methyltransferase. (A) Sequence alignment of the predicted *Eo*PLMT (m.314600) and its homologs. Full-length amino acid sequences were aligned with Clustal Omega. Amino acids are colored according to the RasMol color scheme. The predicted *Eo*PLMT transmembrane domains (TMHMM v.2.0, blue lines) and conserved amino acids corresponding to the human PLMT SAM-binding residues (red triangles) are indicated. Homolog selection was based on Hirashima et al. (2018). The corresponding NCBI accession numbers are: *Chlamydomonas debaryana* NIES-2212: BBC28426.1; *Chlamydomonas sphaeroides* NIES-2242: BBC28426.1; *Chlorella variabilis*: XP_005851476.1; *Auxenochlorella protothecoides*: XP_011400892.1; *Coccomyxa subellipsoidea* C-169: XP_005647515.1; *Arabidopsis thaliana*: NP_565246.1; *Saccharomyces cerevisiae*: NP_012607.1; *Homo sapiens*: NP_680478.1. (B) Pairwise comparison among PLMT homologs listed in (A) shows the percentage identity (upper right values) and number of identical residues (bottom left values

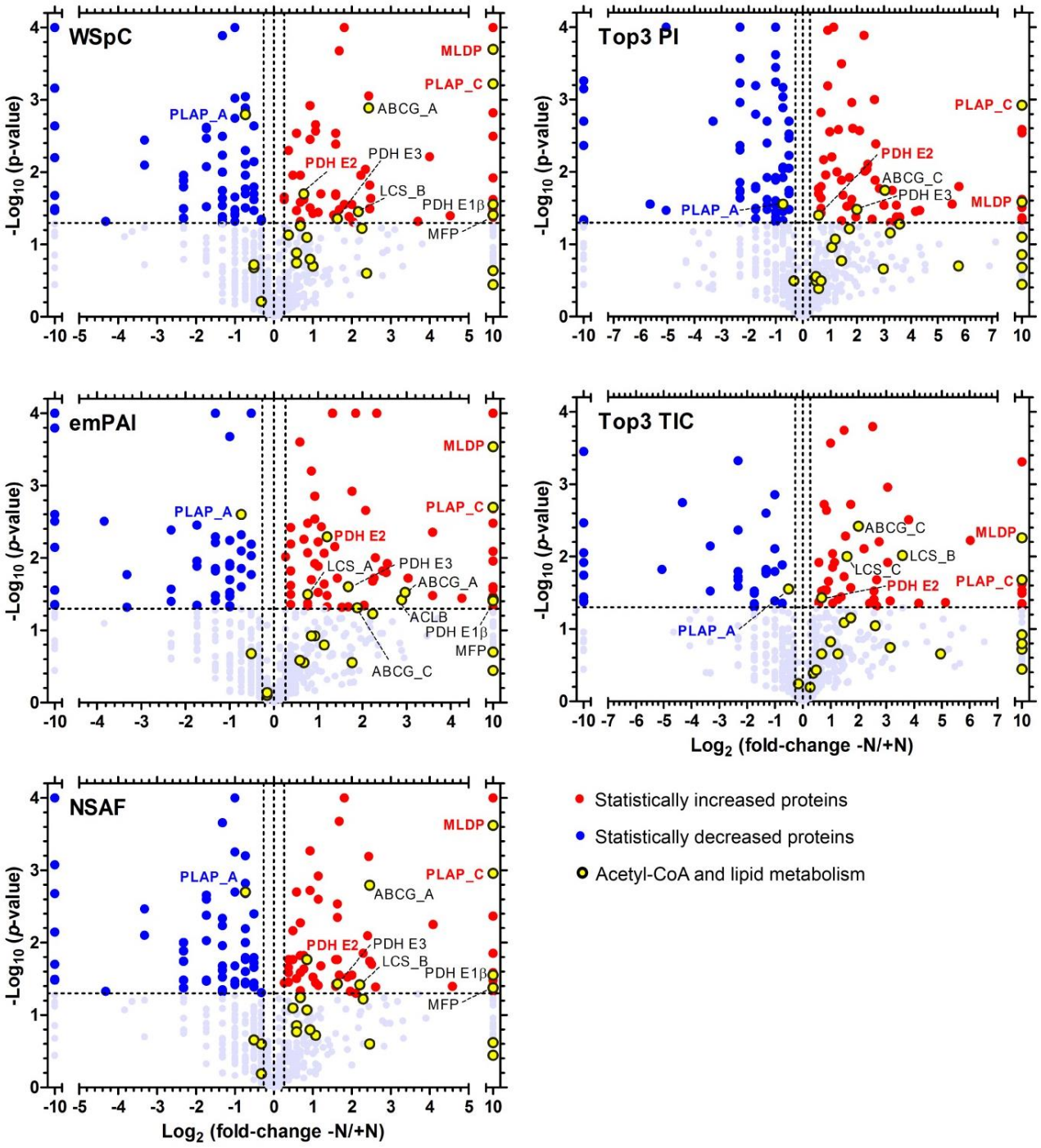

Figure S5.8. Quantification of N depletion-responsive membrane proteins through different label-free approaches. Volcano plots of the 619 proteins identified in *E. oleoabundans* membranes. A volcano plot is provided per each label-free quantification method. Negative $\log_{10}$ of *t*-test *p*-values were plotted against $\log_2$ of the FC between N deprivation and N sufficiency; red: FC ≥ 1.2; *p*-value ≤ 0.05; blue: FC ≤ 0.83; *p*-value ≤ 0.05. Acetyl-CoA and lipid metabolism proteins are indicated (yellow) together with their abbreviations (described in Fig. 5.7); labels of proteins comprised within the core proteins are highlighted (red, increased; blue, decreased)

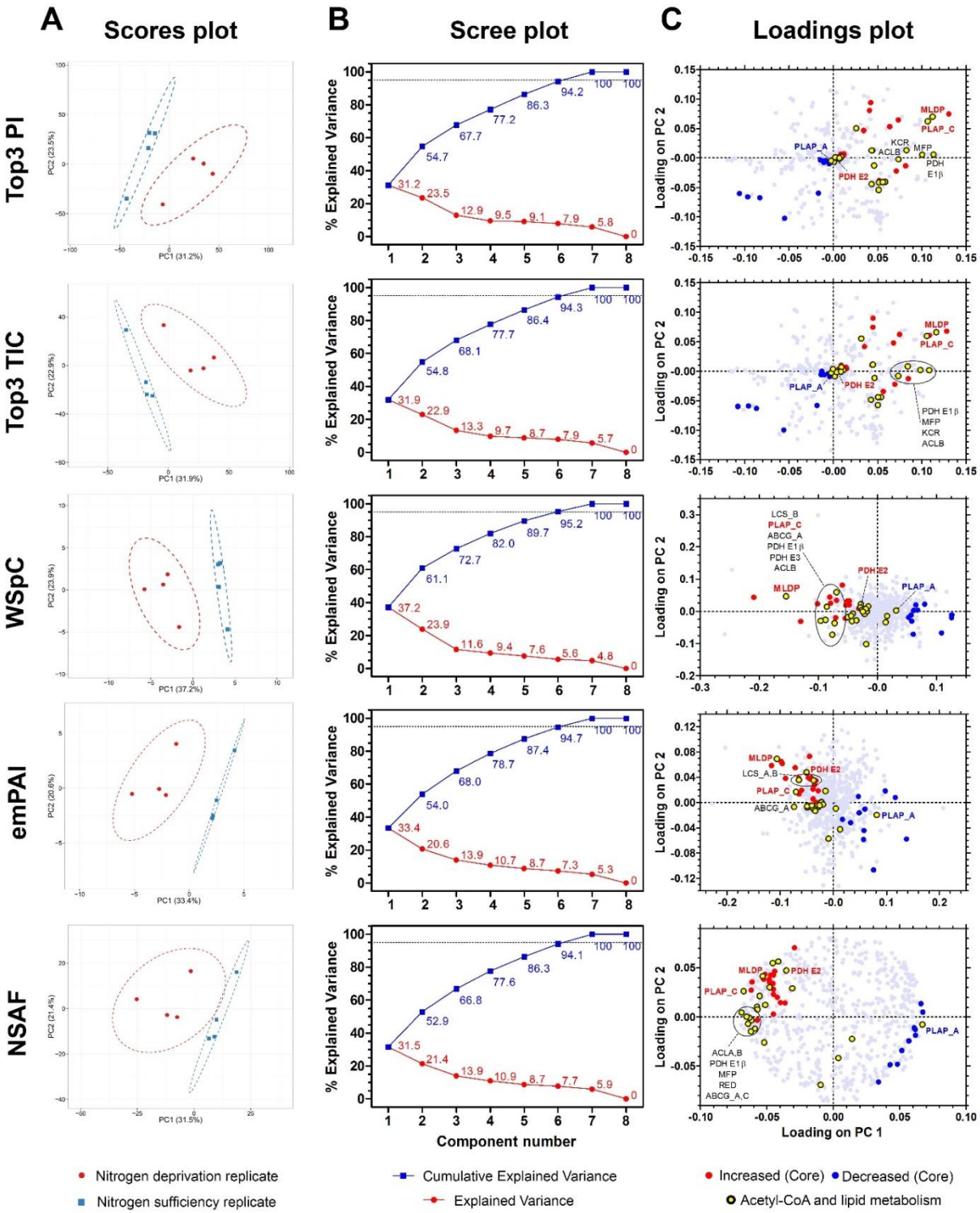

Figure S5.9. PCA of membrane proteomics data analyzed through different label-free quantitation approaches. The dataset corresponding to each label-free method was individually submitted to PCA as indicated in Materials and methods. Plots describing the outputs from each of these analyses are shown. (A) PCA scores plots. Points represent each of the biological replicates (N = 8). The X and Y coordinates represent PC1 and PC2, respectively. Prediction ellipses are such that with probability of 0.95 a new observation from the same group will fall inside the ellipse. (B) PCA scree plots representing the proportion of variance explained by each principal component (red) and the corresponding cumulative variance values (blue). Dashed lines indicate 95% of total variance explained. (C) PCA loadings plots (as described in Fig. 5.7D).

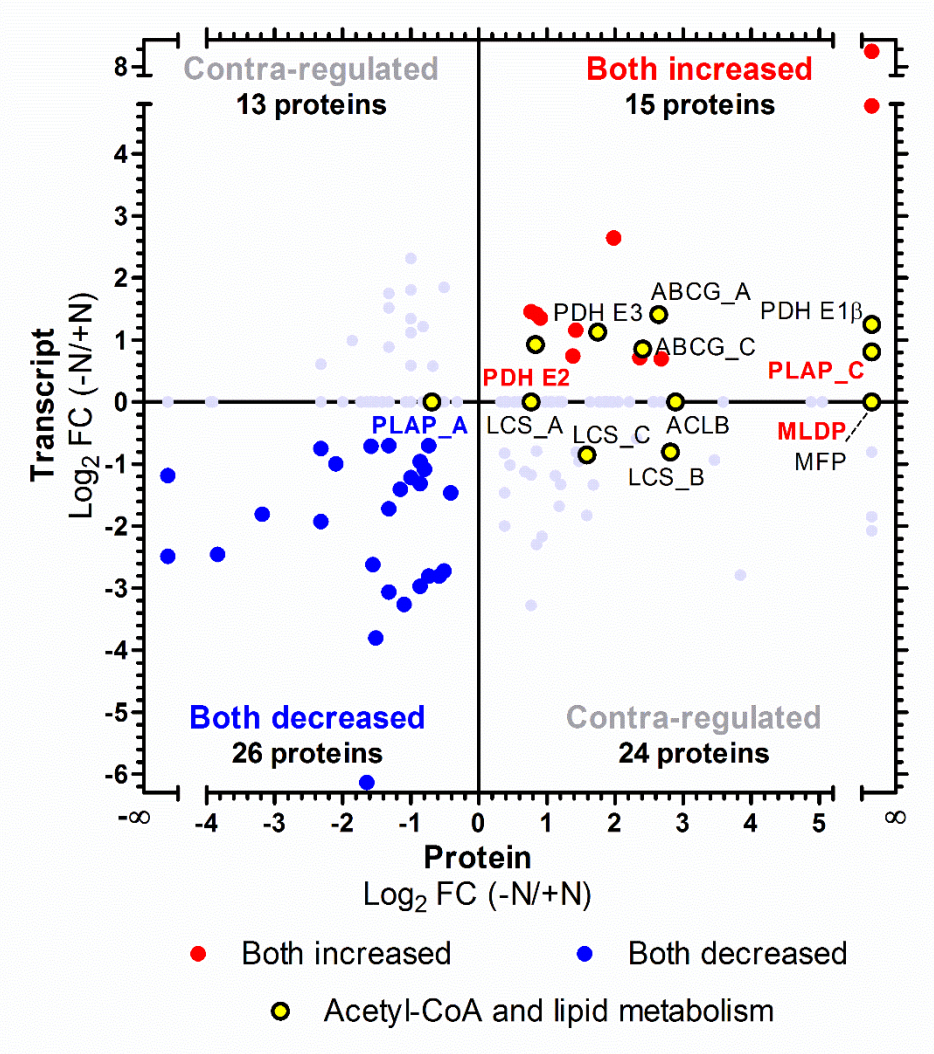

Figure S5.10. Transcriptional regulation of N depletion-responsive membrane proteins. Transcripts corresponding to each of the 157 responsive membrane proteins retrieved, together with their expression values following N deprivation, from Rismani-Yazdi et al. (2010). Both, protein and transcript $\log_2$ FC are plotted; FC: N deprivation (-N) relative to N sufficiency (+N). A $\log_2$ value of zero was considered for non-statistically significant transcript FC values (Benjamini and Hochberg adusted *p*-value: *q*-value > 0.05). Red: protein and transcript levels are statistically increased; blue: protein and transcript levels are statistically decreased; grey: protein levels are changed contrary to their corresponding transcript levels.

B.2. Supplemental tables

Table S5.1. Profiling of *E. oleoabundans* glycerolipid molecular species via ESI-TQ-MS/MS.

Intact ion masses (*m/z* values), sum formulas, and predicted glycerolipid identities are indicated. Values are in nmoles per mg of lipid dry weight, except for SQDG, DAG, and TAG species, whose amounts are expressed as normalized signal per mg of lipid dry weight. Average and standard deviation (SD) values are representative of five biological replicates. Fold-change (N deprivation –minus N- relative to N sufficiency –plus N-) and Student's *t*-test *p*-values are provided. When detection was exclusive to one condition, *p*-values were calculated considering a minimum of 0.001 for one of the replicates, whereas the remaining four were handled with a value of zero. The percentages comprised by every molecular species relative to the total of the corresponding glycerolipid class are also indicated for both tested conditions. The precursor and neutral loss scan modes specific for the identification of different glycerolipid classes are described, as well as the internal standards used in this work.

Lipid Abbreviations

lysoPG	lysophosphatidylglycerol
PG	phosphatidylglycerol
lysoPE	lysophosphatidylethanolamine
PE	phosphatidylethanolamine
lysoPC	lysophosphatidylcholine
PC	phosphatidylcholine
PA	phosphatidic acid
PI	phosphatidylinositol
PS	phosphatidylserine
DGDG	digalactosyldiacylglycerol
MGDG	monogalactosyldiacylglycerol
DAG	diacylglycerol
TAG	triacylglycerol

Prec	precursor
NL	neutral loss

Parameters for Glycerolipid Analysis

Glycerolipid class	Polarity	Precursor ion	Scan Mode
PC, LysoPC	Positive	$[M+H]^+$	+Prec184
PE, LysoPE	Positive	$[M+H]^+$	+NL141
PS	Positive	$[M+NH_4]^+$	+NL185
PI	Positive	$[M+NH_4]^+$	+NL277
PG	Positive	$[M+NH_4]^+$	+NL189
LysoPG	Negative	$[M-H]^-$	-Prec153
PA	Positive	$[M+NH_4]^+$	+NL115
MGDG	Positive	$[M+NH_4]^+$	+NL179
DGDG	Positive	$[M+NH_4]^+$	+NL341
SQDG	Negative	$[M-H]^-$	-Prec225

Lipid Internal Standards

Phospholipids	ion mass	used to quantify	Scan Mode
lysoPG 14:0	455.3	LysoPG	-Prec153
lysoPG 18:0	511.3	LysoPG	-Prec153
Not available		SQDG	-Prec225
di 14:0 PG	684.5	PG	+NL189
di Phy (20:0)PG	852.7	PG	+NL189
lysoPE 14:0	426.3	LysoPE	+NL141
lysoPE 18:0	482.3	LysoPE	+NL141
di 12:0 PE	580.5	PE	+NL141
di 23:0 PE	888.9	PE	+NL141
lysoPC 13:0	454.3	LysoPC	+Prec184
lysoPC 19:0	538.3	LysoPC	+Prec184
di 12:0 PC	622.4	PC	+Prec184
di 24:1 PC	954.9	PC	+Prec184
lysoPA 14:0	400.3	LysoPA	+NL115
lysoPA 18:0	456.3	LysoPA	+NL115
di14:0 PA	610.5	PA	+NL115
di Phy (20:0)PA	778.7	PA	+NL115
di 14:0 PS	680.6	PS	+NL185
di Phy PS	848.8	PS	+NL185
PI 16:0-18:0	856.70	PI	+NL277
PI di 18:0	884.7	PI	+NL277

Galactolipids	ion mass	used to quantify	Scan Mode
DGDG 34:0	938.6	DGDG	+NL341
DGDG 36:0	966.6	DGDG	+NL341
MGDG 34:0	776.5	MGDG	+NL179
MGDG 36:0	804.5	MGDG	+NL179

Neutral Glycerolipids	used to quantify
DAG 15:0	DAG
TAG 17:1	TAG

			Plus N *(nmol per mg dry lipid wt)*		Minus N *(nmol per mg dry lipid wt)*				Plus N *(% of class)*		Minus N *(% of class)*	
Ion Mass *(m/z)*	**Compound Formula**	**Compound Name**	**Average** *(n=5)*	**SD**	**Average** *(n=5)*	**SD**	**Fold-change (Minus/Plus N)**	***t-test* *p*-value**	**Average** *(n=5)*	**SD**	**Average** *(n=5)*	**SD**
898.5	C47H76O15	**DGDG(32:6)**	**0.565**	0.059	**0.234**	0.057	**0.413**	0.0001	**1.660**	0.174	**0.360**	0.058
900.5	C47H78O15	**DGDG(32:5)**	**1.520**	0.151	**1.318**	0.329	**0.867**	0.248	**4.476**	0.572	**2.034**	0.323
902.6	C47H80O15	**DGDG(32:4)**	**0.285**	0.044	**0.429**	0.087	**1.508**	0.0105	**0.829**	0.059	**0.666**	0.090
904.6	C47H82O15	**DGDG(32:3)**	**0.516**	0.020	**0.608**	0.129	**1.179**	0.1528	**1.523**	0.192	**0.941**	0.097
918.6	C48H84O15	**DGDG(33:3)**	**0.404**	0.078	**0.679**	0.127	**1.683**	0.0033	**1.171**	0.142	**1.052**	0.076
926.6	C49H80O15	**DGDG(34:6)**	**14.206**	1.788	**16.124**	1.954	**1.135**	0.1439	**41.453**	1.097	**25.152**	0.861
928.6	C49H82O15	**DGDG(34:5)**	**3.707**	0.447	**7.078**	0.855	**1.909**	0.0001	**10.819**	0.153	**11.066**	0.911
930.6	C49H84O15	**DGDG(34:4)**	**1.754**	0.254	**5.782**	0.683	**3.296**	0.0001	**5.118**	0.439	**9.058**	0.973
932.6	C49H86O15	**DGDG(34:3)**	**1.346**	0.164	**2.689**	0.353	**1.998**	0.0001	**3.943**	0.374	**4.210**	0.492
934.6	C49H88O15	**DGDG(34:2)**	**0.881**	0.099	**2.788**	0.437	**3.164**	0.0001	**2.575**	0.078	**4.343**	0.393
936.6	C49H90O15	**DGDG(34:1)**	**0.716**	0.032	**3.377**	0.590	**4.719**	0.0001	**2.107**	0.215	**5.264**	0.695
954.6	C51H84O15	**DGDG(36:6)**	**4.572**	0.760	**7.745**	1.093	**1.694**	0.0007	**13.282**	0.655	**12.054**	0.278
956.6	C51H86O15	**DGDG(36:5)**	**2.977**	0.548	**10.309**	2.758	**3.463**	0.0004	**8.631**	0.691	**15.844**	2.188
958.6	C51H88O15	**DGDG(36:4)**	**0.757**	0.152	**4.594**	1.404	**6.069**	0.0003	**2.197**	0.308	**7.035**	1.161
960.6	C51H90O15	**DGDG(36:3)**	**0.033**	0.008	**0.485**	0.170	**14.578**	0.0003	**0.099**	0.031	**0.739**	0.149
962.6	C51H92O15	**DGDG(36:2)**	**0.003**	0.002	**0.031**	0.018	**8.879**	0.0094	**0.010**	0.004	**0.047**	0.020
964.7	C51H94O15	**DGDG(36:1)**	**0.002**	0.003	**0.017**	0.013	**7.165**	0.0386	**0.006**	0.008	**0.025**	0.015
982.6	C53H88O15	**DGDG(38:6)**	**0.019**	0.018	**0.029**	0.011	**1.570**	0.2889	**0.053**	0.047	**0.046**	0.018
984.6	C53H90O15	**DGDG(38:5)**	**0.006**	0.006	**0.020**	0.010	**3.394**	0.0322	**0.016**	0.015	**0.031**	0.014
986.6	C53H92O15	**DGDG(38:4)**	**0.008**	0.010	**0.018**	0.008	**2.115**	0.143	**0.023**	0.026	**0.027**	0.010
988.7	C53H94O15	**DGDG(38:3)**	**0.002**	0.003	**0.004**	0.006	**2.366**	0.419	**0.006**	0.009	**0.007**	0.010
Total DGDG			**34.279**	**4.249**	**64.358**	**9.962**	**1.877**	**0.0003**	**100.000**	**0.000**	**100.000**	**0.000**
736.5	C41H66O10	**MGDG(32:6)**	**9.025**	1.946	**2.953**	0.325	**0.327**	0.0001	**3.208**	0.361	**1.332**	0.110
738.5	C41H68O10	**MGDG(32:5)**	**19.239**	3.387	**11.310**	1.521	**0.588**	0.0014	**6.855**	0.510	**5.076**	0.164
740.5	C41H70O10	**MGDG(32:4)**	**3.608**	0.549	**3.022**	0.441	**0.838**	0.0995	**1.290**	0.102	**1.358**	0.125
764.5	C43H70O10	**MGDG(34:6)**	**165.461**	19.953	**100.390**	12.423	**0.607**	0.0003	**59.170**	1.289	**45.097**	0.838
766.5	C43H72O10	**MGDG(34:5)**	**38.590**	4.418	**41.709**	4.674	**1.081**	0.3097	**13.811**	0.652	**18.782**	1.109
768.5	C43H74O10	**MGDG(34:4)**	**8.042**	1.109	**20.694**	2.805	**2.573**	0.0001	**2.884**	0.334	**9.288**	0.326
770.5	C43H76O10	**MGDG(34:3)**	**2.262**	0.278	**5.234**	0.923	**2.314**	0.0001	**0.817**	0.130	**2.340**	0.145
772.6	C43H78O10	**MGDG(34:2)**	**0.332**	0.083	**0.943**	0.210	**2.842**	0.0003	**0.121**	0.034	**0.420**	0.050
774.6	C43H80O10	**MGDG(34:1)**	**0.367**	0.203	**0.560**	0.214	**1.523**	0.1835	**0.136**	0.079	**0.246**	0.070
792.5	C45H74O10	**MGDG(36:6)**	**23.815**	2.949	**18.534**	3.409	**0.778**	0.0307	**8.521**	0.544	**8.275**	0.516
794.5	C45H76O10	**MGDG(36:5)**	**7.458**	1.275	**11.800**	3.389	**1.582**	0.0279	**2.663**	0.343	**5.249**	1.070
796.6	C45H78O10	**MGDG(36:4)**	**1.293**	0.258	**4.671**	1.370	**3.612**	0.0006	**0.461**	0.071	**2.080**	0.427

798.6	C45H80O10	**MGDG(36:3)**	**0.136**	0.037	**0.923**	0.314	**6.763**	0.0005	**0.049**	0.013	**0.409**	0.096
800.6	C45H82O10	**MGDG(36:2)**	**0.000**	0.000	**0.080**	0.021	**INF**	0.0001	**0.000**	0.000	**0.036**	0.006
802.6	C45H84O10	**MGDG(36:1)**	**0.005**	0.006	**0.005**	0.007	**0.969**	0.9733	**0.002**	0.002	**0.002**	0.003
820.6	C47H78O10	**MGDG(38:6)**	**0.017**	0.009	**0.011**	0.004	**0.664**	0.2134	**0.006**	0.003	**0.005**	0.002
822.6	C47H80O10	**MGDG(38:5)**	**0.014**	0.005	**0.004**	0.004	**0.308**	0.009	**0.005**	0.002	**0.002**	0.002
824.6	C47H82O10	**MGDG(38:4)**	**0.005**	0.005	**0.006**	0.004	**1.118**	0.8474	**0.002**	0.002	**0.002**	0.001
826.6	C47H84O10	**MGDG(38:3)**	**0.002**	0.002	**0.001**	0.001	**0.332**	0.1791	**0.001**	0.001	**0.000**	0.001
Total MGDG			**279.672**	**33.206**	**222.849**	**29.772**	**0.797**	**0.0215**	**100.000**	**0.000**	**100.000**	**0.000**
710.5	C36H69O10P	**PG(30:1)**	**0.025**	0.016	**0.005**	0.007	**0.185**	0.0304	**0.014**	0.008	**0.004**	0.006
712.5	C36H71O10P	**PG(30:0)**	**0.088**	0.031	**0.041**	0.021	**0.468**	0.0225	**0.049**	0.015	**0.036**	0.021
736.5	C38H71O10P	**PG(32:2)**	**0.652**	0.393	**0.205**	0.084	**0.314**	0.0373	**0.360**	0.191	**0.166**	0.053
738.5	C38H73O10P	**PG(32:1)**	**6.783**	1.158	**3.652**	0.430	**0.538**	0.0005	**3.815**	0.454	**3.082**	0.492
740.5	C38H75O10P	**PG(32:0)**	**9.749**	2.580	**11.783**	1.842	**1.209**	0.1892	**5.461**	1.109	**9.892**	1.610
752.5	C39H75O10P	**PG(33:1)**	**0.829**	0.268	**0.644**	0.077	**0.776**	0.1749	**0.463**	0.118	**0.541**	0.073
754.5	C39H77O10P	**PG(33:0)**	**1.368**	0.448	**1.903**	0.337	**1.391**	0.0653	**0.764**	0.203	**1.580**	0.101
760.5	C40H71O10P	**PG(34:4)**	**41.663**	4.836	**12.876**	2.215	**0.309**	0.0001	**23.571**	2.684	**10.683**	0.489
762.5	C40H73O10P	**PG(34:3)**	**63.045**	3.685	**27.989**	5.476	**0.444**	0.0001	**35.611**	0.846	**23.161**	1.266
764.5	C40H75O10P	**PG(34:2)**	**42.812**	4.052	**40.993**	9.080	**0.958**	0.6933	**24.155**	1.458	**33.765**	1.837
766.5	C40H77O10P	**PG(34:1)**	**5.224**	0.865	**16.682**	3.967	**3.193**	0.0002	**2.937**	0.309	**13.740**	1.733
768.5	C40H79O10P	**PG(34:0)**	**0.135**	0.077	**0.068**	0.067	**0.501**	0.1789	**0.076**	0.044	**0.061**	0.060
774.5	C41H73O10P	**PG(35:4)**	**0.994**	0.125	**0.447**	0.115	**0.449**	0.0001	**0.561**	0.060	**0.367**	0.057
776.5	C41H75O10P	**PG(35:3)**	**2.025**	0.323	**1.389**	0.277	**0.686**	0.0103	**1.137**	0.107	**1.150**	0.096
778.5	C41H77O10P	**PG(35:2)**	**1.593**	0.474	**1.589**	0.529	**0.998**	0.9912	**0.889**	0.206	**1.301**	0.319
788.5	C42H75O10P	**PG(36:4)**	**0.092**	0.006	**0.157**	0.061	**1.714**	0.1917	**0.052**	0.005	**0.128**	0.038
790.5	C42H77O10P	**PG(36:3)**	**0.056**	0.012	**0.128**	0.056	**2.293**	0.043	**0.031**	0.007	**0.104**	0.043
792.5	C42H79O10P	**PG(36:2)**	**0.056**	0.033	**0.232**	0.096	**4.174**	0.0224	**0.031**	0.018	**0.190**	0.061
794.6	C42H81O10P	**PG(36:1)**	**0.041**	0.027	**0.057**	0.039	**1.386**	0.0047	**0.023**	0.014	**0.045**	0.031
814.5	C44H77O10P	**PG(38:5)**	**0.001**	0.003	**0.005**	0.005	**3.704**	0.4773	**0.001**	0.002	**0.004**	0.004
Total PG			**177.229**	**13.193**	**120.845**	**22.300**	**0.682**	**0.0012**	**100.000**	**0.000**	**100.000**	**0.000**
500.3	C22H43O9P	**LPG(16:1)**	**0.009**	0.019	**0.011**	0.024	**1.256**	0.8773	**0.517**	1.156	**0.780**	1.744
502.3	C22H45O9P	**LPG(16:0)**	**0.192**	0.121	**0.525**	0.335	**2.729**	0.0707	**11.356**	7.741	**46.472**	22.148
516.3	C23H47O9P	**LPG(17:0)**	**0.094**	0.083	**0.176**	0.135	**1.876**	0.2793	**4.967**	4.052	**16.613**	12.718
524.3	C24H43O9P	**LPG(18:3)**	**0.005**	0.011	**0.015**	0.022	**2.926**	0.3972	**0.210**	0.470	**1.179**	1.815
526.3	C24H45O9P	**LPG(18:2)**	**0.012**	0.017	**0.015**	0.020	**1.222**	0.8301	**0.683**	0.963	**1.326**	1.884
528.3	C24H47O9P	**LPG(18:1)**	**0.000**	0.000	**0.038**	0.055	**INF**	0.1652	**0.000**	0.000	**3.501**	5.275
536.3	C25H43O9P	**LPG(19:2)**	**1.395**	0.376	**0.278**	0.096	**0.200**	0.0002	**78.603**	7.320	**26.129**	9.022
568.3	C27H51O9P	**LPG(21:0)**	**0.063**	0.045	**0.042**	0.041	**0.662**	0.4564	**3.663**	2.622	**4.000**	3.739
Total LysoPG			**1.770**	**0.427**	**1.099**	**0.196**	**0.621**	**0.0128**	**100.000**	**0.000**	**100.000**	**0.000**

468.3	C22H46O7PN	**LPC(14:0)**	**0.000**	0.000	**0.001**	0.002	**INF**	0.4554	**0.000**	0.000	**0.248**	0.556
480.3	C23H46O7PN	**LPC(15:1)**	**0.000**	0.000	**0.000**	0.001	**INF**	0.6666	**0.000**	0.000	**0.066**	0.148
482.3	C23H48O7PN	**LPC(15:0)**	**0.001**	0.002	**0.000**	0.000	**0.000**	0.5447	**0.051**	0.114	**0.000**	0.000
494.3	C24H48O7PN	**LPC(16:1)**	**0.013**	0.007	**0.012**	0.008	**0.898**	0.7541	**1.043**	0.548	**1.847**	1.622
496.3	C24H50O7PN	**LPC(16:0)**	**0.083**	0.022	**0.065**	0.036	**0.781**	0.3556	**6.750**	1.774	**9.243**	3.024
508.3	C25H50O7PN	**LPC(17:1)**	**0.001**	0.002	**0.000**	0.001	**0.457**	0.5927	**0.082**	0.184	**0.066**	0.148
510.4	C25H52O7PN	**LPC(17:0)**	**0.002**	0.004	**0.000**	0.000	**0.000**	0.2874	**0.174**	0.322	**0.000**	0.000
518.3	C26H48O7PN	**LPC(18:3)**	**0.861**	0.058	**0.311**	0.114	**0.361**	0.0001	**70.063**	2.457	**47.415**	3.005
520.3	C26H50O7PN	**LPC(18:2)**	**0.262**	0.037	**0.213**	0.077	**0.813**	0.2335	**21.210**	1.598	**32.886**	6.193
522.4	C26H52O7PN	**LPC(18:1)**	**0.005**	0.007	**0.050**	0.028	**10.183**	0.0087	**0.387**	0.563	**7.716**	4.002
524.4	C26H54O7PN	**LPC(18:0)**	**0.003**	0.003	**0.003**	0.005	**1.131**	0.8788	**0.240**	0.219	**0.513**	0.705
Total LysoPC			**1.230**	**0.094**	**0.654**	**0.231**	**0.532**	**0.0009**	**100.000**	**0.000**	**100.000**	**0.000**
440.3	C20H42O7PN	**LPE(15:0)**	**0.000**	0.000	**0.002**	0.004	**INF**	0.4028	**0.000**	0.000	**0.494**	1.104
452.3	C21H42O7PN	**LPE(16:1)**	**0.012**	0.026	**0.000**	0.000	**0.000**	0.3544	**1.613**	3.607	**0.000**	0.000
454.3	C21H44O7PN	**LPE(16:0)**	**0.267**	0.054	**0.174**	0.065	**0.651**	**0.0384**	**50.483**	3.507	**49.133**	15.633
466.3	C22H44O7PN	**LPE(17:1)**	**0.001**	0.003	**0.000**	0.000	**0.000**	0.4208	**0.194**	0.433	**0.000**	0.000
468.3	C22H46O7PN	**LPE(17:0)**	**0.004**	0.008	**0.004**	0.006	**1.118**	0.8955	**0.688**	1.538	**1.189**	1.630
476.3	C23H42O7PN	**LPE(18:3)**	**0.125**	0.046	**0.037**	0.016	**0.297**	**0.0037**	**23.680**	6.414	**11.240**	6.352
478.3	C23H44O7PN	**LPE(18:2)**	**0.112**	0.039	**0.107**	0.020	**0.954**	0.7873	**21.222**	6.628	**31.559**	9.113
480.3	C23H46O7PN	**LPE(18:1)**	**0.011**	0.012	**0.022**	0.015	**1.930**	0.2656	**2.121**	2.307	**6.386**	4.224
Total LysoPE			**0.532**	**0.125**	**0.345**	**0.036**	**0.649**	**0.0124**	**100.000**	**0.000**	**100.000**	**0.000**
650.5	C34H68O8PN	**PC(26:0)**	**0.035**	0.008	**0.087**	0.018	**2.465**	0.0004	**0.028**	0.006	**0.072**	0.024
676.5	C36H70O8PN	**PC(28:1)**	**0.023**	0.009	**0.076**	0.010	**3.252**	0.0001	**0.018**	0.007	**0.063**	0.018
678.5	C36H72O8PN	**PC(28:0)**	**0.007**	0.007	**0.037**	0.015	**5.638**	0.0031	**0.006**	0.006	**0.031**	0.013
702.5	C38H72O8PN	**PC(30:2)**	**0.045**	0.009	**0.064**	0.023	**1.417**	0.1314	**0.035**	0.004	**0.052**	0.019
704.5	C38H74O8PN	**PC(30:1)**	**0.050**	0.016	**0.082**	0.021	**1.624**	0.0289	**0.038**	0.007	**0.065**	0.017
706.5	C38H76O8PN	**PC(30:0)**	**0.005**	0.002	**0.010**	0.008	**2.178**	0.1632	**0.004**	0.002	**0.008**	0.007
716.5	C39H74O8PN	**PC(31:2)**	**0.093**	0.024	**0.116**	0.018	**1.244**	0.1285	**0.072**	0.013	**0.093**	0.011
718.5	C39H76O8PN	**PC(31:1)**	**0.057**	0.019	**0.115**	0.032	**2.026**	0.0082	**0.043**	0.010	**0.090**	0.012
720.5	C39H78O8PN	**PC(31:0)**	**0.005**	0.004	**0.013**	0.009	**2.984**	0.0898	**0.003**	0.003	**0.010**	0.007
730.5	C40H76O8PN	**PC(32:2)**	**1.641**	0.324	**1.608**	0.240	**0.980**	0.856	**1.274**	0.103	**1.285**	0.057
732.5	C40H78O8PN	**PC(32:1)**	**0.889**	0.116	**1.564**	0.358	**1.759**	0.0039	**0.695**	0.031	**1.237**	0.078
734.6	C40H80O8PN	**PC(32:0)**	**0.020**	0.015	**0.035**	0.022	**1.714**	0.2665	**0.016**	0.012	**0.030**	0.022
744.5	C41H78O8PN	**PC(33:2)**	**0.720**	0.207	**0.996**	0.164	**1.384**	0.0476	**0.553**	0.085	**0.795**	0.044
746.6	C41H80O8PN	**PC(33:1)**	**0.328**	0.073	**0.670**	0.092	**2.040**	0.0002	**0.254**	0.023	**0.536**	0.024
748.6	C41H82O8PN	**PC(33:0)**	**0.035**	0.015	**0.038**	0.030	**1.096**	0.8254	**0.028**	0.014	**0.030**	0.022
752.5	C42H74O8PN	**PC(34:5)**	**3.132**	0.451	**1.656**	0.238	**0.529**	0.0002	**2.441**	0.038	**1.326**	0.100
754.5	C42H76O8PN	**PC(34:4)**	**2.590**	0.427	**2.400**	0.417	**0.926**	0.4959	**2.015**	0.127	**1.910**	0.020

756.5	C42H78O8PN	**PC(34:3)**	**23.966**	2.784	**20.199**	3.333	**0.843**	0.0884	**18.741**	0.748	**16.104**	0.766
758.6	C42H80O8PN	**PC(34:2)**	**11.126**	1.858	**17.906**	3.000	**1.609**	0.0026	**8.655**	0.409	**14.278**	0.709
760.6	C42H82O8PN	**PC(34:1)**	**0.313**	0.067	**3.334**	0.888	**10.644**	0.0001	**0.247**	0.059	**2.627**	0.338
770.6	C43H80O8PN	**PC(35:3)**	**1.590**	0.349	**1.640**	0.259	**1.032**	0.802	**1.229**	0.118	**1.309**	0.048
772.6	C43H82O8PN	**PC(35:2)**	**0.699**	0.138	**1.221**	0.130	**1.745**	0.0003	**0.542**	0.038	**0.986**	0.125
778.5	C44H76O8PN	**PC(36:6)**	**32.284**	4.201	**11.132**	1.964	**0.345**	0.0001	**25.211**	0.972	**8.875**	0.712
780.5	C44H78O8PN	**PC(36:5)**	**29.175**	4.311	**21.021**	4.488	**0.721**	0.019	**22.739**	1.392	**16.663**	1.147
782.6	C44H80O8PN	**PC(36:4)**	**8.718**	1.027	**18.659**	3.442	**2.140**	0.0003	**6.826**	0.575	**14.843**	0.525
784.6	C44H82O8PN	**PC(36:3)**	**2.096**	0.250	**10.931**	2.440	**5.215**	0.0001	**1.649**	0.217	**8.658**	0.619
786.6	C44H84O8PN	**PC(36:2)**	**0.267**	0.041	**2.506**	0.593	**9.376**	0.0001	**0.208**	0.016	**1.985**	0.189
788.6	C44H86O8PN	**PC(36:1)**	**0.080**	0.021	**0.342**	0.141	**4.299**	0.0033	**0.064**	0.024	**0.268**	0.089
796.6	C45H82O8PN	**PC(37:4)**	**3.344**	0.882	**1.904**	0.453	**0.569**	0.0118	**2.591**	0.461	**1.510**	0.186
798.6	C45H84O8PN	**PC(37:3)**	**1.413**	0.212	**1.708**	0.232	**1.208**	0.0692	**1.110**	0.148	**1.378**	0.219
806.6	C46H80O8PN	**PC(38:6)**	**0.312**	0.105	**0.170**	0.059	**0.544**	0.0297	**0.242**	0.062	**0.134**	0.035
808.6	C46H82O8PN	**PC(38:5)**	**0.299**	0.089	**0.134**	0.026	**0.448**	0.004	**0.231**	0.044	**0.110**	0.029
810.6	C46H84O8PN	**PC(38:4)**	**0.302**	0.086	**0.259**	0.052	**0.857**	0.3686	**0.233**	0.048	**0.207**	0.027
812.6	C46H86O8PN	**PC(38:3)**	**0.293**	0.048	**0.346**	0.054	**1.178**	0.1474	**0.228**	0.016	**0.280**	0.061
814.6	C46H88O8PN	**PC(38:2)**	**0.091**	0.031	**0.185**	0.034	**2.033**	0.0018	**0.070**	0.016	**0.150**	0.037
820.6	C47H82O8PN	**PC(39:6)**	**1.278**	0.307	**1.091**	0.065	**0.854**	0.2182	**0.989**	0.135	**0.884**	0.113
822.6	C47H84O8PN	**PC(39:5)**	**0.674**	0.123	**1.155**	0.143	**1.715**	0.0005	**0.523**	0.030	**0.932**	0.133
836.6	C48H86O8PN	**PC(40:5)**	**0.072**	0.029	**0.072**	0.025	**0.994**	0.9728	**0.056**	0.017	**0.056**	0.013
838.6	C48H88O8PN	**PC(40:4)**	**0.078**	0.041	**0.091**	0.033	**1.174**	0.5804	**0.058**	0.024	**0.072**	0.025
840.6	C48H90O8PN	**PC(40:3)**	**0.034**	0.013	**0.044**	0.015	**1.279**	0.3121	**0.026**	0.008	**0.035**	0.009
842.7	C48H92O8PN	**PC(40:2)**	**0.011**	0.010	**0.028**	0.015	**2.568**	0.0713	**0.009**	0.009	**0.022**	0.012
Total PC			**128.191**	**17.103**	**125.644**	**22.044**	**0.980**	**0.8434**	**100.000**	**0.000**	**100.000**	**0.000**
606.4	C31H60O8PN	**PE(26:1)**	**0.024**	0.015	**0.006**	0.005	**0.265**	0.0411	**0.079**	0.057	**0.023**	0.021
608.4	C31H62O8PN	**PE(26:0)**	**0.389**	0.130	**0.213**	0.071	**0.547**	0.0287	**1.187**	0.335	**0.759**	0.291
632.4	C33H62O8PN	**PE(28:2)**	**0.072**	0.029	**0.052**	0.019	**0.727**	0.2417	**0.221**	0.080	**0.190**	0.086
634.4	C33H64O8PN	**PE(28:1)**	**0.061**	0.024	**0.079**	0.013	**1.302**	0.1683	**0.192**	0.081	**0.284**	0.072
660.5	C35H66O8PN	**PE(30:2)**	**0.010**	0.007	**0.002**	0.001	**0.153**	0.0241	**0.030**	0.016	**0.006**	0.005
662.5	C35H68O8PN	**PE(30:1)**	**0.015**	0.025	**0.001**	0.002	**0.099**	0.2488	**0.039**	0.057	**0.005**	0.008
664.5	C35H70O8PN	**PE(30:0)**	**0.012**	0.008	**0.004**	0.004	**0.352**	0.0931	**0.035**	0.018	**0.015**	0.016
674.5	C36H68O8PN	**PE(31:2)**	**0.006**	0.006	**0.007**	0.005	**1.184**	0.783	**0.020**	0.021	**0.022**	0.016
676.5	C36H70O8PN	**PE(31:1)**	**0.003**	0.005	**0.002**	0.003	**0.753**	0.7753	**0.007**	0.012	**0.007**	0.012
678.5	C36H72O8PN	**PE(31:0)**	**0.001**	0.001	**0.001**	0.002	**2.440**	0.5988	**0.002**	0.003	**0.005**	0.007
686.5	C37H68O8PN	**PE(32:3)**	**1.229**	0.206	**1.022**	0.107	**0.831**	0.081	**3.727**	0.334	**3.621**	0.370
688.5	C37H70O8PN	**PE(32:2)**	**0.569**	0.445	**0.352**	0.038	**0.620**	0.3114	**1.609**	0.911	**1.251**	0.159
690.5	C37H72O8PN	**PE(32:1)**	**0.642**	1.197	**0.148**	0.038	**0.230**	0.383	**1.599**	2.795	**0.515**	0.065

692.5	C37H74O8PN	**PE(32:0)**	**0.023**	0.046	**0.000**	0.000	**0.000**	0.2899	**0.058**	0.108	**0.000**	0.000
702.5	C38H72O8PN	**PE(33:2)**	**0.378**	0.110	**0.235**	0.048	**0.623**	0.0293	**1.125**	0.134	**0.830**	0.144
704.5	C38H74O8PN	**PE(33:1)**	**0.040**	0.058	**0.022**	0.007	**0.565**	0.5123	**0.104**	0.133	**0.078**	0.017
706.5	C38H76O8PN	**PE(33:0)**	**0.010**	0.001	**0.002**	0.002	**0.192**	0.0001	**0.031**	0.008	**0.007**	0.007
708.5	C39H66O8PN	**PE(34:6)**	**0.494**	0.104	**0.187**	0.052	**0.378**	0.0004	**1.494**	0.203	**0.655**	0.153
710.5	C39H68O8PN	**PE(34:5)**	**0.426**	0.127	**0.262**	0.042	**0.614**	0.0255	**1.265**	0.137	**0.924**	0.122
712.5	C39H70O8PN	**PE(34:4)**	**0.270**	0.054	**0.266**	0.046	**0.985**	0.9028	**0.814**	0.033	**0.936**	0.084
714.5	C39H72O8PN	**PE(34:3)**	**5.000**	0.930	**3.330**	0.417	**0.666**	0.0064	**15.090**	0.684	**11.740**	0.681
716.5	C39H74O8PN	**PE(34:2)**	**7.254**	1.396	**6.911**	0.932	**0.953**	0.6604	**21.877**	0.941	**24.322**	0.632
718.5	C39H76O8PN	**PE(34:1)**	**0.066**	0.064	**0.150**	0.056	**2.296**	0.0551	**0.178**	0.168	**0.518**	0.119
720.5	C39H78O8PN	**PE(34:0)**	**0.138**	0.032	**0.091**	0.014	**0.657**	0.0163	**0.443**	0.172	**0.322**	0.049
726.5	C40H72O8PN	**PE(35:4)**	**0.086**	0.023	**0.072**	0.021	**0.839**	0.3509	**0.257**	0.046	**0.251**	0.065
728.5	C40H74O8PN	**PE(35:3)**	**0.234**	0.054	**0.170**	0.018	**0.724**	0.0348	**0.702**	0.048	**0.602**	0.079
730.5	C40H76O8PN	**PE(35:2)**	**0.286**	0.081	**0.243**	0.033	**0.847**	0.2915	**0.852**	0.119	**0.855**	0.065
732.5	C40H78O8PN	**PE(35:1)**	**0.017**	0.013	**0.029**	0.011	**1.691**	0.1622	**0.049**	0.029	**0.099**	0.030
734.6	C40H80O8PN	**PE(35:0)**	**0.420**	0.110	**0.237**	0.056	**0.565**	0.0108	**1.305**	0.375	**0.834**	0.173
736.5	C41H70O8PN	**PE(36:6)**	**1.332**	0.326	**0.657**	0.090	**0.493**	0.0021	**3.992**	0.369	**2.315**	0.195
738.5	C41H72O8PN	**PE(36:5)**	**3.219**	0.790	**2.444**	0.367	**0.759**	0.0818	**9.631**	0.736	**8.596**	0.473
740.5	C41H74O8PN	**PE(36:4)**	**3.409**	0.733	**4.662**	0.646	**1.368**	0.0209	**10.261**	1.011	**16.400**	0.241
742.5	C41H76O8PN	**PE(36:3)**	**0.784**	0.112	**2.096**	0.329	**2.675**	0.0001	**2.413**	0.463	**7.371**	0.574
744.5	C41H78O8PN	**PE(36:2)**	**0.076**	0.015	**0.205**	0.060	**2.681**	0.0016	**0.236**	0.057	**0.720**	0.172
746.6	C41H80O8PN	**PE(36:1)**	**0.011**	0.010	**0.031**	0.011	**2.744**	0.0198	**0.035**	0.035	**0.109**	0.041
748.6	C41H82O8PN	**PE(36:0)**	**0.028**	0.013	**0.013**	0.009	**0.460**	0.0718	**0.083**	0.033	**0.043**	0.025
752.5	C42H74O8PN	**PE(37:5)**	**0.081**	0.018	**0.044**	0.011	**0.548**	0.0044	**0.245**	0.049	**0.155**	0.030
754.5	C42H76O8PN	**PE(37:4)**	**0.332**	0.059	**0.237**	0.053	**0.713**	0.0274	**1.006**	0.095	**0.826**	0.083
756.5	C42H78O8PN	**PE(37:3)**	**3.650**	0.621	**2.113**	0.291	**0.579**	0.001	**11.044**	0.609	**7.438**	0.210
758.6	C42H80O8PN	**PE(37:2)**	**0.000**	0.000	**0.005**	0.007	**INF**	0.2391	**0.000**	0.000	**0.017**	0.030
760.6	C42H82O8PN	**PE(37:1)**	**0.066**	0.027	**0.085**	0.037	**1.290**	0.3763	**0.204**	0.081	**0.295**	0.118
762.6	C42H84O8PN	**PE(37:0)**	**0.029**	0.018	**0.012**	0.008	**0.417**	0.0996	**0.089**	0.055	**0.042**	0.026
764.5	C43H74O8PN	**PE(38:6)**	**0.031**	0.019	**0.005**	0.004	**0.172**	0.0228	**0.087**	0.043	**0.018**	0.014
766.5	C43H76O8PN	**PE(38:5)**	**0.061**	0.016	**0.010**	0.007	**0.171**	0.0002	**0.183**	0.032	**0.036**	0.025
768.5	C43H78O8PN	**PE(38:4)**	**0.065**	0.021	**0.020**	0.007	**0.299**	0.0017	**0.193**	0.032	**0.068**	0.022
770.6	C43H80O8PN	**PE(38:3)**	**0.115**	0.035	**0.054**	0.024	**0.472**	0.0138	**0.339**	0.048	**0.189**	0.078
772.6	C43H82O8PN	**PE(38:2)**	**0.070**	0.011	**0.057**	0.008	**0.815**	0.0538	**0.212**	0.028	**0.201**	0.029
774.6	C43H84O8PN	**PE(38:1)**	**0.000**	0.000	**0.003**	0.004	**INF**	0.1302	**0.000**	0.000	**0.012**	0.016
776.6	C43H86O8PN	**PE(38:0)**	**0.023**	0.009	**0.009**	0.009	**0.404**	0.0434	**0.067**	0.016	**0.034**	0.032
778.5	C44H76O8PN	**PE(39:6)**	**0.558**	0.122	**0.301**	0.051	**0.539**	0.0024	**1.682**	0.150	**1.066**	0.195
780.5	C44H78O8PN	**PE(39:5)**	**0.579**	0.079	**0.516**	0.068	**0.892**	0.2165	**1.762**	0.167	**1.820**	0.136

782.6	C44H80O8PN	**PE(39:4)**	**0.494**	0.082	**0.660**	0.095	**1.335**	0.0184	**1.542**	0.409	**2.326**	0.177
798.6	C45H84O8PN	**PE(40:3)**	**0.043**	0.012	**0.014**	0.009	**0.333**	0.0029	**0.137**	0.050	**0.050**	0.029
800.6	C45H86O8PN	**PE(40:2)**	**0.010**	0.011	**0.000**	0.001	**0.041**	0.0686	**0.036**	0.039	**0.002**	0.004
826.6	C47H88O8PN	**PE(42:3)**	**0.015**	0.006	**0.007**	0.003	**0.486**	0.0223	**0.047**	0.018	**0.027**	0.012
828.6	C47H90O8PN	**PE(42:2)**	**0.026**	0.017	**0.042**	0.010	**1.628**	0.1163	**0.082**	0.068	**0.147**	0.033
Total PE			**33.280**	**6.974**	**28.399**	**3.626**	**0.853**	**0.2024**	**100.000**	**0.000**	**100.000**	**0.000**
796.5	C39H71O13P	**PI(30:2)**	**0.021**	0.011	**0.049**	0.021	**2.289**	0.0326	**0.275**	0.132	**0.287**	0.105
798.5	C39H73O13P	**PI(30:1)**	**0.000**	0.001	**0.005**	0.005	**10.112**	0.0821	**0.006**	0.013	**0.027**	0.025
800.5	C39H75O13P	**PI(30:0)**	**0.002**	0.001	**0.002**	0.001	**1.235**	0.6137	**0.023**	0.015	**0.013**	0.007
810.5	C40H73O13P	**PI(31:2)**	**0.003**	0.001	**0.002**	0.001	**0.819**	0.7599	**0.034**	0.009	**0.012**	0.007
812.5	C40H75O13P	**PI(31:1)**	**0.001**	0.001	**0.002**	0.001	**1.826**	0.308	**0.015**	0.014	**0.012**	0.007
814.5	C40H77O13P	**PI(31:0)**	**0.002**	0.002	**0.001**	0.002	**0.535**	0.5237	**0.030**	0.031	**0.006**	0.009
822.5	C41H73O13P	**PI(32:3)**	**0.347**	0.056	**0.317**	0.055	**0.913**	0.4123	**4.647**	0.605	**1.871**	0.175
824.5	C41H75O13P	**PI(32:2)**	**0.150**	0.024	**0.148**	0.031	**0.984**	0.8936	**2.012**	0.263	**0.872**	0.116
826.5	C41H77O13P	**PI(32:1)**	**0.065**	0.007	**0.131**	0.023	**2.022**	0.0003	**0.876**	0.160	**0.773**	0.073
828.5	C41H79O13P	**PI(32:0)**	**0.043**	0.017	**0.039**	0.006	**0.908**	0.616	**0.579**	0.217	**0.235**	0.042
838.5	C42H77O13P	**PI(33:2)**	**0.043**	0.008	**0.071**	0.015	**1.651**	0.007	**0.574**	0.095	**0.422**	0.092
840.5	C42H79O13P	**PI(33:1)**	**0.041**	0.024	**0.122**	0.036	**2.986**	0.0029	**0.531**	0.293	**0.721**	0.185
842.5	C42H81O13P	**PI(33:0)**	**0.000**	0.001	**0.003**	0.003	**6.422**	0.129	**0.006**	0.013	**0.016**	0.017
848.5	C43H75O13P	**PI(34:4)**	**0.071**	0.013	**0.166**	0.038	**2.329**	0.0008	**0.953**	0.149	**0.970**	0.082
850.5	C43H77O13P	**PI(34:3)**	**1.895**	0.186	**1.694**	0.207	**0.894**	0.1454	**25.378**	0.803	**10.044**	0.405
852.5	C43H79O13P	**PI(34:2)**	**2.683**	0.216	**3.652**	0.500	**1.361**	0.0041	**35.976**	0.907	**21.632**	1.051
854.5	C43H81O13P	**PI(34:1)**	**0.646**	0.079	**5.923**	1.123	**9.169**	0.0001	**8.651**	0.706	**34.868**	1.696
866.5	C44H81O13P	**PI(35:2)**	**0.157**	0.029	**0.377**	0.071	**2.403**	0.0002	**2.109**	0.352	**2.230**	0.260
868.6	C44H83O13P	**PI(35:1)**	**0.034**	0.022	**0.437**	0.087	**12.879**	0.0001	**0.453**	0.276	**2.579**	0.283
870.6	C44H85O13P	**PI(35:0)**	**0.032**	0.009	**0.020**	0.008	**0.631**	0.0588	**0.431**	0.114	**0.125**	0.057
872.5	C45H75O13P	**PI(36:6)**	**0.111**	0.032	**0.171**	0.041	**1.544**	0.0322	**1.465**	0.370	**1.010**	0.199
874.5	C45H77O13P	**PI(36:5)**	**0.220**	0.016	**0.336**	0.035	**1.531**	0.0002	**2.954**	0.233	**2.028**	0.399
876.5	C45H79O13P	**PI(36:4)**	**0.155**	0.060	**0.851**	0.121	**5.475**	0.0001	**2.040**	0.711	**5.046**	0.345
878.5	C45H81O13P	**PI(36:3)**	**0.083**	0.024	**0.991**	0.133	**11.995**	0.0001	**1.098**	0.275	**5.869**	0.110
880.6	C45H83O13P	**PI(36:2)**	**0.009**	0.012	**1.144**	0.214	**129.683**	0.0001	**0.124**	0.170	**6.735**	0.399
882.6	C45H85O13P	**PI(36:1)**	**0.003**	0.003	**0.033**	0.027	**9.630**	0.043	**0.047**	0.045	**0.196**	0.159
892.6	C46H83O13P	**PI(37:3)**	**0.626**	0.061	**0.213**	0.067	**0.341**	0.0001	**8.408**	0.751	**1.283**	0.438
908.6	C47H87O13P	**PI(38:2)**	**0.023**	0.031	**0.019**	0.018	**0.808**	0.7898	**0.298**	0.381	**0.111**	0.110
912.6	C47H91O13P	**PI(38:0)**	**0.001**	0.001	**0.001**	0.003	**1.908**	0.6666	**0.008**	0.018	**0.007**	0.015
Total PI			**7.466**	**0.688**	**16.918**	**2.526**	**2.266**	**0.0001**	**100.000**	**0.000**	**100.000**	**0.000**
708.5	C36H70O10PN	**PS(30:0)**	**0.001**	0.002	**0.001**	0.001	**0.558**	0.7404	**0.018**	0.040	**0.010**	0.022
730.5	C38H68O10PN	**PS(32:3)**	**0.122**	0.023	**0.083**	0.012	**0.680**	0.0095	**2.364**	0.383	**1.797**	0.202

732.5	C38H70O10PN	**PS(32:2)**	**0.035**	0.011	**0.031**	0.009	**0.891**	0.5843	**0.677**	0.201	**0.665**	0.154
734.5	C38H72O10PN	**PS(32:1)**	**0.010**	0.004	**0.006**	0.001	**0.625**	0.0508	**0.190**	0.076	**0.131**	0.023
736.5	C38H74O10PN	**PS(32:0)**	**0.038**	0.007	**0.021**	0.009	**0.561**	0.0089	**0.733**	0.115	**0.470**	0.231
746.5	C39H72O10PN	**PS(33:2)**	**0.057**	0.009	**0.039**	0.017	**0.693**	0.0751	**1.095**	0.129	**0.840**	0.301
748.5	C39H74O10PN	**PS(33:1)**	**0.004**	0.005	**0.003**	0.003	**0.874**	0.7599	**0.076**	0.090	**0.078**	0.074
750.5	C39H76O10PN	**PS(33:0)**	**0.001**	0.001	**0.002**	0.002	**2.720**	0.2936	**0.015**	0.022	**0.042**	0.042
756.5	C40H70O10PN	**PS(34:4)**	**0.032**	0.015	**0.021**	0.015	**0.651**	0.2695	**0.601**	0.262	**0.429**	0.287
758.5	C40H72O10PN	**PS(34:3)**	**1.126**	0.054	**0.894**	0.121	**0.795**	0.0046	**21.807**	0.552	**19.226**	0.582
760.5	C40H74O10PN	**PS(34:2)**	**1.400**	0.092	**1.315**	0.172	**0.939**	0.3576	**27.109**	0.625	**28.294**	1.189
762.5	C40H76O10PN	**PS(34:1)**	**0.014**	0.016	**0.076**	0.017	**5.250**	0.0004	**0.280**	0.294	**1.625**	0.272
764.5	C40H78O10PN	**PS(34:0)**	**0.005**	0.004	**0.001**	0.003	**0.269**	0.0919	**0.092**	0.070	**0.033**	0.073
774.5	C41H76O10PN	**PS(35:2)**	**0.073**	0.019	**0.054**	0.004	**0.735**	0.0519	**1.411**	0.311	**1.168**	0.099
776.5	C41H78O10PN	**PS(35:1)**	**0.002**	0.003	**0.012**	0.013	**5.867**	0.1199	**0.040**	0.060	**0.260**	0.251
778.6	C41H80O10PN	**PS(35:0)**	**0.003**	0.003	**0.001**	0.001	**0.375**	0.2095	**0.054**	0.049	**0.023**	0.031
780.5	C42H70O10PN	**PS(36:6)**	**0.155**	0.028	**0.151**	0.028	**0.977**	0.8417	**2.995**	0.523	**3.255**	0.474
782.5	C42H72O10PN	**PS(36:5)**	**0.303**	0.029	**0.380**	0.059	**1.254**	0.0308	**5.866**	0.286	**8.174**	0.614
784.5	C42H74O10PN	**PS(36:4)**	**0.345**	0.034	**0.580**	0.086	**1.680**	0.0005	**6.685**	0.544	**12.465**	0.767
786.5	C42H76O10PN	**PS(36:3)**	**0.054**	0.011	**0.106**	0.022	**1.953**	0.0016	**1.045**	0.172	**2.297**	0.510
788.5	C42H78O10PN	**PS(36:2)**	**0.019**	0.009	**0.019**	0.013	**0.986**	0.9332	**0.371**	0.172	**0.390**	0.235
790.6	C42H80O10PN	**PS(36:1)**	**0.000**	0.000	**0.000**	0.001	**INF**	0.6666	**0.000**	0.000	**0.011**	0.025
792.6	C42H82O10PN	**PS(36:0)**	**0.002**	0.003	**0.003**	0.003	**1.400**	0.7256	**0.043**	0.070	**0.063**	0.066
808.5	C44H74O10PN	**PS(38:6)**	**0.000**	0.001	**0.000**	0.000	**0.000**	0.6666	**0.007**	0.015	**0.000**	0.000
810.5	C44H76O10PN	**PS(38:5)**	**0.000**	0.000	**0.000**	0.001	**INF**	0.6666	**0.000**	0.000	**0.011**	0.025
812.5	C44H78O10PN	**PS(38:4)**	**0.000**	0.000	**0.001**	0.001	**INF**	0.5447	**0.000**	0.000	**0.012**	0.026
814.6	C44H80O10PN	**PS(38:3)**	**0.030**	0.019	**0.000**	0.000	**0.000**	**0.0081**	**0.566**	0.366	**0.000**	0.000
816.6	C44H82O10PN	**PS(38:2)**	**0.029**	0.015	**0.001**	0.001	**0.020**	**0.0028**	**0.556**	0.271	**0.012**	0.026
818.6	C44H84O10PN	**PS(38:1)**	**0.001**	0.001	**0.000**	0.001	**0.606**	0.5447	**0.016**	0.022	**0.011**	0.025
840.6	C46H82O10PN	**PS(40:4)**	**0.000**	0.000	**0.000**	0.001	**INF**	0.6666	**0.000**	0.000	**0.011**	0.024
842.6	C46H84O10PN	**PS(40:3)**	**0.293**	0.025	**0.038**	0.028	**0.130**	0.0001	**5.663**	0.282	**0.849**	0.656
844.6	C46H86O10PN	**PS(40:2)**	**0.398**	0.028	**0.063**	0.043	**0.158**	0.0001	**7.725**	0.641	**1.372**	0.963
846.6	C46H88O10PN	**PS(40:1)**	**0.004**	0.006	**0.003**	0.003	**0.704**	0.6075	**0.085**	0.113	**0.069**	0.064
870.6	C48H88O10PN	**PS(42:3)**	**0.207**	0.015	**0.155**	0.018	**0.751**	0.0011	**4.021**	0.374	**3.356**	0.283
872.6	C48H90O10PN	**PS(42:2)**	**0.356**	0.036	**0.370**	0.058	**1.039**	0.6627	**6.936**	1.016	**8.005**	1.249
874.6	C48H92O10PN	**PS(42:1)**	**0.005**	0.005	**0.004**	0.006	**0.885**	0.8768	**0.090**	0.099	**0.090**	0.146
898.6	C50H92O10PN	**PS(44:3)**	**0.016**	0.014	**0.053**	0.036	**3.323**	0.0003	**0.318**	0.295	**1.189**	0.837
900.7	C50H94O10PN	**PS(44:2)**	**0.023**	0.018	**0.153**	0.045	**6.576**	0.0693	**0.453**	0.346	**3.268**	0.658
Total PS			**5.163**	**0.250**	**4.644**	**0.530**	**0.899**	**0.083**	**100.000**	**0.000**	**100.000**	**0.000**
660.4	C35H63O8P	**PA(32:3)**	**0.130**	0.067	**0.096**	0.030	**0.743**	0.338	**5.964**	1.793	**3.670**	0.822

662.4	C35H65O8P	**PA(32:2)**	**0.044**	0.030	**0.014**	0.004	**0.317**	0.0525	**2.033**	1.294	**0.577**	0.284
664.5	C35H67O8P	**PA(32:1)**	**0.021**	0.012	**0.032**	0.029	**1.518**	0.4532	**1.000**	0.461	**1.182**	1.080
666.5	C35H69O8P	**PA(32:0)**	**0.022**	0.010	**0.038**	0.019	**1.748**	0.1324	**1.134**	0.583	**1.438**	0.630
682.4	C37H61O8P	**PA(34:6)**	**0.033**	0.029	**0.014**	0.006	**0.430**	0.1835	**1.452**	0.745	**0.580**	0.285
684.4	C37H63O8P	**PA(34:5)**	**0.039**	0.007	**0.040**	0.023	**1.030**	0.9019	**1.919**	0.361	**1.433**	0.579
686.4	C37H65O8P	**PA(34:4)**	**0.053**	0.023	**0.023**	0.015	**0.441**	0.0422	**2.613**	1.256	**0.940**	0.599
688.5	C37H67O8P	**PA(34:3)**	**0.515**	0.124	**0.429**	0.066	**0.832**	0.2043	**24.974**	1.676	**16.598**	2.018
690.5	C37H69O8P	**PA(34:2)**	**0.678**	0.184	**0.872**	0.169	**1.286**	0.1204	**32.656**	2.291	**33.376**	0.849
692.5	C37H71O8P	**PA(34:1)**	**0.042**	0.022	**0.139**	0.038	**3.308**	0.0012	**2.134**	1.325	**5.253**	0.816
710.4	C39H65O8P	**PA(36:6)**	**0.091**	0.027	**0.049**	0.025	**0.541**	0.0364	**4.344**	0.767	**1.788**	0.744
712.5	C39H67O8P	**PA(36:5)**	**0.189**	0.095	**0.191**	0.058	**1.013**	0.9628	**8.695**	1.597	**7.313**	1.533
714.5	C39H69O8P	**PA(36:4)**	**0.184**	0.079	**0.415**	0.100	**2.255**	0.0038	**8.603**	2.167	**15.771**	0.823
716.5	C39H71O8P	**PA(36:3)**	**0.044**	0.018	**0.208**	0.065	**4.714**	0.0006	**2.243**	1.087	**7.808**	1.030
718.5	C39H73O8P	**PA(36:2)**	**0.002**	0.002	**0.058**	0.035	**34.196**	0.0068	**0.075**	0.089	**2.150**	1.064
720.5	C39H75O8P	**PA(36:1)**	**0.002**	0.005	**0.004**	0.008	**1.558**	0.7885	**0.161**	0.360	**0.123**	0.275
Total PA			**2.088**	**0.612**	**2.623**	**0.562**	**1.256**	**0.1883**	**100.000**	**0.000**	**100.000**	**0.000**
787.5	C41H72O12S	**SQDG(32:3)**	**0.026**	0.022	**0.025**	0.021	**0.944**	0.8983	**2.369**	0.867	**2.359**	1.025
789.5	C41H74O12S	**SQDG(32:2)**	**0.016**	0.017	**0.014**	0.009	**0.857**	0.7849	**1.280**	0.606	**1.415**	0.617
791.5	C41H76O12S	**SQDG(32:1)**	**0.017**	0.019	**0.012**	0.009	**0.696**	0.5743	**1.367**	0.737	**1.268**	0.835
793.5	C41H78O12S	**SQDG(32:0)**	**0.286**	0.224	**0.227**	0.129	**0.793**	0.6215	**27.110**	1.845	**24.160**	2.023
809.5	C43H70O12S	**SQDG(34:6)**	**0.008**	0.009	**0.016**	0.013	**2.050**	0.2634	**0.913**	0.667	**1.628**	0.693
811.5	C43H72O12S	**SQDG(34:5)**	**0.007**	0.009	**0.003**	0.004	**0.449**	0.3514	**0.692**	0.409	**0.391**	0.381
813.5	C43H74O12S	**SQDG(34:4)**	**0.006**	0.006	**0.009**	0.006	**1.587**	0.4226	**0.678**	0.504	**1.076**	0.497
815.5	C43H76O12S	**SQDG(34:3)**	**0.493**	0.343	**0.355**	0.174	**0.720**	0.4458	**49.322**	2.568	**38.943**	2.075
817.5	C43H78O12S	**SQDG(34:2)**	**0.068**	0.062	**0.113**	0.059	**1.648**	0.2826	**6.000**	2.309	**12.301**	2.367
819.5	C43H80O12S	**SQDG(34:1)**	**0.019**	0.015	**0.054**	0.027	**2.900**	0.0327	**2.265**	1.506	**5.937**	0.888
837.5	C45H74O12S	**SQDG(36:6)**	**0.055**	0.039	**0.056**	0.030	**1.012**	0.9789	**5.500**	1.303	**5.940**	1.373
839.5	C45H76O12S	**SQDG(36:5)**	**0.017**	0.014	**0.025**	0.012	**1.423**	0.4032	**1.977**	1.589	**2.727**	0.455
841.5	C45H78O12S	**SQDG(36:4)**	**0.005**	0.005	**0.012**	0.010	**2.575**	0.1845	**0.354**	0.235	**1.238**	0.907
843.5	C45H80O12S	**SQDG(36:3)**	**0.000**	0.001	**0.002**	0.002	**7.722**	0.1078	**0.063**	0.141	**0.221**	0.213
845.6	C45H82O12S	**SQDG(36:2)**	**0.001**	0.002	**0.000**	0.001	**0.529**	0.5927	**0.046**	0.103	**0.041**	0.093
847.6	C45H84O12S	**SQDG(36:1)**	**0.000**	0.001	**0.003**	0.003	**7.752**	0.1021	**0.064**	0.143	**0.355**	0.350
Total SQDG			**1.026**	**0.758**	**0.926**	**0.487**	**0.903**	**0.8117**	**100.000**	**0.000**	**100.000**	**0.000**
764.6745	C47H90O6N	**44:2**	**0.124**	0.016	**0.122**	0.038	**0.988**	0.9328	**47.297**	3.566	**21.600**	3.626
766.6901	C47H92O6N	**44:1**	**0.027**	0.013	**0.075**	0.033	**2.818**	0.0158	**9.922**	4.643	**12.353**	3.250
768.7057	C47H94O6N	**44:0**	**0.009**	0.005	**0.031**	0.017	**3.604**	0.0228	**3.289**	2.035	**5.582**	2.752
790.6901	C49H92O6N	**46:3**	**0.048**	0.014	**0.135**	0.049	**2.828**	0.0052	**18.448**	5.740	**23.808**	6.111
792.7057	C49H94O6N	**46:2**	**0.014**	0.006	**0.095**	0.066	**7.005**	0.0262	**5.057**	1.653	**15.900**	8.946

796.7369	C49H98O6N	**46:0**	**0.025**	0.004	**0.050**	0.037	**2.010**	0.171	**9.540**	1.268	**8.453**	4.180
818.7213	C51H96O6N	**48:3**	**0.001**	0.001	**0.055**	0.031	**69.712**	0.0047	**0.288**	0.463	**9.576**	4.388
844.7369	C53H98O6N	**50:4**	**0.017**	0.011	**0.015**	0.014	**0.872**	0.7879	**6.159**	3.540	**2.727**	2.378
Total TAG NL215 12:1 acyl containing			**0.263**	**0.041**	**0.578**	**0.177**	**2.197**	**0.0047**	**100.000**	**0.000**	**100.000**	**0.000**
790.6901	C49H92O6N	**46:3**	**0.013**	0.004	**0.027**	0.012	**2.066**	0.0416	**38.927**	7.404	**17.873**	4.016
792.7057	C49H94O6N	**46:2**	**0.018**	0.003	**0.051**	0.008	**2.772**	0.0001	**55.501**	5.529	**35.886**	8.685
794.7213	C49H96O6N	**46:1**	**0.000**	0.000	**0.048**	0.026	**351.110**	0.0033	**0.444**	0.993	**30.426**	13.279
816.7057	C51H94O6N	**48:4**	**0.002**	0.001	**0.023**	0.013	**12.681**	0.007	**5.128**	3.595	**15.814**	8.273
Total TAG +NL217 12:0 acyl containing			**0.033**	**0.006**	**0.149**	**0.043**	**4.453**	**0.0003**	**100.000**	**0.000**	**100.000**	**0.000**
764.6745	C47H90O6N	**44:2**	**0.018**	0.005	**0.012**	0.003	**0.680**	0.0678	**1.128**	0.141	**0.323**	0.163
792.7057	C49H94O6N	**46:2**	**0.002**	0.001	**0.031**	0.011	**19.082**	0.0004	**0.098**	0.037	**0.712**	0.092
806.7576	C51H100O5N	**47:2**	**0.044**	0.014	**0.076**	0.019	**1.753**	0.0145	**2.814**	0.930	**1.892**	0.646
810.7888	C51H104O5N	**47:0**	**0.001**	0.001	**0.115**	0.051	**96.298**	0.0011	**0.071**	0.068	**2.611**	0.493
816.7057	C51H94O6N	**48:4**	**0.003**	0.002	**0.105**	0.022	**32.200**	0.0001	**0.201**	0.135	**2.549**	0.604
818.7213	C51H96O6N	**48:3**	**0.006**	0.004	**0.129**	0.048	**20.913**	0.0005	**0.388**	0.218	**3.017**	0.587
820.7369	C51H98O6N	**48:2**	**0.028**	0.011	**0.322**	0.146	**11.687**	0.002	**1.763**	0.724	**7.247**	1.365
830.7576	C53H100O5N	**49:4**	**0.034**	0.011	**0.089**	0.020	**2.638**	0.0006	**2.108**	0.328	**2.129**	0.274
832.7732	C53H102O5N	**49:3**	**0.035**	0.011	**0.100**	0.028	**2.824**	0.0013	**2.203**	0.441	**2.337**	0.284
834.7888	C53H104O5N	**49:2**	**1.023**	0.274	**1.754**	0.568	**1.714**	0.0321	**64.013**	2.930	**40.706**	1.409
836.8044	C53H106O5N	**49:1**	**0.027**	0.007	**0.067**	0.026	**2.497**	0.011	**1.761**	0.685	**1.586**	0.634
838.82	C53H108O5N	**49:0**	**0.015**	0.014	**0.080**	0.021	**5.389**	0.0004	**0.906**	0.725	**1.895**	0.267
844.7369	C53H98O6N	**50:4**	**0.002**	0.002	**0.211**	0.091	**87.283**	0.0009	**0.165**	0.105	**4.768**	0.938
846.7525	C53H100O6N	**50:3**	**0.004**	0.004	**0.307**	0.167	**87.641**	0.0036	**0.204**	0.185	**6.847**	2.513
848.7681	C53H102O6N	**50:2**	**0.016**	0.008	**0.062**	0.024	**3.947**	0.0033	**0.932**	0.312	**1.423**	0.359
856.7732	C55H102O5N	**51:5**	**0.212**	0.064	**0.371**	0.092	**1.745**	0.0137	**13.223**	1.506	**8.780**	0.708
858.7888	C55H104O5N	**51:4**	**0.097**	0.028	**0.280**	0.078	**2.888**	0.0011	**6.119**	1.461	**6.704**	1.253
860.8044	C55H106O5N	**51:3**	**0.029**	0.004	**0.186**	0.033	**6.346**	0.0001	**1.904**	0.458	**4.475**	0.683
Total TAG +NL243 14:1 acyl containing			**1.596**	**0.406**	**4.298**	**1.324**	**2.693**	**0.0024**	**100.000**	**0.000**	**100.000**	**0.000**
764.6745	C47H90O6N	**44:2**	**0.055**	0.008	**0.060**	0.029	**1.099**	0.6837	**18.522**	1.491	**1.463**	0.551
768.7057	C47H94O6N	**44:0**	**0.012**	0.006	**0.029**	0.013	**2.340**	0.0276	**4.223**	1.927	**0.670**	0.237
790.6901	C49H92O6N	**46:3**	**0.003**	0.003	**0.082**	0.032	**28.265**	0.0005	**0.889**	0.799	**1.965**	0.560
792.7057	C49H94O6N	**46:2**	**0.005**	0.002	**0.058**	0.033	**10.991**	0.0071	**1.833**	0.815	**1.275**	0.430
794.7213	C49H96O6N	**46:1**	**0.004**	0.001	**0.060**	0.017	**15.365**	0.0001	**1.343**	0.312	**1.497**	0.590
796.7369	C49H98O6N	**46:0**	**0.015**	0.009	**0.061**	0.024	**3.981**	0.0042	**5.113**	3.050	**1.425**	0.318
806.7576	C51H100O5N	**47:2**	**0.013**	0.005	**0.053**	0.019	**4.198**	0.0016	**4.281**	1.911	**1.246**	0.273
808.7732	C51H102O5N	**47:1**	**0.007**	0.004	**0.052**	0.026	**7.845**	0.0048	**2.111**	0.927	**1.224**	0.445
816.7057	C51H94O6N	**48:4**	**0.001**	0.001	**0.192**	0.064	**381.629**	0.0002	**0.187**	0.417	**4.504**	0.720
818.7213	C51H96O6N	**48:3**	**0.027**	0.014	**0.287**	0.102	**10.747**	0.0005	**8.630**	2.642	**6.863**	1.896

820.7369	C51H98O6N	**48:2**	**0.019**	0.011	**0.405**	0.129	**21.751**	0.0002	**6.340**	3.936	**9.654**	2.144
822.7525	C51H100O6N	**48:1**	**0.009**	0.007	**0.848**	0.362	**98.487**	0.0008	**2.703**	1.654	**18.912**	1.321
832.7732	C53H102O5N	**49:3**	**0.001**	0.001	**0.042**	0.019	**28.831**	0.0012	**0.481**	0.304	**1.016**	0.339
834.7888	C53H104O5N	**49:2**	**0.020**	0.011	**0.057**	0.018	**2.784**	0.0045	**6.646**	2.827	**1.359**	0.330
836.8044	C53H106O5N	**49:1**	**0.086**	0.009	**0.223**	0.077	**2.577**	0.0044	**29.364**	3.694	**5.152**	0.992
844.7369	C53H98O6N	**50:4**	**0.002**	0.002	**0.396**	0.136	**229.270**	0.0002	**0.556**	0.650	**9.406**	2.204
846.7525	C53H100O6N	**50:3**	**0.001**	0.002	**0.530**	0.221	**539.626**	0.0007	**0.268**	0.439	**11.850**	1.059
848.7681	C53H102O6N	**50:2**	**0.001**	0.001	**0.781**	0.480	**926.492**	0.0066	**0.300**	0.290	**16.192**	6.039
850.7837	C53H104O6N	**50:1**	**0.001**	0.001	**0.107**	0.062	**181.309**	0.0051	**0.148**	0.330	**2.253**	0.817
858.7888	C55H104O5N	**51:4**	**0.012**	0.007	**0.034**	0.017	**2.783**	0.0288	**3.907**	1.688	**0.808**	0.325
860.8044	C55H106O5N	**51:3**	**0.006**	0.003	**0.024**	0.018	**4.030**	0.054	**2.091**	1.047	**0.569**	0.420
862.82	C55H108O5N	**51:2**	**0.000**	0.000	**0.036**	0.033	**184.501**	0.0413	**0.064**	0.140	**0.698**	0.575
Total TAG +NL245 14:0 acyl containing			**0.299**	**0.059**	**4.418**	**1.735**	**14.767**	**0.0007**	**100.000**	**0.000**	**100.000**	**0.000**
764.6745	C47H90O6N	**44:2**	**4.163**	0.714	**4.264**	1.316	**1.024**	0.8841	**72.620**	1.626	**17.981**	3.914
766.6901	C47H92O6N	**44:1**	**0.567**	0.115	**1.050**	0.326	**1.853**	0.014	**9.858**	0.545	**4.422**	1.016
768.7057	C47H94O6N	**44:0**	**0.225**	0.085	**0.885**	0.273	**3.923**	0.0009	**3.837**	0.729	**3.699**	0.661
776.7108	C49H94O5N	**45:3**	**0.001**	0.001	**0.046**	0.048	**35.788**	0.0724	**0.021**	0.016	**0.157**	0.145
778.7264	C49H96O5N	**45:2**	**0.009**	0.005	**0.038**	0.024	**4.223**	0.0293	**0.153**	0.059	**0.139**	0.044
780.742	C49H98O5N	**45:1**	**0.008**	0.005	**0.024**	0.018	**2.892**	0.0887	**0.160**	0.107	**0.095**	0.041
790.6901	C49H92O6N	**46:3**	**0.002**	0.002	**0.054**	0.028	**27.528**	0.0033	**0.037**	0.043	**0.227**	0.095
792.7057	C49H94O6N	**46:2**	**0.417**	0.088	**0.526**	0.198	**1.261**	0.294	**7.248**	0.568	**2.252**	0.718
794.7213	C49H96O6N	**46:1**	**0.088**	0.027	**0.257**	0.085	**2.914**	0.0029	**1.518**	0.193	**1.181**	0.581
796.7369	C49H98O6N	**46:0**	**0.016**	0.010	**0.089**	0.021	**5.440**	0.0001	**0.271**	0.126	**0.414**	0.208
806.7576	C51H100O5N	**47:2**	**0.006**	0.003	**0.020**	0.015	**3.546**	0.0734	**0.097**	0.051	**0.076**	0.035
808.7732	C51H102O5N	**47:1**	**0.005**	0.008	**0.043**	0.018	**7.859**	0.0031	**0.095**	0.127	**0.175**	0.034
810.7888	C51H104O5N	**47:0**	**0.065**	0.010	**0.321**	0.074	**4.924**	0.0001	**1.149**	0.173	**1.379**	0.341
816.7057	C51H94O6N	**48:4**	**0.006**	0.003	**0.632**	0.243	**111.749**	0.0004	**0.100**	0.060	**2.618**	0.541
818.7213	C51H96O6N	**48:3**	**0.006**	0.003	**0.288**	0.106	**45.402**	0.0004	**0.114**	0.059	**1.185**	0.209
820.7369	C51H98O6N	**48:2**	**0.016**	0.008	**0.282**	0.105	**17.639**	0.0005	**0.283**	0.157	**1.163**	0.221
822.7525	C51H100O6N	**48:1**	**0.017**	0.009	**0.414**	0.171	**24.180**	0.0008	**0.296**	0.145	**1.681**	0.281
830.7576	C53H100O5N	**49:4**	**0.002**	0.001	**0.092**	0.044	**58.068**	0.0017	**0.031**	0.021	**0.365**	0.084
832.7732	C53H102O5N	**49:3**	**0.020**	0.007	**0.113**	0.044	**5.771**	0.0016	**0.342**	0.134	**0.467**	0.096
834.7888	C53H104O5N	**49:2**	**0.002**	0.004	**0.139**	0.034	**57.670**	0.0001	**0.047**	0.067	**0.610**	0.201
836.8044	C53H106O5N	**49:1**	**0.003**	0.003	**0.091**	0.049	**29.593**	0.004	**0.053**	0.055	**0.363**	0.118
838.82	C53H108O5N	**49:0**	**0.005**	0.005	**0.798**	0.315	**160.600**	0.0005	**0.087**	0.084	**3.244**	0.530
844.7369	C53H98O6N	**50:4**	**0.020**	0.010	**1.119**	0.512	**57.212**	0.0014	**0.329**	0.120	**4.506**	0.773
846.7525	C53H100O6N	**50:3**	**0.039**	0.013	**1.643**	0.684	**42.542**	0.0008	**0.667**	0.144	**6.542**	0.431
848.7681	C53H102O6N	**50:2**	**0.004**	0.004	**3.047**	1.553	**744.972**	0.0023	**0.075**	0.070	**11.548**	1.716

850.7837	C53H104O6N	**50:1**	**0.001**	0.001	**0.049**	0.032	**41.934**	0.01	**0.020**	0.024	**0.184**	0.094
856.7732	C55H102O5N	**51:5**	**0.000**	0.000	**0.046**	0.021	**INF**	0.0013	**0.000**	0.000	**0.189**	0.059
858.7888	C55H104O5N	**51:4**	**0.001**	0.001	**0.100**	0.037	**120.719**	0.0003	**0.014**	0.013	**0.425**	0.139
860.8044	C55H106O5N	**51:3**	**0.005**	0.005	**0.155**	0.054	**29.386**	0.0003	**0.085**	0.069	**0.636**	0.094
862.82	C55H108O5N	**51:2**	**0.000**	0.000	**0.235**	0.121	**5697.448**	0.0025	**0.001**	0.001	**0.910**	0.214
866.8512	C55H112O5N	**51:0**	**0.003**	0.002	**0.159**	0.033	**47.479**	0.0001	**0.058**	0.027	**0.708**	0.252
868.7369	C55H98O6N	**52:6**	**0.004**	0.002	**0.304**	0.153	**70.155**	0.0023	**0.072**	0.033	**1.175**	0.151
870.7525	C55H100O6N	**52:5**	**0.007**	0.005	**1.465**	0.646	**213.171**	0.001	**0.117**	0.095	**5.760**	0.295
872.7681	C55H102O6N	**52:4**	**0.001**	0.001	**2.133**	1.151	**1543.703**	0.0032	**0.024**	0.014	**7.982**	1.797
874.7837	C55H104O6N	**52:3**	**0.003**	0.003	**3.621**	2.392	**1103.111**	0.0096	**0.060**	0.053	**12.859**	5.083
876.7993	C55H106O6N	**52:2**	**0.002**	0.003	**0.549**	0.400	**294.422**	0.0157	**0.033**	0.046	**1.877**	1.032
886.82	C57H108O5N	**53:4**	**0.001**	0.001	**0.059**	0.057	**61.572**	0.0527	**0.018**	0.011	**0.190**	0.172
888.8356	C57H110O5N	**53:3**	**0.000**	0.000	**0.084**	0.081	**INF**	0.0504	**0.000**	0.000	**0.291**	0.238
900.7993	C57H106O6N	**54:4**	**0.000**	0.001	**0.048**	0.034	**107.455**	0.0144	**0.009**	0.019	**0.170**	0.083
902.8149	C57H108O6N	**54:3**	**0.000**	0.000	**0.045**	0.038	**INF**	0.0301	**0.000**	0.000	**0.157**	0.106
Total TAG +NL271 16:1 acyl containing			**5.742**	**1.061**	**25.328**	**10.758**	**4.411**	**0.0037**	**100.000**	**0.000**	**100.000**	**0.000**
764.6745	C47H90O6N	**44:2**	**0.152**	0.036	**0.334**	0.129	**2.190**	0.0165	**4.466**	0.238	**0.233**	0.076
766.6901	C47H92O6N	**44:1**	**0.181**	0.032	**0.658**	0.331	**3.627**	0.0124	**5.363**	0.189	**0.423**	0.082
768.7057	C47H94O6N	**44:0**	**0.033**	0.010	**0.223**	0.137	**6.726**	0.0147	**1.011**	0.354	**0.134**	0.015
776.7108	C49H94O5N	**45:3**	**0.022**	0.005	**0.194**	0.139	**8.774**	0.0245	**0.657**	0.110	**0.108**	0.025
778.7264	C49H96O5N	**45:2**	**0.018**	0.007	**1.024**	1.130	**57.976**	0.0816	**0.505**	0.140	**0.457**	0.397
780.742	C49H98O5N	**45:1**	**0.007**	0.004	**0.241**	0.232	**34.897**	0.0542	**0.215**	0.144	**0.119**	0.066
782.7576	C49H100O5N	**45:0**	**0.010**	0.004	**0.117**	0.076	**11.973**	0.0135	**0.298**	0.138	**0.069**	0.020
790.6901	C49H92O6N	**46:3**	**0.030**	0.008	**0.190**	0.098	**6.314**	0.0066	**0.897**	0.227	**0.126**	0.042
792.7057	C49H94O6N	**46:2**	**0.042**	0.008	**0.771**	0.717	**18.158**	0.0527	**1.262**	0.181	**0.401**	0.195
794.7213	C49H96O6N	**46:1**	**0.038**	0.011	**0.312**	0.141	**8.251**	0.0025	**1.116**	0.253	**0.209**	0.055
796.7369	C49H98O6N	**46:0**	**0.034**	0.010	**0.168**	0.091	**4.932**	0.0111	**1.037**	0.326	**0.108**	0.027
802.7264	C51H96O5N	**47:4**	**0.002**	0.002	**0.026**	0.017	**12.058**	0.0143	**0.057**	0.054	**0.016**	0.005
804.742	C51H98O5N	**47:3**	**0.008**	0.003	**0.126**	0.048	**16.021**	0.0006	**0.234**	0.083	**0.090**	0.031
806.7576	C51H100O5N	**47:2**	**0.179**	0.035	**0.366**	0.176	**2.047**	0.0482	**5.292**	0.520	**0.238**	0.046
808.7732	C51H102O5N	**47:1**	**0.048**	0.006	**0.263**	0.122	**5.484**	0.0042	**1.434**	0.166	**0.173**	0.044
810.7888	C51H104O5N	**47:0**	**0.085**	0.022	**0.230**	0.110	**2.723**	0.0195	**2.477**	0.299	**0.154**	0.042
816.7057	C51H94O6N	**48:4**	**0.025**	0.008	**0.686**	0.240	**27.650**	0.0003	**0.717**	0.111	**0.513**	0.235
818.7213	C51H96O6N	**48:3**	**0.076**	0.026	**2.672**	1.120	**34.949**	0.0008	**2.257**	0.555	**1.893**	0.700
820.7369	C51H98O6N	**48:2**	**0.089**	0.022	**1.466**	0.570	**16.531**	0.0006	**2.595**	0.287	**1.040**	0.378
822.7525	C51H100O6N	**48:1**	**0.043**	0.007	**1.941**	0.815	**45.208**	0.0008	**1.280**	0.183	**1.345**	0.430
824.7681	C51H102O6N	**48:0**	**0.050**	0.009	**0.407**	0.208	**8.200**	0.005	**1.473**	0.190	**0.257**	0.034
830.7576	C53H100O5N	**49:4**	**0.048**	0.013	**0.145**	0.057	**3.038**	0.0056	**1.389**	0.117	**0.105**	0.044

832.7732	C53H102O5N	**49:3**	**0.028**	0.005	**0.433**	0.154	**15.589**	0.0004	**0.833**	0.167	**0.338**	0.177
834.7888	C53H104O5N	**49:2**	**1.059**	0.221	**2.456**	0.743	**2.320**	0.0038	**31.180**	1.211	**1.853**	0.852
836.8044	C53H106O5N	**49:1**	**0.286**	0.059	**2.018**	0.751	**7.057**	0.0009	**8.422**	0.606	**1.448**	0.541
838.82	C53H108O5N	**49:0**	**0.088**	0.020	**0.519**	0.215	**5.879**	0.0021	**2.595**	0.250	**0.356**	0.112
844.7369	C53H98O6N	**50:4**	**0.044**	0.010	**5.005**	2.472	**112.732**	0.002	**1.320**	0.249	**3.236**	0.636
846.7525	C53H100O6N	**50:3**	**0.126**	0.042	**7.153**	2.986	**56.732**	0.0008	**3.667**	0.667	**5.028**	1.787
848.7681	C53H102O6N	**50:2**	**0.174**	0.061	**12.242**	5.909	**70.160**	0.0018	**5.121**	1.279	**7.957**	1.552
850.7837	C53H104O6N	**50:1**	**0.067**	0.022	**29.847**	17.691	**446.305**	0.0055	**1.958**	0.436	**17.577**	0.742
852.7993	C53H106O6N	**50:0**	**0.011**	0.004	**0.017**	0.038	**1.481**	0.7514	**0.352**	0.134	**0.006**	0.014
856.7732	C55H102O5N	**51:5**	**0.001**	0.001	**0.125**	0.076	**133.002**	0.0064	**0.028**	0.016	**0.079**	0.023
858.7888	C55H104O5N	**51:4**	**0.001**	0.001	**0.297**	0.117	**261.036**	0.0005	**0.031**	0.030	**0.205**	0.062
860.8044	C55H106O5N	**51:3**	**0.013**	0.005	**0.660**	0.246	**49.443**	0.0004	**0.392**	0.121	**0.487**	0.213
862.82	C55H108O5N	**51:2**	**0.021**	0.010	**1.440**	0.626	**69.977**	0.001	**0.595**	0.285	**0.979**	0.278
864.8356	C55H110O5N	**51:1**	**0.022**	0.006	**2.750**	1.893	**123.505**	0.0122	**0.661**	0.146	**1.575**	0.276
866.8512	C55H112O5N	**51:0**	**0.002**	0.002	**0.133**	0.106	**58.911**	0.0254	**0.066**	0.069	**0.077**	0.024
868.7369	C55H98O6N	**52:6**	**0.033**	0.009	**0.939**	0.411	**28.406**	0.0012	**0.967**	0.174	**0.699**	0.334
870.7525	C55H100O6N	**52:5**	**0.051**	0.018	**2.629**	1.006	**51.326**	0.0004	**1.502**	0.478	**1.913**	0.804
872.7681	C55H102O6N	**52:4**	**0.043**	0.013	**12.829**	6.282	**301.277**	0.0019	**1.247**	0.304	**8.351**	1.723
874.7837	C55H104O6N	**52:3**	**0.022**	0.010	**18.883**	11.672	**854.514**	0.0068	**0.633**	0.276	**10.865**	0.900
876.7993	C55H106O6N	**52:2**	**0.023**	0.008	**46.135**	34.135	**2011.192**	0.0165	**0.683**	0.234	**24.271**	7.147
878.8149	C55H108O6N	**52:1**	**0.010**	0.003	**5.013**	3.857	**491.740**	0.0199	**0.311**	0.110	**2.498**	1.129
880.8305	C55H110O6N	**52:0**	**0.003**	0.003	**0.112**	0.072	**35.358**	0.0092	**0.088**	0.070	**0.068**	0.034
884.8044	C57H106O5N	**53:5**	**0.000**	0.000	**0.031**	0.026	**INF**	0.0322	**0.000**	0.000	**0.021**	0.011
886.82	C57H108O5N	**53:4**	**0.016**	0.008	**0.261**	0.172	**16.600**	0.0126	**0.516**	0.352	**0.147**	0.019
888.8356	C57H110O5N	**53:3**	**0.015**	0.005	**0.463**	0.360	**31.663**	0.0236	**0.430**	0.123	**0.251**	0.078
890.8512	C57H112O5N	**53:2**	**0.002**	0.002	**1.501**	1.708	**654.422**	0.0854	**0.077**	0.077	**0.703**	0.558
892.8668	C57H114O5N	**53:1**	**0.002**	0.001	**0.424**	0.368	**216.467**	0.0334	**0.056**	0.026	**0.211**	0.101
900.7993	C57H106O6N	**54:4**	**0.001**	0.001	**0.062**	0.025	**59.457**	0.0005	**0.031**	0.030	**0.043**	0.017
902.8149	C57H108O6N	**54:3**	**0.003**	0.003	**0.131**	0.091	**39.844**	0.0138	**0.086**	0.068	**0.071**	0.015
904.8305	C57H110O6N	**54:2**	**0.003**	0.003	**0.785**	0.809	**244.758**	0.0626	**0.097**	0.075	**0.384**	0.240
906.8461	C57H112O6N	**54:1**	**0.000**	0.001	**0.112**	0.076	**224.611**	0.011	**0.017**	0.022	**0.061**	0.015
908.8617	C57H114O6N	**54:0**	**0.000**	0.000	**0.018**	0.016	**116.477**	0.0456	**0.006**	0.013	**0.008**	0.005
918.8824	C59H116O5N	**55:1**	**0.000**	0.000	**0.050**	0.065	**INF**	0.1266	**0.000**	0.000	**0.021**	0.024
Total TAG +NL273 16:0 acyl containing			**3.392**	**0.661**	**168.034**	**98.095**	**49.541**	**0.0056**	**100.000**	**0.000**	**100.000**	**0.000**
764.6745	C47H90O6N	**44:2**	**1.034**	0.147	**1.098**	0.293	**1.062**	0.6751	**26.751**	1.928	**1.982**	0.523
766.6901	C47H92O6N	**44:1**	**0.084**	0.024	**0.224**	0.107	**2.670**	0.021	**2.124**	0.326	**0.363**	0.054
768.7057	C47H94O6N	**44:0**	**0.042**	0.015	**0.134**	0.032	**3.215**	0.0004	**1.066**	0.281	**0.245**	0.071
776.7108	C49H94O5N	**45:3**	**0.007**	0.003	**0.035**	0.028	**5.220**	0.0513	**0.170**	0.076	**0.051**	0.020

782.7576	C49H100O5N	**45:0**	**0.010**	0.005	**0.032**	0.015	**3.228**	0.0128	**0.248**	0.089	**0.054**	0.023
790.6901	C49H92O6N	**46:3**	**0.009**	0.004	**0.060**	0.021	**6.447**	0.0008	**0.239**	0.077	**0.108**	0.038
792.7057	C49H94O6N	**46:2**	**0.151**	0.023	**0.197**	0.067	**1.305**	0.1853	**3.895**	0.217	**0.353**	0.115
794.7213	C49H96O6N	**46:1**	**0.028**	0.009	**0.060**	0.022	**2.136**	0.0173	**0.715**	0.142	**0.115**	0.056
796.7369	C49H98O6N	**46:0**	**0.110**	0.017	**0.132**	0.060	**1.199**	0.4461	**2.852**	0.391	**0.237**	0.089
802.7264	C51H96O5N	**47:4**	**0.009**	0.006	**0.043**	0.023	**4.901**	0.0122	**0.217**	0.122	**0.074**	0.028
804.742	C51H98O5N	**47:3**	**0.002**	0.003	**0.027**	0.012	**15.373**	0.0016	**0.045**	0.075	**0.047**	0.009
806.7576	C51H100O5N	**47:2**	**0.006**	0.005	**0.033**	0.014	**5.659**	0.0044	**0.148**	0.115	**0.060**	0.022
810.7888	C51H104O5N	**47:0**	**0.002**	0.002	**0.082**	0.034	**39.565**	0.0008	**0.055**	0.040	**0.141**	0.040
816.7057	C51H94O6N	**48:4**	**0.003**	0.001	**0.184**	0.053	**66.501**	0.0001	**0.069**	0.023	**0.335**	0.100
818.7213	C51H96O6N	**48:3**	**0.009**	0.005	**0.212**	0.091	**24.608**	0.001	**0.220**	0.110	**0.380**	0.126
820.7369	C51H98O6N	**48:2**	**0.007**	0.006	**0.052**	0.023	**7.248**	0.0029	**0.185**	0.134	**0.087**	0.014
824.7681	C51H102O6N	**48:0**	**0.012**	0.006	**0.033**	0.018	**2.767**	0.041	**0.323**	0.186	**0.054**	0.022
830.7576	C53H100O5N	**49:4**	**0.038**	0.009	**0.122**	0.046	**3.227**	0.0038	**0.972**	0.183	**0.209**	0.036
832.7732	C53H102O5N	**49:3**	**0.011**	0.008	**0.183**	0.052	**16.849**	0.0001	**0.270**	0.190	**0.347**	0.145
834.7888	C53H104O5N	**49:2**	**1.154**	0.221	**2.882**	0.850	**2.498**	0.0023	**29.591**	1.469	**5.149**	1.205
836.8044	C53H106O5N	**49:1**	**0.052**	0.018	**0.762**	0.270	**14.650**	0.0004	**1.317**	0.358	**1.366**	0.396
838.82	C53H108O5N	**49:0**	**0.010**	0.008	**0.722**	0.268	**71.282**	0.0003	**0.244**	0.171	**1.256**	0.243
844.7369	C53H98O6N	**50:4**	**0.024**	0.012	**1.106**	0.402	**45.505**	0.0003	**0.595**	0.257	**1.929**	0.362
846.7525	C53H100O6N	**50:3**	**0.051**	0.019	**2.014**	0.964	**39.573**	0.0019	**1.270**	0.320	**3.398**	0.576
848.7681	C53H102O6N	**50:2**	**0.009**	0.007	**0.018**	0.019	**1.938**	0.3589	**0.234**	0.179	**0.029**	0.024
850.7837	C53H104O6N	**50:1**	**0.133**	0.036	**0.159**	0.051	**1.189**	0.3865	**3.497**	0.950	**0.282**	0.068
852.7993	C53H106O6N	**50:0**	**0.090**	0.014	**0.169**	0.048	**1.868**	0.0074	**2.347**	0.294	**0.305**	0.090
856.7732	C55H102O5N	**51:5**	**0.197**	0.060	**0.724**	0.240	**3.678**	0.0014	**4.980**	1.068	**1.272**	0.270
858.7888	C55H104O5N	**51:4**	**0.037**	0.018	**0.481**	0.125	**13.158**	0.0001	**0.953**	0.436	**0.903**	0.350
860.8044	C55H106O5N	**51:3**	**0.015**	0.007	**0.393**	0.151	**25.618**	0.0005	**0.389**	0.158	**0.708**	0.221
862.82	C55H108O5N	**51:2**	**0.068**	0.007	**2.029**	0.644	**30.056**	0.0001	**1.773**	0.315	**3.653**	1.023
864.8356	C55H110O5N	**51:1**	**0.034**	0.014	**1.353**	0.504	**39.894**	0.0004	**0.836**	0.296	**2.331**	0.339
866.8512	C55H112O5N	**51:0**	**0.031**	0.012	**6.445**	3.409	**208.285**	0.003	**0.779**	0.249	**10.176**	1.488
868.7369	C55H98O6N	**52:6**	**0.063**	0.030	**4.089**	1.915	**64.679**	0.0015	**1.563**	0.639	**6.687**	0.246
870.7525	C55H100O6N	**52:5**	**0.055**	0.024	**3.859**	1.653	**70.417**	0.0009	**1.373**	0.577	**6.492**	0.601
872.7681	C55H102O6N	**52:4**	**0.029**	0.017	**11.423**	5.695	**398.086**	0.0021	**0.709**	0.369	**18.400**	1.084
874.7837	C55H104O6N	**52:3**	**0.013**	0.014	**0.225**	0.166	**17.168**	0.0218	**0.326**	0.299	**0.322**	0.185
876.7993	C55H106O6N	**52:2**	**0.007**	0.008	**0.052**	0.027	**7.309**	0.0071	**0.204**	0.241	**0.089**	0.050
878.8149	C55H108O6N	**52:1**	**0.001**	0.001	**0.030**	0.011	**25.497**	0.0005	**0.027**	0.029	**0.055**	0.022
880.8305	C55H110O6N	**52:0**	**0.003**	0.003	**0.153**	0.075	**47.043**	0.0022	**0.079**	0.068	**0.250**	0.022
882.7888	C57H104O5N	**53:6**	**0.006**	0.004	**0.307**	0.124	**52.195**	0.0006	**0.150**	0.105	**0.531**	0.099
884.8044	C57H106O5N	**53:5**	**0.012**	0.006	**0.356**	0.148	**29.731**	0.0008	**0.299**	0.161	**0.617**	0.127

886.82	C57H108O5N	**53:4**	**0.003**	0.001	**0.911**	0.449	**289.654**	0.0019	**0.087**	0.047	**1.471**	0.122
888.8356	C57H110O5N	**53:3**	**0.000**	0.001	**0.043**	0.021	**93.647**	0.0021	**0.011**	0.025	**0.076**	0.048
890.8512	C57H112O5N	**53:2**	**0.031**	0.006	**0.387**	0.156	**12.294**	0.0009	**0.822**	0.177	**0.666**	0.115
892.8668	C57H114O5N	**53:1**	**0.025**	0.014	**0.457**	0.182	**18.194**	0.0007	**0.634**	0.327	**0.827**	0.286
894.7525	C57H100O6N	**53:0**	**0.017**	0.011	**2.325**	0.924	**136.941**	0.0005	**0.415**	0.283	**3.964**	0.473
896.7681	C57H102O6N	**54:6**	**0.008**	0.006	**3.219**	1.597	**383.813**	0.002	**0.210**	0.154	**5.183**	0.328
898.7837	C57H104O6N	**54:5**	**0.002**	0.002	**7.910**	4.664	**3463.388**	0.0053	**0.060**	0.044	**12.078**	3.157
900.7993	C57H106O6N	**54:4**	**0.003**	0.002	**2.215**	1.579	**794.953**	0.014	**0.069**	0.031	**3.164**	1.371
908.8617	C57H114O6N	**54:0**	**0.088**	0.006	**0.143**	0.049	**1.623**	0.0361	**2.346**	0.609	**0.257**	0.070
910.82	C59H108O5N	**55:6**	**0.016**	0.003	**0.105**	0.053	**6.608**	0.0054	**0.419**	0.116	**0.176**	0.042
912.8356	C59H110O5N	**55:5**	**0.000**	0.001	**0.172**	0.128	**505.287**	0.0169	**0.008**	0.018	**0.245**	0.137
914.8512	C59H112O5N	**55:4**	**0.000**	0.000	**0.059**	0.032	**268.649**	0.0036	**0.005**	0.012	**0.093**	0.020
924.7993	C59H106O6N	**56:6**	**0.024**	0.018	**0.062**	0.025	**2.642**	0.0231	**0.594**	0.371	**0.117**	0.055
926.8149	C59H108O6N	**56:5**	**0.008**	0.007	**0.109**	0.051	**13.782**	0.0021	**0.217**	0.177	**0.178**	0.021
928.8305	C59H110O6N	**56:4**	**0.000**	0.000	**0.041**	0.024	**714.365**	0.0059	**0.002**	0.003	**0.063**	0.013
Total TAG +NL18:3 acyl containing			**3.893**	**0.662**	**60.852**	**27.875**	**15.632**	**0.0018**	**100.000**	**0.000**	**100.000**	**0.000**
764.6745	C47H90O6N	**44:2**	**0.042**	0.013	**0.145**	0.054	**3.495**	0.0031	**2.491**	0.546	**0.207**	0.088
766.6901	C47H92O6N	**44:1**	**0.079**	0.011	**0.190**	0.072	**2.398**	0.0089	**4.892**	0.883	**0.264**	0.101
768.7057	C47H94O6N	**44:0**	**0.041**	0.016	**0.156**	0.049	**3.803**	0.001	**2.532**	0.933	**0.234**	0.118
776.7108	C49H94O5N	**45:3**	**0.009**	0.005	**0.173**	0.147	**18.812**	0.0382	**0.583**	0.337	**0.176**	0.076
778.7264	C49H96O5N	**45:0**	**0.008**	0.003	**0.050**	0.047	**6.404**	0.0828	**0.481**	0.173	**0.052**	0.030
790.6901	C49H92O6N	**46:3**	**0.005**	0.003	**0.190**	0.104	**42.014**	0.0041	**0.271**	0.158	**0.232**	0.037
792.7057	C49H94O6N	**46:2**	**0.012**	0.009	**0.110**	0.037	**9.059**	0.0004	**0.742**	0.532	**0.157**	0.064
794.7213	C49H96O6N	**46:1**	**0.020**	0.007	**0.046**	0.012	**2.244**	0.0039	**1.294**	0.541	**0.075**	0.047
796.7369	C49H98O6N	**46:0**	**0.062**	0.007	**0.098**	0.048	**1.598**	0.1276	**3.784**	0.515	**0.140**	0.064
802.7264	C51H96O5N	**47:4**	**0.008**	0.008	**0.193**	0.187	**25.111**	0.0576	**0.450**	0.446	**0.176**	0.129
804.742	C51H98O5N	**47:3**	**0.005**	0.003	**0.079**	0.054	**14.430**	0.0165	**0.339**	0.192	**0.094**	0.028
806.7576	C51H100O5N	**47:2**	**0.002**	0.002	**0.041**	0.018	**19.398**	0.0014	**0.118**	0.096	**0.059**	0.029
808.7732	C51H102O5N	**47:1**	**0.006**	0.002	**0.019**	0.016	**3.022**	0.1079	**0.384**	0.082	**0.022**	0.011
816.7057	C51H94O6N	**48:4**	**0.010**	0.006	**0.261**	0.135	**25.624**	0.0033	**0.636**	0.340	**0.318**	0.038
818.7213	C51H96O6N	**48:3**	**0.002**	0.001	**0.215**	0.085	**93.500**	0.0005	**0.144**	0.070	**0.290**	0.090
820.7369	C51H98O6N	**48:2**	**0.009**	0.010	**0.330**	0.140	**38.474**	0.0009	**0.492**	0.521	**0.483**	0.233
822.7525	C51H100O6N	**48:1**	**0.007**	0.006	**0.018**	0.010	**2.447**	0.0729	**0.421**	0.314	**0.029**	0.018
830.7576	C53H100O5N	**49:4**	**0.131**	0.016	**0.178**	0.066	**1.353**	0.1654	**8.132**	1.501	**0.255**	0.110
832.7732	C53H102O5N	**49:3**	**0.006**	0.005	**0.098**	0.051	**17.846**	0.0039	**0.383**	0.450	**0.152**	0.089
834.7888	C53H104O5N	**49:2**	**0.012**	0.008	**0.274**	0.095	**22.414**	0.0003	**0.708**	0.420	**0.413**	0.229
836.8044	C53H106O5N	**49:1**	**0.340**	0.073	**1.500**	0.536	**4.413**	0.0014	**20.566**	2.004	**2.116**	0.835
838.82	C53H108O5N	**49:0**	**0.004**	0.005	**0.370**	0.099	**96.904**	0.0001	**0.220**	0.277	**0.555**	0.284

844.7369	C53H98O6N	**50:4**	**0.051**	0.017	**2.173**	1.131	**42.813**	0.003	**2.998**	0.766	**2.657**	0.344
846.7525	C53H100O6N	**50:3**	**0.019**	0.007	**1.659**	0.766	**85.506**	0.0014	**1.168**	0.319	**2.124**	0.454
848.7681	C53H102O6N	**50:2**	**0.072**	0.024	**3.907**	1.941	**54.622**	0.0022	**4.359**	1.157	**4.941**	1.092
852.7993	C53H106O6N	**50:0**	**0.062**	0.011	**0.093**	0.041	**1.489**	0.1447	**3.886**	0.983	**0.127**	0.048
856.7732	C55H102O5N	**51:5**	**0.019**	0.016	**0.339**	0.136	**17.819**	0.0008	**1.088**	0.875	**0.492**	0.226
858.7888	C55H104O5N	**51:4**	**0.043**	0.016	**0.448**	0.196	**10.500**	0.0018	**2.539**	0.758	**0.588**	0.153
860.8044	C55H106O5N	**51:3**	**0.013**	0.007	**0.645**	0.237	**50.532**	0.0003	**0.770**	0.374	**0.902**	0.338
862.82	C55H108O5N	**51:2**	**0.016**	0.009	**0.776**	0.324	**48.729**	0.0008	**0.942**	0.419	**1.076**	0.411
864.8356	C55H110O5N	**51:1**	**0.028**	0.011	**1.204**	0.428	**43.112**	0.0003	**1.726**	0.644	**1.705**	0.686
866.8512	C55H112O5N	**51:0**	**0.020**	0.007	**1.114**	0.428	**55.482**	0.0004	**1.229**	0.395	**1.527**	0.556
868.7369	C55H98O6N	**52:6**	**0.015**	0.010	**2.499**	1.262	**170.909**	0.0023	**0.850**	0.496	**3.097**	0.464
870.7525	C55H100O6N	**52:5**	**0.050**	0.019	**4.889**	2.482	**97.044**	0.0024	**3.045**	1.005	**6.039**	0.879
872.7681	C55H102O6N	**52:4**	**0.000**	0.000	**6.334**	3.526	**INF**	0.0039	**0.000**	0.000	**7.478**	0.381
874.7837	C55H104O6N	**52:3**	**0.013**	0.012	**18.976**	11.627	**1405.964**	0.0065	**0.798**	0.697	**21.410**	1.519
876.7993	C55H106O6N	**52:2**	**0.012**	0.013	**1.080**	0.765	**93.725**	0.0142	**0.629**	0.643	**1.121**	0.330
878.8149	C55H108O6N	**52:1**	**0.000**	0.000	**0.040**	0.027	**INF**	0.0105	**0.000**	0.000	**0.044**	0.015
880.8305	C55H110O6N	**52:0**	**0.000**	0.001	**0.028**	0.005	**85.201**	0.0001	**0.027**	0.061	**0.045**	0.027
882.7888	C57H104O5N	**53:6**	**0.002**	0.002	**0.110**	0.057	**64.279**	0.0027	**0.102**	0.127	**0.138**	0.027
884.8044	C57H106O5N	**53:5**	**0.006**	0.002	**0.318**	0.140	**54.841**	0.0011	**0.347**	0.116	**0.441**	0.177
886.82	C57H108O5N	**53:4**	**0.011**	0.006	**0.574**	0.273	**54.440**	0.0017	**0.614**	0.333	**0.727**	0.136
888.8356	C57H110O5N	**53:3**	**0.011**	0.008	**1.521**	0.876	**133.600**	0.0049	**0.739**	0.520	**1.768**	0.072
890.8512	C57H112O5N	**53:2**	**0.001**	0.001	**0.146**	0.092	**138.447**	0.0076	**0.061**	0.061	**0.172**	0.046
892.8668	C57H114O5N	**53:1**	**0.011**	0.005	**0.259**	0.109	**24.311**	0.0009	**0.648**	0.246	**0.393**	0.216
894.7525	C57H100O6N	**53:0**	**0.030**	0.011	**0.744**	0.323	**24.511**	0.0011	**1.786**	0.466	**1.024**	0.379
896.7681	C57H102O6N	**54:6**	**0.013**	0.007	**3.465**	1.695	**264.623**	0.0019	**0.797**	0.406	**4.397**	0.907
898.7837	C57H104O6N	**54:5**	**0.004**	0.006	**5.305**	3.467	**1313.312**	0.0091	**0.237**	0.327	**5.787**	0.866
900.7993	C57H106O6N	**54:4**	**0.003**	0.002	**17.365**	12.644	**6823.850**	0.0153	**0.174**	0.166	**17.710**	5.679
902.8149	C57H108O6N	**54:3**	**0.005**	0.004	**3.595**	2.690	**668.238**	0.0175	**0.316**	0.275	**3.557**	1.365
904.8305	C57H110O6N	**54:2**	**0.004**	0.004	**0.159**	0.119	**38.123**	0.0198	**0.256**	0.222	**0.158**	0.062
908.8617	C57H114O6N	**54:0**	**0.024**	0.011	**0.052**	0.019	**2.187**	0.0227	**1.441**	0.628	**0.084**	0.054
910.82	C59H108O5N	**55:6**	**0.110**	0.023	**0.304**	0.185	**2.761**	0.0489	**6.679**	1.007	**0.404**	0.160
912.8356	C59H110O5N	**55:5**	**0.010**	0.009	**0.184**	0.139	**17.998**	0.024	**0.622**	0.495	**0.187**	0.066
914.8512	C59H112O5N	**55:4**	**0.001**	0.001	**0.370**	0.357	**264.781**	0.0498	**0.079**	0.080	**0.341**	0.229
916.8668	C59H114O5N	**55:3**	**0.000**	0.000	**0.137**	0.100	**INF**	0.0159	**0.000**	0.000	**0.143**	0.047
924.7993	C59H106O6N	**56:6**	**0.016**	0.010	**0.059**	0.033	**3.797**	0.0224	**0.921**	0.476	**0.079**	0.039
926.8149	C59H108O6N	**56:5**	**0.090**	0.031	**0.143**	0.032	**1.594**	0.0293	**5.442**	1.401	**0.220**	0.116
928.8305	C59H110O6N	**56:4**	**0.008**	0.006	**0.183**	0.152	**22.352**	0.0329	**0.523**	0.351	**0.184**	0.079
930.8461	C59H112O6N	**56:3**	**0.001**	0.002	**0.113**	0.080	**147.387**	0.0133	**0.041**	0.079	**0.127**	0.041

940.8668	C61H114O5N	**57:5**	**0.010**	0.008	**0.011**	0.004	**1.160**	0.7818	**0.559**	0.422	**0.021**	0.017
942.8824	C61H116O5N	**57:4**	**0.011**	0.007	**0.013**	0.010	**1.226**	0.6665	**0.649**	0.380	**0.017**	0.008
956.8617	C61H114O6N	**58:4**	**0.013**	0.012	**0.012**	0.007	**0.937**	0.8729	**0.760**	0.688	**0.015**	0.005
958.8773	C61H116O6N	**58:3**	**0.002**	0.003	**0.035**	0.027	**22.242**	0.0222	**0.091**	0.144	**0.035**	0.020
Total TAG +NL297 18:2 acyl containing			**1.648**	**0.277**	**86.116**	**49.621**	**52.240**	**0.0052**	**100.000**	**0.000**	**100.000**	**0.000**
764.6745	C47H90O6N	**44:2**	**0.210**	0.027	**0.394**	0.171	**1.877**	0.0446	**33.536**	4.399	**0.194**	0.085
766.6901	C47H92O6N	**44:1**	**0.017**	0.009	**0.163**	0.088	**9.675**	0.0061	**2.607**	1.110	**0.074**	0.026
768.7057	C47H94O6N	**44:0**	**0.004**	0.002	**0.036**	0.019	**9.674**	0.0055	**0.581**	0.214	**0.023**	0.018
776.7108	C49H94O5N	**45:3**	**0.001**	0.001	**0.082**	0.072	**58.711**	0.0365	**0.203**	0.195	**0.025**	0.012
778.7264	C49H96O5N	**45:2**	**0.005**	0.001	**0.539**	0.591	**105.193**	0.0778	**0.857**	0.396	**0.160**	0.115
780.742	C49H98O5N	**45:1**	**0.006**	0.005	**0.098**	0.080	**15.575**	0.0339	**0.938**	0.676	**0.035**	0.010
782.7576	C49H100O5N	**45:0**	**0.003**	0.003	**0.026**	0.028	**9.155**	0.0959	**0.448**	0.493	**0.008**	0.006
790.6901	C49H92O6N	**46:3**	**0.001**	0.002	**0.148**	0.091	**109.096**	0.007	**0.234**	0.321	**0.064**	0.021
792.7057	C49H94O6N	**46:2**	**0.020**	0.005	**0.482**	0.297	**24.655**	0.0083	**3.056**	0.372	**0.198**	0.038
794.7213	C49H96O6N	**46:1**	**0.004**	0.005	**0.158**	0.095	**39.688**	0.007	**0.592**	0.722	**0.070**	0.022
796.7369	C49H98O6N	**46:0**	**0.003**	0.003	**0.031**	0.023	**9.686**	0.0314	**0.490**	0.363	**0.014**	0.006
802.7264	C51H96O5N	**47:4**	**0.003**	0.003	**0.137**	0.121	**41.607**	0.0383	**0.501**	0.332	**0.043**	0.021
804.742	C51H98O5N	**47:3**	**0.001**	0.001	**0.759**	0.861	**537.300**	0.0848	**0.229**	0.178	**0.207**	0.186
806.7576	C51H100O5N	**47:2**	**0.002**	0.004	**0.194**	0.174	**92.814**	0.0391	**0.336**	0.658	**0.064**	0.026
808.7732	C51H102O5N	**47:1**	**0.001**	0.003	**0.078**	0.052	**66.935**	0.0107	**0.159**	0.351	**0.036**	0.015
816.7057	C51H94O6N	**48:4**	**0.000**	0.001	**0.193**	0.073	**389.593**	0.0004	**0.085**	0.119	**0.102**	0.056
818.7213	C51H96O6N	**48:3**	**0.001**	0.001	**0.480**	0.389	**426.116**	0.0249	**0.174**	0.162	**0.181**	0.050
820.7369	C51H98O6N	**48:2**	**0.001**	0.001	**0.393**	0.203	**351.513**	0.0025	**0.182**	0.159	**0.181**	0.063
822.7525	C51H100O6N	**48:1**	**0.008**	0.006	**0.654**	0.260	**85.194**	0.0005	**1.139**	0.816	**0.340**	0.177
830.7576	C53H100O5N	**49:4**	**0.001**	0.002	**0.101**	0.045	**76.258**	0.0011	**0.211**	0.269	**0.054**	0.033
832.7732	C53H102O5N	**49:3**	**0.019**	0.012	**0.168**	0.100	**8.621**	0.0111	**2.975**	1.855	**0.073**	0.023
834.7888	C53H104O5N	**49:2**	**0.001**	0.001	**0.155**	0.071	**176.713**	0.0012	**0.145**	0.137	**0.076**	0.037
836.8044	C53H106O5N	**49:1**	**0.002**	0.002	**0.451**	0.177	**255.319**	0.0005	**0.263**	0.329	**0.247**	0.153
838.82	C53H108O5N	**49:0**	**0.109**	0.015	**1.275**	0.534	**11.697**	0.0012	**17.499**	3.101	**0.649**	0.315
844.7369	C53H98O6N	**50:4**	**0.007**	0.006	**2.709**	1.336	**362.454**	0.0019	**1.117**	0.744	**1.287**	0.506
846.7525	C53H100O6N	**50:3**	**0.018**	0.009	**2.199**	1.146	**123.128**	0.0028	**2.736**	1.216	**0.994**	0.324
848.7681	C53H102O6N	**50:2**	**0.005**	0.003	**3.223**	1.789	**704.887**	0.0038	**0.692**	0.419	**1.392**	0.333
850.7837	C53H104O6N	**50:1**	**0.018**	0.007	**8.979**	5.250	**499.421**	0.0051	**2.835**	0.941	**3.763**	0.753
852.7993	C53H106O6N	**50:0**	**0.000**	0.000	**0.028**	0.015	**INF**	0.0034	**0.000**	0.000	**0.018**	0.021
856.7732	C55H102O5N	**51:5**	**0.005**	0.005	**0.102**	0.048	**19.566**	0.002	**0.875**	0.831	**0.055**	0.033
858.7888	C55H104O5N	**51:4**	**0.001**	0.001	**0.425**	0.198	**291.033**	0.0014	**0.256**	0.247	**0.221**	0.124
860.8044	C55H106O5N	**51:3**	**0.014**	0.003	**0.634**	0.265	**46.454**	0.0008	**2.169**	0.298	**0.327**	0.167
862.82	C55H108O5N	**51:2**	**0.001**	0.002	**1.469**	0.779	**1286.630**	0.0029	**0.216**	0.334	**0.656**	0.194

864.8356	C55H110O5N	**51:1**	**0.002**	0.002	**1.084**	0.506	**713.626**	0.0014	**0.234**	0.287	**0.533**	0.262
866.8512	C55H112O5N	**51:0**	**0.007**	0.005	**4.879**	2.550	**664.827**	0.0027	**1.138**	0.776	**2.222**	0.740
868.7369	C55H98O6N	**52:6**	**0.003**	0.003	**1.909**	0.919	**639.065**	0.0017	**0.466**	0.394	**0.897**	0.332
870.7525	C55H100O6N	**52:5**	**0.007**	0.007	**5.250**	3.015	**789.705**	0.0046	**1.009**	1.095	**2.227**	0.479
872.7681	C55H102O6N	**52:4**	**0.025**	0.010	**10.886**	5.675	**439.472**	0.0027	**3.847**	1.412	**4.953**	1.621
874.7837	C55H104O6N	**52:3**	**0.042**	0.011	**16.964**	10.450	**404.845**	0.0068	**6.532**	0.911	**6.828**	0.875
876.7993	C55H106O6N	**52:2**	**0.023**	0.008	**67.291**	47.275	**2947.496**	0.013	**3.563**	1.004	**24.431**	1.973
878.8149	C55H108O6N	**52:1**	**0.003**	0.003	**1.591**	1.252	**530.845**	0.0219	**0.464**	0.507	**0.504**	0.212
880.8305	C55H110O6N	**52:0**	**0.000**	0.000	**0.284**	0.194	**INF**	0.0112	**0.000**	0.000	**0.107**	0.009
882.7888	C57H104O5N	**53:6**	**0.000**	0.001	**0.073**	0.049	**322.122**	0.0112	**0.033**	0.073	**0.035**	0.018
884.8044	C57H106O5N	**53:5**	**0.000**	0.001	**0.276**	0.149	**1167.954**	0.0032	**0.039**	0.087	**0.123**	0.041
886.82	C57H108O5N	**53:4**	**0.001**	0.000	**0.802**	0.438	**1491.676**	0.0035	**0.094**	0.088	**0.375**	0.152
888.8356	C57H110O5N	**53:3**	**0.001**	0.002	**1.254**	0.692	**1227.801**	0.0037	**0.165**	0.275	**0.544**	0.134
890.8512	C57H112O5N	**53:2**	**0.003**	0.004	**4.072**	2.828	**1457.424**	0.0123	**0.399**	0.575	**1.491**	0.094
892.8668	C57H114O5N	**53:1**	**0.000**	0.001	**0.206**	0.128	**547.733**	0.0072	**0.061**	0.123	**0.083**	0.016
894.7525	C57H100O6N	**53:0**	**0.001**	0.001	**0.808**	0.373	**664.955**	0.0013	**0.186**	0.118	**0.432**	0.246
896.7681	C57H102O6N	**54:6**	**0.004**	0.003	**2.285**	1.121	**571.523**	0.0019	**0.643**	0.431	**1.100**	0.470
898.7837	C57H104O6N	**54:5**	**0.005**	0.003	**12.137**	6.991	**2493.022**	0.0047	**0.747**	0.364	**5.133**	1.077
900.7993	C57H106O6N	**54:4**	**0.002**	0.002	**22.828**	15.537	**10321.892**	0.0111	**0.367**	0.377	**8.457**	0.460
902.8149	C57H108O6N	**54:3**	**0.003**	0.004	**63.426**	47.642	**21535.386**	0.0177	**0.551**	0.853	**21.441**	4.822
904.8305	C57H110O6N	**54:2**	**0.003**	0.002	**15.569**	12.317	**5458.968**	0.0223	**0.471**	0.316	**4.920**	1.843
906.8461	C57H112O6N	**54:1**	**0.000**	0.000	**0.200**	0.234	**INF**	0.0934	**0.000**	0.000	**0.077**	0.054
908.8617	C57H114O6N	**54:0**	**0.000**	0.000	**0.064**	0.062	**INF**	0.0488	**0.000**	0.000	**0.020**	0.011
910.82	C59H108O5N	**55:6**	**0.001**	0.001	**0.034**	0.026	**62.373**	0.0211	**0.081**	0.114	**0.013**	0.005
912.8356	C59H110O5N	**55:5**	**0.002**	0.001	**0.169**	0.107	**100.199**	0.0084	**0.300**	0.272	**0.066**	0.015
914.8512	C59H112O5N	**55:4**	**0.000**	0.000	**0.441**	0.349	**INF**	0.0223	**0.000**	0.000	**0.152**	0.037
916.8668	C59H114O5N	**55:3**	**0.000**	0.001	**1.340**	1.354	**2839.580**	0.0581	**0.078**	0.173	**0.397**	0.256
918.8824	C59H116O5N	**55:2**	**0.000**	0.000	**0.392**	0.349	**INF**	0.0363	**0.000**	0.000	**0.125**	0.054
920.898	C59H118O5N	**55:1**	**0.000**	0.000	**0.037**	0.027	**INF**	0.0188	**0.000**	0.000	**0.012**	0.003
926.8149	C59H108O6N	**56:5**	**0.001**	0.001	**0.065**	0.037	**72.911**	0.0047	**0.135**	0.137	**0.030**	0.013
928.8305	C59H110O6N	**56:4**	**0.000**	0.000	**0.160**	0.119	**INF**	0.017	**0.000**	0.000	**0.057**	0.011
930.8461	C59H112O6N	**56:3**	**0.000**	0.001	**0.679**	0.549	**1475.889**	0.0245	**0.063**	0.140	**0.227**	0.065
932.8617	C59H114O6N	**56:2**	**0.000**	0.000	**0.278**	0.194	**INF**	0.0125	**0.000**	0.000	**0.103**	0.016
934.8773	C59H116O6N	**56:1**	**0.000**	0.000	**0.051**	0.042	**INF**	0.0274	**0.000**	0.000	**0.015**	0.009
944.898	C61H118O5N	**57:3**	**0.000**	0.000	**0.028**	0.035	**INF**	0.1149	**0.000**	0.000	**0.007**	0.008
960.8929	C61H118O6N	**58:2**	**0.000**	0.000	**0.049**	0.043	**INF**	0.0356	**0.000**	0.000	**0.014**	0.009
974.9448	C63H124O5N	**59:2**	**0.000**	0.000	**0.027**	0.029	**INF**	0.0731	**0.000**	0.000	**0.008**	0.007
988.9241	C63H122O6N	**60:2**	**0.000**	0.000	**0.035**	0.028	**INF**	0.0255	**0.000**	0.000	**0.011**	0.005

Total TAG +NL299 18:1 acyl containing			0.633	0.100	264.883	176.523	418.604	0.0101	100.000	0.000	100.000	0.000
764.6745	C47H90O6N	44:2	0.465	0.066	0.482	0.151	1.037	0.821	49.659	2.838	1.189	0.813
766.6901	C47H92O6N	44:1	0.039	0.003	0.085	0.037	2.194	0.0224	4.204	0.672	0.184	0.096
768.7057	C47H94O6N	44:0	0.012	0.012	0.051	0.022	4.144	0.0087	1.284	1.378	0.113	0.072
776.7108	C49H94O5N	45:3	0.005	0.008	0.041	0.037	8.188	0.0669	0.439	0.614	0.046	0.034
780.742	C49H98O5N	45:1	0.003	0.002	0.220	0.226	64.286	0.0654	0.401	0.289	0.286	0.191
782.7576	C49H100O5N	45:0	0.006	0.005	0.052	0.047	9.292	0.0588	0.535	0.412	0.087	0.046
792.7057	C49H94O6N	46:2	0.083	0.018	0.143	0.053	1.722	0.0428	8.769	0.744	0.325	0.201
794.7213	C49H96O6N	46:1	0.031	0.012	0.172	0.091	5.623	0.0087	3.165	0.776	0.336	0.138
796.7369	C49H98O6N	46:0	0.008	0.005	0.053	0.034	7.052	0.0164	0.802	0.623	0.115	0.065
804.742	C51H98O5N	47:3	0.001	0.001	0.030	0.042	25.047	0.1643	0.128	0.143	0.034	0.043
806.7576	C51H100O5N	47:2	0.001	0.002	0.309	0.359	248.084	0.0909	0.128	0.166	0.356	0.359
808.7732	C51H102O5N	47:1	0.002	0.003	0.070	0.053	28.165	0.0224	0.255	0.250	0.126	0.049
810.7888	C51H104O5N	47:0	0.002	0.004	0.037	0.015	21.175	0.001	0.144	0.322	0.088	0.060
818.7213	C51H96O6N	48:3	0.001	0.001	0.033	0.022	55.062	0.0109	0.054	0.076	0.059	0.021
820.7369	C51H98O6N	48:2	0.003	0.003	0.178	0.175	52.724	0.0552	0.388	0.354	0.243	0.145
822.7525	C51H100O6N	48:1	0.002	0.001	0.079	0.043	44.443	0.004	0.192	0.146	0.149	0.050
824.7681	C51H102O6N	48:0	0.004	0.001	0.091	0.049	22.784	0.0043	0.442	0.198	0.200	0.112
834.7888	C53H104O5N	49:2	0.026	0.004	0.063	0.049	2.429	0.1304	2.774	0.398	0.096	0.033
836.8044	C53H106O5N	49:1	0.001	0.001	0.030	0.023	40.701	0.0224	0.085	0.147	0.044	0.010
838.82	C53H108O5N	49:0	0.001	0.001	0.029	0.013	26.909	0.0015	0.127	0.131	0.099	0.105
844.7369	C53H98O6N	50:4	0.001	0.001	0.114	0.093	149.767	0.0268	0.065	0.097	0.204	0.137
846.7525	C53H100O6N	50:3	0.002	0.002	0.547	0.315	341.429	0.0047	0.147	0.163	1.042	0.382
848.7681	C53H102O6N	50:2	0.008	0.003	0.333	0.217	41.473	0.0101	0.882	0.394	0.543	0.063
850.7837	C53H104O6N	50:1	0.005	0.001	0.618	0.404	119.218	0.0095	0.556	0.143	1.016	0.129
852.7993	C53H106O6N	50:0	0.012	0.003	0.543	0.479	46.734	0.0382	1.229	0.294	1.226	0.861
856.7732	C55H102O5N	51:5	0.015	0.005	0.027	0.033	1.825	0.4335	1.559	0.504	0.051	0.042
858.7888	C55H104O5N	51:4	0.002	0.003	0.024	0.011	12.757	0.0025	0.221	0.317	0.056	0.041
860.8044	C55H106O5N	51:3	0.002	0.001	0.087	0.044	51.585	0.0025	0.195	0.158	0.181	0.087
862.82	C55H108O5N	51:2	0.002	0.002	0.112	0.048	56.868	0.0009	0.211	0.193	0.264	0.168
864.8356	C55H110O5N	51:1	0.001	0.001	0.263	0.167	406.618	0.0079	0.067	0.084	0.452	0.116
866.8512	C55H112O5N	51:0	0.001	0.001	0.060	0.050	77.571	0.0293	0.094	0.092	0.175	0.175
868.7369	C55H98O6N	52:6	0.001	0.001	1.655	1.053	1278.893	0.0079	0.140	0.140	2.831	0.585
870.7525	C55H100O6N	52:5	0.001	0.001	0.651	0.391	566.855	0.006	0.110	0.106	1.150	0.352
872.7681	C55H102O6N	52:4	0.001	0.001	1.533	0.976	1663.322	0.008	0.104	0.106	2.563	0.384
874.7837	C55H104O6N	52:3	0.010	0.006	1.995	1.235	197.392	0.007	1.019	0.386	3.603	1.405
876.7993	C55H106O6N	52:2	0.154	0.057	4.518	2.637	29.421	0.006	15.976	3.296	8.091	2.039
878.8149	C55H108O6N	52:1	0.008	0.009	13.442	9.479	1591.958	0.0132	0.902	0.930	20.311	1.360

882.7888	C57H104O5N	**53:6**	**0.000**	0.000	**0.059**	0.055	**INF**	0.0438	**0.000**	0.000	**0.067**	0.055
886.82	C57H108O5N	**53:4**	**0.000**	0.001	**0.067**	0.041	**298.327**	0.0062	**0.022**	0.049	**0.125**	0.068
888.8356	C57H110O5N	**53:3**	**0.000**	0.000	**0.160**	0.101	**INF**	0.0077	**0.000**	0.000	**0.311**	0.132
890.8512	C57H112O5N	**53:2**	**0.000**	0.000	**0.323**	0.208	**2377.302**	0.0085	**0.017**	0.023	**0.551**	0.111
892.8668	C57H114O5N	**53:1**	**0.010**	0.005	**0.958**	0.670	**97.012**	0.0133	**1.039**	0.445	**1.544**	0.278
894.7525	C57H100O6N	**53:0**	**0.000**	0.000	**0.041**	0.057	**87.508**	0.1534	**0.044**	0.036	**0.051**	0.055
896.7681	C57H102O6N	**54:6**	**0.000**	0.000	**0.252**	0.114	**956.546**	0.0011	**0.027**	0.029	**0.578**	0.352
898.7837	C57H104O6N	**54:5**	**0.000**	0.001	**0.563**	0.371	**2240.690**	0.0095	**0.029**	0.065	**1.016**	0.330
900.7993	C57H106O6N	**54:4**	**0.001**	0.001	**3.919**	2.384	**4005.164**	0.0063	**0.096**	0.084	**6.851**	1.505
902.8149	C57H108O6N	**54:3**	**0.001**	0.001	**6.123**	4.390	**4791.817**	0.0143	**0.129**	0.112	**9.065**	0.873
904.8305	C57H110O6N	**54:2**	**0.002**	0.002	**19.660**	14.850	**12567.517**	0.0181	**0.168**	0.196	**27.485**	5.892
906.8461	C57H112O6N	**54:1**	**0.003**	0.003	**2.280**	1.891	**740.219**	0.0274	**0.330**	0.319	**2.838**	1.338
908.8617	C57H114O6N	**54:0**	**0.004**	0.004	**0.085**	0.086	**20.347**	0.0692	**0.406**	0.327	**0.217**	0.177
914.8512	C59H112O5N	**55:4**	**0.000**	0.000	**0.051**	0.045	**INF**	0.0369	**0.000**	0.000	**0.060**	0.036
916.8668	C59H114O5N	**55:3**	**0.001**	0.001	**0.132**	0.120	**219.076**	0.0398	**0.070**	0.157	**0.167**	0.100
918.8824	C59H116O5N	**55:2**	**0.000**	0.000	**0.455**	0.499	**2586.609**	0.0756	**0.023**	0.052	**0.528**	0.490
920.898	C59H118O5N	**55:1**	**0.000**	0.000	**0.134**	0.114	**649.641**	0.0305	**0.024**	0.054	**0.172**	0.085
930.8461	C59H112O6N	**56:3**	**0.000**	0.001	**0.041**	0.033	**180.927**	0.0243	**0.022**	0.049	**0.054**	0.021
932.8617	C59H114O6N	**56:2**	**0.001**	0.002	**0.214**	0.193	**246.114**	0.0385	**0.101**	0.226	**0.276**	0.150
934.8773	C59H116O6N	**56:1**	**0.000**	0.000	**0.067**	0.055	**INF**	0.0266	**0.000**	0.000	**0.110**	0.041
Total TAG +NL301 18:0 acyl containing			**0.944**	**0.187**	**64.354**	**43.913**	**68.177**	**0.0121**	**100.000**	**0.000**	**100.000**	**0.000**
764.6745	C47H90O6N	**44:2**	**0.244**	0.056	**0.244**	0.066	**1.002**	0.988	**77.448**	3.481	**18.191**	7.770
766.6901	C47H92O6N	**44:1**	**0.014**	0.003	**0.030**	0.012	**2.090**	0.0237	**4.652**	1.085	**2.319**	1.301
792.7057	C49H94O6N	**46:2**	**0.023**	0.002	**0.042**	0.019	**1.819**	0.0553	**7.565**	0.953	**3.154**	1.563
834.7888	C53H104O5N	**49:2**	**0.009**	0.004	**0.026**	0.015	**2.928**	0.0372	**2.796**	1.039	**1.528**	0.180
872.7681	C55H102O6N	**52:4**	**0.000**	0.001	**0.047**	0.037	**206.142**	0.0231	**0.065**	0.145	**2.444**	1.226
878.8149	C55H108O6N	**52:1**	**0.001**	0.001	**0.053**	0.029	**88.667**	0.0038	**0.220**	0.323	**3.360**	0.666
898.7837	C57H104O6N	**54:5**	**0.000**	0.000	**0.049**	0.037	**236.322**	0.0187	**0.077**	0.172	**2.903**	1.126
900.7993	C57H106O6N	**54:4**	**0.001**	0.001	**0.071**	0.036	**114.300**	0.0025	**0.156**	0.349	**4.593**	0.749
902.8149	C57H108O6N	**54:3**	**0.021**	0.007	**0.182**	0.081	**8.628**	0.0022	**6.899**	2.551	**12.213**	2.817
904.8305	C57H110O6N	**54:2**	**0.000**	0.000	**0.306**	0.187	**INF**	0.0064	**0.000**	0.000	**17.879**	3.180
918.8824	C59H116O5N	**55:2**	**0.000**	0.000	**0.046**	0.041	**INF**	0.0365	**0.000**	0.000	**2.372**	1.564
926.8149	C59H108O6N	**56:5**	**0.000**	0.001	**0.062**	0.037	**187.274**	0.0061	**0.122**	0.274	**4.029**	1.270
928.8305	C59H110O6N	**56:4**	**0.000**	0.000	**0.074**	0.055	**INF**	0.0171	**0.000**	0.000	**4.298**	1.600
930.8461	C59H112O6N	**56:3**	**0.000**	0.000	**0.319**	0.233	**INF**	0.0157	**0.000**	0.000	**17.093**	6.997
932.8617	C59H114O6N	**56:2**	**0.000**	0.000	**0.071**	0.061	**INF**	0.0333	**0.000**	0.000	**3.623**	2.237
Total TAG +NL327 20:1 acyl containing			**0.313**	**0.059**	**1.621**	**0.852**	**5.175**	**0.009**	**100.000**	**0.000**	**100.000**	**0.000**
Total TAG *signal*			**18.757**	**3.318**	**680.631**	**406.321**	**36.286**	**0.0066**				

556.5	C33H66O5N	**30:1**	**0.036**	0.039	**0.000**	0.000	**0.000**	0.0769	**8.404**	7.863	**0.000**	0.000
558.5	C33H68O5N	**30:0**	**0.024**	0.032	**0.051**	0.083	**2.123**	0.5169	**5.318**	8.172	**13.023**	20.485
584.5	C35H70O5N	**32:1**	**0.018**	0.021	**0.019**	0.022	**1.066**	0.9321	**4.137**	4.275	**4.772**	5.115
586.5	C35H72O5N	**32:0**	**0.129**	0.065	**0.099**	0.094	**0.767**	0.5704	**29.440**	16.316	**37.400**	43.021
606.5	C37H68O5N	**34:4**	**0.127**	0.109	**0.035**	0.064	**0.273**	0.1412	**23.274**	20.382	**8.079**	13.695
608.5	C37H70O5N	**34:3**	**0.069**	0.155	**0.000**	0.000	**0.000**	0.3479	**5.553**	12.417	**0.000**	0.000
610.5	C37H72O5N	**34:2**	**0.016**	0.022	**0.000**	0.000	**0.000**	0.1491	**2.183**	3.506	**0.000**	0.000
612.6	C37H74O5N	**34:1**	**0.013**	0.029	**0.030**	0.066	**2.307**	0.6144	**1.034**	2.313	**7.353**	16.441
656.5	C41H70O5N	**38:7**	**0.019**	0.019	**0.009**	0.018	**0.501**	0.4478	**3.484**	1.643	**7.517**	12.504
658.5	C41H72O5N	**38:6**	**0.018**	0.026	**0.003**	0.007	**0.161**	0.2504	**2.593**	3.026	**0.629**	1.406
688.6	C43H78O5N	**40:5**	**0.020**	0.019	**0.002**	0.005	**0.115**	0.0744	**6.332**	9.205	**11.354**	25.388
Total DAG NL243 14:1 acyl containing			**0.489**	**0.374**	**0.248**	**0.154**	**0.507**	**0.2195**	**100.000**	**0.000**	**100.000**	**0.000**
556.5	C33H66O5N	**30:1**	**0.074**	0.033	**0.089**	0.046	**1.201**	0.5692	**12.064**	2.133	**10.648**	6.461
558.5	C33H68O5N	**30:0**	**0.057**	0.050	**0.070**	0.035	**1.217**	0.6588	**12.343**	13.905	**7.439**	2.900
584.5	C35H70O5N	**32:1**	**0.076**	0.037	**0.266**	0.065	**3.515**	0.0005	**14.135**	10.873	**29.124**	2.963
586.5	C35H72O5N	**32:0**	**0.310**	0.206	**0.367**	0.109	**1.183**	0.6008	**46.871**	26.750	**40.161**	8.671
606.5	C37H68O5N	**34:4**	**0.018**	0.013	**0.002**	0.004	**0.096**	0.03	**3.324**	2.570	**0.238**	0.531
610.5	C37H72O5N	**34:2**	**0.014**	0.018	**0.008**	0.008	**0.552**	0.502	**2.055**	2.030	**0.830**	0.809
636.6	C39H74O5N	**36:3**	**0.005**	0.004	**0.026**	0.020	**5.386**	0.0464	**0.709**	0.523	**2.639**	1.599
640.6	C39H78O5N	**36:1**	**0.019**	0.004	**0.015**	0.013	**0.759**	0.5004	**3.664**	1.967	**1.618**	1.410
656.5	C41H70O5N	**38:7**	**0.007**	0.006	**0.020**	0.013	**2.665**	0.0833	**1.496**	1.212	**2.227**	1.322
684.6	C43H74O5N	**40:7**	**0.011**	0.006	**0.022**	0.023	**1.982**	0.3542	**1.901**	1.248	**2.289**	2.354
686.6	C43H76O5N	**40:6**	**0.009**	0.009	**0.025**	0.017	**2.642**	0.1058	**1.439**	1.119	**2.787**	1.987
Total DAG NL245 14:0 acyl containing			**0.602**	**0.204**	**0.908**	**0.182**	**1.508**	**0.0366**	**100.000**	**0.000**	**100.000**	**0.000**
556.5	C33H66O5N	**30:1**	**0.419**	0.158	**0.507**	0.261	**1.209**	0.5403	**8.268**	2.420	**5.471**	2.772
558.5	C33H68O5N	**30:0**	**0.045**	0.083	**0.030**	0.068	**0.680**	0.7717	**0.754**	1.314	**0.378**	0.844
584.5	C35H70O5N	**32:1**	**1.158**	0.204	**1.770**	0.423	**1.529**	0.0194	**23.125**	3.645	**19.424**	3.323
586.5	C35H72O5N	**32:0**	**0.562**	0.136	**0.372**	0.187	**0.662**	0.1036	**11.121**	1.938	**4.023**	2.142
606.5	C37H68O5N	**34:4**	**1.823**	0.301	**2.488**	0.779	**1.364**	0.1134	**36.349**	5.021	**27.141**	5.923
608.5	C37H70O5N	**34:3**	**0.812**	0.133	**2.009**	0.596	**2.472**	0.0023	**16.217**	2.214	**21.755**	2.570
610.5	C37H72O5N	**34:2**	**0.111**	0.092	**1.824**	0.526	**16.365**	0.0001	**2.182**	1.907	**19.713**	3.176
612.6	C37H74O5N	**34:1**	**0.051**	0.037	**0.056**	0.044	**1.095**	0.8506	**0.991**	0.725	**0.632**	0.401
630.5	C39H68O5N	**36:6**	**0.016**	0.013	**0.018**	0.015	**1.120**	0.8422	**0.336**	0.275	**0.179**	0.120
636.6	C39H74O5N	**36:3**	**0.022**	0.027	**0.044**	0.028	**1.941**	0.2632	**0.398**	0.411	**0.458**	0.236
664.6	C41H78O5N	**38:3**	**0.006**	0.008	**0.027**	0.030	**4.517**	0.168	**0.124**	0.179	**0.284**	0.300
684.6	C43H74O5N	**40:7**	**0.007**	0.004	**0.044**	0.027	**6.539**	0.0135	**0.132**	0.079	**0.542**	0.376
Total DAG NL271 16:1 acyl containing			**5.034**	**0.743**	**9.189**	**2.221**	**1.825**	**0.0041**	**100.000**	**0.000**	**100.000**	**0.000**
556.5	C33H66O5N	**30:1**	**0.090**	0.035	**0.164**	0.043	**1.820**	0.0179	**0.425**	0.172	**0.361**	0.136

558.5	C33H68O5N	**30:0**	**0.037**	0.029	**0.057**	0.052	**1.539**	0.4724	**0.176**	0.140	**0.122**	0.121
584.5	C35H70O5N	**32:1**	**0.827**	0.139	**1.157**	0.224	**1.399**	0.0232	**3.823**	0.283	**2.463**	0.234
586.5	C35H72O5N	**32:0**	**2.943**	0.829	**6.840**	1.908	**2.324**	0.003	**13.546**	2.807	**14.331**	1.382
606.5	C37H68O5N	**34:4**	**0.015**	0.009	**0.015**	0.010	**1.040**	0.9212	**0.071**	0.055	**0.032**	0.016
608.5	C37H70O5N	**34:3**	**6.025**	0.645	**5.681**	1.616	**0.943**	0.6705	**28.059**	2.080	**12.014**	2.059
610.5	C37H72O5N	**34:2**	**9.283**	0.989	**16.510**	4.276	**1.779**	0.0062	**43.156**	1.868	**34.710**	1.877
612.6	C37H74O5N	**34:1**	**1.979**	0.408	**15.994**	3.460	**8.083**	0.0001	**9.144**	1.237	**33.871**	2.064
630.5	C39H68O5N	**36:6**	**0.072**	0.043	**0.081**	0.016	**1.129**	0.6675	**0.342**	0.234	**0.182**	0.063
636.6	C39H74O5N	**36:3**	**0.005**	0.007	**0.036**	0.021	**7.099**	0.0143	**0.025**	0.034	**0.078**	0.039
638.6	C39H76O5N	**36:2**	**0.032**	0.024	**0.063**	0.032	**2.003**	0.1122	**0.140**	0.093	**0.130**	0.045
640.6	C39H78O5N	**36:1**	**0.122**	0.048	**0.330**	0.165	**2.703**	0.0266	**0.562**	0.185	**0.693**	0.296
656.5	C41H70O5N	**38:7**	**0.058**	0.041	**0.288**	0.109	**4.948**	0.0023	**0.271**	0.178	**0.615**	0.243
658.5	C41H72O5N	**38:6**	**0.004**	0.002	**0.024**	0.024	**6.783**	0.0968	**0.016**	0.010	**0.054**	0.060
660.6	C41H74O5N	**38:5**	**0.013**	0.008	**0.023**	0.019	**1.824**	0.2816	**0.057**	0.032	**0.050**	0.040
684.6	C43H74O5N	**40:7**	**0.021**	0.023	**0.074**	0.052	**3.521**	0.0698	**0.100**	0.112	**0.151**	0.078
686.6	C43H76O5N	**40:6**	**0.014**	0.018	**0.032**	0.035	**2.358**	0.3175	**0.060**	0.075	**0.071**	0.079
688.6	C43H78O5N	**40:5**	**0.006**	0.008	**0.032**	0.024	**5.577**	0.0455	**0.028**	0.040	**0.071**	0.052
Total DAG NL273 16:0 acyl containing			**21.544**	**2.512**	**47.402**	**11.039**	**2.200**	**0.0009**	**100.000**	**0.000**	**100.000**	**0.000**
556.5	C33H66O5N	**30:1**	**0.000**	0.000	**0.027**	0.037	**INF**	0.1446	**0.000**	0.000	**0.085**	0.122
558.5	C33H68O5N	**30:0**	**0.049**	0.033	**0.044**	0.019	**0.893**	0.7609	**0.270**	0.161	**0.142**	0.075
584.5	C35H70O5N	**32:1**	**0.078**	0.031	**0.071**	0.035	**0.915**	0.7623	**0.446**	0.172	**0.215**	0.103
586.5	C35H72O5N	**32:0**	**0.339**	0.057	**0.282**	0.084	**0.830**	0.2411	**1.911**	0.160	**0.832**	0.227
606.5	C37H68O5N	**34:4**	**1.489**	0.707	**1.836**	0.880	**1.233**	0.5108	**8.427**	4.094	**5.188**	1.556
608.5	C37H70O5N	**34:3**	**9.293**	0.982	**9.432**	2.568	**1.015**	0.9129	**52.701**	3.285	**27.337**	1.666
610.5	C37H72O5N	**34:2**	**0.004**	0.008	**0.021**	0.047	**5.733**	0.4378	**0.018**	0.041	**0.088**	0.198
612.6	C37H74O5N	**34:1**	**0.025**	0.021	**0.036**	0.050	**1.451**	0.6546	**0.144**	0.118	**0.118**	0.175
630.5	C39H68O5N	**36:6**	**3.210**	0.762	**4.077**	1.242	**1.270**	0.22	**17.960**	2.767	**11.713**	1.207
632.5	C39H70O5N	**36:5**	**1.894**	0.595	**4.775**	1.320	**2.521**	0.0021	**10.652**	3.283	**13.800**	0.542
634.5	C39H72O5N	**36:4**	**1.110**	0.296	**13.527**	3.431	**12.188**	0.0001	**6.173**	1.002	**39.262**	1.629
636.6	C39H74O5N	**36:3**	**0.152**	0.035	**0.321**	0.120	**2.105**	0.0165	**0.858**	0.155	**0.934**	0.213
656.5	C41H70O5N	**38:7**	**0.013**	0.017	**0.007**	0.015	**0.497**	0.5155	**0.074**	0.092	**0.015**	0.033
658.5	C41H72O5N	**38:6**	**0.026**	0.043	**0.027**	0.039	**1.018**	0.9881	**0.145**	0.233	**0.079**	0.108
662.6	C41H76O5N	**38:4**	**0.030**	0.046	**0.044**	0.044	**1.468**	0.642	**0.155**	0.236	**0.149**	0.174
688.6	C43H78O5N	**40:5**	**0.012**	0.019	**0.018**	0.036	**1.574**	0.724	**0.067**	0.103	**0.043**	0.078
Total DAG NL295 18:3 acyl containing			**17.724**	**2.460**	**34.544**	**9.274**	**1.949**	**0.0044**	**100.000**	**0.000**	**100.000**	**0.000**
556.5	C33H66O5N	**30:1**	**0.013**	0.028	**0.001**	0.002	**0.077**	0.3856	**0.066**	0.148	**0.002**	0.004
558.5	C33H68O5N	**30:0**	**0.028**	0.014	**0.032**	0.027	**1.124**	0.8085	**0.141**	0.064	**0.049**	0.037
584.5	C35H70O5N	**32:1**	**0.104**	0.028	**0.114**	0.060	**1.100**	0.74	**0.552**	0.177	**0.168**	0.067

586.5	C35H72O5N	**32:0**	**0.413**	0.087	**0.392**	0.048	**0.949**	0.6466	**2.149**	0.395	**0.624**	0.117
606.5	C37H68O5N	**34:4**	**0.722**	0.194	**2.362**	0.395	**3.271**	0.0001	**3.679**	0.481	**3.705**	0.276
608.5	C37H70O5N	**34:3**	**0.483**	0.134	**1.636**	0.493	**3.391**	0.001	**2.498**	0.584	**2.537**	0.448
610.5	C37H72O5N	**34:2**	**13.181**	1.853	**24.708**	7.382	**1.875**	0.0095	**68.190**	2.223	**37.874**	2.771
630.5	C39H68O5N	**36:6**	**0.031**	0.034	**0.075**	0.048	**2.398**	0.1373	**0.151**	0.160	**0.113**	0.077
632.5	C39H70O5N	**36:5**	**1.678**	0.391	**3.753**	1.172	**2.236**	0.0056	**8.572**	0.942	**5.833**	1.431
634.5	C39H72O5N	**36:4**	**1.731**	0.484	**8.876**	1.963	**5.128**	0.0001	**8.790**	1.432	**13.775**	0.507
636.6	C39H74O5N	**36:3**	**0.789**	0.202	**22.024**	4.608	**27.912**	0.0001	**4.048**	0.643	**34.329**	3.358
638.6	C39H76O5N	**36:2**	**0.199**	0.066	**0.543**	0.120	**2.733**	0.0005	**1.014**	0.249	**0.849**	0.120
662.6	C41H76O5N	**38:4**	**0.008**	0.010	**0.020**	0.019	**2.373**	0.2732	**0.039**	0.047	**0.028**	0.025
664.6	C41H78O5N	**38:3**	**0.022**	0.032	**0.073**	0.023	**3.282**	0.0214	**0.111**	0.167	**0.114**	0.030
Total DAG NL297 18:2 acyl containing			**19.401**	**3.160**	**64.609**	**15.167**	**3.330**	**0.0002**	**100.000**	**0.000**	**100.000**	**0.000**
556.5	C33H66O5N	**30:1**	**0.088**	0.025	**0.178**	0.046	**2.024**	0.0053	**1.379**	0.408	**0.195**	0.054
558.5	C33H68O5N	**30:0**	**0.017**	0.010	**0.009**	0.009	**0.557**	0.2382	**0.286**	0.188	**0.011**	0.013
584.5	C35H70O5N	**32:1**	**0.234**	0.097	**0.450**	0.110	**1.925**	0.0108	**3.716**	1.533	**0.496**	0.145
586.5	C35H72O5N	**32:0**	**0.577**	0.181	**0.452**	0.068	**0.783**	0.1849	**8.793**	1.957	**0.508**	0.155
606.5	C37H68O5N	**34:4**	**0.176**	0.089	**1.132**	0.309	**6.416**	0.0002	**2.715**	1.140	**1.223**	0.218
608.5	C37H70O5N	**34:3**	**0.158**	0.047	**1.147**	0.210	**7.253**	0.0001	**2.391**	0.377	**1.251**	0.200
610.5	C37H72O5N	**34:2**	**0.171**	0.034	**1.411**	0.292	**8.235**	0.0001	**2.667**	0.459	**1.529**	0.199
612.6	C37H74O5N	**34:1**	**2.887**	0.600	**17.605**	3.745	**6.098**	0.0001	**44.325**	1.850	**18.970**	1.564
632.5	C39H70O5N	**36:5**	**0.036**	0.018	**0.090**	0.040	**2.487**	0.026	**0.525**	0.222	**0.105**	0.071
634.5	C39H72O5N	**36:4**	**0.921**	0.208	**8.280**	2.222	**8.991**	0.0001	**14.052**	0.696	**9.071**	2.375
636.6	C39H74O5N	**36:3**	**0.791**	0.245	**16.781**	3.572	**21.216**	0.0001	**11.886**	1.437	**18.025**	0.541
638.6	C39H76O5N	**36:2**	**0.373**	0.086	**44.255**	12.580	**118.618**	0.0001	**5.743**	0.704	**46.811**	4.904
640.6	C39H78O5N	**36:1**	**0.079**	0.025	**1.654**	0.575	**21.060**	0.0003	**1.237**	0.445	**1.732**	0.278
658.5	C41H72O5N	**38:6**	**0.007**	0.009	**0.018**	0.009	**2.712**	0.0767	**0.113**	0.136	**0.020**	0.008
662.6	C41H76O5N	**38:4**	**0.005**	0.005	**0.027**	0.009	**5.063**	0.0024	**0.079**	0.077	**0.029**	0.008
664.6	C41H78O5N	**38:3**	**0.007**	0.007	**0.022**	0.012	**3.304**	0.0412	**0.092**	0.095	**0.023**	0.011
Total DAG NL299 18:1 acyl containing			**6.527**	**1.359**	**93.511**	**21.571**	**14.328**	**0.0001**	**100.000**	**0.000**	**100.000**	**0.000**
556.5	C33H66O5N	**30:1**	**0.016**	0.022	**0.031**	0.019	**1.916**	0.2698	**0.970**	1.145	**0.346**	0.194
558.5	C33H68O5N	**30:0**	**0.030**	0.015	**0.030**	0.027	**0.976**	0.9665	**2.156**	1.348	**0.350**	0.311
584.5	C35H70O5N	**32:1**	**0.199**	0.071	**0.215**	0.041	**1.079**	0.6868	**12.907**	3.348	**2.416**	0.159
586.5	C35H72O5N	**32:0**	**0.386**	0.124	**0.384**	0.133	**0.996**	0.9848	**25.637**	7.795	**4.274**	0.885
608.5	C37H70O5N	**34:3**	**0.052**	0.020	**0.174**	0.066	**3.337**	0.0042	**3.492**	1.484	**1.909**	0.415
610.5	C37H72O5N	**34:2**	**0.084**	0.059	**0.193**	0.087	**2.306**	0.0481	**5.193**	3.064	**2.091**	0.693
612.6	C37H74O5N	**34:1**	**0.098**	0.077	**0.147**	0.027	**1.496**	0.2197	**6.157**	3.702	**1.723**	0.599
630.5	C39H68O5N	**36:6**	**0.009**	0.007	**0.012**	0.008	**1.342**	0.5439	**0.644**	0.575	**0.150**	0.130
632.5	C39H70O5N	**36:5**	**0.021**	0.021	**0.021**	0.013	**1.010**	0.9859	**1.526**	1.793	**0.240**	0.138

634.5	C39H72O5N	**36:4**	**0.012**	0.009	**0.039**	0.026	**3.371**	0.0566	**0.760**	0.612	**0.475**	0.358
636.6	C39H74O5N	**36:3**	**0.252**	0.064	**0.802**	0.177	**3.178**	0.0002	**16.996**	4.749	**9.144**	2.077
638.6	C39H76O5N	**36:2**	**0.216**	0.045	**1.406**	0.201	**6.498**	0.0001	**14.304**	1.546	**15.990**	2.171
640.6	C39H78O5N	**36:1**	**0.103**	0.048	**5.162**	1.233	**49.922**	0.0001	**7.045**	3.486	**57.398**	4.970
656.5	C41H70O5N	**38:7**	**0.009**	0.005	**0.084**	0.037	**9.846**	0.002	**0.541**	0.311	**0.936**	0.342
684.6	C43H74O5N	**40:7**	**0.026**	0.016	**0.235**	0.117	**9.035**	0.0041	**1.672**	0.918	**2.558**	1.089
Total DAG NL301 18:0 acyl containing			**1.514**	**0.291**	**8.935**	**1.783**	**5.902**	**0.0001**	**100.000**	**0.000**	**100.000**	**0.000**
558.5	C33H68O5N	**30:0**	**0.024**	0.020	**0.007**	0.003	**0.303**	0.1177	**2.445**	2.210	**0.688**	0.434
584.5	C35H70O5N	**32:1**	**0.156**	0.058	**0.137**	0.052	**0.880**	0.6003	**17.246**	8.497	**13.863**	9.540
586.5	C35H72O5N	**32:0**	**0.316**	0.051	**0.246**	0.074	**0.779**	0.1173	**34.453**	11.184	**23.466**	14.182
612.6	C37H74O5N	**34:1**	**0.013**	0.009	**0.020**	0.016	**1.540**	0.392	**1.465**	1.093	**1.891**	1.136
630.5	C39H68O5N	**36:6**	**0.023**	0.023	**0.081**	0.046	**3.463**	0.0375	**2.578**	2.404	**7.633**	5.377
632.5	C39H70O5N	**36:5**	**0.041**	0.018	**0.027**	0.026	**0.654**	0.3383	**4.358**	2.315	**1.844**	0.818
634.5	C39H72O5N	**36:4**	**0.082**	0.038	**0.144**	0.085	**1.767**	0.1728	**8.304**	2.945	**10.769**	2.811
656.5	C41H70O5N	**38:7**	**0.099**	0.076	**0.138**	0.137	**1.396**	0.5927	**9.481**	6.489	**8.794**	6.165
658.5	C41H72O5N	**38:6**	**0.075**	0.095	**0.216**	0.224	**2.860**	0.234	**6.616**	7.317	**13.720**	10.023
660.6	C41H74O5N	**38:5**	**0.090**	0.094	**0.184**	0.139	**2.037**	0.2484	**8.108**	6.750	**12.499**	8.041
662.6	C41H76O5N	**38:4**	**0.031**	0.037	**0.061**	0.060	**1.943**	0.3737	**2.741**	2.985	**3.841**	3.555
664.6	C41H78O5N	**38:3**	**0.021**	0.013	**0.012**	0.013	**0.578**	0.3311	**2.203**	1.407	**0.992**	1.184
Total DAG NL321 20:4 acyl containing			**0.971**	**0.238**	**1.273**	**0.666**	**1.310**	**0.368**	**100.000**	**0.000**	**100.000**	**0.000**
556.5	C33H66O5N	**30:1**	**0.017**	0.026	**0.038**	0.047	**2.313**	0.3889	**1.122**	1.464	**2.706**	3.778
558.5	C33H68O5N	**30:0**	**0.017**	0.011	**0.027**	0.026	**1.554**	0.4537	**1.370**	0.882	**1.949**	1.789
584.5	C35H70O5N	**32:1**	**0.257**	0.093	**0.196**	0.104	**0.763**	0.3613	**20.171**	6.343	**16.928**	11.532
586.5	C35H72O5N	**32:0**	**0.456**	0.061	**0.390**	0.202	**0.855**	0.5064	**36.012**	6.148	**27.232**	5.223
630.5	C39H68O5N	**36:6**	**0.079**	0.015	**0.069**	0.026	**0.870**	0.4652	**6.267**	1.511	**6.582**	5.561
632.5	C39H70O5N	**36:5**	**0.038**	0.021	**0.042**	0.038	**1.088**	0.8668	**2.902**	1.566	**2.212**	1.547
634.5	C39H72O5N	**36:4**	**0.029**	0.011	**0.049**	0.062	**1.672**	0.5174	**2.353**	1.059	**3.042**	2.241
636.6	C39H74O5N	**36:3**	**0.031**	0.026	**0.032**	0.042	**1.030**	0.9649	**2.424**	1.790	**2.896**	3.315
658.5	C41H72O5N	**38:6**	**0.276**	0.086	**0.280**	0.217	**1.013**	0.9719	**20.969**	1.854	**14.370**	8.748
660.6	C41H74O5N	**38:5**	**0.052**	0.095	**0.230**	0.168	**4.428**	0.0723	**3.260**	5.348	**12.308**	8.141
662.6	C41H76O5N	**38:4**	**0.033**	0.071	**0.158**	0.148	**4.838**	0.1259	**1.897**	4.057	**7.872**	5.383
664.6	C41H78O5N	**38:3**	**0.018**	0.018	**0.037**	0.036	**2.041**	0.3222	**1.253**	1.165	**1.904**	1.965
Total DAG NL323 20:3 acyl containing			**1.302**	**0.330**	**1.546**	**0.883**	**1.187**	**0.5788**	**100.000**	**0.000**	**100.000**	**0.000**
556.5	C33H66O5N	**30:1**	**0.019**	0.014	**0.057**	0.058	**3.020**	0.193	**0.417**	0.328	**1.311**	1.591
558.5	C33H68O5N	**30:0**	**0.273**	0.034	**0.125**	0.087	**0.457**	0.0077	**5.624**	0.694	**3.365**	1.710
584.5	C35H70O5N	**32:1**	**0.195**	0.070	**0.153**	0.061	**0.783**	0.3375	**3.966**	1.089	**4.238**	1.796
586.5	C35H72O5N	**32:0**	**4.007**	0.663	**2.851**	1.396	**0.712**	0.133	**81.732**	2.732	**69.619**	2.362
608.5	C37H70O5N	**34:3**	**0.012**	0.014	**0.072**	0.046	**6.019**	0.0238	**0.256**	0.305	**1.502**	0.889

612.6	C37H74O5N	**34:1**	**0.014**	0.007	**0.010**	0.013	**0.689**	0.5504	**0.293**	0.184	**0.222**	0.325
630.5	C39H68O5N	**36:6**	**0.008**	0.008	**0.017**	0.020	**2.140**	0.393	**0.161**	0.167	**0.301**	0.344
632.5	C39H70O5N	**36:5**	**0.071**	0.041	**0.077**	0.052	**1.082**	0.8494	**1.429**	0.775	**1.687**	0.604
634.5	C39H72O5N	**36:4**	**0.010**	0.008	**0.085**	0.045	**8.592**	0.0059	**0.192**	0.114	**2.130**	0.477
636.6	C39H74O5N	**36:3**	**0.017**	0.006	**0.113**	0.066	**6.590**	0.0113	**0.354**	0.120	**2.821**	1.166
638.6	C39H76O5N	**36:2**	**0.115**	0.021	**0.218**	0.118	**1.895**	0.0919	**2.391**	0.595	**4.990**	1.993
660.6	C41H74O5N	**38:5**	**0.061**	0.039	**0.124**	0.066	**2.050**	0.0997	**1.298**	0.865	**3.143**	0.829
662.6	C41H76O5N	**38:4**	**0.038**	0.044	**0.060**	0.068	**1.571**	0.561	**0.821**	0.900	**1.149**	1.246
664.6	C41H78O5N	**38:3**	**0.051**	0.037	**0.152**	0.084	**2.987**	0.0392	**1.068**	0.807	**3.521**	0.982
Total DAG NL325 20:2 acyl containing			**4.890**	**0.691**	**4.114**	**2.005**	**0.841**	**0.4367**	**100.000**	**0.000**	**100.000**	**0.000**
556.5	C33H66O5N	**30:1**	**0.028**	0.016	**0.037**	0.035	**1.311**	0.6204	**0.848**	0.444	**1.047**	0.617
558.5	C33H68O5N	**30:0**	**0.205**	0.039	**0.100**	0.071	**0.489**	0.0196	**6.230**	0.645	**2.728**	1.278
584.5	C35H70O5N	**32:1**	**0.145**	0.054	**0.107**	0.058	**0.737**	0.3153	**4.359**	1.269	**3.915**	1.983
586.5	C35H72O5N	**32:0**	**2.249**	0.478	**1.541**	1.037	**0.685**	0.2025	**67.783**	5.053	**38.927**	22.768
606.5	C37H68O5N	**34:4**	**0.011**	0.009	**0.033**	0.039	**2.986**	0.2595	**0.327**	0.265	**0.747**	0.766
608.5	C37H70O5N	**34:3**	**0.017**	0.009	**0.010**	0.013	**0.570**	0.3333	**0.567**	0.380	**0.302**	0.443
610.5	C37H72O5N	**34:2**	**0.026**	0.017	**0.051**	0.028	**1.979**	0.1212	**0.822**	0.651	**1.781**	0.757
630.5	C39H68O5N	**36:6**	**0.012**	0.008	**0.013**	0.006	**1.107**	0.7969	**0.348**	0.285	**0.566**	0.424
632.5	C39H70O5N	**36:5**	**0.029**	0.021	**0.026**	0.024	**0.909**	0.8481	**0.923**	0.733	**1.582**	1.950
634.5	C39H72O5N	**36:4**	**0.021**	0.014	**0.065**	0.071	**3.061**	0.2101	**0.602**	0.360	**1.724**	1.163
636.6	C39H74O5N	**36:3**	**0.012**	0.011	**0.048**	0.023	**3.916**	0.0124	**0.387**	0.367	**1.630**	0.418
638.6	C39H76O5N	**36:2**	**0.074**	0.032	**0.127**	0.072	**1.720**	0.1697	**2.170**	0.701	**4.014**	0.633
640.6	C39H78O5N	**36:1**	**0.444**	0.170	**0.936**	0.450	**2.111**	0.0513	**13.195**	4.246	**36.393**	21.510
662.6	C41H76O5N	**38:4**	**0.017**	0.008	**0.055**	0.046	**3.171**	0.1131	**0.529**	0.284	**1.409**	0.681
664.6	C41H78O5N	**38:3**	**0.032**	0.021	**0.136**	0.120	**4.249**	0.0922	**0.910**	0.560	**3.235**	2.301
Total DAG NL327 20:1 acyl containing			**3.323**	**0.706**	**3.286**	**1.848**	**0.989**	**0.9673**	**100.000**	**0.000**	**100.000**	**0.000**
556.5	C33H66O5N	**30:1**	**0.007**	0.009	**0.020**	0.036	**2.809**	0.4578	**0.413**	0.532	**0.673**	1.069
558.5	C33H68O5N	**30:0**	**0.145**	0.074	**0.099**	0.073	**0.683**	0.3514	**6.629**	1.402	**3.691**	1.882
584.5	C35H70O5N	**32:1**	**0.282**	0.074	**0.312**	0.223	**1.105**	0.7842	**14.080**	5.149	**14.695**	13.411
586.5	C35H72O5N	**32:0**	**1.075**	0.407	**0.754**	0.430	**0.701**	0.2594	**50.134**	5.607	**29.650**	9.836
606.5	C37H68O5N	**34:4**	**0.231**	0.082	**0.299**	0.176	**1.291**	0.4607	**11.105**	3.525	**11.497**	3.541
608.5	C37H70O5N	**34:3**	**0.011**	0.011	**0.047**	0.025	**4.163**	0.0194	**0.587**	0.513	**1.900**	0.870
610.5	C37H72O5N	**34:2**	**0.011**	0.009	**0.043**	0.019	**4.015**	0.0082	**0.481**	0.377	**1.861**	1.003
612.6	C37H74O5N	**34:1**	**0.083**	0.027	**0.098**	0.032	**1.172**	0.4633	**4.266**	1.786	**4.278**	1.733
630.5	C39H68O5N	**36:6**	**0.018**	0.014	**0.015**	0.013	**0.811**	0.694	**0.847**	0.650	**0.676**	0.693
632.5	C39H70O5N	**36:5**	**0.037**	0.018	**0.037**	0.048	**0.986**	0.9731	**1.755**	0.771	**1.327**	1.328
634.5	C39H72O5N	**36:4**	**0.007**	0.009	**0.027**	0.028	**3.829**	0.1729	**0.331**	0.494	**0.938**	0.774
636.6	C39H74O5N	**36:3**	**0.003**	0.004	**0.034**	0.015	**9.675**	0.0023	**0.181**	0.179	**1.467**	0.798

638.6	C39H76O5N	36:2	0.008	0.005	0.020	0.020	2.495	0.232	0.394	0.272	0.693	0.589
656.5	C41H70O5N	38:7	0.010	0.011	0.074	0.076	7.755	0.0974	0.419	0.503	3.726	4.286
658.5	C41H72O5N	38:6	0.094	0.046	0.313	0.160	3.319	0.0188	4.574	2.513	12.714	5.306
686.6	C43H76O5N	40:6	0.077	0.055	0.239	0.141	3.107	0.0437	3.804	2.861	10.213	6.529
Total DAG NL345 22:6 acyl containing			2.101	0.571	2.429	0.764	1.156	0.4646	100.000	0.000	100.000	0.000
558.5	C33H68O5N	30:0	0.016	0.010	0.009	0.006	0.566	0.2514	0.739	0.469	0.351	0.231
584.5	C35H70O5N	32:1	0.385	0.084	0.464	0.480	1.205	0.7268	18.425	4.958	19.602	19.731
586.5	C35H72O5N	32:0	0.306	0.132	0.348	0.066	1.135	0.5491	14.087	3.727	13.978	3.634
606.5	C37H68O5N	34:4	0.006	0.006	0.027	0.037	4.467	0.2473	0.282	0.275	0.843	0.988
608.5	C37H70O5N	34:3	0.881	0.216	0.769	0.542	0.873	0.679	41.122	5.954	26.721	9.579
610.5	C37H72O5N	34:2	0.273	0.064	0.421	0.259	1.542	0.2487	12.781	1.453	15.038	4.580
612.6	C37H74O5N	34:1	0.029	0.016	0.186	0.140	6.395	0.037	1.496	1.035	6.556	3.374
630.5	C39H68O5N	36:6	0.033	0.024	0.042	0.030	1.246	0.6451	1.453	0.667	1.461	0.649
632.5	C39H70O5N	36:5	0.026	0.016	0.019	0.019	0.719	0.5274	1.296	0.864	0.707	0.657
634.5	C39H72O5N	36:4	0.008	0.008	0.015	0.013	1.772	0.3963	0.407	0.380	0.520	0.330
640.6	C39H78O5N	36:1	0.095	0.063	0.198	0.146	2.087	0.1838	4.184	2.200	6.732	2.854
658.5	C41H72O5N	38:6	0.013	0.015	0.024	0.030	1.831	0.477	0.536	0.489	0.814	0.835
660.6	C41H74O5N	38:5	0.049	0.026	0.131	0.089	2.672	0.0829	2.513	1.465	4.564	1.737
684.6	C43H74O5N	40:7	0.005	0.003	0.027	0.020	5.269	0.0465	0.234	0.134	0.951	0.792
686.6	C43H76O5N	40:6	0.010	0.008	0.030	0.015	2.885	0.0336	0.446	0.260	1.161	0.593
Total DAG NL347 22:5 acyl containing			2.136	0.445	2.708	1.123	1.268	0.3208	100.000	0.000	100.000	0.000
584.5	C35H70O5N	32:1	0.113	0.027	0.110	0.085	0.979	0.9533	24.291	10.296	5.221	3.281
586.5	C35H72O5N	32:0	0.125	0.130	0.126	0.064	1.002	0.9976	21.060	13.740	6.521	1.061
610.5	C37H72O5N	34:2	0.020	0.016	0.065	0.059	3.243	0.1396	3.683	2.331	2.908	1.860
612.6	C37H74O5N	34:1	0.017	0.014	0.029	0.022	1.659	0.3633	3.410	2.952	1.649	1.128
630.5	C39H68O5N	36:6	0.021	0.022	0.039	0.030	1.833	0.315	4.030	4.095	2.643	2.310
632.5	C39H70O5N	36:5	0.058	0.023	0.437	0.179	7.580	0.0015	12.204	5.777	23.179	3.965
634.5	C39H72O5N	36:4	0.013	0.010	0.006	0.008	0.436	0.2186	3.072	2.093	0.261	0.323
656.5	C41H70O5N	38:7	0.025	0.003	0.256	0.122	10.402	0.0028	5.131	1.141	12.942	2.071
658.5	C41H72O5N	38:6	0.023	0.007	0.707	0.323	30.749	0.0015	4.729	1.606	37.537	7.091
660.6	C41H74O5N	38:5	0.007	0.007	0.052	0.039	6.959	0.042	1.570	1.817	3.116	2.097
662.6	C41H76O5N	38:4	0.009	0.003	0.022	0.019	2.397	0.1911	1.820	0.554	1.195	0.895
684.6	C43H74O5N	40:7	0.072	0.042	0.028	0.022	0.395	0.0711	13.526	4.051	1.612	1.016
686.6	C43H76O5N	40:6	0.007	0.011	0.029	0.031	4.290	0.1679	1.473	2.330	1.215	1.157
Total DAG NL349 22:4 acyl containing			0.511	0.196	1.906	0.819	3.733	0.006	100.000	0.000	100.000	0.000
Total DAG signal			88.070	11.746	276.607	61.536	3.141	0.0001				
Total Neutral Glycerolipid (DAG+TAG) signal			106.827	14.674	957.238	432.151	8.961	0.0023				

Table S5.2. N deprivation-responsive proteins in *E. oleoabundans* membranes.

N deprivation-responsive proteins are described according to the main biological process to which they are related: (1) Photosynthesis; (2) Oxidative phosphorylation; (3) Energy and redox homeostasis; (4) Carbon metabolism; (5) Protein and N compound metabolism; (6) Other biological processes; (7) Proteins of unknown function. Responsive proteins were identified by at least two unique peptides in not less than three out of four biological replicates of either N-deprived (-N) or N-sufficient (+N) conditions. Curated protein annotations are provided according to Garibay-Hernández et al. (2017), with additional manual annotation. Common abbreviations (Abbr.) and calculated molecular masses (MM) are indicated. Relative quantitation of protein abundance was performed by different label-free methods (WSpC, emPAI, NSAF, Top3 PI, Top3 TIC). The fold-changes (FC) are shown for each method; for those proteins exclusively detected under –N, FC are reported as infinity (INF), whereas FC values of zero are given to those exclusively identified in +N. The label-free methods in which the responsive proteins showed a statistical significant (p-value ≤ 0.05) FC ≥ 1.2 or ≤ 0.83 are highlighted in gray. The average of statistically significant FC is provided per each protein. The corresponding transcriptional regulation under -N is indicated according to Rismani-Yazdi et al. (2010). Statistically significant (q-value < 0.05) transcript changes are highlighted

(1) Photosynthesis

Major category	Specific category	Protein identifier	Curated description	Abbr.	MM (kDa)	Protein abundance (FC: -N/+N)						Transcript abundance	
						Average FC	WSpC	emPAI	NSAF	Top3 PI	Top3 TIC	Log_2 FC (+N/-N)	*q*-value
Photosynthetic core complexes	PSI core protein	m.253815	Photosystem I P700 chlorophyll a apoprotein A2	PSAB	82	**1.30**	1.1	1.3	1.1	1.3	1.7	0.40	0.34782
		m.420934	Photosystem I reaction center subunit II	PSAD	22	**0.45**	0.9	0.9	0.9	0.5	0.4	**1.41**	0.00302
		m.396598	Photosystem I reaction center subunit IV	PSAE	14	**0.58**	0.6	0.5	0.6	0.6	1.9	**1.09**	0.00302
		m.375289	Photosystem I reaction center subunit N	PSAN	18	**0.60**	0.8	1.1	0.8	0.6	0.6	-0.63	0.05166
	Cytochrome b6f complex	m.186165	Cytochrome b6, chloroplastic	PETB	24	**1.25**	1.2	1.2	1.3	2.5	1.6	0.61	0.07023
	Chloroplast ATP synthase	gi|416678	ATP synthase subunit beta, chloroplastic	ATPB	52	**0.70**	0.9	0.8	1.0	0.7	0.5	NA	NA
Antenna proteins	LHCI peripheral antenna	m.365254	LHCI chlorophyll a/b-binding protein LHCA5	LHCA5	30	**1.80**	1.3	1.7	1.3	1.9	1.3	**-1.42**	0.00000
		m.353942	LHCI chlorophyll a/b-binding protein LHCA6	LHCA6	29	**1.33**	1.3	1.3	1.4	2.1	2.2	0.72	0.08307
		m.382652	LHCI chlorophyll a/b-binding protein LHCA7	LHCA7	29	**1.60**	0.9	1.2	0.9	1.6	0.8	**1.12**	0.00383
	LHCII antenna proteins	m.416614	Major LHCII type I chlorophyll a/b binding protein A	LHCBMt1_A	26	**1.90**	2.0	0.9	2.1	1.6	1.4	**2.17**	0.00000
		m.421136	Major LHCII type I chlorophyll a/b-binding protein B	LHCBMt1_B	18	**1.80**	1.6	0.9	1.6	1.9	1.7	**2.30**	0.00000
		m.418152	Major LHCII type III chlorophyll a/b binding protein	LHCBMt3	29	**2.08**	2.1	1.2	2.2	2.2	1.8	0.74	0.14083

		m.418258	Major LHCII type IV chlorophyll a/b binding protein	LHCBMt4	24	**1.55**	1.7	1.3	1.7	1.5	5.1	-0.28	0.65566
Photoprotection	PSII biogenesis and/or repair factor	m.207905	Photosystem II 11 kD protein	PSB27	21	**0.55**	0.8	0.9	0.8	0.5	0.6	**1.32**	0.00000
		m.202007	Protein THYLAKOID FORMATION1, chloroplastic	PSB29	31	**1.73**	1.6	2.0	1.6	1.5	1.5	0.10	0.87346
		m.308390	Probable zinc metalloprotease EGY1, chloroplastic	EGY1	71	**0.23**	0.2	0.3	0.2	0.4	0.6	**1.00**	0.00058
		m.316237	Protein LOW PSII ACCUMULATION 1, chloroplastic	LPA1	49	**0.60**	0.6	0.6	0.6	0.8	0.8	**0.70**	0.00434
		m.376520	Protein M-ENRICHED THYLAKOID 1, chloroplastic	MET1	39	**0.55**	0.6	0.5	0.6	0.5	0.9	**0.96**	0.00051
		m.337748	Probable MPH1 protein, chloroplastic	MPH1	16	**0.33**	0.4	0.4	0.4	0.2	0.2	-0.09	0.86709
		m.170274	PsbP-like protein 1, chloroplastic	PPL1	27	**0.50**	0.5	0.5	0.5	0.4	0.5	**1.22**	0.00000
		m.157685	Rubredoxin, chloroplastic	RBD	25	**1.30**	1.1	1.3	1.2	1.0	1.1	**0.83**	0.00048
	Activation of rapid reversible NPQ	m.373663	Voltage-dependent chloride channel_A, chloroplastic	VCCN_A	51	**2.30**	1.7	2.3	1.8	2.1	1.4	**1.33**	0.00474
		m.388425	Voltage-dependent chloride channel B, chloroplastic	VCCN_B	50	**1.30**	1.1	1.3	1.1	1.4	1.5	**1.47**	0.00016
	Cyclic electron flow	m.115949	Ferredoxin-NADP reductase, chloroplastic	FNR	39	**0.50**	0.8	0.8	0.8	0.5	0.6	**-2.31**	0.00000
		m.264998	PGR5-like protein, chloroplastic	PGRL1	33	**2.25**	2.1	2.7	2.2	2.0	1.7	0.28	0.52470
		m.384354	Protein THYLAKOID RHODANESE-LIKE, chloroplastic	TROL	43	**1.50**	1.1	1.3	1.2	1.5	1.5	0.56	0.14397
		m.403196	Type-II NAD(P)H dehydrogenase, chloroplastic	NDH-2	67	**4.98**	3.2	3.6	3.2	9.9	8.2	**0.59**	0.04400

	Zeaxanthin-dependent NPQ	m.405041	Violaxanthin de-epoxidase, chloroplastic	VDE	50	**0.60**	0.6	0.7	0.6	0.8	1.2	-0.18	0.62254
	Photoprotecion	m.117393	Serine protease SPPA, chloroplastic	SPPA	80	**6.40**	5.5	8.2	5.5	13.0	13.0	**-0.69**	0.01949
Chlorophyll biosynthesis	Chlorophyll biosynthesis	m.19173	Protochlorophyllide reductase, chloroplastic	POR	43	**0.70**	0.7	0.7	0.7	0.8	0.7	**-1.85**	0.00000

(2) Oxidative phosphorylation

Major category	Specific category	Protein identifier	Curated description	Abbr.	MM (kDa)	Protein abundance (FC: -N/+N)						Transcript abundance	
						Average FC	WSpC	emPAI	NSAF	Top3 PI	Top3 TIC	Log_2 FC (+N/-N)	*q*-value
Oxidative phosphorylation	Complex I, NADH:ubiquinone oxidoreductase	m.355155	NADH dehydrogenase [ubiquinone] iron-sulfur protein 6, mitochondrial	**NDUFS6**	16	**0.25**	0.3	0.4	0.3	0.2	0.3	-0.19	0.76907
		m.390039	NADH dehydrogenase [ubiquinone] 1 beta subcomplex subunit 10, mitochondrial	**PDSW**	17	**0.50**	0.6	0.7	0.7	0.5	0.6	0.40	0.30548
	Complex III, ubiquinol: cytochrome *c* oxidorecductase (bc_1 complex)	m.384751	Mitochondrial-processing peptidase subunit alpha	**MPPA**	55	**2.10**	1.5	1.7	1.5	2.4	2.2	-0.06	0.93288
		m.415214	Mitochondrial-processing peptidase subunit beta	**QCR1**	54	**1.70**	1.6	1.6	1.6	1.7	2.0	**1.18**	0.01833
		m.365842	Cytochrome b-c1 complex subunit 4, mitochondrial	**CYC1**	33	**4.62**	4.0	5.8	4.0	5.3	4.0	0.35	0.47446
		m.421237	Cytochrome b-c1 complex subunit Rieske, mitochondrial	**RIP1**	27	**5.90**	2.7	2.5	2.6	4.2	5.9	0.56	0.15765
	Complex IV, cytochrome *c* oxidase	m.110997	Cytochrome c oxidase subunit 2, mitochondrial	**COX2**	23	**1.57**	1.4	1.9	1.4	3.5	2.7	0.14	0.84417
		m.356410	Cytochrome c oxidase subunit 6B, mitochondrial	**COX6B**	16	**0.60**	0.7	0.6	0.7	0.8	0.6	-0.42	0.27634
	Complex V, ATP synthase	m.347310	ATP synthase subunit alpha, mitochondrial	**ATPα**	55	**1.80**	1.6	2.2	1.6	2.5	2.2	**0.79**	0.00503
		m.366102	ATP synthase subunit beta, mitochondrial	**ATPβ**	52	**1.70**	1.3	1.7	1.3	1.3	1.6	-0.58	0.30935
		m.415370	ATP synthase subunit gamma, mitochondrial	**ATPγ**	37	**1.82**	1.7	1.8	1.7	2.1	1.8	0.36	0.48185

		m.381548	ATP synthase subunit delta', mitochondrial	**ATPδ**	22	**1.65**	1.4	1.4	1.5	1.8	1.5	0.49	0.17007
		m.417976	ATP synthase subunit F_Ad, mitochondrial	**ATPFAD**	26	**2.77**	1.6	2.2	1.6	3.3	2.8	**0.95**	0.01655
		m.161014	ATP synthase subunit d, N-terminal peptide, mitochondrial	**ATP*d***	12	**3.68**	1.5	2.0	1.5	7.1	6.3	0.12	0.78531
		m.364530	ATP synthase subunit d, C-terminal peptide, mitochondrial	**ATP*d***	9	**3.66**	1.9	2.5	1.9	6.3	5.7	0.29	0.55528

(3) Energy and redox homeostasis

Major category	Specific category	Protein identifier	Curated description	Abbr.	MM (kDa)	Protein abundance (FC: -N/+N)						Transcript abundance	
						Average FC	WSpC	emPAI	NSAF	Top3 PI	Top3 TIC	Log_2 FC (+N/-N)	*q*-value
Regulation of energy homeostasis	Energy homeostasis	m.331511	Adenylate kinase, mitochondrial	**ADKm**	28	**0.50**	0.5	0.5	0.5	0.5	0.5	**-0.59**	0.02796
		m.414529	ADP/ATP carrier protein, chloroplastic	**AAA**	64	**1.25**	1.2	1.4	1.3	1.3	0.9	0.18	0.78043
		m.418026	ADP/ATP carrier protein, mitochondrial	**AAC**	37	**1.30**	1.2	1.3	1.2	1.7	1.3	**2.00**	0.00006
		m.358988	Mitochondrial phosphate carrier protein	**MPT**	40	**3.20**	3.0	3.2	3.1	3.5	2.2	**1.34**	0.00099
	Reducing power homeostasis	m.377074	NAD(P) transhydrogenase, mitochondrial	**NNT**	113	**3.85**	3.8	4.5	3.9	14.0	34.0	0.82	0.07687
Regulation of redox homeostasis	Redox signaling and oxidative stress	m.370006	2-cys peroxiredoxin BAS1, chloroplastic	**BAS1**	27	**3.10**	1.9	2.3	2.0	3.9	2.9	-0.39	0.35367
		m.267965	Glutaredoxin, chloroplastic	**GRX**	64	**5.88**	3.0	3.4	3.1	5.9	14.0	0.52	0.23487
		m.418074	Protein disulfide isomerase	**PDI**	56	**3.90**	2.1	2.2	2.1	3.9	3.1	0.54	0.27499

(4) Carbon metabolism

Major category	Specific category	Protein identifier	Curated description	Abbr.	MM (kDa)	Protein abundance (FC: -N/+N)						Transcript abundance	
						Average FC	WSpC	emPAI	NSAF	Top3 PI	Top3 TIC	Log_2 FC (+N/-N)	*q*-value
One carbon metabolism	Carbon concentrating mechanism	m.370606	Putative inorganic carbon transporter HLA3	**HLA3**	149	**1.70**	1.9	2.3	1.9	2.7	1.7	**3.28**	0.00000
		m.310144	Alpha carbonic anhydrase, chloroplastic	**CAH3**	39	**0.40**	0.4	0.5	0.4	0.2	0.5	**3.06**	0.00000
	Photorespiration	m.352886	Serine hydroxymethyltransferase, mitochondrial	**SHMT**	57	**1.60**	1.1	1.4	1.1	1.6	1.5	0.72	0.08350
	SAM metabolism	m.357300	Adenosylhomocysteinase	**SAH1**	54	**11.00**	4.6	3.8	4.7	11.0	12.0	**0.93**	0.02084
Calvin Cycle	Calvin Cycle	m.382809	Phosphoglycerate kinase, chloroplastic	**PGK**	50	**2.27**	1.6	1.7	1.6	2.7	2.4	**1.68**	0.00000
		m.372822	Transketolase, chloroplastic	**TKL**	80	**14.33**	13.0	8.9	13.0	12.0	18.0	**2.79**	0.00000
Acetyl-CoA biosynthesis	Acetyl-CoA biosynthesis	m.371437	Pyruvate dehydrogenase E1 component subunit beta, chloroplastic	**PDH E1β**	41	**INF**	INF	INF	INF	INF	INF	**-1.25**	0.00000
		m.130266	Pyruvate dehydrogenase E2 component, chloroplastic	**PDH E2**	50	**1.78**	1.7	2.3	1.8	1.5	1.6	**-0.93**	0.00055
		m.324850	Pyruvate dehydrogenase E3 component, chloroplastic	**PDH E3**	63	**3.35**	3.1	3.2	3.1	4.0	2.8	**-1.12**	0.00002
Lipid metabolism	Acyl-lipid biosynthesis	m.368848	Long-chain acyl-CoA synthetase A	**LCS_A**	71	**1.70**	1.3	1.7	1.4	1.4	1.3	-0.51	0.24833
		m.224985	Long chain acyl-CoA synthetase_B	**LCS_B**	76	**7.03**	4.5	4.7	4.6	9.4	12.0	**0.81**	0.00727
	Lipid droplet structural protein	m.392627	Probable plastid-lipid associated protein A, chloroplastic	**PLAP_A**	59	**0.62**	0.6	0.6	0.6	0.6	0.7	-0.10	0.86550
		m.244306	Probable plastid-lipid associated protein_C, chloroplastic	**PLAP_C**	23	**INF**	INF	INF	INF	INF	INF	**-0.81**	0.00347
		m.413736	Major lipid droplet protein	**MLDP**	34	**INF**	INF	INF	INF	INF	INF	-0.49	0.28114
	Lipid trafficking	m.417181	ABC transporter G family member_A	**ABCG_A**	70	**6.23**	5.4	7.8	5.5	12.0	6.1	**-1.41**	0.00041

(5) Protein and N compound metabolism

Major category	Specific category	Protein identifier	Curated description	Abbr.	MM (kDa)	Protein abundance (FC: -N/+N)						Transcript abundance	
						Average FC	WSpC	emPAI	NSAF	Top3 PI	Top3 TIC	Log_2 FC (+N/-N)	*q*-value
Nitrogen compound metabolism	Nitrogen assimilation	m.413648	High affinity nitrate transporter 2	**NRT2**	56	**INF**	INF	INF	INF	INF	INF	**-8.17**	0.00000
		m.360553	Ammonium transporter 1_A	**AMT1_A**	55	**INF**	INF	INF	INF	INF	INF	**-4.77**	0.00000
		m.363330	Choline transporter-like protein	**CTL**	31	**INF**	INF	INF	INF	INF	INF	**1.85**	0.00002
		m.415635	Glutamine synthetase, cytosolic	**GLN1**	41	**3.94**	3.5	5.0	3.5	4.8	2.9	**-2.65**	0.00000
	Amino acid metabolism	m.367066	Carbamoyl-phosphate synthase large chain, chloroplastic	**CARB**	132	**33.00**	16.0	12.0	17.0	55.0	65.0	0.43	0.45854
Chloroplastic translation	Regulation of chloroplastic translation	m.405364	Chloroplast elongation factor Ts pro-protein	**PETs**	88	**0.20**	0.2	0.2	0.2	0.2	0.6	**1.93**	0.00000
	Chloroplast ribosome, large subunit	m.147308	50S ribosomal protein L4	**CL4**	26	**0.50**	0.5	0.5	0.5	0.5	0.9	**-1.12**	0.00000
Cytosolic translation	Regulation of cytosolic translation	m.360936	Eukaryotic translation initiation factor 4A	**EIF4A**	49	**1.97**	1.9	2.0	2.0	2.1	1.8	0.30	0.61189
		m.410544	Eukaryotic translation initiation factor 3 subunit J	**EIF3J**	24	**0.20**	0.3	0.3	0.3	0.3	0.2	-0.02	0.95698
		m.137660	Eukaryotic translation initiation factor 3 subunit G	**EIF3G**	36	**0.00**	0.0	0.0	0.0	0.0	0.0	0.01	0.97867
		m.414715	Elongation factor 1-alpha	**EF1A**	51	**0.70**	0.7	0.9	0.7	1.2	1.5	0.42	0.67798
	Cytosolic ribosome, small subunit	m.366080	40S ribosomal protein S4	**RPS4**	29	**2.34**	1.9	1.9	1.9	2.7	3.3	-0.41	0.56527
	Cytosolic ribosome, large subunit	m.416054	60S acidic ribosomal protein P0	**RPLP0**	33	**1.60**	0.9	1.1	0.9	0.9	1.6	0.23	0.73858
		m.384792	60S acidic ribosomal protein P2	**RPLP2**	10	**0.60**	0.8	0.7	0.8	0.6	1.0	0.07	0.93348

		m.415487	60S ribosomal protein L4	**RPL4**	43	**0.67**	0.7	0.7	0.7	0.6	0.8	0.11	0.90120
		m.416634	60S ribosomal protein L5	**RPL5**	34	**0.70**	0.7	0.8	0.7	0.7	0.8	0.31	0.68100
		m.417233	60S ribosomal protein L6	**RPL6**	27	**0.70**	0.7	0.7	0.7	0.7	1.0	0.44	0.50406
		m.358078	60S ribosomal protein L7	**RPL7**	27	**0.70**	0.8	0.8	0.8	0.7	0.9	-0.18	0.86624
		m.415229	60S ribosomal protein L9	**RPL9**	23	**0.60**	0.6	0.8	0.6	0.7	0.7	-0.24	0.77162
		m.413488	60S ribosomal protein L11	**RPL11**	21	**0.70**	0.9	0.8	0.9	0.7	1.1	0.06	0.95336
		m.373292	60S ribosomal protein L12	**RPL12**	20	**0.60**	0.9	0.9	0.9	0.6	0.9	0.32	0.60924
		m.415461	60S ribosomal protein L19	**RPL19**	18	**0.38**	0.4	0.4	0.4	0.3	0.3	0.25	0.75776
		m.418238	60S ribosomal protein L21	**RPL21**	16	**0.50**	0.5	0.6	0.5	0.7	0.6	0.29	0.66683
		m.418624	60S ribosomal protein L23	**RPL23**	14	**0.50**	0.5	0.5	0.5	0.7	0.7	-0.19	0.78598
		m.416193	60S ribosomal protein L37	**RPL37**	10	**0.60**	0.7	0.9	0.7	0.6	0.7	0.07	0.92890

(6) Other biological processes

Major category	Specific category	Protein identifier	Curated description	Abbr.	MM (kDa)	Protein abundance (FC: -N/+N)						Transcript abundance	
						Average FC	WSpC	emPAI	NSAF	Top3 PI	Top3 TIC	Log_2 FC (+N/-N)	*q*-value
Membrane organization	Thylakoid membrane organization	m.244283	FZO-like protein, chloroplastic	**FZL**	109	**0.00**	0.0	0.0	0.0	0.0	0.0	0.20	0.58625
		m.216464	Vesicle-inducing protein in plastids1	**VIPP1**	33	**2.18**	1.6	2.1	1.6	3.5	2.1	**1.19**	0.00004
	Cytoskeleton organization	m.381961	Tubulin beta chain	**TUBB**	54	**1.38**	1.2	1.5	1.3	1.2	1.5	**1.02**	0.00277
Cell division	Cell division	m.309971	ERBB-3 binding protein 1 EBP1	**EBP1**	41	**0.20**	0.2	0.3	0.2	0.2	0.2	-0.23	0.61027
		m.391974	Protein RETARDED ROOT GROWTH, mitochondrial	**RRG**	45	**INF**	INF	INF	INF	INF	INF	0.54	0.12145
Signal transduction	Signal transduction	m.413740	14-3-3 protein	**14-3-3**	29	**3.58**	3.0	4.8	3.0	4.3	2.8	-0.51	0.35359
		m.420836	Calcium-dependent protein kinase	**CDPK**	60	**2.70**	1.7	1.5	1.7	2.7	1.7	**0.81**	0.02174
		m.413885	Hypersensitive-induced response protein	**HIR**	32	**3.00**	3.0	4.8	3.0	4.5	2.4	**1.83**	0.00000
Regulation of transcription	Regulation of transcription	m.323842	GCN5-related N-acetyltransferase, chloroplastic	**GNAT**	23	**5.94**	5.4	4.2	5.4	6.4	8.3	-0.16	0.70894
		m.339185	HLA8-like nuclease	**HLA8**	21	**0.34**	0.3	0.3	0.3	0.3	0.5	**2.62**	0.00000
	RNA processing	m.235791	rRNA 2'-O-methyltransferase fibrillarin	**FIB**	33	**0.40**	0.4	0.4	0.4	0.4	0.6	**-1.52**	0.00000
Nucleosome assembly	Nucleosome assembly	m.166547	Histone H4	**H4**	14	**1.70**	1.1	1.3	1.2	1.7	1.6	-0.28	0.59188
		m.135435	Histone H5 family protein	**H5**	69	**0.07**	0.1	0.1	0.1	0.0	0.1	**2.46**	0.00000
Iron assimilation	Iron assimilation	m.360182	Transferrin	**TTF1**	121	**0.30**	0.4	0.4	0.4	0.1	0.2	-1.01	0.09834
		m.136962	Ferric reduction oxidase	**FRE**	87	**0.07**	0.1	0.1	0.1	0.0	0.1	0.50	0.06126
		m.413714	Ferritin, chloroplastic	**FER**	31	**1.43**	1.2	1.4	1.2	1.6	1.5	0.48	0.33174
		m.357380	ABC transporter B family member	**ABCB**	81	**6.40**	4.7	4.7	4.9	11.0	6.7	0.01	0.99797

Other transmembrane transporters	ATP-coupled transmembrane transport	m.352416	Proton-efflux P-type ATPase, plasma membrane-type A	**H+ATPase_A**	112	**1.96**	1.5	1.9	1.5	2.8	2.1	-0.75	0.19110
		m.363780	Proton-efflux P-type ATPase, plasma membrane-type B	**H+ATPase_B**	113	**3.40**	3.1	4.5	3.1	3.4	2.7	-0.05	0.96987
	Porin-like channel protein	m.421753	Outer envelope pore protein 24 A, chloroplastic	**OEP24_A**	29	**0.32**	0.4	0.4	0.4	0.2	0.2	**6.13**	0.00000
		m.341627	Outer envelope pore protein 24 B, chloroplastic	**OEP24_B**	24	**0.40**	0.4	0.4	0.4	0.4	0.6	-0.26	0.44244
		m.378383	Voltage-dependent anion-selective channel protein, mitochondrial	**VDAC**	30	**0.75**	0.8	0.7	0.8	0.7	0.8	**1.46**	0.00015
	Major facilitator superfamily antiporter	m.29156	Probable hexose phosphate transport protein, chloroplastic	**HPT**	62	**2.60**	1.2	1.2	1.2	3.1	2.1	**-0.74**	0.01283

(7) Proteins of unknown function

Major category	Specific category	Protein identifier	Curated description	Abbr.	MM (kDa)	Protein abundance (FC: -N/+N)						Transcript abundance	
						Average FC	WSpC	emPAI	NSAF	Top3 PI	Top3 TIC	Log_2 FC (+N/-N)	*q*-value
Identified proteins of unknown function	Probable cell wall protein	m.372532	FAS1 domain-containing protein	NA	28	**INF**	INF	INF	INF	INF	INF	**2.08**	0.00000
		m.270148	Proline-rich extensin signature-containing protein B	NA	60	**0.40**	0.6	0.8	0.6	0.4	0.5	**0.70**	0.03351
	Nucleic acid binding protein	m.222753	KH domain-contaning protein	NA	39	**12.00**	8.6	13.0	9.0	12.0	8.4	0.16	0.76264
		m.262528	SAP domain-containing protein	NA	86	**0.07**	0.1	0.1	0.1	0.1	0.1	-0.04	0.95415
	NAD(P)-binding domain-containing proteins	m.314583	Galactose-binding domain-like, CIA-30 and Rossmann-fold NAD(P)-binding domain-containing protein A, chloroplastic	NA	76	**0.57**	0.5	0.9	0.5	0.7	1.0	**-1.22**	0.00000
		m.13924	NAD(P)-binding Rossmann-fold superfamily protein B, chloroplastic	NA	54	**0.48**	0.5	0.4	0.5	0.5	0.5	0.00	0.98558
		m.66681	NAD(P)-binding Rossmann-fold superfamily protein C, chloroplastic	NA	36	**0.80**	0.8	0.8	0.8	0.6	1.1	0.37	0.18420
	Rhodanese-like domain-containing protein	m.269266	Rhodanese-like domain containing protein A, chloroplastic	NA	29	**1.87**	1.3	1.8	1.3	2.5	1.8	**-1.35**	0.00000
		m.58086	Rhodanese-like domain containing protein B, chloroplastic	NA	69	**0.33**	0.4	0.5	0.4	0.2	0.2	**0.72**	0.01514
		m.381311	Rhodanese-like domain containing protein D, chloroplastic	NA	26	**0.50**	0.6	0.6	0.6	0.3	0.4	**-1.80**	0.00000
	Other identified proteins	m.302725	COBW domain-containing protein, chloroplastic	NA	56	**0.20**	0.2	0.3	0.2	0.1	0.1	**0.75**	0.00179
		m.243853	DUF1517 family protein, chloroplastic	NA	47	**4.13**	2.2	2.9	2.2	8.0	5.9	0.25	0.54418
		m.230740	DUF1995 domain-containing protein	NA	42	**5.14**	5.6	4.9	5.7	4.9	4.6	**-0.72**	0.01137
		m.419428	Glyoxal/galactose oxidase	**GOX**	48	**INF**	INF	INF	INF	INF	INF	**0.81**	0.01888
		m.286009	MORN repeat-containing protein	NA	48	**0.50**	0.8	0.8	0.9	0.5	0.7	0.39	0.25849
		m.317171	NTF2-like domain-containing protein, mitochondrial	NA	31	**2.68**	2.3	2.6	2.3	3.6	2.6	**-1.16**	0.00003
		m.362403	PLAC8 family protein	NA	19	**0.28**	0.3	0.4	0.3	0.2	0.3	**-0.99**	0.01917

		m.184707	Pollen allergen Poa pIX/PhI pVI family protein	NA	19	**0.70**	0.7	0.8	0.7	0.9	1.3	**2.72**	0.00000
		m.178172	Streptococcal non-M secreted SibA family protein	**SIBA**	27	**0.32**	0.3	0.3	0.3	0.2	0.5	0.14	0.70739
		m.274860	TraB family protein, chloroplastic	NA	71	**0.40**	0.4	0.5	0.4	0.3	0.7	**-0.89**	0.00258
Unknown proteins	Unknown proteins	m.412999	Unknown protein_AB	**UAB**	21	**0.35**	0.5	0.6	0.5	0.3	0.4	**3.81**	0.00000
		m.389943	Unknown protein_F	**UF**	29	**0.40**	0.4	0.5	0.4	0.4	0.3	**1.72**	0.00000
		m.135510	Unknown protein_I	**UI**	49	**0.00**	0.0	0.0	0.0	0.0	0.0	**2.49**	0.00000
		m.239299	Unknown protein_J	**UJ**	21	**0.50**	0.5	0.5	0.5	0.6	0.9	**-1.34**	0.00000
		m.349190	Unknown protein_K	**UK**	30	**0.00**	0.0	0.0	0.0	0.0	0.0	**1.19**	0.00002
		m.364518	Unknown protein_L	**UL**	22	**0.11**	0.2	0.1	0.2	0.0	0.0	**1.81**	0.00000
		m.169592	Unknown protein_P	**UP**	16	**0.57**	0.5	0.6	0.6	0.6	0.8	-0.02	0.96073